Cranfield Institute of Technology
School of Mechanical Engineering

Ph.D Thesis

Academic Year 1989-90

Ameen Ahmed Nassar Al-Edani

Efficient Fracture Mechanics Programming System for Linear and Non-Linear Proplems Using Finite-Element and Boundary-Element Methods

Supervisor:	**Dr A M El-Zafrany**
External Examiner:	**Dr R Fenner, D.Sc.**
Internal Examinar:	**Prof R L Elder**

This Thesis is Submitted in Candidature for the Degree of Doctor of Philosophy.

June 1990

TO MY

FAMILY

ACKNOWLEDGEMENTS

The author would like to express his most sincere gratitude and thanks to **Dr A M EL-Zafrany**, for his stimulating supervision, valuable guidance and human co-operation throughout this work.

The author would like to express his gratitude to **Professor R A Cookson** for his useful help and guidance during the early stages of development of this work.

Words are not enough to express the author's gratitude and sincere thanks to his government for all the help and support offered throughout his study in the UK.

Finally, the author would like to thank all members of his family for their moral support and help during the course of this work. He also wishes to thank his friends and colleagues for the useful discussions offered throughout this study.

SUMMARY

An attempt has been made, in this work, to design an efficient, linear-elastic and elasto-plastic, fracture mechanics package based upon finite and boundary element methods. The package contains many useful facilities such as, pre- and post-processors, different types of loading including inertial and thermal loading, and different types of finite and boundary elements. New crack-tip elements, and efficient algorithms for the analysis of J-integrals, have been derived. Elasto-plastic boundary element programs with different types of loading, and using a new subregion facility have also been developed. The package was employed for fracture mechanics analysis of some case studies with elastic, thermo-elastic, and elasto-plastic conditions, and with one and two modes of fracture. The results have proved that the package is very reliable and controllable, and new facilities and techniques, developed in this work, can provide useful tools for fracture mechanics analysis.

CONTENTS

CHAPTER 1

INTRODUCTION

1.1 General Introduction:

In many engineering problems, failure of loaded structures is frequently caused by the growth of cracks or crack-like flaws in the structure. For complex structures and loading conditions, no analytical solution is available for failure prediction due to the difficulty encountered in evaluating the field parameters at the crack tip. Therefore, numerical methods such as the finite element method *(FEM)* and the boundary element method *(BEM)* are more likely to be considered for such situations.

The usefulness of linear-elastic fracture mechanics *(LEFM)* and the elasto-plastic fracture mechanics *(EPFM)* has become widely recognized in the current trends towards the design of large and small size structures, with the increasing use of high strength materials, and with the development of welding techniques.

Fracture mechanics parameters such as stress intensity factors, *J*-integrals, and crack-opening displacements have become important parameters when evaluating the strength of a cracked structure, since they can represent the strength of the stress field at the crack tip and have critical values which determine whether or not the crack will propagate.

In the past, fracture mechanics parameters had been calculated for some geometrical shapes of cracks by using various analytical and experimental methods. However, such results are limited to geometrically simple shapes of cracks and structures.

Engineering problems with more complex shapes and boundary conditions may require investigation by means of methods offering greater flexibility than existing analytical and experimental techniques. The major two of such methods are the finite element method and the boundary element method, and

their accuracy and efficiency for the stress analysis of two and three dimensional problems are now undenied.

1.2 Objectives of the Work:

Using the finite element method and the boundary element method to solve fracture mechanics problems may require special elements and additional facilities. These elements and facilities are not fully recognized in most of the commercial packages available on the market, especially the boundary element packages. Therefore, the main objective of this work is to develop an efficient finite element and boundary element package specially designed to deal with static, elastic and elasto-plastic, two-dimensional, problems of fracture mechanics. Other complementary objectives are summarized as follows:

1. Special isoparametric finite and boundary crack-tip elements are to be developed and implemented in the package.

2. Facilities for efficient meshing, such as transition elements and transition blocks are to be included in the programming package.

3. The package would be capable of dealing with different types of loading, such as concentrated, pressure, inertial, centrifugal and thermal loading.

4. Efficient solvers such as the frontal solver are to be employed in the package.

5. Due to the sensitivity of the *BEM* to the geometrical shape of the problem and the applied loading and boundary conditions, an attempt should be made to improve the

accuracy of the boundary element elastic and elasto-plastic solutions. A subregion technique is to be employed for both elastic and elasto-plastic analyses. Efficiency measures aiming at reducing computer *CPU* time and/or human being effort should also be considered.

6. Methods for the calculation of fracture mechanics parameters will be thoroughly investigated so as to improve their accuracy, and new ideas should also be explored.

7. Relevant pre- and post-processing facilities are to be developed for efficient mesh generation, plotting and useful graphical representation of results.

8. Developed programming facilities must be thoroughly validated so as to assure the reliability of the programming package.

9. Some case studies will be analyzed aiming at, evaluating the efficiency of the package developed, and making a useful comparison between finite element and boundary element techniques.

1.3 Layout of the Thesis:

This work is based upon three basic aspects, finite element methods, boundary element methods, and their applications to fracture mechanics. The thesis starts with a general introduction and a summary of the basic objectives of the work. A detailed literature review of the development of different fracture mechanics aspects is summarized in the next chapter.

For the completion of the thesis material, the basic principles of stress analysis, linear-elastic fracture mechanics, and

elasto-plastic fracture mechanics are reviewed in chapter 3. However, a separate chapter, chapter 4, is devoted to the discussion of a generalized derivation for the *J*-integral parameter, and some interesting ideas will be introduced there.

A review of the basic theory of the finite element method for linear-elastic, and elasto-plastic, fracture mechanics analysis is presented in chapter 5, together with the derivation of some efficient crack-tip finite elements.

Chapter 6 contains a summary of the theory of the boundary element method for elastic and elasto-plastic analyses. Some accuracy measures, together with the subregion technique will be explained.

The use of the finite element and boundary element results for the calculation of various fracture mechanics parameters is investigated in chapter 7. Some interesting new ideas for improving the accuracy of those parameters are also introduced.

It was not possible to describe the details of the programming package developed in this work without exceeding volume limits. Hence, it was decided to present a brief description of the basic programs constituting the package, in chapter 8.

Different validation cases and other case studies are described in chapter 9, together with their results obtained by means of the package compared, according to each case, with corresponding solutions available in the literature.

Finally, the major conclusions and recommendations for future work are summarized in chapter 10.

CHAPTER 2

LITERATURE REVIEW

2.1 General Review in Fracture Mechanics:

The earliest investigation into fracture mechanics would appear to be that of Leonardo da Vinci, in his study mentioned in Ref.[1]. The study dealt with the variation of the failure strength of iron wire, using different lengths of wire with the same diameter.

It was mentioned in Ref.[2], that in 1835 Lloyd and Hodkinson studied the same effects but for the case of iron bars. It was until 1939, when it was explained by Weibull, using statistical analysis, that those effects were due to flaws in material under test [Ref.3].

The first attempt at applying a mathematical approach to fracture was carried out by Inglis in 1913 [Ref.4], followed by Griffith in 1920 [Ref.5], and then Westergaard in 1939 [Ref.6].

The main work of Inglis lies in the determination of the stress around a hole in a plate, the hole being elliptic in form. He claimed that the results obtained were exact and consequently applicable to the extreme limits of the form which an ellipse can assume.

Griffith [Ref.5] formulated the well-known concept that an existing crack will propagate if thereby the total energy of the system is lowered. He assumed that there is a simple energy balance, consisting of a decrease in elastic strain energy within the stressed body as the crack extends, counteracted by the energy needed to create the new crack surface. His theory allows for the estimation of the theoretical strength of brittle solids and also gives the correct relationship between fracture strength and defect size.

Westergaard [Ref.6] treated crack problems by employing the complex variable technique. He used a complex stress function which satisfied the nominal requirement of compatibility *(bi-harmonic equation)* in order to determine the displacements and stresses in the immediate neighbourhood of a crack in an

infinite plate subjected to a remote bi-axial stress.

Griffith's concept was first related to brittle fracture of metallic materials by Zener and Hollomon in 1944 [Ref.7]. Soon after, Irwin [Ref.8] pointed out that a Griffith-type energy balance should exist between the stored strain energy and the surface energy plus the work done in plastic deformation. Irwin also recognized that for relatively ductile materials the energy required to form new crack surface is generally insignificant compared to the work done in plastic deformation, and he defined a material property G as the total energy absorbed during cracking per unit increase in crack length and per unit thickness. This parameter was called the *'energy release rate'* or *'crack driving force'*.

In the middle of 1950s Irwin [Ref.9] contributed another major advance by showing that the energy approach is equivalent to the stress intensity approach, according to which fracture occurs when a critical stress distribution ahead of the crack tip is reached. The material property governing fracture may therefore be stated as a critical stress intensity K_c, or in terms of energy as a critical value G_c.

Demonstration of the equivalence of G and K has provided the basis for the development of disciplines for linear-elastic fracture mechanics *(LEFM)*. This is because the form of the stress distribution around and close to a crack tip is always the same.

The beginning of elasto-plastic fracture mechanics *(EPFM)* can be traced to the early development of *LEFM*, notably Wells's work on crack opening displacement *(COD)*, which was published in 1961. However, the greater complexity of the problems of analysis has unavoidably led to somewhat slower progress. *EPFM* is still very much an evolving discipline.

During the seventies numerical methods such as the finite element method *(FEM)*, and later on the boundary element method *(BEM)* have provided greater flexibility than the existing

analytical techniques in analyzing engineering problems with more complex shapes and loading conditions. For fracture mechanics problems special finite and boundary element formulations have been developed. The development of such formulations as well as the development of fracture mechanics techniques will be reviewed in the following sections.

2.2 Review on the Development of Singular Crack-Tip Elements:

The implementation of the finite and boundary element methods in fracture mechanics problems is difficult due to the stress field singularity which exists at the crack tip. The two most successful methods of approach to solve this problem, would appear to be the so-called energy technique and the singularity function formulation.

To overcome the necessity for excessive mesh refinements, several elements containing the proper form of singularity have been developed during 1971 to 1987.

In 1971, Tracey [Ref.10] introduced a new type of finite element, which embodied the inverse square root singularity present near a crack in an elastic medium. He selected the displacement function of the element such that the displacements are continuous everywhere and the near-tip displacements are proportional to the square root of the distance from the crack tip.

Blackburn [Ref.11], in 1973, developed special singularity elements with square root displacement variation radiating from the crack tip and they conformed with adjacent standard displacement elements. These elements were extended to three dimensions by Blackburn and Hellen in 1977 [Ref.12].

In 1975, an alternative procedure to achieve the singularity has been introduced by Henshell and Shaw [Ref.13], as well as Barsoum [Ref.14]. These two references showed independently

that the quadratic isoparametric elements can possess the required singularity by moving the mid-side nodes on the two sides meeting at the crack tip to the quarter points. This movement will be carried out in the cartesian plane without any effect on element intrinsic shape functions. Hence, Henshell and Shaw concluded that special finite elements for crack tips are not necessary for plane stress/strain analyses, since the whole structure can be analyzed using absolutely standard 8-node elements, where the elements adjacent to the crack tip are to be distorted to produce the proper singularity.

Barsoum carried out a comparison between two types of those elements, and showed numerically that the crack-tip 6-node, triangular element gives better results than the crack-tip 8-node, quadrilateral element, because, as he claimed [Ref.14], that the strain energy of the later element is unbounded.

In the same year, Hibbitt [Ref.15] offered a possible explanation for such behaviour based on the proof that the strain energy and hence the stiffness of such a quadrilateral element is unbounded.

Tracey and Cook [Ref.16], in 1977, described a finite element formulation with a special 3-node triangular element encircled the singularity and focused to share a common node at the singular point. The shape functions of the element have the appropriate r^n variation mode $(0<n<1)$ and a smooth angular mode expressed in element natural coordinates. The conditions of continuity, low order solution capability, and numerical integration of the singularity element have been discussed.

In the same year, Barsoum [Ref.17] showed that the triangular and the prismatic quadratic isoparametric elements, formed by collapsing one side and placing the mid-side nodes near the crack tip at the quarter points, contained the $1/\sqrt{r}$ singularity of elastic fracture mechanics and the $1/r$ singularity of perfect plasticity. He concluded that the proposed elements have wide applications in fracture mechanics analysis of structures where ductile fracture is investigated.

In 1978, Gallagher Ref.[18] reviewed the past developments in finite element calculation of design parameters for linear fracture mechanics. The component aspects of singularity element development were identified as stiffness formulation based on classical-solution displacement fields, polynomial displacement fields, and isoparametric concepts as well as hybrid formulations.

In the same year, Stern and Becker published a paper [Ref.19], in which the shape functions for a 6-node triangular element with $\sqrt{r}$ displacement field were given. Also numerical results were presented, as well as the shape functions for a 15-node three-dimensional element.

Also in 1978, it was shown [Ref.20] that, for a 12-node quadrilateral isoparametric element, the inverse square root singularity of the strain field at the crack tip can be obtained by collapsing the quadrilateral element into a triangular element around the crack tip and placing the two nodes of two sides of the triangle at 1/9 and 4/9 of the length of the side from the tip. This was analogous to placing the mid-side nodes at the quarter points in the vicinity of a crack tip for the quadratic isoparametric elements. The authors of this reference concluded that with this method the displacement compatibility is satisfied throughout the region, and there is no need for special crack-tip elements.

In 1979, the use of 8-node parabolic isoparametric element as a crack-tip element was tested by Fawkes and Owen [Ref.21], who demonstrated the use of a hybrid element as a special case for the boundary integral method.

In the same year, Heymann [Ref.22] reviewed the usefulness of the standard elements for fracture mechanics with most emphasis being placed on linear elastic plane analysis. He concluded that the iterative method used by Swedlow in 1978 would still be used due to the inability of linear elastic methods to account for the changing of singularity surrounding the crack

tip, and it was an interesting alternative to use high order elements, and to place nodes iteratively to obtain the correct order of singularity.

Also in 1979, Morris and Wait [Ref.23] showed how the standard transformation for singular isoparametric elements can be combined with non-standard reference elements. Such reference elements may have nodes which are not symmetrically placed along the sides, and they may have curved sides.

Lin and Tong [Ref.24], in 1980, formulated special notch elements to account for the singular stress around the tip of a sharp V-notched plate. They concluded that the special notch elements could be matched compatibly with the standard isoparametric elements outside the notch-tip region.

In 1981, Blanford [Ref.25] presented a multi-domain boundary element formulation for the analysis of general two-dimensional plane stress/strain crack problems. The analysis was performed using traction singular quarter-point boundary elements on each side of the crack tip with and without transition elements. Blanford concluded that the use of transition elements in conjunction with the traction singular quarter-point elements gives improved results with coarse meshes for the mixed mode crack problems, while the use of transition elements for *mode I* problems yields approximately the same results as obtained without transition elements for both tension and bending crack problems.

In 1982, the boundary integral equation method *(BIEM)* was used for the analysis of centrally cracked plate [Ref26]. The authors concluded that a further development and validation were necessary before the *BIEM* could be applied with complete confidence to the treatment of stress singularities.

In the same year, Smith and Mason [Ref.27] presented a general formulation of the boundary element method for applications of both straight and curved crack problems in two dimensions. A technique was adopted, in which the region was subdivided along

the line of the crack, and traction singular quarter-point elements were used to provide an accurate crack-tip representation of displacement and traction. The authors concluded that the *BEM* could be applied successfully to curved crack problems, with a recommendation to use traction singular quarter-point elements.

Reference [28], presented in 1984, a historical overview on the use and development of crack-tip isoparametric elements. Also a recommendation was made, concerning the use and installation of such elements when modelling a crack tip.

In the same year, Banks-Sills and Bortman [Ref.29] re-examined the quarter-point 8-node isoparametric serendipity element. They concluded that the stresses were square-root singular in a small region adjacent to the crack tip, and that the strain energy, and hence the stiffness of the above element were bounded. Also they recommended the use of quarter-point quadrilateral elements, and claimed that these elements yields excellent results without any poor behaviour.

In 1985, Wahba [Ref.30] investigated special displacement crack-tip elements. These elements are based on 6-node quadratic triangular isoparametric elements, and have a singular stress proportional to the reciprocal of the square root of the radial distance from the crack tip. The singular elements were used in the region surrounding the crack tip, for a problem of an infinite isotropic plate containing a straight-through crack, subjected to a constant out-of-plane bending. Wahba concluded that the singular elements have satisfied the essential convergence criteria, namely, continuity of displacements, inter-element compatibility, constant-strain modes, and rigid-body motion modes.

Hellen [Ref.31], introduced, in 1986, a new approach to match the classical crack-tip behaviour of displacements in the vicinity of a crack tip. In his approach, instead of using special elements containing the tip node and the required displacement variations, as given by the classical crack-tip

equations of elasticity, generalized constraints were specified to relate individual degrees of freedom along rays emanating from the tip. He concluded that the developed relations have reflected the classical behaviour and could be extended to include a secondary term due to such effects, as thermal strains.

In 1987, Al-Edani [Ref.32] studied the use of three types of singular isoparametric crack-tip elements using the finite and boundary element methods. Also he introduced a new crack-tip element, the Lagrangian 9-node quadrilateral element with mid-side nodes of two adjacent sides moved to the quarter points. The new element was tested and a conclusion was drawn, that the results obtained by using such an element are more accurate than those obtained by using the 8-node and the 6-node isoparametric crack-tip elements.

2.3 Review on the Methods of Calculating Stress Intensity Factors:

Stress intensity factors represent very useful parameters in linear-elastic fracture mechanics, since they can be used for the description of the stress field in the vicinity of a crack tip. They can also be compared with material critical values to assess its strength against brittle or sudden failure. During the past years, several methods have been developed to calculate such parameters.

In 1971, Tracey [Ref.10] used the finite element method with the inverse square-root singularity elements to calculate the stress intensity factors. He showed that by using the above elements near the crack tip in two typical crack configurations, stress intensity factors within 5% of the accepted values had been obtained, with meshes having as few as 25 degrees of freedom.

Cartwright and Rooke [Ref.33], in 1974, developed a *'compounding'* method for calculating stress intensity factors at the tips of cracks in structures having complex geometrical configurations. This method was based on the systematic evaluation of the effects on one particular crack tip in the presence of other cracks, holes, and structural boundaries.

In 1977, Mendelson [Ref.34] presented a boundary integral equation method to calculate the stress intensity factor directly. This *BIEM* included the crack-tip singularities, so that the stress intensity factor became just one more unknown in the set of boundary unknowns, so it could be calculated directly to avoid the uncertainties of plotting and extrapolation. The method was applied to problems of notched beams in tension and bending.

Takao and Kawata [Ref.35], in 1979, applied the boundary collocation procedure to the plane elastic problem of a rectangular tensile cracked plate with ends being considered as free from shear and constrained to a uniform vertical displacement. They concluded that for the calculated stress intensity factors, it seemed that there were two characteristic effects of the specimen length/width ratio.

Vainshtok [Ref.36], in 1980, proposed a procedure of virtual crack variation technique for calculating stress intensity factors for mixed mode cracks. He pointed out that this technique was based on curvilinear crack theory developed by Cherepanov in 1974 and Hellen in 1975. Also he concluded that the above procedure had yielded similar results compared with the energy method of calculating stress intensity factors for mixed mode cracks.

In 1982, a method for the determination of stress intensity factors of a cracked body using a conic-section simulation model of the crack surface was presented in Ref.[37]. The authors claimed that this method has improved the accuracy of the stress intensity factor values, and they mentioned that it is simple enough to be used with most standard isoparametric

finite element programs, and it eliminates the necessity of extrapolation to estimate the stress intensity factors at the crack tip.

Rooke and Hutchins [Ref.38], introduced, in 1984, an integral transform technique to evaluate stress intensity factors for a crack at the edge of a hole subjected, on its perimeter, to a localized force, either radial or tangential. These stress intensity factors can be used as numerical Green's functions to obtain both K_I and K_{II} stress intensity factors. They concluded that this Green's function technique involves simple summation methods which do not require large expensive computing facilities and the developed technique and similar techniques, have been used successfully to analyze experimental data on crack growth under fretting conditions.

In 1985, a constrained finite element for the two-dimensional crack problems in common with other elliptic problems containing a boundary singularity was introduced [Ref.39]. The method has been summarized such that the singularity was surrounded by a super element containing a refined mesh whose interior nodal values were constrained to agree with the first few terms of the known expansion for the solution. The authors claimed that the calculation yields the expansion coefficients directly, and the method has been applied to determine stress intensity factors for a variety of configurations and the results are in excellent agreement with those obtained by other methods.

In the same year, Walsh and Pipes [Ref.40] used the finite element method and the energy release rate principle for the determination of *mode I* stress intensity factors for selected crack configurations. This approach relates the change in the strain energy resulting from crack advancement, to the change in the stiffness matrix of the structure containing the crack. The method was tested and the generated solutions were compared with analytical solutions.

In 1986, Ref.[41] presented a finite element technique to calculate *mode I* stress intensity factors within the framework of plane linear-elastic fracture mechanics. Also it has been shown that the ratio of K for two separate crack problems can be approximated by the ratio of crack opening displacements near the crack tips, as obtained from conventional finite element solutions.

In the same year, a comparison between three methods for calculating stress intensity factors was shown in Ref.[42]. These methods were the displacement extrapolation, the J-integral and Griffith's energy calculations, and the stiffness derivative technique. The authors observed that the stiffness derivative method yields the most accurate results, whereas displacement extrapolation is the easiest method to implement and still gives reasonable accuracy.

Also in 1986, Baker and Parker [Ref.43] used the boundary element method with several methods for calculating stress intensity factors in linear-elastic fracture mechanics, the methods were based on utilizing the classical crack-tip solutions for stresses and displacements. They concluded that the methods based on the displacement values are more accurate than the stress methods, and the displacement extrapolation method is consistently accurate for two-dimensional and axisymmetric fracture mechanics problems.

2.4 Review on the Development of J-Integral and Crack Opening Displacement Approaches:

The crack opening displacement *(COD)* approach was first introduced by Wells [Ref.44] in 1961. The philosophy behind the approach is that, in the regimes of fracture-dominant failure, the stresses and strains in the vicinity of a crack or defect are responsible for failure. For practical engineering problems the stresses always exceed the yield strength at crack tips and

plastic deformation occurs. Thus failure is brought about by stresses and hence plastic strains exceeding certain respective limits [Ref.7].

In 1966, Burdekin and Stone [Ref.45] provided an improved basis for the *COD* concept. They used Dugdale's strip yield model to find an expression for the crack opening displacement.

The path independent *J*-integral proposed by Rice [Ref.46], in 1968, has been used as a fracture criterion, and as a technique for calculating stress intensity factors, since under *LEFM* conditions, the *J* value may be equated to the strain energy release rate G, which can be related by a simple expression to the stress intensity factor *K*. This technique has now been widely recognized and used for both linear and nonlinear fracture mechanics.

In 1975, Knott [Ref.47] discussed the problems in applying *LEFM* to the fracture of metals. He mentioned that the crack opening displacement and the *J*-integral approaches could be employed to characterize fracture in some ways which may be open to discussion, but should be tested by experiment, also the calculation of the *COD* or *J* could be carried out using finite element techniques, but a part of the assumption is that, if failure is controlled by fracture in a test piece, it is controlled by a similar type of fracture in the structure.

In the same year, Turner [Ref.48] mentioned that the crack opening displacement, δ, and the *J*-integral are two proposals for describing the stresses and deformation at the tip of a sharp crack embodied in a region of a yielding material. Also he showed that the two concepts can be related in the form $J = MY\delta$, where Y is the uniaxial yield stress of the material, and M a factor with value between about 1.0 to 2.5. Finally, he concluded that either *COD* or *J* offers a reasonable one term description of the conditions at the tip of an elasto-plastic crack.

In 1979, Ref.[49] presented the path independent *J*-integral as the energy release rate during crack extension, also it showed the usefulness of the *J*-integral in fracture problems, where numerical values of the *J*-integral in the presence of body forces, thermal strains, inertia effects, and preloadings were evaluated using the finite element method.

In the same year, Miyoshi and Shiratori [Ref.50] described a finite element analysis, which showed the correlation between the *J*-integral and the crack opening displacement.

Again in 1979, the authors of Ref.[51] investigated experimentally and numerically *(by means of the finite element method)* the calculation of crack opening displacements from crack-mouth opening displacement *(CMOD)* by measuring it at different distances from the crack tip, and then by extrapolating the results to the crack tip.

In 1980, a method for estimating the dynamic stress intensity factor by using the finite element method and the path independent *J*-integral was developed [Ref.52]. The authors concluded that the results of the computation for the stress intensity factors of pure and mixed modes have agreed well with analytical solutions published, also they recommended this method because it does not require neither a fine mesh near the crack tip nor an element of special type.

Dodds, Read, and Wellman [Ref.53], presented,in 1983, some experimental and finite element results for the *J*-integral and the *CMOD* response for tensile panels containing short single-edge cracks. The experimental *J*-integral values were obtained by integrating strain and displacement quantities measured along an instrumented contour. The authors concluded that the short cracks $(a/w<0.25)$ in tensile panels have a radically different *J*-integral behaviour than that observed in tests with more traditional specimen geometries $(a/w>0.5)$. Also they claimed that conventional finite element and limit load approaches for *J*-integral prediction are inadequate for short

cracks commonly encountered in practice.

In the same year, Sladek and Sladek [Ref.54] formulated boundary integral equations, which give the relation between the crack opening displacement and the traction on the surface of a crack embedded in an infinite isotropic elastic body. The integral equations were transformed into spherical and cylindrical surfaces respectively, so as to be converted into a system of algebraic equations. Also the dependence of the stress intensity factor on the curvature of the cracks has been numerically calculated for a spherical crack with a circular contour under a constant load.

In 1984, Ref.[55] examined, in preliminary studies, the accuracy of solutions obtained by the boundary element method based on direct and indirect formulation. Also a formulation of the *J*-integral calculation by using the indirect method was performed, and applications were made on the analysis of a number of typical crack problems. The authors concluded that the *J*-integral method has given excellent accuracy for the selected problems.

Dodds and Read [Ref.56], in 1985, repeated the same study carried out by them in 1983 [Ref.53], with the introduction of a small stiffened zone near the crack tip, and by using plane-strain elements. They concluded that the results of the finite element *J*-integral and *CMOD* values are in a close agreement with experimental values, and the large geometry changes near the crack tip have a negligible effect on the finite element *J*-integral and crack-mouth opening displacement values.

2.5 Review on the Development of Elasto-Plastic Fracture Mechanics Concepts:

In 1969, Zenkiewicz, Valliappan, and King [Ref.57] presented a general formulation of the elasto-plastic matrix for evaluating stress increments from those of stresses for any yield surface with an associated flow rule, also an *'intial stress'* computational process was proposed, which, as the authors claimed, showed to give a more rapid convergence than other approaches, to permit large load increments without violating the yield criteria, and to establish lower bound solutions. Several solutions demonstrated stress distribution, strain development, and growth of plastic enclaves were presented for both von Mises and Coulomb *(Druker)* type yield criteria.

In 1971, the use of the finite element method applied to elasto-plastic analysis of a cracked plate was demonstrated [Ref.58]. In this demonstration , first, the effect of the plate thickness on the growth of the plastic zone and the stress distributions along the leading edge of the crack tip were studied, second, the cyclic behaviour of the element near the crack tip and the deformation of the crack surface were analyzed for pulsating and completely reversed loads.

Tracey [Ref.59], in 1976, carried out an incremental plasticity finite element formulation for the analysis of a complete field problem including the extensively deformed elasto-plastic region near the crack tip, and the remote elastic region. He claimed that the formulation has general applicability and can be used to solve small scale yielding problems for a set of material hardening exponents. The distribution of the *COD* at the crack tip and through the elasto-plastic zone was presented as a function of the elastic stress intensity factor and material properties.

In 1979, Ref.[60] presented some results of an elasto-plastic finite element analysis on a centrally cracked plate. A comparison was made, on features like crack tip plastic zone,

intensities of plastic strain near the tip, the major principle stress in the crack tip region, crack opening displacements, values of the *J*-integral, and crack separation energy rates, all corresponding to different biaxial stress states.

In the same year, Hammouda and Miller [Ref.61] showed an elasto-plastic analysis of notches. The authors concluded that it is possible to predict the effect of notch plasticity on the behaviour of short propagating cracks, and a crack may initially propagate at a decreasing rate until it generates crack tip plasticity which is greater than the elastic threshold stress intensity condition.

Pilcer and Ohlson [Ref.62], carried out, in 1983, experimental and numerical investigations to discuss the relation problems between fracture toughness parameters (*COD*, *J*, *K*). It was found that generally known relations valid in linear elasticity, can be extended into the elasto-plastic range through the use of certain factors, which take into account the strain hardening exponent. The authors concluded that the numerical evaluations together with the experimental investigations showed that the measured and calculated plastic components of the clip gage displacements suggested a presence of plane-strain during experiments, even when some of the requirements of recommended testing procedure in the *COD* testing were not fulfilled.

In 1985, Ref.[63] introduced an elasto-plastic finite element analysis for a three-point bend specimen geometry. The elasto-plastic parameters, such as *CTOD* and *J*, were determined from results of 2D and 3D finite element analyses. Analytical *CTOD* values were determined from the finite element model displacements. The authors concluded that the *J*-integral values determined from the 2D finite element results using direct contour integration were used in conjunction with the corresponding *CTOD* values to develop an improved correlation between *J* and *CTOD* for a wide range of material characteristics.

In the same year, a new alternative to subincrementation technique for the analysis of solid media with rate independent elasto-plastic material behaviour was presented [Ref.64]. The new procedure was called the ζ-method. The authors concluded that the numerical results obtained for an assortment problems by the finite element method had showed an improved numerical efficiency.

Again in 1985, Ref.[65] demonstrated the applicability of the selective reduced integration/penalty function method for the analysis of two and three dimensional fully-plastic fracture problems. The fully-plastic solutions for cylinders with a circumferential through-wall crack, and plates with a semi-elliptical surface crack subjected to remote uniform tension were calculated as a function of the hardening exponent.

Cruse and Polch [Ref.66], also in 1985, extended the boundary integral equation method of 2D elastic fracture mechanics to the elasto-plastic problems. The formulation is based upon a special elastic Green's function for the crack, thereby eliminating the need to model the crack itself. Application of the general formulation was made to problems of localized or limited plasticity. The authors concluded that, in those problems, the elastic stress intensity factor still provides a useful characterization for cyclic crack growth predictions.

In 1986, Ref.[67] presented an incremental implicit mechanical formulation for elasto-plastic problems, and two numerical resolution algorithms of the equation system. The authors concluded that the solutions obtained with the two algorithms are the same, since the mechanical formulation is separated from the resolution algorithms, also this method requires less computer time than the initial stress method in the case of elasto-plasticity with work hardening, and it is easy to implement in an elasto-plastic program based on the initial stress method.

In the same year, Cruse and Polch [Ref.68] republished the work they carried out in 1985 [Ref.66] with the use of a new algorithm for crack-tip plasticity modelling. This algorithm was explored for small and large-scale plasticity conditions.

Also in 1986, they presented a paper in two parts. Part one of this paper [Ref.69] deals with the formulation of a boundary integral equation model for fracture mechanics analysis of cracked plates, subjected to elasto-plastic behaviour or other, related body force problems. The basis of this formulation contrasts with other boundary integral equation elasto-plastic formulations, in the use of the Green's function for an infinite plate containing a stress free crack. Part two [Ref.70] covers the numerical implementation of the developed algorithm. An iteration solution scheme was adopted which eliminated the need for recalculation of the boundary integral equation matrices. The stability and accuracy of the algorithm were demonstrated for an uncracked, notch geometry, and a comparison with finite element results was made for a centrally cracked panel.

Cruse [Ref.71] presented, in 1988, a fundamental treatment of the boundary integral equation method and its application to fracture mechanics problems. Two and three dimensional, elastic, and elasto-plastic formulations and applications were presented. He concluded that the treatment includes all of the past as well as the current boundary element applications to fracture mechanics problems.

2.6 General Discussions and Conclusions:

It is clear from this literature review that a great amount of experimental, and finite element analyses have been carried out, and a variety of approaches and methods have been developed to estimate or to find valid relations, which can describe or relate certain fracture parameters such as stress

intensity factors, *J*-integrals, crack opening displacements, and fracture toughness. Also it is clear that there is no general relation, method, or criterion which can be valid for all fracture problems, because of the influence of other parameters such as plasticity, yielding, loading conditions, crack configurations, and material behaviour. Hence it can be concluded that further investigations and tests whether experimental or numerical are still necessary and required.

Other conclusion remarks can be summarized as follows:

a. A small amount of work for the solution of fracture problems by the boundary element method, has been carried out, compared with that based on the use of the finite element method.

b. A variety of singular crack-tip finite elements have been developed. The boundary crack-tip elements and the higher order elements need to be considered and tested. Singular elements with shape-function singularity may be advantageous to be developed, since they do not require any distortion in the mesh used.

c. The energy method for calculating stress intensity factors ought to be reviewed and tested against different crack configuration and loading conditions.

d. The *J*-integral technique should be generalized and applied to different crack problems with different loading conditions, such as inertial loading, thermal strains, and elasto-plastic behaviour, with the use of finite and boundary element methods, because no clear derivation or implementation of this technique to the finite or boundary element methods has been given in the literature.

e. The use of crack opening displacement technique in finite and boundary element methods requires further investigations and testing.

f. Finally, the elasto-plastic fracture mechanics approach with the use of finite and boundary element methods requires more attention and development, and further investigations to improve the applicability and the accuracy of such an approach is still very much valid and required.

CHAPTER 3

INTRODUCTORY CONCEPTS OF FRACTURE MECHANICS

3.1 Introduction:

In the process of designing structural or machine components one of the important steps is the selection of the material in such a way that under given loading and environmental conditions the component will perform its function properly. This is usually carried out by applying a "*failure criterion*" which is in general a comparison of a critical load intensity of the component with the characteristic strength parameter of the material. It is, therefore, clear that in order to predict failure of engineering structures, it is necessary to understand the basic concepts of stress analysis, linear-elastic fracture mechanics, and elasto-plastic fracture mechanics, and to link these via physical principles. Some of these concepts are summarized in this chapter.

3.2 Basic Concepts of Stress Analysis:

3.2.1 Stress:

Consider a three-dimensional body in equilibrium under the action of external forces F_n (n = 1,2,3,...) as shown in Fig.(3.1). Suppose that the body be sliced at a cross section C, with actual internal forces being kept on the surface of the cut to maintain equilibrium. Confining the attention to a small area δA on one of the cut surfaces, the proportion of the total internal force over the cross section acting on δA may be named δF. The force δF may be resolved into two components, one δP normal to the area, and the other δQ in the plane of the area as shown in Fig.(3.2). The intensity of these forces (*force per unit area*) at a point is termed the "*stress*". There are stresses associated with both the normal and the tangential components of the force δF, and these are given by:

$$\textit{direct stress,} \quad \sigma = \lim_{\delta A \to 0} \frac{\delta P}{\delta A} \qquad (3.1)$$

shear stress, $$\tau = \lim_{\delta A \to 0} \frac{\delta Q}{\delta A} \qquad (3.2)$$

In general, an infinitesimal prism element within a three-dimensional body has both direct and shear stresses acting on each of its six faces. In order to form a coherent reference system it is necessary to resolve the stress on each face in accordance with the coordinate system. This produces nine stress components, which may be represented by the following matrix:

$$\begin{bmatrix} \sigma_x & \tau_{xy} & \tau_{xz} \\ \tau_{yx} & \sigma_y & \tau_{yz} \\ \tau_{zx} & \tau_{zy} & \sigma_z \end{bmatrix}$$

where a single subscript indicates a direct stress, and a double subscript indicates a shear stress, and from moment equilibrium of the element, it can be deduced that:

$$\tau_{zx} = \tau_{xz},\ \tau_{zy} = \tau_{yz},\ \tau_{yx} = \tau_{xy} \qquad (3.3)$$

For some cases of configurations which possess geometrical or loading symmetries it may be advantageous to use cylindrical polar coordinates as shown in Fig.(3.3). The corresponding stress matrix is given as follows:

$$\begin{bmatrix} \sigma_r & \tau_{r\theta} & \tau_{rz} \\ \tau_{\theta r} & \sigma_\theta & \tau_{\theta z} \\ \tau_{zr} & \tau_{z\theta} & \sigma_z \end{bmatrix}$$

with

$$\tau_{r\theta} = \tau_{\theta r},\ \tau_{\theta z} = \tau_{z\theta},\ \tau_{zr} = \tau_{rz} \tag{3.4}$$

3.2.2 Equations of Equilibrium:

Consider an infinitesimal element with sides of lengths δx, δy, δz, respectively, being subjected to a general stress system in which increments of stress may occur. If only the forces in the x-direction have been considered, then the stress system is as shown in Fig.(3.4). Considering body forces, the equilibrium in the x-direction is satisfied by:

$$\frac{\partial \sigma_x}{\partial x} + \frac{\partial \tau_{xy}}{\partial y} + \frac{\partial \tau_{xz}}{\partial z} + X = 0 \tag{3.5}$$

Similarly y- and z-directions equilibrium is satisfied by:

$$\begin{aligned} \frac{\partial \sigma_y}{\partial y} + \frac{\partial \tau_{yz}}{\partial z} + \frac{\partial \tau_{yx}}{\partial x} + Y &= 0 \\ \frac{\partial \sigma_z}{\partial z} + \frac{\partial \tau_{zx}}{\partial x} + \frac{\partial \tau_{zy}}{\partial y} + Z &= 0 \end{aligned} \tag{3.6}$$

where X, Y, Z are the body force intensities *(force per unit volume)* in the x-, y-, and z-directions, respectively.

3.2.3 Boundary Equilibrium:

Consider a structure subjected to surface loads. Let ΔA be an infinitesimal surface area at a point on the boundary of the structure and $\Delta \vec{F}$ be the part of the external surface load which acts through ΔA. The traction vector $\vec{T}$ at such a point is defined as follows:

$$\vec{T} = \lim_{\Delta A \to 0} \frac{\Delta \vec{F}}{\Delta A} = \frac{d\vec{F}}{dA} \tag{3.7}$$

and it can be expressed in terms of its components in the x-, y-, and z-directions as follows:

$$\vec{T} = T_x\, i + T_y\, j + T_z\, k \tag{3.8}$$

Hence, at any part of the boundary where there is no acting load, it can be deduced that:

$$T_x = T_y = T_z = 0 \tag{3.9}$$

Employing equilibrium conditions between external surface load and internal surface stresses, it can be proved that:

$$\begin{aligned} T_x &= \ell\, \sigma_x + m\, \tau_{xy} + n\, \tau_{zx} \\ T_y &= \ell\, \tau_{xy} + m\, \sigma_y + n\, \tau_{yz} \\ T_z &= \ell\, \tau_{zx} + m\, \tau_{yz} + n\, \sigma_z \end{aligned} \tag{3.10}$$

where ℓ, m, n are the directional cosines of the outside normal to the surface at the considered point.

3.2.4 Strain:

There are many different methods for the definition of the direct strain. The simplest and oldest measure for direct strain is the Cauchy's engineering strain, which is defined as the ratio of the change of length to the original length, i.e.

$$\varepsilon_1 = \frac{\Delta S - \Delta S_o}{\Delta S_o} \tag{3.11}$$

Alternatively, the Green's strain is defined as follows:

$$\varepsilon_2 = \frac{\overline{\Delta S}^2 - \overline{\Delta S}_o^2}{2\, \overline{\Delta S}_o^2} \tag{3.12}$$

Considering the different components of strain, a strain matrix $[\varepsilon_{ij}]$ can be defined such that:

$$\overline{\Delta S}^2 - \overline{\Delta S}_o^2 = 2\ \Delta \underline{S}_o^t\ [\varepsilon_{ij}]\ \Delta \underline{S}_o \qquad (3.13)$$

where

$$[\varepsilon_{ij}] = \begin{bmatrix} \varepsilon_x & \varepsilon_{xy} & \varepsilon_{xz} \\ \varepsilon_{yx} & \varepsilon_y & \varepsilon_{yz} \\ \varepsilon_{zx} & \varepsilon_{zy} & \varepsilon_z \end{bmatrix}$$

$$\Delta \underline{S}_o = \{\ \Delta x \quad \Delta y \quad \Delta z\ \}\ ,$$

and Δx, Δy, Δz are the components of the vector with infinitesimal length ΔS_o.

Green's strain matrix can be defined explicitly in terms of the following components [Ref.72]:

$$\varepsilon_x = \frac{\partial u}{\partial x} + \frac{1}{2}\left[\left(\frac{\partial u}{\partial x}\right)^2 + \left(\frac{\partial v}{\partial x}\right)^2 + \left(\frac{\partial w}{\partial x}\right)^2 \right]$$

$$\varepsilon_y = \frac{\partial v}{\partial y} + \frac{1}{2}\left[\left(\frac{\partial u}{\partial y}\right)^2 + \left(\frac{\partial v}{\partial y}\right)^2 + \left(\frac{\partial w}{\partial y}\right)^2 \right]$$

$$\varepsilon_z = \frac{\partial w}{\partial z} + \frac{1}{2}\left[\left(\frac{\partial u}{\partial z}\right)^2 + \left(\frac{\partial v}{\partial z}\right)^2 + \left(\frac{\partial w}{\partial z}\right)^2 \right]$$

$$\varepsilon_{xy} = \frac{1}{2}\left(\frac{\partial v}{\partial x} + \frac{\partial u}{\partial y} \right) + \frac{1}{2}\left[\frac{\partial u}{\partial x}\frac{\partial u}{\partial y} + \frac{\partial v}{\partial x}\frac{\partial v}{\partial y} + \frac{\partial w}{\partial x}\frac{\partial w}{\partial y} \right]$$

$$\varepsilon_{yz} = \frac{1}{2}\left(\frac{\partial w}{\partial y} + \frac{\partial v}{\partial z} \right) + \frac{1}{2}\left[\frac{\partial u}{\partial y}\frac{\partial u}{\partial z} + \frac{\partial v}{\partial y}\frac{\partial v}{\partial z} + \frac{\partial w}{\partial y}\frac{\partial w}{\partial z} \right]$$

$$\varepsilon_{zx} = \frac{1}{2}\left(\frac{\partial u}{\partial z} + \frac{\partial w}{\partial x} \right) + \frac{1}{2}\left[\frac{\partial u}{\partial z}\frac{\partial u}{\partial x} + \frac{\partial v}{\partial z}\frac{\partial v}{\partial x} + \frac{\partial w}{\partial z}\frac{\partial w}{\partial x} \right]$$

where u, v, w are the displacement components in x-, y-, and z-directions, respectively.

Due to the symmetry of the strain matrix $[\varepsilon_{ij}]$, it can be represented in terms of an engineering 6-component vector $\underline{\varepsilon}$, where:

$$\underline{\varepsilon} = \{ \varepsilon_x \quad \varepsilon_y \quad \varepsilon_z \quad \gamma_{xy} \quad \gamma_{yz} \quad \gamma_{zx} \}$$

and

$$\gamma_{xy} = 2\,\varepsilon_{xy},\ \gamma_{yz} = 2\,\varepsilon_{yz},\ \text{and}\ \gamma_{zx} = 2\,\varepsilon_{zx}.$$

For the special case of two-dimensional problems, the strain vector may be reduced to:

$$\underline{\varepsilon} = \{ \varepsilon_x \quad \varepsilon_y \quad \gamma_{xy} \} \tag{3.14}$$

and by neglecting the high-order terms, the small-strain or Cauchy's strain components may be defined as follows:

$$\varepsilon_x = \frac{\partial u}{\partial x}, \quad \varepsilon_y = \frac{\partial v}{\partial y}, \quad \gamma_{xy} = \frac{\partial u}{\partial y} + \frac{\partial v}{\partial x}$$

Since the three components of strain are derived from two components of displacement for two-dimensional problems, some restrains must be placed on "*allowable*" strains, the strains must be compatible. By differentiating the components of equation (3.14), the following can be obtained:

$$\frac{\partial^2 \varepsilon_x}{\partial y^2} + \frac{\partial^2 \varepsilon_y}{\partial x^2} - \frac{\partial^2 \gamma_{xy}}{\partial x \partial y} = 0 \tag{3.15}$$

The above equation is the compatibility requirement expressed in terms of strains.

3.2.5 Stress-Strain Relations:

The relationship between stress and strain for an elastic homogeneous, isotropic material, termed generalized Hooke's law, is well known, and for a three-dimensional case it is given by:

$$\varepsilon_x = \frac{1}{E}\left[\sigma_x - \nu\,(\sigma_y + \sigma_z)\right], \quad \varepsilon_{xy} = \frac{1+\nu}{E}\,\tau_{xy},$$

$$\varepsilon_y = \frac{1}{E}\left[\sigma_y - \nu\,(\sigma_z + \sigma_x)\right], \quad \varepsilon_{yz} = \frac{1+\nu}{E}\,\tau_{yz}, \qquad (3.16)$$

$$\varepsilon_z = \frac{1}{E}\left[\sigma_z - \nu\,(\sigma_x + \sigma_y)\right], \quad \varepsilon_{zx} = \frac{1+\nu}{E}\,\tau_{zx}.$$

where E is Young's modulus *(modulus of elasticity)*, and ν is Poisson's ratio.

3.2.6 Plane Deformation:

The problem of evaluation of stresses and displacements at points within a loaded structure is considerably simplified if it can be assumed, that there is no change along the z-direction in the distribution of either stress or strain, over the x-y plane. In other words, the displacement components u and v are functions of x and y only, whilst the displacement component w is either negligible or dependent on u and v. Such cases will be denoted here as *"plane deformation"* cases, and the two familiar cases of plane deformation are as follows:

(a) Plane stress:

This is the state of stress which may be assumed to exist in a thin sheet, or plate, which is considered incapable of supporting stresses through the thickness *(the z-direction)*. Thus any stress having a z subscript may be ignored, yielding:

$$\sigma_z = \tau_{zx} = \tau_{zy} = 0 \qquad (3.17)$$

which reduces the stress-strain relationships, equations (3.16), to:

$$\varepsilon_x = \frac{1}{E}(\sigma_x - \nu\,\sigma_y)$$

$$\varepsilon_y = \frac{1}{E}(\sigma_y - \nu\,\sigma_x) \qquad (3.18)$$

$$\varepsilon_{xy} = \frac{1}{E}(1 + \nu)\,\tau_{xy}$$

(b) *Plane strain:*

This case models a plane-symmetric structure which is sufficiently thick to prevent through-the-thickness strains. Thus with appropriate loading and boundary conditions any strain having a z subscript may be set to zero, giving:

$$\varepsilon_z = \varepsilon_{zx} = \varepsilon_{zy} = 0 \qquad (3.19)$$

and reducing the stress-strain relationships, after some manipulation to:

$$\varepsilon_x = \frac{1-\nu^2}{E}\left(\sigma_x - \frac{\nu}{1-\nu}\,\sigma_y\right)$$

$$\varepsilon_y = \frac{1-\nu^2}{E}\left(\sigma_y - \frac{\nu}{1-\nu}\,\sigma_x\right) \qquad (3.20)$$

$$\varepsilon_{xy} = \frac{1-\nu^2}{E}\left(1 + \frac{\nu}{1-\nu}\right)\tau_{xy}$$

These equations can be obtained from plane stress equations (3.18), if E is replaced by $E/(1-\nu^2)$ and ν replaced by $\nu/(1-\nu)$.

3.2.7 Elasto-Plastic Behaviour:

The actual elasto-plastic behaviour of a material is usually investigated experimentally for uniaxial stress conditions, whilst fundamental criteria, based often upon some experimental evidence, are employed so as to predict the behaviour of the

material under multiaxial stress conditions. A typical σ-ε diagram for annealed mild steel is shown in Fig.(3.5), and it is clear that the material starts yielding at point C, after which a permanent plastic deformation will be generated with the increase of the applied force.

Most metals and alloys do not show such a clearly marked initial yield as that seen in Fig.(3.5). For such materials, the change form elastic to elasto-plastic state is gradual and it is common practice to use a stress broadly equivalent to the yield stress, known as the proof stress which represents a stress value corresponding to a permanent strain *(or plastic strain)* equal to a specified percentage of the original gauge length, as shown in Fig.(3.6). Some examples of σ-ε diagrams for useful engineering materials are given in Fig.(3.7) [Ref.88].

3.3 Linear-Elastic Fracture Mechanics Concepts:

3.3.1 Introductory Concepts:

(i) The Energy Balance Concept:

In an elastic solid such as that considered by Griffith [Ref.5], if W and U respectively refer to the work done by the external forces and the elastic energy, and if U_γ is the specific surface tension energy of the solid, then according to the energy balance concept adopted by Griffith the necessary condition for fracture propagation may be expressed as:

$$\frac{d}{dA}(W-U) = U_\gamma \qquad (3.21)$$

where A is the surface area of the crack.

In equation (3.21) the left-hand side is the specific energy available for fracture, and the right-hand side represents the

resistance of the solid to fracture and for a given system of loading, the stability of *(quasi-static)* fracture propagation may be determined from:

$$\frac{d}{dA}\left[\frac{d}{dA}(W-U) - U_{\gamma}\right] \begin{cases} > 0 & \textit{unstable fracture.} \\ = 0 & \textit{neutral equilibrium.} \\ < 0 & \textit{stable fracture.} \end{cases} \qquad (3.22)$$

(ii) *Griffith Energy Balance Approach:*

For an infinite plate with unit thickness containing a through-thickness crack of length $2a$ and being subjected to a uniform tensile stress σ, applied at infinity, as shown approximately in Fig.(3.8), the total energy χ of the cracked plate may be written as:

$$\chi = U_o + U_a + U_{\gamma} - W \qquad (3.23)$$

where,

U_o = elastic energy of the loaded uncracked plate *(a constant)*,

U_a = change in the elastic energy caused by introducing the crack in the plate,

U_{γ} = change in the elastic surface energy by the formation of the crack surfaces,

W = work performed by external forces.

Griffith showed that for the plate with unit thickness the value of U_a is given by:

$$U_a = -\frac{\pi \sigma^2 a^2}{E} \qquad (3.24)$$

Moreover, the elastic surface energy, U_{γ}, is equal to the product of the elastic surface energy of the material, γ_o, and the new surface area of the crack:

$$U_\gamma = 4\,a\,\gamma_e \tag{3.25}$$

For the case where no work is done by external forces, the so-called fixed grip condition, W = 0, the total energy χ of the cracked plate can be written as:

$$\chi = U_o - \frac{\pi\,\sigma^2 a^2}{E} + 4\,a\,\gamma_e \tag{3.26}$$

Since U_o is constant, dU_o/da is zero, and the equilibrium condition for crack extension is obtained by setting $d\chi/da$ equal to zero, i.e.

$$\frac{d}{da}\left(-\frac{\pi\,\sigma^2 a^2}{E} + 4\,a\,\gamma_e\right) = 0 \tag{3.27}$$

The above equation shows that, when the elastic energy released due to a potential increment of crack growth, da, outweighs the demand for surface energy for the same crack growth, the introduction of a crack will lead to its unstable propagation. From the equilibrium condition, the following can be obtained:

$$\frac{2\,\pi\,\sigma^2 a}{E} = 4\,\gamma_e \tag{3.28}$$

which can be rearranged to:

$$\sigma\sqrt{a} = \left(\frac{2E\gamma_e}{\pi}\right)^{1/2} \tag{3.29}$$

The above equation indicates that crack extension in ideally brittle materials is governed by the product of the remotely applied stress and the square root of the crack length and by material properties. Because E and γ_e are material properties, the right-hand side of equation (3.29) indicates that crack extension in such materials occurs when the product $\sigma\sqrt{a}$ reaches certain critical value.

(iii) Irwin's Modification to Griffith Theory:

In 1948 Irwin suggested that Griffith theory for ideally brittle materials could be modified and applied to both brittle materials and metals that exhibit plastic deformation. The modification recognized that material resistance to crack extension can be measured in terms of the elastic surface energy and the plastic strain work γ_p accompanying crack extension. Consequently, equation (3.28) may be modified to:

$$\frac{\pi \sigma^2 a}{E} = 2 (\gamma_e + \gamma_p) \qquad (3.30)$$

For relatively ductile materials $\gamma_p \gg \gamma_e$.

(iv) Modes of Fracture:

All stress systems in the vicinity of a crack tip may be derived from three modes of loading as illustrated in Fig.(3.9). These modes are as follows:

(a) The Opening Mode:

The crack surfaces move directly apart under a tensile stress perpendicular to these surfaces.

(b) The Sliding Mode:

The crack surfaces move normal to the crack front and remain in the crack plane under a shearing stress parallel to this plane.

(c) The Tearing Mode:

The crack surfaces move parallel to the crack front and remain in the crack plane under a shearing stress perpendicular to this plane.

3.3.2 The Stress Intensity Approach:

Irwin's second important contribution was on providing the technique for the calculation of the rate of the energy (W-U). He observed that the symmetric crack solutions given by Westergaard and Sneddon may be generalized to include asymptotic expressions for all crack problems in which the plane of the crack is a plane of symmetry and showed that, by introducing a constant G, for small values of the distance r from the crack tip the cleavage stress and the crack surface displacement in the plane of the crack may be expressed as [Ref.74]:

$$\sigma_y(r,0) \cong \frac{K}{\sqrt{2r}} \tag{3.31}$$

$$v(r,\pi) \cong \left[\frac{1+\kappa}{4\mu} \right] K \sqrt{2r} \tag{3.32}$$

where,

$$K = \left[\frac{8\mu}{1+\kappa} \cdot \frac{G}{\pi} \right]^{1/2},$$

$$\mu = E/2(1+\nu),$$

$$\kappa = \begin{cases} (3-\nu)/(1+\nu) & \textit{for plane stress.} \\ (3-4\nu) & \textit{for plane strain.} \end{cases}$$

and (r,θ) are the polar coordinate with the origin at the crack tip.

For a small crack extension da in the plane of the crack, in a symmetric problem, the strain energy release under fixed grip conditions can be calculated through the crack closure energy as follows [Ref.74]:

$$d(W-U) = 2 \int_0^{da} \frac{1}{2} \sigma_y(r,0)\, v(da-r,\pi)\, dr \tag{3.33}$$

which, by substituting from (3.31) and (3.32), gives:

$$\frac{d}{da}(W-U) = G \qquad (3.34)$$

Hence, it is clear that the energy available for fracture per unit crack extension may be directly related to the parameter K which Irwin called the "*stress-intensity factor*".

In the middle of 1950s Irwin made a major advance by developing this stress intensity approach. Using linear elastic theory he showed that the stresses in the vicinity of a crack tip may be expressed in the form:

$$\sigma_{ij} = \frac{K}{\sqrt{2\pi r}} f_{ij}(\theta) + \ldots . \qquad (3.35)$$

where (r,θ) are the polar coordinates of a point with respect to the crack tip, as shown in Fig.(3.10), and K is the stress intensity factor which can define the elastic stress field at the crack tip.

Then, it can be seen that if the elasticity solution of the crack problem is available, the stress intensity factors may be evaluated by means of expressions of the form:

$$K = \lim_{x \to a} [\, 2\,(x-a)^{1/2}\, \sigma_{ij}(x,0)\,] \qquad (3.36)$$

If the problem has symmetry with respect to loading and geometry, then the following expression can be obtained:

$$G = \frac{1+k}{8\mu} K^2 \qquad (3.37)$$

Then the parameter governing the fracture process may be expressed as a critical stress intensity value, K_c, instead of a critical energy value G_c. For tensile loading conditions the relationship between K_c and G_c may be stated as:

$$G_c = \frac{K_c^2}{\mathbb{E}} \qquad (3.38)$$

where,

$\mathbb{E} = E$ *for plane stress,*

$\mathbb{E} = E/(1-\nu^2)$ *for plane strain.*

From equations (3.37) it is clear that under *mode I* condition the specific energy available to create a unit crack surface is G_I. Irwin has designated the corresponding "*critical strength parameter*" of the material by G_{IC} and called it the "*fracture toughness*" of the material. For *mode I* fracture, the necessary condition for fracture (*failure criterion*) may be expressed as:

$$G_I = \frac{1+k}{8\mu} K_I^2 = G_{IC} \qquad (3.39)$$

Since G_{IC} is a material constant, the stability of fracture propagation can be determined by the sign of dG_I/da, where a positive sign corresponds to an unstable fracture condition.

The critical value of K_I can now be expressed as K_{IC} (*corresponding to* G_{IC}) which is called the "*critical stress intensity factor*". Therefore, the failure criterion equation (3.39) can be replaced by:

$$K_I = K_{IC} = \left(\frac{8\mu}{1+k} G_{IC}\right)^{1/2} \qquad (3.40)$$

Again, since K_{IC} is a material constant, the sign of dK_I/da determines the stability of fracture propagation.

3.3.3 Elastic Field Equations around Crack Tips:

The elastic field equations around the crack tip for a plane-loaded infinite plate containing a crack (Fig. 3.11) can be written in terms of cartesian coordinates [Ref.75], as follows:

$$\sigma_x = \frac{K_I}{(2\pi r)^{1/2}} \cos\left(\frac{\theta}{2}\right) \left[1 - \sin\left(\frac{\theta}{2}\right) \sin\left(\frac{3\theta}{2}\right) \right]$$

$$+ \frac{K_{II}}{(2\pi r)^{1/2}} \sin\left(\frac{\theta}{2}\right) \left[2 + \cos\left(\frac{\theta}{2}\right) \cos\left(\frac{3\theta}{2}\right) \right] \qquad (3.41)$$

$$\sigma_y = \frac{K_I}{(2\pi r)^{1/2}} \cos\left(\frac{\theta}{2}\right) \left[1 + \sin\left(\frac{\theta}{2}\right) \sin\left(\frac{3\theta}{2}\right) \right]$$

$$- \frac{K_{II}}{(2\pi r)^{1/2}} \cos\left(\frac{\theta}{2}\right) \sin\left(\frac{\theta}{2}\right) \cos\left(\frac{3\theta}{2}\right) \qquad (3.42)$$

$$\tau_{xy} = \frac{K_I}{(2\pi r)^{1/2}} \cos\left(\frac{\theta}{2}\right) \sin\left(\frac{\theta}{2}\right) \cos\left(\frac{3\theta}{2}\right)$$

$$- \frac{K_{II}}{(2\pi r)^{1/2}} \cos\left(\frac{\theta}{2}\right) \left[1-\sin\left(\frac{\theta}{2}\right) \sin\left(\frac{3\theta}{2}\right) \right] \qquad (3.43)$$

$$u = \left(\frac{K_I}{4\mu} \right) \left(\frac{r}{2\pi} \right)^{1/2} \left[(2k-1) \cos\left(\frac{\theta}{2}\right) - \cos\left(\frac{3\theta}{2}\right) \right]$$

$$- \left(\frac{K_{II}}{4\mu} \right) \left(\frac{r}{2\pi} \right)^{1/2} \left[(2k+3) \sin\left(\frac{\theta}{2}\right) + \sin\left(\frac{3\theta}{2}\right) \right] \qquad (3.44)$$

$$v = \left(\frac{K_I}{4\mu} \right) \left(\frac{r}{2\pi} \right)^{1/2} \left[(2k+1) \sin\left(\frac{\theta}{2}\right) - \sin\left(\frac{3\theta}{2}\right) \right]$$

$$+ \left(\frac{K_{II}}{4\mu} \right) \left(\frac{r}{2\pi} \right)^{1/2} \left[(2k-3) \cos\left(\frac{\theta}{2}\right) + \cos\left(\frac{3\theta}{2}\right) \right] \qquad (3.45)$$

where (r,θ) are the polar coordinates of the crack tip based on the right-hand crack tip as shown in Fig.(3.11).

3.3.4 Fracture under Combined Loading:

Engineering structures subjected to a combined loading of tension, shear, and torsional loading usually experience mixed

mode cracking. The combination of in-plane tension and shear gives a mixture of *mode I* and *mode II*. It is clear that under *mode II* condition only the fracture failure takes place when K_{II} reaches a critical value K_{IIC}. With mixed mode loading conditions, failure may occur when the value of certain combination of the two stress intensity modes reaches a critical magnitude.

Using the elastic energy balance criterion, the total energy release rate G can be written as follows:

$$G = G_I + G_{II} + G_{III} \tag{3.46}$$

For *I-II* mixed loading condition $G_{III} = 0$, and:

$$G_I = \frac{\kappa+1}{8\mu} K_I^2 , \quad G_{II} = \frac{\kappa+1}{8\mu} K_{II}^2$$

An equivalent stress intensity factor K_E can be defined [Ref.75] such that:

$$K_E^2 = \frac{8\mu}{\kappa+1} (G_I + G_{II}) \tag{3.47}$$

Hence, fracture may occur when the following condition is satisfied:

$$K_I^2 + K_{II}^2 = K_E^2 \tag{3.48}$$

Comparing K_E with only K_{IC} may provide a conservative solution, since usually $K_E \geq K_I$.

In practice $K_{IC} \neq K_{IIC}$, therefore, the fracture failure condition can be modified as follows:

$$\left(\frac{K_I}{K_{IC}} \right)^2 + \left(\frac{K_{II}}{K_{IIC}} \right)^2 = 1 \tag{3.49}$$

Since K_{IIC} is difficult to predict, it can be approximated [Ref.76] as follows:

$$K_{IIC} \simeq 0.75\ K_{IC} \qquad (3.50)$$

Equation (3.49) is the locus of an ellipse, and fracture failure takes place when K_I and K_{II} reach values sufficient to fulfill such an equation.

3.3.5 Crack-Tip Plasticity:

The elastic stress field in the vicinity of a crack tip, as given by equation (3.35), shows that as r tends to zero the stresses become infinite (*i.e. there is a stress singularity at the crack tip*). Since many structural materials deform plastically above the yield stress, there will be in reality a plastic zone surrounding the crack tip, and the elastic solution is no longer applicable for such situations, which may require modification to some of the linear-elastic fracture mechanics concepts.

The two physically acceptable yield criteria for metals and alloys are the well-known *Tresca* and *von Mises* yield criteria. The Tresca criterion states that yielding will occur when the maximum value of shear stress approaches a critical value. In terms of principal stresses ($\sigma_1 > \sigma_2 > \sigma_3$), Tresca's criterion predicts yielding when:

$$| \sigma_1 - \sigma_3 | = Y \qquad (3.51)$$

where Y is the uniaxial yield stress of the material.

The von Mises criterion requires that the distortion energy per unit volume approaches a critical value. This criterion can be expressed in terms of principal stresses as follows:

$$(\sigma_1 - \sigma_2)^2 + (\sigma_2 - \sigma_3)^2 + (\sigma_3 - \sigma_1)^2 = 2\ Y^2 \qquad (3.52)$$

In order to apply a proper yield criterion, the crack-tip

stress field equations (3.41-3.43), should be deduced in terms of principal stresses, and since *mode I* is the most predominant stress situation in many practical cases, then the stress field equations for this mode can be deduced as follows:

$$\sigma_1 = \frac{K_I}{(2\pi r)^{1/2}} \cos\left(\frac{\theta}{2}\right)\left[1+\sin\left(\frac{\theta}{2}\right)\right]$$

$$\sigma_2 = \frac{K_I}{(2\pi r)^{1/2}} \cos\left(\frac{\theta}{2}\right)\left[1-\sin\left(\frac{\theta}{2}\right)\right] \qquad (3.53)$$

$$\sigma_3 = \begin{cases} \nu(\sigma_1+\sigma_2) & \textit{for plane strain.} \\ 0 & \textit{for plane stress.} \end{cases}$$

By substituting the above equations into Tresca and von Mises criteria equations (3.51, 3.52), expressions for the plastic zone boundary as a function of θ, can be obtained. Considering the derivation given in Ref.[76], these expressions can be stated as follows:

For Tresca criterion:

$$r_p(\theta) = \frac{K_I^2}{2\pi Y^2} \cos^2\left(\frac{\theta}{2}\right)\left[1+\sin\left(\frac{\theta}{2}\right)\right]^2 \qquad \textit{plane stress,} \qquad (3.54)$$

$$r_p(\theta) = \frac{K_I^2}{2\pi Y^2} \cos^2\left(\frac{\theta}{2}\right)\left[1-2\nu+\sin\left(\frac{\theta}{2}\right)\right]^2 \qquad \textit{plane strain.} \qquad (3.55)$$

For von Mises criterion:

$$r_p(\theta) = \frac{K_I^2}{4\pi Y^2}\left[1+\frac{3}{2}\sin^2\theta+\cos\theta\right] \qquad \textit{plane stress,} \qquad (3.56)$$

$$r_p(\theta) = \frac{K_I^2}{4\pi Y^2}\left[\frac{3}{2}\sin^2\theta+(1-2\nu)^2(1+\cos\theta)\right] \qquad \textit{plane strain.} \qquad (3.57)$$

3.4 Elasto-Plastic Fracture Mechanics Concepts:

The concepts of linear-elastic fracture mechanics can be used satisfactorily with brittle materials and may be safely applied to ductile materials as long as the plastic zone is small compared to the crack size. This usually occurs at stresses extremely below the yield stress of the material in use. In such a case the fracture can be characterized by K_{IC} or G_{IC}. If, however, the plastic zone is large compared to the crack size, linear-elastic fracture mechanics can no longer be valid, and elasto-plastic fracture mechanics should be considered instead. The basic approaches to elasto-plastic fracture mechanics are summarized in the following sections.

3.4.1 The Crack Opening Displacement Approach:

The crack opening displacement (*COD*) approach which was first introduced by Wells [Ref.44] in 1961, has been used as a criterion to characterize failure of cracked specimens in the presence of moderate plasticity. By using the Dugdale strip yield model, an expression for the *COD*, δ, can be found as follows [Ref.75]:

$$\delta = \frac{8Y}{\pi E}\, a\, \ell og_e\left[\sec\left(\frac{\pi\sigma}{2Y}\right)\right] \qquad (3.58)$$

Expanding the above equation in series form, the following can be obtained:

$$\delta = \frac{8Y}{\pi E}\, a\left[\frac{1}{2}\left(\frac{\pi\sigma}{2Y}\right)^2 + \frac{1}{12}\left(\frac{\pi\sigma}{2Y}\right)^4 + \frac{1}{45}\left(\frac{\pi\sigma}{2Y}\right)^6 + \ldots.\right] \qquad (3.59)$$

A reasonable approximation to δ can be deduced by using a remote load of $\sigma < 0.7\ Y$, as follows:

$$\delta = \frac{\pi\ \sigma^2 a}{E\ Y} \qquad (3.60)$$

and since $K_I = \sigma(\pi a)^{1/2}$, then $\delta = K_I^2/EY$.

In general, a critical crack-opening displacement, δ_c, can be defined as follows:

$$\delta_c = \frac{K_{Ic}^2}{\lambda E Y} \qquad (3.61)$$

where λ is a constraint factor [Ref.76].

3.4.2 The *J*-Integral Approach:

The path independent *J*-integral concept has first been introduced by Rice [Ref.46] in 1968. This concept is based on the energy balance approach discussed earlier in this chapter. Considering the energy balance given in equation (3.23), as long as this energy balance remains valid, an instability condition can be derived as follows [Ref.7]:

$$\frac{d}{da}(W-U_a) \geq \frac{dU_\gamma}{da} \qquad (3.62)$$

Hence, a nonlinear elastic parameter equivalent to G can be defined as follows:

$$J = \frac{d}{da}(W-U_a) \qquad (3.63)$$

where for elastic behaviour $J = G$.

Referring again to equation (3.23), the potential energy U_p can be defined as:

$$U_p = U_o + U_a - W \qquad (3.64)$$

which means that:

$$\chi = U_p + U_\gamma \qquad (3.65)$$

Equation (3.64), shows that U_p contains the basic energy terms that may contribute to nonlinear material behaviour. Since U_o is a constant, differentiation of U_p gives:

$$\frac{dU_p}{da} = \frac{d}{da}(U_a - W) = -\frac{d}{da}(W - U_a) \qquad (3.66)$$

Thus, from equation (3.63) it can be shown that:

$$J = -\frac{dU_p}{da} \qquad (3.67)$$

Now consider a line integral along a contour Γ surrounding the crack tip, starting from the lower crack surface, and moving anti-clockwise to the upper surface, as shown in Fig.(3.12), J can be redefined as:

$$J = \oint_{\Gamma} \left[W\, dy - \underline{T}^t \left(\frac{\partial \underline{u}}{\partial x} \right) ds \right] \qquad (3.68)$$

where,

$$W = \int_{\underline{0}}^{\underline{\varepsilon}} \underline{\sigma}^t \, d\underline{\varepsilon}$$

$\underline{\sigma}$ = Stress vector,

$\underline{\varepsilon}$ = Strain vector,

$\underline{T}$ = Traction vector,

$\underline{u}$ = Displacement vector.

Rice has shown that in case of a closed contour *ABCDEF* as shown in Fig.(3.13), $J = 0$. Since no contribution is gained from *CD* and *AF* on the crack surface ($\underline{T} = \underline{0}$, $dy = 0$), the integral along *ABC* must be equal and opposite to that along *DEF*. Therefore, the *J*-integral taken along an unclosed anti-clockwise contour between unloaded crack surfaces is *path independent* [Ref.76].

The path independency of the *J*-integral allows its calculation along contours remote from the crack tip. Such contours can be chosen to contain only elastic stresses and displacements. Thus

an elasto-plastic energy release rate can be obtained from an elastic expression in terms of stresses and displacements.

For a cracked structure, the J values may be compared to a critical value, J_c, which is a characteristic of the material, analogous to G_c in linear-elastic fracture mechanics. Finally, a number of expressions relating J and δ can be found in the literature, most of these expressions take the form:

$$J = M \delta Y \tag{3.69}$$

where M varies from 1.15 to 2.95 [Ref.7].

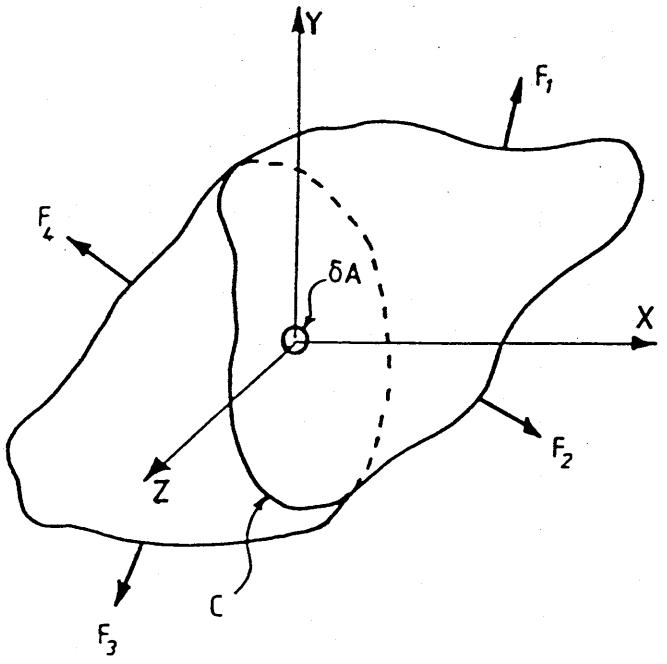

Fig.(3.1) Three-dimensional body under general loading system.

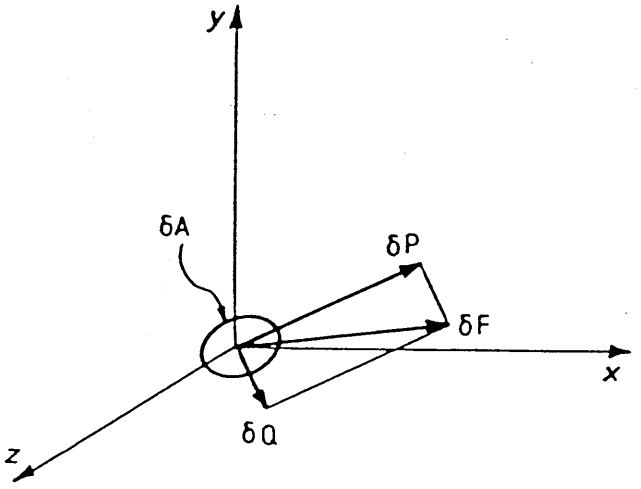

Fig.(3.2) Normal and tangential force components.

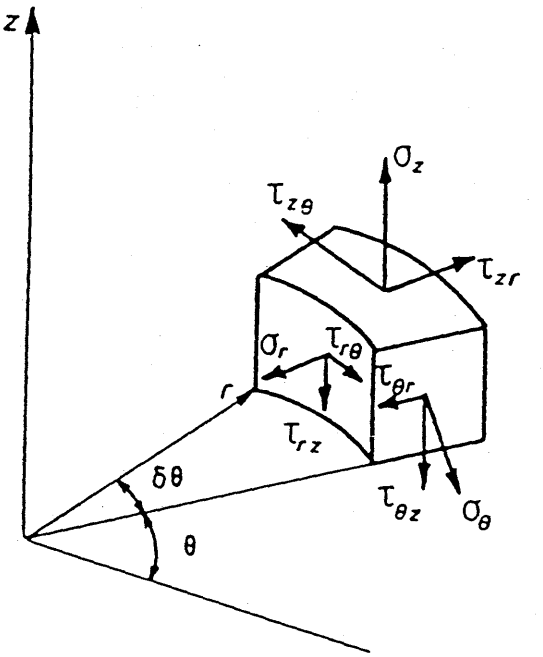

Fig.(3.3) Cylindrical polar stress system.

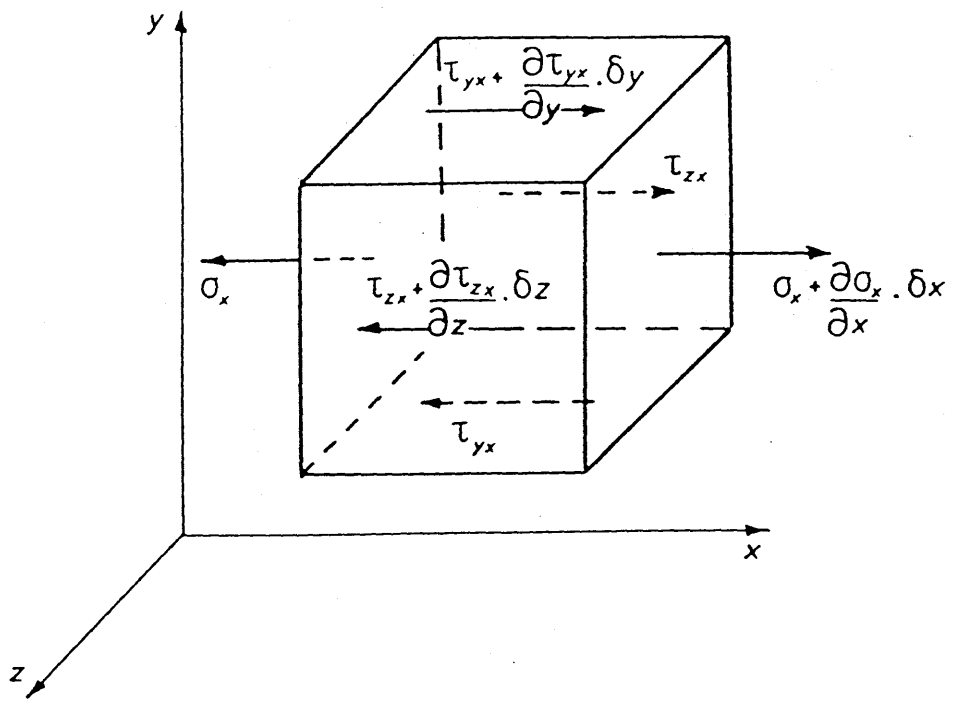

Fig.(3.4) Stress equilibrium in the x-direction.

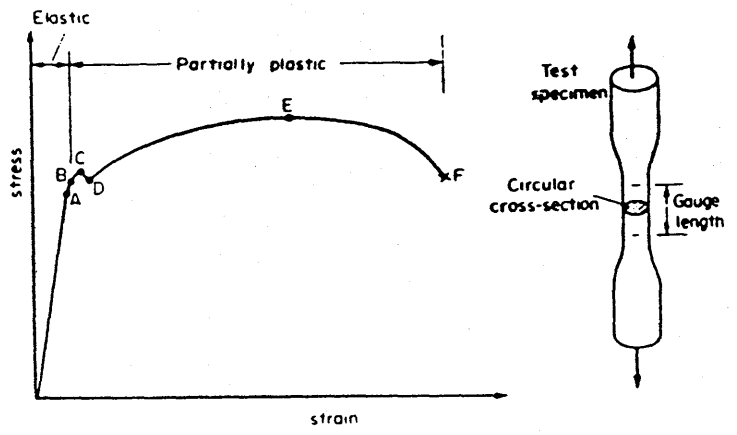

Fig.(3.5) Typical tensile test curve for mild steel.

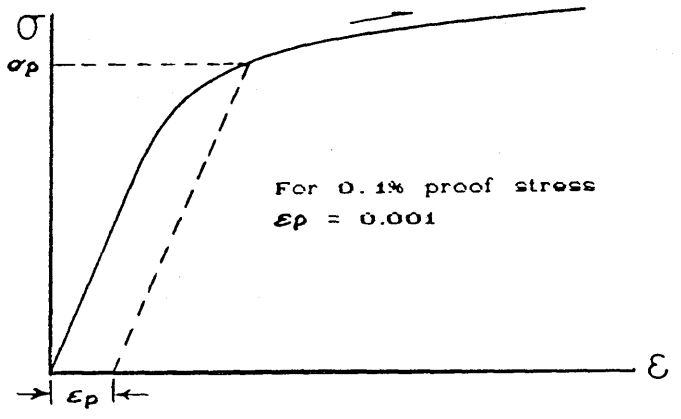

Fig.(3.6) Proof stress representation.

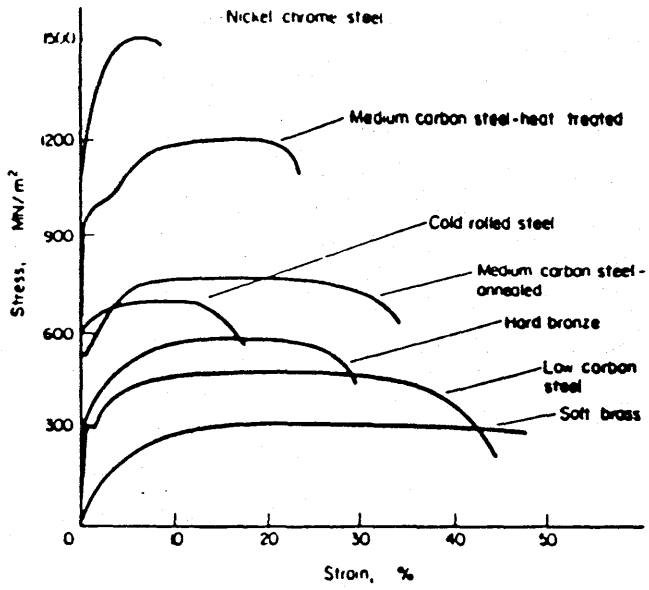

Fig.(3.7) Tensile test curves for various metals.

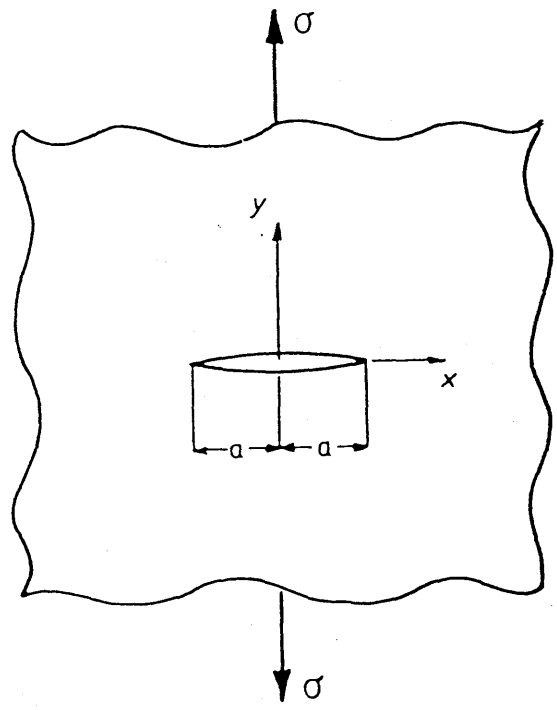

Fig.(3.8) A through-thickness crack in an infinite plate.

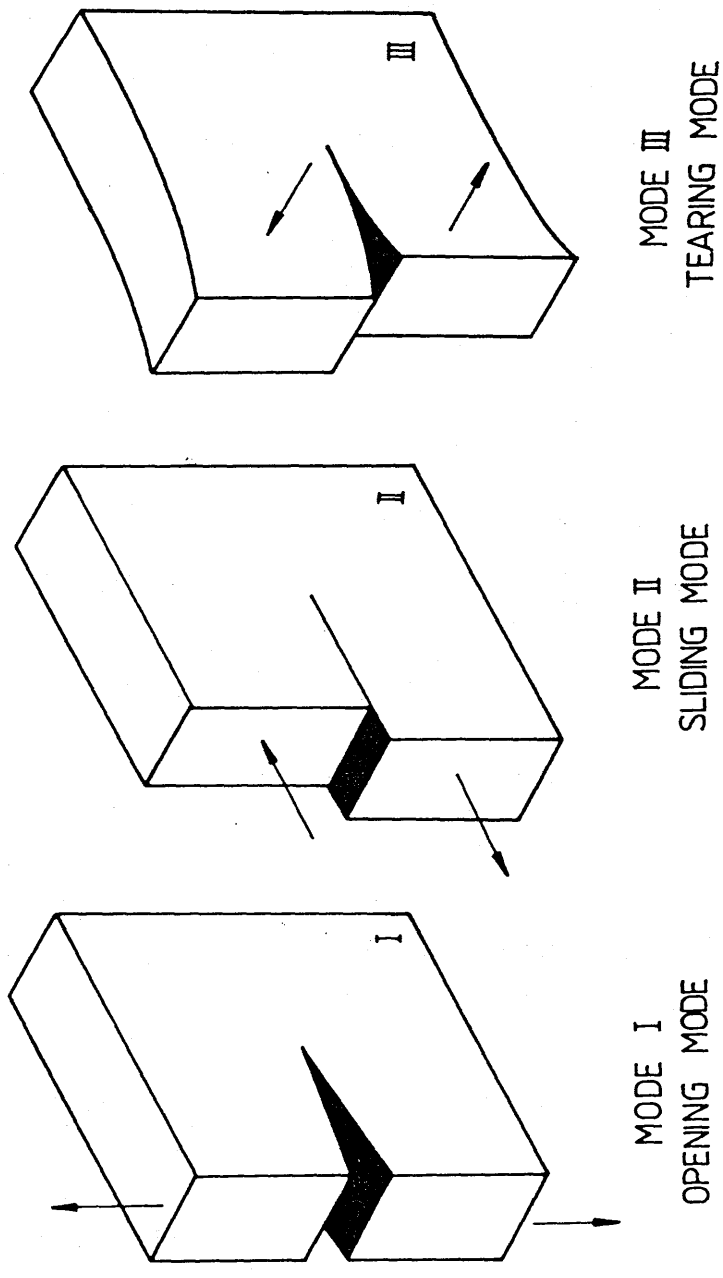

Fig.(3.9) Fundamental modes of fracture.

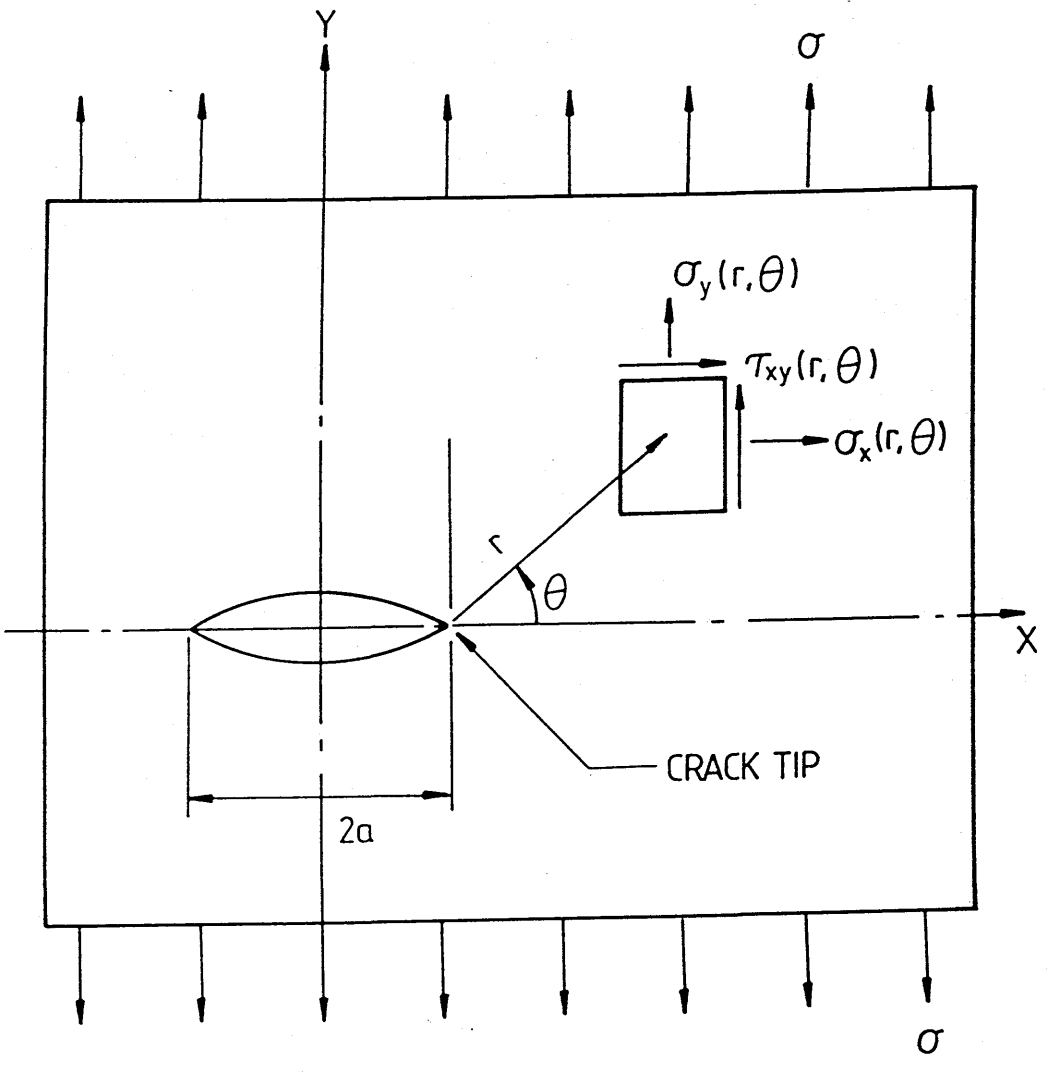

Fig.(3.10) Crack-tip coordinates system.

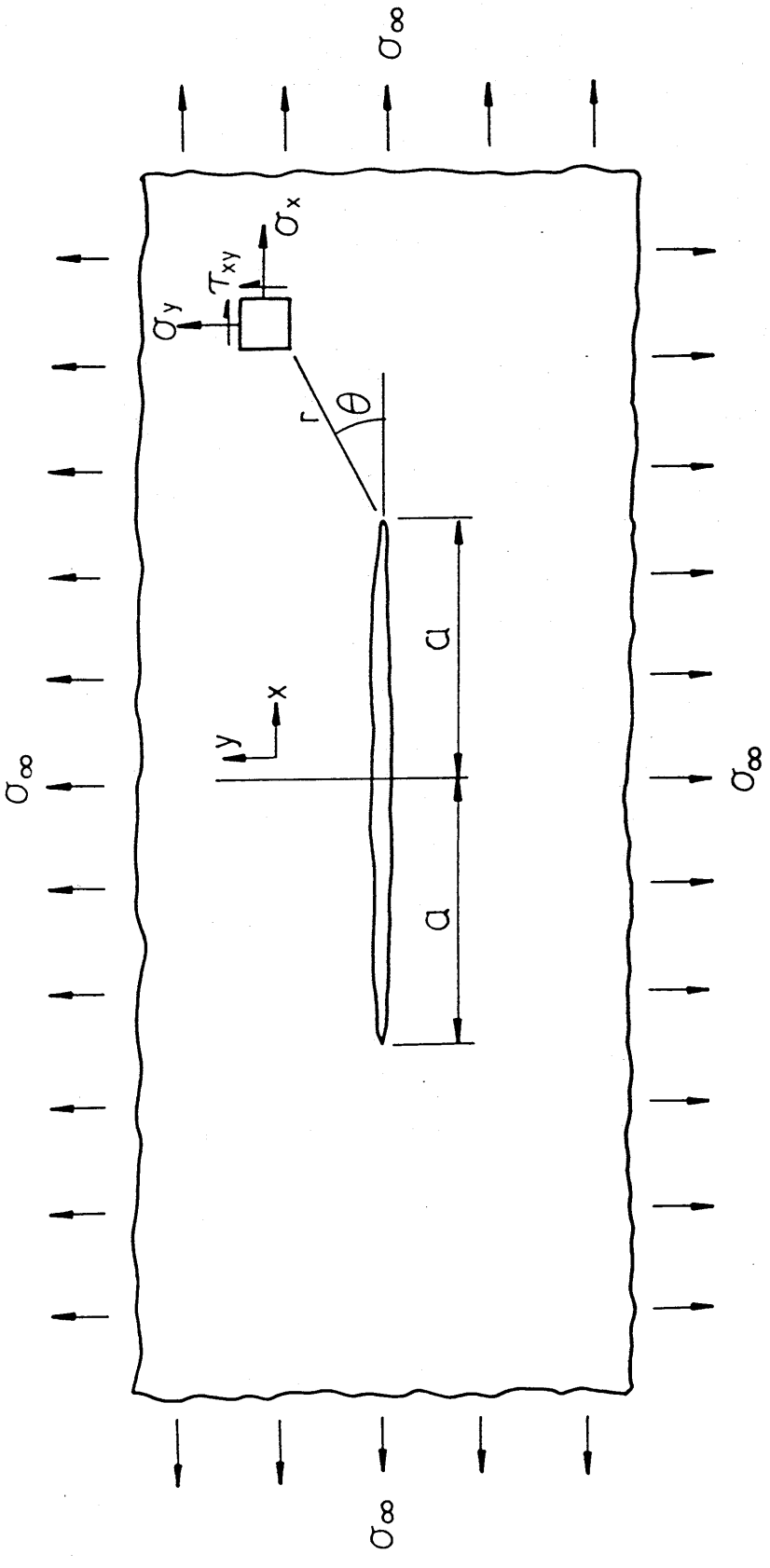

Fig.(3.11) A loaded infinite plate containing a crack.

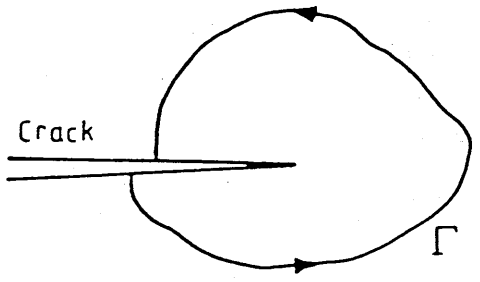

Fig.(3.12) Unclosed contour around the crack tip.

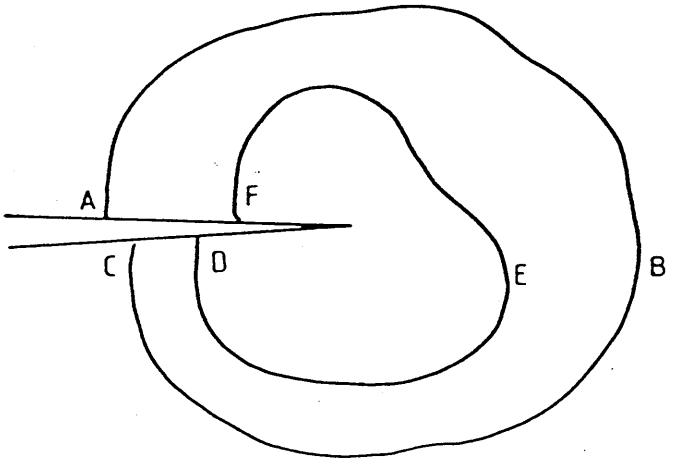

Fig.(3.13) Closed contour at the crack tip.

CHAPTER 4

DERIVATION OF GENERALISED J-INTEGRAL FOR 2D FRACTURE MECHANICS PROBLEMS

4.1 Introduction:

It is clear from the literature that Eshelby [Ref.75] was the first to derive a number of contour integrals including the so-called *J*-integral. Cherepanov [Ref.76] and Rice [Refs.46, 77] were apparently the first to apply such an integral to crack problems.

The basic advantage of the *J*-integral is that it is independent of the integration path, and hence it can be evaluated over contours which are far from a crack tip so as to avoid singularities and nonlinearities often encountered in the vicinity of the crack tip. Unfortunately, many of the algorithms suggested in the literature, for the estimation of *J*-integral values are either crude or lack the generality.

In this work an attempt is made to derive the *J*-integral expressions for cases with general loading conditions. Some useful ideas for saving computer *CPU* time and/or improving the accuracy of the *J*-integrals are summarized. A new procedure for the calculation of *J*-integrals, based upon boundary element characteristics will be introduced in chapter 7.

4.2 Introductory Definitions and Relations:

Consider a two-dimensional structure defined in terms of a domain Ω in the x-y plane and a thickness t in the z-direction.

At any point (x,y) inside Ω, the following parameters can be defined:

1. Displacement vector:

$$\underline{u} = \begin{bmatrix} u \\ v \end{bmatrix} = \{ u \quad v \} \tag{4.1}$$

2. *Domain loading intensity vector:*

$$\underline{X} = \begin{bmatrix} X \\ Y \end{bmatrix} = \{ X \quad Y \} \tag{4.2}$$

3. *Stress vector:*

$$\underline{\sigma} = \{ \sigma_x \quad \sigma_y \quad \tau_{xy} \} \tag{4.3}$$

4. *Strain vector:*

$$\underline{\varepsilon} = \{ \varepsilon_x \quad \varepsilon_y \quad \gamma_{xy} \} \tag{4.4}$$

5. *Traction vector:*

$$\underline{T} = \begin{bmatrix} T_x \\ T_y \end{bmatrix} = \begin{bmatrix} l\sigma_x + m\tau_{xy} \\ l\tau_{xy} + m\sigma_y \end{bmatrix} \tag{4.5}$$

4.3 Energy Principles and Relations:

Consider a domain as that shown by Fig.(4.1). This domain can be divided into an equivalent system of subdomains, if each subdomain has its contribution of internal loading to be acting as external loads on the subdomain boundary together with its share of existing boundary and loading conditions. This consideration has been used successfully in the finite element method and it has been pointed out that the subdomain should obey the same physical principles and constitutive relationships as the parent domain.

From the first law of thermodynamics:

$$\chi = K_E + D_E + U + V = \textit{stationary}. \tag{4.6}$$

where,

χ = Total energy of the subdomain,

K_E = Kinetic energy of the subdomain,

D_E = Dissipation energy of the subdomain,

U = Strain energy of the subdomain,

V = Potential energy of the subdomain.

For a subdomain Ω with boundary Γ, the following parameters can be defined:

1. *Kinetic Energy:*

$$K_E = \frac{1}{2} \int (\dot{u}^2 + \dot{v}^2) \, dm$$

$$= \frac{1}{2} \iint_{\Omega} t (\dot{u}^2 + \dot{v}^2) \rho \, dA \qquad (4.7)$$

2. *Strain Energy:*

$$U = \iiint W \, dvol \qquad (4.8)$$

where,

$$W = \int_{\underline{0}}^{\underline{\varepsilon}} \underline{\sigma}^t \, d\underline{\varepsilon} \qquad (4.9)$$

3. *Potential Energy:*

In the absence of magnetic, electric,...., fields, the potential energy is equal to minus the work done by external loads, and can be defined as follows:

(i) *Due to surface traction:*

An increment of force due to surface traction can be written as:

$$d\vec{F} = \vec{T}\, t\, ds$$

where, $\vec{T} = T_x \vec{i} + T_y \vec{j}$, and the corresponding increment of the potential energy due to the above force is given by:

$$dV_\Gamma = - \vec{u} \cdot d\vec{F}$$

where, $\vec{u} = u\, \vec{i} + v\, \vec{j}$.

Therefore, the total potential energy due to traction can be evaluated as:

$$V_\Gamma = - \oint_\Gamma \vec{u} \cdot d\vec{F} = \oint_\Gamma t \langle \vec{T} \cdot \vec{u} \rangle ds$$

Using matrix notation, V_Γ can be rewritten as:

$$V_\Gamma = - \oint_\Gamma t\, \underline{T}^t\, \underline{u}\, ds \qquad (4.10)$$

(ii) Due to domain loading:

The rate of force due to domain loading can be expressed as:

$$d\vec{F} = \vec{X}\, dvol$$

where, $\vec{X} = X\, \vec{i} + Y\, \vec{j}$. Then the rate of change of potential energy due to such force is equal to:

$$dV_\Omega = - \vec{u} \cdot d\vec{F} = - \vec{u} \cdot \vec{X}\, dvol$$

i.e.

$$V_\Omega = - \iint_\Omega t \langle \vec{u} \cdot \vec{X} \rangle dA$$

and by using matrix notation:

$$V_{\Omega} = - \iint_{\Omega} t \, \underline{X}^{t} \, \underline{u} \, dA \qquad (4.11)$$

4. Energy Densities:

The strain energy density W can be defined as:

$$W = \frac{dU}{dvol} \qquad (4.12)$$

or for two-dimensional problems:

$$W = \frac{1}{t} \frac{dU}{dA} \qquad (4.13)$$

i.e.

$$U = \iint_{\Omega} t \, W \, dA \qquad (4.14)$$

Other similar energy densities can be defined as follows:

(i) *Kinetic energy density:*

$$\mathcal{K} = \frac{dK_{E}}{dvol} \qquad (4.15)$$

i.e.

$$\mathcal{K} = \frac{1}{2} \rho \, \dot{\underline{u}}^{t} \, \dot{\underline{u}} \qquad (4.16)$$

where $\dot{\underline{u}}$ represents the vector of velocity components, then:

$$K_{E} = \iint_{\Omega} t \, \mathcal{K} \, dA \qquad (4.17)$$

(ii) *Surface work density:*

$$\psi = \frac{\text{d(Surface Work)}}{\text{d(Surface Area)}}$$

The surface work can be defined as:

$$V_\Gamma = \int_\Gamma t \left(\int_{\underline{o}}^{\underline{u}} \underline{T}^t \, d\underline{u} \right) ds \qquad (4.18)$$

therefore,

$$\psi = \int_{\underline{o}}^{\underline{u}} \underline{T}^t \, d\underline{u} \qquad (4.19)$$

i.e.

$$V_\Gamma = \int_\Gamma t \, \psi \, ds \qquad (4.20)$$

For surface forces being independent of $\underline{u}$:

$$\Delta\psi = \underline{T}^t \, \Delta\underline{u} \qquad (4.21)$$

(iii) *Body work density:*

$$\mathcal{B} = \frac{\text{(work done by body forces)}}{\text{dvol}}$$

Since the work done by body forces is:

$$V_\Omega = \iint_\Omega t \left(\int_{\underline{o}}^{\underline{u}} \underline{X}^t \, d\underline{u} \right) dA \qquad (4.22)$$

it can be deduced that:

$$\mathcal{B} = \int_{\underline{o}}^{\underline{u}} \underline{X}^t \, d\underline{u} \qquad (4.23)$$

i.e.

$$V_\Omega = \iint_\Omega t\, \mathcal{B}\, dA \qquad (4.24)$$

If the domain forces are independent of $\underline{u}$, then:

$$\Delta\mathcal{B} = \underline{X}^t\, \Delta\underline{u} \qquad (4.25)$$

4.4 Derivation of the J-Integral Expressions:

4.4.1 The Physical Concept:

Consider a two-dimensional structure which contain a crack of original length a_o. The total energy of the structure may be expressed as follows:

$$\chi(a) = K_E + D_E + \Pi + S$$

where,

$\Pi = U + V$ as defined before,

S = energy required to form the crack.

Now, if the crack grows by Δa, then from energy conservation:

$$\chi(a+\Delta a) = (\Pi+\Delta\Pi) + (S+\Delta S) + (K_E+\Delta K_E) + (D_E+\Delta D_E)$$

Hence, from energy balance:

$$\lim_{\Delta a \to o} \frac{(a+\Delta a) - \chi(a)}{\Delta a} = 0$$

i.e.

$$\lim_{\Delta a \to o} \frac{\Delta \Pi}{\Delta a} + \lim_{\Delta a \to o} \frac{\Delta S}{\Delta a} + \lim_{\Delta a \to o} \frac{\Delta K_E}{\Delta a} + \lim_{\Delta a \to o} \frac{\Delta D_E}{\Delta a} = 0$$

Thus,

$$\frac{d\Pi}{da} + \frac{dS}{da} + \frac{dK_E}{da} + \frac{dD_E}{da} = 0$$

or

$$\frac{dS}{da} = - \left(\frac{d\Pi}{da} + \frac{dK_E}{da} + \frac{dD_E}{da} \right) \qquad (4.26)$$

If the changes of kinetic and dissipation energies can be ignored, then:

$$\frac{dS}{da} \cong - \frac{d\Pi}{da}$$

or for two-dimensional problems:

$$\frac{1}{t} \frac{dS}{da} = - \frac{1}{t} \frac{d\Pi}{da} \qquad (4.27)$$

For linear-elastic analysis, $\frac{1}{t} \frac{dS}{da}$ represents the energy release rate G, and it can be shown that [Ref.78]:

$$G = \frac{1}{E'} (K_I^2 + K_{II}^2) + \frac{(1+\nu)}{E} K_{III} \qquad (4.28)$$

where,

$E' = E$ *for plane stress,*

$= \frac{E}{1-\nu^2}$ *for plane strain.*

For elasto-plastic analysis, $\frac{1}{t} \frac{dS}{da}$ still represents the energy release rate, and it will be denoted by J. Although $J = G$, equation (4.28) is only valid for linear-elastic fracture mechanics.

4.4.2. Change of Coordinates:

If (ξ,η) are used such that their origin is located at a crack tip which has a length a, and is growing in the x-direction, as shown in Fig.(4.2), where:

$$x = a + \xi$$
$$y = \eta \qquad (4.29)$$

The x-y coordinates system is always independent of the crack growth, i.e. x, y, and a are independent or:

$$\frac{dx}{da} = \frac{dy}{da} = 0 \qquad (4.30)$$

From equations (4.29) and (4.30), it can show that:

$$\frac{d\xi}{da} = \frac{dx}{da} - 1 = -1 \qquad (4.31)$$

$$\frac{d\xi}{dx} = 1 - \frac{da}{dx} = 1 \qquad (4.32)$$

Consider a function $f(a,x,y)$ which is continuous and has a continuous first order partial derivatives in the reference domain. From,

$$df = \frac{\partial f}{\partial a}\,da + \frac{\partial f}{\partial x}\,dx + \frac{\partial f}{\partial y}\,dy$$

it can be deduced that:

$$\frac{df}{da} = \frac{\partial f(a,x,y)}{\partial a} \qquad (4.33)$$

$$\frac{df}{dx} = \frac{\partial f(a,x,y)}{\partial x} \qquad (4.34)$$

By using $x = a+\xi$, then $f(a,x,y) \rightarrow f(a,\xi,y)$, and,

$$df = \frac{\partial f(a,\xi,y)}{\partial a}\,da + \frac{\partial f(a,\xi,y)}{\partial \xi}\,d\xi + \frac{\partial f(a,\xi,y)}{\partial y}\,dy$$

then, it can be shown that:

$$\frac{df}{da} = \frac{\partial f(a,\xi,y)}{\partial a} + \frac{\partial f(a,\xi,y)}{\partial \xi}\frac{d\xi}{da}$$

and

$$\frac{df}{dx} = \frac{\partial f(a,\xi,y)}{\partial \xi}\frac{d\xi}{dx}$$

From equations (4.31) and (4.32), the above equations can be reduced to:

$$\frac{df}{da} = \frac{\partial f(a,\xi,y)}{\partial a} - \frac{\partial f(a,\xi,y)}{\partial \xi} \qquad (4.35)$$

$$\frac{df}{dx} = \frac{\partial f(a,\xi,y)}{\partial \xi} \qquad (4.36)$$

Comparing equations (4.35), (4.36) with (4.33) and (4.34), it can be proved that:

$$\frac{df}{da} = \frac{\partial f(a,\xi,y)}{\partial a} - \frac{\partial f(a,x,y)}{\partial x} \qquad (4.37)$$

4.4.3. Case of a Closed Contour:

Consider a domain Ω, with a closed contour Γ (*the domain is actually a substructure of a cracked structure as described before*), Fig.(4.1). Hence,

$$\frac{1}{t}\frac{d\chi}{da} = \frac{1}{t}\left[\frac{dU}{da} + \frac{dK_E}{da} + \frac{dD_E}{da} + \frac{dV}{da} + \frac{dS}{da}\right] = 0$$

Neglecting the rate of the change of the dissipation energy, then:

$$J = \frac{1}{t}\frac{dS}{da} = -\frac{1}{t}\left[\frac{dU}{da} + \frac{dK_E}{da} + \frac{dV}{da}\right] \qquad (4.38)$$

Using the expressions in terms of energy densities, it can be shown that:

$$J = -\left[\iint_{\Omega} \left(\frac{dW}{da} + \frac{d\mathcal{K}}{da} \right) dA - \oint_{\Gamma} \frac{d\psi}{da} ds - \iint_{\Omega} \frac{d\mathcal{B}}{da} dA \right] \qquad (4.39)$$

Substituting from equation (4.37) into (4.39), it can be deduced that:

$$J = -J_a + J_x \qquad (4.40)$$

where,

$$J_a = \iint_{\Omega} \left(\frac{\partial W}{\partial a} + \frac{\partial \mathcal{K}}{\partial a} \right) dA - \oint_{\Gamma} \frac{\partial \psi}{\partial a} ds - \iint_{\Omega} \frac{\partial \mathcal{B}}{\partial a} dA \qquad (4.41)$$

and

$$J_x = \iint_{\Omega} \left(\frac{\partial W}{\partial x} + \frac{\partial \mathcal{K}}{\partial x} \right) dA - \oint_{\Gamma} \frac{\partial \psi}{\partial x} ds - \iint_{\Omega} \frac{\partial \mathcal{B}}{\partial x} dA \qquad (4.42)$$

Comparing equations (4.41) and (4.42) with equation (A.6) [Appendix A], it is clear that:

$$J_a = J_x = 0$$

Equation (4.42) has an interesting reduction, as follows:

$$J_x = \iint_{\Omega} \frac{\partial}{\partial x} (W+\mathcal{K}) dA - \oint_{\Gamma} \frac{\partial \psi}{\partial x} ds - \iint_{\Omega} \frac{\partial \mathcal{B}}{\partial x} dA \qquad (4.43)$$

Using integration by-part theorem (A.1) [Appendix A], it can be shown that:

$$J = J_x = \oint_{\Gamma} (W+\mathcal{K}) dy - \oint_{\Gamma} \frac{\partial \psi}{\partial x} ds - \oint_{\Gamma} \mathcal{B} dy = 0 \qquad (4.44)$$

The above reduction is only possible if the contour Γ does not contain any singularity (*i.e. derivation of* W, $\mathcal{K}$, *and* $\mathcal{B}$ *are continuous over* Γ) which is not the case of a contour containing a crack tip.

Consider next a domain with contour Γ which does not contain a crack tip, as shown in Fig.(4.3), where:

$$\Gamma = \overline{abc} + \overline{cd} + \overline{def} + \overline{fa}$$

and define Γ_1 and Γ_2 such that:

$$\Gamma_1 \equiv \overline{abc} \quad , \quad \Gamma_2 \equiv \overline{fed}$$

From equation (4.44), it can deduced that:

$$J = \oint_{\Gamma} (W+\mathcal{K}-\mathcal{B})\, dy - \oint_{\Gamma} \frac{\partial \psi}{\partial x}\, ds = 0$$

i.e.

$$J = \int_{\Gamma_1} (W+\mathcal{K}-\mathcal{B})\, dy + \int_{\overline{cd}} (W+\mathcal{K}-\mathcal{B})\, dy + \int_{\overline{def}} (W+\mathcal{K}-\mathcal{B})\, dy + \int_{\overline{fa}} (W+\mathcal{K}-\mathcal{B})\, dy$$

$$- \int_{\Gamma_1} \frac{\partial \psi}{\partial x}\, ds - \int_{\overline{cd}} \frac{\partial \psi}{\partial x}\, ds - \int_{\overline{def}} \frac{\partial \psi}{\partial x}\, ds - \int_{\overline{fa}} \frac{\partial \psi}{\partial x}\, ds$$

Now, for small crack opening, $dy \to 0$ over $\overline{cd}$ and $\overline{fa}$, i.e.

$$\int_{\overline{cd}} (W+\mathcal{K}-\mathcal{B})\, dy = \int_{\overline{fa}} (W+\mathcal{K}-\mathcal{B})\, dy = 0 \qquad (4.45)$$

and on the crack surfaces $\overline{cd}$ and $\overline{fa}$, $T_x = T_y = 0$, i.e.

$$\int_{\overline{cd}} \frac{\partial \psi}{\partial x}\, ds = \int_{\overline{fa}} \frac{\partial \psi}{\partial x}\, ds = 0 \qquad (4.46)$$

and

$$\int_{\overline{def}} f\, ds = - \int_{\overline{fed}} f\, ds = - \int_{\Gamma_2} f\, ds \qquad (4.47)$$

Hence, from equations (4.45), (4.46), and (4.47), it can be deduced that:

$$\int_{\Gamma_1} (W+\mathcal{K}-\mathcal{B})\, dy - \int_{\Gamma_1} \frac{\partial \psi}{\partial x}\, ds - \int_{\Gamma_2} (W+\mathcal{K}-\mathcal{B})\, dy + \int_{\Gamma_2} \frac{\partial \psi}{\partial x}\, ds = 0$$

Defining:

$$J_1 = \int_{\Gamma_1} (W+\mathcal{K}-\mathcal{B})\, dy - \int_{\Gamma_1} \frac{\partial \psi}{\partial x}\, ds$$

$$J_2 = \int_{\Gamma_2} (W+\mathcal{K}-\mathcal{B})\, dy - \int_{\Gamma_2} \frac{\partial \psi}{\partial x}\, ds$$

gives, $J_1 - J_2 = 0$, i.e.

$$J_1 = J_2 \qquad (4.48)$$

This interesting result shows that such integrals over contours from lower surface of the crack to the upper surface of the crack are independent of the integration path. Since the contour is not closed, then for any open contour Γ_o *(similar to* Γ_1, *or* Γ_2*)* the following integral can be defined:

$$J_o = \oint_{\Gamma_o} (W+\mathcal{K}-\mathcal{B})\, dy - \oint_{\Gamma_o} \frac{\partial \psi}{\partial x}\, ds \qquad (4.49)$$

From equation (4.48), it is clear that such quantity is independent of Γ_o.

Taking Γ_o very near to the crack tip, it can be shown that:

(i) *for a crack with blunt edge (Fig. 4.4):*

$$J_o = \lim_{\Gamma_o \to \Gamma_t} \left[\oint_{\Gamma_o} (W+\mathcal{K}-\mathcal{B})\, dy - \oint_{\Gamma_o} \frac{\partial \psi}{\partial x}\, ds \right] \to \oint_{\Gamma_t} (W+\mathcal{K}-\mathcal{B})\, dy \qquad (4.50)$$

(ii) for a crack with sharp edge (Fig. 4.5):

$$J_o = \lim_{\Gamma_o \to o} \left[\oint_{\Gamma_o} (W+\mathcal{K}-\mathcal{B})\, dy - \oint_{\Gamma_o} \frac{\partial \psi}{\partial x}\, ds \right]$$

$$= - \lim_{\Gamma_o \to o} \oint_{\Gamma_o} \frac{\partial \psi}{\partial x}\, ds \qquad (4.51)$$

Using polar coordinates such that:

$$\xi = r\cos\theta \quad , \quad x = a + r\cos\theta$$
$$\eta = r\sin\theta \quad , \quad y = r\sin\theta$$

Ignoring crack edge and angle, then:

$$J_o \cong \lim_{r \to o} \left[\int_{-\pi}^{\pi} (W+\mathcal{K}-\mathcal{B})\, r\sin\theta\, d\theta - \int_{-\pi}^{\pi} \frac{\partial \psi}{\partial x}\, r\, d\theta \right] \qquad (4.52)$$

It is clear that up till now J_o has not yet been related with the term $\frac{1}{t}\, ds/da$.

4.4.4. Case of a Blunt Crack:

If there is a crack with a smooth blunt edge, as shown in Fig.(4.6), then there is no singularity related to surface tractions, which means that $T_x = T_y = 0$ *(for old and developed crack surface)*, then:

$$\frac{1}{t}\,\Delta\chi = \iint_{\Omega+\Delta\Omega} \left[(W+\Delta W) + (\mathcal{K}+\Delta\mathcal{K}) - (\mathcal{B}+\Delta\mathcal{B}) \right] dA$$

$$- \iint_{\Omega} (W+\mathcal{K}-\mathcal{B})\, dA - \oint_{\Gamma} \Delta\psi\, ds + \frac{1}{t}\,\Delta S = 0$$

Dividing by Δa, and taking the limit $\Delta a \to 0$, the following can be obtained:

$$\lim_{\Delta a \to o} \iint_{\Omega+\Delta\Omega} \left(\frac{\Delta W}{\Delta a} + \frac{\Delta \mathcal{K}}{\Delta a} - \frac{\Delta \mathcal{B}}{\Delta a} \right) dA - \lim_{\Delta a \to o} \frac{1}{\Delta a} \iint_{\Delta\Omega} (W+\mathcal{K}-\mathcal{B})\, dA$$

$$- \oint_{\Gamma} \frac{\partial \psi}{\partial x}\, ds + \frac{1}{t} \frac{dS}{da} = 0$$

i.e.

$$- \frac{1}{t} \frac{dS}{da} = \iint_{\Omega} \left(\frac{dW}{da} + \frac{d\mathcal{K}}{da} - \frac{d\mathcal{B}}{da} \right) dA$$

$$- \oint_{\Gamma} \frac{\partial \psi}{\partial x}\, ds - \lim_{\Delta a \to o} \frac{1}{\Delta a} \iint_{\Delta\Omega} (W+\mathcal{K}-\mathcal{B})\, dA$$

From equation (A.6) [Appendix A], it can be deduced that:

$$\iint_{\Omega} \left(\frac{dW}{da} + \frac{d\mathcal{K}}{da} - \frac{d\mathcal{B}}{da} \right) dA - \oint_{\Gamma} \frac{\partial \psi}{\partial x}\, ds = 0$$

Hence,

$$\frac{1}{t} \frac{dS}{da} = \lim_{\Delta a \to o} \frac{1}{\Delta a} \iint_{\Delta\Omega} (W+\mathcal{K}-\mathcal{B})\, dA$$

$$= \lim_{\Delta a \to o} \frac{1}{\Delta a} \iint_{\Delta\Omega} (W+\mathcal{K}-\mathcal{B})\, da\, dy = \int_{\Gamma_t} (W+\mathcal{K}-\mathcal{B})\, dy$$

where Γ_t is the crack tip boundary.

Comparing this result with equations (4.50) and (4.38), it is clear that:

$$J = J_o = \frac{1}{t} \frac{dS}{da} \qquad (4.53)$$

which means that J is not zero on a contour which contain a crack tip and it can be evaluated at any open contour Γ_o starting from lower crack surface up to the upper surface of the crack.

4.4.5. Case of a Sharp Crack:

Initially,

$$\frac{1}{t}\,\chi = \frac{1}{t}\,S + \iint_{\Omega} (W+\mathcal{K}-\mathcal{B})\,dA - \int_{\Gamma_o} \psi\,ds$$

where Γ_o represents the free surface of the boundary Γ, as shown in Fig.(4.7).

If the crack is very sharp and grows by Δa, without any change of Ω, then:

$$\frac{1}{t}\,(\chi+\Delta\chi) = \frac{1}{t}\,(S+\Delta S) + \iint_{\Omega} \left[(W+\Delta W) + (\mathcal{K}+\Delta\mathcal{K}) - (\mathcal{B}+\Delta\mathcal{B}) \right] dA$$

$$- \int_{\Gamma_o} (\psi+\Delta\psi)\,ds$$

Dividing the difference of the above equations by Δa, and taking the limit $\Delta a \to 0$, it can be deduced that:

$$\frac{1}{t}\,\frac{d\chi}{da} = \frac{1}{t}\,\frac{dS}{da} + \iint_{\Omega} \left(\frac{dW}{da} + \frac{d\mathcal{K}}{da} - \frac{d\mathcal{B}}{da} \right) dA - \int_{\Gamma_o} \frac{\partial\psi}{\partial x}\,ds = 0$$

If only the tractions are assumed singular at the crack tip, then from equation (A.6) [Appendix A]:

$$\iint_{\Omega} \left(\frac{dW}{da} + \frac{d\mathcal{K}}{da} - \frac{d\mathcal{B}}{da} \right) dA = \oint_{\Gamma} \frac{\partial\psi}{\partial x}\,ds$$

i.e.

$$\frac{1}{t}\,\frac{dS}{da} + \oint_{\Gamma} \frac{d\psi}{da}\,ds - \int_{\Gamma_o} \frac{d\psi}{da}\,ds = 0$$

or

$$\frac{1}{t}\frac{dS}{da} + \int_{\Gamma_c} \frac{d\psi}{da}\, ds = 0$$

Since the tractions are zeros on the surface of the crack, then:

$$J = \frac{1}{t}\frac{dS}{da} = - \lim_{\Delta\Gamma \to o} \int_{\Delta\Gamma} \frac{d\psi}{da}\, ds$$

Now, at the crack tip, $\frac{d\psi}{da} \to \frac{d\psi}{dx}$, therefore, comparing with equation (4.51), it can be shown that:

$$J = J_o = - \lim_{\Gamma_o \to o} \oint_{\Gamma_o} \frac{\partial\psi}{\partial x}\, ds \qquad (4.54)$$

4.4.6 Energy Changes Due to Crack Growth:

Let the effect of a crack growth Δa on displacement, stress, and traction vectors be $\Delta\underline{u}$, $\Delta\underline{\sigma}$, and $\Delta\underline{T}$ respectively. Hence,

$$\Delta U = \iint_{\Omega} t \left(\underline{\sigma} + \alpha\, \Delta\underline{\sigma} \right)^t \Delta\underline{\varepsilon}\, dA$$

$$\Delta V_{\Gamma} = - \int_{\Gamma} t \left(\underline{T} + \beta\, \Delta\underline{T} \right)^t \Delta\underline{u}\, ds$$

$$\Delta V_{\Omega} = \iint_{\Omega} t\, \underline{X}^t\, \Delta\underline{u}\, dA$$

where, $0 < \alpha < 1$, $0 < \beta < 1$.

Neglecting second order terms, then:

$$\Delta U \cong \iint_{\Omega} t\ \underline{\sigma}^{t}\ \Delta\underline{\varepsilon}\ dA$$

$$\Delta V_{\Gamma} \cong \int_{\Gamma} t\ \underline{T}^{t}\ \Delta\underline{u}\ ds$$

therefore,

$$\frac{dU}{da} = \lim_{\Delta a \to 0} \frac{\Delta U}{\Delta a} = \iint_{\Omega} t\ \underline{\sigma}^{t}\ \frac{d\underline{\varepsilon}}{da}\ dA \qquad (4.55)$$

$$\frac{dV_{\Gamma}}{da} = \lim_{\Delta a \to 0} \frac{\Delta V_{\Gamma}}{\Delta a} = \int_{\Gamma} t\ \underline{T}^{t}\ \frac{d\underline{u}}{da}\ ds \qquad (4.56)$$

$$\frac{dV_{\Omega}}{da} = \lim_{\Delta a \to 0} \frac{\Delta V_{\Omega}}{\Delta a} = \iint_{\Omega} t\ \underline{X}^{t}\ \frac{d\underline{u}}{da}\ ds \qquad (4.57)$$

Substituting from equations (4.55) and (4.56) into (4.38) and employing the previous approximation, it can be deduced that:

$$J = -\left[\iint_{\Omega} \underline{\sigma}^{t}\ \frac{d\underline{\varepsilon}}{da}\ dA - \int_{\Gamma} \underline{T}^{t}\ \frac{d\underline{u}}{da}\ ds - \iint_{\Omega} \underline{X}^{t}\ \frac{d\underline{u}}{da}\ dA \right] \qquad (4.58)$$

An interesting (*similar*) result can be obtained by applying the following theorem:

Theorem:

Consider that u, v are functions of a parameter ζ, then:

$$\frac{dU}{d\zeta} = \oint_{\Gamma} t \left(T_x \frac{du}{d\zeta} + T_y \frac{dv}{d\zeta} \right) ds + \iint_{\Omega} t \left(X \frac{du}{d\zeta} + Y \frac{dv}{d\zeta} \right) dx\ dy \qquad (4.59)$$

4.4.7. The *J*-Integral as a Contour Integral:

From equation (4.58), it can be shown that:

$$J = -\iint_{\Omega} \frac{dW}{da}\, dx\, dy + \int_{\Gamma_o} \left(T_x \frac{du}{da} + T_y \frac{dv}{da} \right) ds + \iint_{\Omega} \left(X \frac{du}{da} + Y \frac{dv}{da} \right) dx\, dy$$

Hence, from previous analysis (Equ. 4.49), it can be deduced that:

$$J = \oint_{\Gamma} W\, dy - \int_{\Gamma_o} \left(T_x \frac{\partial u}{\partial x} + T_y \frac{\partial v}{\partial x} \right) ds - \iint_{\Omega} \left(X \frac{\partial u}{\partial x} + Y \frac{\partial v}{\partial x} \right) dx\, dy$$

If the crack is taken as explained before, then $dy \to 0$ over Γ_c (Γ_c *is the crack surface*), i.e.

$$\oint_{\Gamma} W\, dy = \int_{\Gamma_o} W\, dy + \int_{\Gamma_c} W\, dy \to \int_{\Gamma_o} W\, dy$$

which leads to:

$$J = \int_{\Gamma_o} W\, dy - \int_{\Gamma_o} \left(T_x \frac{\partial u}{\partial a} + T_y \frac{\partial v}{\partial a} \right) ds - \iint_{\Omega} \left(X \frac{\partial u}{\partial x} + Y \frac{\partial v}{\partial x} \right) dx\, dy \qquad (4.60)$$

4.5 Useful Expressions for Domain Loading Term in J-Integral:

4.5.1 Reduction of Domain Integrals for Special Cases:

Defining the domain loading term as:

$$D_L = \iint_{\Omega} \left(X \frac{\partial u}{\partial x} + Y \frac{\partial v}{\partial x} \right) dA \qquad (4.61)$$

then, from the equations of equilibrium:

$$D_L = \iint_{\Omega} \left\{ \frac{\partial u}{\partial x} \left(\frac{\partial \sigma_x}{\partial x} + \frac{\partial \tau_{xy}}{\partial y} \right) + \frac{\partial v}{\partial x} \left(\frac{\partial \tau_{xy}}{\partial x} + \frac{\partial \sigma_y}{\partial y} \right) \right\} dA$$

Using integration by-parts theorems [Appendix A], it can be proved that:

$$D_L = - \oint_{\Gamma} \left(\frac{\partial u}{\partial x} T_x + \frac{\partial v}{\partial x} T_y \right) ds$$

$$+ \iint_{\Omega} \left\{ \sigma_x \frac{\partial^2 u}{\partial x^2} + \tau_{xy} \left(\frac{\partial^2 u}{\partial x \partial y} + \frac{\partial^2 v}{\partial x^2} \right) + \sigma_y \frac{\partial^2 v}{\partial x \partial y} \right\} dA$$

i.e.

$$D_L = - \oint_{\Gamma} \left(\frac{\partial u}{\partial x} T_x + \frac{\partial v}{\partial x} T_y \right) ds + \iint_{\Omega} \underline{\sigma}^t \frac{\partial \underline{\varepsilon}}{\partial x} dx\, dy$$

which can be written as follows:

$$D_L = \int_{\Gamma_o} \frac{\partial W}{\partial x} dy - \oint_{\Gamma} \left(\frac{\partial u}{\partial x} T_x + \frac{\partial v}{\partial x} T_y \right) ds \qquad (4.62)$$

where Γ is the complete boundary contour for Ω.

Special cases of symmetric cracks can be considered as follows:

(a) Case of One Crack Tip:

For the case shown in Fig.(4.8), it can be shown that:

$$\frac{1}{2} J = \int_{\Gamma_o} W \, dy - \int_{\Gamma_o} \left(T_x \frac{\partial u}{\partial x} + T_y \frac{\partial v}{\partial x} \right) ds$$

$$- \iint_{\Omega} \left(X \frac{\partial u}{\partial x} + Y \frac{\partial v}{\partial x} \right) dx \, dy$$

Hence, from equation (4.62), it can be written that:

$$\frac{1}{2} J \equiv - \int_{\Gamma_o} \left(T_x \frac{\partial u}{\partial x} + T_y \frac{\partial v}{\partial x} \right) ds + \oint_{\Gamma} \left(T_x \frac{\partial u}{\partial x} + T_y \frac{\partial v}{\partial x} \right) ds$$

i.e.

$$\frac{1}{2} J = \int_{a}^{b} \left(T_x \frac{\partial u}{\partial x} + T_y \frac{\partial v}{\partial x} \right) ds \qquad (4.63)$$

The above equation is a simplified expression for J, but it contains a singular point *(i.e. the crack tip)*.

(b) Case of Two Crack Tips:

Using Fig.(4.9), for crack tip 1, it can be shown that:

$$J_1 = \int_{\Gamma_1} W \, dy - \int_{\Gamma_1} \underline{\underline{T}}^t \frac{\partial \underline{\underline{u}}}{\partial x} ds - \iint_{\Omega_1} \underline{\underline{X}}^t \frac{\partial \underline{\underline{u}}}{\partial x} dx \, dy$$

For crack tip 2, x is in the opposite direction, and hence the contour should be in the clockwise direction, i.e., it can be proved that:

$$- J_2 = \int_{\Gamma_2} W \, dy - \int_{\Gamma_2} \underline{\underline{T}}^t \frac{\partial \underline{\underline{u}}}{\partial x} ds - \iint_{\Omega_2} \underline{\underline{X}}^t \frac{\partial \underline{\underline{u}}}{\partial x} dx \, dy$$

Therefore, it can be deduced that:

$$J_1 - J_2 = \int_{\Gamma_1+\Gamma_2} W \, dy - \int_{\Gamma_1+\Gamma_2} \underline{T}^t \frac{\partial \underline{u}}{\partial x} \, ds - \iint_{\Omega_1+\Omega_2} \underline{X}^t \frac{\partial \underline{u}}{\partial x} \, dx \, dy$$

or, it can be written that:

$$J_1 - J_2 = \int_{\Gamma} W \, dy - \int_{\Gamma} \underline{T}^t \frac{\partial \underline{u}}{\partial x} \, ds - \iint_{\Omega} \underline{X}^t \frac{\partial \underline{u}}{\partial x} \, dx \, dy \qquad (4.64)$$

For the special case of symmetric crack $J_1 = J_2$, and it can be proved that:

$$\int_{\Gamma} W \, dy - \int_{\Gamma} \underline{T}^t \frac{\partial \underline{u}}{\partial x} \, ds - \iint_{\Omega} \underline{X}^t \frac{\partial \underline{u}}{\partial x} \, dx \, dy = 0 \qquad (4.65)$$

Now, the following results can be deduced:

(i) *Result (1):*

Since for a closed contour Γ enclosing a domain Ω:

$$\iint_{\Omega} \underline{X}^t \frac{\partial \underline{u}}{\partial x} \, dx \, dy = - \oint_{\Gamma} \underline{T}^t \frac{\partial \underline{u}}{\partial x} + \iint_{\Omega} \underline{\sigma}^t \frac{\partial \underline{\varepsilon}}{\partial x} \, dx \, dy$$

$$= - \oint_{\Gamma} \underline{T}^t \frac{\partial \underline{u}}{\partial x} + \oint_{\Gamma} W \, dy \qquad (4.66)$$

Generally speaking, it is clear from equation (4.64) that the result obtained by equation (4.65) is only correct if there is no crack tip inside Γ. For the special case of a symmetric crack inside the closed contour Γ, equation (4.66) should be valid.

(ii) *Result (2):*

For symmetric crack, surrounded by symmetric contour Γ, it can be proved that:

$$\int_{\Gamma} W \, dy = 0, \quad \int_{\Gamma} \underline{T}^{t} \frac{\partial \underline{u}}{\partial x} \, ds = 0, \quad \iint_{\Omega} \underline{X}^{t} \frac{\partial \underline{u}}{\partial x} \, dx \, dy = 0 \qquad (4.67)$$

since, $\int_{\Gamma_1} W \, dy = - \int_{\Gamma_2} W \, dy,$

and $\int_{\Gamma_1+\Gamma_2} W \, dy = 0 = \int_{\Gamma} W \, dy$, etc.

4.5.2 First Integration of Domain Loading Term:

Using integration by-parts theorems [Appendix A1], equation (4.61) can be written as:

$$D_L = \int_{\Gamma_o} \left(X \, u + Y \, v \right) dy - \iint_{\Omega} \left(\frac{\partial X}{\partial x} u + \frac{\partial Y}{\partial x} v \right) dx \, dy \qquad (4.68)$$

For domain loading due to translational or rotational inertia, it can be shown that:

$$X = a_o + a_1 x + a_2 y$$

$$Y = b_o + b_1 x + b_2 y \qquad (4.69)$$

Hence, using the above equations, it can be deduced that:

$$D_L = \int_{\Gamma_o} \left(X \, u + Y \, v \right) dy - \iint_{\Omega} \left(a_1 u + b_1 v \right) dx \, dy \qquad (4.70)$$

The domain integration is evaluated in terms of integration cells within the whole domain, including the crack tip. For most cases, the strain parameters $\partial u/\partial x$ and $\partial v/\partial x$ are singular at the crack tip, whilst u and v are not. Hence, it is clear that using equation (4.70) for the calculation of domain loading term does not involve any singular parameters and should lead to more accurate values.

Note also that for the special case of translational inertia, or rotation with respect to the x-axis, $a_1 = b_1 = 0$, the domain integral term in equation (4.70) vanishes, leading to a simple contour integration, i.e.

$$D_L = \int_{\Gamma_o} \left[X\, u + Y\, v \right] dy \qquad (4.71)$$

4.5.3 Domain Loading Term for Rotational Inertia around Z-Axis:

For the special case of a structure rotating around the z-axis, the corresponding domain loading intensities can be expressed as follows:

$$X = a_o + a_1 x$$
$$Y = b_o + b_2 y \qquad (4.72)$$

Hence, from equation (4.61) and by using Integration by-parts theorems [Appendix A], it can be shown that:

$$\iint_{\Omega} Y \frac{\partial v}{\partial x}\, dA = \oint_{\Gamma} Y\, v\, dy - \iint_{\Omega} v \frac{\partial Y}{\partial x}\, dx\, dy$$

and from equation (4.72), its clear that $\partial Y/\partial x = 0$, which means:

$$\iint_{\Omega} Y \frac{\partial v}{\partial x}\, dA = \oint_{\Gamma} Y\, v\, dy \qquad (4.73)$$

The remaining problem is to reduce the term $\iint_{\Omega} X \frac{\partial u}{\partial x}\, dA$.

Considering the equilibrium equation in terms of displacements [Ref.79], then:

$$\nabla^2 u + \frac{1}{1-2\nu'} \frac{\partial}{\partial x} \left[\frac{\partial u}{\partial x} + \frac{\partial v}{\partial x} \right] + \frac{X}{\mu} = 0 \qquad (4.74)$$

where,

$\nu' = \nu$ *for plane strain,*

$= \nu/1+\nu$ *for plane stress.*

$\mu = E/2(1+\nu)$

Define a function $f(x)$ such that:

$$\frac{\partial f}{\partial x} = X$$

$$\frac{\partial f}{\partial y} = 0 \qquad (4.75)$$

The simplest form of such function is:

$$f(x) = a_o x + \frac{1}{2} a_1 x^2 \qquad (4.76)$$

Hence,

$$\nabla^2 u + \frac{1}{1-2\nu'} \left[\frac{\partial^2 u}{\partial x^2} + \frac{\partial^2 v}{\partial x \partial y} \right] + \frac{1}{\mu} \frac{\partial f}{\partial x} = 0$$

i.e.

$$\frac{2(1-\nu')}{1-2\nu'} \frac{\partial^2 u}{\partial x^2} + \frac{\partial^2 u}{\partial y^2} + \frac{1}{1-2\nu'} \frac{\partial^2 v}{\partial x \partial y} + \frac{1}{\mu} \frac{\partial f}{\partial x} = 0$$

or

$$\frac{\partial^2 u}{\partial x^2} + \frac{1-2\nu'}{2(1-\nu')} \frac{\partial^2 u}{\partial y^2} + \frac{1}{2(1-\nu')} \frac{\partial^2 v}{\partial x \partial y} + \frac{1-2\nu'}{2(1-\nu')\mu} \frac{\partial f}{\partial x} = 0$$

For more simplifications:

$$(1-2\nu') \frac{\partial^2 u}{\partial x^2} + \frac{\partial^2 v}{\partial x \partial y} = (1-2\nu') \left[\frac{\partial^2 u}{\partial y^2} + \frac{\partial^2 v}{\partial x \partial y} \right] + 2\nu' \frac{\partial^2 v}{\partial x \partial y}$$

Now, the equilibrium equation may be rewritten as follows:

$$\frac{\partial^2 u}{\partial x^2} + \frac{1}{2(1-\nu')} \frac{\partial}{\partial y} \left[(1-2\nu') \gamma_{xy} + 2\nu' \frac{\partial v}{\partial x} \right] + \frac{1-2\nu'}{2(1-\nu')\mu} \frac{\partial f}{\partial x} = 0$$

Defining,

$$C_1 = \frac{1-2\nu'}{4(1-\nu')\mu} = \frac{1-2\nu'}{2(1-\nu')} \frac{1+\nu}{E}$$

$$C_2 = \frac{1-2\nu'}{2(1-\nu')}$$

$$C_3 = \frac{\nu'}{1-\nu'}$$

Hence, the equilibrium equation can be expressed as:

$$\frac{\partial^2 u}{\partial x^2} + \frac{\partial}{\partial y} \left[C_2 \gamma_{xy} + C_3 \frac{\partial v}{\partial x} \right] + 2 C_1 \frac{\partial f}{\partial x} = 0 \qquad (4.77)$$

Considering $f(x)$ to be a weighting function, then:

$$\iint_\Omega f(x) \left[\frac{\partial^2 u}{\partial x^2} + \frac{\partial}{\partial y} \left[C_2 \gamma_{xy} + C_3 \frac{\partial v}{\partial x} \right] + 2 C_1 \frac{\partial f}{\partial x} \right] dx\, dy = 0$$

i.e.

$$\iint_\Omega f(x) \frac{\partial^2 u}{\partial x^2} dx\, dy + \iint_\Omega f(x) \frac{\partial}{\partial y} \left[C_2 \gamma_{xy} + C_3 \frac{\partial v}{\partial x} \right] dx\, dy$$

$$+ \iint_\Omega C_1 \frac{\partial}{\partial x} \left[f(x) \right]^2 dx\, dy = 0$$

Using integration by-parts theorems [Appendix A], it can be deduced that:

$$\oint_\Gamma f(x) \frac{\partial u}{\partial x} dy - \iint_\Omega \frac{\partial f}{\partial x} \frac{\partial u}{\partial x} dx\, dy - \oint_\Gamma f(x) \left[C_2 \gamma_{xy} + C_3 \frac{\partial v}{\partial x} \right] dx$$

$$- \iint_\Omega \frac{\partial f}{\partial y} \left[C_2 \gamma_{xy} + C_3 \frac{\partial v}{\partial x} \right] dx\, dy + \oint_\Gamma C_1 f^2(x)\, dy = 0$$

Now, by using equations (4.75), it can be proved that the above expression may be reduced to:

$$\oint_{\Gamma} f(x) \frac{\partial u}{\partial x}\, dy - \iint_{\Omega} X \frac{\partial u}{\partial x}\, dx\, dy - \oint_{\Gamma} f(x) \left[C_2 \gamma_{xy} + C_3 \frac{\partial v}{\partial x} \right] dx + \oint_{\Gamma} C_1 f^2(x)\, dy = 0$$

i.e.

$$\iint_{\Omega} X \frac{\partial u}{\partial x}\, dx\, dy = \oint_{\Gamma} f(x) \frac{\partial u}{\partial x}\, dy - \oint_{\Gamma} f(x) \left[C_2 \gamma_{xy} + C_3 \frac{\partial v}{\partial x} \right] dx + \oint_{\Gamma} C_1 f^2(x)\, dy$$

or

$$\iint_{\Omega} X \frac{\partial u}{\partial x}\, dx\, dy = \oint_{\Gamma} f(x) \left[\frac{\partial u}{\partial x} + C_1 f(x) \right] dy - \oint_{\Gamma} f(x) \left[C_2 \gamma_{xy} + C_3 \frac{\partial v}{\partial x} \right] dx \qquad (4.78)$$

Hence, from equations (4.61), (4.73) and (4.78), it can shown that:

$$\iint_{\Omega} \underline{X}^t \frac{\partial \underline{u}}{\partial x}\, dA = \oint_{\Gamma_o} f(x) \left[\frac{\partial u}{\partial x} + C_1 f(x) \right] dy - \oint_{\Gamma} f(x) \left[C_2 \gamma_{xy} + C_3 \frac{\partial v}{\partial x} \right] dx + \oint_{\Gamma_o} Y v\, dy \qquad (4.79)$$

4.6 Cases with Thermal & Plastic Strains:

4.6.1 Case with Thermal Strains:

Consider a case with a thermal loading represented by $\underline{\varepsilon}_o$, where,

$$\underline{\varepsilon}_o = \begin{bmatrix} \varepsilon_x \\ \varepsilon_y \\ \gamma_{xy} \end{bmatrix} = \alpha' \begin{bmatrix} T \\ T \\ 0 \end{bmatrix} \qquad (4.80)$$

and

$\alpha' = \alpha$ *for plane stress,*

$= (1+\nu)\alpha$ *for plane strain,*

α = Coefficient of thermal expansion,

T = Temperature difference.

For such a case, the strain energy term in the J-integral equation, may be written as follows:

$$\int_{\Gamma_o} W \, dy = \iint_{\Omega} \underline{\sigma}^t \frac{\partial \underline{\varepsilon}}{\partial x} \, dx \, dy \qquad (4.81)$$

Where $\underline{\varepsilon}$ represents the total strain vector.

From the elastic stress-strain relationship, it can be shown that:

$$\underline{\sigma} = \underline{D} (\underline{\varepsilon} - \underline{\varepsilon}_o) = \underline{D} \, \underline{\varepsilon}_e$$

where,

$$\underline{\varepsilon}_e = \underline{\varepsilon} - \underline{\varepsilon}_o$$

i.e.

$$d\underline{\varepsilon} = d\underline{\varepsilon}_{\circ} + d\underline{\varepsilon}_{\circ}$$

Hence, it can be deduced that:

$$\iint_{\Omega} \underline{\sigma}^{t} \frac{\partial \underline{\varepsilon}}{\partial x}\, dx\, dy = \iint_{\Omega} \underline{\varepsilon}_{\circ}^{t}\, \underline{D} \left(\frac{\partial \underline{\varepsilon}_{\circ}}{\partial x} + \frac{\partial \underline{\varepsilon}_{\circ}}{\partial x} \right) dx\, dy$$

which can be rearranged as follows:

$$\iint_{\Omega} \underline{\sigma}^{t} \frac{\partial \underline{\varepsilon}}{\partial x}\, dx\, dy = \frac{1}{2} \iint_{\Omega} \frac{\partial}{\partial x} \left(\underline{\varepsilon}_{\circ}^{t}\, \underline{D}\, \underline{\varepsilon}_{\circ} \right) dx\, dy$$

$$+ \iint_{\Omega} \underline{\varepsilon}_{\circ}^{t}\, \underline{D}\, \frac{\partial \underline{\varepsilon}_{\circ}}{\partial x}\, dx\, dy$$

The above expression can now be written as follows:

$$\iint_{\Omega} \underline{\sigma}^{t} \frac{\partial \underline{\varepsilon}}{\partial x}\, dx\, dy = \frac{1}{2} \iint_{\Omega} \frac{\partial}{\partial x} \left(\underline{\sigma}^{t}\, \underline{\varepsilon}_{\circ} \right) dx\, dy$$

$$+ \iint_{\Omega} \underline{\sigma}^{t} \frac{\partial \underline{\varepsilon}_{\circ}}{\partial x}\, dx\, dy$$

Using integration by-parts theorem, then it can be shown that:

$$\iint_{\Omega} \underline{\sigma}^{t} \frac{\partial \underline{\varepsilon}}{\partial x}\, dx\, dy = \int_{\Gamma_{\circ}} W_{\circ}\, dy + \iint_{\Omega} \underline{\sigma}^{t} \frac{\partial \underline{\varepsilon}_{\circ}}{\partial x}\, dx\, dy \qquad (4.82)$$

where,

$$W_{\circ} = \frac{1}{2}\, \underline{\sigma}^{t}\, \underline{\varepsilon}_{\circ}$$

4.6.2 Case with Plastic Strains:

For this case the change in strain energy can be defined as follows:

$$dW = \underline{\sigma}^t \, d\underline{\varepsilon} = \underline{\sigma}^t \, d\underline{\varepsilon}_e + \underline{\sigma}^t \, d\underline{\varepsilon}_p \qquad (4.83)$$

where,

$d\underline{\varepsilon}_e$ = Elastic strains component,

$d\underline{\varepsilon}_p$ = Plastic strains component.

Now, the strain energy rate W, can be written as:

$$W = W_e + W_p \qquad (4.84)$$

where,

$$W_e = \int_{\underline{0}}^{\underline{\varepsilon}_e} \underline{\sigma}^t \, d\underline{\varepsilon}_e = \frac{1}{2} \underline{\sigma}^t \, \underline{\varepsilon}_e$$

$$W_p = \int_{\underline{0}}^{\underline{\varepsilon}_p} \underline{\sigma}^t \, d\underline{\varepsilon}_p$$

Hence, the total strain energy can be deduced as follows:

$$\iint_{\Omega} \underline{\sigma}^t \frac{\partial \underline{\varepsilon}}{\partial x} \, dx \, dy = \iint_{\Omega} \left(\frac{\partial W_e}{\partial x} + \frac{\partial W_p}{\partial x} \right) dx \, dy \qquad (4.85)$$

Finally, the following can be deduced:

$$\iint_{\Omega} \underline{\sigma}^t \frac{\partial \underline{\varepsilon}}{\partial x} \, dx \, dy = \oint_{\Gamma} (W_e + W_p) \, dy \qquad (4.86)$$

The plastic work intensity W_p can be calculated within incremental finite or boundary element analysis.

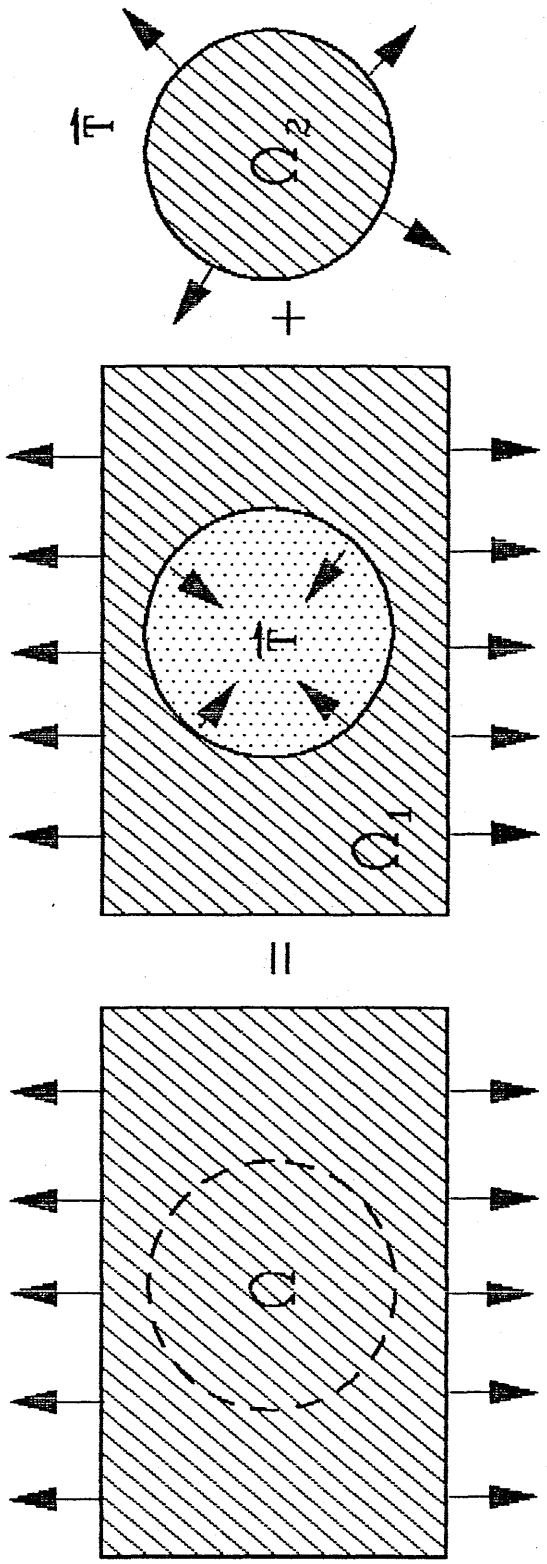

Fig.(4.1) Domain Piecewise Discretization.

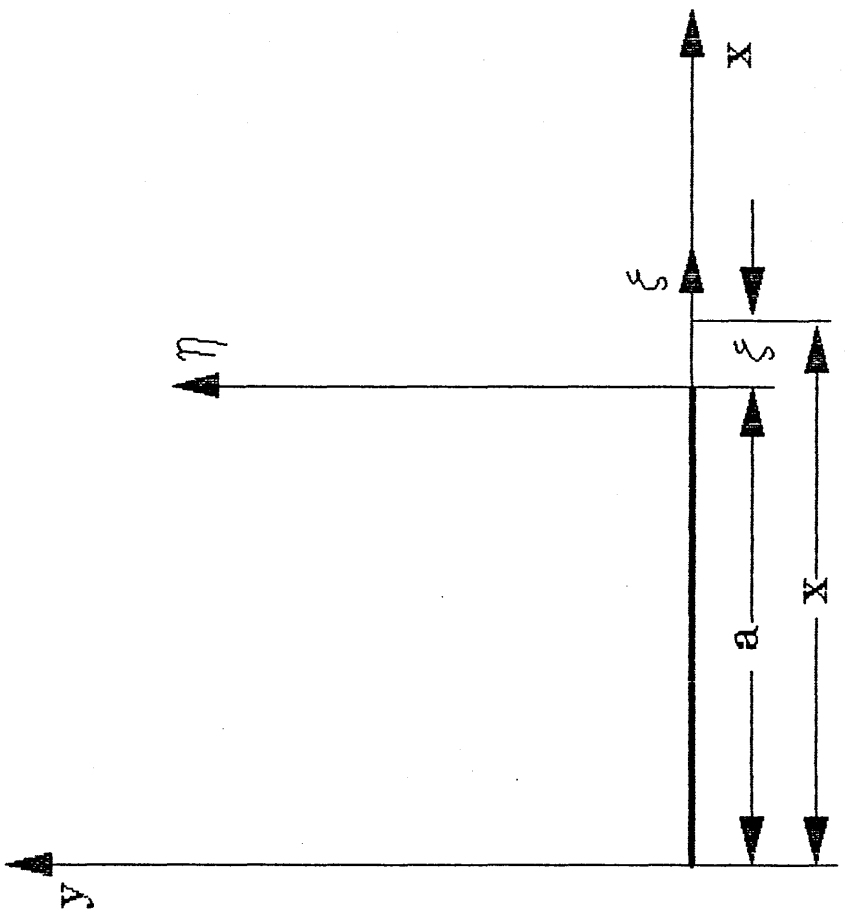

Fig.(4.2) Change of Coordinates.

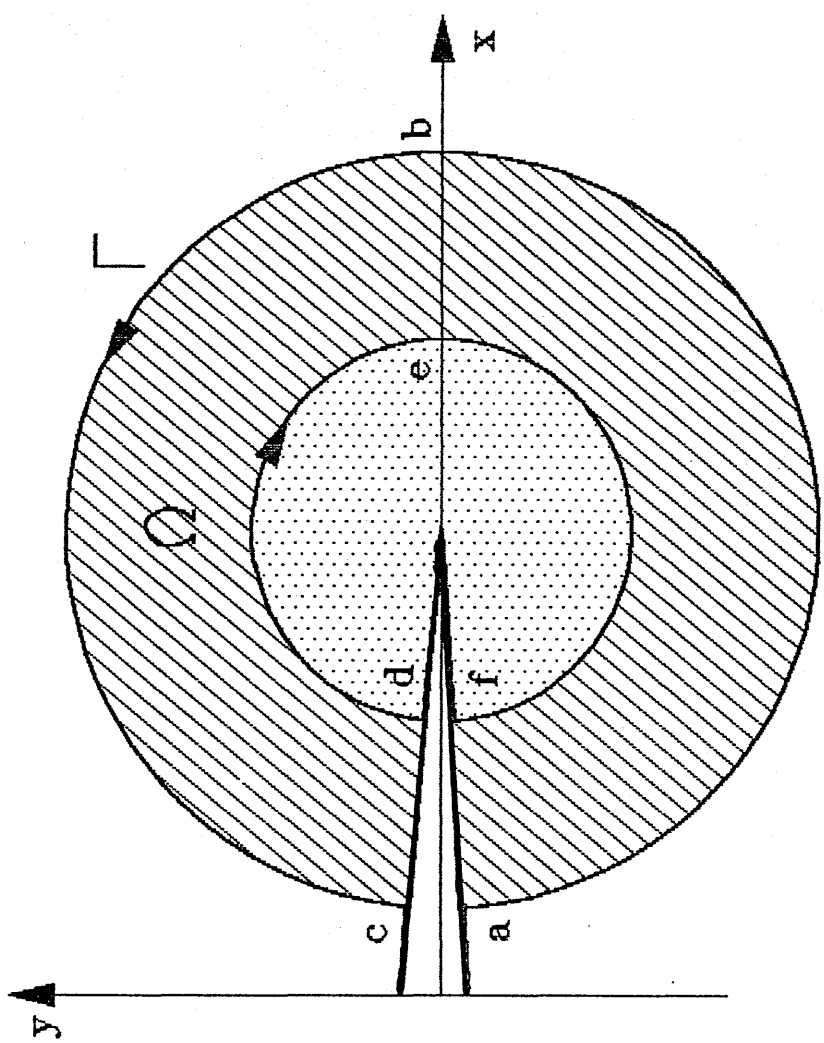

Fig.(4.3) Closed Contour Around the Crack Tip.

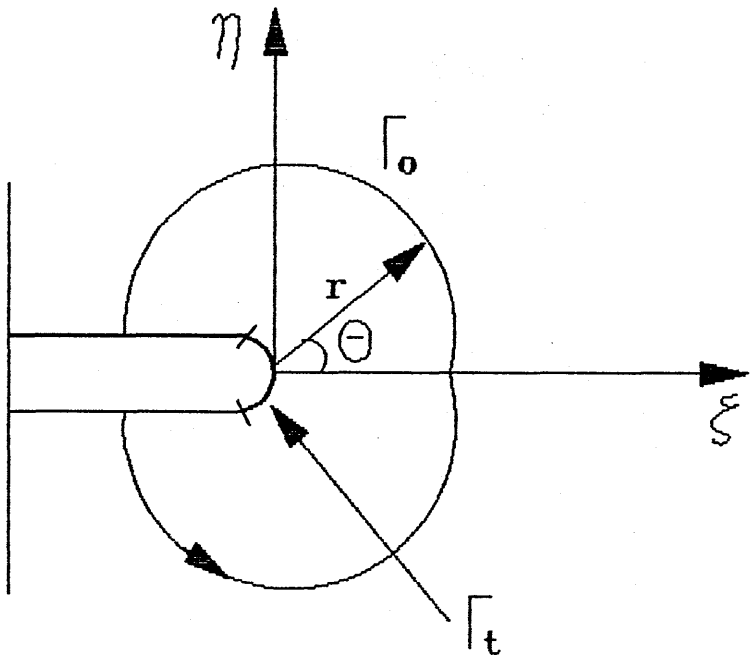

Fig.(4.4) Crack with Blunt Edge.

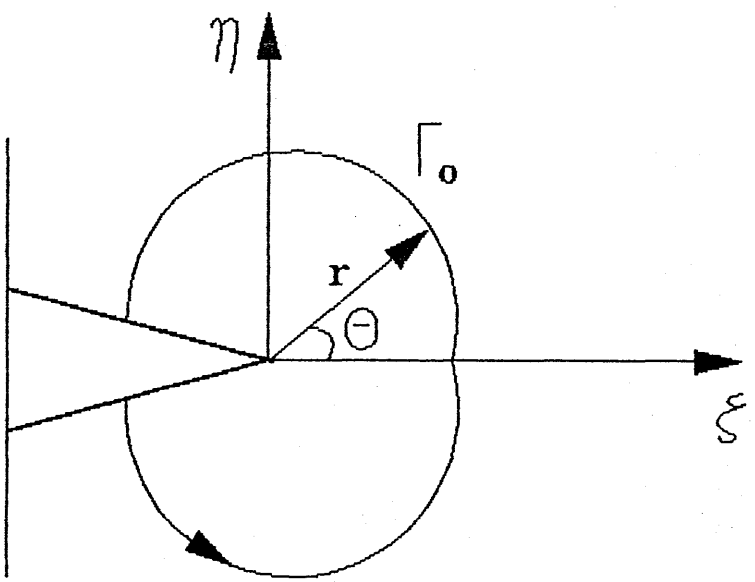

Fig.(4.5) Crack with Sharp Edge.

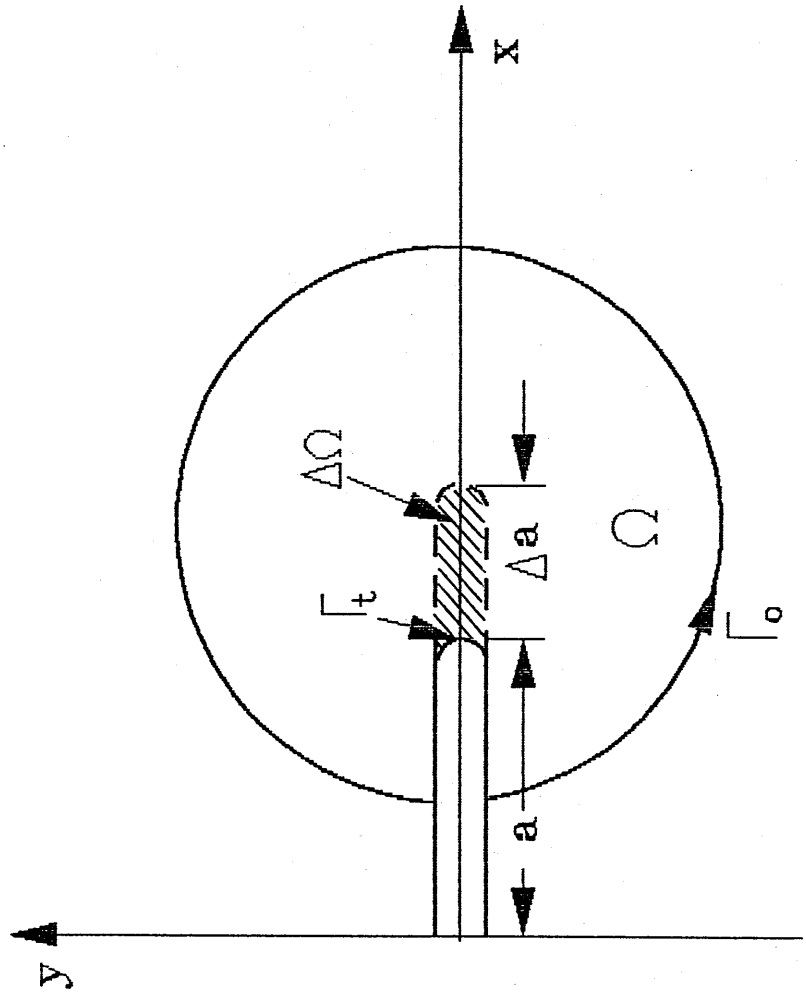

Fig.(4.6) Case of a Blunt Crack.

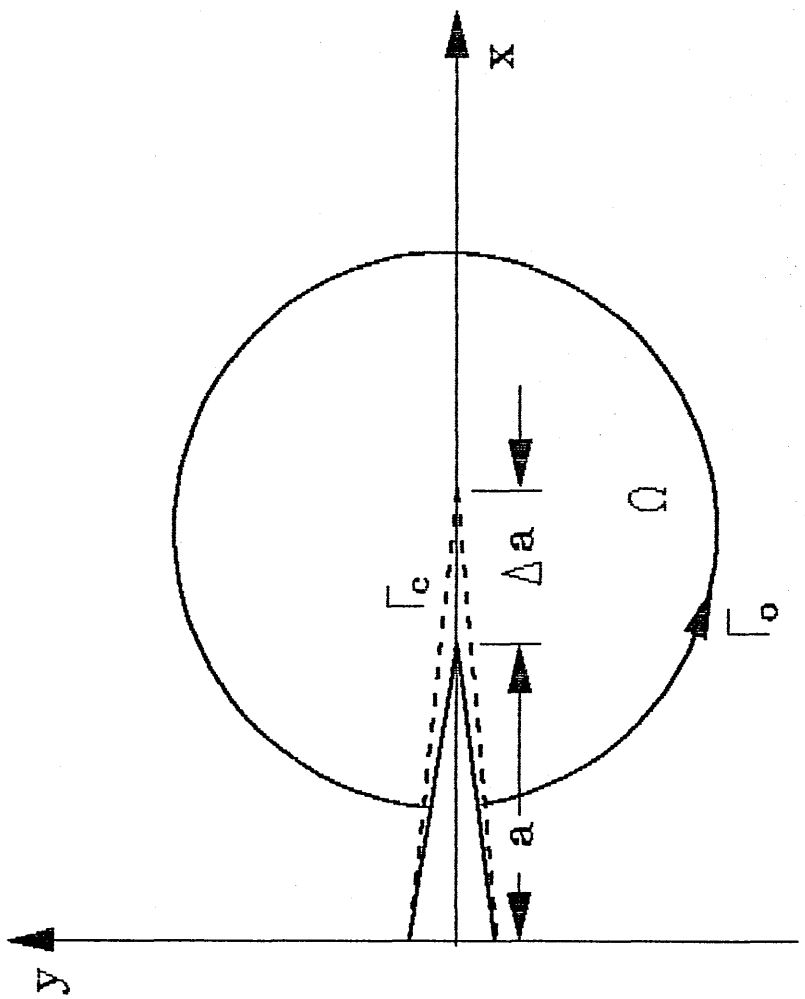

Fig.(4.7) Case of a Sharp Crack.

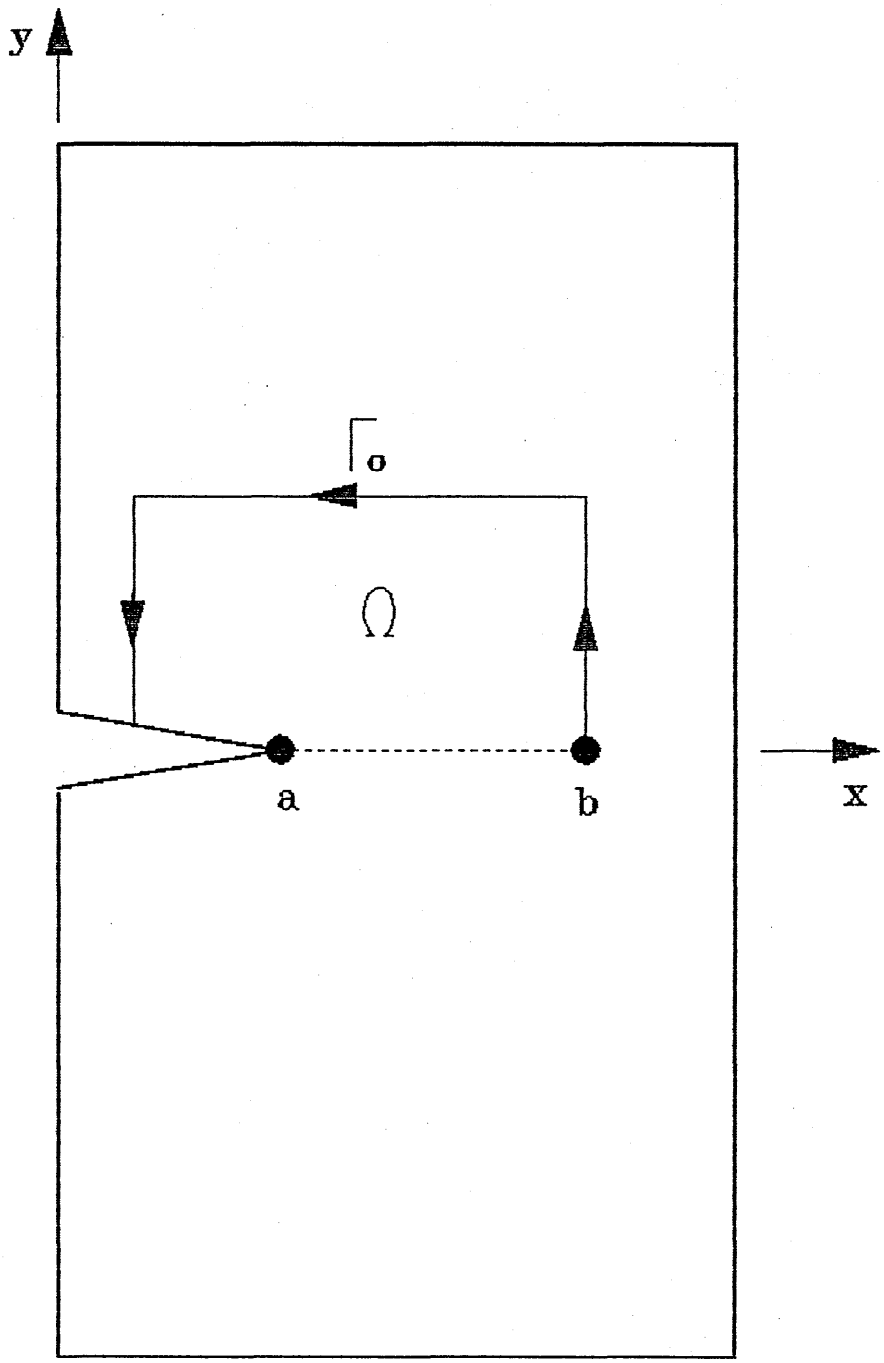

Fig.(4.8) Case of One Crack Tip.

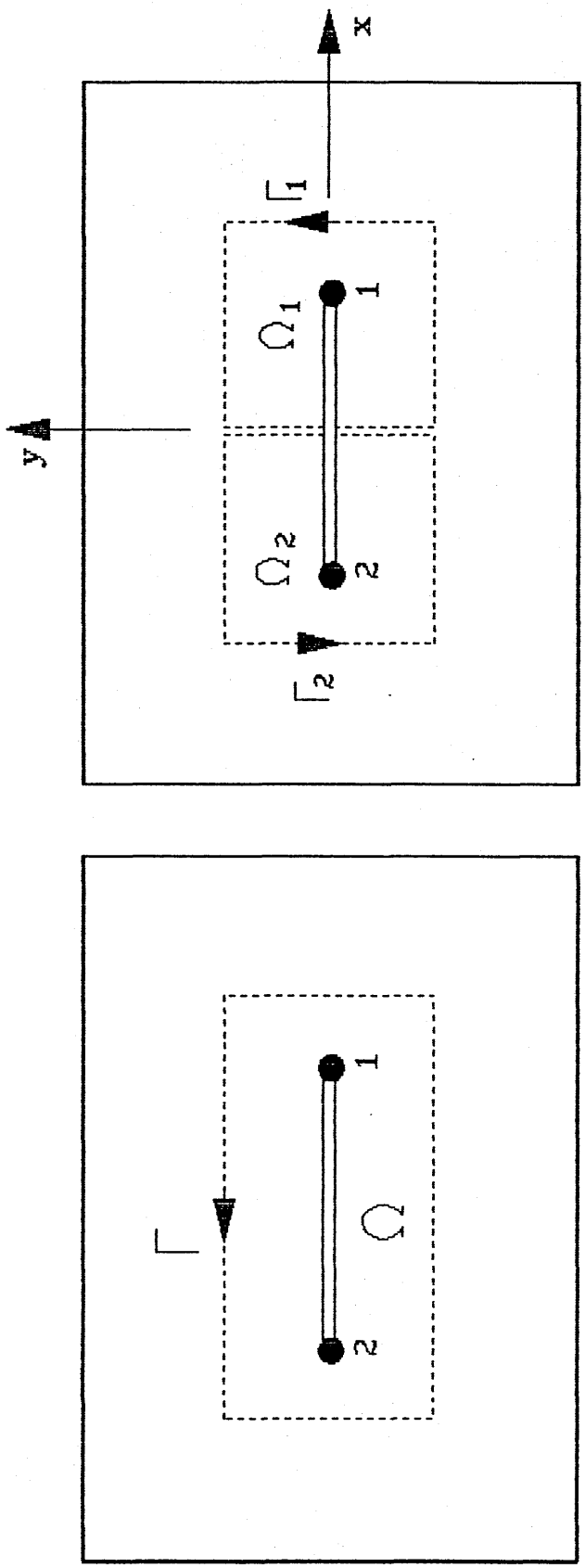

Fig.(4.9) Case of Two Crack Tips.

CHAPTER 5

THE FINITE ELEMENT METHOD FOR FRACTURE MECHANICS PROBLEMS

5.1 Introduction:

There are many engineering problems which may be considered as boundary value problems *(BVP)*. A typical boundary value problem is governed by one or more *'differential'* or *'integral'* equations within a specified domain, together with some conditions over the boundary of the domain.

For complex boundary value problems or complex boundary conditions an analytical or closed-form solution might be difficult to discover, and there is therefore no other choice but to employ an approximate procedure for the solution of such problems.

With the advent of high-speed digital computers, approximate numerical procedures have become very accurate and reliable for the solution of linear and nonlinear boundary value problems. Currently, the most dominant numerical techniques for engineering analysis are the finite element method *(FEM)*, and the boundary element method *(BEM)*.

The finite element method is based upon integral formulations for the governing equation of the given *BVP*. Discretizing the problem domain piecewise into a number of subdomains, or finite elements, the governing equations for each element can be obtained by means of variational or weighted residual approaches. Assembling the subdomains equations together, a simple algebraic system of equations can be obtained and solved.

In this chapter the procedures of linear-elastic and elasto-plastic finite element analyses are reviewed together with different types of loading conditions. New formulations of the standard crack-tip finite elements are presented, also new crack-tip singular finite elements are developed in this work.

5.2 Finite Element Analysis of Linear-Elastic 2D Problems:

5.2.1 Outline of the FEM for 2D Problems:

The process of solving a two-dimensional linear-elastic fracture mechanics problem by the finite element method can be conveniently summarized into the following steps for the so-called '*displacement*' or '*stiffness*' formulation.

Step (1):
Discretization of the Domain (Piecewise discretization).

In this step the whole domain is divided into subdomains (*finite elements*) which are connected together at specified nodes. The field variables on the finite element model is lumped on the specified nodes, i.e. the infinite number of system degrees of freedom is substituted by a finite number of degrees of freedom which represent the values of the field variables at the nodes.

Fig.(5.1) shows the discretization procedure for a plate subjected to an in-plane tensile load at one end and fixed at the other end. Fig.(5.1-a) shows the whole domain as global while Fig.(5.1-b) shows the discretized domain with two finite elements connected by nodes.

The essential points which should be taken into consideration in this step are:

(*a*) The rate of change of the field variables.
(*b*) The boundary and loading conditions.
(*c*) The discontinuity in the geometry and material.

The above points affect the selection of the shape, size, number, and configuration of the elements, which consequently affect the accuracy of the results, and the computer *CPU* time.

Step (2):

Selection of Field Variable Models (Pointwise discretization).

After discretizing the domain into subdomains, each subdomain will be treated separately. The field function over the subdomain is represented in terms of its values at the given nodes and of element shape functions. The shape functions are used for the interpolation of the field variables and may be linear, quadratic, cubic, etc.

For the case shown in Fig.(5.1), the field variable is the displacement component, so at any point the displacement component is expressed in terms of nodal displacements and shape functions.

The displacement vector $\underline{u}$ at any point (x,y) can be expressed as follows:

$$\underline{u}(x,y) = \sum_{i=1}^{n} \underline{u}_i \, N_i(x,y) \qquad (5.1)$$

where,

$\underline{u}(x,y)$ = Displacement vector,

$N_i(x,y)$ = Element shape functions,

n = Number of nodes,

i = 1, 2, 3, ...

The function chosen to describe the field variable pattern within a specified element must meet certain criteria, usually the same function is used for all of the elements over the discretized domain, but if more than one type of elements is used in the same domain, it will be clear that these functions will need to be different for different types of elements.

Step (3):

Formulation of Element Stiffness Matrices and Vectors.

In this step the relation between the source and the field variable is obtained *(i.e. between the applied force acting on the nodes and the nodal displacement)*.

The element stiffness matrix for two-dimensional elasticity problem is given in Ref.[80] as follows:

$$\underline{K}_{(e)} = \int_y \int_x \underline{B}^t \, \underline{D} \, \underline{B} \, t \, dx \, dy \qquad (5.2)$$

where,

$\underline{K}_{(e)}$ = Element stiffness matrix,

$\underline{B}$ = The matrix which relates the strain vector to the nodal displacement vector *(matrix containing the derivatives of the element shape functions with respect to the cartesian coordinates)*,

$\underline{D}$ = The stress-strain matrix *(matrix containing the element properties such as, Young's modulus and Possion's ratio)*,

t = Thickness in the z-direction.

Since the shape functions N_i are expressed in terms of the intrinsic coordinates (ξ,η), it is useful to deduce the derivatives with respect to cartesian coordinates in terms of the intrinsic derivatives. This is possible by means of the chain rule of partial differentiation with the following result:

$$\begin{bmatrix} \frac{\partial N_i}{\partial \xi} \\ \\ \frac{\partial N_i}{\partial \eta} \end{bmatrix} = \underline{J} \begin{bmatrix} \frac{\partial N_i}{\partial x} \\ \\ \frac{\partial N_i}{\partial y} \end{bmatrix} \qquad (5.3)$$

where $\underline{J}$ is the Jacobian matrix which can be defined as:

$$\underline{J} = \begin{bmatrix} \frac{\partial x}{\partial \xi} & \frac{\partial y}{\partial \xi} \\ \frac{\partial x}{\partial \eta} & \frac{\partial y}{\partial \eta} \end{bmatrix}$$

$$= \begin{bmatrix} \frac{\partial N_1}{\partial \xi} & \frac{\partial N_2}{\partial \xi} & \cdots \\ \frac{\partial N_1}{\partial \eta} & \frac{\partial N_2}{\partial \eta} & \cdots \end{bmatrix} \begin{bmatrix} x_1 & y_1 \\ x_2 & y_2 \\ \vdots & \vdots \end{bmatrix} \qquad (5.4)$$

The area relationship between the cartesian coordinates and the intrinsic coordinates is expressed as follows:

$$dx\ dy = |\underline{J}|\ d\xi\ d\eta \qquad (5.5)$$

Thus, equation (5.2) can be rewritten in terms of the intrinsic coordinates coordinates (ξ,η) as follows:

$$\underline{K}_{(e)} = \int_{\eta}\int_{\xi} \underline{B}^t\ \underline{D}\ \underline{B}\ |\underline{J}|\ t\ d\xi\ d\eta \qquad (5.6)$$

Step (4):

Assembly of the Element Matrices and Vectors.

In this step all of the subdomains are assembled together to build the whole domain, the procedure of the assembly is based on the requirement of *'Compatibility'* at element nodes. For the case of stress analysis, two conditions must be satisfied, which are:

(i) To satisfy the equilibrium condition, the global load on a node is equal to the summation of all element forces joining at this node.

(ii) To satisfy the continuity condition, the global displacement of each node has the same value for all the elements joining at this node.

Hence, the nodal stiffness and nodal loads for each of the elements sharing the same node are added to each others to obtain the net stiffness and the net load at the specified node, so the global stiffness matrix can be expressed as:

$$\underline{K} = \sum_{e=1}^{n_e} \underline{K}_{(e)} \qquad (5.7)$$

and the global force vector as:

$$\underline{F} = \sum_{e=1}^{n_e} \underline{F}_{(e)} \qquad (5.8)$$

where,

$\underline{F}_{(e)}$ = Element force vector,

n_e = Number of elements.

Step (5):

Application of the Boundary Conditions.

The overall system of equations for the domain can be written as follows:

$$\underline{K} \cdot \underline{U} = \underline{F} \qquad (5.9)$$

where $\underline{U}$ is the global displacement vector.

In order to solve the above system of equations the following boundary conditions are applied:

(i) At loaded nodes the displacement is unknown and the applied force is known.

(ii) At restrained nodes the load is unknown and the displacement is known.

After applying the above two boundary conditions the system of equations can be partitioned as follows:

$$\begin{bmatrix} \underline{K}_{uu} & \underline{K}_{up} \\ \underline{K}_{pu} & \underline{K}_{pp} \end{bmatrix} \begin{bmatrix} \underline{U}_u \\ \underline{U}_p \end{bmatrix} = \begin{bmatrix} \underline{F}_u \\ \underline{F}_p \end{bmatrix} \qquad (5.10)$$

where,

$\underline{U}_u$ = Unknown displacement vector,
$\underline{U}_p$ = Prescribed displacement vector,
$\underline{F}_u$ = Prescribed force vector,
$\underline{F}_p$ = Unknown force vector.

Hence, from the above equation it can be show that:

$$\underline{K}_{uu}\ \underline{U}_u + \underline{K}_{up}\ \underline{U}_p = \underline{F}_u$$
$$\underline{K}_{pu}\ \underline{U}_u + \underline{K}_{pp}\ \underline{U}_p = \underline{F}_p \qquad (5.11)$$

i.e.

$$\underline{K}_{uu}\ \underline{U}_u = \underline{F}_u - \underline{K}_{up}\ \underline{U}_p \qquad (5.12)$$

which represents a reduced system of equations.

Step (6):

Solution of the Resulting Reduced Equations.

To solve equation (5.12), one of the following solvers can be employed:

(a) Gauss elimination ordinary solver.
(b) Choleski factorization ordinary solver.
(c) Banded Gauss or Choleski solver.
(d) Gauss elimination frontal solver.

The above solvers are available in the finite element package developed in this work.

Step (7):
Determination of nodal Strains and Stresses.

Once the nodal displacements have been determined from the above step, the element strains and stresses can be calculated using strain-displacement, and stress-strain relations, such as:

$$\underline{\varepsilon} = \underline{B}\ \underline{U} \qquad (5.13)$$

and

$$\underline{\sigma} = \underline{D}\ \underline{\varepsilon} \qquad (5.14)$$

Hence, it can be shown that:

$$\underline{\sigma} = \underline{D}\ \underline{B}\ \underline{U} \qquad (5.15)$$

The $\underline{D}$ matrix can be expressed for plane stress and plane strain linear-elastic conditions as follows:

For plane stress:

$$\underline{D} = \frac{E}{1-\nu^2}\begin{bmatrix} 1 & \nu & 0 \\ \nu & 1 & 0 \\ 0 & 0 & \frac{1-\nu}{2} \end{bmatrix} \qquad (5.16)$$

For plane strain:

$$\underline{D} = \frac{E}{(1+\nu)(1-2\nu)} \begin{bmatrix} 1-\nu & \nu & 0 \\ \nu & 1-\nu & 0 \\ 0 & 0 & \frac{1-2\nu}{2} \end{bmatrix} \qquad (5.17)$$

where,

E = Young's modulus of elasticity,

ν = Poisson's ratio.

The $\underline{B}$ matrix for linear-elastic conditions is defined as follows:

$$\underline{B} = \begin{bmatrix} \ldots\ldots & \frac{\partial N_i}{\partial x} & 0 & \ldots\ldots \\ \ldots\ldots & 0 & \frac{\partial N_i}{\partial y} & \ldots\ldots \\ \ldots\ldots & \frac{\partial N_i}{\partial y} & \frac{\partial N_i}{\partial x} & \ldots\ldots \end{bmatrix} \qquad (5.18)$$

Using intrinsic coordinates, the following can be deduced:

$$\begin{bmatrix} \frac{\partial N_i}{\partial x} \\ \\ \frac{\partial N_i}{\partial y} \end{bmatrix} = \underline{J}^{-1} \begin{bmatrix} \frac{\partial N_i}{\partial \xi} \\ \\ \frac{\partial N_i}{\partial \eta} \end{bmatrix} \qquad (5.19)$$

The stresses are then obtained by means of Hooke's law, and since they are proportional to the derivatives of the displacements they will not be as accurate as the displacements themselves. Accurate values for stresses can be obtained at gaussian quadrature points as suggested by Ref.[80].

5.2.2 Library of Two-Dimensional Elements:

The library of the two-dimensional elements, available in the developed finite element module, consists of two families as follows:

(a) The Standard Family:

1. The 4-node Isoparametric Quadrilateral Element.
2. The 6-node Isoparametric Quadrilateral Element.
3. The 8-node serendipity Quadrilateral Element.
4. The 9-node Lagrangian Quadrilateral Element.
5. The 8-node Isoparametric Quadrilateral Element.
6. The 10-node Isoparametric Quadrilateral Element.
7. The 12-node Serendipity Quadrilateral Element.
8. The 3-node Isoparametric Triangular Element.
9. The 6-node Isoparametric Triangular Element.
10. The 10-node Lagrangian Triangular Element.

(b) The Transition Family:

11. The 5-node Quadrilateral Element.
12. The 6-node Quadrilateral Element.
13. The 11-node Lagrangian Quadrilateral Element.
14. The 13-node Lagrangian Quadrilateral Element.
15. The 10-node Quadrilateral Element.
16. The 12-node Quadrilateral Element.
17. The 4-node Triangular Element.
18. The 8-node Triangular Element.

The above families of elements are shown in Fig.(5.2) and Fig.(5.3) respectively. Also the shape functions of the elements are given in Appendix [B].

5.2.3 Initial and Domain Type Loading:

The total potential energy of a two-dimensional subdomain under general loading conditions can be written as follows:

$$\chi = \frac{1}{2}\,\underline{U}^t \left(\iint_{Element} \underline{B}^t\ \underline{D}\ \underline{B}\ t\ dx\ dy \right) \underline{U} - \underline{U}^t\ \underline{F} \qquad (5.20)$$

The total force vector $\underline{F}$ can be expressed as follows:

$$\underline{F} = \underline{F}_E + \underline{F}_\varepsilon + \underline{F}_\sigma \qquad (5.21)$$

where,

$$\underline{F}_\varepsilon = \iint_{Element} \underline{B}^t\ \underline{D}\ \underline{\varepsilon}_o\ t\ dx\ dy$$

$$\underline{F}_\sigma = -\iint_{Element} \underline{B}^t\ \underline{\sigma}_o\ t\ dx\ dy$$

where $\underline{\varepsilon}_o$ and $\underline{\sigma}_o$ are the initial strain and stress vectors, and the above loading vectors are defined as follows:

$\underline{F}_\varepsilon$ = A nodal loading vector equivalent to initial and/or thermal strains.

$\underline{F}_\sigma$ = A nodal loading vector equivalent to initial stresses.

$\underline{F}_E$ = A nodal loading vector equivalent to any other type of loading such as body forces, pressure, etc.

In the presence of body forces the problem can be solved by obtaining the nodal loading vector which is equivalent to a given force field, represented by the following intensity vector:

$$\underline{\omega} = \left\{ \omega_{x_1} \; \omega_{y_1} \quad \omega_{x_2} \; \omega_{y_2} \; \ldots \; \omega_{x_n} \; \omega_{y_n} \right\} \tag{5.22}$$

where $(\omega_x,\omega_y)_i$ are the components of the body force intensity *(force per unit area)* at the i^{th} node.

Now, if the equivalent nodal loading vector is written as:

$$\underline{\Omega} = \left\{ \Omega_{x_1} \; \Omega_{y_1} \quad \Omega_{x_2} \; \Omega_{y_2} \; \ldots \; \Omega_{x_n} \; \Omega_{y_n} \right\} \tag{5.23}$$

then, it can be shown that [Ref.80]:

$$\begin{aligned} \Omega_{x_i} &= \sum_{j=1}^{n} Q_{ij} \; \omega_{x_i} \\ \Omega_{y_i} &= \sum_{j=1}^{n} Q_{ij} \; \omega_{y_i} \end{aligned} \tag{5.24}$$

where,

$$Q_{ij} = \iint_{element} N_i \; N_j \; dx \; dy$$

For the special case of a uniform body force, i.e.

$$\omega_{x_1} = \omega_{x_2} = \ldots = \omega_x$$

$$\omega_{y_1} = \omega_{y_2} = \ldots = \omega_y$$

it can be deduced that:

$$\begin{aligned} \Omega_{x_i} &= Q_i \; \omega_x \\ \Omega_{y_i} &= Q_i \; \omega_y \end{aligned} \tag{5.25}$$

where,

$$Q_i = \iint_{Element} N_i \, dx \, dy$$

Now, from the definition of $\underline{F}_E$, it can be deduced that:

$$\underline{\Omega} \equiv \underline{F}_E$$

i.e.

$$\underline{F} = \underline{\Omega} + \underline{F}_\varepsilon + \underline{F}_\sigma \qquad (5.26)$$

Applying the minimum total potential energy theorem, such that:

$$\chi(\underline{U}) = minimum$$

or

$$\frac{\partial \chi}{\partial \underline{U}} = \underline{0}$$

leads to the same system of equations, as shown by Equ.(5.9).

5.2.4 Pressure Type Loading:

Consider a two-dimensional finite element having a side under a pressure P which is uniform in the thickness direction *(z-direction)*, i.e.

$$P = P(x,y) \qquad (5.27)$$

The force acting on an infinitesimal length Δs of the loaded side of the element can be expressed as follows:

$$\Delta\vec{F} = - P \, \Delta s \, t \, \hat{n} \qquad (5.28)$$

where,

t = The thickness of the element.

$\hat{n}$ = The outward unit vector normal to Δs.

Writing the outward normal unit vector as:

$$\hat{n} = \ell\, i + m\, j$$

where $\ell = dy/ds$ and $m = -\, dx/ds$, it can be shown that:

$$\Delta\vec{F} = P\, t\, (-\, \Delta y\, i + \Delta x\, j) \qquad (5.29)$$

Hence, the increment of the change in work done by $\Delta\vec{F}$ due to a virtual displacement $\delta\vec{q}$ can be expressed as follows:

$$\delta(\Delta W) = \Delta\vec{F} \cdot \delta\vec{q} = P\, t\, (-\, \delta u\, \Delta y + \delta v\, \Delta x) \qquad (5.30)$$

In order to model geometrically the loaded boundary of the finite element a compatible one dimensional pressure *(boundary)* element should be used, such that the number of nodes of this element is equal to the number of nodes on the loaded side of the parent finite element.

From the properties of two-dimensional shape functions, the choice of compatible pressure elements will lead to the same interpolation of the field functions over the loaded boundaries *(This is due to the Co continuity of two dimensional interpolation expressions).*

The equation of the pressure element in the x-y plane can be represented in terms of the following parametric equations:

$$x(\xi) = \sum_{i=1}^{n} x_i\, N_i(\xi)$$

$$y(\xi) = \sum_{i=1}^{n} y_i\, N_i(\xi) \qquad (5.31)$$

where,

$$N_i(\xi) = \mathcal{L}_i^n(\xi) = \prod_{\substack{r=1 \\ r \neq i}}^{n} \left[\frac{(n-1)\,\xi - (r-1)}{i - r} \right] \tag{5.32}$$

The displacement components can be interpolated over the pressure element, as follows:

$$\begin{aligned} \delta u &= \sum_{i=1}^{n} \delta u_i \; N_i(\xi) \\ \delta v &= \sum_{i=1}^{n} \delta v_i \; N_i(\xi) \end{aligned} \tag{5.33}$$

Hence, the increment of the work done by pressure forces due to $\delta\vec{q}$ can be obtained form equation (5.30) as follows:

$$\delta W = \int_{\substack{\text{Pressure} \\ \text{Element}}} P \; t \; (-\,\delta u \; dy + \delta v \; dx) \tag{5.34}$$

Now, substituting from equations (5.33) into (5.34), it can be shown that:

$$\delta W = \sum_{i=1}^{n} \left[\int_{\substack{\text{Pressure} \\ \text{Element}}} P \; t \; N_i \; (-\,\delta u_i \; dy + \delta v_i \; dx) \right] \tag{5.35}$$

The work done by the equivalent nodal forces due to $\delta\vec{q}$ can also be written as follows:

$$\delta W = \sum_{i=1}^{n} \left[F_{x_i} \; \delta u_i + F_{y_i} \; \delta v_i \right] \tag{5.36}$$

Comparing equations (5.35) and (5.36), it can be proved that:

$$F_{x_i} = - \int P\ t\ N_i(\xi)\ dy$$

$$F_{y_i} = + \int P\ t\ N_i(\xi)\ dx \qquad (5.37)$$

Using equations (5.31), the above equations can be rewritten for a pressure element in the intrinsic system ($0 \le \xi \le 1$), as follows:

$$F_{x_i} = - \int_0^1 P\ t\ N_i(\xi) \left[\frac{dy}{d\xi} \right] d\xi$$

$$F_{y_i} = + \int_0^1 P\ t\ N_i(\xi) \left[\frac{dx}{d\xi} \right] d\xi \qquad (5.38)$$

The resulting vector $\underline{F}$ is acting on the nodes of the pressure element and it can be added to the global nodal loading vector by means of the topology array of the pressure element, in the usual way.

5.3 Crack-Tip Finite Elements:

5.3.1 Basic Concept of Singular Isoparametric Elements:

The geometry of an isoparametric two-dimensional element can be mapped into a normalized element ($0 \le \xi \le 1, 0 \le \eta \le 1$) in the intrinsic ξ-η space, through the following transformation:

$$x = \sum_{i=1}^{n} N_i(\xi,\eta)\ x_i$$

$$y = \sum_{i=1}^{n} N_i(\xi,\eta)\ y_i \qquad (5.39)$$

where,

n	= Number of element nodes.
$N_i(\xi,\eta)$	= The shape functions in the (ξ,η) space.
(x_i,y_i)	= The nodal cartesian coordinates.

Displacement components at any point within the element are interpolated in terms of the corresponding nodal values as follows:

$$u = \sum_{i=1}^{n} N_i(\xi,\eta)\ u_i$$

$$v = \sum_{i=1}^{n} N_i(\xi,\eta)\ v_i \qquad (5.40)$$

The form of $N_i(\xi,\eta)$ in all isoparametric elements are algebraic polynomials [Ref.14], and hence, $\partial N_i/\partial\xi$, $\partial N_i/\partial\eta$, are non-singular.

On the other hand, the strain in equation (5.13) can be written by combining equations (5.13), (5.18) and (5.19), in the following form:

$$\underline{\varepsilon} = \hat{\underline{J}}^{-1}\ \hat{\underline{B}}(\xi,\eta)\ \underline{U} \qquad (5.41)$$

where $\hat{\underline{B}}(\xi,\eta)$ is the $\underline{B}$ matrix with respect to the (ξ,η) system, and $\hat{\underline{J}}^{-1}$ is a 3x3 matrix formed from $\underline{J}^{-1}$.

Therefore, a crack-tip singularity could be achieved by making the Jacobian matrix $\underline{J}$ singular at the crack tip, or in other words, if the determinant of the Jacobian $|\underline{J}|$ vanishes at the crack tip, where from equation (5.4):

$$|\underline{J}| = \frac{\partial x}{\partial\xi}\frac{\partial y}{\partial\eta} - \frac{\partial x}{\partial\eta}\frac{\partial y}{\partial\xi} \qquad (5.42)$$

It was found [Ref.13,14,25,27,29] that by placing the mid-side

node of the appropriate elements at the quarter point of two sides, the Jacobian matrix $\underline{J}$ become singular, at the common corner between those sides. Consequently, the values of strain and stress vectors go to infinite values, at such a corner, which should, of course, be set at the crack tip.

5.3.2 The Quadratic-Side Crack-Tip Elements:

(a) The Eight-Node Quadrilateral Singular Element:

This element is an eight-node quadrilateral with the mid-side nodes of two sides being placed in the x-y plane at the quarter points as shown in Fig.(5.4-a).

Using $(0\le\xi\le1, 0\le\eta\le1)$ system, the shape functions for this element are the same as those used for standard serendipity element and can be expressed explicitly as follows:

$$
\begin{aligned}
N_1 &= (1-\xi)\,(1-\eta)\,(1-2\xi-2\eta)\\
N_2 &= 4\,\xi\,(1-\xi)\,(1-\eta)\\
N_3 &= \xi\,(1-\eta)\,(-1+2\xi+2\eta)\\
N_4 &= 4\,\xi\,\eta\,(1-\eta)\\
N_5 &= \xi\,\eta\,(-3+2\xi+2\eta)\\
N_6 &= 4\,\xi\,(1-\xi)\,\eta\\
N_7 &= (1-\xi)\,\eta\,(-1-2\xi+2\eta)\\
N_8 &= 4\,(1-\xi)\,\eta\,(1-\eta)
\end{aligned}
\qquad (5.43)
$$

For simplicity, the strength of the singularity will be found along the line 1-3, as shown in Fig.(5.4).

The shape functions along the line 1-3 can be evaluated by setting $\eta = 0$, as follows:

$$
\begin{aligned}
N_1 &= (1-\xi)\,(1-2\xi)\\
N_2 &= 4\,\xi\,(1-\xi)\\
N_3 &= \xi\,(2\xi-1)
\end{aligned}
\qquad (5.44)
$$

Using equations (5.39), it can be shown that:

$$x(\xi) = (1-\xi)(1-2\xi)\, x_1 + 4\,\xi\,(1-\xi)\, x_2 + \xi\,(2\xi-1)\, x_3 \qquad (5.45)$$

For the quarter-point element in the x-y plane, the cartesian x-coordinates of nodes 1, 2, and 3 are:

$$x_1 = 0,\ x_2 = L_x/4,\ x_3 = L_x$$

Substituting the above values in equation (5.45), it can be deduced that:

$$x(\xi) = L_x\,(1-\xi) + L_x\,\xi\,(2\xi-1) \qquad (5.46)$$

and by rearranging the terms, it can be proved that:

$$x = L_x\,\xi^2 \qquad (5.47)$$

therefore,

$$\xi = +\sqrt{x / L_x} \qquad (5.48)$$

In the Jacobian matrix the term $\partial x/\partial \xi$ will then be given by:

$$\frac{\partial x}{\partial \xi} = 2\,L_x\,\xi = 2\sqrt{x\,L_x} \qquad (5.49)$$

Now, it is clear from equation (5.49), that the Jacobian matrix becomes singular at ($x = 0$, $\xi = 0$).

Considering only the nodes 1, 2, and 3 the displacement u along the line 1-3 can be written according to equations (5.40) as follows:

$$u = (1-\xi)(1-2\xi)\, u_1 + 4\,\xi\,(1-\xi)\, u_2 + \xi\,(2\xi-1)\, u_3 \qquad (5.50)$$

In terms of x, equation (5.50) will be as follows:

$$u = \left[1 - 3\sqrt{x/L_x} + 2\, x/L_x \right] u_1 + \left[4\sqrt{x/L_x} - 4\, x/L_x \right] u_2$$

$$+ \left[2\, x/L_x - \sqrt{x/L_x} \right] u_3 \qquad (5.51)$$

Since the strain in the x-direction can be expressed as follows:

$$\varepsilon_x = \frac{\partial u}{\partial x} = \underline{J}^{-1} \frac{\partial u}{\partial \xi} = \frac{\partial \xi}{\partial x} \frac{\partial u}{\partial \xi}$$

therefore,

$$\varepsilon_x = \left[\frac{3}{2\sqrt{x\, L_x}} + \frac{2}{L_x} \right] u_1 + \left[\frac{2}{\sqrt{x\, L_x}} - \frac{4}{L_x} \right] u_2$$

$$+ \left[\frac{2}{L_x} - \frac{1}{2\sqrt{x\, L_x}} \right] u_3 \qquad (5.52)$$

Measuring x from the crack tip as r, it is clear from the above equation that the strain singularity along the line 1-3 is $1/\sqrt{r}$, which is the required singularity for linear elastic fracture analysis.

(b) *The Six-Node Triangular singular Element:*

This is an isoparametric element with the mid-side nodes of two sides being placed at the quarter points, as shown in Fig.(5.5-a).

Using Argyris theorem [Ref.80], the shape functions for the element can be expressed in terms of area coordinates (L_1, L_2, L_3) as follows:

$$
\begin{aligned}
N_1 &= L_1\ (2L_1-1)\\
N_2 &= 4\ L_1\ L_2\\
N_3 &= L_2\ (2L_2-1)\\
N_4 &= 4\ L_2\ L_3\\
N_5 &= L_3\ (2L_3-1)\\
N_6 &= 4\ L_3\ L_1
\end{aligned}
\qquad (5.53)
$$

Alternatively, they can be expressed in terms of the intrinsic coordinates (ξ,η) by using the following relations:

$$
\begin{aligned}
L_1 &= 1-\xi-\eta\\
L_2 &= \xi\\
L_3 &= \eta
\end{aligned}
\qquad (5.54)
$$

Hence, the shape functions with respect to the $(0\le\xi\le1, 0\le\eta\le1)$ system, can be expressed as follows:

$$
\begin{aligned}
N_1 &= (1-\xi-\eta)\ (1-2\xi-2\eta)\\
N_2 &= 4\ \xi\ (1-\xi-\eta)\\
N_3 &= \xi\ (2\xi-1)\\
N_4 &= 4\ \xi\ \eta\\
N_5 &= \eta\ (2\eta-1)\\
N_6 &= 4\ \eta\ (1-\xi-\eta)
\end{aligned}
\qquad (5.55)
$$

For this element, the singularity can be investigated along the side 1-3 (Fig.5.5) in the same manner as shown in section (5.3.2-a).

5.3.3 The Nine-Node Lagrangian Crack-Tip Element:

This element has been derived by the current author and it has been used, for the first time, as a crack-tip element. The element has mid-side nodes of two adjacent sides at the quarter points, as shown in Fig.(5.6). The inside node of the element has been deduced, using the equations of the intersected lines, as follows:

$$x = a + \frac{2\alpha}{1+2\alpha} L_x$$

$$y = b + \frac{2\alpha}{1+2\alpha} L_y$$

where (a,b) are the coordinates of node 1, and for quarter-point element $\alpha = 1/4$.

The type of singularity for this element can be investigated using the $(0\le\xi\le1, 0\le\eta\le1)$ system by applying equations (5.39) to the element, and using the coordinate system described in Fig.(5.7), it can be deduced that:

$$x(\xi,\eta) = a + L_x \left\{ \mathcal{L}_3^3(\xi) + \mathcal{L}_2^3(\xi) \left[\alpha\, \mathcal{L}_1^3(\eta) + \left(\frac{2\alpha}{1+2\alpha}\right) \mathcal{L}_2^3(\eta) + \frac{1}{2}\, \mathcal{L}_3^3(\eta) \right] \right\} \qquad (5.56)$$

similarly, it can be proved that:

$$y(\xi,\eta) = b + L_y \left\{ \mathcal{L}_3^3(\eta) + \mathcal{L}_2^3(\eta) \left[\alpha\, \mathcal{L}_1^3(\xi) + \left(\frac{2\alpha}{1+2\alpha}\right) \mathcal{L}_2^3(\xi) + \frac{1}{2}\, \mathcal{L}_3^3(\xi) \right] \right\} \qquad (5.57)$$

At the crack tip, $(\xi=0,\ \eta=0)$, the derivatives with respect to ξ and η can be found as follows:

$$\frac{\partial x}{\partial \xi} = L_x\,(4\alpha-1)\ ,\quad \frac{\partial x}{\partial \eta} = 0$$

$$\frac{\partial y}{\partial \eta} = L_y\,(4\alpha-1)\ ,\quad \frac{\partial y}{\partial \xi} = 0 \qquad (5.58)$$

Now, from equation (5.4), it can be shown that, at the crack tip:

$$\underline{J} = \begin{bmatrix} L_x\,(4\alpha-1) & 0 \\ 0 & Ly\,(4\alpha-1) \end{bmatrix} \qquad (5.59)$$

It is clear from equation (5.59) that for a quarter-point element (α=1/4) the Jacobian matrix $\underline{J}$ vanishes, which gives the required singularity.

The explicit shape functions for this element can be written as follows:

$$\begin{aligned}
N_1 &= (1-\xi)\,(1-2\xi)\,(1-\eta)\,(1-2\eta) \\
N_2 &= 4\,\xi\,(1-\xi)\,(1-\eta)\,(1-2\eta) \\
N_3 &= \xi\,(2\xi-1)\,(1-\eta)\,(1-2\eta) \\
N_4 &= 4\,\xi\,(2\xi-1)\,\eta\,(1-\eta) \\
N_5 &= \xi\,(2\xi-1)\,\eta\,(2\eta-1) \\
N_6 &= 4\,\xi\,(1-\xi)\,\eta\,(2\eta-1) \\
N_7 &= (1-\xi)\,(1-2\xi)\,\eta\,(2\eta-1) \\
N_8 &= 4\,(1-\xi)\,(1-2\xi)\,\eta\,(1-\eta) \\
N_9 &= 16\,\xi\,(1-\xi)\,\eta\,(1-\eta)
\end{aligned} \qquad (5.60)$$

Now, from equations (5.60) it can be proved that the strength of the singularity along the line 1-3, is $1/\sqrt{r}$, which is the required singularity for linear-elastic fracture mechanics.

5.3.4 The $1/\sqrt{2}$ Singular Crack-Tip Element:

One of the disadvantages of standard isoparametric crack-tip elements is that the distortion should be carried out in the x-y plane by the package user. Hence, an alternative family of crack-tip isoparametric elements, in which the distortion is only in the intrinsic ξ-η plane would be more useful.

This element, which also has been derived by the current author for the first time, is one of such a family of elements, and it

is based upon the 9-node Lagrangian isoparametric element.

Consider a one-dimensional element on the ξ-line, as shown in Fig.(5.8-a). Using the Lagrangian multiplier as:

$$\mathcal{L}^{n}_{i=1}(\xi) = \prod^{n}_{\substack{r=1 \\ r\neq i}} \left(\frac{\xi - \xi_r}{\xi_i - \xi_r} \right) \qquad (5.61)$$

the shape functions for this element can be deduced as follows:

$$N_1 = \mathcal{L}^{3}_{1}(\xi) = \frac{1}{\alpha}(1-\xi)(\alpha-\xi)$$

$$N_2 = \mathcal{L}^{3}_{2}(\xi) = \frac{1}{\alpha(1-\alpha)}\xi(1-\xi) \qquad (5.62)$$

$$N_3 = \mathcal{L}^{3}_{3}(\xi) = -\frac{1}{1-\alpha}\xi(\alpha-\xi)$$

Now, consider the same element on the x-line, as shown in Fig.(5.8-b). Using the isoparametric transformation given by equations (5.39), and assuming that $x_1 = a$, $x_2 = a + L/2$, and $x_3 = a + L$, it can be deduced that:

$$x = a + \frac{L}{2\alpha(1-\alpha)}\xi(1-\xi) - \frac{L}{1-\alpha}\xi(\alpha-\xi)$$

By rearranging the terms, it can be shown that:

$$x = a + \frac{L}{2\alpha(1-\alpha)}\xi\left[(1-2\alpha^2) + (2\alpha-1)\xi\right] \qquad (5.63)$$

The condition for having the coefficient of ξ, in the above expression, equal to zero is:

$$1 - 2\alpha^2 = 0$$

which gives,

$$\alpha = 1/\sqrt{2} \tag{5.64}$$

Substituting back in equation (5.63), and setting $\alpha = 0$, it can be shown that:

$$x = L\,\xi^2 \tag{5.65}$$

Comparing equation (5.65) with equation (5.47), it is clear that equation (5.65) gives the singularity required for the analysis of linear elastic fracture mechanics.

Now, at $\alpha = 1/\sqrt{2}$ the shape functions for the one-dimensional element are deduced as follows:

$$\begin{aligned} N_1 &= (1-\xi)\,(1-\sqrt{2}\,\xi) \\ N_2 &= 2\,(\sqrt{2}+1)\,\xi\,(1-\xi) \\ N_3 &= -\,(\sqrt{2}+1)\,\xi\,(1-\sqrt{2}\,\xi) \end{aligned} \tag{5.66}$$

In order to check the element shape function derivations the following condition should be satisfied:

$$\sum_{i=1}^{n} N_i(\xi) = 1 \tag{5.67}$$

Substituting equations (5.66) in the left-hand side of equation (5.67), it can be shown that:

$$N_1 + N_2 + N_3 = 1 \tag{5.68}$$

Hence, equations (5.66) represent the correct shape functions for an element on the ξ-line. Notice also that the above shape functions can be used for a crack-tip boundary element from the same family.

Similarly, for an element on the η-line the shape functions are as follows:

$$
\begin{aligned}
N_1(\eta) &= (1-\eta)\ (1-\sqrt{2}\ \eta) \\
N_2(\eta) &= 2\ (\sqrt{2}+1)\ \eta\ (1-\eta) \\
N_3(\eta) &= -\ (\sqrt{2}+1)\ \eta\ (1-\sqrt{2}\ \eta)
\end{aligned}
\qquad (5.69)
$$

Now, consider a nine-node element in two-dimensional plane as shown in Fig.(5.9). The shape functions for this element can be deduced as follows:

$$
\begin{aligned}
N_1(\xi,\eta) &= N_1(\xi)\ N_1(\eta) \\
N_2(\xi,\eta) &= N_2(\xi)\ N_1(\eta) \\
N_3(\xi,\eta) &= N_3(\xi)\ N_1(\eta) \\
N_4(\xi,\eta) &= N_3(\xi)\ N_2(\eta) \\
N_5(\xi,\eta) &= N_3(\xi)\ N_3(\eta) \\
N_6(\xi,\eta) &= N_2(\xi)\ N_3(\eta) \\
N_7(\xi,\eta) &= N_1(\xi)\ N_3(\eta) \\
N_8(\xi,\eta) &= N_1(\xi)\ N_2(\eta) \\
N_9(\xi,\eta) &= N_2(\xi)\ N_2(\eta)
\end{aligned}
\qquad (5.70)
$$

Substituting from equations (5.66) and (5.69) into (5.70), the shape functions for the 9-node $1/\sqrt{2}$ singular crack-tip element can be deduced in explicit form as follows:

$$
\begin{aligned}
N_1 &= (1-\xi)\ (1-\sqrt{2}\ \xi)\ (1-\eta)\ (1-\sqrt{2}\ \eta) \\
N_2 &= 2\ (\sqrt{2}+1)\ \xi\ (1-\xi)\ (1-\eta)\ (1-\sqrt{2}\ \eta) \\
N_3 &= -\ (\sqrt{2}+1)\ \xi\ (1-\sqrt{2}\ \xi)\ (1-\eta)\ (1-\sqrt{2}\ \eta) \\
N_4 &= -\ 2\ (\sqrt{2}+1)^2\ \xi\ (1-\sqrt{2}\ \xi)\ \eta\ (1-\eta) \\
N_5 &= (\sqrt{2}+1)^2\ \xi\ (1-\sqrt{2}\ \xi)\ \eta\ (1-\sqrt{2}\ \eta) \\
N_6 &= -\ 2\ (\sqrt{2}+1)^2\ \xi\ (1-\xi)\ \eta\ (1-\sqrt{2}\ \eta) \\
N_7 &= -\ (\sqrt{2}+1)\ (1-\xi)\ (1-\sqrt{2}\ \xi)\ \eta\ (1-\sqrt{2}\ \eta) \\
N_8 &= 2\ (\sqrt{2}+1)\ (1-\xi)\ (1-\sqrt{2}\ \xi)\ \eta\ (1-\eta) \\
N_9 &= 4\ (\sqrt{2}+1)^2\ \xi\ (1-\xi)\ \eta\ (1-\eta)
\end{aligned}
\qquad (5.71)
$$

5.3.5 The Collapsed Six-Node Triangular Crack-Tip Elements:

The collapsed triangular crack-tip elements given in the literature are based upon distorting the quadrilateral elements in the cartesian x-y plane such that one of their sides diminishes [Refs.13,17,20,87]. Alternatively, singular triangular elements can be generated by collapsing the quadrilateral elements in the ξ-η plane.

Collapsed 6-Node triangular crack-tip elements have been derived in this work using different transformations, one of these elements is generated and described in this section, whilst the derivations of other collapsed elements can be reviewed in Appendix [B].

Consider an 8-Node isoparametric element in the (ξ',η') system as shown in Fig.(5.10-a). This element can be collapsed to a 6-Node triangular element, Fig.(5.10-b) using the following transformation:

$$\xi' = \frac{\xi}{1-\eta} \quad , \quad \eta' = \eta \tag{5.72}$$

Hence, the shape functions for this collapsed element can be written as follows:

$$\begin{aligned} N_1 &= N'_5 + N'_6 + N'_7 \\ N_2 &= N'_8 \\ N_3 &= N'_1 \\ N_4 &= N'_2 \\ N_5 &= N'_3 \\ N_6 &= N'_4 \end{aligned} \tag{5.73}$$

Now, substituting from equations (5.43) and equation (5.72) into the above equations, the shape functions for this element can be deduced explicitly, as follows:

$$
\begin{aligned}
N_1 &= \eta\,(2\eta-1)\\
N_2 &= 4\,\eta\,(1-\xi-\eta)\\
N_3 &= (1-\xi-\eta)\,(1-2\eta) - 2\xi + \frac{2\xi^2}{1-\eta}\\
N_4 &= 4\xi - \frac{4\xi^2}{1-\eta}\\
N_5 &= -\xi\,(1+2\eta) + \frac{2\xi^2}{1-\eta}\\
N_6 &= 4\,\xi\,\eta
\end{aligned}
\qquad (5.74)
$$

Notice that some of the shape functions and their derivatives, for such an element, are singular at $\eta = 1$, which should be set at the crack tip.

Another crack-tip element can be deduced from the previous one by locating the mid-side nodes of two sides at quarter points, as shown in Fig.(5.10-c).

5.3.6 The Cubic-Side Crack-Tip Elements:

Two singular cubic crack-tip finite elements can be generated from the standard 12-node quadrilateral and 10-node triangular elements, by moving the two internal side nodes of two intersecting sides in both elements to 1/9 and 4/9 locations with respect to the length of the side [Ref.20]. These elements can be derived for the ($0\le\xi\le1, 0\le\eta\le1$) system as will be shown in the following subsections.

(a) The Twelve-Node Quadrilateral Singular Element:

The shape functions of this element along the line 1-4 ($\eta=0$), as shown in Fig.(5.11), can be written explicitly as:

$$N_1 = (1-\xi)\left[\,1 - \frac{9}{2}\,\xi\,(1-\xi)\,\right]$$

$$N_2 = \frac{9}{2}\,\xi\,(1-\xi)\,(2-3\xi) \qquad (5.75)$$

$$N_3 = -\,\frac{9}{2}\,\xi\,(1-\xi)\,(1-3\xi)$$

$$N_4 = \xi\left[\,1 - \frac{9}{2}\,\xi\,(1-\xi)\,\right]$$

Using the isoparametric transformation equations (5.39), and setting $x_1 = 0$, $x_2 = 1/9\ L_x$, $x_3 = 4/9\ L_x$, and $x_4 = L_x$ gives:

$$x(\xi) = \frac{1}{2}\,\xi\,(1-\xi)\,(2-3\xi)\,L_x + 2\,\xi\,(1-\xi)\,(3\xi-1)\,L_x + \xi\,(1 - \frac{9}{2}\,\xi + \frac{9}{2}\,\xi^2)\,L_x \qquad (5.76)$$

which leads to,

$$x(\xi) = \xi^2\,L_x \qquad (5.77)$$

where,

$$\xi = \sqrt{\frac{x}{L_x}} \qquad (5.78)$$

Now, from equations (5.77) and (5.78), it can be shown that:

$$\frac{\partial x}{\partial \xi} = 2\,\sqrt{x\,L_x} \qquad (5.79)$$

Comparing equation (5.79) with equation (5.49), it is clear that the element can produce the same order of singularity required for linear-elastic fracture mechanics, which is the $1/\sqrt{r}$.

(b) *The 10-Node Triangular Crack-Tip Element:*

This element is again derived by the current author as a crack tip element for the first time. The shape functions of this element in the ξ-line (η=0) for the line 1-4, as shown in Fig.(5.12), are as follows:

$$N_1 = \frac{1}{2}(1-\xi)(2-3\xi)(1-3\xi)$$

$$N_2 = \frac{9}{2}\xi(1-\xi)(2-3\xi)$$

$$N_3 = -\frac{9}{2}\xi(1-\xi)(1-3\xi) \qquad (5.80)$$

$$N_4 = \frac{1}{2}\xi(2-3\xi)(1-3\xi)$$

Now, setting $x_1 = 0$, $x_2 = 1/9\ L_x$, $x_3 = 4/9\ L_x$, $x_4 = L_x$ and using equations (5.39), the following can be deduced:

$$x(\xi) = \frac{1}{2}\xi(1-\xi)(2-3\xi)L_x + 2\xi(1-\xi)(3\xi-1)L_x + \frac{1}{2}\xi(2-3\xi)(1-3\xi)L_x \qquad (5.81)$$

which leads to,

$$x(\xi) = \xi^2 L_x \qquad (5.82)$$

Comparing equation (5.82) with equation (5.77), it is obvious that this element can generate the same order of singularity required for the analysis of linear-elastic fracture mechanics.

5.4 Finite Element Analysis of Elasto-Plastic 2D Problems:

The complexity of elasto-plastic fracture mechanics problems has necessarily led to the use of a numerical method such as the finite element method to determine the field parameters *(i.e. displacements, stresses, etc.)* required to evaluate fracture mechanics parameters such as the *J*-integral, and the crack-opening displacement *COD*.

The elasto-plastic behaviour of any engineering material can be modelled for a multiaxial stress state from a uniaxial stress state by means of the following conditions:

(1) An initial yield condition which defines the elastic limit of the material.

(2) A flow rule which relates any plastic strain increment to stresses and stress increments.

(3) A hardening rule to define the subsequent yield condition from a plastic state.

5.4.1 Derivation of Elasto-Plastic Stress-Strain Matrix:

In general, the yield surface of many engineering materials can be expressed as follows:

$$F(\underline{\sigma} , \underline{k}) = 0 \qquad (5.83)$$

where $\underline{k}$ is a measure of the degree of work hardening.

The hardening vector $\underline{k}$ is generally a function of the plastic strain $\underline{\varepsilon}_p$ and a history parameter k. Thus, equation (5.83) can be written as:

$$F(\underline{\sigma} , \underline{\varepsilon}_p, k) = 0 \qquad (5.84)$$

The Drucker's postulate states that the work done by an external agency during a complete cycle of loading and unloading must be non-negative. Hence, the following requirements must be satisfied [Ref.80]:

(1) *The instantaneous yield surface is convex with respect to the origin in the stress space.*

(2) *The plastic strain increment vector is on the outward normal to the instantaneous yield surface.*

The second condition is known as the normality principle, which provides a means by which a constitutive relationship may be obtained. This constitutive relationship, known as the *flow rule*, can be written for materials with associated plasticity as follows:

$$d\underline{\varepsilon}_p = d\lambda \frac{\partial F}{\partial \underline{\sigma}} = d\lambda \, \underline{a} \tag{5.85}$$

where,

$$\underline{a} = \frac{\partial F}{\partial \underline{\sigma}} = \left[\frac{\partial F}{\partial \sigma_x} \quad \frac{\partial F}{\partial \sigma_y} \quad \cdots\cdots\cdots \quad \frac{\partial F}{\partial \tau_{zx}} \right] \tag{5.86}$$

Now, from equation (5.84) it can be shown that:

$$dF = \left(\frac{\partial F}{\partial \underline{\sigma}} \right)^t d\underline{\sigma} + \left(\frac{\partial F}{\partial \underline{\varepsilon}_p} \right)^t d\underline{\varepsilon}_p + \frac{\partial F}{\partial k} dk = 0 \tag{5.87}$$

The above equation can be simplified by grouping hardening terms as follows:

$$A = - \left[\left(\frac{\partial F}{\partial \underline{\varepsilon}_p} \right)^t d\underline{\varepsilon}_p + \frac{\partial F}{\partial k} dk \right] / d\lambda \tag{5.88}$$

Hence, equation (5.87) can be written as:

$$dF = \left(\frac{\partial F}{\partial \underline{\sigma}} \right)^t d\underline{\sigma} - A \, d\lambda = 0 \tag{5.89}$$

The total strain vector can be expressed in two parts, elastic and plastic, as follows:

$$d\underline{\varepsilon} = d\underline{\varepsilon}_e + d\underline{\varepsilon}_p \qquad (5.90)$$

where,

$$d\underline{\varepsilon}_e = \underline{D}^{-1}\, d\underline{\sigma}$$

and

$$d\underline{\varepsilon}_p = d\lambda\, \underline{a}$$

Hence, equation (5.90) can be written as:

$$d\underline{\varepsilon} = \underline{D}^{-1}\, d\underline{\sigma} + d\lambda\, \underline{a} \qquad (5.91)$$

Now, from the above equation it can be shown that:

$$d\underline{\sigma} = \underline{D}\, d\underline{\varepsilon} - d\lambda\, (\underline{D}\, \underline{a}) \qquad (5.92)$$

Multiplying both sides of equation (5.92) by $\underline{a}^t$ and substituting $A\, d\lambda$ for $\underline{a}^t\, d\underline{\sigma}$ as deduced by equation (5.89), the following can be obtained:

$$A\, d\lambda = \underline{a}^t\, \underline{D}\, d\underline{\varepsilon} - d\lambda\, (\underline{a}^t\, \underline{D}\, \underline{a}) \qquad (5.93)$$

from which, it can be deduced that:

$$d\lambda = \frac{\underline{a}^t\, \underline{D}}{A + \underline{a}^t\, \underline{D}\, \underline{a}}\, d\underline{\varepsilon} \qquad (5.94)$$

Hence, equation (5.92) can be expressed as follows:

$$d\underline{\sigma} = \underline{D}\, d\underline{\varepsilon} - \frac{(\underline{D}\, \underline{a})\, (\underline{D}\, \underline{a})^t}{A + \underline{a}^t\, \underline{D}\, \underline{a}}\, d\underline{\varepsilon} \qquad (5.95)$$

i.e.

$$d\underline{\sigma} = \underline{D}_{ep}\, d\underline{\varepsilon} \qquad (5.96)$$

where,

$$\underline{D}_{ep} = \underline{D} - \underline{D}_{p}$$

and

$$\underline{D}_{p} = \frac{(\underline{D}\ \underline{a})\ (\underline{D}\ \underline{a})^{t}}{A + \underline{a}^{t}\ \underline{D}\ \underline{a}} \qquad (5.97)$$

The $\underline{D}_{ep}$ matrix is known as the elasto-plastic stress-strain matrix.

5.4.2 Hardening Rules:

(a) Euler's Theorem:

Euler's theorem on homogeneous functions states that if $F(\underline{x})$ is homogeneous and of degree n, then:

$$\left[\frac{\partial F}{\partial x}\right]^{t} \underline{x} = n\ F \qquad (5.98)$$

For a homogeneous yield surface in $\underline{\sigma}$ and $\underline{k}$, $F(\underline{\sigma}, \underline{k}) = 0$, and:

$$\left[\frac{\partial F}{\partial \sigma}\right]^{t} \underline{\sigma} + \left[\frac{\partial F}{\partial k}\right]^{t} \underline{k} = n\ F \qquad (5.99)$$

(b) H' Definition:

Given the uniaxial stress-strain diagram of a material, as shown in Fig.(5.13), the parameter H' is defined as follows:

$$H' = d\sigma/d\varepsilon_p \qquad (5.100)$$

The total strain is defined as:

$$\varepsilon = \varepsilon_e + \varepsilon_p \qquad (5.101)$$

where,

$$\varepsilon_e = \sigma/E_o$$

and E_o is Young's modulus of the material, defined as the tangential modulus at $\sigma = 0$, $\varepsilon = 0$.

Thus,

$$\varepsilon_p = \varepsilon - \sigma/E_o \qquad (5.102)$$

Now, differentiating the above equation with respect to ε, it can be deduced that:

$$\frac{d\varepsilon_p}{d\varepsilon} = 1 - \frac{1}{E_o}\frac{d\sigma}{d\varepsilon} \qquad (5.103)$$

Hence, from equation (5.100), it can be shown that:

$$H' = \frac{d\sigma}{d\varepsilon}\frac{d\varepsilon}{d\varepsilon_p} = \frac{d\sigma / d\varepsilon}{d\varepsilon_p / d\varepsilon} = \frac{d\sigma / d\varepsilon}{1 - \frac{1}{E_o}\frac{d\sigma}{d\varepsilon}} \qquad (5.104)$$

Defining the tangential modulus E_t such that:

$$E_t = \frac{d\sigma}{d\varepsilon} \qquad (5.105)$$

Now, the hardening parameter H' can be written as:

$$H' = \frac{E_t}{1 - E_t/E_o} \qquad (5.106)$$

(c) *Isotropic Hardening:*

The theory of isotropic hardening states that during plastic flow the instantaneous yield surface expands uniformly in the stress space around the origin, maintaining the same shape, centre, and orientation as the initial yield surface. The subsequent yield surface equation may be written as follows:

$$F(\underline{\sigma} , Y(\&)) = 0 \qquad (5.107)$$

where,

$\&$ = A hardening parameter,

$Y(\&)$ = The instantaneous, uniaxial yield stress of the material.

In order to define the hardening parameter $\&$, one of the following two hypotheses may be used:

(i) *The Work-Hardening Hypothesis:*

This hypothesis considers that the amount of hardening depends only upon the total plastic work, and it is independent of the strain path. i.e.

$$d\&_1 = dW_p = \underline{\sigma}^t \, d\underline{\varepsilon}_p \qquad (5.108)$$

where, W_p is the total plastic work.

(ii) *The Strain-Hardening Hypothesis:*

This hypothesis employs an expression, known as the effective plastic strain $\bar{\varepsilon}_p$, as a measure of work hardening. i.e.

$$d\&_2 = d\bar{\varepsilon}_p \qquad (5.109)$$

For the case of the von Mises yield criterion the above two hypotheses are equivalent.

Since the work hardening hypothesis is the more general one from thermodynamics point of view, a useful expression between the uniaxial and the multiaxial cases arises if the following assumption is made:

$$dW_p = \underline{\sigma}^t \, d\underline{\varepsilon}_p = Y \, d\bar{\varepsilon}_p$$

or

$$dW_p = Y \, d\bar{\varepsilon}_p = (d\underline{\varepsilon}_p)^t \, \underline{\sigma} = d\lambda \, \underline{a}^t \, \underline{\sigma} \qquad (5.110)$$

(d) The Relation between A and H' :

For isotropic hardening, where $\partial F/\partial \underline{\varepsilon}_p = 0$, equation (5.88) reduced to:

$$A = - \left[\frac{\partial F}{\partial k} \right] \frac{\partial k}{\partial \lambda} \qquad (5.111)$$

which can be written as:

$$A = - \frac{\partial F}{\partial Y} \frac{\partial Y}{\partial \underline{\varepsilon}_p} \frac{d\underline{\varepsilon}_p}{dk} \frac{dk}{d\lambda} \qquad (5.112)$$

With further reduction to the above equation, the following can obtained:

$$A = \left[\frac{\partial F}{\partial Y} \right]^2 H' \qquad (5.113)$$

where,

$$H' = \frac{dY}{d\varepsilon_p}$$

For the special case of $f(\underline{\sigma}) - Y = 0$, the following can be deduced:

$$A = H' = \frac{E_t}{1 - E_t/E_o} \qquad (5.114)$$

5.4.3 Outline of the Finite Element Elasto-Plastic Theory:

(a) Formulation of Finite Element Equations:

The minimum energy theory states that:

$$\chi = U - W = \textit{Minimum}$$

where,

U = Strain energy,

W = Work done by external loads.

thus,

$$d\chi = dU - dW = 0 \qquad (5.115)$$

The total strain energy U, can be defined as follows:

$$U = \iiint \left(\int \underline{\sigma}^t \, d\underline{\varepsilon} \right) dv \qquad (5.116)$$

Then, the variation of the strain energy can be written as:

$$dU = \iiint d\underline{\varepsilon}^t \, \underline{\sigma} \, dv \qquad (5.117)$$

Similarly, it can be shown that:

$$dW = d\underline{\delta}^t \, \underline{F} \qquad (5.118)$$

where $\underline{\delta}$ is the nodal displacement vector.

Hence, equation (5.115) can be rewritten as follows:

$$d\chi = \iiint d\underline{\varepsilon}^t \, \underline{\sigma} \, dv - d\underline{\delta}^t \, \underline{F} = 0 \qquad (5.119)$$

The strain-displacement matrix $\underline{B}$ is defined such that:

$$d\underline{\varepsilon} = \underline{B} \, d\underline{\delta} \qquad (5.120)$$

Thus, equation (5.119) can be restated as follows:

$$d\chi = d\underline{\delta}^t \left(\iiint \underline{B}^t \, \underline{\sigma} \, dv - \underline{F} \right) = 0 \qquad (5.121)$$

Hence, for an arbitrary variation $d\underline{\delta}$, it can be deduced that:

$$\iiint \underline{B}^t \, \underline{\sigma} \, dv - \underline{F} = \underline{0}$$

i.e.

$$\iiint \underline{B}^t \, \underline{\sigma} \, dv = \underline{F} \qquad (5.122)$$

The above equation represents, a generalized equilibrium equation, which is valid for both linear and non-linear situations.

(b) *Linearization of Non-Linear equations:*

Let a vectorial function $\underline{\psi}$ be defined such that:

$$\underline{\psi} = \underline{\psi}(\underline{\delta}) = \iiint \underline{B}^t(\underline{\delta}) \, \underline{\sigma}(\underline{\delta}) \, dv - \underline{F} \qquad (5.123)$$

and $\underline{\psi} = \underline{0}$ when $\underline{\delta}$ = the exact solution.

For non-linear cases, an approximate solution $\underline{\delta}_o$ may be found such that:

$$\underline{\psi}(\underline{\delta}_o) = \iiint \underline{B}^t(\underline{\delta}_o) \, \underline{\sigma}(\underline{\delta}_o) \, dv - \underline{F} = - \underline{R}_o \qquad (5.124)$$

where $\underline{R}_o$ is a residual vector or error vector.

In general, the residual vector can be expressed as follows:

$$\underline{R} = \underline{F} - \iiint \underline{B}^t \, \underline{\sigma} \, dv \qquad (5.125)$$

Now, let an incremental vector $\Delta\underline{\delta}$ exist such that:

$$\underline{\psi}(\underline{\delta}_o + \Delta\underline{\delta}) = \underline{0} \tag{5.126}$$

Defining:

$$\underline{\psi}(\underline{\delta}_o + \Delta\underline{\delta}) = \underline{\psi}(\underline{\delta}_o) + \Delta\underline{\psi}$$

$$\underline{B}^t(\underline{\delta}_o + \Delta\underline{\delta}) = \underline{B}^t(\underline{\delta}_o) + \Delta\underline{B}^t \tag{5.127}$$

$$\underline{\sigma}(\underline{\delta}_o + \Delta\underline{\delta}) = \underline{\sigma}(\underline{\delta}_o) + \Delta\underline{\sigma}$$

then, it can be shown that:

$$\underline{\psi}(\underline{\delta}_o) + \Delta\underline{\psi} \cong - \underline{R}_o + \iiint \underline{B}^t \, \Delta\underline{\sigma} \, dv + \iiint \Delta\underline{B}^t \, \underline{\sigma} \, dv = \underline{0} \tag{5.128}$$

For the case of small deflection,

$$\Delta\underline{B}^t = \underline{0} \quad \text{and} \quad \Delta\underline{\sigma} = \underline{D}_{ep} \, \underline{B} \, \Delta\underline{\delta}$$

Then from equation (5.128), it can be stated that:

$$\left(\iiint \underline{B}^t \, \underline{D}_{ep} \, \underline{B} \, dv \right) \Delta\underline{\delta} = \underline{R}_o \tag{5.129}$$

or

$$\underline{K}_{ep} \, \Delta\underline{\delta} = \underline{R}_o \tag{5.130}$$

where $\underline{K}_{ep}$ is the elasto-plastic stiffness matrix.

Thus, for a finite element mesh:

$$\underline{K}_{ep} = \sum_{e=1}^{n_e} (\underline{K}_{ep})_e \tag{5.131}$$

where,

$$(\underline{K}_{ep})_e = \iiint_{Element} \underline{B}^t \, \underline{D}_{ep} \, \underline{B} \, dv$$

and

$$\underline{R}_o = \underline{F} - \sum_{e=1}^{n_e} \iiint_{Element} \underline{B}^t \, \underline{\sigma} \, dv \qquad (5.132)$$

The summations can be carried out using ordinary finite element assembly rules.

(c) *Solution Algorithms:*

i. *Interpolative, "Newton-Raphson" Scheme:*

Step (1): **Initiation.**

Before applying the first/next load increment, the following vectors are assumed to be known from the previous increment, or they are zeros.

$\underline{\varepsilon}_o$ = The total strain vector, at every Gaussian point.
$\underline{\sigma}_o$ = The total stress vector, at every Gaussian point.
$\underline{\delta}_o$ = The total nodal displacement vector.

The load increment vectors are defined as follows:

$\Delta\underline{F}_1$ = The increment of equivalent nodal loading vector.

$\Delta\underline{\eta}_1$ = The vector of initial and thermal strains, during a given load increment, at the stress points.

Step (2): **Incremental solution.**

(1) Calculation of the elasto-plastic stress-strain matrix at all of the stress points.

$$\underline{D}_o = \underline{D}_{ep}(\underline{\sigma}_o, \underline{\varepsilon}_o)$$

(2) Calculation of the element stiffness matrix for every element in the mesh.

$$\underline{K}_{o(e)} = \iiint_{Element} \underline{B}^t \, \underline{D}_o \, \underline{B} \, dv$$

(3) Assembly of the stiffness matrix for the whole structure.

$$\underline{K}_o = \sum_{e=1}^{n_e} \underline{K}_{o(e)}$$

(4) Solution of the following incremental equation.

$$\underline{K}_o \, \Delta\underline{\delta}_1 = \Delta\underline{F}_1$$

(5) Calculation of the resulting strain increment at each stress point.

$$\Delta\underline{\varepsilon}_1 = \underline{B} \, \Delta\underline{\delta}_1 - \Delta\underline{\eta}_1$$

(6) Evaluation of the corresponding stress increment.

$$\Delta\underline{\sigma}'_1 = \underline{D}_o \, \Delta\underline{\varepsilon}_1$$

The upper dash is written to indicate that $\Delta\underline{\sigma}'_1$ may not be equal to the actual $\Delta\underline{\sigma}_1$.

Step (3): **Total Solution.**

The calculation of the total vectors are as follows:

(1) $\underline{\delta}_1 = \underline{\delta}_o + \Delta\underline{\delta}_1$

(2) $\underline{\varepsilon}_1 = \underline{\varepsilon}_o + \Delta\underline{\varepsilon}_1$

(3) $\underline{\sigma}'_1 = \underline{\sigma}_o + \Delta\underline{\sigma}'_1$

Step (4): **Plasticity Check.**

In this step, each stress point in turn is checked for yield using a given yield criterion. If none of the stress points have yielded, then no more calculations are required. Otherwise, the following procedure must be employed, assuming that there is no unloading.

If a point has yielded from an initial elastic state, a parameter ξ can be assumed such that:

$$Y = f(\underline{\sigma}_o + \xi\ \Delta\underline{\sigma}'_1)$$

The value of ξ can be either calculated directly or found by an iterative approach. With ξ being known, the completely elastic part of the stress and strain increment can be expressed as follows:

$$\Delta\underline{\sigma}_e = \xi\ \Delta\underline{\sigma}'_1$$

$$\Delta\underline{\varepsilon}_e = \xi\ \Delta\underline{\varepsilon}_1$$

and the elasto-plastic parts as:

$$\Delta\underline{\sigma}'_{ep} = (1-\xi)\ \Delta\underline{\sigma}'_1$$

$$\Delta\underline{\varepsilon}_{ep} = (1-\xi)\,\Delta\underline{\varepsilon}_{1}$$

Notice that $\xi = 0$, if the initial state has already exceeded the initial yielding condition.

Step (5): **Stress Correction.**

In this procedure, the strain increment is assumed to be correct and a correction of the stress is to be carried out so as to match the stress-strain behaviour of the material. The correction algorithm is as follows:

(1) Assume $\Delta\underline{\sigma}_{ep} = \Delta\underline{\sigma}'_{ep}$

(2) $\underline{\varepsilon}_{m} = \underline{\varepsilon}_{o} + \Delta\underline{\varepsilon}_{e} + \Delta\underline{\varepsilon}_{ep} / 2$

(3) $\underline{\sigma}_{m} = \underline{\sigma}_{o} + \Delta\underline{\sigma}_{e} + \Delta\underline{\sigma}_{ep} / 2$

(4) $\underline{D}_{ep} = \underline{D}_{ep}(\underline{\sigma}_{m}, \underline{\varepsilon}_{m})$

(5) $\Delta\underline{\sigma}_{ep} = \underline{D}_{ep}\,\Delta\underline{\varepsilon}_{ep}$

(6) If $| \Delta\underline{\sigma}_{ep(new)} - \Delta\underline{\sigma}_{ep(old)} |$ > a permissible error, then go to step (3).

(7) $\underline{\sigma}_{1} = \underline{\sigma}_{o} + \Delta\underline{\sigma}_{e} + \Delta\underline{\sigma}_{ep}$

(8) The error in the stress increment is $\Delta\underline{\sigma}_{ER} = \underline{\sigma}_{1} - \underline{\sigma}'_{1}$.

(9) The required equivalent nodal force to restore equilibrium is:

$$\Delta\underline{F} = -\sum_{e=1}^{n_e} \iiint \underline{B}^{t}\,\Delta\underline{\sigma}_{ER}\,dv$$

Step (6): **Iteration Control.**

The corrected load is to be applied and the previous steps are to repeated, with all of the numerical subscripts increased by one, until at least one of the following conditions is satisfied.

(1) An acceptable error in the displacement. Such an error can be measured by the following norm:

$$Er_1 = (\Delta\underline{\delta}_i^t \cdot \Delta\underline{\delta}_i) / (\underline{\delta}_i^t \cdot \underline{\delta}_i)$$

(2) An acceptable error in the corrected load. This error can be measured as follows:

$$Er_2 = (\Delta\underline{F}_i^t \cdot \Delta\underline{F}_i) / (\underline{F}_i^t \cdot \underline{F}_i)$$

(3) Divergence. When the structure has become unstable.

(4) Vibratory divergence. This is the case when the problem has failed to reach the required error tolerance within a given number of iterations.

ii. *Iterative, Modified "Newton-Raphson" Scheme:*

In this scheme, a constant value of $\underline{K}$, based upon the elastic stress strain matrix $\underline{D}_o$ is used. A procedure similar to the previous one, can be employed with:

$$\Delta\underline{\delta}_1 = \underline{K}_o^{-1} \Delta\underline{F}_1$$

$$\Delta\underline{\sigma}'_1 = \underline{D}_o \Delta\underline{\varepsilon}_1$$

where for any element in the mesh, $\underline{K}_o$ is defined as follows:

$$\underline{K}_{o(e)} = \iiint \underline{B}^t \underline{D}_o \underline{B} \, dv$$

The procedure requires more iterations than the interpolative scheme, but there is no need to update $\underline{K}_o$.

iii. *The Combined Scheme:*

In this approach, the $\underline{K}$ and $\underline{D}$ matrices are assumed to be fixed *(similar to the modified Newton-Raphson Scheme)*, however their values are the tangential or the elasto-plastic values at the start of the new load increment. This procedure is perhaps the best, being a compromise of the previous two, the stiffness matrix is updated only once for every new load increment which may save time and accelerate the iterative procedure.

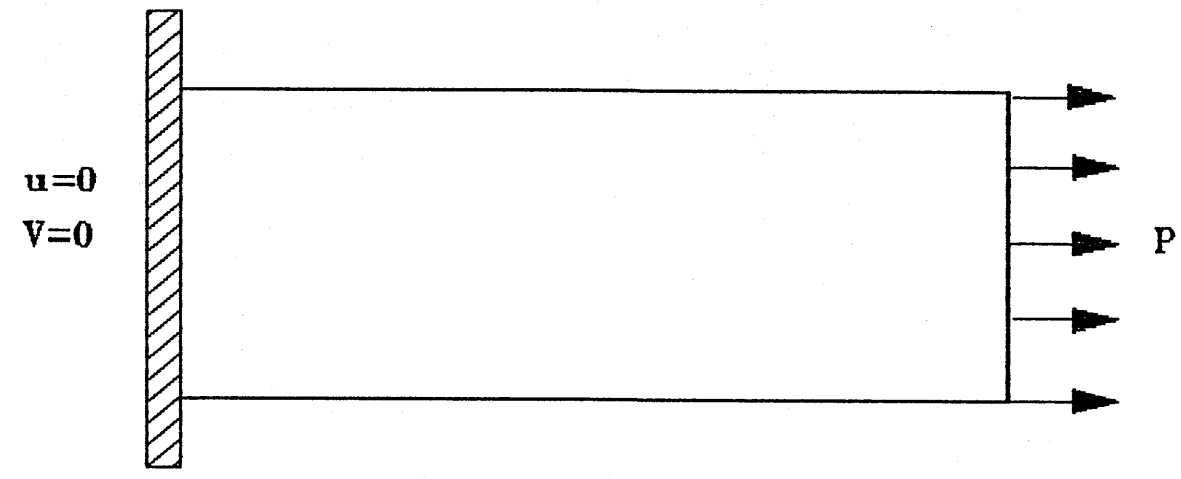

(a)

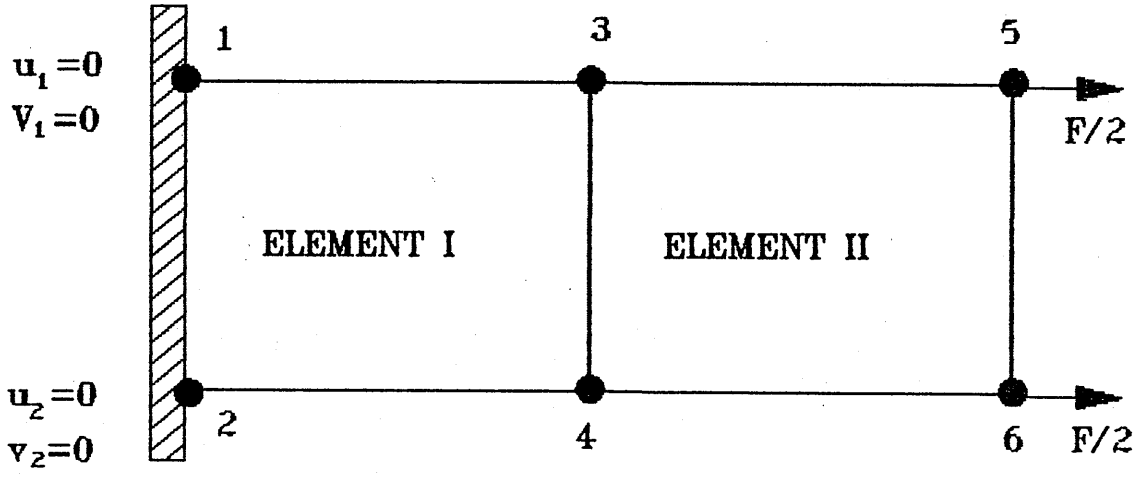

(b)

Fig.(5.1) The Finite-Element Model for a Plate in Tension.

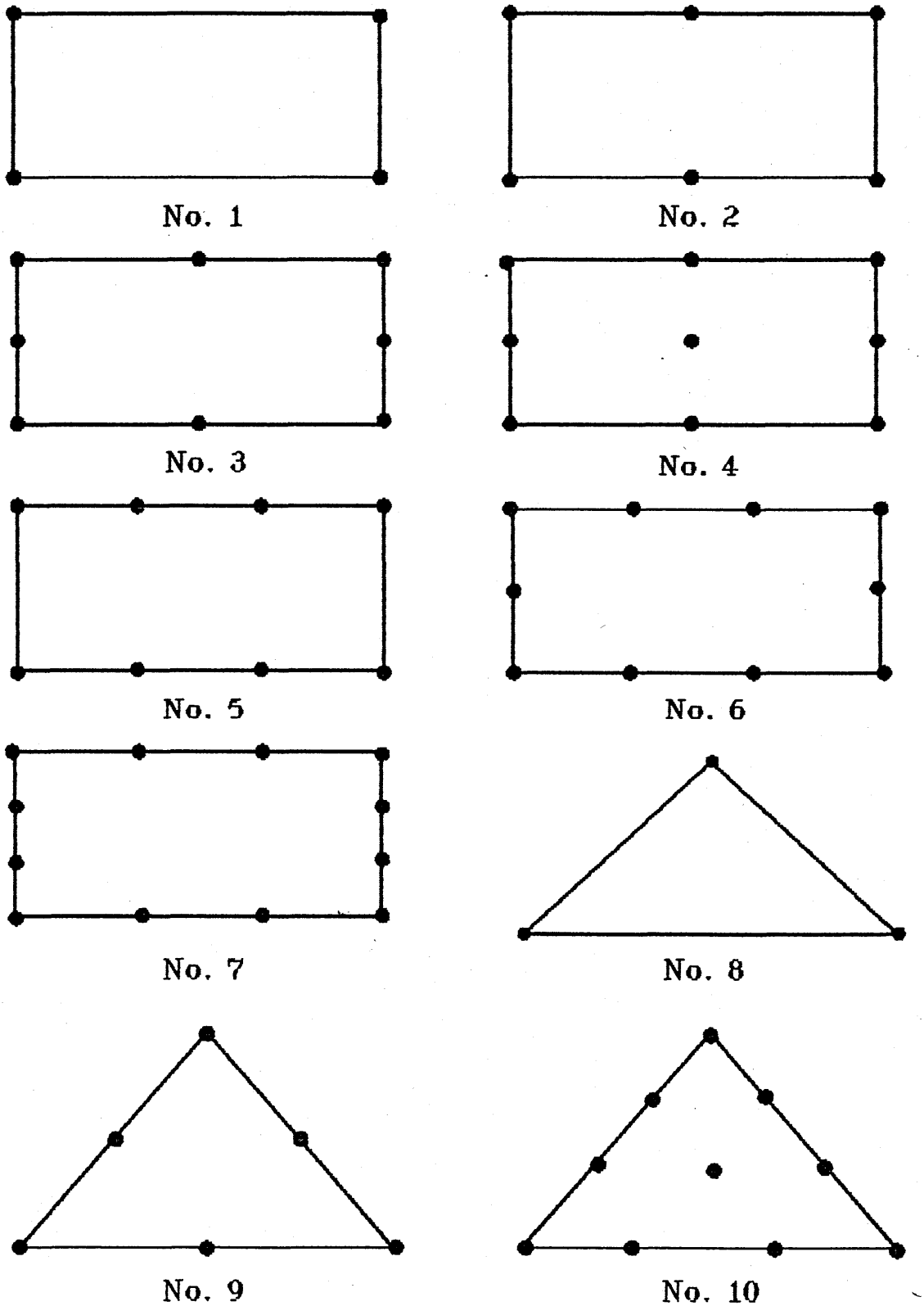

Fig.(5.2) The Standard Family of Finite Elements.

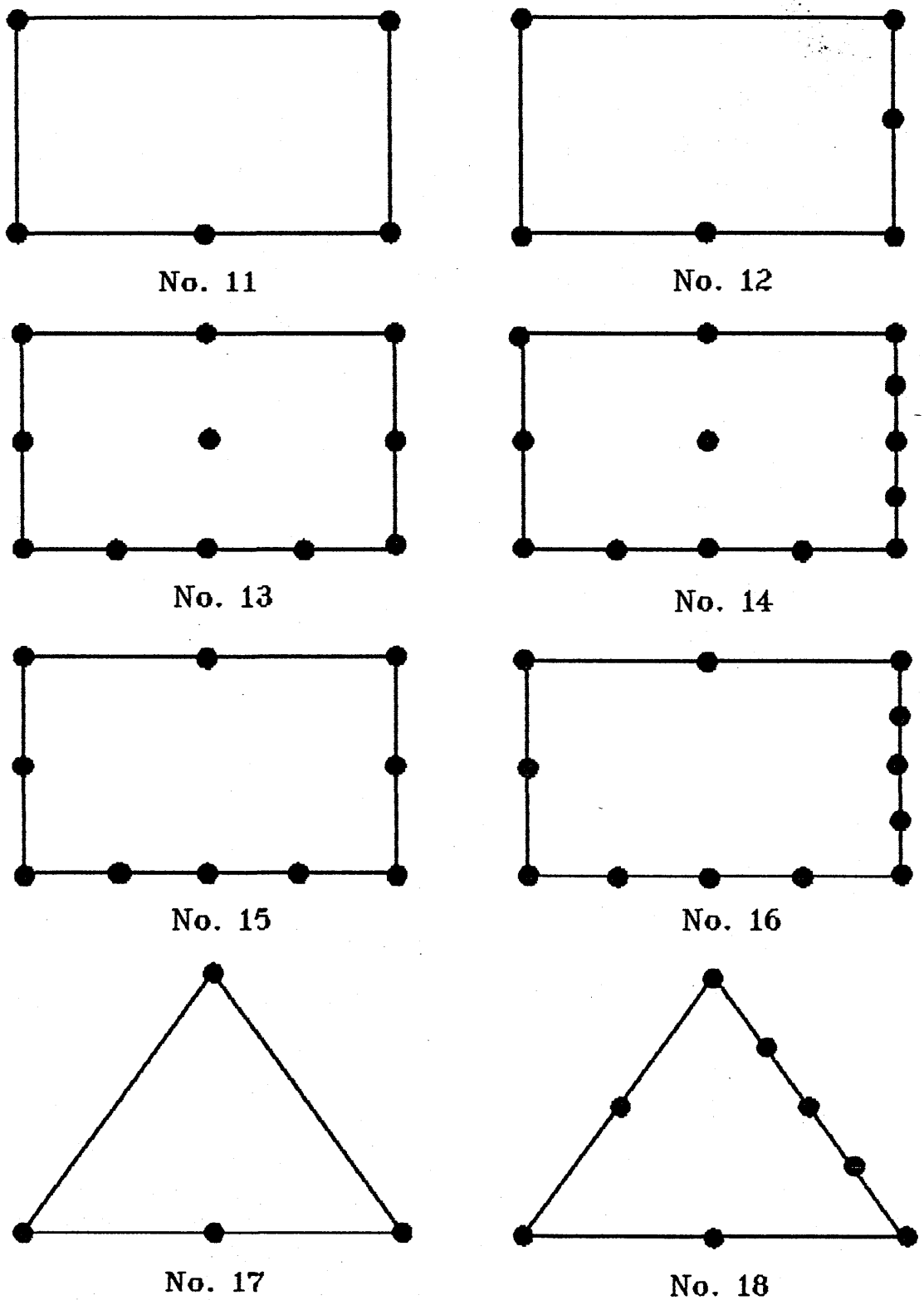

Fig.(5.3) The Transition Family of Finite Elements.

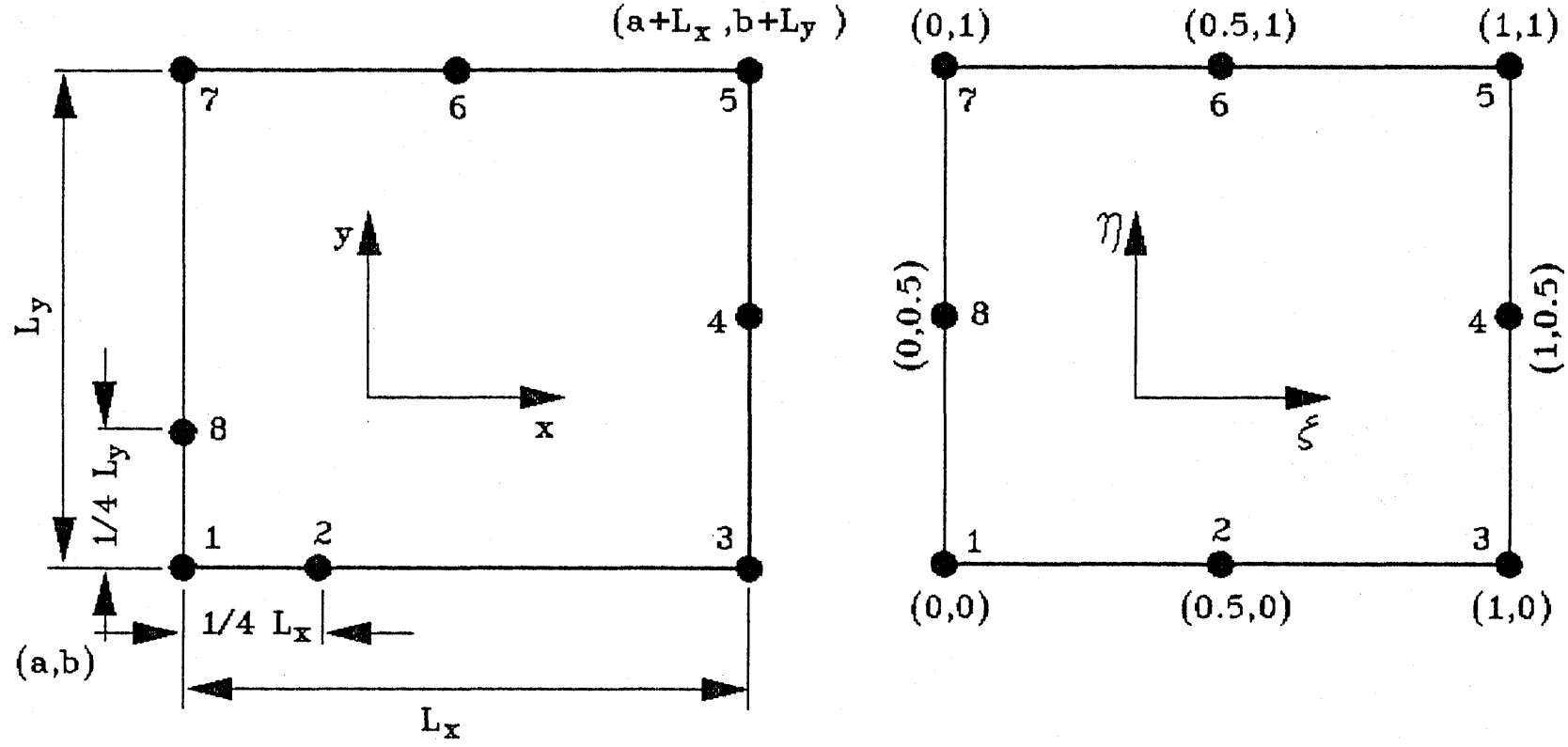

a) CRACK-TIP ELEMENT

b) STANDARD ELEMENT

Fig.(5.4) The 8-Node Quadrilateral Singular Crack-Tip Element.

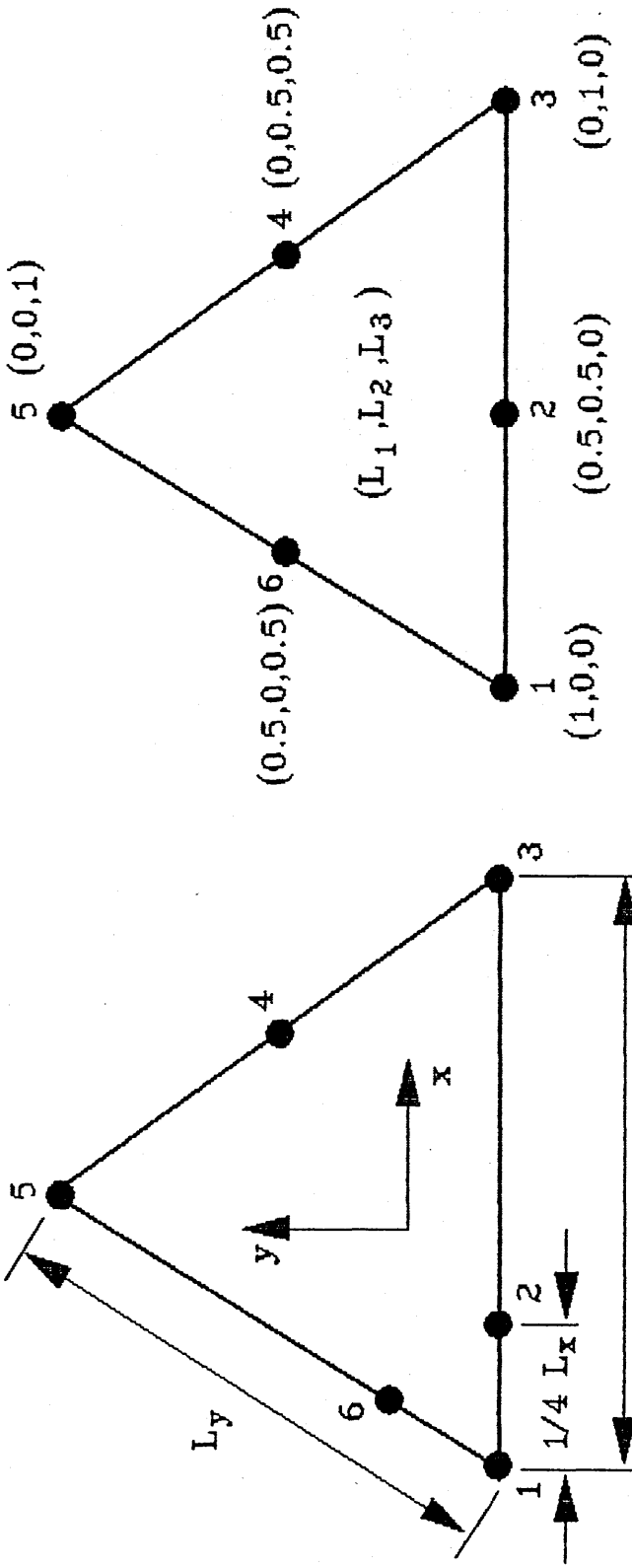

a) CRACK-TIP ELEMENT

b) STANDARD ELEMENT

Fig.(5.5) The 6-Node Triangular Singular Crack-Tip Element.

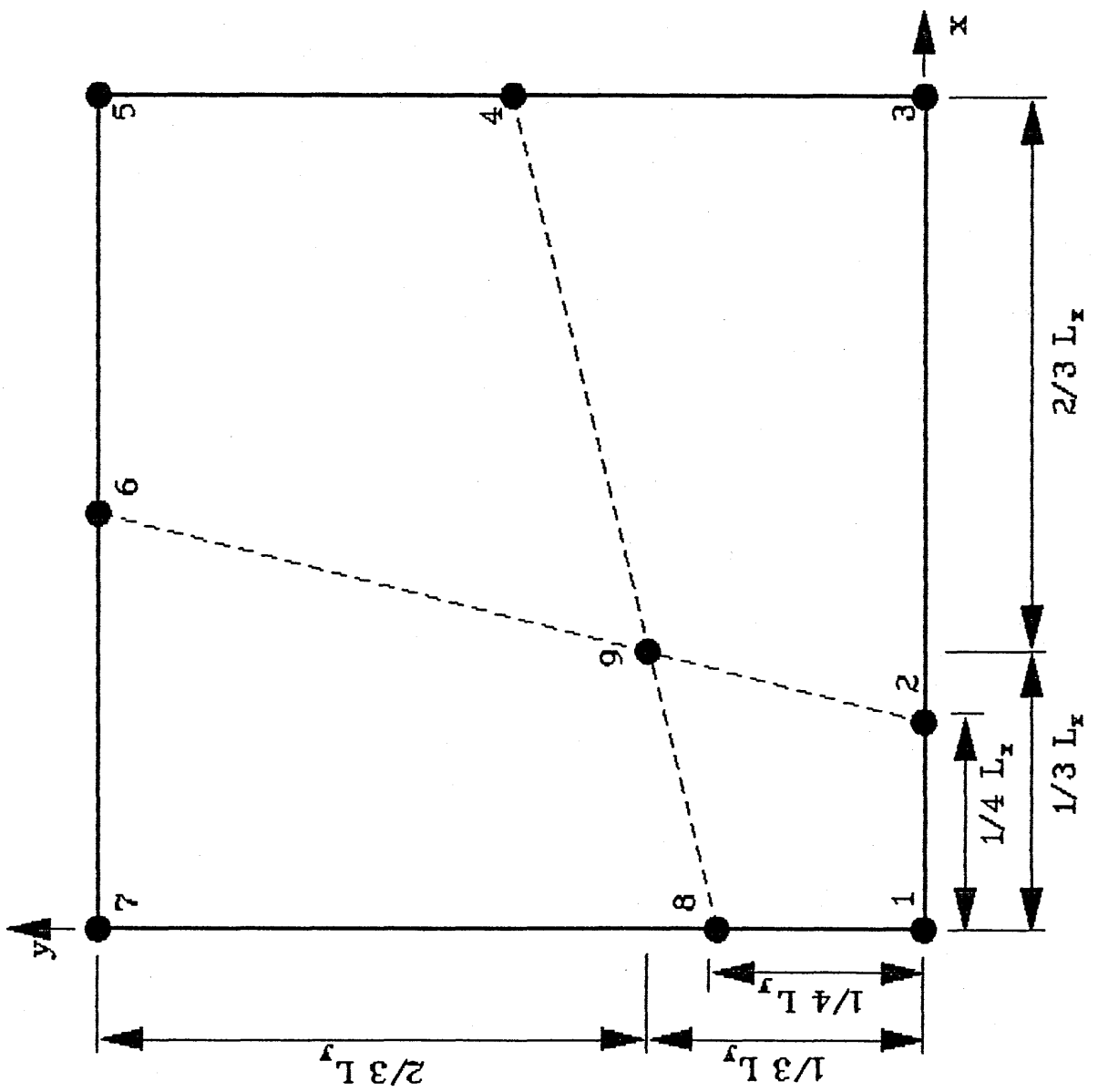

Fig.(5.6) The 9-Node Lagrangian Crack-Tip Element.

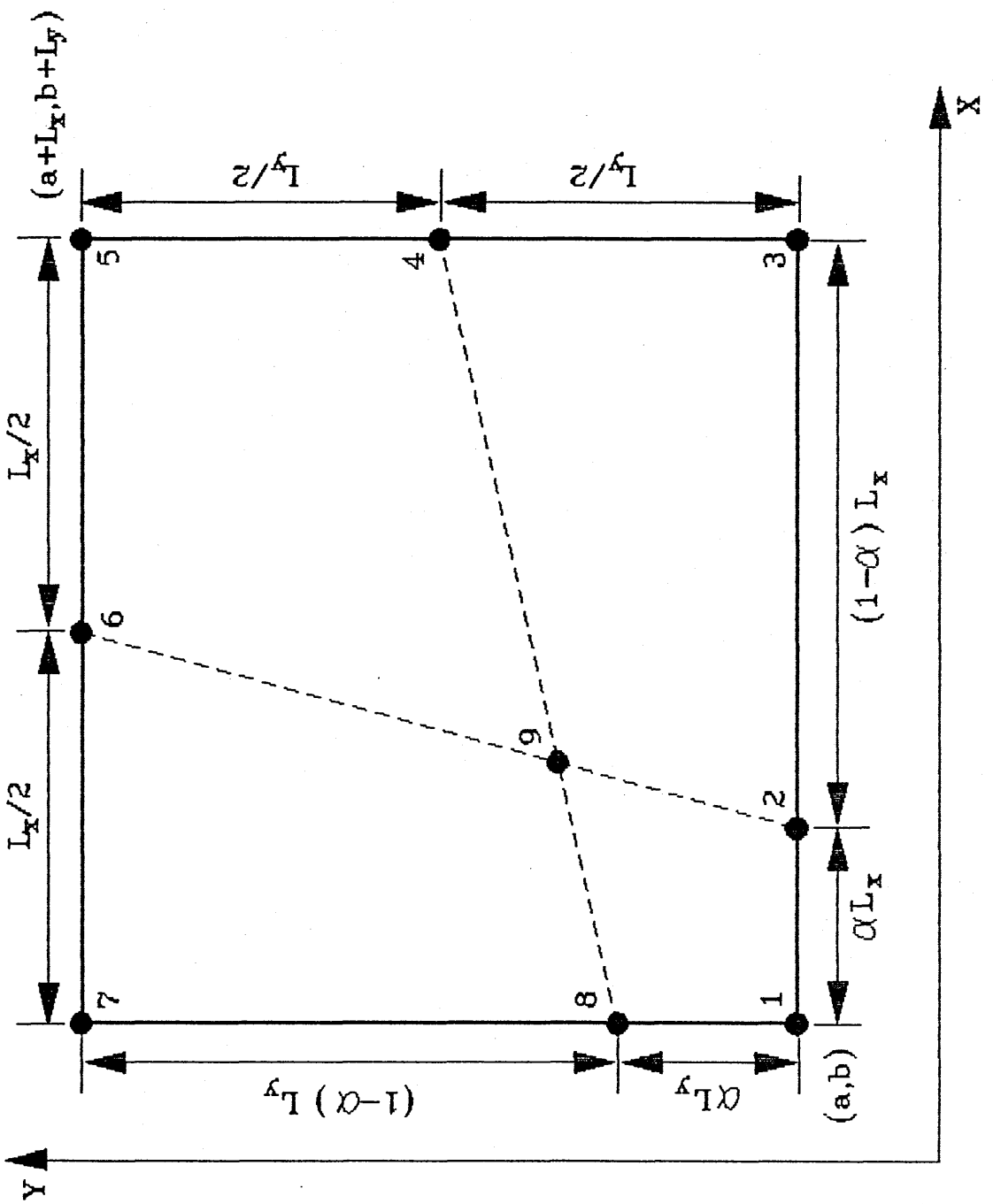

Fig.(5.7) Coordinates System for the 9-Node Lagrangian Crack-Tip Singular Element.

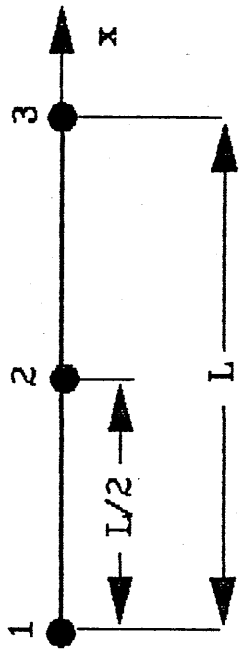

b) X-Line

a) ξ-Line

Fig.(5.8) One-Dimensional Quadratic Element.

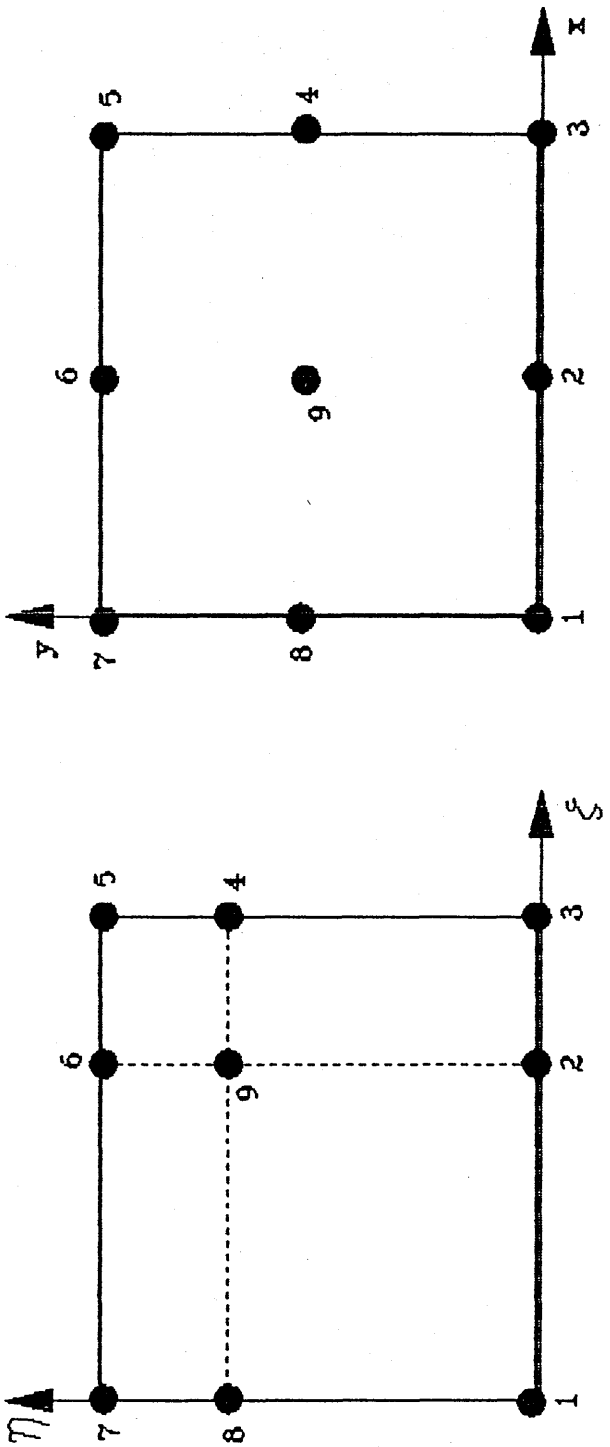

a) CRACK-TIP ELEMENT

b) STANDARD ELEMENT

Fig.(5.9) The $1/\sqrt{2}$ Singular Crack-Tip Element.

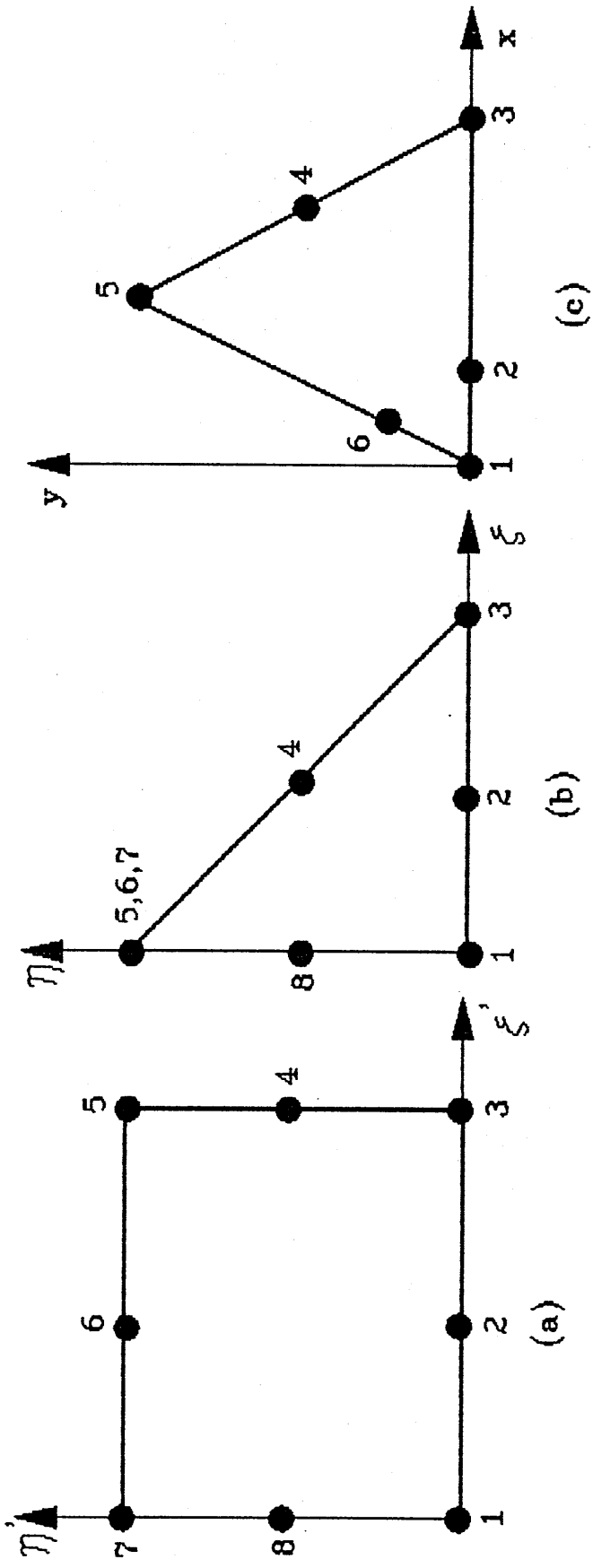

Fig.(5.10) Collapsed 6-Node Crack-Tip Elements.

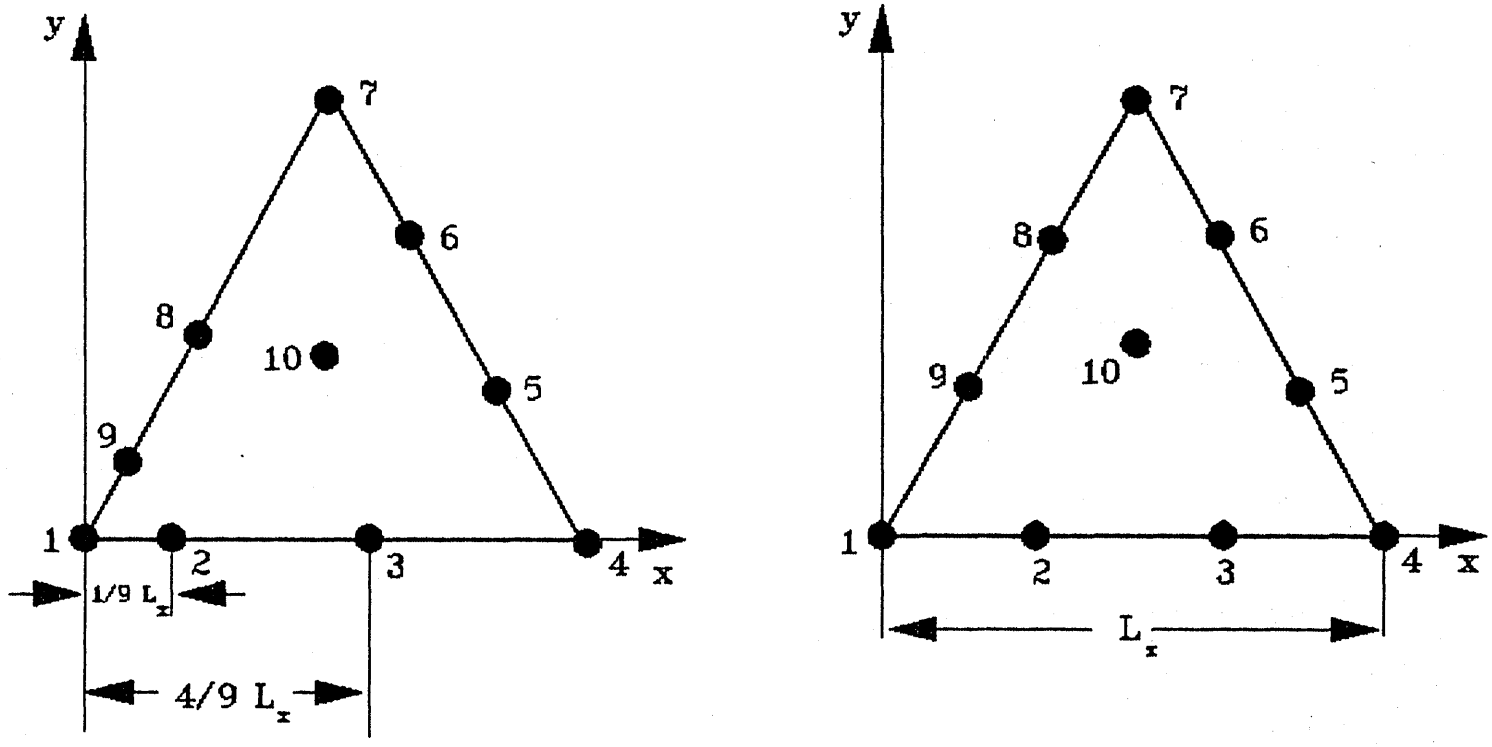

a) CRACK-TIP ELEMENT

b) STANDARD ELEMENT

Fig.(5.12) The 10-Node Singular Crack-Tip Element.

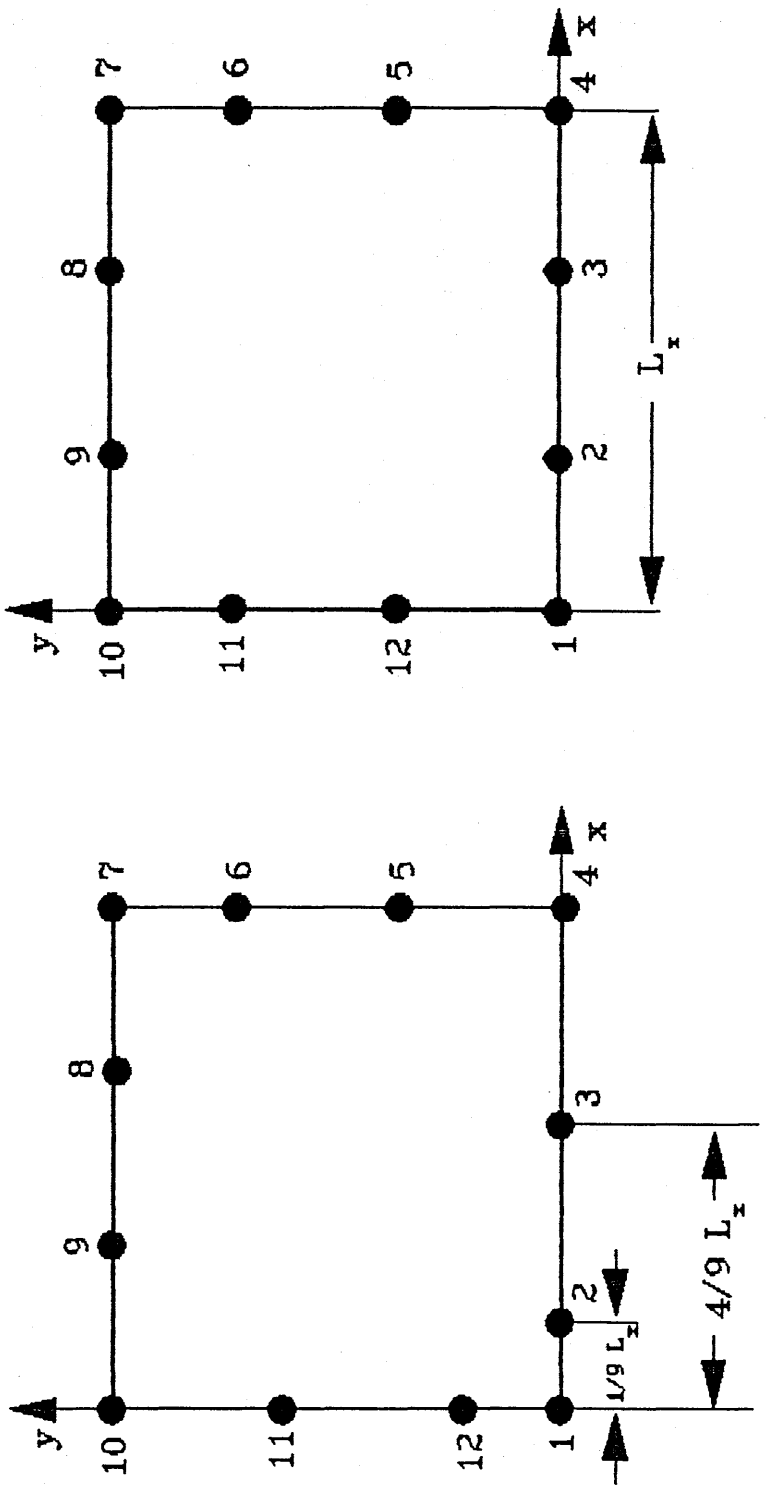

a) CRACK-TIP ELEMENT

b) STANDARD ELEMENT

Fig.(5.11) The 12-Node Singular Crack-Tip Element.

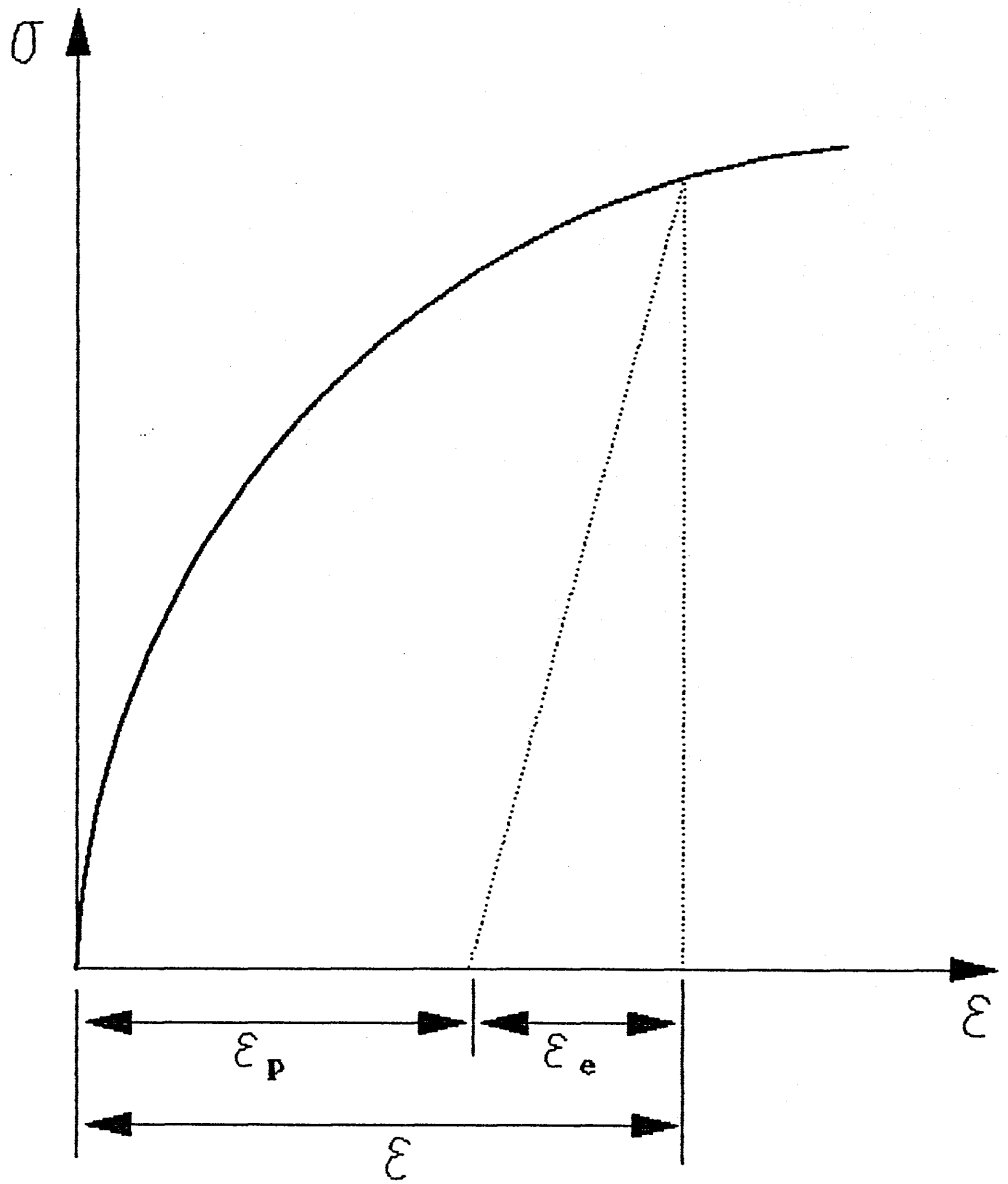

Fig.(5.13) Uniaxial Stress–Strain Diagram.

CHAPTER 6

THE BOUNDARY ELEMENT METHOD FOR FRACTURE MECHANICS PROBLEMS

6.1 Introduction:

An alternative approach to the domain type solution is to integrate the weighted residual expressions of the governing differential equations analytically before introducing any approximation procedure. Using some mathematical techniques, an integral equation within a specified domain can be transformed into a boundary integral equation over the boundary of the domain.

The boundary integral equation *(BIE)* can be solved numerically by means of piece-wise discretization, whereby the boundary of the domain is divided into sub-boundaries *(boundary elements)*. The equations of the boundary elements, are assembled together to form a system of algebraic equations in terms of the values of field function parameters over the boundary. Solving such system of equations, the values of the field function at any point inside the domain can be obtained in terms of its boundary values, and this involves the evaluation of some boundary integrals.

This approach is known as the boundary element method *(BEM)* [Ref.81], and it has many advantages, compared with other numerical methods. Such advantages are given in Ref.[82] as follows:

1. *It reduces the dimensionality of the problem by one, resulting in a smaller system of equations and a considerable reduction in the data required for the analysis.*

2. *It offers continuous interior modelling within the solution domain, and the values of the solution variables can be calculated at any selected interior point.*

3. *The method is well suited to problems of infinite domains, such as fracture mechanics, soil mechanics, hydraulics, stress analysis, for which the classical domain methods are unsuitable.*

Since most of the fracture mechanics problems are considered as boundary-type problems *(i.e. the field parameters are only required on the boundary of the structure)* then a numerical technique such as the boundary element method can be very advantageous and can save computer time and human effort when used to solve such problems.

There are, however, some difficulties associated with the boundary element method which must be taken into consideration. The integrands of the boundary integrals usually contain singular terms such as $\ell n r$, r^{-1}, r^{-2}, which approach infinite values as r goes to zero. Also for geometries like narrow strips, the wide variation in r can cause computer rounding errors which may lead to inaccurate solutions. In this work an attempt has been made to overcome those problems and others such as corner effects, edges, etc, in two-dimensional boundary element programs utilizing general isoparametric elements. The outlines of the boundary element method for linear and nonlinear problems with different types of loading and boundary conditions are reviewed in this chapter.

6.2 Outline of the BEM for 2D Linear-Elastic Problems:

The basic procedure for the boundary element method can be stated in a standard algorithm, which can be summarized for two-dimensional linear-elastic fracture problems in the following steps.

Step (1):

Discretization of the boundary.

Considering a typical two-dimensional problem within a specified domain Ω, as shown in Fig.(6.1), the boundary Γ of the domain is to be discretized in terms of boundary elements connected by boundary nodes. i.e.

$$\Gamma = \bigcup_{e=1}^{n_e} \Gamma_e \qquad (6.1)$$

where n_e is number of boundary elements.

The boundary nodes are to be defined in terms of their cartesian coordinates, and the boundary elements are defined by the number of element nodes and a topology array. The topology array of the external boundary should be defined in an anti-clockwise direction whilst it should be in a clockwise direction for any internal boundary, as shown in Fig.(6.2), in order to obtain the boundary normals in the outward direction with respect to the domain.

The field parameters u, v, T_x, and T_y are defined for each element in terms of their elemental nodal values. The nodal displacement and traction vectors are as follows:

$$\underline{\delta} = \{ u_1 \; v_1 \quad u_2 \; v_2 \; .... \; u_m \; v_m \}$$
$$\underline{T} = \{ (T_x)_1 \; (T_y)_1 \quad (T_x)_2 \; (T_y)_2 \; ... \; (T_x)_m \; (T_y)_m \} \qquad (6.2)$$

where m is number of the boundary nodes over Γ.

For isoparametric elements, the nodes are placed at the ends of the element and along its length such that if there are n nodes on the element, the j^{th} node has ξ value of $(j-1)/(n-1)$. The shape functions $N_j(\xi)$ are the standard Lagrangian multipliers given by:

$$N_j(\xi) = \mathcal{L}_j^n(\xi) = \prod_{\substack{r=1 \\ r \neq j}}^{n} \left(\frac{(n-1)\,\xi - (r-1)}{j-r} \right) \qquad (6.3)$$

Taking the field function u as an example, it can be approximated over the element as follows:

$$u = \sum_{j=1}^{n} N_j(\xi)\, u_j \qquad (6.4)$$

where u_j are the nodal values.

Step (2):

Formulation of the Boundary Element Matrices $\underline{\theta}^{\circ}$, $\underline{h}^{\circ}$.

The element matrices can generally be defined for an n-node boundary element with respect to a source point (x_i, y_i) [Ref.83], as follows:

$$\theta^{\circ}_{\alpha,2(j-1)+\beta}(x_i,y_i) = \int_0^1 G_{\alpha\beta}(x-x_i, y-y_i)\, N_j(\xi)\, |\underline{J}|\, d\xi$$

$$h^{\circ}_{\alpha,2(j-1)+\beta}(x_i,y_i) = \int_0^1 F_{\alpha\beta}(x-x_i, y-y_i)\, N_j(\xi)\, |\underline{J}|\, d\xi \qquad (6.5)$$

where,

$G_{\alpha\beta}$, $F_{\alpha\beta}$ are fundamental solution parameters,

j = The local number of a node on the e^{th} element,

$\alpha = 1, 2$, $\beta = 1, 2$,

$$|\underline{J}| = \sqrt{\left(\frac{\partial x}{\partial \xi}\right)^2 + \left(\frac{\partial y}{\partial \xi}\right)^2}$$

The above integrations may be obtained numerically by means of a Gaussian quadrature technique.

Step (3):

Assembly of the Matrix Equation for the Whole Boundary.

Employing the concept of boundary discretization and the definitions of element matrices $\underline{g}^{\circ}$, $\underline{h}^{\circ}$, and considering all of the boundary equations for the total number of nodes m, it can be shown, in the absence of domain-type loading, that the boundary integral equation is represented by:

$$C_{2I-1,2I-1}\ u_I + \sum_{J=1}^{m} \Big[H_{2I-1,2J-1}\ u_J + H_{2I-1,2J}\ v_J - G_{2I-1,2J-1}\ (T_x)_J - G_{2I-1,2J}\ (T_y)_J \Big] = 0 \qquad (6.6)$$

$$C_{2I,2I}\ v_I + \sum_{J=1}^{m} \Big[H_{2I,2J-1}\ u_J + H_{2I,2J}\ v_J - G_{2I,2J-1}\ (T_x)_J - G_{2I,2J}\ (T_y)_J \Big] = 0 \qquad (6.7)$$

Defining the topology array TA, such that TA(e,j) is the global number of the j^{th} local node on the e^{th} element, an assembly rule can be deduced as follows:

$$C_{2(I-1)+\alpha,2(J-1)+\beta} = \delta_{2(I-1)+\alpha,\,2(J-1)+\beta}\ C_i \qquad (6.8)$$

$$H_{2(I-1)+\alpha,2(J-1)+\beta} = \sum_{e} h^{\circ}_{\alpha,2(j-1)+\beta}(x_i, y_i) \qquad (6.9)$$

$$G_{2(I-1)+\alpha,2(J-1)+\beta} = \sum_{e} g^{\circ}_{\alpha,2(j-1)+\beta}(x_i, y_i) \qquad (6.10)$$

where,

$I = 1$

$\alpha = 1, 2$

$\beta = 1, 2$

$J = TA(e,j)$

$j = 1, 2, \ldots, n.$

and the summations are carried out on relevant elements.

Now, for I = 1, 2, ..., m, the equations generated from equations (6.6) and (6.7), can be expressed in the following matrix form:

$$\underline{C}\ \underline{\delta} + \underline{H}\ \underline{\delta} - \underline{G}\ \underline{T} = \underline{0} \qquad (6.11)$$

From the rigid translation condition, the $\underline{C}$ matrix can obtained as follows:

$$C_{i,i} = -\sum_{j=1}^{2m} H_{i,j} \qquad \textit{for finite domains.}$$

$$C_{i,i} = +\sum_{j=1}^{2m} H_{i,j} \qquad \textit{for infinite domains.} \qquad (6.12)$$

where, i = 1, 2, ..., 2m.

Step (4):

Application of the Boundary Conditions.

Defining a matrix $\hat{\underline{H}}$ such that, $\hat{\underline{H}} = \underline{C} + \underline{H}$, then the system of equations given by equation (6.11) can be written as follows:

$$\hat{\underline{H}}\ \underline{\delta} = \underline{G}\ \underline{T} \qquad (6.13)$$

In order to solve the above system of equations, 2m values of $\underline{\delta}$ and $\underline{T}$ should be prescribed. So the nodal vectors $\underline{\delta}$ and $\underline{T}$ can be participated as follows:

$$\underline{\delta} = \{ \underline{\delta}_u \ \underline{\delta}_p \}$$

$$\underline{T} = \{ \underline{T}_u \ \underline{T}_p \} \qquad (6.14)$$

where,

$\underline{\delta}_u$, $\underline{T}_p$ are the unknown parts of $\underline{\delta}$ and $\underline{T}$,
$\underline{\delta}_p$, $\underline{T}_u$ are the prescribed parts of $\underline{\delta}$ and $\underline{T}$.

Hence, equation (6.13) can be partitioned as follows:

$$\begin{bmatrix} \hat{\underline{H}}_{uu} & \hat{\underline{H}}_{up} \\ \hat{\underline{H}}_{pu} & \hat{\underline{H}}_{pp} \end{bmatrix} \begin{bmatrix} \underline{\delta}_u \\ \underline{\delta}_p \end{bmatrix} = \begin{bmatrix} \underline{G}_{uu} & \underline{G}_{up} \\ \underline{G}_{pu} & \underline{G}_{pp} \end{bmatrix} \begin{bmatrix} \underline{T}_u \\ \underline{T}_p \end{bmatrix} \qquad (6.15)$$

and it can be rearranged as follows:

$$\begin{bmatrix} \hat{\underline{H}}_{uu} & -\underline{G}_{up} \\ \hat{\underline{H}}_{pu} & -\underline{G}_{pp} \end{bmatrix} \begin{bmatrix} \underline{\delta}_u \\ \underline{T}_p \end{bmatrix} = \begin{bmatrix} \underline{G}_{uu} & -\hat{\underline{H}}_{up} \\ \underline{G}_{pu} & -\hat{\underline{H}}_{pp} \end{bmatrix} \begin{bmatrix} \underline{T}_u \\ \underline{\delta}_p \end{bmatrix} \qquad (6.16)$$

Now, equation (6.16) can be rewritten as:

$$\underline{A} \ \underline{X} = \underline{B} \ \underline{P} \qquad (6.17)$$

where,

$$\underline{A} = \begin{bmatrix} \hat{\underline{H}}_{uu} & -\underline{G}_{up} \\ \hat{\underline{H}}_{pu} & -\underline{G}_{pp} \end{bmatrix}$$

$$\underline{B} = \begin{bmatrix} \underline{G}_{uu} & -\hat{\underline{H}}_{up} \\ \underline{G}_{pu} & -\hat{\underline{H}}_{pp} \end{bmatrix}$$

$\underline{X} = \{ \underline{\delta}_u \ \underline{T}_p \}$, which is a vector of the unknown nodal values.

$\underline{P} = \{ \underline{T}_u \ \underline{\delta}_p \}$, which is a vector of the prescribed nodal values.

Defining a vector $\underline{Y}$ such that, $\underline{Y} = \underline{B}\ \underline{P}$, then equation (6.17) can be written as follows:

$$\underline{A}_{2mx2m}\ \underline{X}_{2mx1} = \underline{Y}_{2mx1} \qquad (6.18)$$

Step (5):

Solution at Boundary Nodes.

The matrix equation given by equation (6.18) represents a system of 2m simultaneous equations in 2m unknowns. These equations are generally neither symmetric nor banded and an ordinary Gauss elimination solver may, therefore, be used for solving such system of equations.

Step (6):

Solution at Internal Nodes.

(a) Displacement Components:

Consider a point (x_t,y_t) which is inside the domain, the equation for the displacement components can be expressed [Ref.83], as follows:

$$u_t = \oint_\Gamma G_{11}\ T_x\ ds + \oint_\Gamma G_{21}\ T_y\ ds - \oint_\Gamma F_{11}\ u\ ds - \oint_\Gamma F_{21}\ v\ ds \qquad (6.19)$$

$$v_t = \oint_\Gamma G_{12}\ T_x\ ds + \oint_\Gamma G_{22}\ T_y\ ds - \oint_\Gamma F_{12}\ u\ ds - \oint_\Gamma F_{22}\ v\ ds$$

where,

$u_t = u(x_t,y_t)$

$v_t = v(x_t,y_t)$

$G_{rs} = G_{rs}(x-x_t,y-y_t)$

$F_{rs} = F_{rs}(x-x_t,y-y_t)$

$r = 1, 2$

$s = 1, 2$

Using element matrices $\underline{g}^e(x_t,y_t)$, $\underline{h}^e(x_t,y_t)$, and boundary discretization concepts, the displacement components can be expressed in matrix form as follows:

$$\begin{bmatrix} u_t \\ v_t \end{bmatrix} = \sum_{e=1}^{n_e} [\ \underline{g}^e(x_t,y_t)\ \underline{T}_e - \underline{h}^e(x_t,y_t)\ \underline{\delta}_e\ ] \qquad (6.20)$$

where for n-node isoparametric boundary element:

$$\underline{T}_e = \{\ (T_x)_1\ (T_y)_1\ \ (T_x)_2\ (T_y)_2\ \dots\ (T_x)_n\ (T_y)_n\ \}_e \qquad (6.21)$$

$$\underline{\delta}_e = \{\ u_1\ v_1\ \ u_2\ v_2\ \dots\ u_n\ v_n\ \}_e \qquad (6.22)$$

(b) *Strain Components:*

The strain components at the internal point (x_t,y_t), are stated in Ref.[83] as follows:

$$\varepsilon_j(x_t,y_t) = \oint_\Gamma Q_{1j}(x-x_t,y-y_t)\ T_x\ ds + \oint_\Gamma Q_{2j}(x-x_t,y-y_t)\ T_y\ ds$$

$$- \oint_\Gamma P_{1j}(x-x_t,y-y_t)\ u\ ds - \oint_\Gamma P_{2j}(x-x_t,y-y_t)\ v\ ds \qquad (6.23)$$

where,

$j = 1, 2, 3.$

$\varepsilon_1 \equiv \varepsilon_x,\ \varepsilon_2 \equiv \varepsilon_y,\ \varepsilon_3 \equiv \gamma_{xy}.$

The element matrices $\underline{Q}^e$ and $\underline{P}^e$ can be expressed with respect to a source point (x_i,y_i) as follows:

$$Q^e_{\alpha,2(j-1)+\beta}(x_i,y_i) = \int_0^1 Q_{\alpha\beta}(x-x_i,y-y_i)\, N_j(\xi)\, |\underline{J}|\, d\xi$$

$$P^e_{\alpha,2(j-1)+\beta}(x_i,y_i) = \int_0^1 P_{\alpha\beta}(x-x_i,y-y_i)\, N_j(\xi)\, |\underline{J}|\, d\xi \qquad (6.24)$$

Using the discretization concepts, the strain components can be expressed in matrix form as follows:

$$\underline{\varepsilon}(x_t,y_t) = \sum_{e=1}^{n_e} [\ \underline{Q}^e(x_t,y_t)\ \underline{T}_e - \underline{P}^e(x_t,y_t)\ \underline{\delta}_e\ ] \qquad (6.25)$$

where $\underline{T}_e$ and $\underline{\delta}_e$ are as defined in equations (6.21) and (6.22) respectively.

(c) *Stress Components:*

The stress vector at a point (x_t,y_t) inside the domain can be obtained in terms of the strain vector at the point, as follows:

$$\underline{\sigma}(x_t,y_t) = \underline{D}\ \underline{\varepsilon}(x_t,y_t) \qquad (6.26)$$

where,

$$\underline{\sigma} = \{\ \sigma_x \quad \sigma_y \quad \tau_{xy}\ \}$$

and the $\underline{D}$ matrix can be expressed as follows:

$$\underline{D} = \frac{2\mu}{(1-2\nu')} \begin{bmatrix} 1-\nu' & \nu' & 0 \\ \nu' & 1-\nu' & 0 \\ 0 & 0 & \frac{1-2\nu'}{2} \end{bmatrix} \qquad (6.27)$$

where,

μ = Shear modulus,

ν' = ν *for plane strain,*

= $\frac{\nu}{1-\nu}$ *for plane stress,*

ν = Poisson's ratio.

6.3 Families of Standard and Crack-Tip Boundary Elements:

6.3.1 Family of Standard Elements:

This family contain two types of elements, as follows:

(a) The Constant Element:

This is a one-node element defined in terms of two geometrical points, as shown in Fig.(6.3-a), and is called the constant element because the field parameters of this element are approximated in the node on the middle of the element. The shape functions of this element are approximated as follows:

$$N_j(\xi) = 1 \qquad (6.28)$$

where j = 1, and the field parameters for this element can be expressed as follows:

$$\underline{T}_o = \begin{bmatrix} (T_x)_o \\ (T_y)_o \end{bmatrix} \qquad (6.29)$$

$$\underline{\delta}_{o} = \begin{bmatrix} u_{o} \\ v_{o} \end{bmatrix} \qquad (6.30)$$

(b) *The General n-node Element:*

This is an n-node isoparametric element, as shown in Fig.(6.3-b), and its shape functions are as given in equation (6.3), where n = 2, 3, 4, 5, etc. The field parameters for this element are expressed in equations (6.21) and (6.22) respectively.

6.3.2 Family of Crack-Tip Boundary Elements:

This family contains three types of crack-tip elements as follows:

(a) *The 3-Node Isoparametric Crack-tip Element:*

This element is a three-node isoparametric one-dimensional element with its mid-side node being at the quarter point, as shown in Fig.(6.4-a).

The element can be represented in the intrinsic ξ-system ($0 \le \xi \le 1$), and it has the following shape functions:

$$\begin{aligned} N_{1} &= (1-\xi)\,(1-2\xi) \\ N_{2} &= 4\,\xi\,(1-\xi) \\ N_{3} &= \xi\,(2\xi-1) \end{aligned} \qquad (6.31)$$

The above equations are the same as equations (5.32), therefore this element can provide the same strain singularity which is required for linear-elastic fracture analysis, i.e. the $1/\sqrt{r}$ singularity.

(b) *The 4-Node Isoparametric Crack-Tip Element:*

This element is a four-node isoparametric with the two internal nodes of the element being moved to 1/9 and 4/9 locations with respect to the length of the element, as shown in Fig.(6.4-b). The shape functions for this element are as follows:

$$N_1 = (1-\xi)\left[\,1 - \frac{9}{2}\,\xi\,(1-\xi)\,\right]$$

$$N_2 = \frac{9}{2}\,\xi\,(1-\xi)\,(2-3\xi) \qquad (6.32)$$

$$N_3 = -\frac{9}{2}\,\xi\,(1-\xi)\,(1-3\xi)$$

$$N_4 = \xi\left[\,1 - \frac{9}{2}\,\xi\,(1-\xi)\,\right]$$

Comparing the above equations with equations (5.61), it is clear that this element can produce the same singularity required for linear-elastic fracture mechanics.

(c) *The $1/\sqrt{\xi}$ Singular Crack-tip Boundary Element:*

This element has been derived and used by the current author for the first time. The derivation of this element can be reviewed in section (5.3.4). The shape functions for this element in the ξ-system ($0 \le \xi \le 1$) are as follows:

$$N_1 = (1-\xi)\,(1-\sqrt{2}\,\xi)$$

$$N_2 = 2\,(\sqrt{2}+1)\,\xi\,(1-\xi) \qquad (6.33)$$

$$N_3 = -\,(\sqrt{2}+1)\,\xi\,(1-\sqrt{2}\,\xi)$$

which are the same as equations (5.54).

6.4 Boundary Integral Expressions for Domain Loading:

In the presence of domain loading, the boundary integral equations are given in Ref.[83] as follows:

$$c_i\, u_i + \oint_\Gamma F_{11}\, u\, ds + \oint_\Gamma F_{21}\, v\, ds - \oint_\Gamma G_{11}\, T_x\, ds - \oint_\Gamma G_{21}\, T_y\, ds - U_i = 0 \qquad (6.34)$$

$$c_i\, v_i + \oint_\Gamma F_{12}\, u\, ds + \oint_\Gamma F_{22}\, v\, ds - \oint_\Gamma G_{12}\, T_x\, ds - \oint_\Gamma G_{22}\, T_y\, ds - V_i = 0$$

where,

$$U_i = \iint_\Omega (X\, G_{11} + Y\, G_{21})\, dx\, dy$$

$$V_i = \iint_\Omega (X\, G_{12} + Y\, G_{22})\, dx\, dy$$

From the above equations, the one remaining domain integral is the body force integral. In practice this integral has to be evaluated numerically, increasing the amount of data preparation and the *CPU* time required to solve such a problem. However, it has been shown [Ref.83], that for most of the commonly used body forces such as gravity, rotational inertia, or steady thermal loading, the domain integral may be reduced to a boundary integral by further application of the divergence theorem.

For two-dimensional problems the reduced domain integral equations are given in Ref.[83] as follows:

(a) For Translational Inertia:

$$U = \frac{1}{2a}\left(\int_{\Gamma} X \left[\ell \frac{\partial g^*}{\partial x} - 2(1-\nu) \frac{\partial g^*}{\partial n} \right] ds + \int_{\Gamma} Y \left[m \frac{\partial g^*}{\partial x} \right] ds \right)$$

(6.35)

$$V = \frac{1}{2a}\left(\int_{\Gamma} Y \left[m \frac{\partial g^*}{\partial y} - 2(1-\nu) \frac{\partial g^*}{\partial n} \right] ds + \int_{\Gamma} X \left[\ell \frac{\partial g^*}{\partial y} \right] ds \right)$$

(a) For Rotational Inertia:

$$U = \frac{1}{2a}\left(\int_{\Gamma} X \left[\ell \frac{\partial g^*}{\partial x} - 2(1-\nu) \frac{\partial g^*}{\partial n} \right] ds + \int_{\Gamma} Y \left[m \frac{\partial g^*}{\partial x} \right] ds \right.$$
$$\left. - \int_{\Gamma} g^* \left[\ell \frac{\partial X}{\partial x} - 2(1-\nu) \frac{\partial X}{\partial n} \right] ds - \int_{\Gamma} g^* \left[\ell \frac{\partial Y}{\partial y} \right] \right) ds$$

(6.36)

$$V = \frac{1}{2a}\left(\int_{\Gamma} Y \left[m \frac{\partial g^*}{\partial y} - 2(1-\nu) \frac{\partial g^*}{\partial n} \right] ds + \int_{\Gamma} X \left[\ell \frac{\partial g^*}{\partial y} \right] ds \right.$$
$$\left. - \int_{\Gamma} g^* \left[m \frac{\partial Y}{\partial y} - 2(1-\nu) \frac{\partial Y}{\partial n} \right] ds - \int_{\Gamma} g^* \left[m \frac{\partial X}{\partial x} \right] \right) ds$$

where $a = 8\pi\mu(1-\nu^2)$, and $g^* = r^2 \ell o g r$.

To produce programmable equations, specific values for the body force terms X and Y have been considered as follows:

(i) Rotation about the z-axis:

$$X = \rho (x-x_o) \omega_z^2$$
$$Y = \rho (y-y_o) \omega_z^2 \qquad (6.37)$$

(ii) Rotation about an axis in the x-y plane:

$$X = \rho \left[(x-x_o)\,\omega_y^2 - (y-y_o)\,\omega_x\,\omega_y \right]$$
$$Y = \rho \left[(y-y_o)\,\omega_x^2 - (x-x_o)\,\omega_x\,\omega_y \right] \qquad (6.38)$$

where,

ρ is the density of the material,

x_o, y_o are the coordinates of the centre of rotation,

ω_x, ω_y, ω_z are the angular velocities in the x, y, and z directions.

6.5 Boundary Integral Expressions for Thermal Loading:

In the case of thermal loading the U_i and V_i parameters in the boundary integral equations, (6.34), are given explicitly as follows [Ref.83]:

$$U_i = \iint_\Omega \left[\frac{2\alpha'\mu}{1-2\nu'} \right] T \left[\frac{\partial G_{11}}{\partial x} + \frac{\partial G_{21}}{\partial y} \right] dx\,dy$$
$$V_i = \iint_\Omega \left[\frac{2\alpha'\mu}{1-2\nu'} \right] T \left[\frac{\partial G_{12}}{\partial x} + \frac{\partial G_{22}}{\partial y} \right] dx\,dy \qquad (6.39)$$

where,

$\alpha' = \alpha$ *for plane stress,*

$= (1+\nu)\alpha$ *for plane strain.*

α = Coefficient of thermal expansion.

T = Temperature difference.

and, it can be shown that:

$$\left[\frac{\partial G_{11}}{\partial x} + \frac{\partial G_{21}}{\partial y} \right] = \frac{1-2\nu'}{2\mu(1-\nu')} \frac{\partial}{\partial x}(\nabla^2 G^*)$$

$$\left[\frac{\partial G_{12}}{\partial x} + \frac{\partial G_{22}}{\partial y} \right] = \frac{1-2\nu'}{2\mu(1-\nu')} \frac{\partial}{\partial y}(\nabla^2 G^*)$$

where G^* is a fundamental solution parameter defined as follows:

$$G^* = - \frac{r^2}{8\pi} \ell o g r \qquad (6.40)$$

Hence, it may be deduced that:

$$U_i = \iint_\Omega \frac{\alpha'}{1-\nu'} T \frac{\partial}{\partial x}(\nabla^2 G^*) \, dx \, dy$$

$$V_i = \iint_\Omega \frac{\alpha'}{1-\nu'} T \frac{\partial}{\partial y}(\nabla^2 G^*) \, dx \, dy \qquad (6.41)$$

Now, by using integration by-parts theorems [Appendix A], it can be shown that:

$$\iint_\Omega T \nabla^2\left(\frac{\partial G}{\partial x}^*\right) dx \, dy = \oint_\Gamma T \frac{\partial}{\partial n}\left(\frac{\partial G}{\partial x}^*\right) ds - \oint_\Gamma \frac{\partial T}{\partial n} \left(\frac{\partial G}{\partial x}^*\right) ds + \iint_\Omega (\nabla^2 T) \frac{\partial G}{\partial x}^* dx \, dy \qquad (6.42)$$

$$\iint_\Omega T \nabla^2\left(\frac{\partial G}{\partial y}^*\right) dx \, dy = \oint_\Gamma T \frac{\partial}{\partial n}\left(\frac{\partial G}{\partial y}^*\right) ds - \oint_\Gamma \frac{\partial T}{\partial n} \left(\frac{\partial G}{\partial y}^*\right) ds + \iint_\Omega (\nabla^2 T) \frac{\partial G}{\partial y}^* dx \, dy$$

For steady-state heat condition with no heat generation:

$$\nabla^2 T = 0$$

Hence, it can be proved that:

$$U_i = \frac{\alpha'}{1-\nu'} \left[\oint_\Gamma T \frac{\partial}{\partial n}\left(\frac{\partial G}{\partial x}\right)^* ds - \oint_\Gamma \frac{\partial T}{\partial n}\left(\frac{\partial G}{\partial x}\right)^* ds \right]$$

$$V_i = \frac{\alpha'}{1-\nu'} \left[\oint_\Gamma T \frac{\partial}{\partial n}\left(\frac{\partial G}{\partial y}\right)^* ds - \oint_\Gamma \frac{\partial T}{\partial n}\left(\frac{\partial G}{\partial y}\right)^* ds \right] \qquad (6.43)$$

The thermal strain vector is defined for plane stress/strain problems as follows:

$$\underline{\varepsilon}_T = \{ \alpha' T \quad \alpha' T \quad 0 \}$$

and the corresponding stress vector can be written as:

$$\underline{\sigma} = \underline{D} \, (\underline{\varepsilon} - \underline{\varepsilon}_T)$$

6.6 Accuracy Measure Parameters:

6.6.1 The Singular Integrals:

The mechanics of the boundary element method implies that the magnitude of the basic variables are determined by the influence of a number of source points on the boundary. The effect of each source point on the field point is only a function of the distance r between the two points. Thus when the source point and the field point coincide, a singularity occurs due to terms like $\ell n r$, r^{-1}, and r^{-2}, which approach infinite values when r tends to zero.

Now, in order to improve the accuracy of the solution obtained by the boundary element method, the singularity problems should be solved. A technique developed and employed in this study to solve the $\ell n(\frac{1}{r})$ singularity problem, is based on the quadrature table given in Ref.[84]. This technique is required for the $\underline{g}^\circ$ matrix formulation only.

The term $G_{\alpha\beta}$ which appears in equations (6.5) is defined [Ref.83], as follows:

$$G_{\alpha\beta} = \frac{1}{a}\left[\left[C_1 \log\left(\frac{1}{r}\right) - C_3\right]\delta_{\alpha\beta} + \frac{\partial r}{\partial x_\alpha}\frac{\partial r}{\partial x_\beta}\right] \qquad (6.44)$$

where a, C_1, and C_3 are given constants.

For the special case where the field point coincides with the source point, the value of r in equation (6.44) will go to zero making $\log\left(\frac{1}{r}\right)$ singular. Using the intrinsic coordinate ξ, for any general isoparametric element at node (1), $\xi = 0$, it can be shown that:

$$\log\left(\frac{1}{r}\right) = \log\left(\frac{1}{\xi}\right) + \log\left(\frac{\xi}{r}\right) \qquad (6.45)$$

Hence, for the case of $\alpha = \beta$, and $C_3 = 0$, it can be deduced that:

$$G_{\alpha\alpha} = \frac{1}{a}\left[C_1\left\{\log\left(\frac{1}{\xi}\right) + \log\left(\frac{\xi}{r}\right)\right\} + \left(\frac{\partial r}{\partial x_\alpha}\right)^2\right] \qquad (6.46)$$

For a constant element, the function $G_{\alpha\alpha}$ can be calculated analytically [Ref.83]. However, for an isoparametric element the $G_{\alpha\alpha}$ terms can be split into regular and singular parts as follows:

$$G_{\alpha\alpha} = G^R_{\alpha\alpha} + G^S_{\alpha\alpha} \qquad (6.47)$$

where,

$$G^R_{\alpha\alpha} = \frac{1}{a}\left[C_1 \log\left(\frac{\xi}{r}\right) + \left(\frac{\partial r}{\partial x_\alpha}\right)^2\right] \qquad (6.48)$$

and

$$G^{S}_{\alpha\alpha} = \frac{1}{a}\left[C_1 \log\left(\frac{1}{\xi}\right) \right] \qquad (6.49)$$

Since it can be proved that $\lim_{r\to 0} \log\left(\frac{\xi}{r}\right)$ = *finite value*, equation (6.48) represents a regular function, the integration of which can be obtained by the usual Gauss-Legendre quadrature. On the other hand equation (6.49) represents the singular part in a format suitable to be evaluated by means of the quadrature for the logarithmic kernels given in Ref.[84].

Similarly for node (n), at $\xi = 1$, it can be shown that:

$$\log\left(\frac{1}{r}\right) = \log\left(\frac{1}{1-\xi}\right) + \log\left(\frac{1-\xi}{r}\right) \qquad (6.50)$$

therefore,

$$G^{R}_{\alpha\alpha} = \frac{1}{a}\left[C_1 \log\left(\frac{1-\xi}{r}\right) + \left(\frac{\partial r}{\partial x_\alpha}\right)^2 \right] \qquad (6.51)$$

$$G^{S}_{\alpha\alpha} = \frac{1}{a}\left[C_1 \log\left(\frac{1}{1-\xi}\right) \right] \qquad (6.52)$$

Now, for an interior j^{th} node ξ_j, where $\xi_j = (j-1)/(n-1)$, the element can be divided into two parts as shown in Fig.(6.5), a separate analysis is to be carried out for each parts, as follows:

(a) *Part I:*

For this part, the following can be shown:

$$\log\left(\frac{1}{r}\right) = \log\left[\frac{\xi_j}{\xi_j - \xi} \right] + \log\left[\frac{\xi_j - \xi}{\xi_j\, r} \right] \qquad (6.53)$$

therefore,

$$G^{R}_{\alpha\alpha} = \frac{1}{a}\left[C_1 \log\left[\frac{\xi_j - \xi}{\xi_j\, r} \right] + \left(\frac{\partial r}{\partial x_\alpha}\right)^2 \right] \qquad (6.54)$$

$$G^{S}_{\alpha\alpha} = \frac{1}{a}\left[C_1 \log\left(\frac{\xi_j}{\xi_j - \xi} \right) \right] \qquad (6.55)$$

A parameter ϕ is now defined such that $\phi = 0$ at $\xi = \xi_j$, and $\phi = 1$ at $\xi = 0$, i.e.

$$\phi = \frac{\xi_j - \xi}{\xi_j} \qquad (6.56)$$

resulting in,

$$\xi_I = \xi_j (1-\phi) \qquad (6.57)$$

and

$$\int_0^{\xi_j} f(\xi)\, d\xi = -\int_1^0 \xi_j\, f(\phi)\, d\phi = \int_0^1 \xi_j\, f(\phi)\, d\phi \qquad (6.58)$$

Therefore, the function $G^{S}_{\alpha\alpha}$ can be written as follows:

$$G^{S}_{\alpha\alpha} = \frac{\xi_j}{a}\left[C_1 \log\left(\frac{1}{\phi}\right) \right] \qquad (6.59)$$

(b) *Part II:*

The logarithmic function for the second part is modified as follows:

$$\log\left(\frac{1}{r}\right) = \log\left(\frac{1-\xi_j}{\xi - \xi_j} \right) + \log\left(\frac{\xi - \xi_j}{(1-\xi_j) r} \right) \qquad (6.60)$$

and $G^{R}_{\alpha\alpha'}$, $G^{S}_{\alpha\alpha}$ can be expressed as:

$$G^{R}_{\alpha\alpha} = \frac{1}{a}\left[C_1 \log\left(\frac{\xi - \xi_j}{(1-\xi_j) r} \right) + \left(\frac{\partial r}{\partial x_\alpha}\right)^2 \right] \qquad (6.61)$$

$$G^{s}_{\alpha\alpha} = \frac{1-\xi_j}{a}\left[C_1 \log\left(\frac{1-\xi_j}{\xi-\xi_j} \right) \right] \qquad (6.62)$$

The parameter ϕ is defined such that, $\phi = 0$ at $\xi = \xi_j$ and $\phi = 1$ at $\xi = 1$, i.e.

$$\phi = \frac{\xi-\xi_j}{1-\xi_j} \qquad (6.63)$$

and

$$\xi_{II} = \xi_j + (1-\xi_j)\,\phi \qquad (6.64)$$

Hence, the function $G^{s}_{\alpha\alpha}$ can now be written as:

$$G^{s}_{\alpha\alpha} = \frac{1-\xi_j}{a}\left[C_1 \log\left(\frac{1}{\phi}\right) \right] \qquad (6.65)$$

6.6.2 Corner Jump Functions Technique:

(i) Definitions:

Consider the boundary integral equations given by equations (6.34), and let the boundary Γ contain a corner defined by two nodes a and b ($a \equiv b$), then it can be written that:

$$\oint_{\Gamma} f\, ds = \lim_{a \to b} \left[\int_{\Gamma_b} f\, ds + \int_{a}^{b} f\, ds \right] \qquad (6.66)$$

where $\Gamma_b = \Gamma - \Gamma_c$, as shown in Fig.(6.6).

Now, define $(x_c,y_c) \equiv (x_a,y_a) \equiv (x_b,y_b)$ to represent a boundary node at the corner c. From equations (6.34), it can be shown that:

$$\oint_{\Gamma} F_{\alpha\beta}\, u_{\alpha}\, ds = \int_{\Gamma_b} F_{\alpha\beta}\, u_{\alpha}\, ds + \lim_{a\to b} \int_{a}^{b} F_{\alpha\beta}\, u_{\alpha}\, ds$$

$$= \int_{\Gamma_b} F_{\alpha\beta}\, u_{\alpha}\, ds + \mathcal{F}_{\alpha\beta}(x_i,y_i)\, u_{\alpha}(x_c,y_c) \qquad (6.67)$$

where (x_i,y_i) are the i^{th} source point coordinates, and the term $\mathcal{F}_{\alpha\beta}(x_i,y_i)$ is defined as follows:

$$\mathcal{F}_{\alpha\beta}(x_i,y_i) = \lim_{a\to b} \int_{a}^{b} F_{\alpha\beta}(x-x_i,y-y_i)\, ds \qquad (6.68)$$

Similarly it can be deduced that:

$$\oint_{\Gamma} G_{\alpha\beta}\, T_{\alpha}\, ds = \int_{\Gamma_b} G_{\alpha\beta}\, T_{\alpha}\, ds + \mathcal{G}_{\alpha\beta}(x_i,y_i)\, T_{\alpha}(x_c,y_c) \qquad (6.69)$$

where,

$$\mathcal{G}_{\alpha\beta}(x_i,y_i) = \lim_{a\to b} \int_{a}^{b} G_{\alpha\beta}(x-x_i,y-y_i)\, ds \qquad (6.70)$$

The functions $\mathcal{F}_{\alpha\beta}$ and $\mathcal{G}_{\alpha\beta}$ whenever they exist are called "*Jump Functions*".

(2) *Jump Functions for a Smooth Corner Model:*

Consider a smooth corner model as defined in Fig.(6.7), where (x_c,y_c) are the coordinates of the centre of the circular arc which is tangent to the boundary at points *a* and *b*.

To use this model, two cases should be taken into consideration depending upon the location of the source point. The two cases are as follows:

Case (a):

The Source Point is not a Corner Node.

For such a case there is no singularity in $F_{\alpha\beta}$ and $G_{\alpha\beta}$ terms. Hence:

$$\lim_{a \to b} \int_{a}^{b} f \, ds \to 0 \qquad (6.71)$$

From the above equation it can be deduced that the Jump functions $\mathcal{F}_{\alpha\beta}$ and $\mathcal{G}_{\alpha\beta}$ for this case as defined by equations (6.68) and (6.70) respectively, are zeros.

Case (b):

The Source Point is a Corner Node.

For this case, $F_{\alpha\beta}$ and $G_{\alpha\beta}$ contain singular terms, therefore their integrals should be examined with care. Considering the corner model shown in Fig.(6.7), it can be deduced that the field point (x,y) is moving from point *a* to point *b* on a circular arc centred at *c*, as explained before.

Now, since $x_i = x_c$ and $y_i = y_c$, it can be shown that:

$$r = \sqrt{(x-x_c)^2 + (y-y_c)^2} \qquad (6.72)$$

Using polar coordinates, it can be proved that:

$$x = x_c + r\cos\theta$$

$$y = y_c + r\sin\theta \qquad (6.73)$$

Also it can be shown that:

$$\frac{\partial r}{\partial x} = \cos\theta, \quad \frac{\partial r}{\partial y} = \sin\theta, \quad \frac{\partial r}{\partial n} = 1, \quad \frac{\partial r}{\partial s} = 0 \qquad (6.74)$$

The terms $F_{\alpha\beta}$ and $G_{\alpha\beta}$, as given in Ref.[83], are as follows:

$$F_{\alpha\beta} = -\frac{1}{4\pi(1-p)r}\left[2\frac{\partial r}{\partial n}\frac{\partial r}{\partial x_\alpha}\frac{\partial r}{\partial x_\beta} + (1-2p)\left(\ell_\beta\frac{\partial r}{\partial x_\alpha} - \ell_\alpha\frac{\partial r}{\partial x_\beta}\right) - (1-2p)\frac{\partial r}{\partial n}\delta_{\alpha\beta}\right] \qquad (6.75)$$

$$G_{\alpha\beta} = \frac{1}{8\pi\mu(1-p)}\left\{ -\left[(3-4p)\ell n r + \frac{1}{2}\right]\delta_{\alpha\beta} + \frac{\partial r}{\partial x_\alpha}\frac{\partial r}{\partial x_\beta}\right\} \qquad (6.76)$$

where $\delta_{\alpha\beta}$ is the Kronecher delta.

From equations (6.69), (6.74) and (6.75), it can be shown that:

$$\mathcal{F}_{11}(x_c,y_c) = \lim_{a\to b}\int_{\theta_a}^{\theta_b} F_{11}\, r\, d\theta$$

$$= \lim_{r\to 0}\int_{\theta_a}^{\theta_b}\frac{1}{4\pi(1-p)}\left[2(1-p) + \cos(2\theta)\right] d\theta \qquad (6.77)$$

Therefore, from Fig.(6.7) and equation (6.77), it can be deduced that:

$$\mathcal{F}_{11}(x_c,y_c) = \left(\frac{\alpha}{2\pi} - \frac{1}{2}\right) - \frac{1}{b}\cos(2\gamma)\sin\alpha \qquad (6.78)$$

Similarly, it can be deduced that:

$$\mathcal{F}_{22}(x_c,y_c) = \left(\frac{\alpha}{2\pi} - \frac{1}{2}\right) + \frac{1}{b}\cos(2\gamma)\sin\alpha \qquad (6.79)$$

$$\mathcal{F}_{12}(x_c,y_c) = \mathcal{F}_{21}(x_c,y_c) = -\frac{1}{b}\cos(2\gamma)\sin\alpha \qquad (6.80)$$

where,

$$b = 4\pi(1-p)$$

$$\alpha = \pi + \phi_a - \phi_b$$

$$\gamma = (\theta_a + \theta_b) / 2$$

Using similar procedure, it can be proved that:

$$\mathfrak{G}_{\alpha\beta}(x_c, y_c) = 0 \qquad (6.81)$$

(3) The Modified Boundary Integral Equations:

For a source point (x_i, y_i) being not a corner node, there is no modification required for the boundary integral equations. On the other hand, for (x_i, y_i) being the corner node (x_c, y_c), the following modification is required.

Using the previous corner model, the boundary integral equations may then be rewritten as follows:

$$\left(C_{11}\, u_c + C_{12}\, v_c \right) + \oint_{\Gamma_b} F_{11}\, u\, ds + \oint_{\Gamma_b} F_{21}\, v\, ds$$

$$- \oint_{\Gamma_b} G_{11}\, T_x\, ds - \oint_{\Gamma_b} G_{21}\, T_y\, ds - U_c = 0 \qquad (6.82)$$

$$\left(C_{21}\, u_c + C_{22}\, v_c \right) + \oint_{\Gamma_b} F_{12}\, u\, ds + \oint_{\Gamma_b} F_{22}\, v\, ds$$

$$- \oint_{\Gamma_b} G_{12}\, T_x\, ds - \oint_{\Gamma_b} G_{22}\, T_y\, ds - V_c = 0 \qquad (6.83)$$

where,

$$C_{11} = \frac{1}{2} + \mathfrak{F}_{11}(x_c, y_c) \quad , \quad C_{22} = \frac{1}{2} + \mathfrak{F}_{22}(x_c, y_c)$$

$$C_{12} = \mathfrak{F}_{21}(x_c, y_c) \quad , \quad C_{21} = \mathfrak{F}_{12}(x_c, y_c)$$

6.6.3 Use of Rigid Translation Conditions:

If the structure is moved rigid translations α in the x-direction, and β in the y-direction, then there are no loading and no stresses generated, which means that at any point in the structure, the following can be deduced:

$$T_x = T_y = 0$$
$$U_i = V_i = 0$$
$$u(x,y) = \alpha$$
$$v(x,y) = \beta$$

Then, the boundary integral equations given by equations (6.34) can be rewritten as follows:

$$c_i \alpha + \alpha \oint_\Gamma F_{11}\, ds + \beta \oint_\Gamma F_{21}\, ds = 0$$
$$c_i \beta + \alpha \oint_\Gamma F_{12}\, ds + \beta \oint_\Gamma F_{22}\, ds = 0 \qquad (6.84)$$

For the special case of $\alpha = u_i$ and $\beta = v_i$, the above equations can be restated as follows:

$$c_i u_i + \oint_\Gamma F_{11}\, u_i\, ds + \oint_\Gamma F_{21}\, v_i\, ds = 0$$
$$c_i v_i + \oint_\Gamma F_{12}\, u_i\, ds + \oint_\Gamma F_{22}\, v_i\, ds = 0 \qquad (6.85)$$

Subtracting equations (6.85) from equations (6.34), the boundary integral equations can be rewritten as follows:

$$\oint_\Gamma F_{11}\,(u-u_i)\, ds + \oint_\Gamma F_{21}\,(v-v_i)\, ds - \oint_\Gamma G_{11}\, T_x\, ds$$
$$- \oint_\Gamma G_{21}\, T_y\, ds - U_i = 0 \qquad (6.86)$$

$$\oint_{\Gamma} F_{12}\,(u-u_i)\,ds + \oint_{\Gamma} F_{22}\,(v-v_i)\,ds - \oint_{\Gamma} G_{12}\,T_x\,ds$$

$$- \oint_{\Gamma} G_{22}\,T_y\,ds - V_i = 0 \qquad (6.87)$$

Now, for the special case of having a corner node (x_c,y_c), equations (6.86) and (6.87) can be rewritten as follows:

$$\oint_{\Gamma_b} F_{11}\,(u-u_i)\,ds + (u_c-u_i)\,\mathcal{J}_{11}(x_i-y_i) + \oint_{\Gamma_b} F_{21}\,(v-v_i)\,ds$$

$$+ (v_c-v_i)\,\mathcal{J}_{21} - \oint_{\Gamma_b} G_{11}\,T_x\,ds - \oint_{\Gamma_b} G_{21}\,T_y\,ds - U_i = 0 \qquad (6.88)$$

$$\oint_{\Gamma_b} F_{12}\,(u-u_i)\,ds + (u_c-u_i)\,\mathcal{J}_{12}(x_i-y_i) + \oint_{\Gamma_b} F_{22}\,(v-v_i)\,ds$$

$$+ (u_c-u_i)\,\mathcal{J}_{22} - \oint_{\Gamma_b} G_{12}\,T_x\,ds - \oint_{\Gamma_b} G_{22}\,T_y\,ds - V_i = 0 \qquad (6.89)$$

From the Jump function equations, it can be seen that:

(a) *if* $(x_i,y_i) \neq (x_c,y_c)$, *then* $\mathcal{J}_{\alpha\beta}(x_i,y_i) = 0$.

(b) *if* $(x_i,y_i) \equiv (x_c,y_c)$, *then* $\mathcal{J}_{\alpha\beta}(x_i,y_i) \neq 0$, but $(u_c-u_i) = 0$, *and* $(v_c-v_i) = 0$.

Hence, for any source point (x_i,y_i), it can be deduced that:

$$\lim_{a\to b} \int_a^b F_{\alpha\beta}\,(u-u_i)\,ds = 0 \qquad (6.90)$$

and

$$\lim_{a\to b} \int_a^b F_{\alpha\beta}\,(v-v_i)\,ds = 0 \qquad (6.91)$$

From previous analysis, it can be shown that:

$$\lim_{a \to b} \int_a^b F_{\alpha\beta} (u-u_i) \, ds = (u_c - u_i) \, \mathcal{F}_{\alpha\beta}(x_i, y_i) = 0 \qquad (6.92)$$

and

$$\lim_{a \to b} \int_a^b F_{\alpha\beta} (v-v_i) \, ds = (v_c - v_i) \, \mathcal{F}_{\alpha\beta}(x_i, y_i) = 0 \qquad (6.93)$$

Substituting equations (6.92) and (6.93), into equations (6.88) and (6.89) and using equations (6.90) and (6.91), the boundary integral equations can now be rewritten as follows:

$$\oint_{\Gamma_b} F_{11} (u-u_i) \, ds + \oint_{\Gamma_b} F_{21} (v-v_i) \, ds - \oint_{\Gamma_b} G_{11} T_x \, ds - \oint_{\Gamma_b} G_{21} T_y \, ds - U_i = 0 \qquad (6.94)$$

$$\oint_{\Gamma_b} F_{12} (u-u_i) \, ds + \oint_{\Gamma_b} F_{22} (v-v_i) \, ds - \oint_{\Gamma_b} G_{12} T_x \, ds - \oint_{\Gamma_b} G_{22} T_y \, ds - V_i = 0 \qquad (6.95)$$

The above equations are free from corner effects. The corner can be left as a finite gap in the boundary element mesh. This result justifies the double-node technique of the corner, i.e. representing the corner with two nodes, one with element (1) and the second with element (2), as shown in Fig.(6.8).

For further simplification, defining the factor $C_{\beta\alpha}$ at source point (x_i, y_i), as follows:

$$C_{\beta\alpha}(x_i, y_i) = - \oint_{\Gamma_b} F_{\alpha\beta}(x-x_i, y-y_i) \, ds \qquad (6.96)$$

Then, the boundary integral equations can be expressed as follows:

$$C_{11}(x_i,y_i)\ u_i + C_{12}(x_i,y_i)\ v_i + \oint_{\Gamma_b} F_{11}\ u\ ds + \oint_{\Gamma_b} F_{21}\ v\ ds$$

$$- \oint_{\Gamma_b} G_{11}\ T_x\ ds - \oint_{\Gamma_b} G_{21}\ T_y\ ds - U_i = 0 \qquad (6.97)$$

$$C_{21}(x_i,y_i)\ u_i + C_{22}(x_i,y_i)\ v_i + \oint_{\Gamma_b} F_{12}\ u\ ds + \oint_{\Gamma_b} F_{22}\ v\ ds$$

$$- \oint_{\Gamma_b} G_{12}\ T_x\ ds - \oint_{\Gamma_b} G_{22}\ T_y\ ds - V_i = 0 \qquad (6.98)$$

6.6.4 Boundary Integral Equations for strains:

Although the boundary integral equations for strains exist [Ref.83], the results are not expected to be very accurate, especially near the boundary. This is because the fundamental solutions for the boundary integral equations of strains *(obtained by differentiating the fundamental solutions of the BIE's of displacements)* exhibit a high degree of singularity. In an attempt to improve the accuracy of the results, a number of techniques were developed, their use depending on the position of the source point from the boundary.

Consider the boundary Integral equations given by equations (6.34). Differentiating these equations with respect to x_i and y_i yields the following equations:

$$C_{11}\ \frac{\partial u_i}{\partial x_i} + C_{12}\ \frac{\partial v_i}{\partial x_i} = \phi_x(x_i,y_i) \qquad (6.99)$$

$$C_{21}\frac{\partial u_i}{\partial x_i} + C_{22}\frac{\partial v_i}{\partial x_i} = \psi_x(x_i,y_i) \tag{6.100}$$

$$C_{11}\frac{\partial u_i}{\partial y_i} + C_{12}\frac{\partial v_i}{\partial y_i} = \phi_y(x_i,y_i) \tag{6.101}$$

$$C_{21}\frac{\partial u_i}{\partial y_i} + C_{22}\frac{\partial v_i}{\partial y_i} = \psi_y(x_i,y_i) \tag{6.102}$$

where,

$$\phi_x(x_i,y_i) = \int_{\Gamma_b}\frac{\partial G_{11}}{\partial x_i}T_x\,ds + \int_{\Gamma_b}\frac{\partial G_{21}}{\partial x_i}T_y\,ds - \int_{\Gamma_b}\frac{\partial F_{11}}{\partial x_i}u\,ds - \int_{\Gamma_b}\frac{\partial F_{21}}{\partial x_i}v\,ds + \frac{\partial U_i}{\partial x_i} \tag{6.103}$$

$$\psi_x(x_i,y_i) = \int_{\Gamma_b}\frac{\partial G_{12}}{\partial x_i}T_x\,ds + \int_{\Gamma_b}\frac{\partial G_{22}}{\partial x_i}T_y\,ds - \int_{\Gamma_b}\frac{\partial F_{12}}{\partial x_i}u\,ds - \int_{\Gamma_b}\frac{\partial F_{22}}{\partial x_i}v\,ds + \frac{\partial V_i}{\partial x_i} \tag{6.104}$$

$$\phi_y(x_i,y_i) = \int_{\Gamma_b}\frac{\partial G_{11}}{\partial y_i}T_x\,ds + \int_{\Gamma_b}\frac{\partial G_{21}}{\partial y_i}T_y\,ds - \int_{\Gamma_b}\frac{\partial F_{11}}{\partial y_i}u\,ds - \int_{\Gamma_b}\frac{\partial F_{21}}{\partial y_i}v\,ds + \frac{\partial U_i}{\partial y_i} \tag{6.105}$$

$$\psi_y(x_i,y_i) = \int_{\Gamma_b}\frac{\partial G_{12}}{\partial y_i}T_x\,ds + \int_{\Gamma_b}\frac{\partial G_{22}}{\partial y_i}T_y\,ds - \int_{\Gamma_b}\frac{\partial F_{12}}{\partial y_i}u\,ds - \int_{\Gamma_b}\frac{\partial F_{22}}{\partial y_i}v\,ds + \frac{\partial V_i}{\partial y_i} \tag{6.106}$$

The above system of equations can be solved to obtain the

partial derivatives of u_i and v_i with respect to x_i and y_i, and hence the values of strain at (x_i,y_i). To obtain the values of stress and strain at an internal node using the method outlined above, the rigid translation condition must be used to define the term $C_{\beta\alpha}$.

As mentioned before, the boundary integral equations for strains have singularities in their fundamental solutions. Thus, they are unsuitable for boundary nodes, where these singularities occur. Other techniques exist at such points, where the displacement components at any point on the boundary element can be interpolated as follows:

$$u(\xi) = \sum_{j=1}^{n} u_j \, N_j(\xi)$$

$$v(\xi) = \sum_{j=1}^{n} v_j \, N_j(\xi) \qquad (6.107)$$

The derivatives of the above displacement components with respect to ξ, can be deduced as follows:

$$\frac{du}{d\xi} = \sum_{j=1}^{n} u_j \frac{dN_j}{d\xi}$$

$$\frac{dv}{d\xi} = \sum_{j=1}^{n} v_j \frac{dN_j}{d\xi} \qquad (6.108)$$

From the chain rule of partial differentiation, it can be written that:

$$\frac{du}{d\xi} = \left[\frac{\partial u}{\partial x} \right] \frac{dx}{d\xi} + \left[\frac{\partial u}{\partial y} \right] \frac{dy}{d\xi}$$

$$\frac{dv}{d\xi} = \left[\frac{\partial v}{\partial x} \right] \frac{dx}{d\xi} + \left[\frac{\partial v}{\partial y} \right] \frac{dy}{d\xi} \qquad (6.109)$$

Now, dividing throughout by the Jacobian $|\underline{J}|$, the following expressions can be obtained:

$$\frac{d\mathcal{u}}{d\xi} \Big/ |\underline{J}| = - m \frac{\partial \mathcal{u}}{\partial x} + \ell \frac{\partial \mathcal{u}}{\partial y}$$

$$\frac{d\mathcal{v}}{d\xi} \Big/ |\underline{J}| = - m \frac{\partial \mathcal{v}}{\partial x} + \ell \frac{\partial \mathcal{v}}{\partial y} \qquad (6.110)$$

The surface traction components can be obtained as follows:

$$T_x = \ell \sigma_x + m \tau_{xy}$$

$$T_y = \ell \tau_{xy} + m \sigma_y \qquad (6.111)$$

Substituting the strain values with the appropriate stress/strain coefficients d_{ij}, into equations (6.111), it can be deduced that:

$$T_x = \ell \left[d_{11} \frac{\partial \mathcal{u}}{\partial x} + d_{12} \frac{\partial \mathcal{v}}{\partial y} \right] + m\, d_{33} \left[\frac{\partial \mathcal{v}}{\partial x} + \frac{\partial \mathcal{u}}{\partial y} \right]$$

$$T_y = m \left[d_{21} \frac{\partial \mathcal{u}}{\partial x} + d_{22} \frac{\partial \mathcal{v}}{\partial y} \right] + \ell\, d_{33} \left[\frac{\partial \mathcal{v}}{\partial x} + \frac{\partial \mathcal{u}}{\partial y} \right] \qquad (6.112)$$

If the value of ξ is known for a given (x_i, y_i), then a system of equations can be set up to find the partial derivatives of $\mathcal{u}$ and $\mathcal{v}$ with respect to x_i, y_i. This system can be represented by:

$$\underline{A}\ \underline{x} = \underline{y} \qquad (6.113)$$

where,

$$\underline{A} = \begin{bmatrix} -m & \ell & 0 & 0 \\ 0 & 0 & -m & \ell \\ \ell(d_{11}/E) & m(d_{33}/E) & m(d_{33}/E) & \ell(d_{12}/E) \\ m(d_{12}/E) & \ell(d_{33}/E) & \ell(d_{33}/E) & m(d_{22}/E) \end{bmatrix}$$

$$\underline{x} = \left\{ \begin{array}{cccc} \frac{\partial u}{\partial x} & \frac{\partial u}{\partial y} & \frac{\partial v}{\partial x} & \frac{\partial v}{\partial y} \end{array} \right\}$$

$$\underline{y} = \left\{ \begin{array}{cccc} \frac{\partial u}{\partial \xi} / |\underline{J}| & \frac{\partial v}{\partial \xi} / |\underline{J}| & T_x / E & T_y / E \end{array} \right\}$$

A separate method exists for isoparametric elements if (x_i, y_i) coincides with two different nodes *(double nodes technique)*. The nodes belong to separate elements, say element (1) and (2). Defining (ℓ_1, m_1) and (ℓ_2, m_2) to be the direction cosines for element (1) and (2) respectively, then if $(T_x)_1$ and $(T_y)_1$ are the tractions for the node on element (1) and $(T_x)_2$ and $(T_y)_2$ are similarly defined for the node on element (2), it can be shown that:

$$\begin{aligned} \ell_1 (T_x)_1 - m_1 (T_y)_1 &= \ell_1^2 \sigma_x - m_1^2 \sigma_y \\ \ell_2 (T_x)_2 - m_2 (T_y)_2 &= \ell_2^2 \sigma_x - m_2^2 \sigma_y \end{aligned} \qquad (6.114)$$

The traction components in the above equations can be obtained from the boundary integral equations of displacements, then the equations can be rewritten as follows:

$$\begin{aligned} \ell_1^2 \sigma_x - m_1^2 \sigma_y &= f_1 \\ \ell_2^2 \sigma_x - m_2^2 \sigma_y &= f_2 \end{aligned} \qquad (6.115)$$

where f_1 and f_2 are known parameters.

There are a variety of techniques for solving equations (6.115) depending on the values of the following three determinants:

$$\begin{vmatrix} \ell_1^2 & -m_1^2 \\ \ell_2^2 & -m_2^2 \end{vmatrix}, \quad \begin{vmatrix} \ell_1 \ell_2 & -m_1 m_2 \\ \ell_1^2 & -m_1^2 \end{vmatrix}, \quad \begin{vmatrix} \ell_1 \ell_2 & -m_1 m_2 \\ \ell_2^2 & -m_2^2 \end{vmatrix}$$

6.6.5 Use of Finite Difference Method:

It was clear from many cases tested, that the previous approaches would fail if the source point (x_i,y_i) being very close to the boundary. For such cases, $u(x_i,y_i)$ and $v(x_i,y_i)$ are always very accurate, and the finite difference method can therefore, be employed.

For source point (x_i,y_i), as shown in fig.(6.9), define a, b, c, and d, such that:

$$a \equiv (x_i-\Delta x, y_i)$$
$$b \equiv (x_i+\Delta x, y_i)$$
$$c \equiv (x_i, y_i-\Delta y)$$
$$d \equiv (x_i, y_i+\Delta y)$$

The increments Δx and Δy should be selected such that a, b, c, and d are still inside the domain or on its boundary, but not outside the domain.

For such a case, the following can be deduced:

$$\left[\frac{\partial u}{\partial x}\right]_i \simeq \frac{u_b-u_a}{2\Delta x}, \quad \left[\frac{\partial v}{\partial x}\right]_i \simeq \frac{v_b-v_a}{2\Delta x}$$
$$\left[\frac{\partial u}{\partial y}\right]_i \simeq \frac{u_d-u_c}{2\Delta x}, \quad \left[\frac{\partial v}{\partial y}\right]_i \simeq \frac{v_d-v_c}{2\Delta x} \qquad (6.116)$$

The displacements (u_a,v_a), (u_b,v_b), (u_c,v_c), and (u_d,v_d) will be evaluated from the boundary integral equations. The strain and stress components can be evaluated as follows:

$$(\varepsilon_x)_i = \left[\frac{\partial u}{\partial x}\right]_i, \quad (\varepsilon_y)_i = \left[\frac{\partial v}{\partial y}\right]_i$$
$$(\gamma_{xy})_i = \left[\frac{\partial u}{\partial y}\right]_i + \left[\frac{\partial v}{\partial x}\right]_i \qquad (6.117)$$

and, $\underline{\sigma}_i = \underline{D}\ \underline{\varepsilon}_i$ (6.118)

6.6.6 Use of Subregion Technique:

In many engineering applications it is essential to divide the structure analyzed into several regions known as subregions. This may be due to the existence of cracks, flaws, or because the dimensions of the structure are not regular.

In each of the situations mentioned above, a set of regional boundary equations can be formulated and assembled. These boundary equations are inter-related by the compatibility and equilibrium constraints at the region interfaces, and wherever the traction is discontinuous on an interface boundary the multiple nodes concept, mentioned earlier, can be used.

Consider a structure of two subregions *a* and *b* as shown in Fig.(6.10). For subregion *a* the following can be defined:

$\underline{\delta}_{aa}$ = The displacement vector of the independent boundary nodes of subregion *a*.

$\underline{\delta}_{ab}$ = The displacement vector of the nodes on the interface between subregions *a* and *b*.

Now, the displacement and traction vectors for all boundary nodes of subregion *a* can be defined as follows:

$$\underline{\delta}_{a} = \{ \underline{\delta}_{aa} \quad \underline{\delta}_{ab} \}$$

$$\underline{T}_{a} = \{ \underline{T}_{aa} \quad \underline{T}_{ab} \} \qquad (6.119)$$

Similarly, for subregion *b* , the following can be defined:

$$\underline{\delta}_{b} = \{ \underline{\delta}_{ba} \quad \underline{\delta}_{bb} \}$$

$$\underline{T}_{b} = \{ \underline{T}_{ba} \quad \underline{T}_{bb} \} \qquad (6.120)$$

Consider the matrix equation given by equation (6.11), the matrix equation for subregion *a* and *b* can be written as follows:

$$\underline{C}_a \underline{\delta}_a + \underline{H}_a \underline{\delta}_a - \underline{G}_a \underline{T}_a = 0$$

$$\underline{C}_b \underline{\delta}_b + \underline{H}_b \underline{\delta}_b - \underline{G}_b \underline{T}_b = 0 \qquad (6.121)$$

Therefore, $\underline{C}_a$, $\underline{H}_a$, and $\underline{G}_a$, can be partitioned as follows:

$$\begin{bmatrix} \underline{C}_{aa} & \underline{C}_{ab} \end{bmatrix} \begin{bmatrix} \underline{\delta}_{aa} \\ \underline{\delta}_{ab} \end{bmatrix} + \begin{bmatrix} \underline{H}_{aa} & \underline{H}_{ab} \end{bmatrix} \begin{bmatrix} \underline{\delta}_{aa} \\ \underline{\delta}_{ab} \end{bmatrix}$$

$$- \begin{bmatrix} \underline{G}_{aa} & \underline{G}_{ab} \end{bmatrix} \begin{bmatrix} \underline{T}_{aa} \\ \underline{T}_{ab} \end{bmatrix} = \underline{0} \qquad (6.122)$$

Similarly, for $\underline{C}_b$, $\underline{H}_b$, and $\underline{G}_b$.

Now, since it is assumed to be no relative movement between the subregions (*i.e. no slip or separation*), the conditions of compatibility and equilibrium over the interface must be satisfied. These conditions can be summarized as follows:

(*i*) $\underline{\delta}_{ab} = \underline{\delta}_{ba}$ *for compatibility of displacement.*

(*ii*) $\underline{T}_{ab} = - \underline{T}_{ba}$ *for equilibrium of tractions.*

The above conditions allow the separate subregion matrices to be assembled into a global matrix for the complete boundary. However, before the system can be solved, further conditions must be applied at the multi region interface nodes.

The problem of discontinuity of traction at corners are also encountered at subregion interface nodes, where the normals are not defined. Consider the node *i*, as shown in Fig.(6.10), the total number of variables at this node is six (*i.e. two displacement components, and two traction components for each*

subregion). Now, two component equations, with respect to x and y axes, can be generated for each of the two subregions.

For a unique solution of all the variables, another two extra independent equations are required. To provide these extra independent equations, the multiple nodes concept is used. Auxiliary nodes are defined at the intersection points, where each node is assigned a unique normal. Considering node i again, three auxiliary nodes take the place of this node, as shown in Fig.(6.11), although they are considered to be geometrically coincident, each node is associated with a particular element and hence a unique normal.

This technique also applies to internal interfaces between subregions. For a node at the intersection of three subregions, three nodes should be defined to take the place of the actual node, leading to the auxiliary nodes being only common to two subregions. Thus two equations can be generated from each subregion to correspond to the four unknown variables active at each node.

The subregion technique does have the disadvantage of increasing the total number of active variables, and hence the size of the matrix equation to be solved, also there will be an increase in assembly and solution time, which may mean that for large or complex structures requiring many auxiliary nodes, this method is inefficient. However, using many subregions may lead to a matrix of coefficients diagonally dominant, which facilitates the use of banded solvers.

6.7 Outline of the BEM for 2D Elasto-Plastic Problems:

The outline of the boundary element method for two-dimensional elasto-plastic fracture mechanics problems is summarized in the following sections.

6.7.1 Boundary Integral Equations for Elasto-Plastic Problems:

The boundary integral equations for elasto-plastic problems are given as follows [Ref.83]:

$$c_i\, u_i + \oint_\Gamma \left(F_{11}\, u + F_{21}\, v \right) ds - \oint_\Gamma \left(G_{11}\, T_x + G_{21}\, T_y \right) ds - \iint_\Omega \left(G_{11}\, X + G_{21}\, Y \right) dx\, dy - \iint_\Omega \left(R^*_{11}\, \sigma^p_x + R^*_{21}\, \sigma^p_y + R^*_{31}\, \tau^p_{xy} \right) dx\, dy = 0 \qquad (6.123)$$

$$c_i\, v_i + \oint_\Gamma \left(F_{12}\, u + F_{22}\, v \right) ds - \oint_\Gamma \left(G_{12}\, T_x + G_{22}\, T_y \right) ds - \iint_\Omega \left(G_{12}\, X + G_{22}\, Y \right) dx\, dy - \iint_\Omega \left(R^*_{12}\, \sigma^p_x + R^*_{22}\, \sigma^p_y + R^*_{32}\, \tau^p_{xy} \right) dx\, dy = 0 \qquad (6.124)$$

where,

$$c_i = \iint_\Omega \delta(x-x_i, y-y_i)\, dx\, dy$$

In the above equations the plastic stresses σ^p_x, σ^p_y, and τ^p_{xy} can be defined as follows:

$$\underline{\sigma}^p = \underline{D}\, \underline{\varepsilon}^p = (\underline{D} - \underline{D}_{ep})\, \underline{\varepsilon} \qquad (6.125)$$

where,

$\underline{\sigma}^p = \{ \sigma^p_x \quad \sigma^p_y \quad \tau^p_{xy} \}$,

$\underline{\varepsilon}^p = \{ \varepsilon^p_x \quad \varepsilon^p_y \quad \gamma^p_{xy} \}$, and

$\underline{D}_{ep}$ = Elasto-plastic stress-strain matrix.

6.7.2 Incremental Boundary Integral Equations:

Since the incremental plasticity theory is used, then due to the application of a load increment represented by ΔT_x, ΔT_y, and the load intensity increment ΔX, ΔY, equations (6.123) and (6.124) may be written as follows:

$$C_{11}\,\Delta u_i + C_{12}\,\Delta v_i + \oint_\Gamma \left[F_{11}\,\Delta u + F_{21}\,\Delta v \right] ds$$

$$- \oint_\Gamma \left[G_{11}\,\Delta T_x + G_{21}\,\Delta T_y \right] ds - \iint_\Omega \left[G_{11}\,\Delta X + G_{21}\,\Delta Y \right] dx\,dy$$

$$- \iint_\Omega \left[R^*_{11}\,\Delta\sigma^p_x + R^*_{21}\,\Delta\sigma^p_y + R^*_{31}\,\Delta\tau^p_{xy} \right] dx\,dy = 0 \qquad (6.126)$$

$$C_{21}\,\Delta u_i + C_{22}\,\Delta v_i + \oint_\Gamma \left[F_{12}\,\Delta u + F_{22}\,\Delta v \right] ds$$

$$- \oint_\Gamma \left[G_{12}\,\Delta T_x + G_{22}\,\Delta T_y \right] ds - \iint_\Omega \left[G_{12}\,\Delta X + G_{22}\,\Delta Y \right] dx\,dy$$

$$- \iint_\Omega \left[R^*_{12}\,\Delta\sigma^p_x + R^*_{22}\,\Delta\sigma^p_y + R^*_{32}\,\Delta\tau^p_{xy} \right] dx\,dy = 0 \qquad (6.127)$$

The boundary element calculation of elasto-plastic problems will start always with the elastic solutions, in which the following can be defined:

$$\Delta\underline{\sigma}' = \underline{D}\;\Delta\underline{\varepsilon} \qquad (6.128)$$

Then a correction may be carried out such that:

$$\Delta\underline{\sigma}_{ep} = \underline{D}_{ep}\;\Delta\underline{\varepsilon} \qquad (6.129)$$

Now, from equations (6.125), (6.128), and (6.129), it can be shown that:

$$\Delta\underline{\sigma}^p = \Delta\underline{\sigma}' - \Delta\underline{\sigma}_{ep} \qquad (6.130)$$

The above equation represents the difference between the non-corrected and the corrected stress increments.

6.7.3 Boundary Integral Equations for Strain Components:

The boundary integral equations for strain components can be generated by differentiating equations (6.123) and (6.124) with respect to x_i and y_i as follows:

(1) With respect to x_i:

$$C_{11}\frac{\partial u_i}{\partial x_i} + C_{12}\frac{\partial v_i}{\partial x_i} + \oint_\Gamma \left(\frac{\partial F_{11}}{\partial x_i}(u-u_i) + \frac{\partial F_{21}}{\partial x_i}(v-v_i) \right) ds$$

$$- \oint_\Gamma \left(\frac{\partial G_{11}}{\partial x_i} T_x + \frac{\partial G_{21}}{\partial x_i} T_y \right) ds - \iint_\Omega \left(\frac{\partial G_{11}}{\partial x_i} X + \frac{\partial G_{21}}{\partial x_i} Y \right) dx\, dy$$

$$- \iint_\Omega \left(\frac{\partial R^*_{11}}{\partial x_i} \sigma^p_x + \frac{\partial R^*_{21}}{\partial x_i} \sigma^p_y + \frac{\partial R^*_{31}}{\partial x_i} \tau^p_{xy} \right) dx\, dy = 0 \qquad (6.131)$$

$$C_{21}\frac{\partial u_i}{\partial x_i} + C_{22}\frac{\partial v_i}{\partial x_i} + \oint_\Gamma \left(\frac{\partial F_{12}}{\partial x_i}(u-u_i) + \frac{\partial F_{22}}{\partial x_i}(v-v_i) \right) ds$$

$$- \oint_\Gamma \left(\frac{\partial G_{12}}{\partial x_i} T_x + \frac{\partial G_{22}}{\partial x_i} T_y \right) ds - \iint_\Omega \left(\frac{\partial G_{12}}{\partial x_i} X + \frac{\partial G_{22}}{\partial x_i} Y \right) dx\, dy$$

$$- \iint_\Omega \left(\frac{\partial R^*_{12}}{\partial x_i} \sigma^p_x + \frac{\partial R^*_{22}}{\partial x_i} \sigma^p_y + \frac{\partial R^*_{32}}{\partial x_i} \tau^p_{xy} \right) dx\, dy = 0 \qquad (6.132)$$

(2) With respect to y_i:

$$C_{11}\frac{\partial u_i}{\partial y_i} + C_{12}\frac{\partial v_i}{\partial y_i} + \oint_\Gamma \left[\frac{\partial F_{11}}{\partial y_i}(u-u_i) + \frac{\partial F_{21}}{\partial y_i}(v-v_i) \right] ds$$

$$- \oint_\Gamma \left[\frac{\partial G_{11}}{\partial y_i} T_x + \frac{\partial G_{21}}{\partial y_i} T_y \right] ds - \iint_\Omega \left[\frac{\partial G_{11}}{\partial y_i} X + \frac{\partial G_{21}}{\partial y_i} Y \right] dx\, dy$$

$$- \iint_\Omega \left[\frac{\partial R^*_{11}}{\partial y_i} \sigma^p_x + \frac{\partial R^*_{21}}{\partial y_i} \sigma^p_y + \frac{\partial R^*_{31}}{\partial y_i} \tau^p_{xy} \right] dx\, dy = 0 \qquad (6.133)$$

$$C_{21}\frac{\partial u_i}{\partial y_i} + C_{22}\frac{\partial v_i}{\partial y_i} + \oint_\Gamma \left[\frac{\partial F_{12}}{\partial y_i}(u-u_i) + \frac{\partial F_{22}}{\partial y_i}(v-v_i) \right] ds$$

$$- \oint_\Gamma \left[\frac{\partial G_{12}}{\partial y_i} T_x + \frac{\partial G_{22}}{\partial y_i} T_y \right] ds - \iint_\Omega \left[\frac{\partial G_{12}}{\partial y_i} X + \frac{\partial G_{22}}{\partial y_i} Y \right] dx\, dy$$

$$- \iint_\Omega \left[\frac{\partial R^*_{12}}{\partial y_i} \sigma^p_x + \frac{\partial R^*_{22}}{\partial y_i} \sigma^p_y + \frac{\partial R^*_{32}}{\partial y_i} \tau^p_{xy} \right] dx\, dy = 0 \qquad (6.134)$$

Now, the above equations can be rewritten as follows:

$$C_{11}\frac{\partial u_i}{\partial x_i} + C_{12}\frac{\partial v_i}{\partial x_i} = \aleph_1 \quad , \quad C_{21}\frac{\partial u_i}{\partial x_i} + C_{22}\frac{\partial v_i}{\partial x_i} = \aleph_2$$

$$C_{11}\frac{\partial u_i}{\partial y_i} + C_{12}\frac{\partial v_i}{\partial y_i} = \aleph_3 \quad , \quad C_{21}\frac{\partial u_i}{\partial y_i} + C_{22}\frac{\partial v_i}{\partial y_i} = \aleph_4 \qquad (6.135)$$

where, the parameters $\aleph_1, \aleph_2, \ldots$, can be defined as follows:

$$\gamma_\alpha = -\oint_\Gamma \left[L_{\alpha 1}\,(u-u_i) + L_{\alpha 2}\,(v-v_i) \right] ds$$

$$+ \oint_\Gamma \left[Q_{\alpha 1}\,T_x + Q_{\alpha 2}\,T_y \right] ds + \iint_\Omega \left[Q_{\alpha 1}\,X + Q_{\alpha 2}\,Y \right] dx\,dy$$

$$+ \iint_\Omega \left[S_{\alpha 1}\,\sigma_x^p + S_{\alpha 2}\,\sigma_y^p + S_{\alpha 3}\,\tau_{xy}^p \right] dx\,dy \qquad (6.136)$$

and $\alpha = 1, 2, 3, 4$.

Therefore, from equations (6.135) it can be deduced that:

$$\frac{\partial u_i}{\partial x_i} = (\gamma_1 C_{22} - \gamma_2 C_{12}) / (C_{11} C_{22} - C_{12} C_{21})$$

$$\frac{\partial v_i}{\partial x_i} = (\gamma_2 C_{11} - \gamma_1 C_{21}) / (C_{11} C_{22} - C_{12} C_{21}) \qquad (6.137)$$

Similarly,

$$\frac{\partial u_i}{\partial y_i} = (\gamma_3 C_{22} - \gamma_4 C_{12}) / (C_{11} C_{22} - C_{12} C_{21})$$

$$\frac{\partial v_i}{\partial y_i} = (\gamma_4 C_{11} - \gamma_3 C_{21}) / (C_{11} C_{22} - C_{12} C_{21}) \qquad (6.138)$$

6.7.4 Evaluation of Strain and Stress Increments:

The incremental Boundary integral equation of strain can be written by defining $\Delta\gamma_\alpha$ such that:

$$\Delta\gamma_\alpha = -\oint_\Gamma \left[L_{\alpha 1}\Delta(u-u_i) + L_{\alpha 2}\,\Delta(v-v_i) \right] ds$$

$$+ \oint_\Gamma \left[Q_{\alpha 1}\,\Delta T_x + Q_{\alpha 2}\,\Delta T_y \right] ds + \iint_\Omega \left[Q_{\alpha 1}\,\Delta X + Q_{\alpha 2}\,\Delta Y \right] dx\,dy$$

$$+ \iint_\Omega \left[S_{\alpha 1}\,\Delta\sigma_x^p + S_{\alpha 2}\,\Delta\sigma_y^p + S_{\alpha 3}\,\Delta\tau_{xy}^p \right] dx\,dy \qquad (6.139)$$

Then the incremental equations of strains can be deduced as follows:

$$\begin{aligned} C_{11}\ \Delta U_x + C_{12}\ \Delta V_x &= \Delta \aleph_1 \\ C_{21}\ \Delta U_x + C_{22}\ \Delta V_x &= \Delta \aleph_2 \end{aligned} \qquad (6.140)$$

$$\begin{aligned} C_{11}\ \Delta U_y + C_{12}\ \Delta V_y &= \Delta \aleph_3 \\ C_{21}\ \Delta U_y + C_{22}\ \Delta V_y &= \Delta \aleph_4 \end{aligned}$$

where,

$$U_x = \frac{\partial u}{\partial x} \quad , \quad U_y = \frac{\partial u}{\partial y}$$

$$V_x = \frac{\partial v}{\partial x} \quad , \quad V_y = \frac{\partial v}{\partial y}$$

Now, the increments of strain can be obtained as follows:

$$\begin{aligned} \Delta \varepsilon_x &= \Delta U_x \\ \Delta \varepsilon_y &= \Delta V_y \\ \Delta \gamma_{xy} &= \Delta U_y + \Delta V_x \end{aligned} \qquad (6.141)$$

For elasto-plastic analysis, the increments of stress can be expressed in terms of strain increments as follows:

$$\Delta \underline{\sigma} = \Delta \underline{\sigma}_{ep} = \underline{D}\ \Delta \underline{\varepsilon} - \Delta \underline{\sigma}^p \qquad (6.142)$$

where,

$$\Delta \underline{\sigma} = \{\ \Delta \sigma_x \quad \Delta \sigma_y \quad \Delta \tau_{xy}\ \}$$

and in terms of displacement increments as follows:

$$\begin{aligned} \Delta \sigma_x &= \left[\ d_{11} \frac{\partial \Delta u}{\partial x} + d_{12} \frac{\partial \Delta v}{\partial y}\ \right] - \Delta \sigma_x^p \\ \Delta \sigma_y &= \left[\ d_{21} \frac{\partial \Delta u}{\partial x} + d_{22} \frac{\partial \Delta v}{\partial y}\ \right] - \Delta \sigma_y^p \\ \Delta \tau_{xy} &= d_{33} \left[\ \frac{\partial \Delta u}{\partial y} + \frac{\partial \Delta v}{\partial x}\ \right] - \Delta \tau_{xy}^p \end{aligned} \qquad (6.143)$$

Then the corresponding traction increments can be written as follows:

$$\Delta T_x = \ell \left[d_{11} \Delta U_x + d_{12} \Delta V_y \right] + m\, d_{33} (\Delta U_y + \Delta V_x) - \Delta T_x^P \qquad (6.144)$$

$$\Delta T_y = m \left[d_{21} \Delta U_x + d_{22} \Delta V_y \right] + \ell\, d_{33} (\Delta U_y + \Delta V_x) - \Delta T_y^P$$

where,

$$\ell = \frac{\partial y}{\partial \xi} \Big/ |\underline{J}| \quad , \quad m = - \frac{\partial x}{\partial \xi} \Big/ |\underline{J}|$$

and

$$\Delta T_x^P = \ell\, \Delta \sigma_x^P + m\, \Delta \tau_{xy}^P$$

$$\Delta T_y^P = \ell\, \Delta \tau_{xy}^P + m\, \Delta \sigma_y^P$$

Now, equations (6.144) can be used to form a system of equations similar to that given by equation (6.113), i.e.

$$\underline{A}\ \underline{x} = \underline{y} \qquad (6.145)$$

where $\underline{A}$ and $\underline{x}$ are as defined before, and $\underline{y}$ may be defined as follows:

$$\underline{y} = \left\{ \frac{\partial u}{\partial \xi} \Big/ |\underline{J}| \quad \frac{\partial v}{\partial \xi} \Big/ |\underline{J}| \quad \Delta T_x / E \quad \Delta T_y / E \right\} \qquad (6.146)$$

The solution of the above system of equations involves the use of Gauss elimination solver with a partial pivoting procedure, that due to the zeros in the leading diagonal of matrix $\underline{A}$.

6.7.5 Numerical Integration over N-Node Elements:

(a) Numerical Integration over an N-Node Cell Element:

Consider an integration term as follows:

$$C_o = \iint_{\Omega} \left[f(x-x_i, y-y_i) * p(x,y) \right] dx\, dy \qquad (6.147)$$

where,

$f(x-x_i, y-y_i)$ = A fundamental solution parameter with respect to a source point (x_i, y_i).

$p(x,y)$ = The value of one of the field function parameters *(stress, strain, etc.)*.

Now, for an n-node cell element, as shown in Fig.(6.12-a), the isoparametric interpolation can be employed such that:

$$p(x,y) = \sum_{j=1}^{n} p_j \, N_j(\xi,\eta) \qquad (6.148)$$

where $N_j(\xi,\eta)$ are the shape functions of the corresponding n-node cell element *(finite element)* as given in Appendix [B].

Therefore, the integration in equation (6.147) can be written for the e^{th} element as follows:

$$C_o = \int_0^1 \int_0^{\phi} \left[f\,[x(\xi,\eta)-x_i, y(\xi,\eta)-y_i)] * \sum_{j=1}^{n} p_j \, N_j(\xi,\eta) \right] |\underline{J}| \, d\xi \, d\eta \qquad .....(6.149)$$

where,

ϕ = 1 *for quadrilateral elements,*

= $1-\eta$ *for triangular elements.*

$$|\underline{J}| = \left| \underline{J} \left(\frac{x,y}{\xi,\eta} \right) \right|$$

The numerical evaluation of the above equation can be carried out in a way similar to that used for the finite element method by means of Gaussian quadrature technique.

(b) *Numerical Integration over an N-Node Boundary Element:*

Consider the term,

$$B_e = \int_{\Gamma_e} \left[f(x-x_i, y-y_i) * p(x,y) \right] ds \qquad (6.150)$$

For an n-node isoparametric boundary element, as shown in Fig.(6.12-b), the value of the field function p can be interpolated at point (x,y) as follows:

$$p(x,y) \simeq \sum_{j=1}^{n} p_j \, N_j(\xi) \qquad (6.151)$$

where $N_j(\xi)$ are the shape functions as given by equation (6.3).

Hence, equation (6.150) can now be written as:

$$B_e = \sum_{j=1}^{n} p_j \left\{ \int_0^1 f\,[x(\xi)-x_i, y(\xi)-y_i] * N_j(\xi) \, |\underline{J}| \, d\xi \right\} \qquad (6.152)$$

where,

$$|\underline{J}| = \sqrt{\left(\frac{dx}{d\xi}\right)^2 + \left(\frac{dy}{d\xi}\right)^2}$$

Similarly, the above integration can be evaluated by means of Gaussian quadrature technique.

6.7.6 Solution Algorithm:

The solution algorithm for two-dimensional elasto-plastic boundary element method can be summarized in the following steps.

Step (1): **Initial Calculations.**

The boundary element procedure of elasto-plastic problems starts always with an elastic solution, and matrices like $\underline{H}$, $\underline{G}$, $\underline{A}$, and $\underline{B}$ will be the same throughout the elasto-plastic iterations. To save *CPU* time, these matrices will be calculated once and saved before the start of the load increments.

Step (2): **New Load Increment.**

The initial traction vector $\underline{P}_i$ will be prescribed, so that any new load increment is defined as a ratio of the original vector, i.e.

$$\Delta\underline{P} = \textit{Ratio} \times \underline{P}_i$$

Then the following can be defined:

$$\Delta\underline{Y} = \underline{B}\ \Delta\underline{P}$$

Also at the start of a load increment, the displacement vector $\Delta\underline{u}$ is assumed to be zero, i.e.

$$\Delta\underline{u} = \underline{0}$$

Step (3): **Elastic Solution.**

To define the initial displacement and traction increment vectors $\Delta\underline{\delta}_o$ and $\Delta\underline{T}_o$, the following system of equations should be solved:

$$\underline{A}\ \Delta\underline{X} = \Delta\underline{Y}$$

where $\Delta\underline{X}$ represents a vector of the unknown values.

Step (4): **Results at Integration Cells.**

The domain inside the boundary element will be discritized into a number of integration cells, the extent of the cells need only to cover the area of expected plasticity, but could and normally does cover part or all of the boundary. Each cell is defined in terms of an n-node finite element, the nodes of the cell are defined depending on their position in the domain, i.e. either "*internal node*" or "*boundary node*". Then for each node the vectors $\Delta\underline{u}$, $\Delta\underline{\varepsilon}$, and $\Delta\underline{\sigma}$ should be calculated as follows:

(a) *For Boundary Nodes:*

The above vectors can be calculated using the incremental equations given in section (6.7.4).

(b) *For Internal Nodes:*

The above displacement vectors can be calculated using the boundary integral equations given in section (6.7.2), then the strain and stress vectors can be calculated using either the boundary integral equations for strain increments as given in section (6.7.3) or the finite difference scheme described in section (6.6.5).

Step (5): **Elasto-Plastic Stress Correction.**

By knowing $\Delta\underline{\sigma}'$, $\Delta\underline{\varepsilon}$, $\underline{\sigma}_o$, and $\underline{\varepsilon}_o$ at every internal and boundary node, and using an algorithm similar to that described in steps

(4) and (5) from section (5.4.3-c), a corrected stress vector $\underline{\sigma}$ can be obtained. Hence,

$$\Delta\underline{\sigma}^{p} = \Delta\underline{\sigma}' - \Delta\underline{\sigma}$$

where,

$$\Delta\underline{\sigma} = \underline{D}_{ep}\ \Delta\underline{\varepsilon}$$

Now, if $\Delta\underline{\sigma}^{p}$ is negligible then a new load increment can be applied, and calculations from step (2) in this section are to be repeated.

Step (6): **Elasto-Plastic Iteration.**

The steps of the elasto-plastic iteration can be outlined as follows:

(a) Consider $\Delta\underline{P} = \underline{0}$, and but $\Delta\underline{y} = \Delta\underline{u}$, where $\Delta\underline{u}$ is now calculated in terms of the newly evaluated $\Delta\underline{\sigma}^{p}$.

(b) Solve the system of equations $\underline{A}\ \Delta\underline{x} = \Delta\underline{y}$ to define the additional correction vectors $\Delta\underline{\delta}_{1}$, $\Delta\underline{T}_{1}$, which should be added to $\Delta\underline{\delta}_{o}$, $\Delta\underline{T}_{o}$ respectively.

(c) Due to $\Delta\underline{\delta}_{1}$, $\Delta\underline{T}_{1}$ find the corresponding $\Delta\underline{\varepsilon}_{1}$, and $\Delta\underline{\sigma}'_{1}$. Then calculate $\Delta\underline{\sigma}^{p}$.

(d) Carry on the iterations until, one of the following conditions is encountered:

i. $$\sqrt{\frac{\Delta\underline{\delta}^{t}.\Delta\underline{\delta}}{\underline{\delta}^{t}.\underline{\delta}}} \leq \textit{a permissible error.}$$

ii. $\sqrt{\dfrac{\Delta\underline{T}^t.\Delta\underline{T}}{\underline{T}^t.\underline{T}}} \leq$ *a permissible error.*

iii. Divergence, where the displacement or traction vector ratios begin to increase numerically instead of decrease.

iv. Vibratory Divergence, where the displacement or traction vector ratios failing to reach prescribed values within a given number of iterations

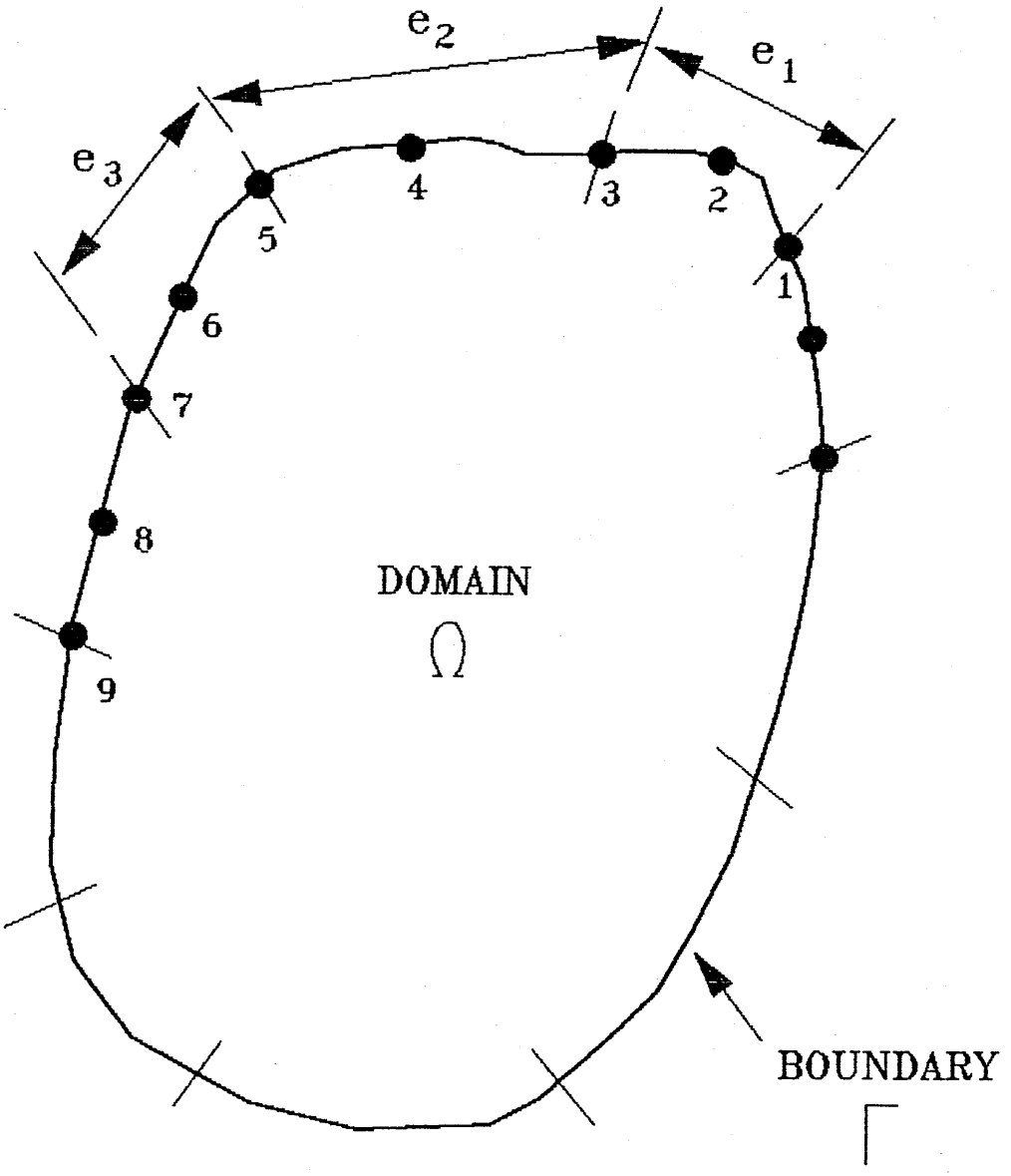

Fig.(6.1) Discretization of the Boundary.

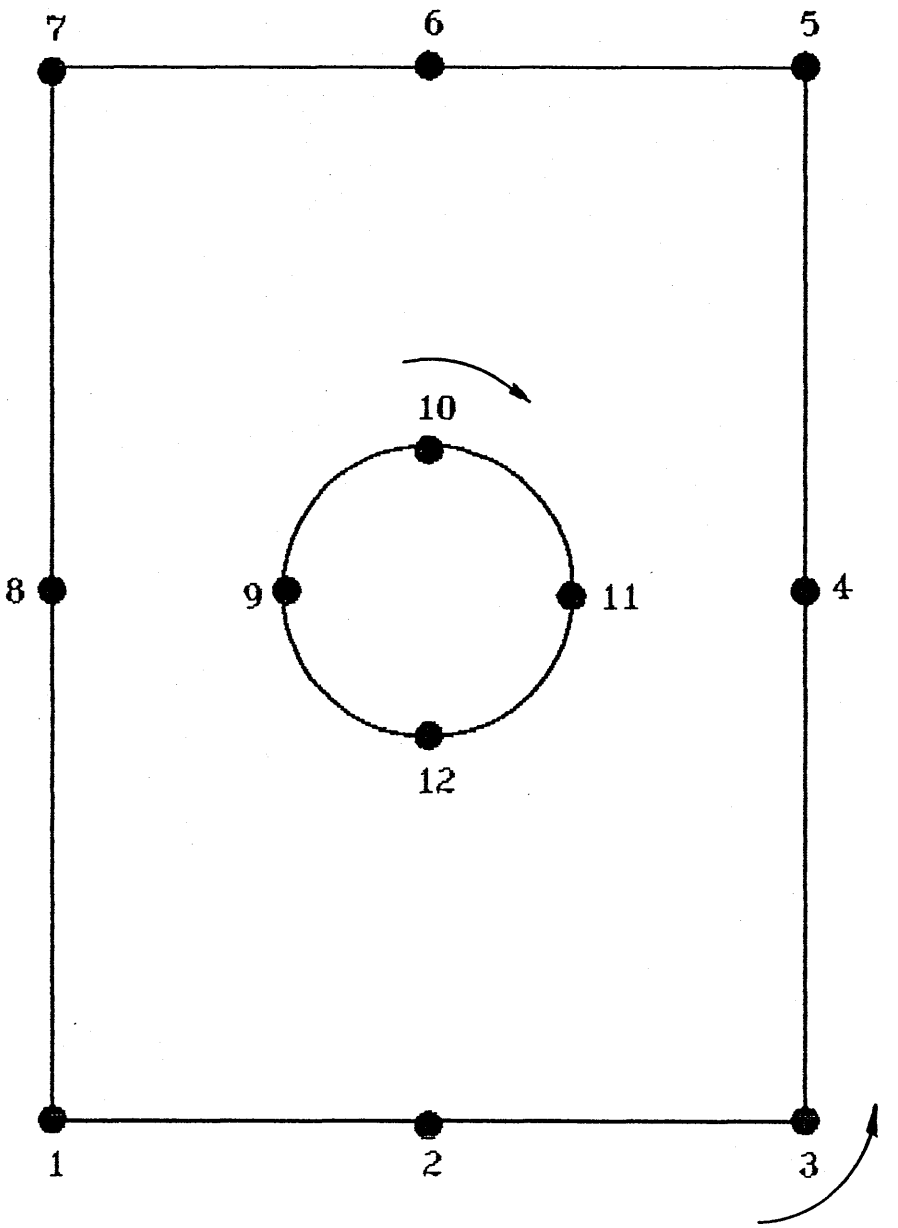

Fig.(6.2) Discretization of Problem with Internal Boundary.

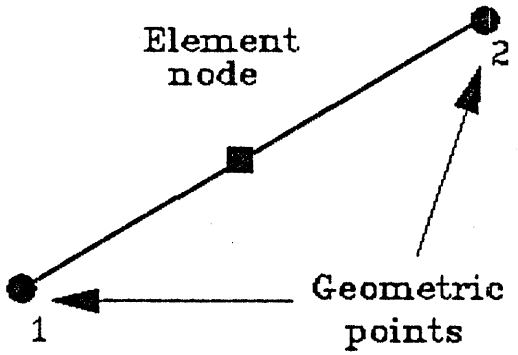

a) Constant Element.

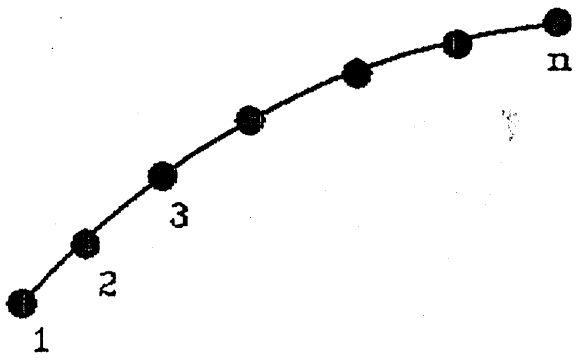

b) General Element.

Fig.(6.3) Family of Standard Boundary Elements.

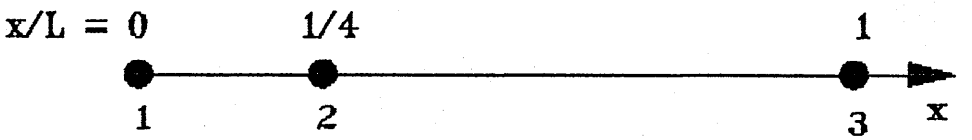

a) 3–Node Singular Element.

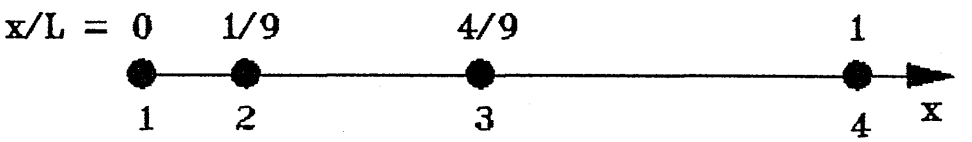

b) 4–Node Singular Element.

c) $1/\sqrt{2}$ Singular Element.

Fig.(6.4) Family of Crack–Tip Boundary Elements.

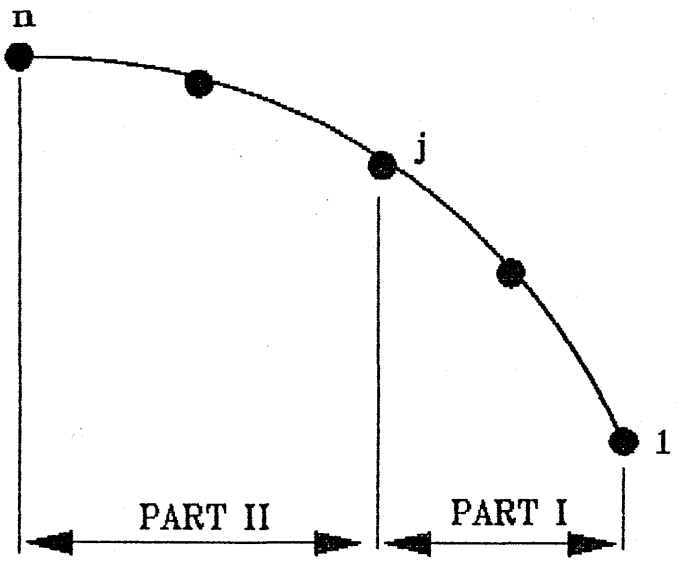

Fig.(6.5) The Two Parts of An Element Essential to the Application of the Singular Integral.

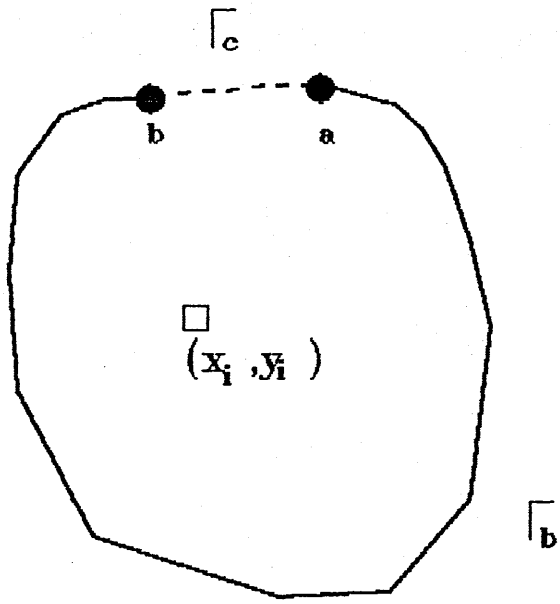

Fig.(6.6) Boundary with a Corner Node.

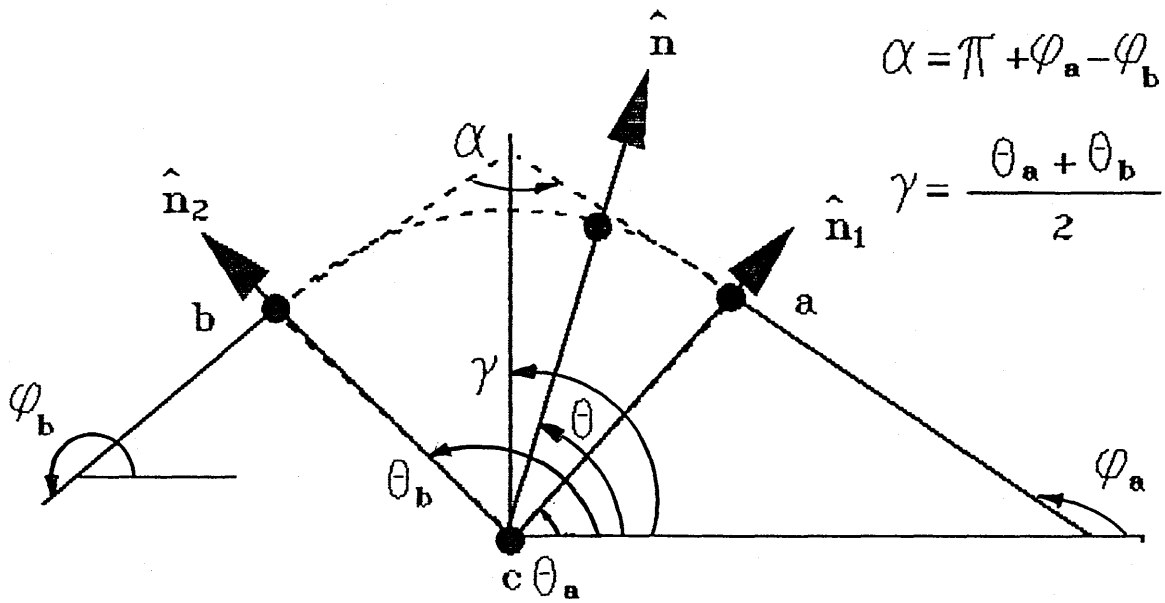

Fig.(6.7) Smooth Corner Model.

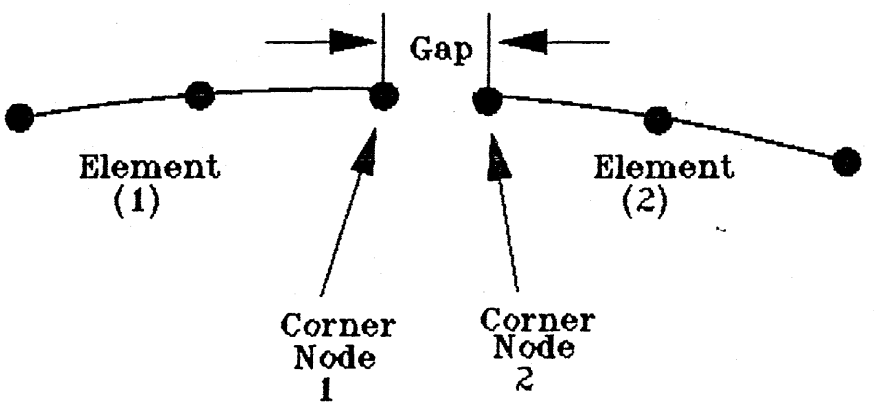

Fig.(6.8) Double Noding for a Corner.

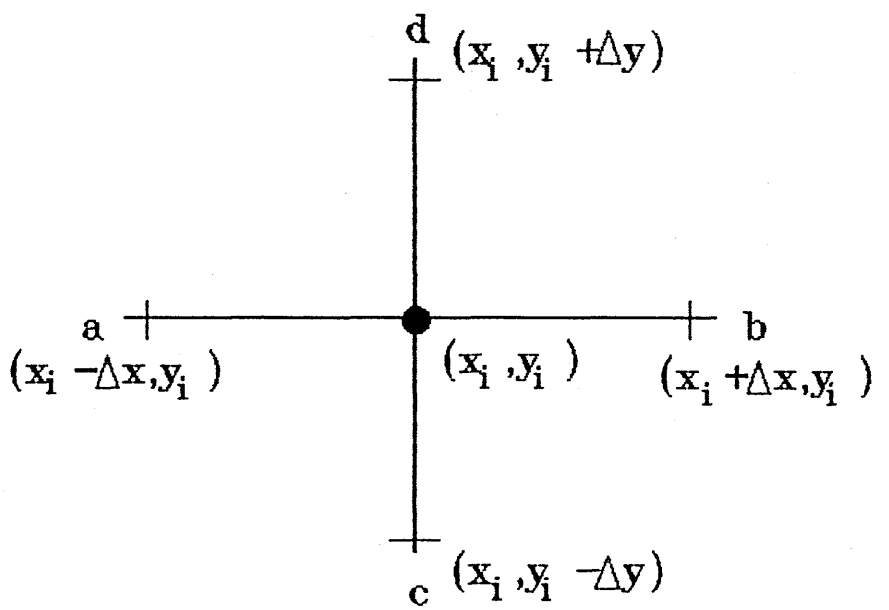

Fig.(6.9) Finite-Difference Points of a Source Point.

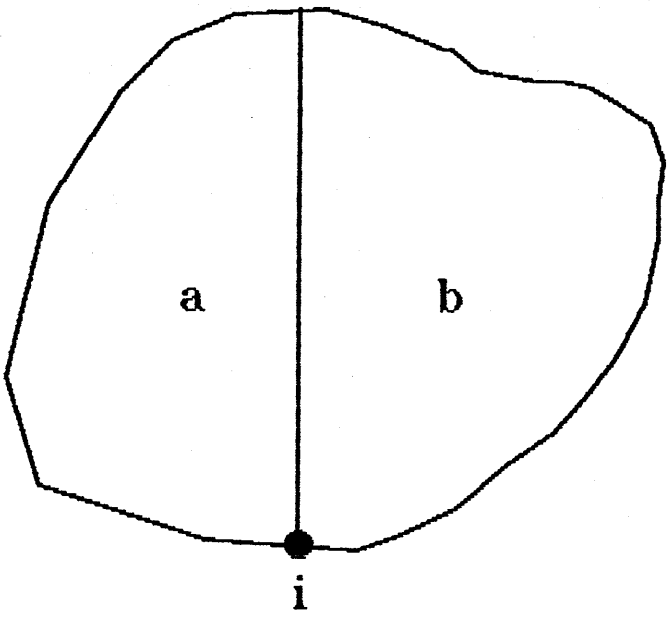

Fig.(6.10) Structure with Two Subregions.

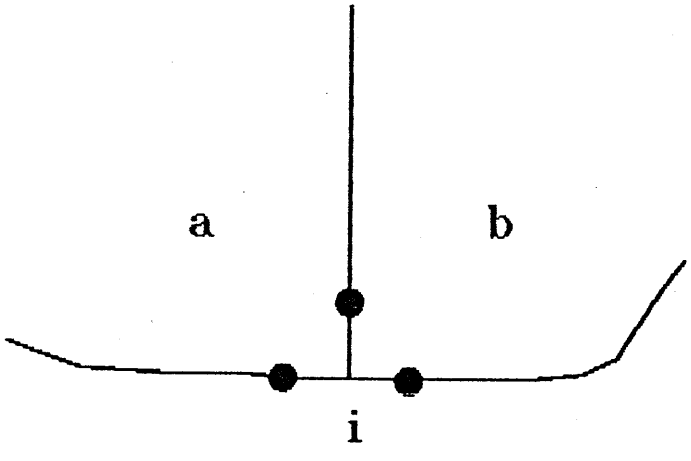

Fig.(6.11) Multiple Nodes at Interface.

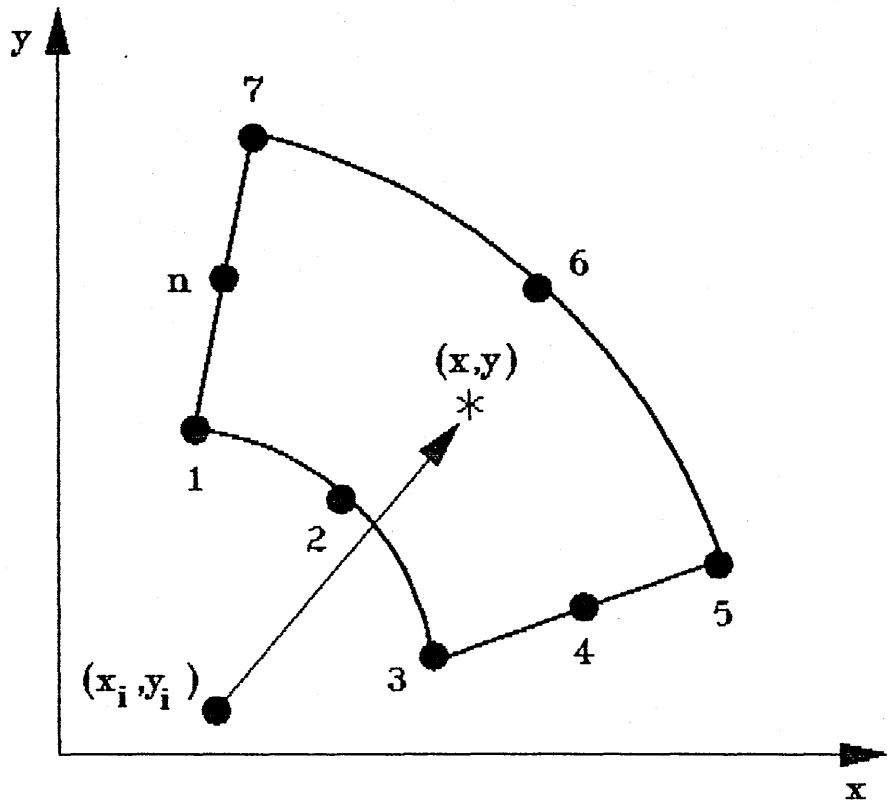

a) N-Node Cell Element.

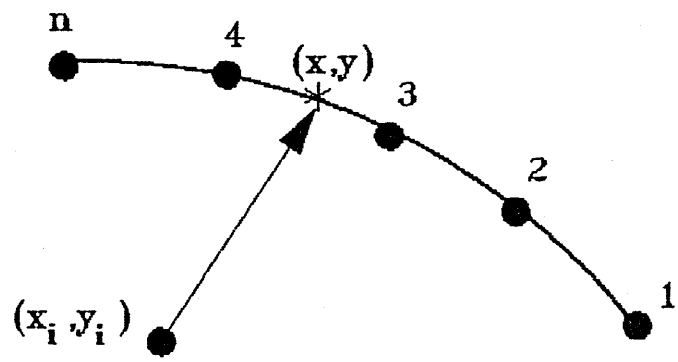

b) N-Node Boundary Element.

Fig.(6.12) N-Node Cell and Boundary Elements.

CHAPTER 7

THE APPLICATIONS OF FEM & BEM IN FRACTURE MECHANICS

7.1 Introduction:

The ability of the finite element and the boundary element methods in providing numerical solutions for some field parameters like displacement, stress, and strain nearly at any point inside or on the boundary of a problem can be very useful for the evaluation of fracture mechanics parameters such as stress intensity factors, crack opening displacements, and *J*-integrals.

To make use of the finite and boundary element solutions in fracture mechanics, several techniques have been developed and employed in this work. Some of these techniques are summarized in the following sections.

7.2 Extrapolation Methods of Stress Intensity Factors:

The extrapolation methods fall into two categories each one associated with the field parameter used for the calculation of the stress intensity factor. These categories are as follows:

7.2.1 Displacement Extrapolation Method:

Considering only the tensile *mode I*, where the crack plane is the plane of symmetry, the analytical expressions for the displacement variation along the radial line emanating from the crack tip can be written, for both plane-stress and plane-strain conditions, as follows:

$$u = \left(\frac{K_I}{4\mu}\right)\left(\frac{r}{2\pi}\right)^{1/2}\left[(2k-1)\cos\left(\frac{\theta}{2}\right) - \cos\left(\frac{3\theta}{2}\right)\right]$$

$$v = \left(\frac{K_I}{4\mu}\right)\left(\frac{r}{2\pi}\right)^{1/2}\left[(2k+1)\sin\left(\frac{\theta}{2}\right) - \sin\left(\frac{3\theta}{2}\right)\right] \qquad (7.1)$$

where,

$$\mu = E/2(1+\nu)$$

$$\kappa = \begin{cases} (3-\nu)/(1+\nu) & \textit{for plane stress,} \\ (3-4\nu) & \textit{for plane strain.} \end{cases}$$

For the purpose of numerical evaluation, a modified parameter K_I^* can be defined as a function of the crack-tip coordinates r, and θ. Consider the finite element mesh given in Fig.(7.1), and using equations (7.1), this parameter can be written as follows:

$$K_I^*(r_i,\theta) = 4\ \mu\ u_i \left[\frac{2\pi}{r_i} \right]^{1/2} / \left[(2\kappa-1) \cos\left[\frac{\theta}{2} \right] - \cos\left[\frac{3\theta}{2} \right] \right]$$

or (7.2)

$$K_I^*(r_i,\theta) = 4\ \mu\ v_i \left[\frac{2\pi}{r_i} \right]^{1/2} / \left[(2\kappa+1) \sin\left[\frac{\theta}{2} \right] - \sin\left[\frac{3\theta}{2} \right] \right]$$

where,

r_i = Nodal radius from the crack tip,
u_i, v_i = Nodal displacements,
i = Node number.

By substituting the nodal point displacement u or v at some nodes on the plane where θ has a constant value between 0° and 180°, and the corresponding radial distance r in the suitable equation, the quantity K_I^* can be calculated at each node and plotted against the radial distance r, as shown in Fig.(7.2).

With suitable refinement of element size the K_I^* curve obtained approaches a constant slope at a point close to the crack tip. The intersection of the tangent to the constant slope position on the curve with the K_I^* axis will define the K_I stress intensity factor. i.e.

$$K_I = \lim_{r \to 0} K_I^*(r_i,\theta) \qquad (7.3)$$

7.2.2 Stress Extrapolation Method:

The stress method for determining crack-tip stress intensity factor is similar to the displacement method.

Equations (3.41-3.43) can be written for *mode I* loading conditions, in a general form, as follows:

$$\sigma_{ij} = \frac{K_I}{\sqrt{2\pi r}} f_{ij}(\theta) \qquad (7.4)$$

where,

i ≡ x, y.

j ≡ x, y.

$$f_{xx}(\theta) = \cos\left(\frac{\theta}{2}\right)\left[1 - \sin\left(\frac{\theta}{2}\right)\sin\left(\frac{3\theta}{2}\right)\right]$$

$$f_{yy}(\theta) = \cos\left(\frac{\theta}{2}\right)\left[1 + \sin\left(\frac{\theta}{2}\right)\sin\left(\frac{3\theta}{2}\right)\right]$$

$$f_{xy}(\theta) = \cos\left(\frac{\theta}{2}\right)\sin\left(\frac{\theta}{2}\right)\sin\left(\frac{3\theta}{2}\right)$$

Now, the K_I^* parameter can be defined as follows:

$$K_I^*(r_k,\theta) = \sqrt{2\pi r_k}\ (\sigma_{ij})_k \ / \ f_{ij}(\theta) \qquad (7.5)$$

where,

$(\sigma_{ij})_k$ = Nodal stresses,

k = Node Number.

Similar to the displacement method, nodal point stress σ_{xx} or σ_{yy} or τ_{xy} can be substituted into equation (7.5) with a suitable $f_{ij}(\theta)$ function to calculate and plot the parameter K_I^*. Then K_I can be estimated from the K_I^* curve in the same way as explained before.

For the case of an oblique crack, both *mode I* and *mode II* loading conditions should be considered. In this case the stress intensity factors K_I and K_{II} can be calculated using the extrapolation methods by solving a system of two simultaneous equations generated from equations (3.41-3.45) by using combinations of two stress or displacement distributions along the line of the crack or any other line with specified crack angle θ.

7.3 Extrapolation Curve-Fitting Technique:

An alternative approach to the graphical extrapolation, described above, is to use an analytical curve fitting for extrapolation. A special extrapolation curve-fitting procedure has been developed in this work to evaluate stress intensity factors as well as crack opening displacements. This technique can be summarized as follows:

Consider a polynomial equation as follows:

$$y(x) = a_1 \phi_1(x) + a_2 \phi_2(x) + a_3 \phi_3(x) + a_n \phi_n(x) \qquad (7.6)$$

where $\phi_i(x)$ can be defined as $\phi_i(x) = x^{i-1}$, $\phi_i(x) = (\log x)^{i-1}$, etc.

Now, for a set of points such as (x_k,y_k), k = 1, 2, ..., m. The above equation can be written as follows:

$$y(x_k) = \sum_{j=1}^{n} a_j \phi_j(x_k) \qquad (7.7)$$

The absolute error ε_k at point (x_k,y_k) can be defined as follows:

$$\varepsilon_k = y(x_k) - y_k = \left[\sum_{j=1}^{n} a_j \phi_j(x_k) \right] - y_k \qquad (7.8)$$

Now, by employing the least-square method, it can be written that:

$$\sum_{k=1}^{m} \varepsilon_k^2 = minimum \qquad (7.9)$$

From the above equation, a functional $\chi(a_1,a_2,...)$ can be defined as follows:

$$\chi = \sum_{k=1}^{m} \varepsilon_k^2$$

i.e.

$$\chi(a_1,a_2,...) = \sum_{k=1}^{m} \left[\sum_{j=1}^{n} a_j \phi_j(x_k) - y_k \right]^2 = min. \qquad (7.10)$$

from which, it can be deduced that $\partial\chi/\partial a_i = 0$. i.e.

$$\sum_{k=1}^{m} \varepsilon_k \left(\frac{\partial \varepsilon_k}{\partial a_i} \right) = 0 \qquad (7.11)$$

Since:

$$\frac{\partial \varepsilon_k}{\partial a_i} = \phi_i(x_k) \qquad (7.12)$$

then, from equations (7.8), (7.11), and (7.12) it can be shown that:

$$\sum_{k=1}^{m} \phi_i(x_k) \left[\sum_{j=1}^{n} a_j \phi_j(x_k) - y_k \right] = 0 \qquad (7.13)$$

Now, the above equation can be rearranged as follows:

$$\sum_{j=1}^{n} a_j \left[\sum_{k=1}^{m} \phi_i(x_k)\ \phi_j(x_k) \right] = \sum_{k=1}^{m} \phi_i(x_k)\ y_k \qquad (7.14)$$

Hence, from equation (7.14), the following parameters can be defined:

$$C_{ij} = \sum_{k=1}^{m} \phi_i(x_k)\ \phi_j(x_k) \qquad (7.15)$$

$$b_i = \sum_{k=1}^{m} \phi_i(x_k)\ y_k \qquad (7.16)$$

where $C_{ji} = C_{ij}$, and i = 1, 2, 3,..., n.

Thus, equation (7.14) can be rewritten as follows:

$$\sum_{j=1}^{n} C_{ij}\ a_j = b_i \ , \ i = 1, 2,\ldots,n \qquad (7.17)$$

and in matrix form as:

$$\underline{C}_{nxn}\ \underline{a}_{nx1} = \underline{b}_{nx1} \qquad (7.18)$$

Solving the above system of equations will provide the coefficients a_1, a_2,...., a_n.

Hence, the intersection of y(x) with the y-axis can be obtained as follows:

$$y(0) = \lim_{x \to 0} \left[\sum_{j=1}^{n} a_j\ \phi_j(x) \right]$$

and for the case of algebraic polynomial:

$$y(0) = a_1 \qquad (7.19)$$

An alternative method to the absolute error approach is to use the relative error, where the following parameter is defined:

$$\bar{\varepsilon}_k = \frac{y(x_k) - y_k}{y_k} \; ; \quad y_k \neq 0 \tag{7.20}$$

and the functional to be minimized is:

$$\bar{\chi} = \sum_{k=1}^{m} \bar{\varepsilon}_k^2$$

from which, the equations parameters can be deduced as follows:

$$\bar{C}_{ij} = C_{ij} \; / \; y_k^2 \tag{7.21}$$

$$\bar{b}_i = b_i \; / \; y_k^2 \tag{7.22}$$

Using the curve fitting procedure explained above, the stress intensity factor can be calculated as follows:

(i) Calculate $K_I^*(r_k,\theta)$ for a given set of r_k, as shown in section (7.2).

(ii) Let $y(x_k) \equiv K_I^*(r_k,\theta)$ and $x_k \equiv r_k$.

(iii) Follow the procedure given above to generate the system of equations given by equation (7.18).

(iv) Solve the generated system of equations by means of Gauss elimination solver, to obtain the coefficients $a_1, \; a_2, \ldots\ldots, \; a_n$.

(v) Finally, substitute the above coefficients into equation (7.6). It is clear from this equation and equation (7.19) that the stress intensity factor at the crack tip can be obtained by putting x = 0. i.e. for an algebraic polynomial $K_I = a_1$.

Similarly, the crack opening displacement can be evaluated by using the model given in Fig.(7.3) as follows:

(i) Evaluate Δv_k for a given set of r_k on the surface of the crack as shown in Fig.(7.3).

(ii) Let $y(x_k) \equiv \Delta v_k$ and $x_k \equiv r_k$.

(iii) Generate and solve the system of equations given by equation (7.18).

(iv) Finally, the crack-tip opening displacement $\delta = 2\ a_1$.

7.4 Numerical Evaluation of the J-Integral:

For the special case of linear-elastic fracture mechanics, the J-integral expression can be written, in the absence of domain loading, as follows:

$$J = \int_{\Gamma_o} \left[W\ dy - \underline{T}^t \frac{\partial \underline{u}}{\partial x}\ ds \right] \qquad (7.23)$$

Using the finite element method or the boundary element method to obtain field parameters such as displacements, stresses, and strains, equation (7.23) can be written in terms of such parameters as follows:

$$J = \int_{\Gamma_o} \left[\frac{1}{2}\ \underline{\sigma}^t\ \underline{\varepsilon}\ dy - \underline{T}^t \frac{\partial \underline{u}}{\partial x}\ ds \right] \qquad (7.24)$$

The numerical evaluation of the above equation can be reviewed in the following subsections.

7.4.1 Piecewise Discretization of Arbitrary Contour:

Consider an arbitrary contour Γ_o around the crack tip. This contour can be divided into n_e sub-contours *(sub-boundaries)* as shown in Fig.(7.4). i.e.

$$\Gamma_o = \sum_{e=1}^{n_e} \Gamma_e \qquad (7.25)$$

Therefore, equation (7.24) can be written as follows:

$$J = \sum_{e=1}^{n_e} \int_{\Gamma_e} \left[\frac{1}{2} \underline{\sigma}^t \underline{\varepsilon} \, dy - \underline{T}^t \frac{\partial \underline{u}}{\partial x} \, ds \right] \qquad (7.26)$$

A parameter J_e can be defined such that:

$$J = \sum_{e=1}^{n_e} J_e \qquad (7.27)$$

where,

$$J_e = \int_{\Gamma_e} \left[\frac{1}{2} \underline{\sigma}^t \underline{\varepsilon} \, dy - \underline{T}^t \frac{\partial \underline{u}}{\partial x} \, ds \right] \qquad (7.28)$$

7.4.2 Characteristics of N-Node Boundary Element:

To evaluate the J_e term numerically, an n-node isoparametric boundary element is employed as a contour element, on the same sub-contour within the x-y plane, as shown in Fig.(7.5). The element may be transformed into a straight line of unit length in the ξ-line, and the parametric equations of the element can, therefore, be expressed as follows:

$$x(\xi) = \sum_{i=1}^{n} x_i \, \mathcal{L}_i^n(\xi)$$

$$y(\xi) = \sum_{i=1}^{n} y_i \, \mathcal{L}_i^n(\xi) \qquad (7.29)$$

For the special case of $\xi_i = (i-1)/(n-1)$, it can be shown that:

$$\mathcal{L}_i^n(\xi) = \prod_{\substack{r=1 \\ r \neq i}} \left[\frac{(n-1)\,\xi - (r-1)}{i - r} \right] \qquad (7.30)$$

Hence, it can be proved that:

$$\frac{dx}{d\xi} = \sum_{i=1}^{n} x_i \left[\frac{d\mathcal{L}_i^n(\xi)}{d\xi} \right]$$

$$\frac{dy}{d\xi} = \sum_{i=1}^{n} y_i \left[\frac{d\mathcal{L}_i^n(\xi)}{d\xi} \right] \qquad (7.31)$$

where,

$$\frac{d\mathcal{L}_i^n(\xi)}{d\xi} = \sum_{\substack{s=1 \\ s \neq i}}^{n} \frac{n-1}{i-s} \prod_{\substack{r=1 \\ r \neq i \\ r \neq s}} \left[\frac{(n-1)\,\xi - (r-1)}{i - r} \right] \qquad (7.32)$$

Now, for n-node boundary element it can be shown that:

$$ds = |\underline{J}| \, d\xi \qquad (7.33)$$

or

$$\frac{ds}{d\xi} = |\underline{J}| \qquad (7.34)$$

where,

$$|\underline{J}| = \sqrt{(\frac{dx}{d\xi})^2 + (\frac{dy}{d\xi})^2}$$

and the directional cosines of the outward normal can be defined as follows:

$$\ell = \frac{dy}{d\xi} \Big/ \frac{ds}{d\xi}$$
$$m = -\frac{dx}{d\xi} \Big/ \frac{ds}{d\xi} \qquad (7.35)$$

7.4.3 Evaluation of the Elemental *J*-Integral:

The evaluation of the elemental *J*-integral J_e is not possible unless the values of $\underline{\sigma}$ and/or $\underline{\varepsilon}$, and $\underline{u}$ are given at the boundary nodes of the corresponding e^{th} element.

Let the e^{th} element be an n-node isoparametric element as described before. Using isoparametric interpolation equations, it can be shown that:

$$\underline{\sigma}(\xi) \cong \sum_{i=1}^{n} \underline{\sigma}_i \, \mathcal{L}_i^n(\xi) \qquad (7.36)$$

$$\underline{\varepsilon}(\xi) = \underline{D}^{-1} \, \underline{\sigma}(\xi) \qquad (7.37)$$

If $\underline{\varepsilon}$ is given instead of $\underline{\sigma}$, the following can be written:

$$\underline{\varepsilon}(\xi) \cong \sum_{i=1}^{n} \underline{\varepsilon}_i \, \mathcal{L}_i^n(\xi) \qquad (7.38)$$

$$\underline{\sigma}(\xi) = \underline{D} \, \underline{\varepsilon}(\xi) \qquad (7.39)$$

Similarly, the displacements can be expressed as follows:

$$u(\xi) \cong \sum_{i=1}^{n} u_i \, \mathcal{L}_i^n(\xi)$$

$$v(\xi) \cong \sum_{i=1}^{n} v_i \, \mathcal{L}_i^n(\xi) \qquad (7.40)$$

Then it can be deduced that:

$$\frac{du}{d\xi} \cong \sum_{i=1}^{n} u_i \left[\frac{d\mathcal{L}_i^n(\xi)}{d\xi} \right]$$

$$\frac{dv}{d\xi} \cong \sum_{i=1}^{n} v_i \left[\frac{d\mathcal{L}_i^n(\xi)}{d\xi} \right] \qquad (7.41)$$

If the values of $\sigma_x(\xi)$, $\sigma_y(\xi)$, and $\tau_{xy}(\xi)$ are known at any ξ. Then, the tractions can be defined as follows:

$$T_x(\xi) = \ell \, \sigma_x(\xi) + m \, \tau_{xy}(\xi)$$

$$T_y(\xi) = \ell \, \tau_{xy}(\xi) + m \, \sigma_y(\xi) \qquad (7.42)$$

Now, from the chain rule of partial differentiation:

$$\frac{du}{d\xi} = \frac{\partial u}{\partial x}\frac{dx}{d\xi} + \frac{\partial u}{\partial y}\frac{dy}{d\xi}$$

$$\frac{dv}{d\xi} = \frac{\partial v}{\partial x}\frac{dx}{d\xi} + \frac{\partial v}{\partial y}\frac{dy}{d\xi} \qquad (7.43)$$

i.e.

$$\frac{du}{d\xi} = \varepsilon_x \frac{dx}{d\xi} + \frac{\partial u}{\partial y}\frac{dy}{d\xi} \qquad (7.44)$$

$$\frac{dv}{d\xi} = \frac{\partial v}{\partial x}\frac{dx}{d\xi} + \varepsilon_y \frac{dy}{d\xi} \qquad (7.45)$$

where $\varepsilon_x = \partial u/\partial x$, $\varepsilon_y = \partial v/\partial y$.

The evaluation of the term $\partial v/\partial x$ in equation (7.45) involves the following two conditions:

(a) *If $dx/d\xi \neq o$ ($m \neq o$):*

From equation (7.45), it can be written that:

$$\frac{\partial v}{\partial x} = \left(\frac{dv}{d\xi} - \frac{dy}{d\xi} \varepsilon_y \right) / \frac{dx}{d\xi}$$

Using equations (7.35) it can be deduced that:

$$\frac{\partial v}{\partial x} = \left(\frac{dv}{d\xi} / \frac{dx}{d\xi} \right) + \ell \varepsilon_y / m \qquad (7.46)$$

(b) *If $dx/d\xi = o$, $dy/d\xi \neq o$ ($\ell \neq o$):*

From equation (7.44), it can be shown that:

$$\frac{\partial u}{\partial y} = \left(\frac{du}{d\xi} / \frac{dy}{d\xi} \right) + m \varepsilon_x / \ell$$

and from $\gamma_{xy} = \frac{\partial u}{\partial y} + \frac{\partial v}{\partial x}$, it can be deduced that:

$$\frac{\partial v}{\partial x} = \gamma_{xy} - \left(\frac{du}{d\xi} / \frac{dy}{d\xi} \right) - m \varepsilon_x / \ell \qquad (7.47)$$

Now, from equation (7.28) it can be written that:

$$J_e = \frac{1}{2} \int_{\Gamma_e} \underline{\sigma}^t \, \underline{\varepsilon} \, dy - \int_{\Gamma_e} \left(T_x \frac{\partial u}{\partial x} + T_y \frac{\partial v}{\partial x} \right) ds \qquad (7.48)$$

Then for an element in the ξ-plane, it can be shown that:

$$J_e = \frac{1}{2} \int_0^1 \underline{\sigma}^t \, \underline{\varepsilon} \frac{dy}{d\xi} \, d\xi - \int_0^1 \left(T_x \frac{\partial u}{\partial x} + T_y \frac{\partial v}{\partial x} \right) |\underline{J}| \, d\xi \qquad (7.49)$$

or

$$J_e = \int_0^1 \left[\frac{1}{2} \ell \, \underline{\sigma}^t \, \underline{\varepsilon} - \left(T_x \frac{\partial u}{\partial x} + T_y \frac{\partial v}{\partial x} \right) \right] |\underline{J}| \, d\xi \qquad (7.50)$$

Using Gaussian quadrature technique, it can be written that:

$$J_e = \sum_{q=1}^{N_Q} \Delta J_e(\xi_q) \qquad (7.51)$$

where,

$$\Delta J_e = W_q \left\{ \left[\frac{1}{2} \ell \, \underline{\sigma}^t \, \underline{\varepsilon} - \left(T_x \frac{\partial u}{\partial x} + T_y \frac{\partial v}{\partial x} \right) \right] |\underline{J}| \right\}_{\xi=\xi_q} \qquad (7.52)$$

7.5 Evaluation of the J-Integral Domain Loading Term:

If the domain loading effect is considered, then a domain loading term can be defined as follows

$$J_D = \iint_\Omega \left(X \frac{\partial u}{\partial x} + Y \frac{\partial v}{\partial x} \right) dA \qquad (7.53)$$

Using the discretization procedure of the finite element method, the above equation can be written as follows:

$$J_D = \sum_{e=1}^{n_e} (J_D)_e \qquad (7.54)$$

where,

$$(J_D)_e = \int_\eta \int_\xi \left(X \frac{\partial u}{\partial x} + Y \frac{\partial v}{\partial x} \right) |\underline{J}| \, d\xi \, d\eta \qquad (7.55)$$

and $\underline{J}$ as given by equation (5.4).

The domain integral in the above equation can be carried out by means of integration cells (*finite elements*). The shape functions for such cells or elements are given in Appendix [B].

Let equation (7.55) be written as follows:

$$(J_D)_e = \int_\eta \int_\xi f(x,y) \; |\underline{J}| \; d\xi \; d\eta \qquad (7.56)$$

where,

$$f(x,y) = \left[X \frac{\partial u}{\partial x} + Y \frac{\partial v}{\partial x} \right]$$

Using quadrilateral cells, the above integration can be evaluated by means of Gaussian quadratures as follows:

$$(J_D)_e = \sum_{s=1}^{N_Q} \sum_{r=1}^{N_Q} f(x_{r,s}, y_{r,s}) \; |\underline{J}| \; W_r \; W_s \qquad (7.57)$$

where $x_{r,s}$, $y_{r,s}$ can be evaluated using the cell shape functions as follows:

$$x_{r,s} = \sum_{j=1}^{n} x_j \; N_j(\xi_r, \eta_s)$$

$$y_{r,s} = \sum_{j=1}^{n} y_j \; N_j(\xi_r, \eta_s) \qquad (7.58)$$

The domain loading components X, Y, can be defined as follows:

(a) *For Transitional Inertia:*

$$X = - \rho \, a_x$$

$$Y = - \rho \, a_y \qquad (7.59)$$

where,

ρ = Material density,

a_x = Rigid acceleration in the x-direction,

a_y = Rigid acceleration in the y-direction.

(b) *For Rotational Inertia about the Z-Axis:*

$$X = \rho \, \omega_z^2 \, (x_{r,s} - x_o)$$

$$Y = \rho \, \omega_z^2 \, (y_{r,s} - y_o) \qquad (7.60)$$

where ω_z is the angular velocity in the z-direction, and (x_o, y_o) are the coordinates of the centre of rotation.

(c) *For Rotational Inertia about a Line in the x-y Plane:*

$$X = \rho \, [\, (x_{r,s} - x_o) \, \omega_y^2 - (y_{r,s} - y_o) \, \omega_x \omega_y \,]$$

$$Y = \rho \, [\, (y_{r,s} - y_o) \, \omega_x^2 - (x_{r,s} - x_o) \, \omega_x \omega_y \,] \qquad (7.61)$$

where ω_x, ω_y are the angular velocities in the x- and y-directions respectively.

A generalized expressions for the domain loading components can be defined [Ref.85], as follows:

$$X = a_1 \, x_{r,s} + a_2 \, y_{r,s} + a_o$$

$$Y = b_1 \, x_{r,s} + b_2 \, y_{r,s} + b_o \qquad (7.62)$$

where,

$$a_1 = \rho\,(\omega_y^2 + \omega_z^2) \quad , \quad b_1 = -\rho\,\omega_x\,\omega_y$$

$$a_2 = -\rho\,\omega_x\,\omega_y \quad , \quad b_2 = \rho\,(\omega_x^2 + \omega_z^2)$$

$$a_o = -(a_1\,x_o + a_2\,y_o) \quad , \quad b_o = -(b_1\,x_o + b_2\,y_o)$$

The above equations are valid for the following conditions:

(i) $\omega_z \neq 0$, $\omega_x = \omega_y = 0$.

(ii) $\omega_z = 0$, $\omega_x \neq 0$, $\omega_y \neq 0$.

7.6 Transformation of J-Integral Domain Loading Term:

The domain integral in equation (7.53) can be transformed to a boundary integral as explained before in chapter 4. i.e.

$$J_D = \int_{\Gamma_o} f(x) \left[\frac{\partial u}{\partial x} + C_1\, f(x) \right] dy$$

$$- \oint_{\Gamma} f(x) \left(C_2\, \gamma_{xy} + C_3\, \frac{\partial v}{\partial x} \right) dx + \int_{\Gamma_o} Y\, v\, dy \qquad (7.63)$$

where $f(x)$, C_1, C_2, and C_3 are as defined in section (4.5.3).

The above transformation is valid for the following cases:

(i) $\omega_z \neq 0$, $\omega_x = \omega_y = 0$.

(ii) $\omega_z = 0$, $\omega_x = 0$, $\omega_y \neq 0$.

Using the first integration approach, discussed in section (4.5.2), then:

$$J_D = \int_{\Gamma_o} \mathcal{B}\, dy - \iint_{\Omega} (a_1\, u + b_1\, v)\, dx\, dy \qquad (7.64)$$

where,

$$\mathcal{B} = \underline{X}^t\, \underline{u} = X\, u + Y\, v$$

For the case of transitional inertia and the case of rotation in the x-y plane when $\omega_y = 0$ *(i.e. only ω_x is considered)*, it can be proved that:

$$J_D = \oint_{\Gamma} \mathcal{B}\, dy \qquad (7.65)$$

Hence, equation (7.28) can be written as follows:

$$J = \sum_{e=1}^{n_e} \int_{\Gamma_e} \left[\left(\frac{1}{2}\, \underline{\sigma}^t\, \underline{\varepsilon} - \underline{X}^t\, \underline{u} \right) dy - \underline{T}^t\, \frac{\partial \underline{u}}{\partial x}\, ds \right] \qquad (7.66)$$

It is clear from equations (7.63) and (7.64) that there is no requirement to use integration cells for the evaluation of the *J*-integral domain loading term, since the domain integral is transformed to a boundary integral. This transformation is very useful for the numerical evaluation of such a term, since it can save computer *CPU* time and reduce the effort required for the preparation of data.

7.7 Evaluation of the J-Integral Thermal Loading Term:

For elastic case with thermal loading, the *J*-integral thermal loading term is given in equation (4.82). The domain integral part of this equation can be written as follows:

$$J_T = \iint_{\Omega} \underline{\sigma}^t \frac{\partial \underline{\varepsilon}_o}{\partial x} \, dx \, dy \qquad (7.67)$$

The double integrals in the above equation can be evaluated by means of integration cells and Gaussian quadrature technique as follows:

$$J_T = \sum_{e=1}^{m_e} (J_T)_e \qquad (7.68)$$

where m_e is the number of integration cells.

The term $(J_T)_e$ can be defined according to equation (7.67) as follows:

$$(J_T)_e = \sum_{s=1}^{N_Q} \sum_{r=1}^{N_Q} f(x_{r,s}, y_{r,s}) \, |\underline{J}| \, W_r \, W_s$$

where,

$$f(x_{r,s}, y_{r,s}) = \underline{\sigma}^t(x_{r,s}, y_{r,s}) \frac{\partial}{\partial x} \underline{\varepsilon}_o(x_{r,s}, y_{r,s})$$

Now, the complete J-integral value due to thermal loading can be evaluated as follows:

$$J = \sum_{e=1}^{n_e} \int_{\Gamma_e} \left[\left(\frac{1}{2} \underline{\sigma}^t \underline{\varepsilon}_e \right) dy - \underline{T}^t \frac{\partial \underline{\underline{u}}}{\partial x} \, ds \right] + J_T \qquad (7.69)$$

7.8 Evaluation of the J-Integral Plastic Loading Term:

For the case of plastic strains the complete *J*-integral expression can be written using equation (4.86) as follows:

$$J = \oint_{\Gamma} \left[(W_e + W_p)\, dy - \underline{T}^t \frac{\partial \underline{u}}{\partial x}\, ds \right] \qquad (7.70)$$

where W_e and W_p are as defined in chapter 4.

Now, to evaluate equation (7.70) numerically, the plastic strain energy component W_p should be evaluated using an elasto-plastic finite element or boundary element programs. Then a numerical procedure similar to that introduced in section (7.4) can be used.

7.9 Evaluation of J-Integral for Oblique Cracks:

All the equations given before for the evaluation of the *J*-integral are with respect to crack axes, the x-axis of which is on *(or parallel to)* the crack surface, as shown in Fig.(7.4).

Consider the case, in which the crack axes (x'-y') are oblique with respect to the structure axes (x-y), by an angle ϕ, as shown in Fig.(7.6). To facilitate the *FEM* or *BEM* analysis, the structure axes will be used in the analysis and to be selected as the best appropriate axes for the finite or boundary element mesh employed, *i.e.* u, v , $\underline{\sigma}$, $\underline{\varepsilon}$ *given to the J-integral program are assumed to be with respect to structural global axes* (x-y). However, according to the derivation of the *J*-integral expression, explained in chapter 4, the expression should now be modified as follows:

$$J = \int_{\Gamma_o} W' \, dy' - \int_{\Gamma_o} \left(\underline{T}'^{t} \frac{\partial \underline{u}'}{\partial x'} \right) ds$$

$$- \iint_{\Omega} \left(\underline{X}'^{t} \frac{\partial \underline{u}'}{\partial x'} \right) dx' \, dy' \qquad (7.71)$$

where the dashed parameters are measured with respect to the crack axes (x'-y').

The directional cosines of the x' and y' axes with respect to the x and y axes, can be obtained as follows:

$$\left.\begin{aligned} \ell_1 &= \cos\phi \\ m_1 &= \sin\phi \end{aligned}\right\} \quad \textit{for } x'\textit{-axis.}$$

$$\left.\begin{aligned} \ell_2 &= -\sin\phi \\ m_2 &= \cos\phi \end{aligned}\right\} \quad \textit{for } y'\textit{-axis.} \qquad (7.72)$$

A vector can be represented in terms of its x-y components as follows:

$$\vec{V} = v_x \, i + v_y \, j = v'_x \, i' + v'_y \, j'$$

From which, it can be deduced that:

$$\underline{V} = \begin{bmatrix} v_x \\ v_y \end{bmatrix} = \begin{bmatrix} \ell_1 & \ell_2 \\ m_1 & m_2 \end{bmatrix} \begin{bmatrix} v'_x \\ v'_y \end{bmatrix} \qquad (7.73)$$

or

$$\underline{V}' = \begin{bmatrix} v'_x \\ v'_y \end{bmatrix} = \begin{bmatrix} \ell_1 & m_1 \\ \ell_2 & m_2 \end{bmatrix} \begin{bmatrix} v_x \\ v_y \end{bmatrix} \qquad (7.74)$$

Using the above equations to represent $d\underline{u}$, $\underline{T}$, $\underline{X}$ in terms of $d\underline{u}'$, $\underline{T}'$, $\underline{X}'$, it can be proved that:

$$\underline{T}'^{t}\, d\underline{u}' = \underline{T}^{t}\, d\underline{u}$$

$$\underline{X}'^{t}\, d\underline{u}' = \underline{X}^{t}\, d\underline{u} \qquad (7.75)$$

From which, the following results are deduced:

$$\int_{\Gamma_o} \underline{T}'^{t}\, \frac{\partial \underline{u}'}{\partial x'}\, ds = \int_{\Gamma_o} \underline{T}^{t}\, \frac{\partial \underline{u}}{\partial x}\, ds \qquad (7.76)$$

and

$$\iint_{\Omega} \underline{X}'^{t}\, \frac{\partial \underline{u}'}{\partial x'}\, dx'\, dy' = \iint_{\Omega} \underline{X}^{t}\, \frac{\partial \underline{u}}{\partial x'}\, dx'\, dy' \qquad (7.77)$$

and from the invariance of the strain energy function, it can be deduced that:

$$W' = W \qquad (7.78)$$

Substituting equations (7.76-7.78) into equation (7.71), the expression for the J-integral can now be written as follows:

$$J = \int_{\Gamma_o} W\, dy' - \int_{\Gamma_o} \left(\underline{T}^{t}\, \frac{\partial \underline{u}}{\partial x'} \right) ds - \iint_{\Omega} \left(\underline{X}^{t}\, \frac{\partial \underline{u}}{\partial x'} \right) dx'\, dy' \qquad (7.79)$$

For the numerical evaluation of J, the following simplifications can be employed:

$$dy' = \frac{dy'}{d\xi}\, d\xi = \left[\frac{\partial y'}{\partial x} \frac{dx}{d\xi} + \frac{\partial y'}{\partial y} \frac{dy}{d\xi} \right] d\xi$$

$$= \left[\ell_2 \frac{dx}{d\xi} + m_2 \frac{dy}{d\xi} \right] d\xi$$

$$\frac{\partial u}{\partial x'} = \frac{\partial u}{\partial x}\frac{\partial x}{\partial x'} + \frac{\partial u}{\partial y}\frac{\partial y}{\partial y'}$$

$$= \ell_1 \varepsilon_x + m_1 \left[\tau_{xy} - \frac{\partial v}{\partial x} \right]$$

$$\frac{\partial v}{\partial x'} = \frac{\partial v}{\partial x}\frac{\partial x}{\partial x'} + \frac{\partial v}{\partial y}\frac{\partial y}{\partial y'}$$

$$= \ell_1 \frac{\partial v}{\partial x} + m_1 \varepsilon_y$$

$$dx'\ dy' = \begin{vmatrix} \ell_1 & m_1 \\ \ell_2 & m_2 \end{vmatrix} dx\ dy \equiv dx\ dy$$

For the case of domain loading, with:

$$X = a_o + a_1 x + a_2 y$$
$$Y = b_o + b_1 x + b_2 y$$

it can be deduced that:

$$\iint_\Omega \left[X \frac{\partial u}{\partial x'} + Y \frac{\partial v}{\partial x'} \right] dx'\ dy' = \int_{\Gamma_o} \left[X u + y v \right] dy'$$

$$- \iint_\Omega \left[\frac{\partial X}{\partial x'} u + \frac{\partial Y}{\partial x'} v \right] dx\ dy \qquad (7.80)$$

where,

$$\frac{\partial X}{\partial x'} = \ell_1 \frac{\partial X}{\partial x} + m_1 \frac{\partial X}{\partial y} = \ell_1 a_1 + m_1 a_2$$

$$\frac{\partial Y}{\partial x'} = \ell_1 \frac{\partial Y}{\partial x} + m_1 \frac{\partial Y}{\partial y} = \ell_1 b_1 + m_1 b_2$$

Finally, for the case thermal loading, the J-integral expression can be written as follows:

$$J = \int_{\Gamma_o} W \, dy' - \int_{\Gamma_o} \left(\underline{T}^t \frac{\partial \underline{\underline{u}}}{\partial x'} \right) ds$$

$$- \iint_{\Omega} \left(\underline{X}^t \frac{\partial \underline{\underline{u}}}{\partial x'} \right) dx' \, dy' + J_T \qquad (7.81)$$

where,

$$J_T = \iint_{\Omega} \underline{\sigma}^t \frac{\partial \underline{\varepsilon}_o}{\partial x'} \, dx' \, dy' \qquad (7.82)$$

Now, for numerical evaluation of J_T, it can proved that:

$$\frac{\partial \underline{\varepsilon}_o}{\partial x'} = \ell_1 \frac{\partial \underline{\varepsilon}_o}{\partial x} + m_1 \frac{\partial \underline{\varepsilon}_o}{\partial y} \qquad (7.83)$$

where,

$$\frac{\partial \underline{\varepsilon}_o}{\partial x} = \sum_{i=1}^{n} (\underline{\varepsilon}_o)_i \frac{\partial N_i}{\partial x}$$

$$\frac{\partial \underline{\varepsilon}_o}{\partial y} = \sum_{i=1}^{n} (\underline{\varepsilon}_o)_i \frac{\partial N_i}{\partial y}$$

Hence, from equations (7.82) and (7.83), it can be written that:

$$J_T = \iint_{\Omega} \underline{\sigma}^t \left(\ell_1 \frac{\partial \underline{\varepsilon}_o}{\partial x} + m_1 \frac{\partial \underline{\varepsilon}_o}{\partial y} \right) dx \, dy \qquad (7.84)$$

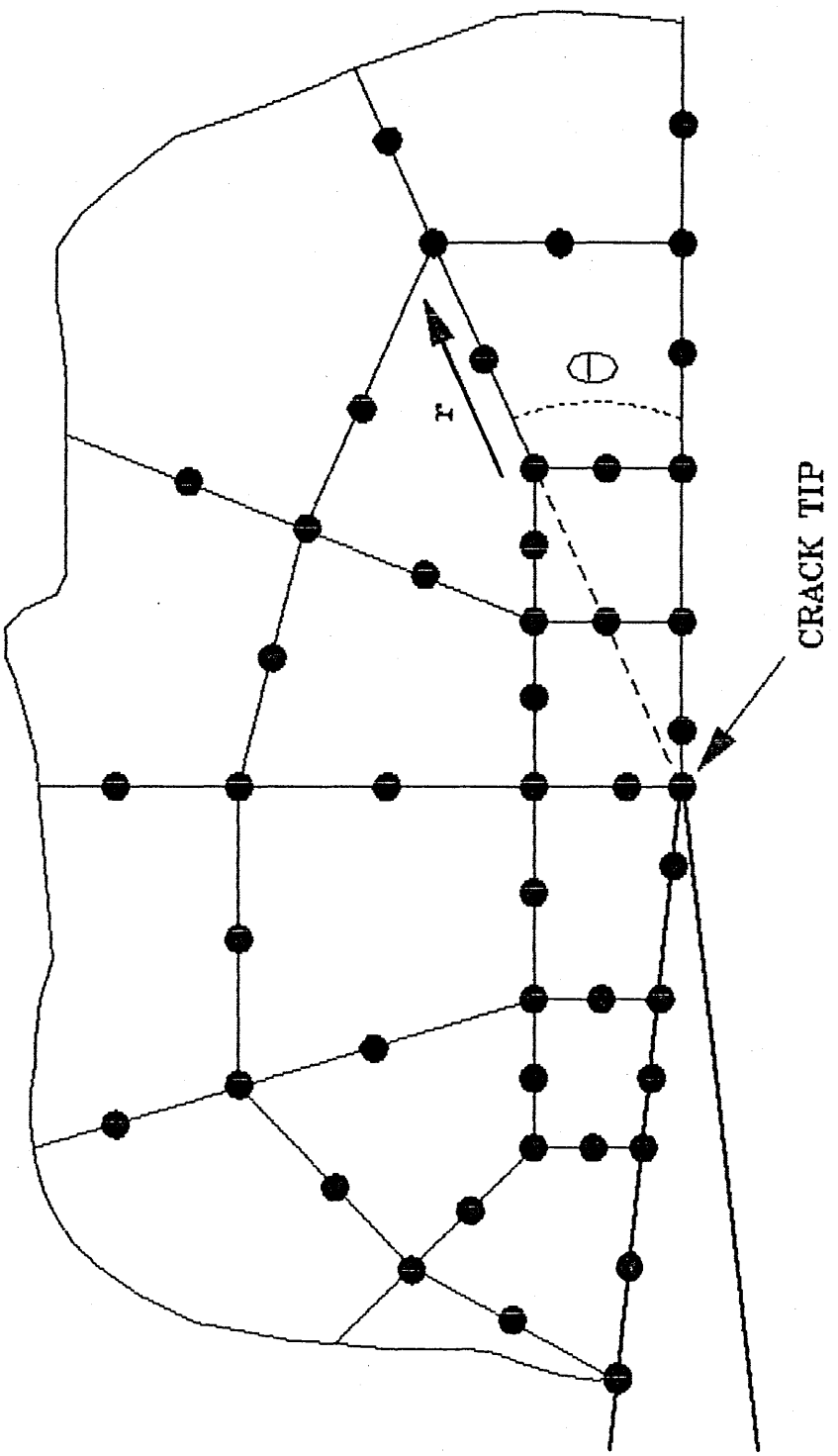

Fig.(7.1) Finite Element Mesh for Cracked Structure.

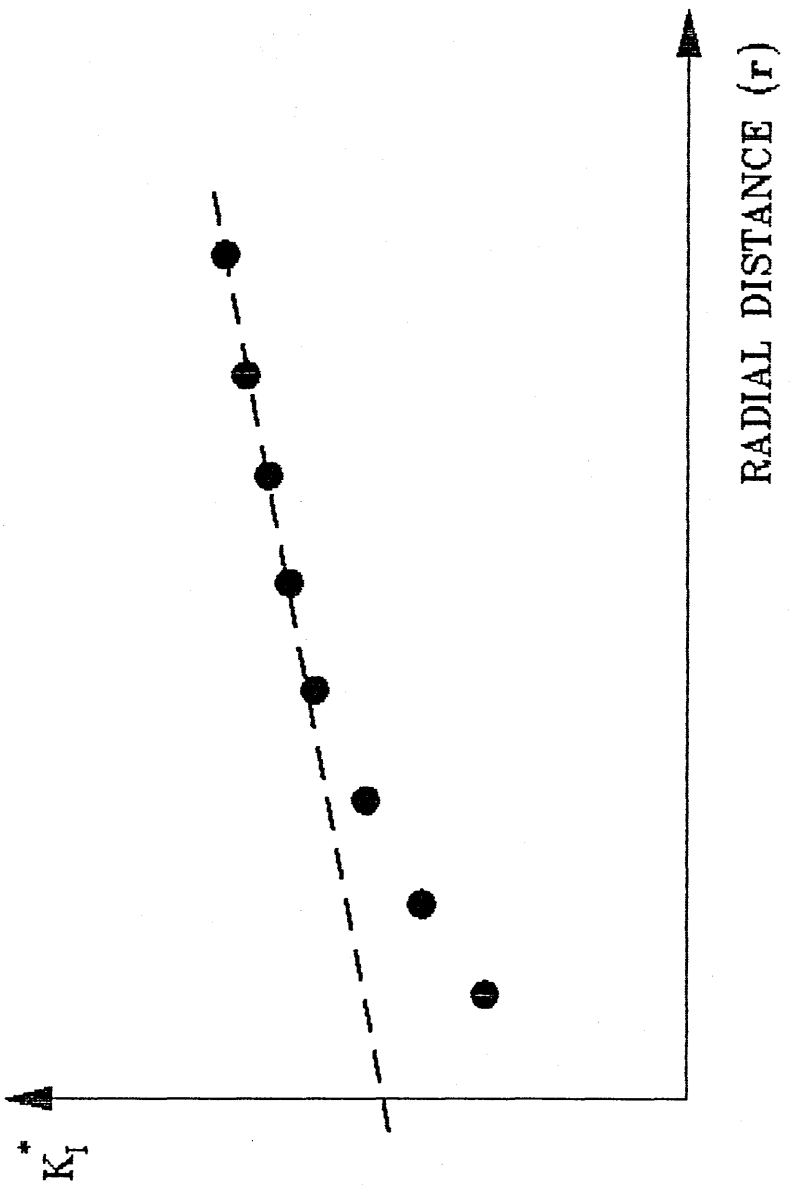

Fig.(7.2) Extrapolation Method of Stress Intensity Factor.

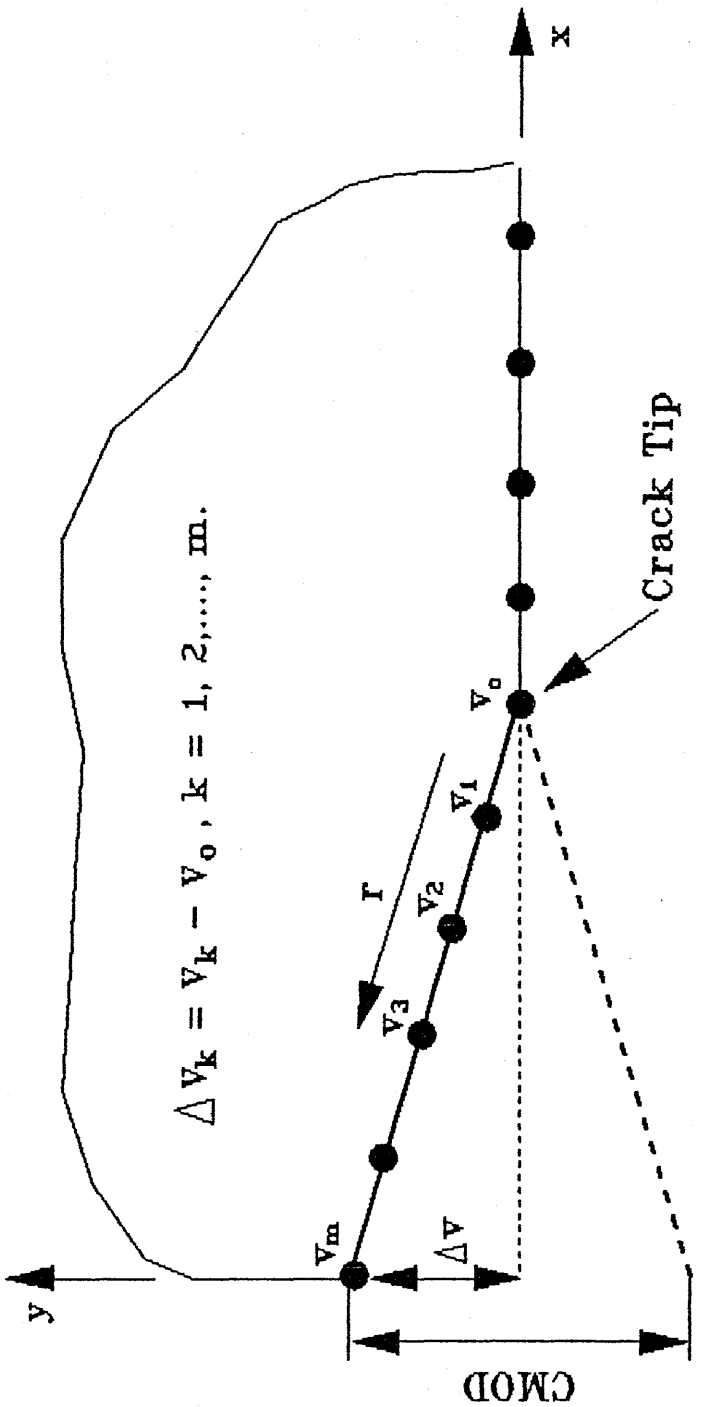

Fig.(7.3) Crack Opening Displacement Model.

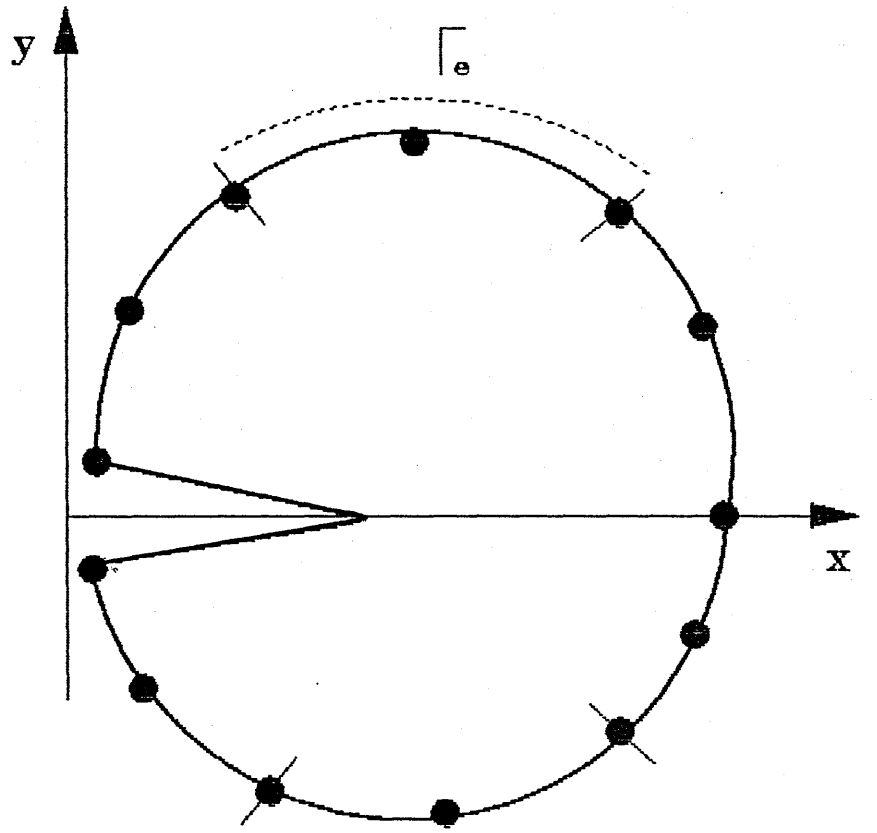

Fig.(7.4) Discretization of a J-Integral Contour.

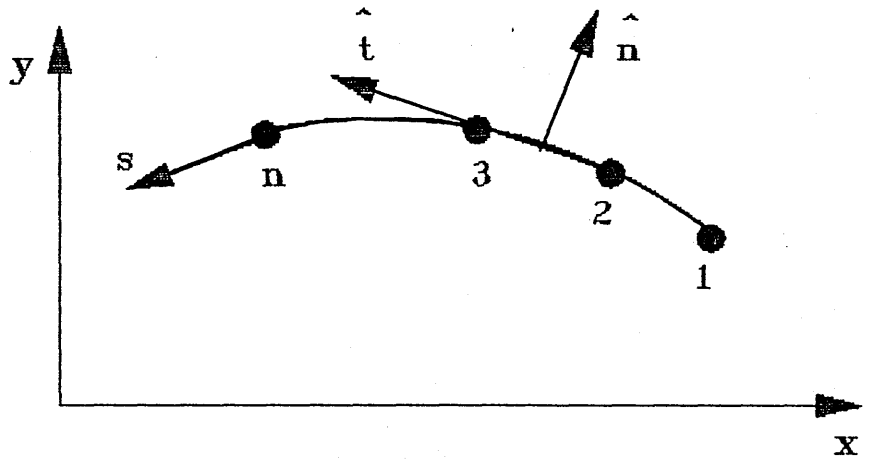

Fig.(7.5) N-Node Boundary Element used as Contour Element.

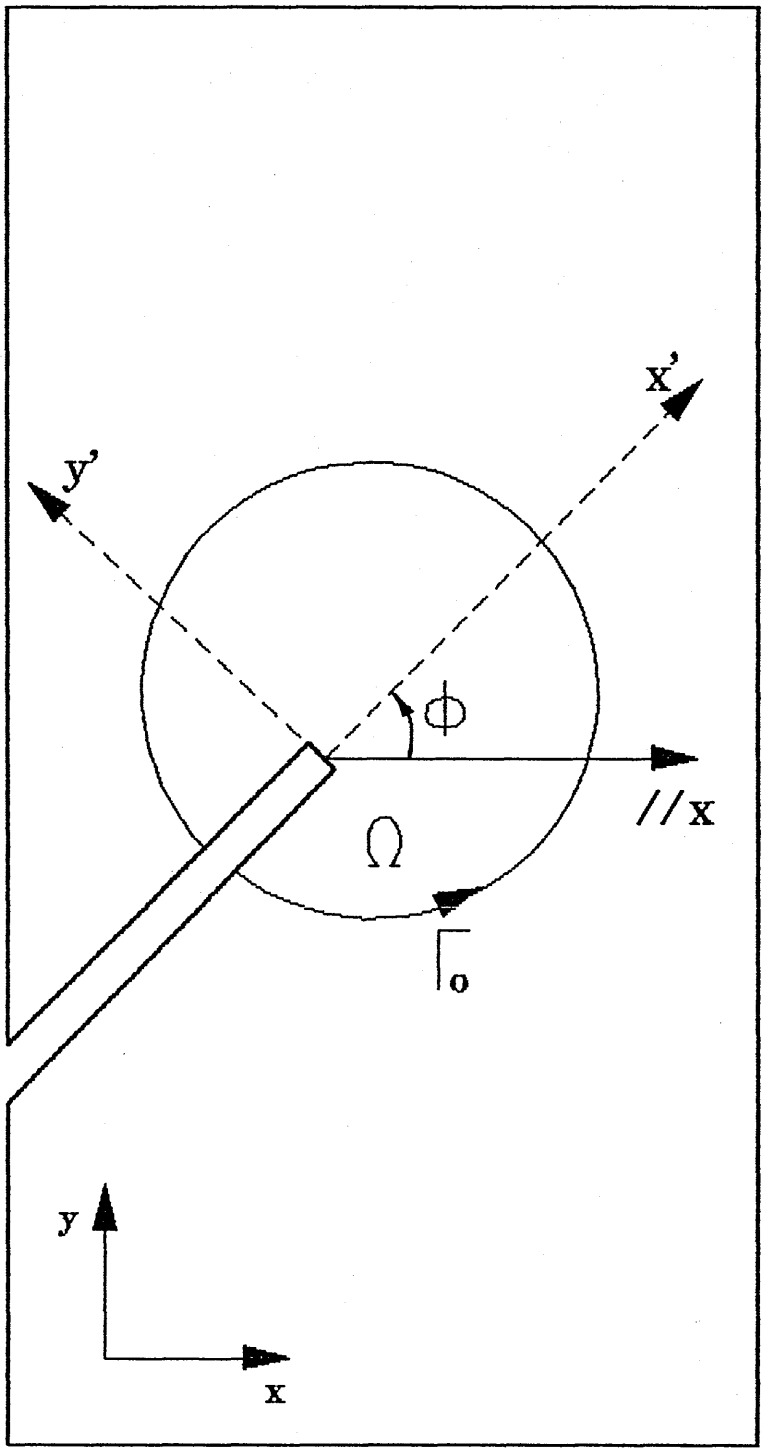

Fig.(7.6) An Oblique Crack with respect to Global Axes.

CHAPTER 8

PROGRAMMING

8.1 Introduction:

A modular approach has been adopted in this work to design the programming system, which is named **FRAMEC** (*FRActure MEChanics*) system. The system consists of five basic modules, each module corresponds to the type of analysis required (*i.e. for example mesh generation, finite element analysis, boundary element analysis, etc.*). The modules are linked together as shown in Fig.(8.1), and each one of them contains a group of programs related to the type of analysis which can be carried out using such a module. The modules and the programs are described in the following sections.

8.2 Pre-Processing Module:

This module consists of two programs namely, a two-dimensional general mesh generator program, and a two-dimensional mesh plotter program. The procedures of these programs are explained in the following subsections.

8.2.1 Two-Dimensional Mesh Generator Program:

This is a general mesh generator program, which is capable of generating finite and boundary element meshes for two-dimensional structures. The structure of the program is given in Fig.(8.2), and the basic steps of the mesh generation procedure can be summarized, for the **FRAMEC** system, as follows:

(a) Block Modelling:

A primary coarse mesh is to be prepared such that, for finite element analysis, multilateral or curved regions are reduced to quadrilateral or triangular blocks, and for boundary element analysis, the boundary is divided into one-dimensional blocks.

The curved domains or boundaries are to be modelled in terms of curved blocks which belong to finite element or boundary element families. The data for blocks can be introduced as mesh data, and the user has the choice, either to employ it directly as the suggested mesh, or to direct the program to generate a new one. Each generated mesh can be considered as a model of blocks for any further generation.

(b) *Intrinsic Transformation:*

Each block is to be transformed into a uniform element inside its own local intrinsic space, by employing an isoparametric transformation as explained in the finite and the boundary element theories.

(c) *Intrinsic Discretization:*

The discretization is carried out using the following two steps:

(i) Division into simple similar elements; the quadrilateral block into 4-node quadrilaterals, the triangular block into 3-node triangles, etc.

(ii) Fitting the required elements, such elements may have different geometry or different nodal systems from the simple ones. The fitting is to be performed recursively, by using the local intrinsic space of every generated simple element.

The final result is to obtain a fully-discretized block in its own intrinsic space.

(d) Transformation to the Global Space:

The global cartesian coordinates of each generated node are obtained by applying the previously-mentioned isoparametric transformation. Hence, the generated elements of every block can be described in the global cartesian space.

(e) Condensation and Compatibility:

The nodes generated on the common boundary between any two blocks may have been repeated. A condensation process is to be performed so that the genuine nodes are to be kept. It is necessary to maintain compatibility at such common boundaries. The geometric points, division numbers, and division ratios should be uniquely specified at these boundaries. The isoparametric transformation itself does not violate any compatibility, as long as the shape functions satisfy the C^{o}-continuity condition over the whole domain.

8.2.2 Two-Dimensional Mesh Plotter Program:

This program has been designed to plot finite and boundary element meshes by using plotting subroutines from the *GINO* library. The structure of the program is given in Fig.(8.3), and the procedure of every subroutine will be described as follows:

(a) ASS TERM Subroutine:

The use of this subroutine is to assign the graphical computer terminal to the *FORTRAN* stream, in order to produce a graphical picture.

(b) DATA Subroutine:

This subroutine reads the output of the mesh generation program, which contains all the information required to run the plotting program *(such as, number of nodes and elements, types of elements, coordinates, topology array, etc.)*.

(c) AMIN & AMAX Functions:

These functions calculate the minimum and the maximum values of the coordinates, which are required by the program to set a graphical view port.

(d) PLOTTER Subroutine:

This is the main subroutine in the program which uses the *GINO* library and the following subroutines to plot the required mesh.

i. QUAD-N Subroutines:

These subroutines are designed according to the quadrilateral family of the finite elements. Every subroutine is capable of plotting one type of element.

ii. TRI-N Subroutines:

The subroutines are designed for the plotting of the triangular family of finite elements, and they are carrying out similar job as in the *QUAD-N* subroutines.

iii. GENBEM Subroutine:

This subroutine is designed to generate the isoparametric boundary elements. It is called by the *PLOTTER* subroutine when

a boundary element mesh with any type of isoparametric elements is required to be plotted.

(e) *NODE Subroutine:*

This subroutine is designed to plot the node number according to the output of the mesh generation program.

8.3 Finite-Element Module:

In this module two general finite element programs are developed, these programs are:

(1) *Linear-Elastic Finite Element Program.*
(2) *Elasto-Plastic Finite Element Program.*

The above programs have the capability of carrying out elastic and elasto-plastic finite element analyses using different types of two-dimensional elements, loading conditions, and boundary conditions. Both programs contain a frontal solver developed in the *Computational Mechanics Group* [Ref.86] to reduce the *CPU* time required for the solution of large matrices, especially in the case of elasto-plasticity where iterations take place. A description of the programs is given in the following sections.

8.3.1 Types of Elements:

The above two programs use a library of elements which contain different families of standard, transition, and crack-tip elements, including the newly developed singular elements. The families of elements are as described in chapter 5, and the shape functions of the standard and transition elements are given in Appendix [B].

8.3.2 Types of Loading:

The previous programs are capable of carrying out elastic and elasto-plastic analyses with different types of loading such as point loading, distributed loading, pressure loading, thermal loading and different types of domain loading *(i.e. inertial, translational, and rotational)*. The above types of loading are described in chapter 5.

8.3.3 Structure of the Linear-Elastic Program:

The structure of the two-dimensional linear-elastic finite element program is given in Fig.(8.4), and can be summarized as follows:

(a) DATA Subroutine:

The data subroutine is designed to read all the information required to run the program such as mesh generated data, material data, boundary conditions data, and the loading data.

(b) DPLOAD Subroutine:

This subroutine assembles the equivalent pressure loading vector and the equivalent domain loading vector which are generated for each element by the following subroutines:

i. EPVG Subroutine:

This subroutine generates the elemental pressure loading vector using the theory described in chapter 5, section 5.2.4, and by calling *GAUSS*, *SHAPEP*, and *JACOBP* subroutines which will be described later.

ii. EDVG Subroutine:

This is a generator for an element domain loading vector using the theory described in chapter 5, section 5.2.3, and it calls *GAUSS*, *JACOB*, and *SHAPEF* subroutines.

(c) INITIATION Subroutine:

This subroutine initiates all the matrices and the vectors required for the frontal solver solution.

(d) FRONT Subroutine:

This subroutine assembles and reduces the system of equations for the whole domain using the approach developed in the *Computational Mechanics Group* [Ref.86]. Each assembled equation is eliminated whenever becoming complete and stored in a direct access file. The subroutine calls *STIFF* subroutine which is designed so as to make the *FRONT* subroutine independent of the type of elements used. *STIFF* subroutine prepares data required for the generation of the stiffness matrix for one element and calls *ESMG* subroutine for carrying out this process.

(e) ESMG Subroutine:

This is an element stiffness matrix generator which uses the following subroutines:

i. DMATRIX Subroutine:

This subroutine generates the $\underline{D}$ matrix which is the stress-strain matrix required for the correlation between stresses and strains.

ii. BMATRIX Subroutine:

This subroutine generates the B matrix in terms of the cartesian derivatives of the element shape functions.

iii. GAUSS Subroutine:

A data file containing the parameters for Gauss quadrature *(up to the 16-point scheme)* is opened by this subroutine, and the parameters for the quadrature scheme selected for an element are read.

iv. MATT, MATM, MATS, MATI Subroutines:

These are matrix operations subroutines, which are required to carry out a number of operations such as transposition, multiplication, initiation, etc.

(f) SOLVER Subroutine:

This subroutine carries out a backward substitution by reading the eliminated equations backward from the direct access file, so as to calculate the nodal displacement vector.

(g) DISP Subroutine:

This subroutine extracts and prints the nodal displacements for the whole number of nodes.

(h) STRESS Subroutine:

This subroutine generates and prints the nodal strains and stresses for the whole number of nodes by using the *DMATRIX* and the following subroutines:

i. INTERCO Subroutine:

This subroutine generates the nodal intrinsic coordinates for all types of standard, transition, and crack-tip elements.

ii. MATV Subroutine:

This subroutine is used for the multiplication of a matrix by a vector, and is required to multiply the $\underline{D}$ matrix by the nodal strain vector to obtain the nodal stress vector.

The remaining subroutines are as follows:

(i) SHAPEP & JACOBP Subroutines:

These subroutines generate the pressure element shape functions and Jacobian matrix using the theory described in chapter 5, section 5.2.4.

(j) SHAPEF Subroutine:

This subroutine uses the developed finite element library to call the type of element required by the *EDVG* subroutine, so as to generate the values of its shape functions at any given point.

(k) CARTD Subroutine:

This subroutine generates the cartesian derivatives of the element shape functions as required for the *BMATRIX* subroutine.

(l) JACOB Subroutine:

This subroutine generates the two-dimensional finite element

Jacobian matrix required by the *CARTD* subroutine.

(m) INTRD Subroutine:

This subroutine uses the finite element library to generate the intrinsic derivatives of the required element shape functions essential to generate the Jacobian matrix.

8.3.4 Structure of the Elasto-Plastic Program:

This is a two-dimensional elasto-plastic finite element program based upon the initial stress incremental method, as described in chapter 5. The program uses the finite element library mentioned before, and incorporates different types of yield criteria, hardening rules, and solution algorithms, as follows:

(a) Yield Criteria:

1. Tresca criterion.
2. Von Mises criterion.
3. Mohr-Coulomb criterion.
4. Druker-Prager criterion.

(b) Hardening Rules:

1. Isotropic hardening.
2. Kinematic hardening.
3. Mixed hardening.

(c) Solution Algorithms:

1. Newton-Raphson interpolative algorithm.
2. Modified Newton-Raphson iterative algorithm.
3. Combined algorithm.

A flow diagram of this program is illustrated in Fig.(8.5). The steps to carry out an elasto-plastic stress analysis using this program are as follows:

(a) *Data Preparation:*

A data subroutine has been designed and implemented in this program to read all the information required for carrying out the elasto-plastic stress analysis using the facilities available in the program.

(b) *Pressure/Domain Loading:*

In this step the program uses the *DPLOAD* subroutine explained earlier to generate the pressure and the domain loading vectors and assemble them in the main force vector, if the analysis involves any pressure and/or domain loading conditions.

(c) *Initiation:*

In this step the program initiates all the vectors and matrices required to carry out a frontal solution, using the *INITIATION* subroutine mentioned earlier in this chapter.

(d) *Load Increments Do-Loop:*

Since the program is based upon an incremental approach, a number of load ratios are specified according to the given number of load increments. The nodal loading vector for every new increment is obtained by multiplying the corresponding ratio by the total nodal loading vector applied.

(e) Assembly & Reduction:

In this step the program uses the *FRONT* subroutine described earlier in this chapter to generate the assembled, reduced, eliminated equations for the whole structure and store their coefficients in a direct access file.

(f) Frontal Solver:

In tis step a backwards substitution procedure is carried out to solve the system of equations generated by the *FRONT* subroutine.

(g) Stress/Strain Calculation:

In this step the displacement-strain relations are used to perform strain calculations at all quadrature and nodal points, similarly the stress-strain relations are used for stress calculations. Also in this step the equivalent stress at every point is checked with the initial yield stress of the material. If no point has exceeded yield, then no plastic calculations are required and a new load increment is to be applied.

(h) Stress Correction:

In this step a stress correction procedure will take place using the theory explained in chapter 5. The structure of the plasticity correction subroutine is shown in Fig.(8.6). This subroutine is common between the elasto-plastic finite element program and the elasto-plastic boundary elements program.

(i) Residual Force/Reaction Calculation:

In this step the equilibrium equations are checked so as to calculate the vector of nodal residual force resulting from stress correction. The subroutine calculates also the reaction forces at restrained nodes.

(j) Convergence Check:

In this stage an error calculation takes place to check the convergence of the displacement and the residual force vectors. If the displacement error or the residual force error is greater than a given value, a new iteration takes place *(according to the iteration algorithm employed)* using the residual force vector as a new load increment.

(k) Print Output:

In this step all the required output such as displacements, stresses, strains, forces, and reactions are printed for all or selected load increments at the nodal and quadrature points.

(l) Unloading Calculation:

After the last load increment for the elasto-plastic calculation, the unloading calculation takes place if required. This calculation involves the evaluation of the residual stresses, strains, and displacements at the nodal and quadrature points.

8.4 Boundary-Element Module:

In this module, six different two-dimensional isoparametric boundary element programs have been developed for linear-elastic and elasto-plastic fracture mechanics problems. These programs are:

(1) Linear-Elastic Boundary Element Program.
(2) Linear-Elastic Domain Loading Boundary Element Program.
(3) Linear-Elastic Subregions Boundary-Element Program.
(4) Elasto-Plastic Boundary Element Program.
(5) Elasto-Plastic Domain Loading Boundary Element Program.
(6) Elasto-Plastic Subregions Boundary-Element Program.

The structures of the above programs are described in the following sections.

8.4.1 Linear-Elastic Boundary Element Program:

This is a two-dimensional isoparametric boundary element program. The structure of the program is illustrated in Fig.(8.7). This program uses different techniques for accuracy measures, such as the singular integration technique, the jump function technique, the corner module technique, and the finite difference scheme. Also a special subroutine has been developed in this work to generate the isoparametric crack-tip boundary element automatically inside the program without the interference of the user. The structure of this program can be explained as follows:

(a) DATA Subroutine:

This subroutine reads all the information required to carry out the analysis, and it calls the following subroutines:

i. GAUSS Subroutine:

The job of this subroutine is similar to that of the *GAUSS* subroutine used for *FEM* analysis, and described earlier.

ii. SING Subroutine:

This subroutine opens a singular quadrature file and reads the quadrature parameters required to carry out a numerical integration for integrands which contain $log(r)$ or $log(\frac{1}{r})$.

iii. TIP ELEMENT Subroutine:

This subroutine has been developed for the purpose of generating crack-tip boundary elements automatically by moving the mid-side node of a 3-node isoparametric element to one quarter of the distance from the crack tip, or for a 4-node isoparametric element by moving the two mid-side nodes to 1/9 and 4/9 the distance from the crack tip. The location of the generated crack-tip elements should be specified by the user in the *DATA* subroutine by giving the global number of the element in the mesh.

(b) GHMAT Subroutine:

In this subroutine $\underline{G}$ and $\underline{H}$ matrices are assembled for all boundary nodes of the whole structure. This subroutine carries out the assembly after calling the *GH* subroutine for every boundary element in the mesh.

(c) GH Subroutine:

This subroutine generates the elemental $\underline{g}$ and $\underline{h}$ matrices with respect to any specified source point. The singular quadrature is invoked whenever the source point lies on the element involved.

(d) JACOB Subroutine:

This subroutine generates the Jacobian matrix required by the *GH* subroutine. The generation of the Jacobian matrix is carried out by calling the following functions:

i. GLAG Function:

This function is used for the generation of Lagrangian shape functions for *n*-node isoparametric boundary element. The required element should be specified by the user in the *DATA* subroutine.

ii. DLAG Function:

This function generates the derivatives of Lagrangian shape functions for *n*-node isoparametric element.

(e) BCO Subroutine:

This subroutine applies the specified boundary conditions to organize the system of equations generated by the *GHMAT* subroutine, so as to form a linear simultaneous system of equations.

(f) SOLVER Subroutine:

This is a Gauss elimination solver used for the solution of equations prepared by the *BCO* subroutine.

(g) OUTPUT Subroutine:

This subroutine extracts and prints the nodal displacements and tractions for the whole boundary.

(h) INTERNAL Subroutine:

This subroutine evaluates the required field parameters such as displacements, tractions, stresses, and strains at given internal nodes. The subroutine incorporates different techniques to improve the accuracy of the results such as jump functions and other techniques which explained before in chapter 6. The subroutine uses *GH* and the following subroutines:

i. CORNER Subroutine:

This subroutine evaluates the $\underline{C}$ matrix required at a corner node. The number of corners on the mesh should be specified by the user and doubling the nodes at each corner is essential to model the corners efficiently.

ii. BOUNDARY Subroutine:

This subroutine calculates the field parameters at any internal node on the boundary of the structure. The subroutine uses a Lagrangian interpolation technique to calculate the location of each node within the nearest element in the mesh, then interpolates the field parameters accordingly.

iii. FINITEDEF Subroutine:

This subroutine uses a finite difference scheme to evaluate the field parameters for internal nodes which are very near to the boundary. At such nodes the boundary integral equations for strains may not lead to accurate answers due to the singular terms involved. However, with the jump function correction, it is possible to obtain accurate displacement values there, and hence it becomes more accurate to evaluate the strains from derivatives obtained from direct finite difference ratios of displacement components, as explained in section (6.6.5).

iv. STRAIN Subroutine:

This subroutine uses the boundary integral equations to evaluate the field parameters for internal nodes which are far enough from the boundary.

v. DMAT Subroutine:

This subroutine generates the elastic $\underline{D}$ matrix which is required to correlate between stresses and strains.

vi. MATVEC Subroutine:

This subroutine carries out a multiplication of a matrix by a vector as follows:

$$\underline{A}_{mxn} \cdot \underline{X}_{nx1} = \underline{Y}_{mx1}$$

(i) EXTERNAL Subroutine:

This subroutine uses the boundary displacements and tractions so as to generate a system of 4 equations in 4 unknowns ($\partial u/\partial x$, $\partial u/\partial y$, $\partial v/\partial x$, $\partial v/\partial y$) at every boundary node by means of subroutine *AMAT*. The equations are solved by using *SOLVER* subroutine, then the strains and stresses are evaluated and printed at each boundary node.

8.4.2 Linear-Elastic Domain Loading Boundary Element Program:

This is a two-dimensional, domain loading, isoparametric, boundary element program which accounts for different types of domain loading such as inertial, rotational, translational, thermal, and concentrated point loading. The structure of this program is illustrated in Fig.(8.8), and it is similar to the elastic boundary element program described above except that

some new extra subroutines are developed and added to the program for dealing with domain loading. The new subroutines are as follows:

(a) *CPLOAD & CPSTRAIN Subroutines:*

These subroutines are developed to generate the equivalent displacement and strain vectors due to a given set of concentrated point loading with respect to any given source point. The *GH* and *STRAIN* subroutines then assemble these vectors to the corresponding boundary integral equations for displacements and strains, respectively.

(b) *BFORCE & BSTRAIN Subroutines:*

These subroutines generate the equivalent displacement and strain vectors due to other types of domain loading at any specified source point, as required by the *GH* and *STRAIN* subroutines to account for the effect of these types of loading on the boundary integral equations for displacements and strains.

8.4.3 Linear-Elastic Subregions Boundary Element Program:

This program is a two-dimensional domain loading boundary element program which incorporates the subregion technique described in chapter 6. The structure of this program is shown in Fig.(8.9), and it is similar to the above program except that some additional subroutines are developed and linked to the program for the assembly of subregions. Also some subroutines such as *BCO*, *OUTPUT*, *EXTERNAL*, and *INTERNAL* have been modified to deal with each subregion separately. The new subroutines are as follows:

(a) SUBDATA Subroutine:

This subroutine is developed to extract the required data for each subregion from the global data provided by the *DATA* subroutine, and also to generate and store a location vector for the nodes in the mesh with respect to each subregion. The location vector is required by the *ASSEMBLER* subroutine to assemble the required matrices for the whole boundary.

(b) ASSEMBLER Subroutine:

This subroutine is designed to assemble the $\underline{G}$ and $\underline{H}$ matrices for the whole structure by calling the *GHMAT* subroutine for every subregion. The *GHMAT* subroutine in this case treats each subregion as a separate boundary element mesh and generates the required matrices by calling other subroutines, as described before.

(c) CONDENSER Subroutine:

Doubling the nodes at generated corners due to subregioning is essential so as to maintain the accuracy gained by using the double-node technique. However, unless a finite tolerance is inserted between the nodes of each corner, a singularity may develop in the generated equations. This tolerance may, unfortunately, reduce the level of accuracy. Alternatively, *CONDENSER* subroutine is developed to condense the equations by eliminating any unknown which is similar to another. A number of similar nodes *(nodes with one or more boundary parameter being similar)* can be specified in the data by the user. This subroutine can also deal with any other similar nodes besides those at generated corners. Using the *CONDENSER* subroutine leads to a reduction in the number of equations required to be solved.

(d) *EXPANDER Subroutine:*

Every time the *CONDENSER* subroutine is used, the program calls *EXPANDER* subroutine, after solving the condensed equations, in order to generate the solution at eliminated nodes, from the specified conditions of similarity. The *CONDENSER* and *EXPANDER* routines can also deal with parameters being equal in magnitude and opposite in direction at specified boundary nodes.

8.4.4 Elasto-Plastic Boundary Element Program:

This is a two-dimensional elasto-plastic boundary element program developed in this work for dealing with elasto-plastic fracture mechanics problems. The program uses the same *CORRECT* subroutine explained before and shown in Fig.(8.6). Also it uses the same library of finite elements as integration cells for the purpose of domain integration required for elasto-plastic analysis. The program flow diagram is shown in Fig.(8.10) and the stages for an elasto-plastic boundary element analysis carried out by this program are as follows:

(a) *Data Preparation:*

In this stage the program reads all the information required to carry out an elasto-plastic boundary element analysis and generates the required vectors such as the prescribed displacement and traction vectors.

(b) *Assembly of G & H Matrices:*

The program in this stage generates and assembles the $\underline{G}$ and $\underline{H}$ matrices for the whole structure to form a system of equations in terms of boundary displacement and traction.

(c) *Boundary Conditions:*

In this stage the boundary conditions are applied to organize the matrices generated by the previous stage, so as to formulate a system of linear equations in terms of the unknown parameters at boundary nodes.

(d) *Load Increments Do-Loop:*

The total load applied to the structure is divided into a number of increments according to some ratios specified by the user in the data. Then the analysis is to be carried out several times by adding one load increment each time till the total load is applied completely. Inside this stage the following steps are carried out:

i. *Tractions Calculations:*

In this step the prescribed traction vector for each load increment is calculated according to the specified load ratio.

ii. *Solver:*

The generated system of equations is solved in terms of the current load increment. Since a large amount of computer *CPU* time is spent in eliminating the matrix of coefficients for equations, provision has been made in the *SOLVER* subroutine used in this program so as to eliminate the matrix only once. For further load increments, only the "*equivalent*" loading vector will be manipulated together with a backward substitution. Using the vector of prescribed values, the nodal displacement and traction vectors are defined for all boundary nodes.

iii. Boundary Calculations:

In this step the strains and stresses are calculated at every boundary node using the technique described in section (6.7.4). Old and new values are stored so as to facilitate stress correction carried out later.

iv. Internal Calculations:

All the field parameters such as displacements, tractions, stresses, and strains at internal nodes are calculated in this step, and old and new values are stored. The equivalent stress at every internal point is calculated and checked against the initial yield stress of the material. If any point has exceeded yield, next step is carried out, otherwise, the procedure goes to step (*f*).

(e) *Iterations Do-Loop:*

In this stage a plasticity check and a correction scheme are applied iteratively till a convergence is met. The steps inside this stage are:

i. Boundary stress correction at the specified boundary nodes.

ii. Internal stress correction at internal nodes defining integration cells.

iii. Estimation of "*equivalent*" residual force: Every integration cell is checked and if some of the nodes of a cell have plastic deformation, then an integration is carried out over the cell to estimate the effect of stress correction on boundary integral equations for every source point, as explained in chapter 6.

The stress correction is carried out using the *CORRECT* subroutine mentioned before, whilst additional subroutines are developed for calling *CORRECT* at boundary and internal nodes and for the estimation of "*equivalent*" residual force.

(f) Print Output:

The required output for each load increment is printed in this stage according to specified switches in the data.

(g) Last Increment:

When the last load increment is applied the program terminates the analysis and stops, unless an unloading calculation is required.

8.5 Fracture Mechanics Module:

This module has been designed for the evaluation of fracture mechanics parameters such as stress intensity factors, *J*-integrals, and crack-opening displacements. The module consists of two types of programs. The first type is programs using the finite element or the boundary element results to calculate the required fracture mechanics parameters. The second type is analytical solution programs based upon well-known analytical solutions to calculate mainly stress intensity factors and crack-opening displacements. In this section only the first type of programs are described, the rest of the programs are not included since they are simple and based upon well-known literature.

8.5.1 The General *J*-Integral Program:

This is a two-dimensional *J*-integral program based upon the algorithm given in chapter 7. The program has been developed in this work to use the finite element or the boundary element results for the evaluation of *J*-integrals for specified contours. It has the ability to calculate elastic, thermo-elastic, elasto-plastic, and domain loading *J*-integrals. The domain loading *J*-integrals are calculated using domain integration or the newly developed techniques of using boundary integrals. The structure of this program is illustrated in Fig.(8.11), and can be described as follows:

(a) DATA Subroutine:

This subroutine reads all the information required to carry out a *J*-integral calculation using finite or boundary element output. It uses the following subroutines to interpolate the field parameters at the Gaussian quadrature points if a domain loading analysis is based upon domain integration.

i- SHF Subroutine:

This subroutine uses the standard library of finite elements to generate shape functions for the integration cells specified by the user in the *DATA* subroutine.

ii- CGAUSS Subroutine:

This subroutine opens one of two Gaussian quadrature files depending upon the type of integration cells employed (*i.e. Quadrilateral or Triangular*), and reads the quadrature parameters for the selected scheme.

(b) INLOAD Subroutine:

This subroutine is designed to evaluate the domain and thermal loading terms in the *J*-integral, if such loading conditions are assumed, by using domain integration. The subroutine uses the *CGAUSS* subroutine described above and the following subroutines:

i. TRANS Subroutine:

This is a transformation subroutine, based upon the theory given in section (7.9), required for the calculation of *J*-integrals for oblique cracks, where the line of the crack is not lying on the x-axis.

ii. BMATRIX, CARTD, CJACOB, and INTRD Subroutines:

These subroutines are similar to the subroutines explained before in the finite element module, and they are used in this program for the same purpose.

(c) JINTI Subroutine:

This is an assembler subroutine which assembles the *J*-integral contour elements and provides the final value of the evaluated *J*-integral for a specified contour. It is also assembles the domain loading term calculated by the domain integration technique provided by the *INLOAD* subroutine. The subroutine calls the following subroutines:

i. JELP Subroutine:

This is a subroutine to generate the elemental plastic *J*-integral term required for an elasto-plastic *J*-integral analysis. The subroutine uses *JACOBC*, *GAUSS*, *GLAG*, and *DLAG*

subroutines, which are the same subroutines explained before in the boundary element module.

ii- JELE Subroutine:

This subroutine generates the the elastic elemental *J*-integral term by calling the same subroutines called by *JELP* subroutine.

(d) *JINT2 Subroutine:*

This subroutine is similar to *JINT1* subroutine but it is used for the calculation of the domain loading term by the boundary integral technique developed in this work. The subroutine uses the next subroutines in order to assemble the final value of the *J*-integral for the required contour.

(e) *JEBP & JEBE Subroutines:*

These subroutines are used for the generation of the elemental elastic and plastic *J*-integral terms required for an elastic or an elasto-plastic *J*-integral evaluation. The subroutines use the *DCOEF* subroutine, which generates the domain loading coefficients required for the boundary integrals.

8.5.2 Extrapolation Method Program for Symmetric Cracks:

This program is based on the theory explained in chapter 7. The program uses the finite and boundary element results such as stresses and displacements to calculate the nodal parameters K_I^* and K_{II}^* for symmetric cracks.

8.5.3 Program for Extrapolation Method of Unsymmetrical Cracks:

This is a program for the calculation of stress intensity factors K_I^* and K_{II}^* required for the extrapolation method and based upon the theory explained in chapter 3. The program uses the finite and the boundary element results to calculate the stress intensity factors for a specified orientation with respect to the crack plane. It employs a stress transformation technique to account for oblique cracks, and uses different combinations of stresses and displacements to generate a system of equations and then solve this system by using Gauss elimination solver. A part from the flow chart of this program is shown in Fig.(8.12), where a combination of σ_x and σ_y stresses have been used to calculate K_I^* and K_{II}^* stress intensity factors.

8.5.4 The General Curve Fitting Program:

This program is based upon the theory explained in chapter 7. The program uses the output of extrapolation method programs to calculate and plot the stress intensity factors K_I and K_{II} at the crack tip. The structure of this program is illustrated in Fig.(8.13) and can be explained as follows:

(a) PDATA Subroutine:

This subroutine reads the information required to carry out a curve fitting using the least-square method.

(b) CFIV Subroutine:

This subroutine reads an interactive data required by the program to select the type of fitting and some other parameters. Then it carries out the curve fitting and plotting by means of the next subroutines.

(c) *GLSQC & PLSQC Subroutines:*

These subroutines are based upon the least-square procedure. The first subroutine is used for the curve fitting in terms of general functions, whilst the second subroutine is used for polynomial curve fitting. Both subroutines use the *BFUN* function to generate the required system of equations.

(d) *SOLVER Subroutine:*

This is a Gauss elimination solver used for the solution of the system of equations generated by one of the above subroutines.

(e) *PLOTTER Subroutine:*

This is a plotting procedure based upon the *GINO* library. The subroutine is used to represent the original data and the fitted data graphically.

8.6 Post-Processing Module:

This module contains a suit of programs, developed in this work, based on *UNIRAS* and *GINO* libraries to represent the results obtained from the previous modules, and to produce hard copies. These programs have been used to create all results-figures presented in this work and they are as follows:

(1) *Graph Plotter based on Uniras Library.*
(2) *Graph Plotter based on Gino Library.*
(3) *Contour Plotter based on Uniras Library.*
(4) *UNIPICT Spooler based on Uniras Library.*

(a) The Graph Plotters:

These plotters are designed to represent a system of functions of one variable. The programs can generate graphs with straight line or curve-fitted segments, and also can draw shaded graphs.

(b) The Contour Plotter:

This program is designed to represent the results in a contour form. It can represent two-dimensional, three-dimensional, shaded, and annotated contours. Also the program can represent cracks, holes or contours within any geometrical shape. This plotter has also been used to plot plastic zones using the output of the finite element or the boundary element module.

(c) The UNIPICT Spooler:

This program has been designed to use the *UNIRAS* standard *UNIPICT* file created by previous programs, so as to produce hard copies or to display the results again without using the original plotters or the original data files.

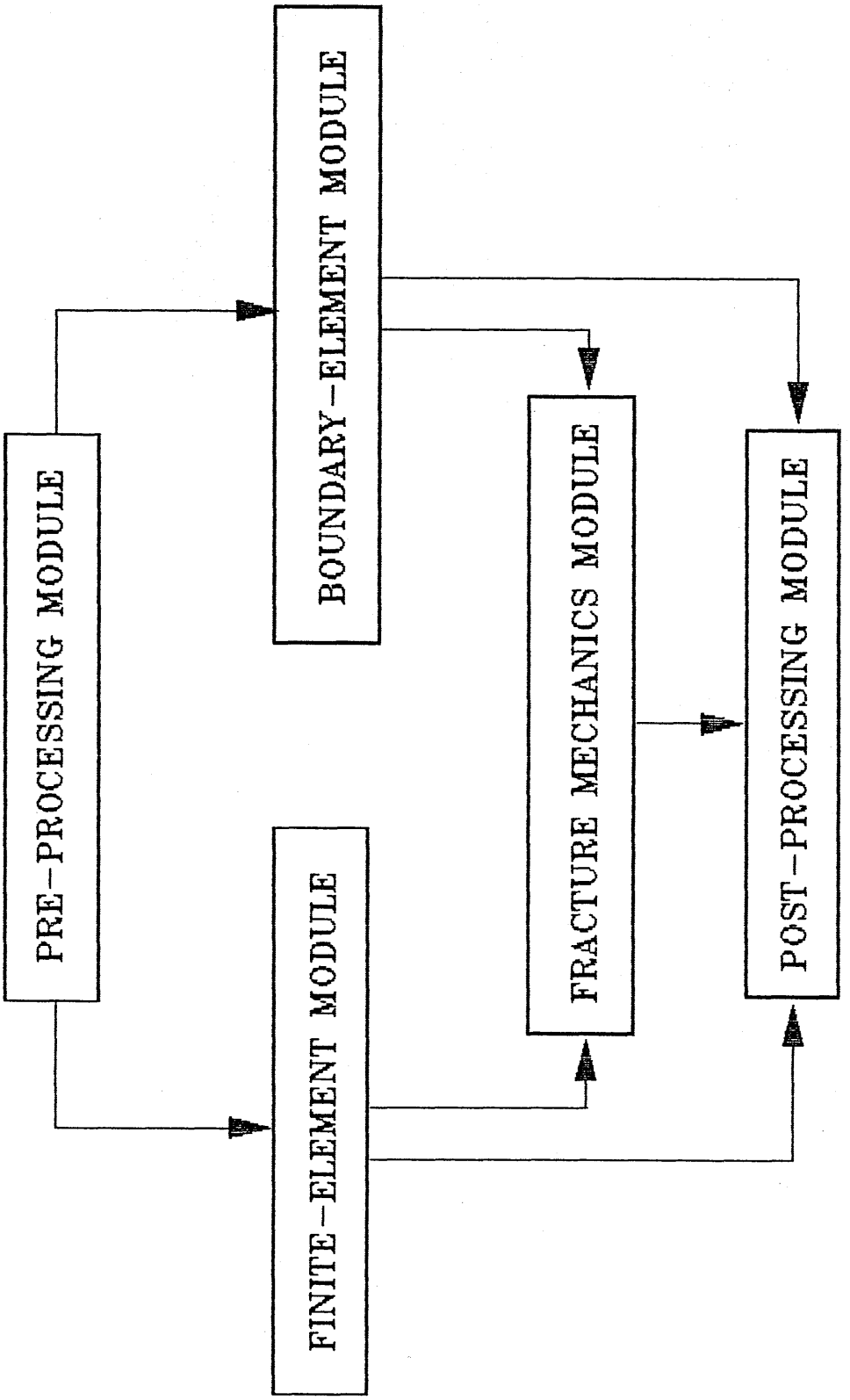

Fig.(8.1) FRAMEC Programming System.

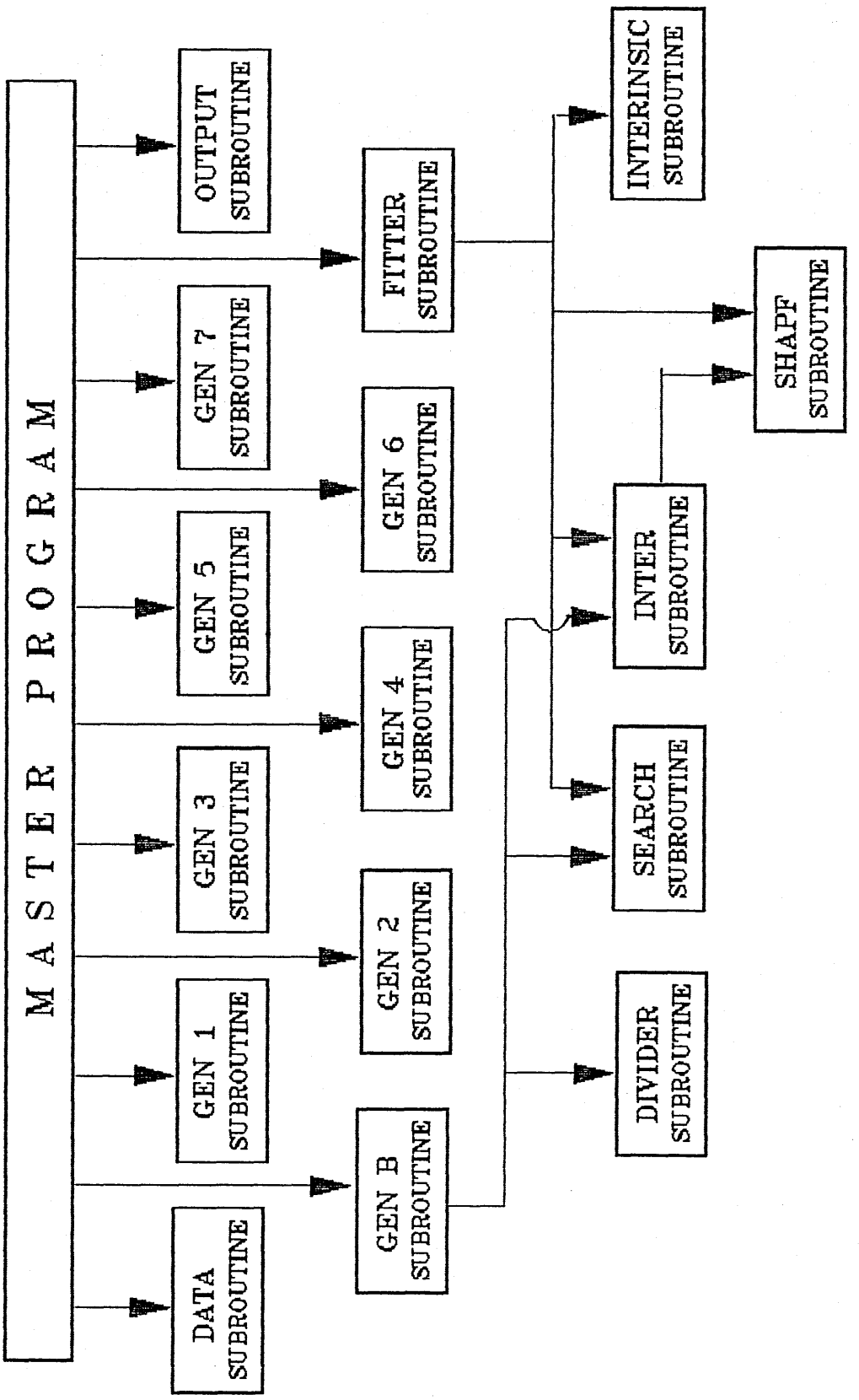

Fig.(8.2) Structure of the Two-Dimensional Mesh Generator Program.

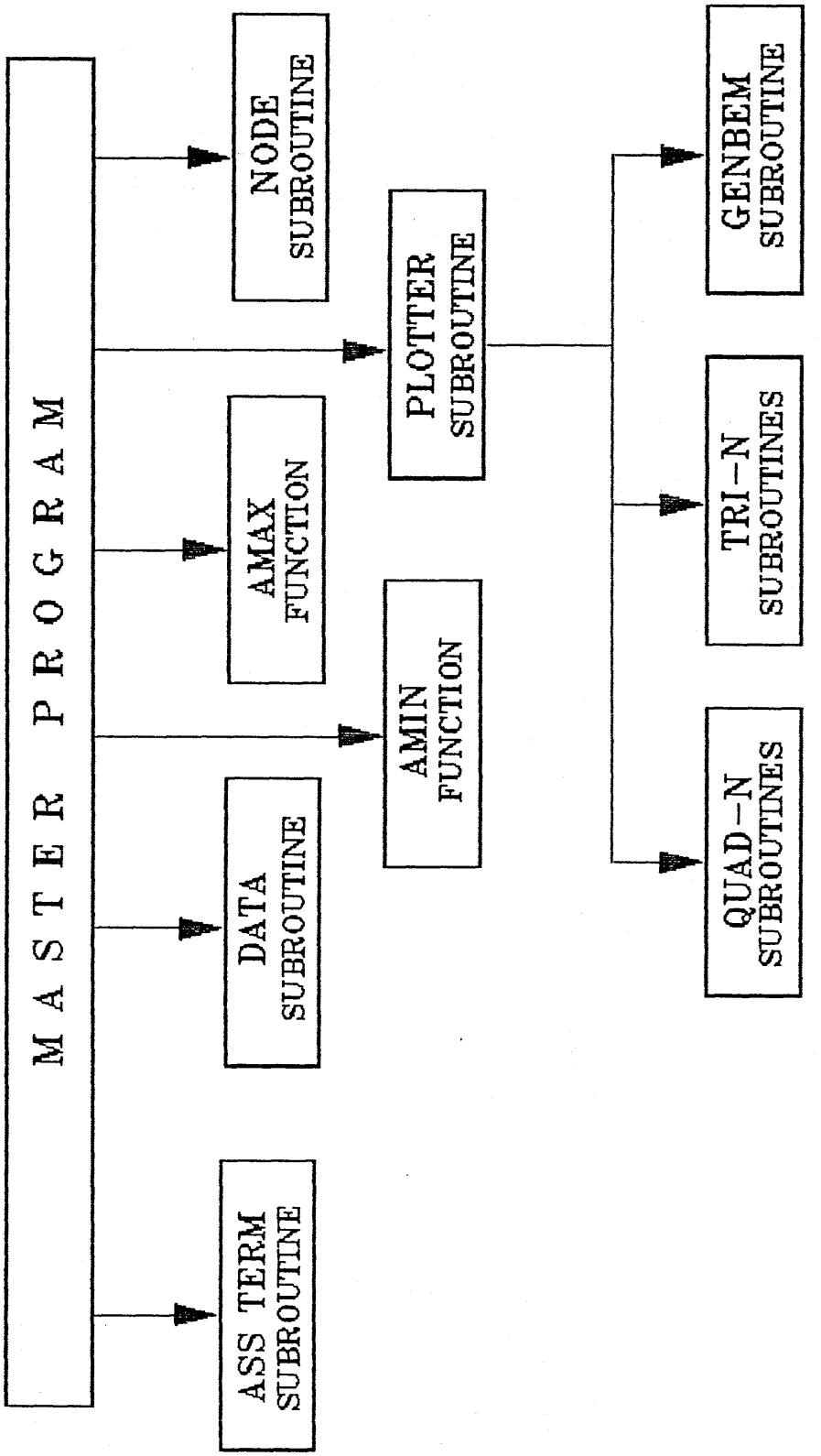

Fig.(8.3) Structure of the Two-Dimensional Mesh Plotter Program.

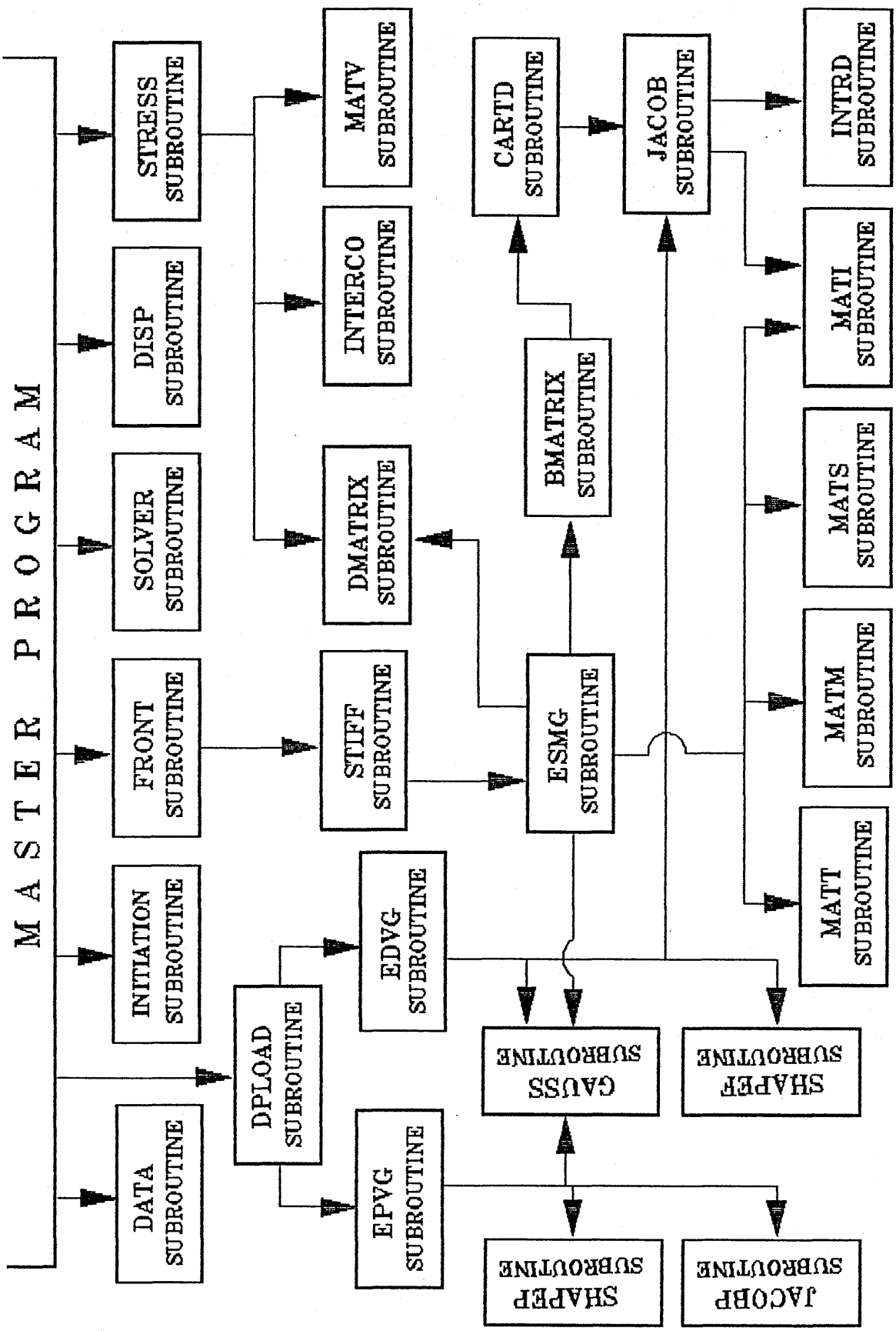

Fig.(8.4) Structure of the 2D Linear-Elastic Finite Element Program.

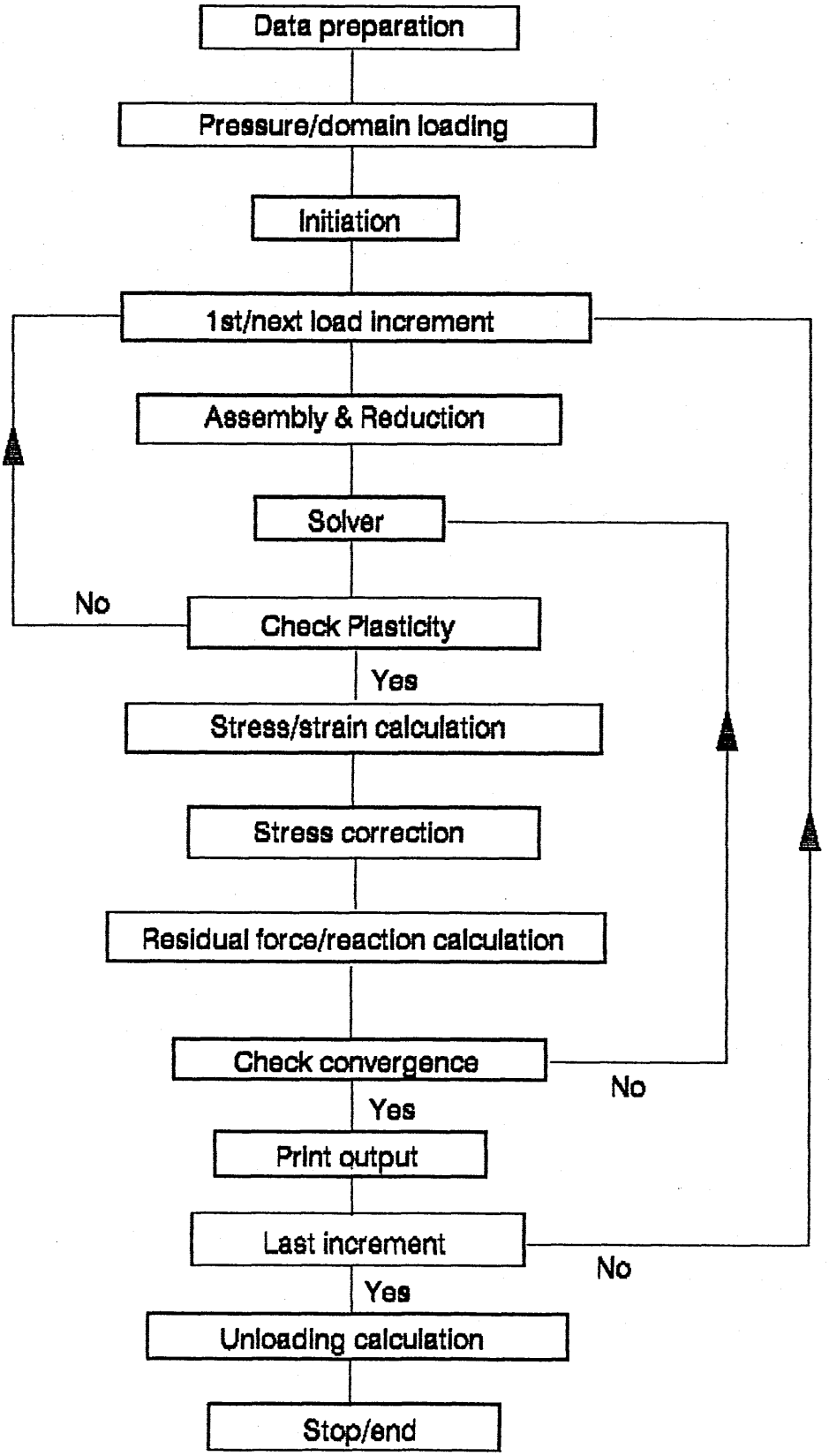

Fig.(8.5) Flow Diagram of the Elasto-Plastic FE Program.

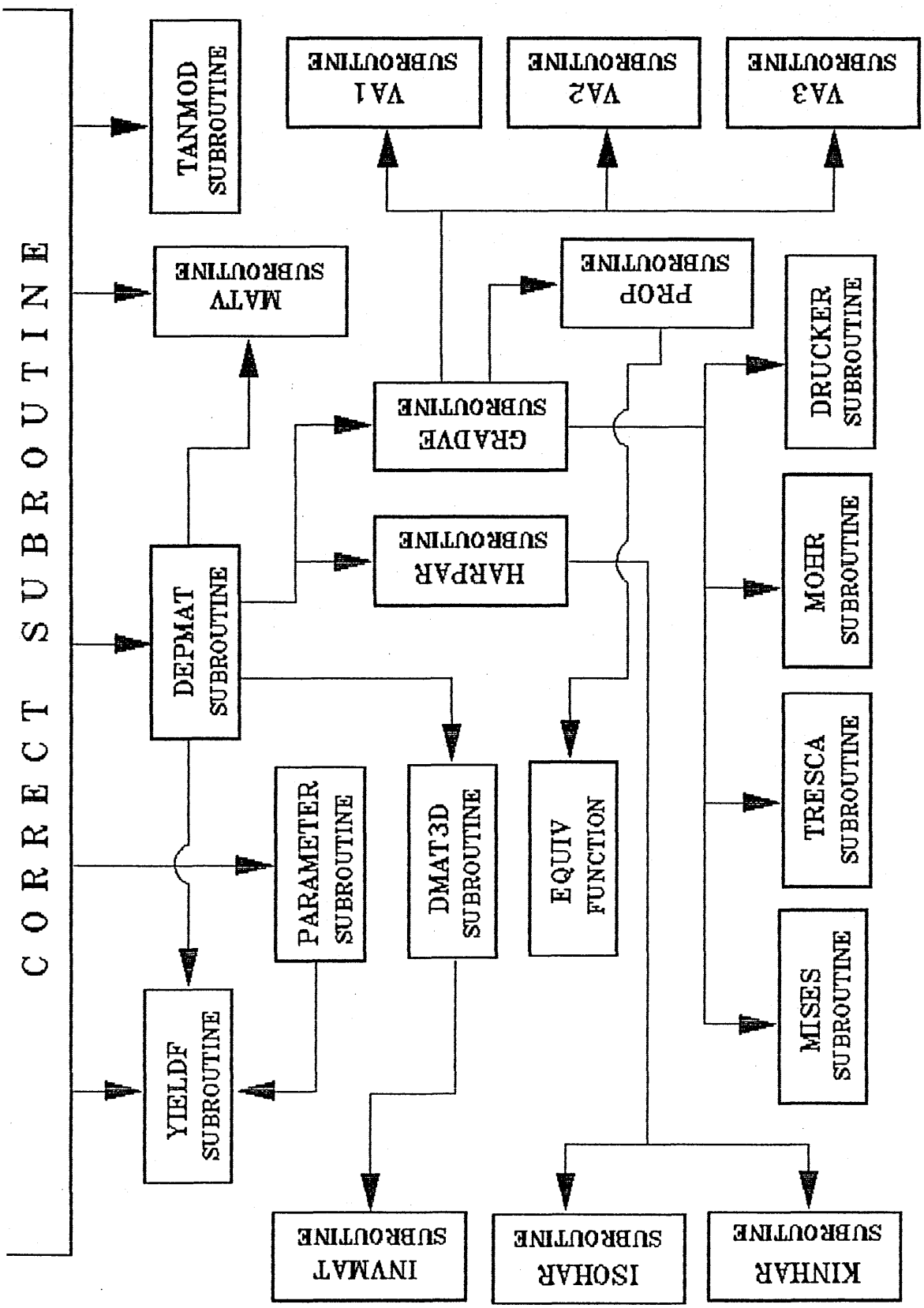

Fig.(8.6) Structure of 2D Plasticity Correction Subroutine.

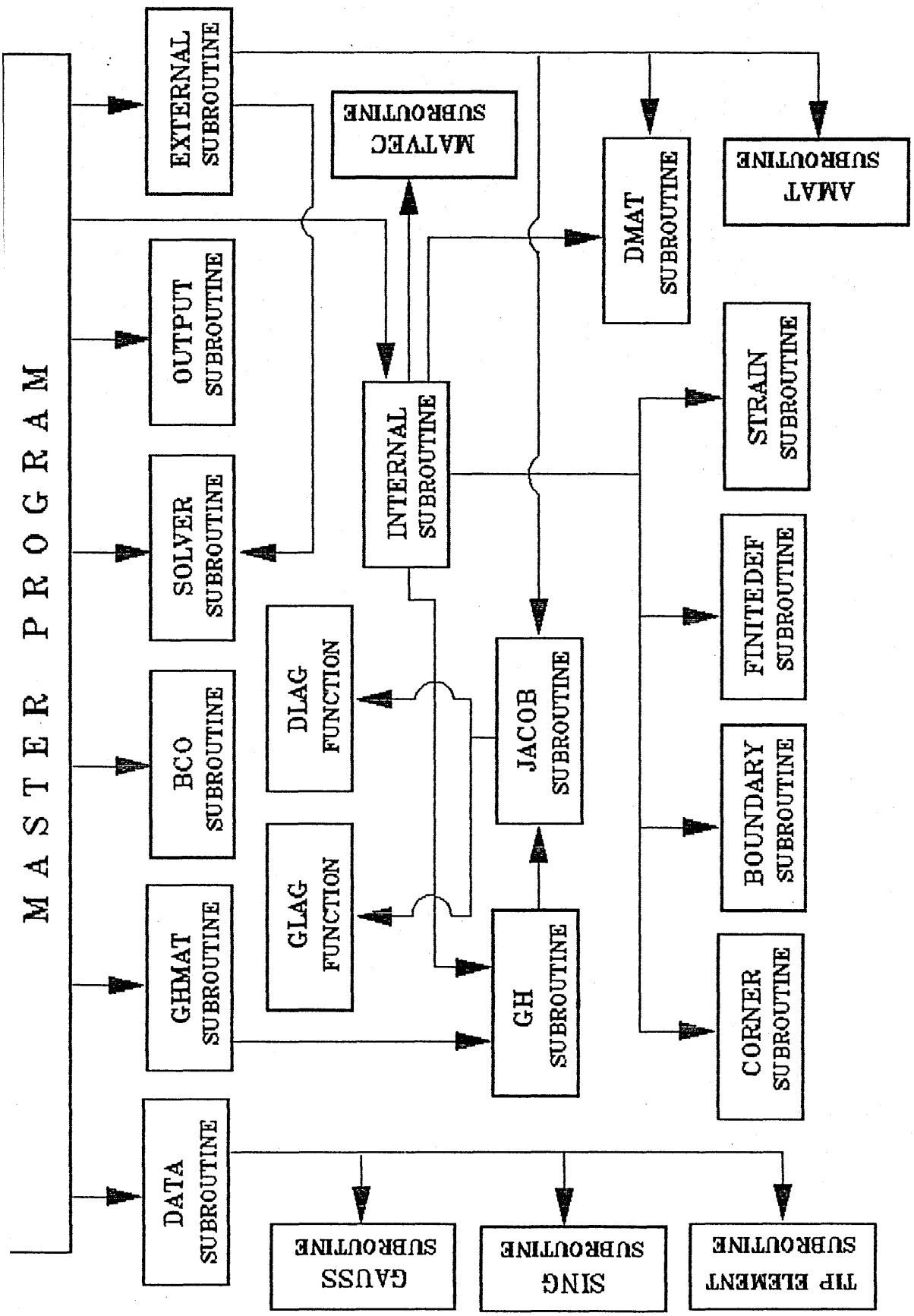

Fig.(8.7) Structure of 2D Linear-Elastic BE Program.

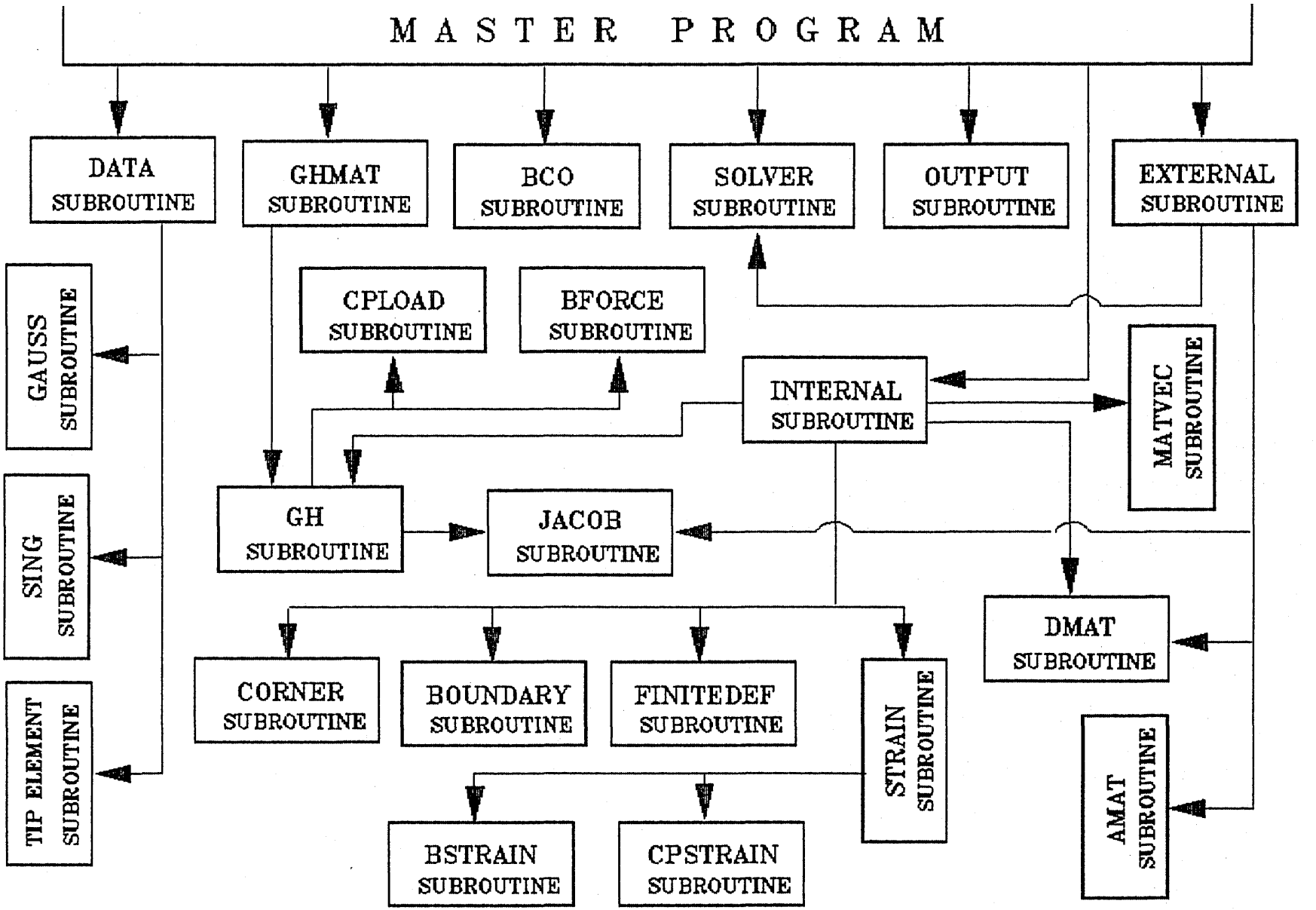

Fig.(8.8) Structure of 2D Domain Loading Elastic BE Program.

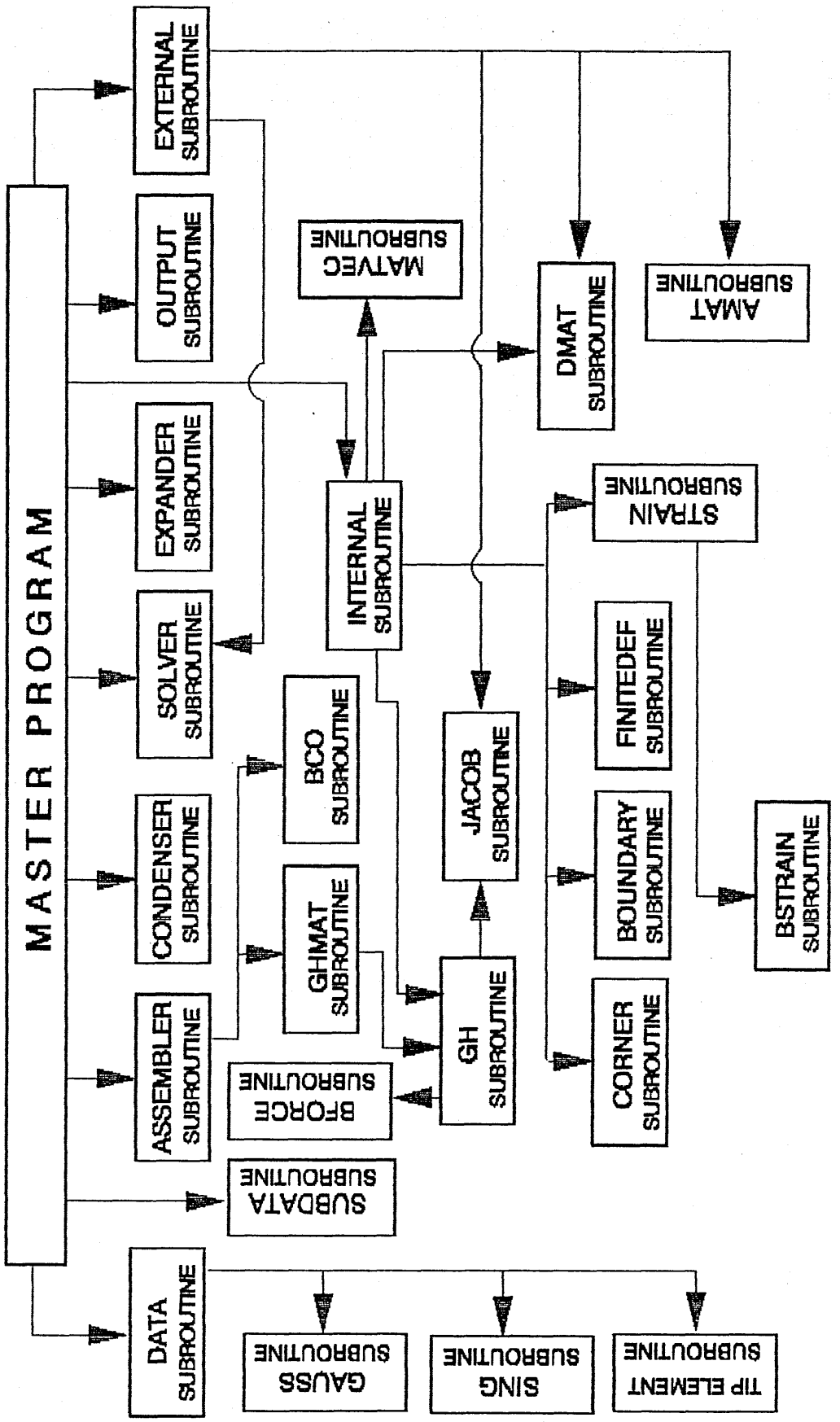

Fig.(8.9) Structure of 2D Subregion Elastic BE Program.

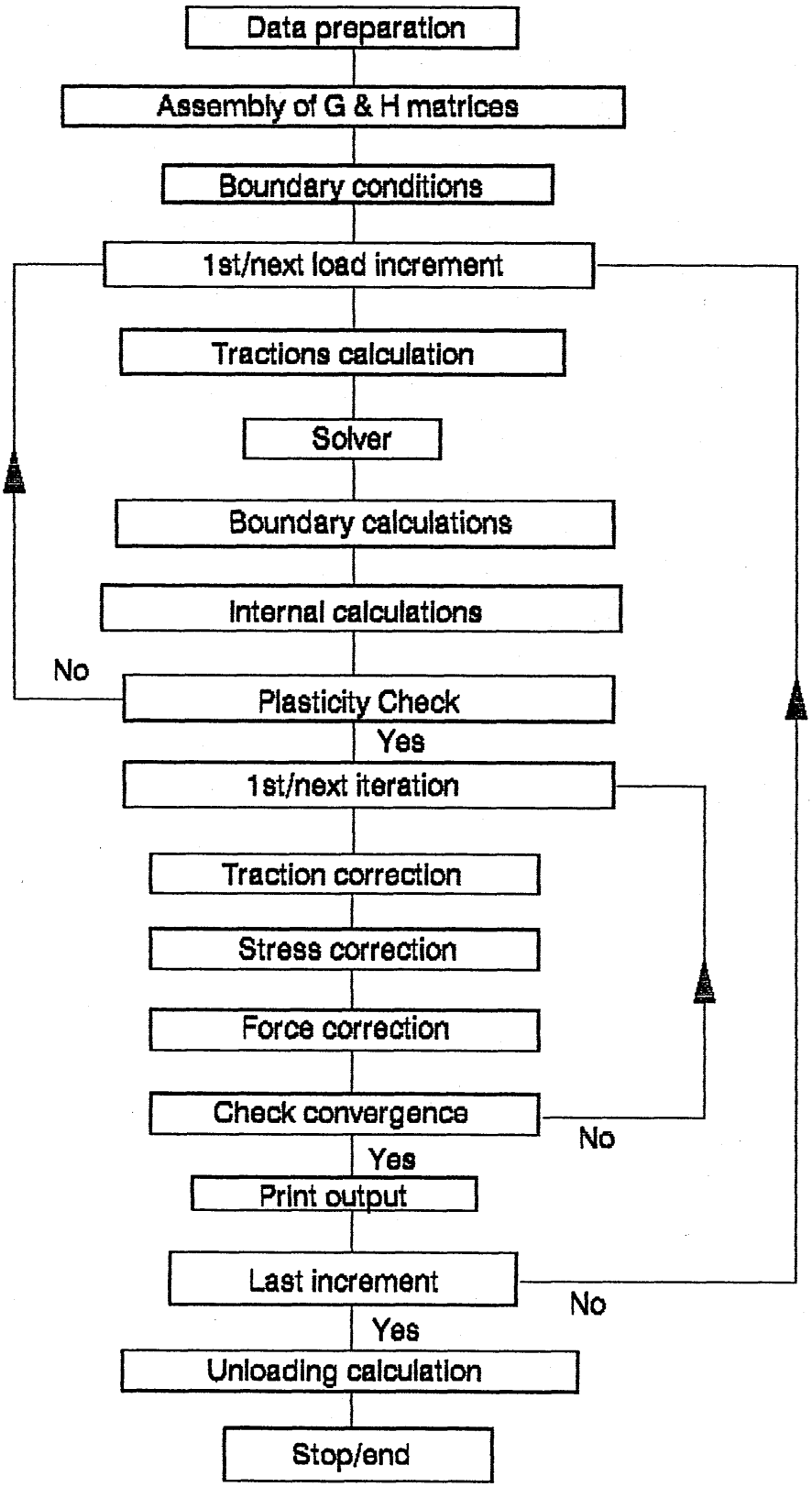

Fig.(8.10) Flow Diagram of the Elasto-Plastic BE Program.

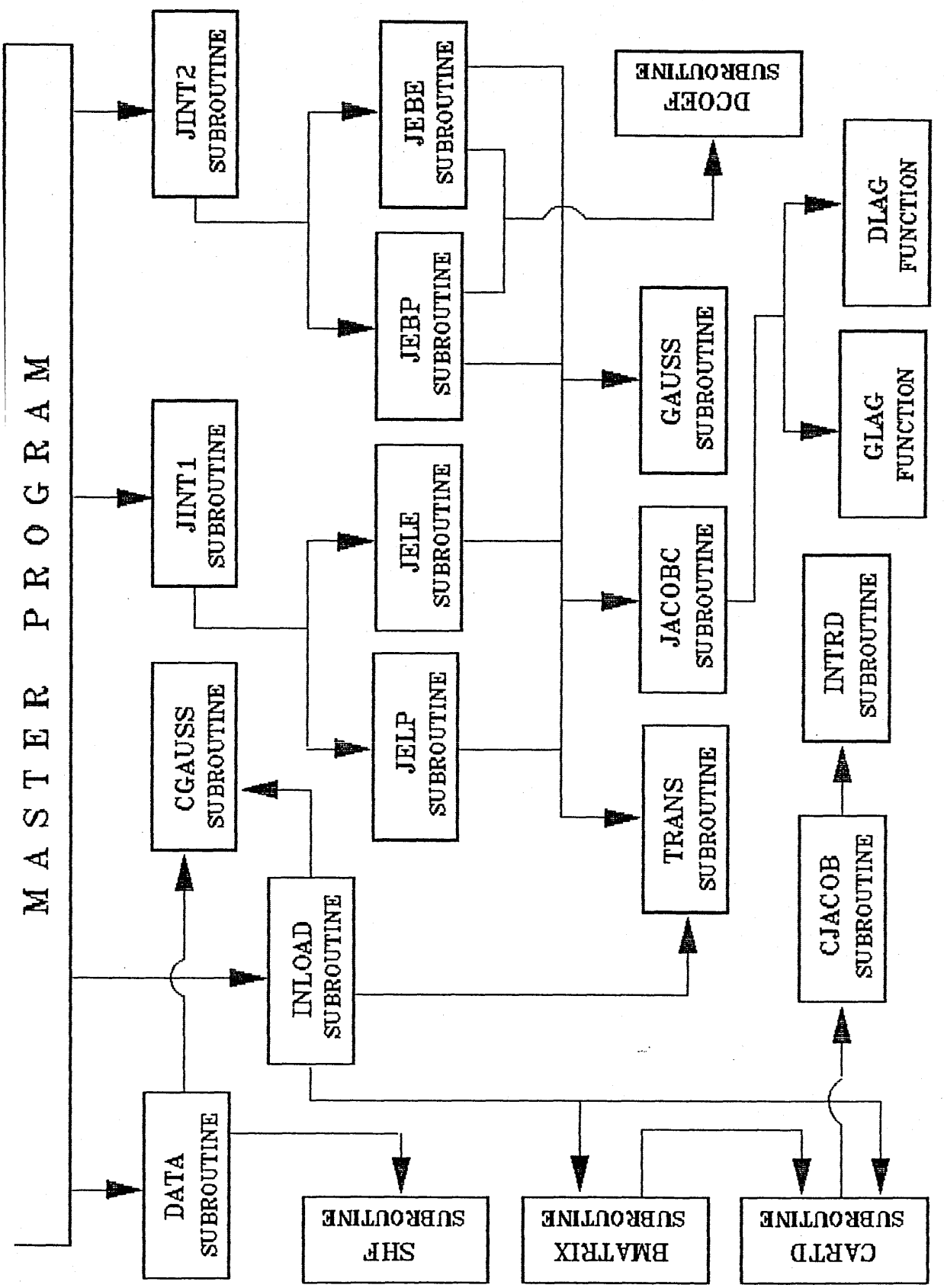

Fig.(8.11) Structure of the General J-Integral Program.

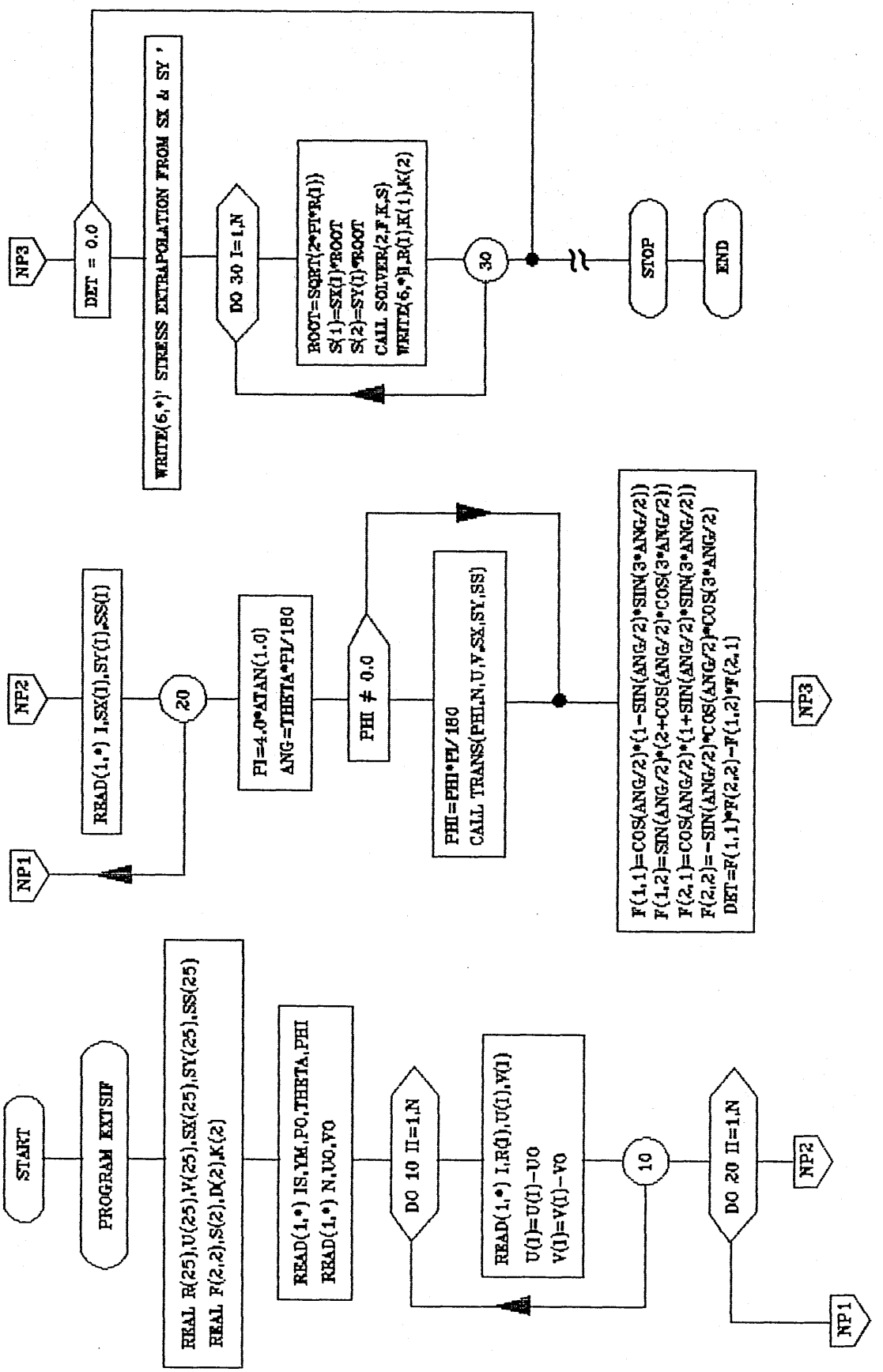

Fig.(8.12) Part from the Flow Chart of the Extrapolation Method Program for Stress Intensity Factors.

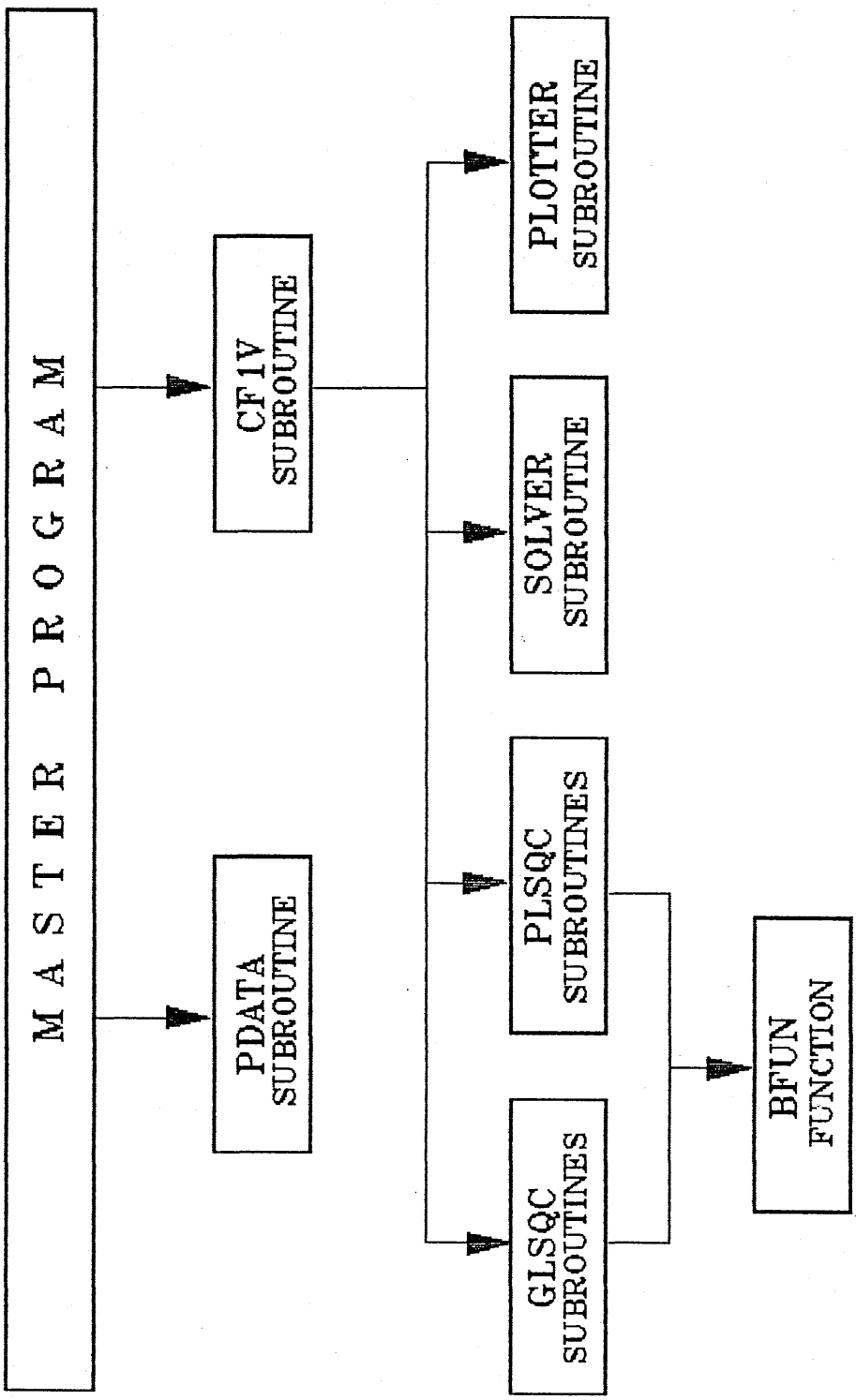

Fig.(8.13) Structure of the General Curve Fitting Program.

CHAPTER 9

RESULTS AND DISCUSSION

9.1 Introduction:

It is clear from chapter 8 that the package, developed in this work, contains many old and new elements and numerous facilities for engineering fracture mechanics analysis. Hence, it was essential to test every developed part, using cases with known analytical or published solutions so as to be sure of its validity. Many of such tests had been carried out in the course of the package development, and some of them will be reported here.

It was vital for such study to assess the efficiency and accuracy of different schemes developed for linear-elastic, and elasto-plastic fracture mechanics. Hence, a number of case studies, most of which have well-known solutions, had been selected, and fracture mechanics parameters such as stress intensity factors and *J*-integrals were evaluated using different methods possible, and some assessment have been carried out.

Since, the *BEM* could offer a numerical technique more efficient than many others, specially for dealing with *LEFM*, a comparison has been made between the *BEM* and its nearest competitor , the *FEM*, for a number of case studies, where accuracy of results, computer *CPU* time, and human being effort were monitored for each of the two methods.

In this chapter, some validation test cases, and case studies are described together with their results obtained by using the **FRAMEC** package developed in this work. The cases are divided into the following two basic sections:

(i) Linear-Elastic Cases.
(ii) Elasto-Plastic Cases.

Although some discussion will be given with every case study, aiming at results interpretation and comparison between

different techniques used, the chapter will end with a rather more general discussion about the efficiency and reliability of the basic facilities available in the package.

9.2 Linear-Elastic Validation and Case Studies:

The following linear-elastic finite and boundary element case studies have been analyzed using FRAMEC system.

9.2.1 Finite Element Simple Validation Test:

The aim of this simple test is to check the validity of the linear-elastic finite element program developed in this work by comparing the results obtained by using it with those obtained be means of an analytical solution. The test was carried out using a thin plate *(Plane-Stress condition)* under a uniform tensile load as shown in Fig.(9.1).

In order to validate the standard elements available in the finite element library used with this program, seven finite element meshes for the plate with different types of elements, as shown in Appendix [C], Figs.(C.1-C.7), have been employed. The meshes were generated and plotted using FRAMEC system pre-processing module.

The displacement distribution on the lower surface of the plate *(along the x-axis)*, as obtained for different meshes, is shown in Fig.(9.2) against the analytical solution. It is clear from the figure that the accuracy of results obtained for different elements tested are beyond any doubt.

The axial stress (σ_x) distribution along the y-axis, on the line $x = 1$, is also plotted for different types of elements against the exact answer for the case used ($\sigma_x = 1$), as shown

in Fig.(9.3) which confirms the validity of the stress routines in the *FEM* program.

It is worth mentioning that several other patch tests for plane-strain cases, cases with different types of loading, and cases with curved boundaries, had been carried out and proved that different facilities available in the *FEM* program are absolutely correct.

9.2.2 Boundary Element Program Validation Test:

The test is carried out to validate the isoparametric linear-elastic boundary element program developed in this work. A pressurized cylinder under a uniform internal pressure, as shown in Fig.(9.4), is used. Different boundary element meshes with different elements are generated for this case and can be reviewed in Appendix [C], Figs.(C.8-C.11).

The results of the boundary element program were compared with the well known Lame's solution. Fig.(9.5) shows the radial displacement distribution along the radius at $\theta = 45^{\circ}$. It is clear from this figure that the results obtained by using the 3-node isoparametric element are more accurate than the results obtained by the use of other elements.

The radial stress distribution along the same radius is shown in Fig.(9.6). It is clear from this figure that the 3-node and the 4-node isoparametric elements have given more accurate results compared with other elements.

Fig.(9.7) shows the hoop stress distribution along the same radius of $\theta = 45^{\circ}$. Again it is clear from this figure that the results obtained by using the 3-node isoparametric element are more accurate than the results obtained from other elements.

It is obvious from the three previous figures that, according

to Lame's solution, the 3-node isoparametric element has provided results more accurate than those obtained by means of the constant and the higher order isoparametric elements. The reason that the higher order elements have less accuracy than the 3-node element is related to the high round-off errors encountered with high-order interpolation within such elements.

Validation of other facilities available in the *BEM* programs such as different types of loading and subregioning will be demonstrated within the analysis of case studies discussed later.

9.2.3 Case Study of Centrally-Cracked Plate in Tension:

This case is as shown in Fig.(9.8) with all of the information required to carry out a finite or boundary element analysis. It is clear from this figure that only one quarter of the plate structure is required to be modelled in order to carry out the analysis, since the structure of the plate is symmetrical with respect to the x any y axes. The meshes for one quarter of the plate with different types of finite and boundary elements are given in Appendix [C], Figs.(C.12-C.17). In these meshes, a modest refinement has been employed in the area around the crack, since crack-tip elements described earlier have been used.

Different analyses were carried out for this case study, and different types of results were obtained. The results are categorized in the following sections.

(a) *Calculation of Stress Distributions:*

The distribution of the stress σ_y along the x-axis was calculated for the case study with a fixed crack length of 60 mm, using different types of standard and crack-tip, finite and

boundary elements, and it has been plotted as shown in Figs.(9.9-9.11), where r represents the distance from the crack tip along the x-axis.

Fig.(9.9) shows the stress distribution calculated by using the 9-node standard element, the 9-node crack-tip element, and the (1/SQR2) singular element developed in this work. It is clear from this figure that the use of one (1/SQR2) element in the left-hand side of the crack-tip has provided better accuracy than the use of two elements in both sides of the crack-tip or than one element in the right-hand side of the crack-tip.

Using the 6-node standard, isoparametric crack-tip, and collapsed crack-tip finite elements, the stress distributions were calculated and plotted as shown in Fig.(9.10), which indicates that the isoparametric crack-tip element and the first collapsed crack-tip element have given better distributions than the rest of the elements. This conclusion will become clearer in the next section where the stress intensity factors are presented and compared with an analytical solution.

The 3-node standard and crack-tip boundary elements were used to calculate the stress distribution for the same case study. This distribution is shown in Fig.(9.11), which proves that the crack-tip boundary element has given a stress value near the area of the crack tip higher than that obtained by using the standard element, especially when only one crack-tip element, located in the left-hand side of the crack-tip, is employed.

(b) *Calculation of SIF using Extrapolation Methods:*

The K_I stress intensity factor was calculated using extrapolation methods with different types of finite and boundary elements for the same case study, and the results are demonstrated in Figs.(9.12-9.21).

Fig.(9.12) shows the K_I stress intensity factor calculated using the 8-node finite, and 3-node boundary, standard elements, at points on the line inclined an angle $\theta = 0^\circ$ from the crack surface. It is clear from this figure that the results obtained by using stress values can easily be extrapolated to an accurate value of K_I, compared with the results obtained from displacement values. Also it can be seen from the figure that the 3-node boundary element has given accuracy much better than that obtained by means of the 8-node finite element with reference to Feddersen's solution [Ref.7].

On the line with angle $\theta = 90^\circ$, the K_I stress intensity factor for the same case study was calculated using the same elements, and the results are shown in Fig.(9.13) and Fig.(9.14), which indicate that both elements have given good results compared with Feddersen's solution mentioned earlier.

Similarly, at $\theta = 180^\circ$, the stress intensity factor K_I was calculated using the displacement extrapolation method, as plotted in Fig.(9.15), which proves that, for this particular case, the results obtained using the 3-node boundary element are more accurate than the results obtained using the 8-node finite element.

The curve fitting technique discussed earlier has been employed with the boundary element results of the stress intensity factor, as shown in Fig.(9.16). It is clear from this figure that the results obtained are more accurate than the results obtained by means of manual fitting as shown in the previous figures.

Different types of elements; old and new, standard and crack-tip, finite and boundary elements have been employed for the analysis of the previous case study and stress and displacement results have been used for the estimation of K_I stress intensity factors. Curves leading, by means of extrapolation, to the value of K_I *(at the crack tip)* are shown

in Figs.(9.17-9.22), and extrapolated values of K_I have been compared with the corresponding Feddersen's solution [Ref.7]. To facilitate the comparison, curves for similar types of elements have been plotted together, and the results can be summarized as follows:

i. For the 8-node standard and crack-tip elements, it is clear from Fig.(9.17) that it is hard to find any appreciable improvement gained by the use of that crack-tip element.

ii. Although the use of the 3-node, crack-tip, boundary element may cause some disturbance in results near the crack tip, as shown in Fig.(9.18), it has been found that the use of one crack-tip element as such in the right-hand side of the crack tip *(material side)* leads to smooth curves which can be extrapolated to a very accurate value for the stress intensity factor K_I.

iii. The 9-node elements developed in this work; the 9-node crack-tip element and the **(1/SQR2)** singular element have shown some improvement of accuracy compared with the standard 9-node element, as demonstrated in Fig.(9.19). Some disturbance of results has occurred near the crack tip, when the **(1/SQR2)** element is used, but this can be avoided if only one of such elements is employed at the left-hand side of the crack tip, or if more refined mesh is used.

iv. Comparing the results obtained by means of several collapsed 6-node elements, developed in this work, against those from standard and crack-tip, 6-node triangular elements, as illustrated in Fig.(9.20), it was proved that the first collapsed element, in which no distortion of node locations is required, has yielded the most accurate answer. It has also shown the minimum disturbance of results near the crack tip.

v. Testing the cubic elements; the 12-node standard and crack-tip quadrilateral elements, and the 10-node standard and crack-tip triangular elements, against one another, as shown in Fig.(9.21), it is clear that crack-tip elements have very little effect on extrapolated answers, except in minimizing the disturbance of results near the crack tip.

vi. When comparing the K_I values obtained by using different types of elements, as demonstrated in Fig.(9.22), it is obvious that most of the new elements developed in this work perform well near the crack tip and lead to some improvement in the accuracy of the extrapolated K_I values. One should deduce that such improvement in accuracy would have become significant if coarser meshes have been used for this analysis.

(c) *Calculation of SIF using the J-Integral Technique:*

Under linear-elastic fracture mechanics conditions the J-integral value is equivalent to the energy release rate G. This correlation can be used to calculate the stress intensity factor K_I as explained before in chapter 3. Using this approach, the stress intensity factors from standard finite and boundary element results have been calculated for the same case study with different crack lengths and compared with the values obtained from five different analytical solutions available in the literature, as shown in Fig.(9.23). It is clear from this figure that the finite and the boundary element results are in good agreement with the analytical solutions for a wide range of crack length.

Using different crack ratios, the non-dimensional stress intensity factors for the same case study have been calculated from finite and boundary element results, as illustrated in Fig.(9.24). This figure shows that the finite and boundary element results are in good agreement with the analytical

solution for crack ratios of values more than 0.1. The reason for this phenomenon is that for the case of a short crack, a very fine mesh should have been used in the vicinity of the crack tip to model accurately the stress distribution in this area.

The same technique has been used to calculate the stress intensity factor K_I for the same case study with a fixed crack length of 60 mm, by means of 9-node and (1/SQR2) elements. A comparison between the stress intensity factors calculated by means of these elements using different *J*-integral contours at different distances from the crack tip is shown in Fig.(9.25), which proves that the use of 9-node standard, crack-tip, and (1/SQR2) elements gives good accuracy compared with Irwin solution. Also this figure indicates that the results of the *J*-integral technique are path independent.

(d) *Calculation of CTOD under Linear-Elastic Conditions:*

The crack-tip opening displacement, δ_t, has been calculated, using the curve fitting technique, from finite and boundary element results for the same case study. The results are shown in Fig.(9.26) and Fig.(9.27) respectively. It is clear from these two figures that the use of the curve fitting technique for the calculation of the *CTOD* has provided an acceptable accuracy compared with Dugdale solution [Ref.7], whilst the use of linear extrapolation, as suggested in the literature and shown in Fig.(9.28), leads to less accurate results.

(e) *Plotting of Displacement and Stress Contours:*

The displacement and stress contours for the same case study have been generated and plotted from the finite element output using post-processing facilities available in the present programming package. Fig.(9.29) shows contours of the

displacement in the y-direction, whilst Fig.(9.30) shows contours of the stress in the y-direction. These two figures show the behaviour of the displacement and stress distributions for a cracked plate under uniform tension, also it is clear from Fig.(9.30) that the highest stress concentration occurs near the area of the crack tip, and this behaviour of stresses agrees well with the theoretical prediction that the stresses at the crack tip have infinite values.

9.2.4 Case Study of Single-Edge Cracked Plate in Tension:

This case is a single-edge cracked plate with an oblique crack at angle $\theta = -45^{\circ}$, as shown in Fig.(9.31), subjected to a uniform tensile loading. Finite and boundary element analyses have been carried out using the meshes shown in Appendix [C], Figs.(C.18-C.19).

Such a case study was very useful for the validation of the subregion technique developed in this work for the *BEM*, and it has been proved, in the course of the analysis, that without such a technique it would become impossible to obtain accurate answers from the *BEM* for any case with an oblique crack being a part of its whole boundary, since it seems that every two opposite boundary elements on the two surfaces of the crack tend to cancel each other.

For such a case study, fracture modes *I* and *II* exist, and this has provided a chance for testing and validating not only the procedures for calculating K_I and K_{II} stress intensity factors, but also the use of the *J*-integral for defining an equivalent stress intensity factor, under linear-elastic conditions.

The stress results obtained by means of the *FEM* and the *BEM* have been used together with different combinations of simultaneous equations given in section (3.3.3), so as to obtain values for K_I^* and K_{II}^* at different distances from the

crack tip, on the line with $\theta = 0$. Due to the nature of the resulting curves, as can be observed in Figs.(9.32-9.34), it was decided to employ the *Extrapolation-Curve-Fitting* technique, developed in this work, so as to obtain the true values of K_I and K_{II}, at the crack tip, which have then been compared with the corresponding analytical solution, as given by Rooke & Cartwright [Ref.33].

The curves for K_I and K_{II} extrapolation, based upon stress components σ_x and σ_y obtained from the finite element and boundary element analyses, are shown in Fig.(9.32) which emphasizes the good agreement of package results compared with the analytical solution.

Using each one of σ_x and σ_y stress components together with τ_{xy} component, for the evaluation of K_I and K_{II} values, two sets of curves have been obtained, as illustrated in Fig.(9.33) and Fig.(9.34), respectively.

One may deduce, from Fig.(9.33), that the σ_x-τ_{xy} combination has led to well-defined curves for K_I, with an extrapolation easier than with corresponding curves in Fig.(9.32), should the manual extrapolation have been used. The figure indicates also that the *FEM* results tend to be extrapolated to answers more accurate than those obtained by extrapolating the corresponding *BEM* results.

Alternatively, the curves resulting from the σ_y-τ_{xy} combination, as represented in Fig.(9.34) have all reasonable curvatures, and the *BEM* extrapolated K_I value seems to be very accurate indeed. One should, of course, have guessed that computer limitations have restricted the usage of very fine meshes required for such cases with irregular geometries.

The equivalent stress intensity factor can be calculated for such a case study, by means of the following formula, suggested in the literature:

$$K_{eq} = \sqrt{K_I^2 + K_{II}^2}$$

Using this formula, the equivalent stress intensity factor for different stress combinations have been calculated from the finite and the boundary element results, and compared with the analytical solution, as can be seen in Fig.(9.35) and Fig.(9.36) respectively. It is clear from these two figures that the best accuracy has been gained from the combination of σ_y and τ_{xy} stress components, where both the finite and the boundary element results have given nearly the same value for K_{eq} stress intensity factor.

Using the *J*-integral technique, the values of K_{eq} were calculated and compared with the analytical solution, as shown in Figures (9.37) and (9.38) . Fig.(9.37) shows the K_{eq} stress intensity factor for this case study calculated using the finite-element results at different contours around the crack tip. It is clear from this figure that the calculated stress intensity factors are in a reasonable agreement with the analytical solution, also it shows that the values of the stress intensity factor calculated at different contours are in close agreement with each other, proving that the *J*-integral values are path independent.

A comparison between the K_{eq} values calculated be means of the *J*-integral technique, and the corresponding value from the analytical solution, is demonstrated in Fig.(9.38) which indicates that the *BEM* value is nearer to the analytical solution of Rooke & Cartwright than the corresponding *FEM* value.

The maximum stress contours for this case study has been generated using finite element results, and plotted in three dimensions as shown in Fig.(9.39), which demonstrates that the maximum stress concentration for this case has occurred at the area near the crack tip, whilst the minimum stress concentration has occurred on the surfaces of the crack itself.

9.2.5 Case Study of Centrally-Cracked Rotating Disc:

In order to verify the calculation of domain loading conditions in FRAMEC system, finite and boundary element analyses have been carried out for the centrally-cracked rotating disc shown in Fig.(9.40). Due to the symmetry of the disc, only one quarter of it has been modelled using the Meshes shown in Appendix [C], Figs.(C.20-C.21).

Using the *J*-integral technique for the case of domain loading, the *J*-values for this case have been calculated from the finite and boundary element results for different crack ratios and compared with the analytical solution of Rooke & Cartwright [Ref.33] as shown in Fig.(9.41), which proves that the *J*-values calculated from the finite and boundary element results are in a very good agreement with the analytical solution values up to a crack ratio of a/R = 0.35, beyond which the analytical solution is no longer valid. Also it is clear from the figure that the finite element and the boundary element results are in a very good agreement with each other.

The K_I stress intensity factor has been calculated for this case study using the *J*-integral values obtained before, and shown in Fig.(9.42). Hence, it is clear that the results of this figure exhibit the same accuracy as demonstrated in the previous one.

In order to study the effect of the crack ratio and the domain loading conditions on the path independency of the *J*-integral, the *J*-values at different contours around the crack tip have been calculated for different crack ratios, as shown in Figs.(9.43-9.46). It is clear from these figures that the domain loading conditions have no effect on the path independency of the *J*-integral. However, the crack ratio has some effect not only on the path independency of the *J*-integral but also on the accuracy of the results compared with the analytical solution. This fact is very clear in Fig.(9.43) when

the crack ratio is very small, and it can be seen that the best agreement with the analytical solution is gained when the crack ratio a/R = 0.25 as seen in Fig.(9.44). Also, it is clear from Figs.(9.45-9.46) that when the crack ratio exceeds the limiting value of a/R = 0.35, the *FEM* and *BEM* *J*-integral values, although converging with each other, start to diverge away from the analytical solution, whilst the path independency of their *J*-integrals improves noticeably.

9.3 Elasto-Plastic Validation and Case Studies:

Before using *FEM* and *BEM* elasto-plastic programs developed in FRAMEC system for the analysis of elasto-plastic fracture mechanics, it was essential to validate such facilities. A number of validation cases, with known analytical solutions, have been tested, and some of them will be reported here, followed by results and discussions for some interesting case studies.

9.3.1 Finite Element Elasto-Plastic Validation Case:

This case is a pressurized cylinder, as shown in Fig.(9.47), with increasing internal pressure and plane-strain conditions. Due to the symmetry of the problem, only one quarter of the structure has been meshed using 8-node finite elements as shown in Appendix [C], Fig.(C.22). The analysis has been carried out in different stages, as follows:

(a) *Analysis with Pressure in the Elastic Range of the Material:*

Since the elasto-plastic analysis is based upon the incremental theory, which requires the loading to start with an increment generating stresses below the yield stress of the material

(i.e. elastic analysis), it was necessary then to verify the elasto-plastic analysis at this stage. Hence, an initial pressure increment of 10 N/mm^2 has been applied to the structure, causing the stresses to be within the elastic range of the material.

Fig.(9.48) shows the elastic radial displacement distribution for this case compared with the analytical solution given in Ref.[72] and with the **ABSEA** finite element package. It is clear from this figure that the results of **FRAMEC** finite element module agree well with the other results. Similar agreement has been achieved for the elastic radial stress and hoop stress distributions as can be observed in Figs.(9.49-9.50).

(b) *Elasto-Plastic Analysis with Pressure Higher than the Elastic Range:*

Increments of pressure leading to plastic deformation have then been applied, and the results for the case with a pressure of 16 N/mm^2, *(causing plasticity up to the radius of 135 mm)*, are demonstrated here. The elasto-plastic radial and hoop stress distributions have been plotted as shown in Fig.(9.51) and Fig.(9.52) respectively, which illustrate that the results of **FRAMEC** system have more or less the same accuracy as the analytical solution and **ABSEA** package, and this agreement in accuracy level may verify that the elasto-plastic procedure employed in **FRAMEC** system is absolutely correct.

Using von Mises yield criterion, the equivalent stress distribution has been calculated and plotted in contour form, as shown in Fig.(9.53), which shows that the maximum equivalent stress distribution occurs in the area near the internal surface of the cylinder, also this figure shows the size of the plastic zone and the plastic zone boundary.

(c) *Elastic Unloading from Pressure Higher than the Elastic Range:*

In order to calculate residual stresses and validate the unloading facility in the **FRAMEC** finite element module, an unloading elasto-plastic analysis has been carried out when the pressure reached the value of 16 N/mm^2. The residual radial and hoop stress distributions have been calculated and shown in Fig.(9.54) and Fig.(9.55) respectively. It is clear from these two figures that the results of **FRAMEC** system are more close to the analytical solution than the results of **ABSEA** system.

The residual radial and hoop stress contours have been plotted as can be seen in Fig.(9.56) and Fig.(9.57) respectively. Fig.(9.56) shows that the maximum residual radial stress distribution occurs in the area near the internal surface of the cylinder, whilst the minimum residual radial stress distribution occurs on the outer surface of the cylinder. Similarly, Fig.(9.57) illustrates that the maximum residual hoop stress distribution occurs in the internal surface of the cylinder, and it ia a compressive stress, which may be useful to improve the strength of the material, if the structure is re-loaded (*Autofrettage*).

(d) *Elasto-Plastic J-Integral Validation with Different Pressure Values:*

Before applying the *J*-integral elasto-plastic algorithm to cracked components, an attempt has been made to validate it, using a reliable solution. The present case study is very useful, since it has an analytical solution for elasto-plastic displacement, stress and strain, but the actual value for any *J*-integral around a closed contour within the cylinder is zero, since it has no crack. Hence, a non-trivial *J*-integral value does exist, if only a part of a complete contour is considered.

An analytical solution for the value of the *J*-integral, considered only around the outer boundary of the cylinder has been derived in this work using Tresca yield criterion, as shown in Appendix [D], and the final expressions of the *J*-integral for plane stress/strain conditions are given as follows:

$$J = \frac{r_o}{2E} y^2 \left[\frac{C}{r_o}\right]^4 \qquad \textit{for plane-stress condition,}$$

$$J = \frac{r_o}{2E} y^2 \left[\frac{C}{r_o}\right]^4 (1-\nu^2) \qquad \textit{for plane-strain condition.}$$

where,

C = The radius of the plastic zone,

r_o = The outer radius of the cylinder.

Elasto-plastic *J*-integral calculations have been carried out using different pressure values ranging from elastic to plastic, for both plane-stress and plane-strain conditions and using Tresca yield criterion. The results are compared with the above analytical solution and shown in Figs.(9.58, 9.59). It is clear from these two figures that the finite element *J*-integral results are in a very good agreement with the analytical solution up to the pressure value of 14 N/mm^2. However, for pressures higher than that, the *FEM* *J*-integral value starts to diverge from the analytical solution. This may be related to the accumulation of errors during the elasto-plastic finite element analysis, and to the growth of the plastic zone at high pressure levels.

9.3.2 Boundary Element Elasto-Plastic Validation Case:

In order to validate different facilities available in the boundary element elasto-plastic programs developed in this work, an analysis has been carried out, using a case similar to the previous one, with different loading conditions, and one

and two subregions. The boundary element meshes and the corresponding integration-cell finite element mesh are shown in Appendix [C], Figs.(C.23-C.25), respectively.

(a) *Case with Pressure Loading Only:*

A boundary element elasto-plastic stress analysis has been carried out for the case study, under different pressure values, assuming the von Mises yield criterion, and ignoring strain-hardening effects.

The resulting hoop and radial stress distributions, for the pressure values of 14 and 16 dN/mm^2 have been compared with the corresponding finite element and analytical solution results, as shown in Figs.(9.60-9.63).

It is clear from figures (9.60) and (9.61), which demonstrate the radial distributions of hoop and radial stresses at the pressure value of 14 dN/mm^2, that the boundary element results are even slightly more accurate than the corresponding finite element results, compared with the analytical solution. This may prove that the boundary element elasto-plastic algorithm is completely reliable. However, the hoop and radial stress distributions at the pressure of 16 dN/mm^2, as can be seen in figures (9.62) and (9.63), indicate a slight drop in accuracy, compared with the analytical solution, due to the accumulation of errors resulting from the increase of the plastic zone.

(b) *Case with Subregions:*

The previous case has also been analyzed using the elasto-plastic, boundary element, subregion program developed in this work. Two different meshes were tested, one with only one subregion and the second with two subregions, as shown in Appendix [C], Figs.(C.23, C.24).

The hoop and radial stress distributions, at pressure 14 dN/mm^2, are presented in figures (9.64) and (9.65), respectively, which prove that subregioning technique leads to an improvement in the accuracy of the *BEM* analysis.

The subregion program contains a facility which allows the user to select one or more subregions to be elastically analyzed only, depending upon his prediction of the expected plastic zone. When such a facility has been tested by considering the case with two subregions, such that only the inner subregion would be analyzed plastically, a significant saving of the computer *CPU* time has been achieved, with the same level of accuracy, proving the usefulness of such a facility which can only be employed with subregioning.

(c) *Case with Pressure and Thermal Loading:*

The previous case of the pressurized cylinder was reconsidered when its inner surface was kept at a temperature of 120 ^{o}C, whilst the outer surface was at 20 ^{o}C.

Boundary element programs for heat conduction, with and without subregions, as developed in this work, have been employed to calculate the values of temperature and its gradient at different nodes, and feed them to the elasto-plastic programs. The resulting hoop and radial stress distributions at pressure 18 dN/mm^2 have been compared with the corresponding finite element solution, validated before, and plotted as shown in figures (9.66) and (9.67) respectively, which prove that, for the case of thermal loading the elasto-plastic boundary element analysis, developed in this work, is as accurate as the finite element analysis.

(d) Case with Domain Loading:

The pressurized cylinder was also analyzed when it was assumed to rotate with a uniform angular speed (ω) around its axis. Different values of ω have been tested, and it may be worth mentioning that, as soon as plasticity occurs, the value of ω can only be increased slightly before divergence occurs in finite element and boundary element elasto-plastic programs. This phenomenon may be explained, since the difference between the value of ω causing complete collapse of the structure and ω which initiates yield is only 11% [Ref.72]. The results for the particular case, with ω = 1 rad/s together with an internal pressure of 11 dN/mm^2 is reported here.

The hoop and radial stress distributions are shown in Fig.(9.68) and Fig.(9.69) respectively, which prove that the boundary element elasto-plastic results are very accurate compared with the corresponding finite element solution, validated earlier.

9.3.3 Case Study of Elasto-Plastic Analysis for Centrally-Cracked Plate:

Having validated the elasto-plastic finite element and boundary element programs, the elasto-plastic fracture mechanics analyses for some case studies of cracked components have been carried out, aiming at comparing the newly-developed boundary element method with the well-established finite element method, in terms of accuracy and computer *CPU* time. The case study, which is shown in Fig.(9.70), is the first case employed for such a purpose.

Due to the symmetry of the problem, only one quarter of the structure has been modelled. The finite element mesh and the boundary element mesh used in this analysis are similar to those given in Appendix [C], Figs.(C.12, C.17).

The σ_y stress distribution along the line of the crack has been calculated and plotted, as shown in Fig.(9.71). This figure shows an acceptable agreement between the finite element and the boundary element results. However, the boundary element results seem to have more singularity *(i.e. higher stress distribution)* in the area near the crack tip.

Using different load values, the *J*-integral values have been calculated, for every load value, and plotted as can be seen in Fig.(9.72). It is clear from this figure that the finite element results and the boundary element results are almost identical.

The *J*-integral values have also been calculated using different contours around the crack tip. The results from the finite and the boundary element programs are shown in Fig.(9.73). It is obvious from these results that the path independency of the *J*-integral has been satisfied, although the boundary element results show a higher *J* value at contour number 1, because the contour has been taken on the outer boundary of the problem, which contains some corners, with less accurate results there.

The von Mises equivalent stress contours around the crack tip has been calculated and plotted in Figs.(9.74-9.76). The scale of the stress contours has been magnified 25 times in order to show the shape of the plastic zone, which is in this case, the area srounded by the 400.0 MN/m^2 contour.

9.3.4 Case Study of Symmetrically Cracked Pressurized Cylinder:

The case has been selected to test the efficiency of boundary element accuracy measures such as subregioning on the performance of the *BEM* elasto-plastic analysis for a cracked component. A pressurized cylinder with two symmetric radial cracks, as shown in Fig.(9.77), was employed for this purpose.

Since, the case has two axes of symmetry, one quarter of it was modelled with a finite element mesh as shown in Fig.(C.26) [Appendix C], and a boundary element mesh with four subregions as illustrated in Fig.(C.27) [Appendix C].

On running the case without any subregions, the *BEM* elasto-plastic analysis had divergence occurring due to the high stress concentration at the crack tip. With the 4-subregion mesh, and limiting plastic check to the inner subregions, it was possible to obtain boundary element results with rapid convergence, for such a relatively coarse mesh.

The boundary integral equation for strains was tested against the finite difference procedure, by changing the length of the finite difference boundary layer thickness from a very small to a very large value, no difference in results has been observed throughout all of the load increments used.

The u_y displacement distribution on the crack surface, and the σ_y stress distribution on the crack line have been plotted, for elastic results, as shown in figures (9.78) and (9.79) respectively, which indicate that *BEM* results have more or less the same accuracy level as *FEM* results. Fig.(9.79) shows also that, without using any crack-tip element, a singularity occurs at the crack tip because of its location as a corner node common between two subregions.

The elasto-plastic *J*-integral values are plotted at different internal pressures, as shown in Fig.(9.80), which shows a reasonable agreement between *FEM* and *BEM* results. The deviation between the results of the two methods increases with the increase of the internal pressure due to plasticity in outer subregions.

9.3.5 Case Study of Cracked Thick-Walled Pressurized Cylinder:

This case is similar to the previous one but with one radial crack only, as shown in Fig.(9.81). Due to the symmetry of the problem around the x-axis, only one half has been analyzed using the mesh given in Appendix [C], Fig.(C.28). The nondimensional *J*-integral for this case study has been calculated for different pressure ratios using the elasto-plastic *FEM* program of **FRAMEC** package and compared with similar results obtained for the same case study by Sumpter [Ref.89], and Tan & Lee [Ref.90].

The output has been plotted, as shown in Fig.(9.82), which proves that the elasto-plastic *J*-integral values obtained by means of **FRAMEC** finite element analysis is in a very good agreement with the published results. The equivalent stress contours for this case study is shown in Fig.(9.83) which can provide a useful illustration for stress concentration and plastic zones.

9.4 General Discussion:

During the course of study, and considering the results obtained for different case studies described before, some general interesting points have been materialized, and they are discussed and reviewed as follows:

(a) Programming Package Facilities:

It was not possible to run the package so easily and smoothly without the help of its control program developed as a *VAX-Command* file which controls different operations of the package. It is also clear that the package pre- and post-processing facilities are very useful tools for data

preparation, mesh generation and plotting, and results presentation. Most of the figures presented in this chapter have been generated by means of those facilities.

Many other facilities have been validated and proved to be very advantageous. Pressure elements may help in reducing data and human effort required for the specification of finite element loading equivalent to pressure loading. The package own finite and boundary element, heat-conduction programs provide thermal data required for thermo-elastic analysis, using the same mesh. An experienced user can employ facilities, such as transition and crack-tip elements, for generating very economical meshes, without affecting accuracy levels required. Some advantages of other facilities may become apparent within next sections.

(b) *Standard Finite and Boundary Elements:*

Although different tests have proved that all of the finite and boundary elements available in the package are correct in derivation, it is clear from the analysis of previous case studies that one should not expect an automatic improvement in accuracy whenever higher order elements are employed. The second order finite elements, elements with one mid-side nodes, and the second order boundary element, the 3-node isoparametric element, provide an optimum choice.

(c) *Package Modularity:*

The package modular design has proved to be extremely useful. The same *J*-integral program can be coupled with results from either *FEM* programs or *BEM* programs without any interference by the user. The elasto-plastic analysis; stress-correction, stress-strain matrix, ...etc, is available in a separate file which can be linked to either *FEM* or *BEM* elasto-plastic programs. It is perhaps best to use the same mesh employed for

FEM analysis as an integration-cell mesh for the *BEM* elasto-plastic analysis, since it will make it possible to have a direct comparison, at the same nodes between the results obtained by means of each method. This idea was not possible without including the same finite element library in elasto-plastic *BEM* programs. Different boundary elements have, similarly, been employed in the *FEM* analysis as pressure elements, they have also been used as contour elements in the *J*-integral programs.

(d) *Assessment of Crack-Tip Elements:*

Many old and new crack-tip elements have been tested, and the results have proved that a crack-tip singularity can be generated within a rather coarse mesh, when such elements are used in the vicinity of a crack tip. Most of the crack-tip elements available in the literature require coordinates distortion for some nodes near to the crack tip, and this may become as a heavy burden to the user generating meshes for cracked components.

However, two of the new elements developed in this work, the **(1/SQR2)** element and the collapsed element require the distortion to be carried out only in the intrinsic plane, keeping the nodal cartesian coordinates untouched. These new elements have also proved to be very accurate compared with other elements. Some crack-tip elements, specially the 3-node boundary element, seem to have a favoured direction, i.e. they cannot be used efficiently except when located at certain side of the crack.

(e) *Methods for Stress Intensity Factor Evaluation:*

Many methods for the evaluation of stress intensity factors have been presented in this work. The extrapolation method,

which is based upon some parameters defined on a line emanating from the crack tip, may require the use of additional internal nodes for the *BEM* analysis. The suitability of generated curves for being extrapolated, may depend upon the parameters used and the inclination of the line from the crack surface. The extrapolation curve-fitting technique, developed in this work, provides a very efficient tool for the evaluation of stress intensity factors, specially when the component contains an oblique crack. Short cracks may require the use of very fine meshes so as to obtain accurate stress intensity factors for them by means of *FEM* or *BEM* results. It may be advantageous to employ the *J*-integral technique for the evaluation of linear-elastic stress intensity factors but it is only capable of providing the value of an equivalent stress intensity factor, whenever the component has multiple modes of fracture.

(*f*) *J-Integral Algorithms:*

The algorithms developed in this work for the calculation of *J*-integral values have proved to be very accurate and efficient. They have performed well for cases with boundary loading, domain loading, and thermal loading and with elastic and elasto-plastic analyses. They have been programmed so as to use directly output files generated by means of the *FEM* or *BEM* programs without any human interference. Transformation of global axes to crack axes have been carried out internally within the *J*-integral programs, and this allows the user to employ the best global axes possible for the *FEM* or *BEM* analysis. New derivations and simplifications of domain-loading terms in *J*-integral expressions have helped in obtaining *J*-integral values accurately and efficiently, and also in reducing computer *CPU* time.

Although the **ABAQUS** finite element package, which contains *J*-integral facilities, is available at Cranfield, no comparison with its results has been presented here, simply because some

tests carried out earlier had proved that the *J*-integral values for domain loading cases, as calculated by means of the **ABAQUS** package, were far from being accurate or path independent.

(g) *BEM Accuracy Measures and Subregioning:*

Some accuracy measures should be observed when using isoparametric boundary elements such as, doubling of corner nodes, using subregions whenever necessary, and defining a boundary layer within which stresses are calculated by means of a finite difference procedure applied to displacement values there.

The subregion technique presented in this work is unique in using double nodes at generated corners, and a condensation algorithm to minimize unknowns at similar nodes. This allows the use of, gaps with zero length at corners, and corner jump-functions which improve the accuracy of the *BEM* analysis. It is clear from previous tests that, in addition to the condensation facility, there are three basic advantages achieved by subregioning:

i. It improves the accuracy of *BEM* results, specially for cases with irregular domains.

ii. It has made it possible for the *BEM* to deal with cases which contain non-symmetric or oblique cracks.

iii. It can be used to reduce the computer *CPU* time for elasto-plastic analysis, by specifying whether every subregion may have plastic analysis or not.

(h) *Finite Element versus Boundary Element for Linear-Elastic Fracture Mechanics:*

It is clear from previous results that the *BEM* has proved to be very advantageous for the analysis of linear-elastic fracture mechanics problems as compared with the *FEM*, due to the following main reasons:

i. For the calculation of *J*-integrals, and stress intensity factors from data along crack surfaces, *FEM* and *BEM* results are only required on the boundary. This represents an ideal situation in favour of the *BEM* since no internal nodes are required for fracture mechanics analysis.

ii. The accuracy of the *BEM* is, without any doubt, as good as that for the *FEM*, or may even be better, for many cases.

iii. Some saving in *CPU* time may be achieved with the use of the *BEM*. However, with the frontal solver being employed only for *FEM*, the actual saving with the *BEM* would be in data-preparation effort and in mesh generation, specially whenever there are non-symmetric or oblique cracks which may require mesh-zooming in the vicinity of crack tips.

iv. Subregioning, if considered instead of a coarse finite element mesh would provide more accurate answers and have banded-matrix characteristic which may then be dealt with by means of efficient solvers.

(i) *Finite Element versus Boundary Element for Elasto-Plastic Fracture Mechanics:*

It is clear from previous cases that there are still some development required to be carried out in order to have the *BEM* being as efficient as the *FEM* for elasto-plastic fracture mechanics analysis. With old and new accuracy measures

considered within the *BEM* analysis, its accuracy has not now become the crucial factor, since accurate *BEM* results could be obtained by one way or another, but the basic disadvantage is that the *CPU* time required for carrying out an accurate *BEM* analysis is larger than that for the corresponding *FEM* analysis. One may, of course, reduce the *BEM CPU* time by means of efficient subregioning. Although the present author, cannot argue against the view that this may not provide enough grounds for the *BEM* to become superior to the *FEM*, for elasto-plastic analysis, he believes that most of the *CPU* of the *BEM*, is spent in pagination required with a virtual memory computer such as *VAX*. Anyway, subregioning techniques provided here may pave the way for generating a hybrid procedure within which the *FEM* and the *BEM* will be coupled together to provide a new technique more efficient than each of the two methods on its own.

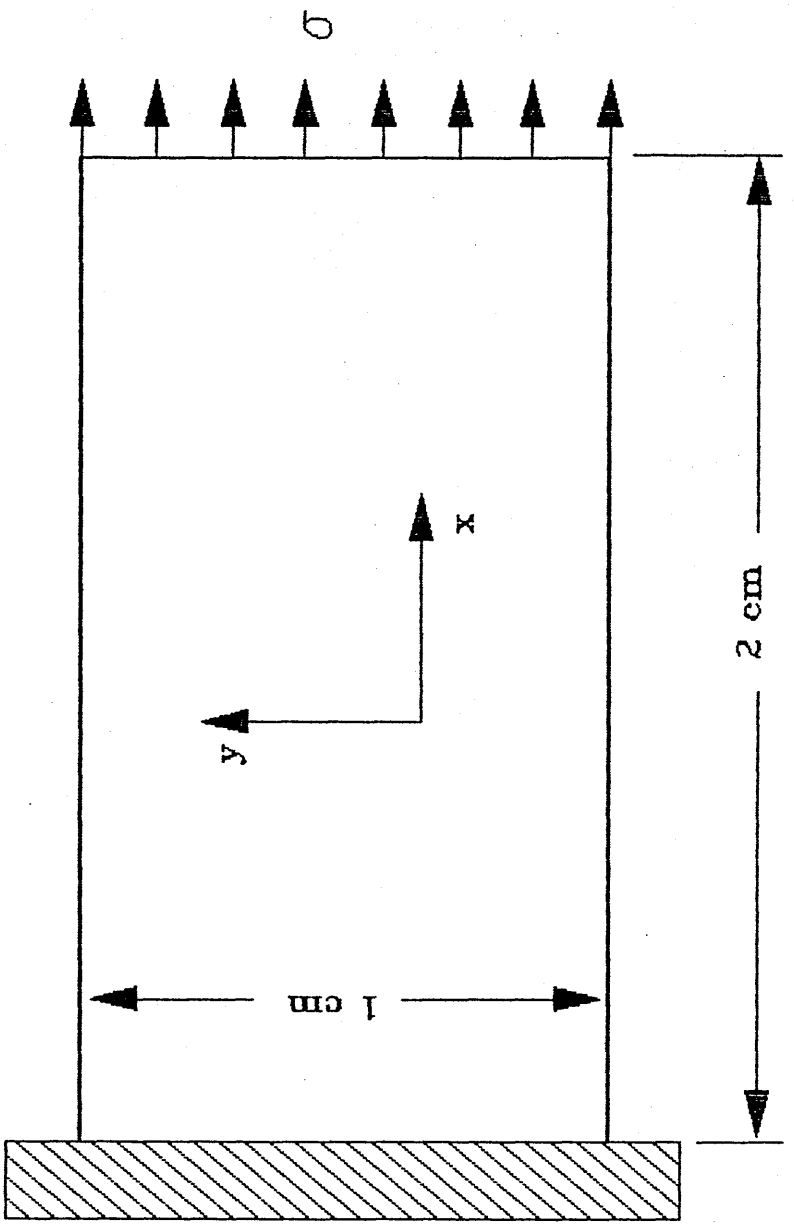

σ = 1.0 N/cm^2

ν = 0.3

E = 1.0 x 10^4 N/cm^2 , Thickness = 0.1 cm

Fig.(9.1) Plate under Tension used for the Validation of the Linear-Elastic Finite-Element Program.

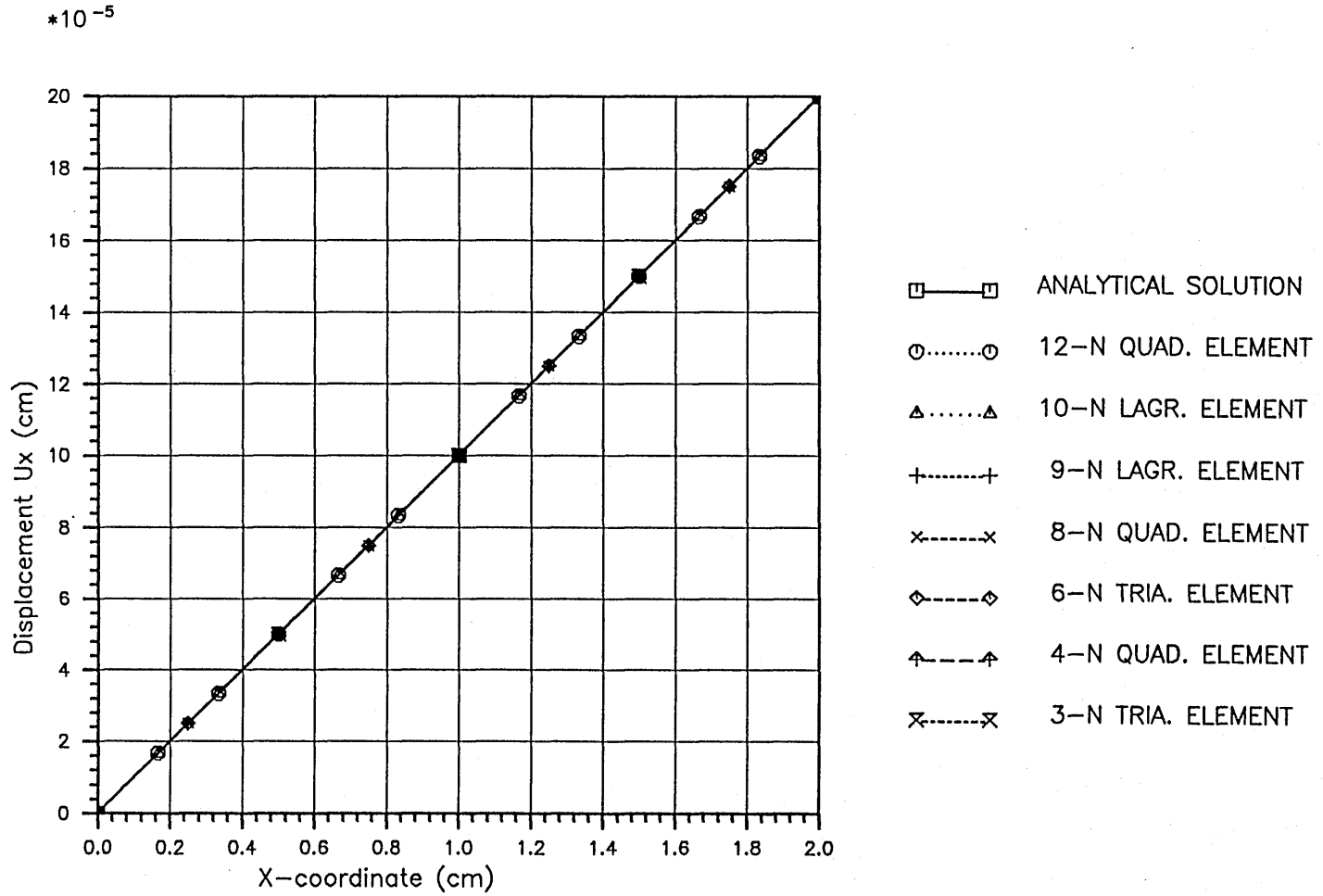

Fig.(9.2) Displacement in the X-direction for Plate under Tension calculated using Different Types of Finite Elements.

FRAMEC

Run on 7-JUN-90, At 16:08:20

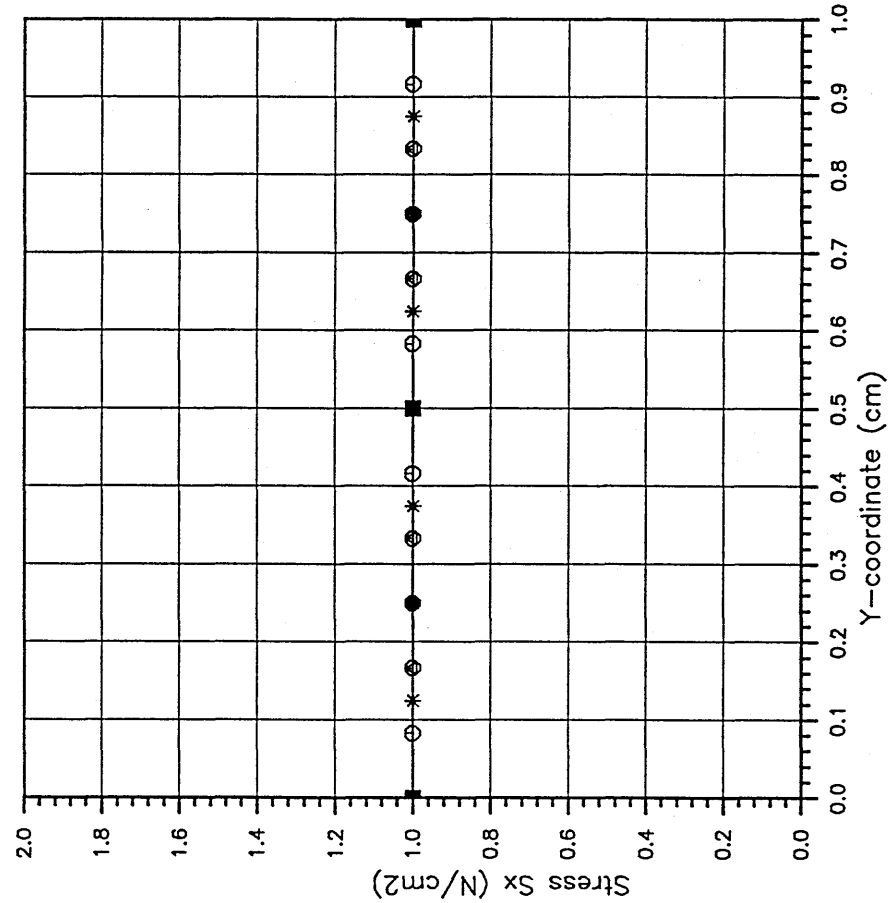

Fig.(9.3) Stress Disribution in the Y-direction for Plate under Tension calculated using Different Types of Finite Elements.

FRAMEC

Run on 7-JUN-90, At 16:13:25

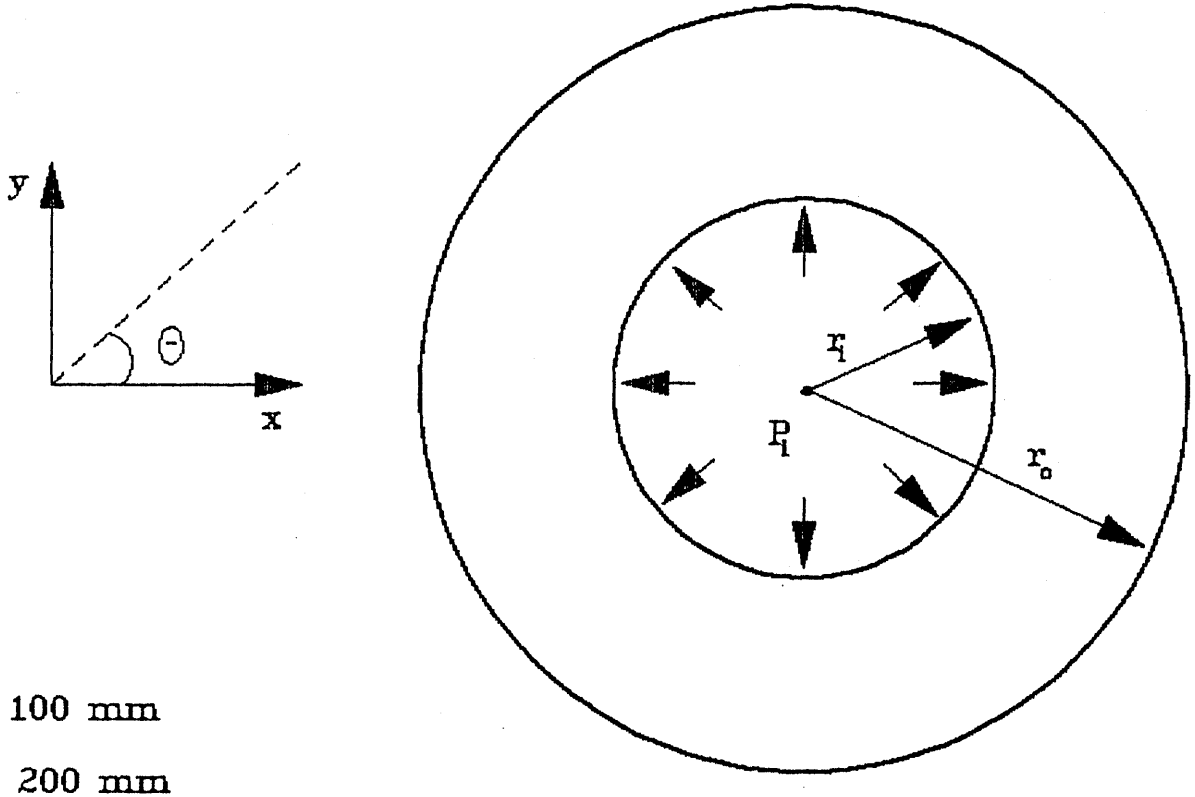

r_i = 100 mm

r_o = 200 mm

P_i = 10 N/mm^2

E = 12.5 x 10^4 N/mm^2, ν = 0.25

Fig.(9.4) Pressurized Cylinder used for the Validation of the Isoparametric Linear-Elastic Boundary-Element Program.

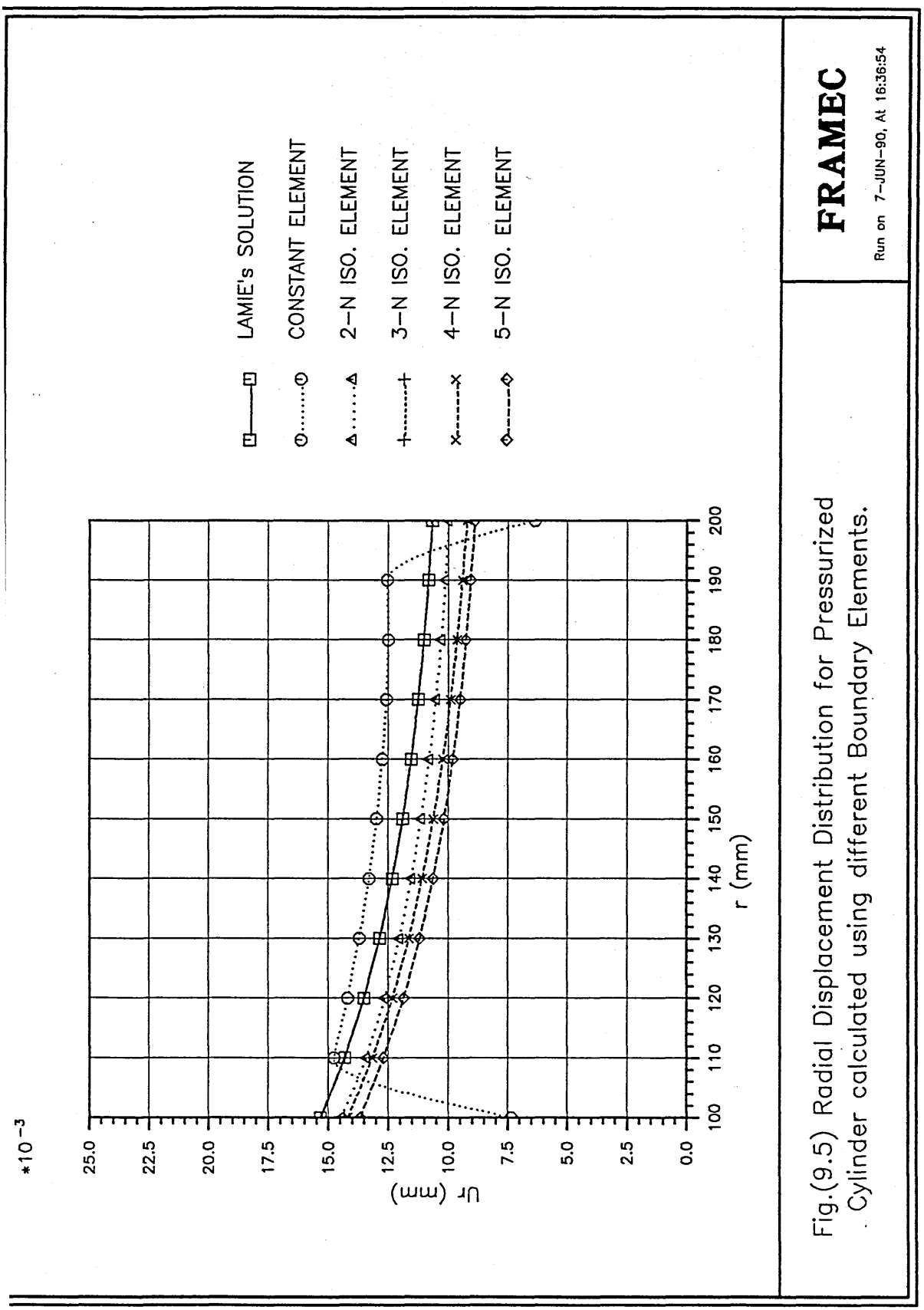

Fig.(9.5) Radial Displacement Distribution for Pressurized Cylinder calculated using different Boundary Elements.

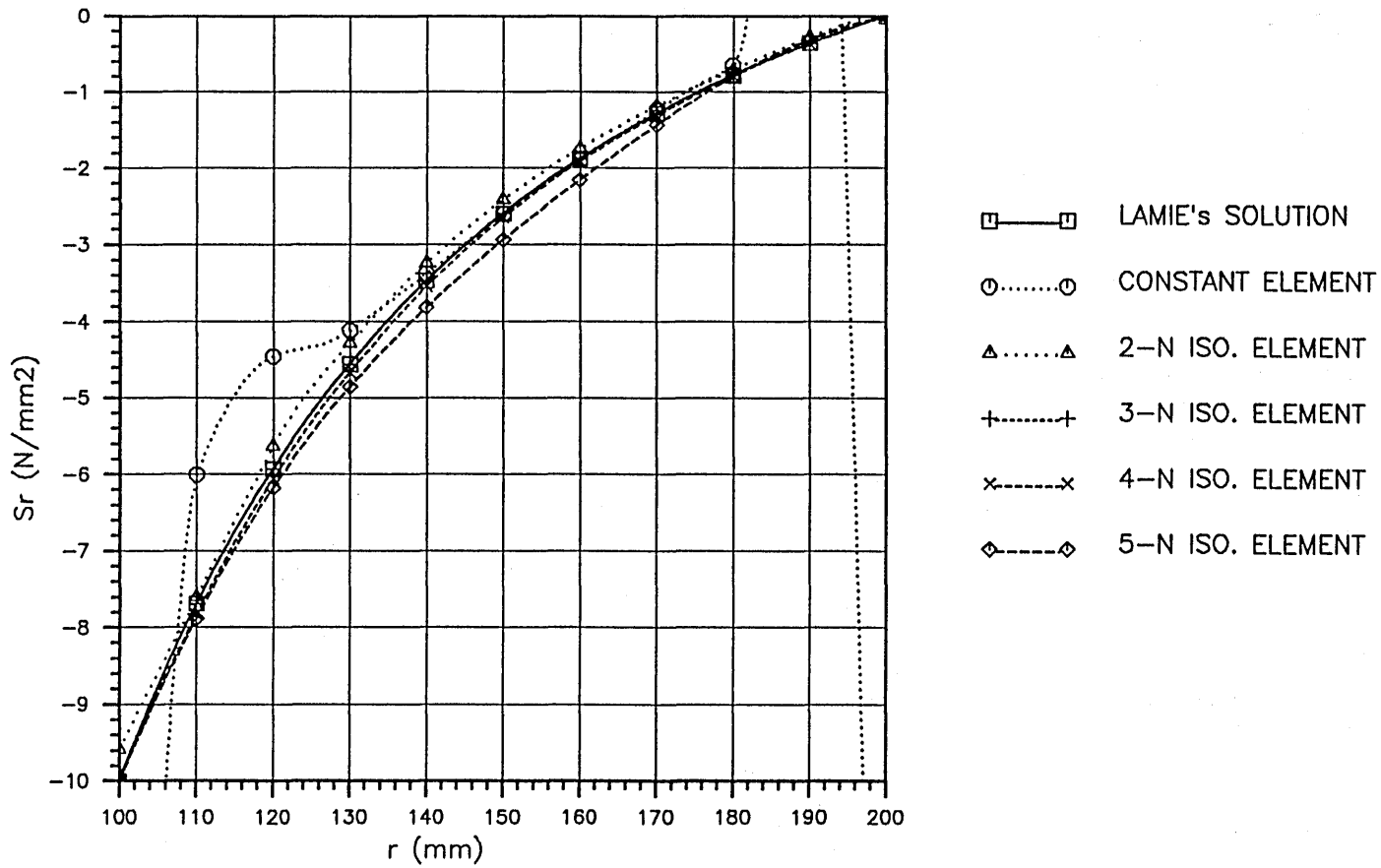

Fig.(9.6) Radial Stress Distribution for Pressurised Cylinder calculated using different Boundary Elements.

FRAMEC

Run on 7-JUN-90, At 16:42:19

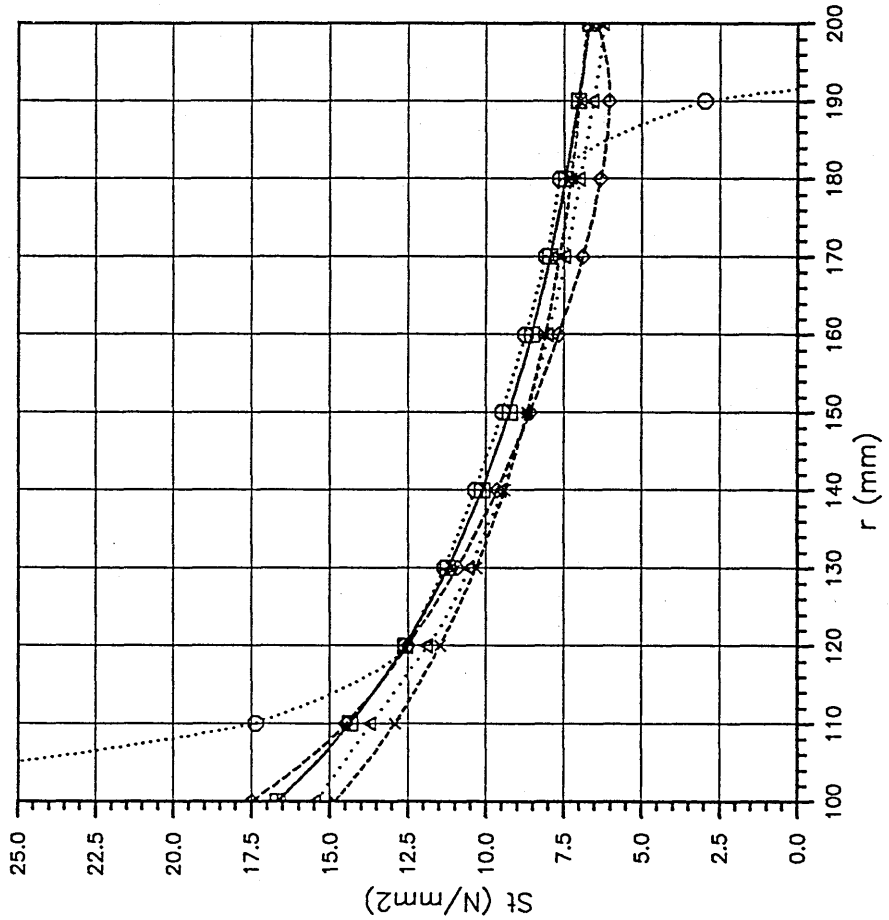

FRAMEC

Run on 7-JUN-90, At 16:49:36

Fig.(9.7) Hoop Stress Distribution for Pressurized Cylinder calculated using different Boundary Elements.

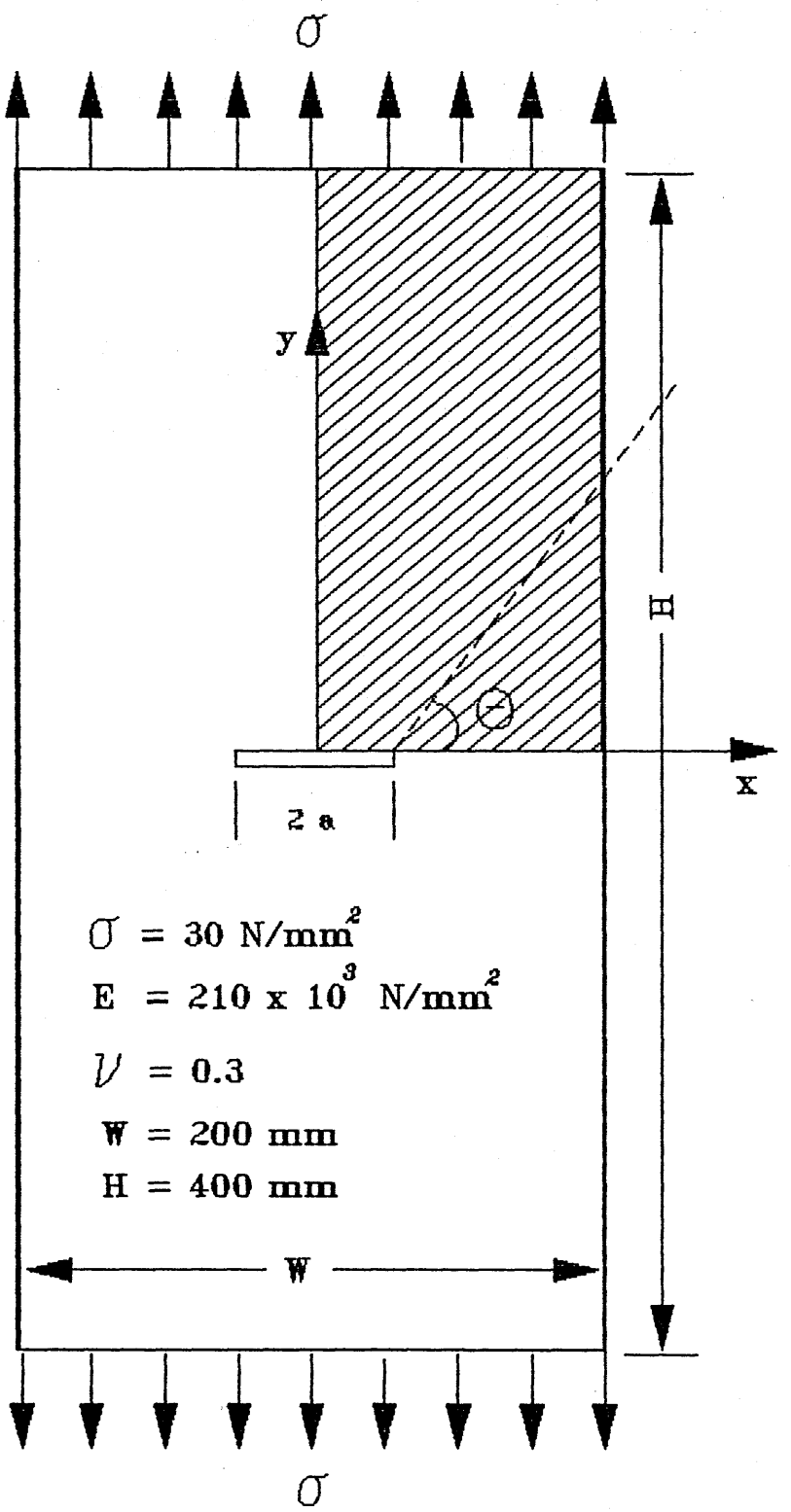

Fig.(9.8) Central-Cracked Plate under Uniform Tension.

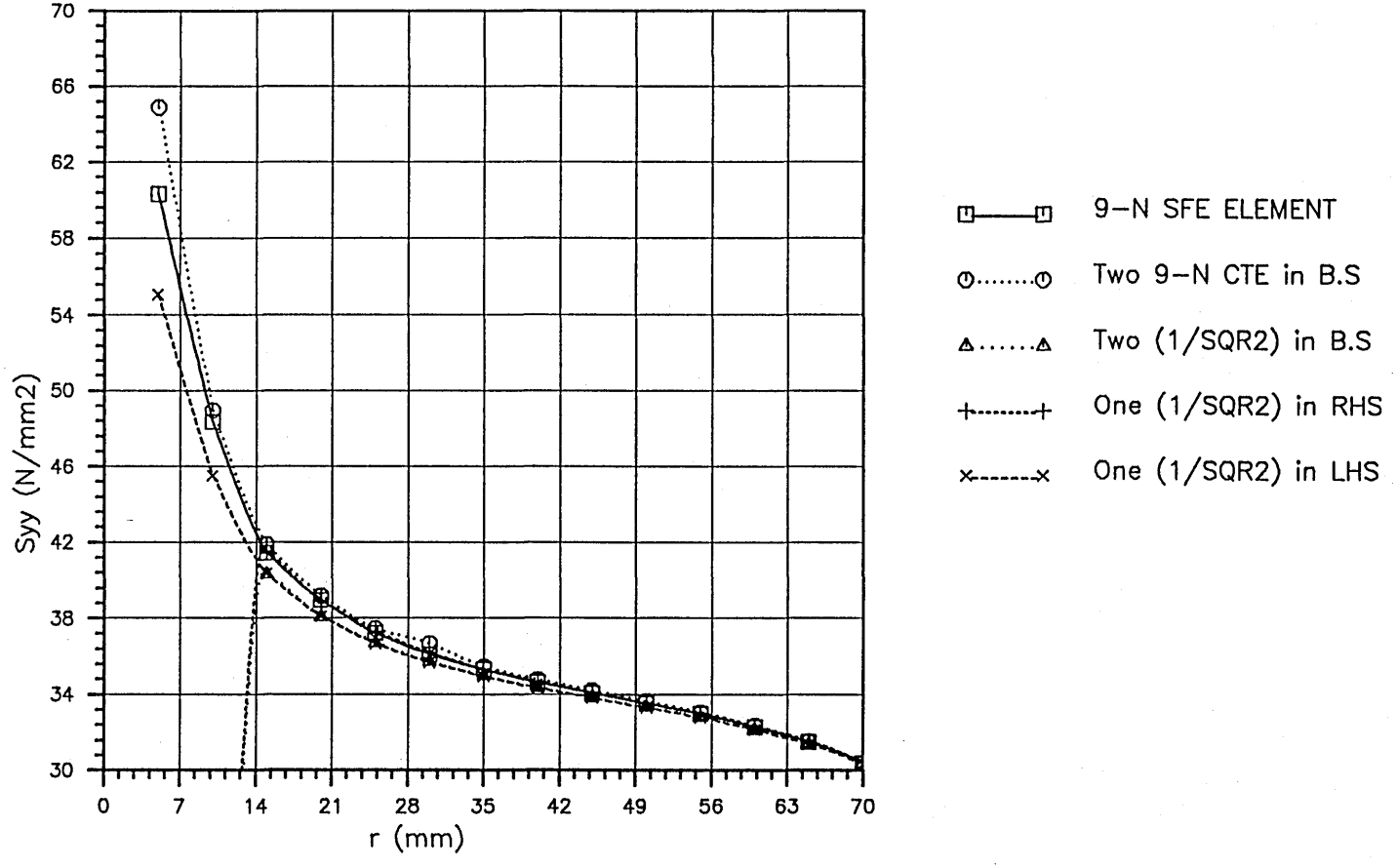

Fig.(9.9) Stress Distribution for CC Plate calculated using Standard and Crack–tip Finite Elements.

FRAMEC

Run on 7–JUN–90, At 17:08:10

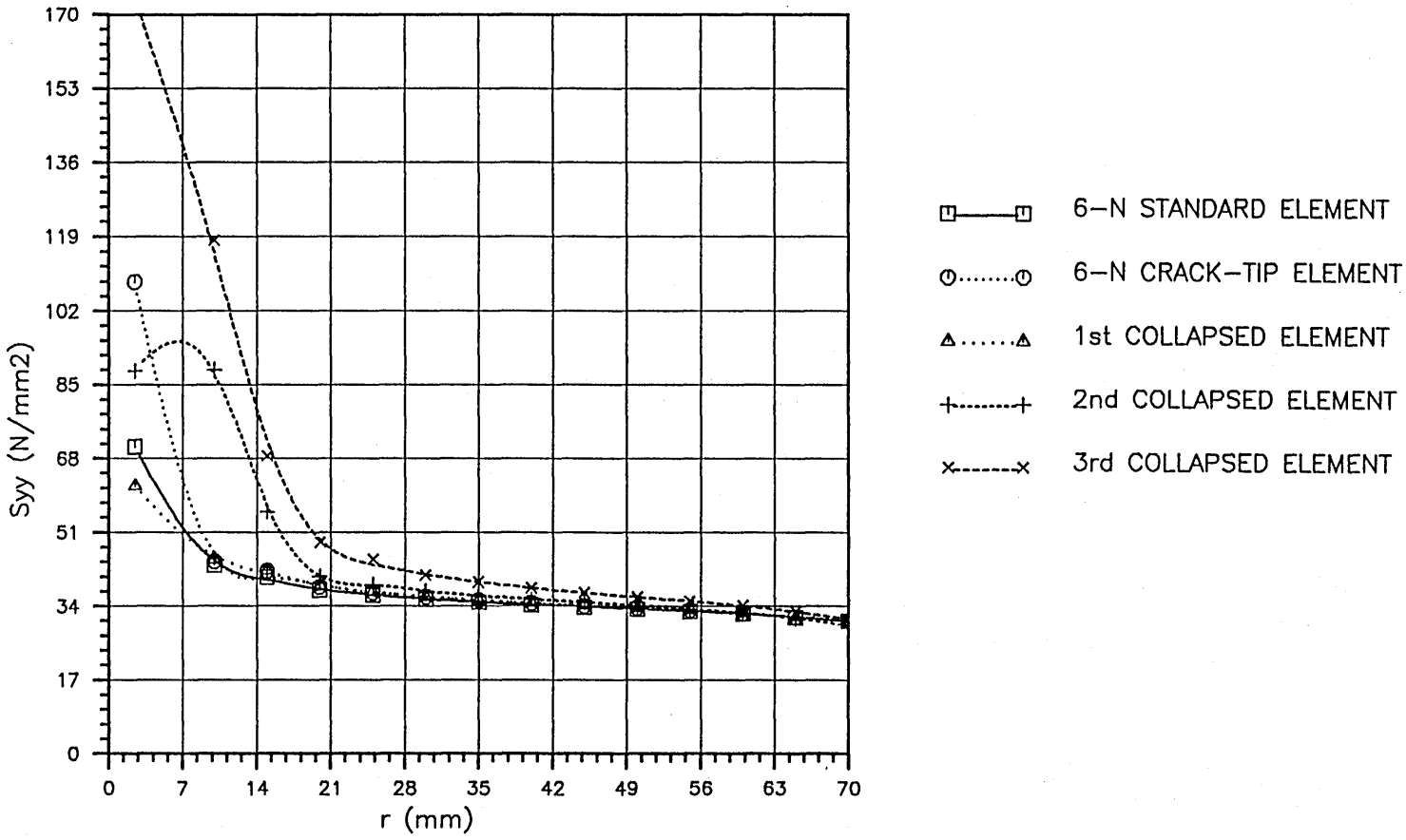

Fig.(9.10) Sigma–Y Stress Distribution for CC Plate calculated using Different Standard and Crack–tip Finite Elements.

FRAMEC

Run on 7–JUN–90, At 18:15:08

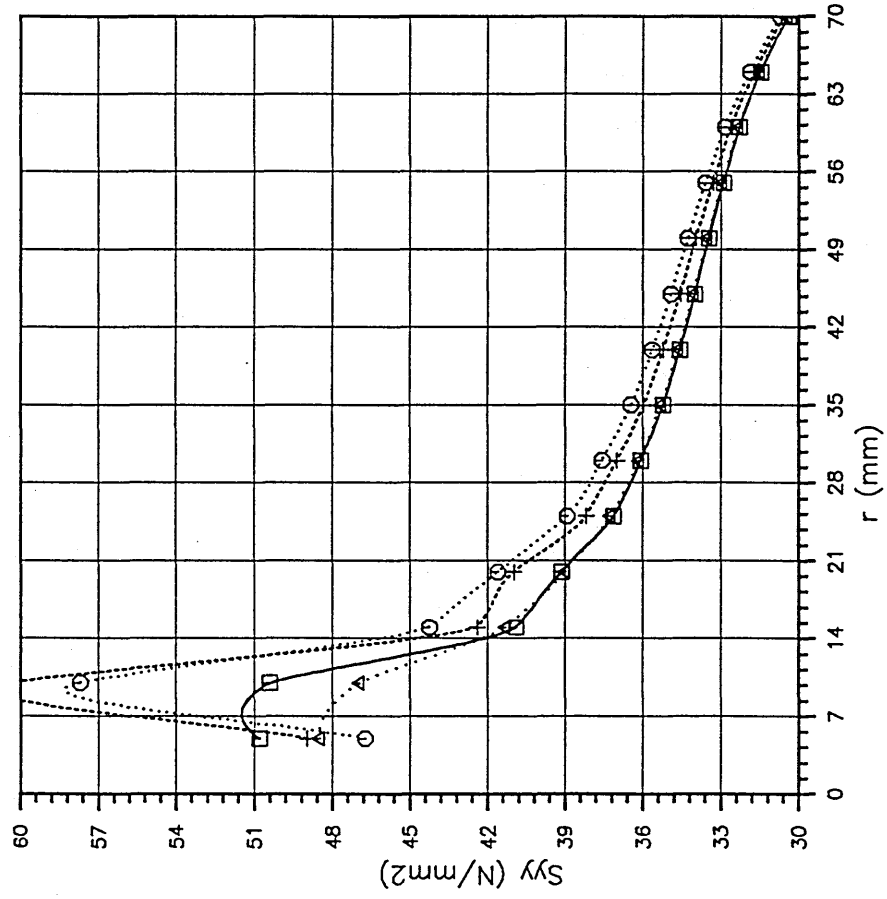

FRAMEC

Run on 7-JUN-90, At 17:25:14

Fig.(9.11) Stress Distribution in the Y-direction for CC Plate calculated using Standard & Crack-tip Boundary Elements.

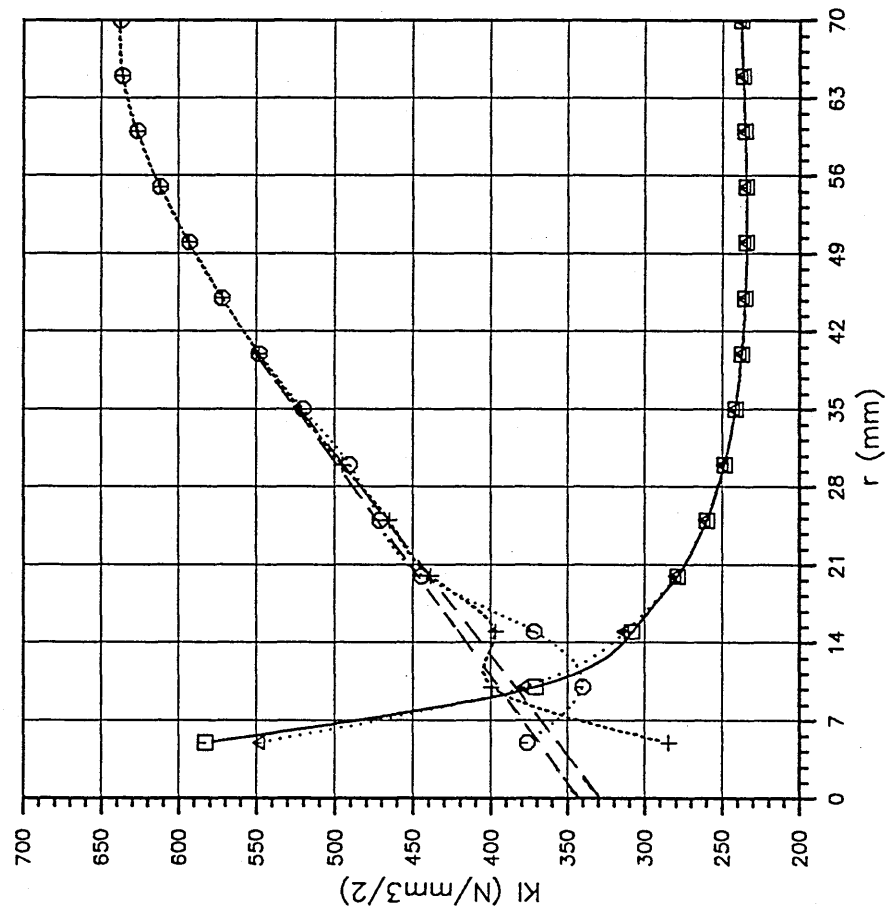

FRAMEC

Run on 7-JUN-90, At 17:30:43

Fig.(9.12) KI SIF for CC Plate calculated by Extrapolation of Finite & Boundary Element Results at an Angle of 0 Deg.

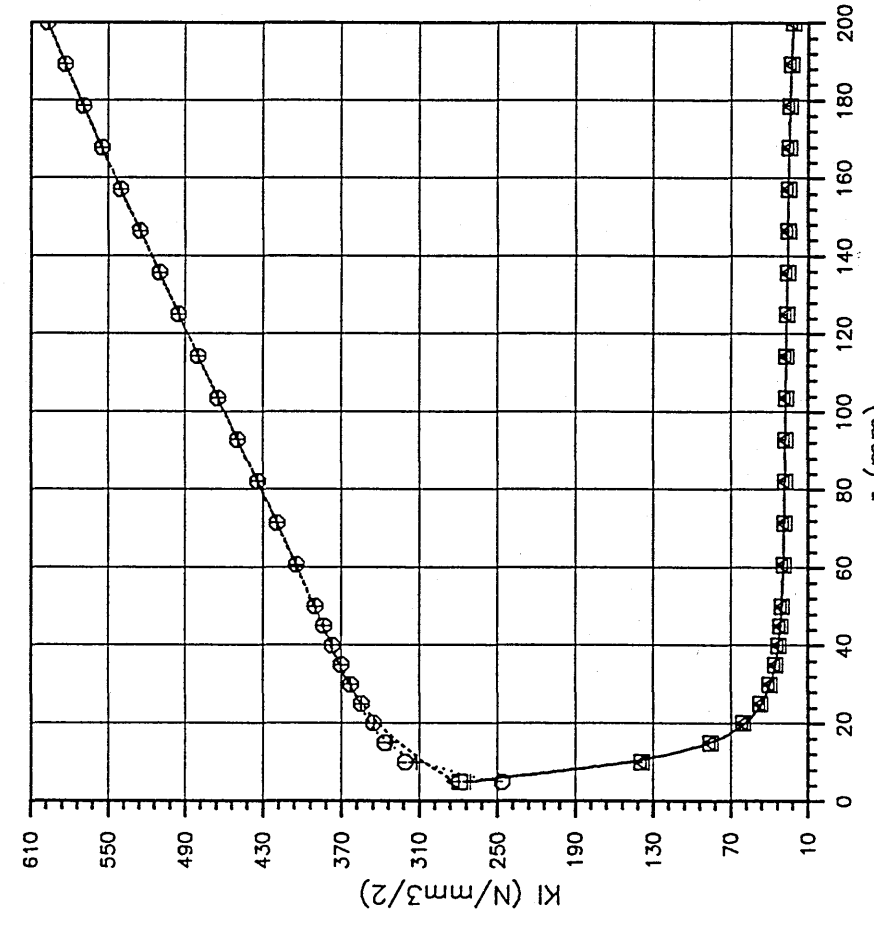

Fig.(9.13) KI SIF for CC Plate calculated from Finite & Boundary Results using Disp. Extrapolation at Angle 90 Deg.

FRAMEC

Run on 7-JUN-90, At 17:38:51

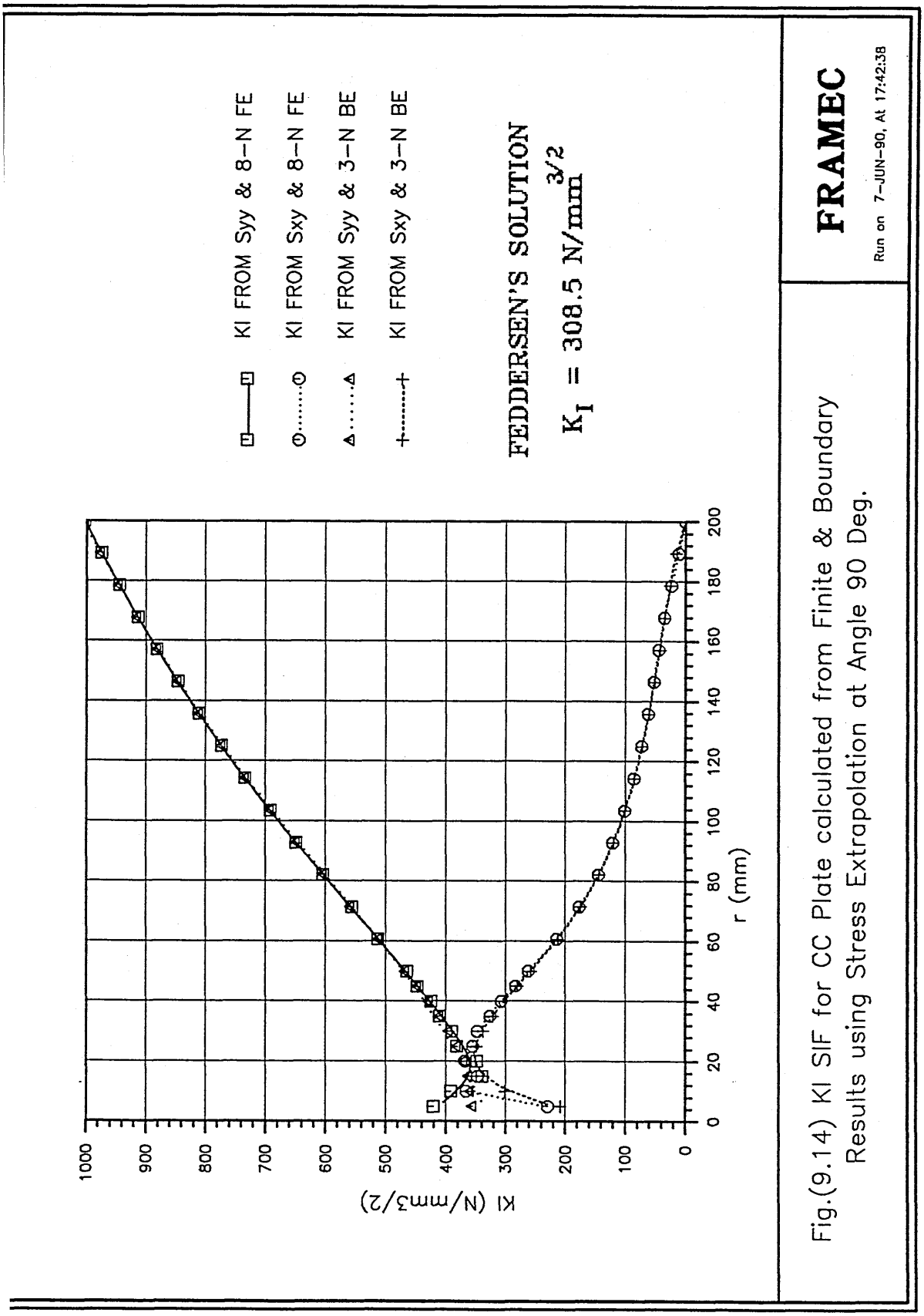

Fig.(9.14) KI SIF for CC Plate calculated from Finite & Boundary Results using Stress Extrapolation at Angle 90 Deg.

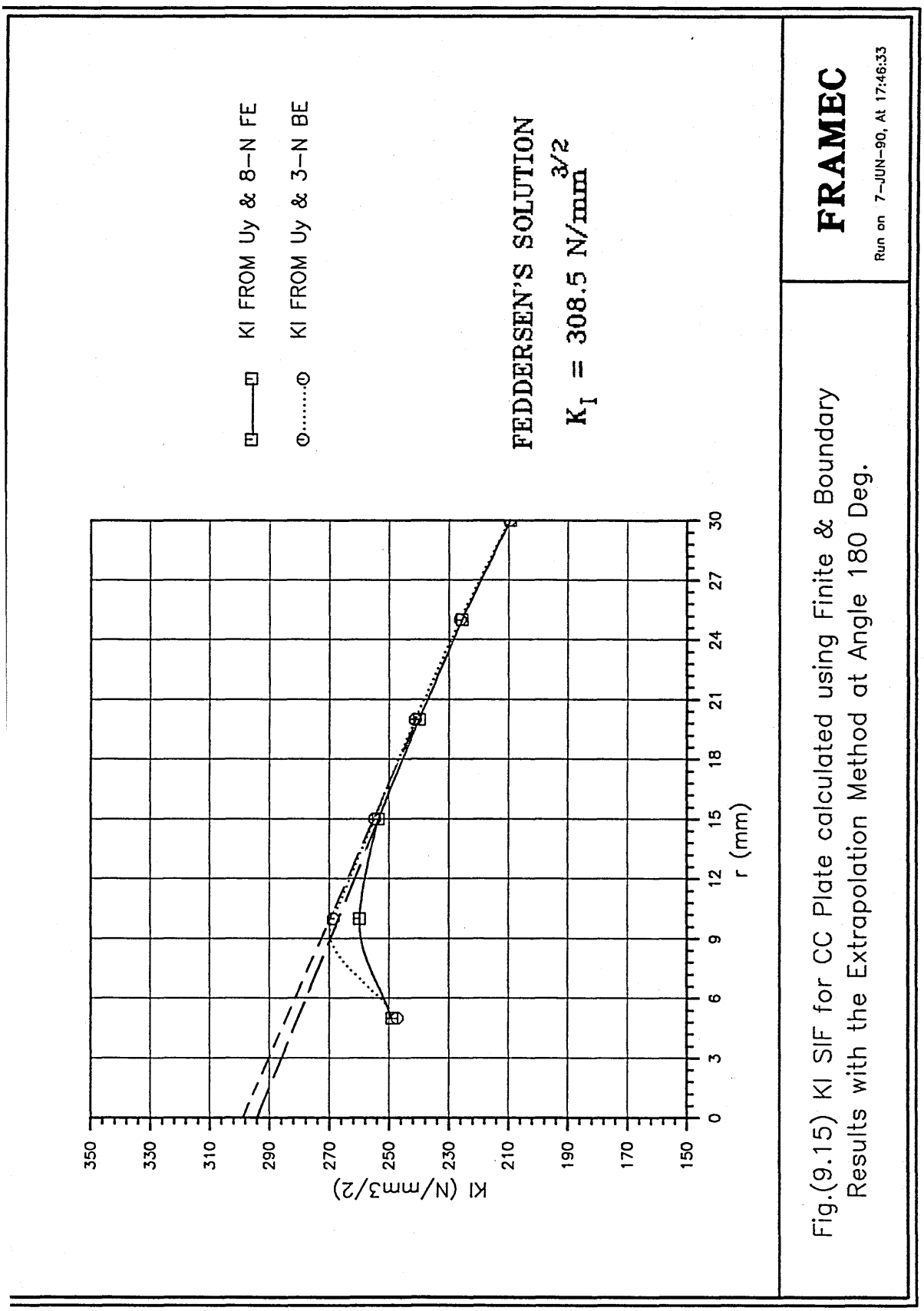

Fig.(9.15) KI SIF for CC Plate calculated using Finite & Boundary Results with the Extrapolation Method at Angle 180 Deg.

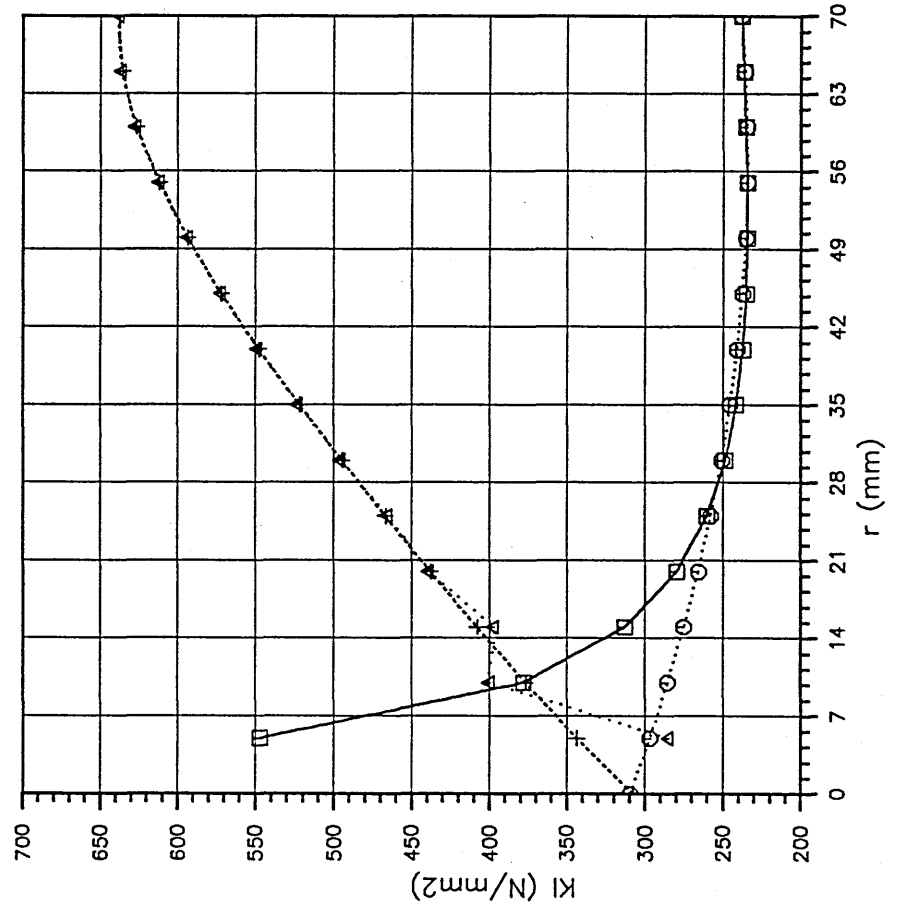

Fig.(9.16) KI SIF for CC Plate calculated from 3-N Boundary Elements by Curve Fitting Extrapolation Technique.

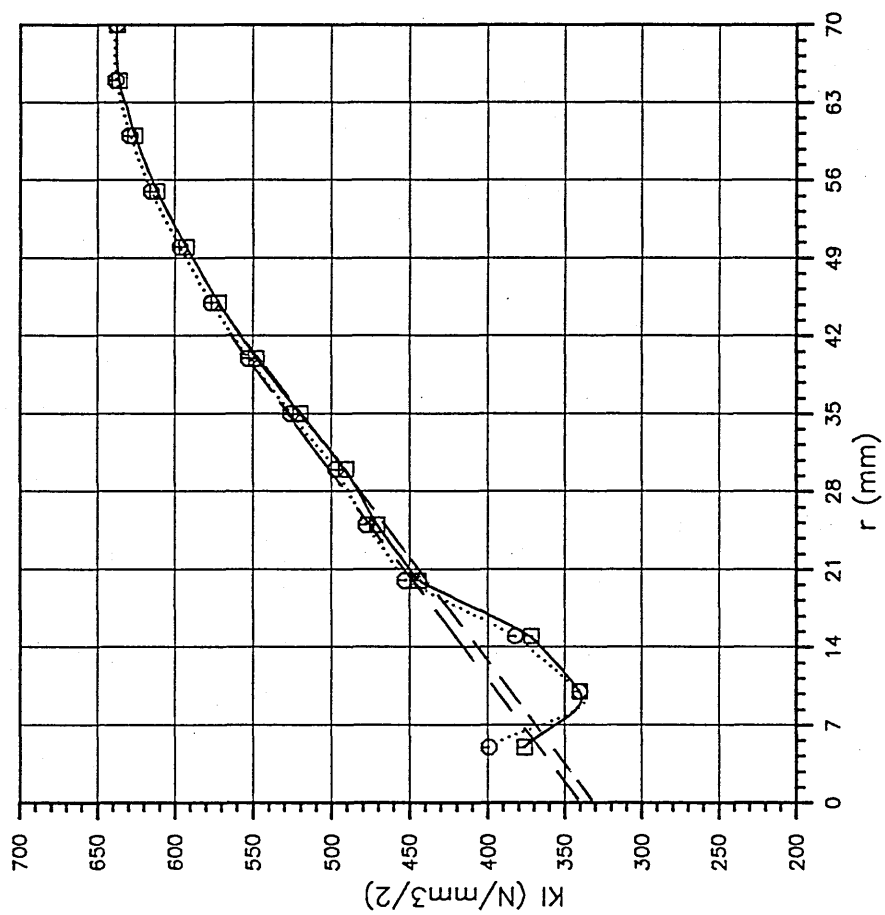

FRAMEC

Run on 7-JUN-90, At 17:57:19

Fig.(9.17) KI SIF for CC Plate calculated by Stress Extrapolation using 8-Node Standard & Crack-tip Finite Elements.

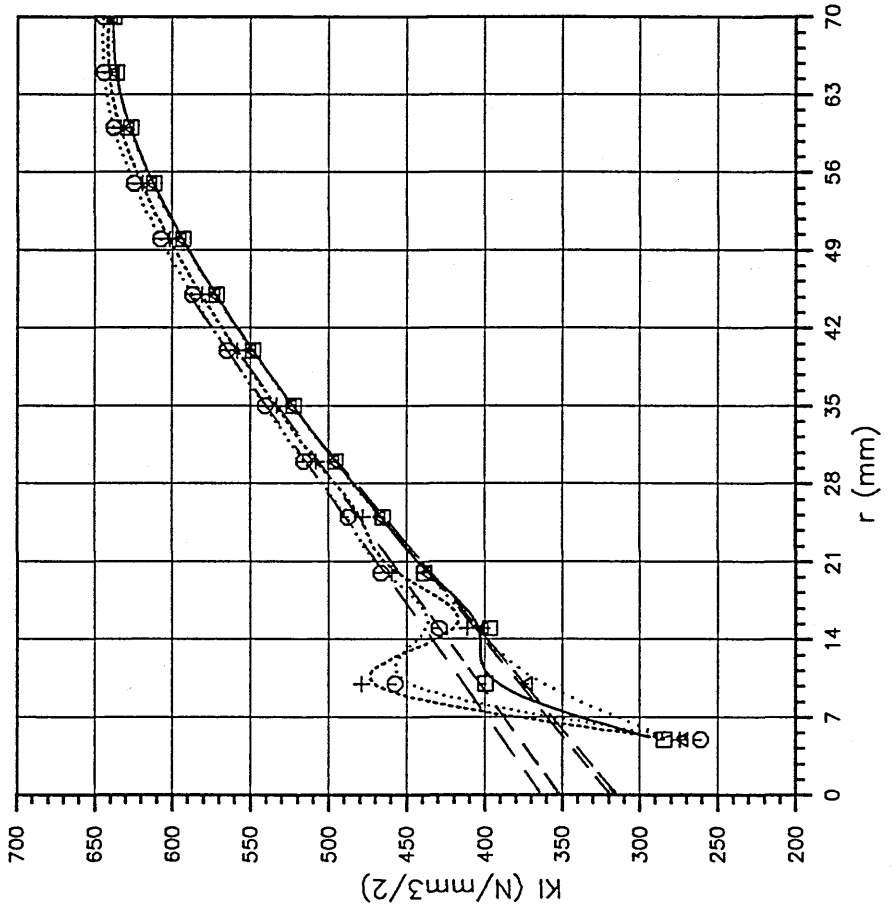

FRAMEC

Run on 7-JUN-90, At 18:01:44

Fig.(9.18) KI SIF for CC Plate calculated by Stress Extrapolation using Standard & Crack-tip Boundary Elements (THETA = 0 Deg.).

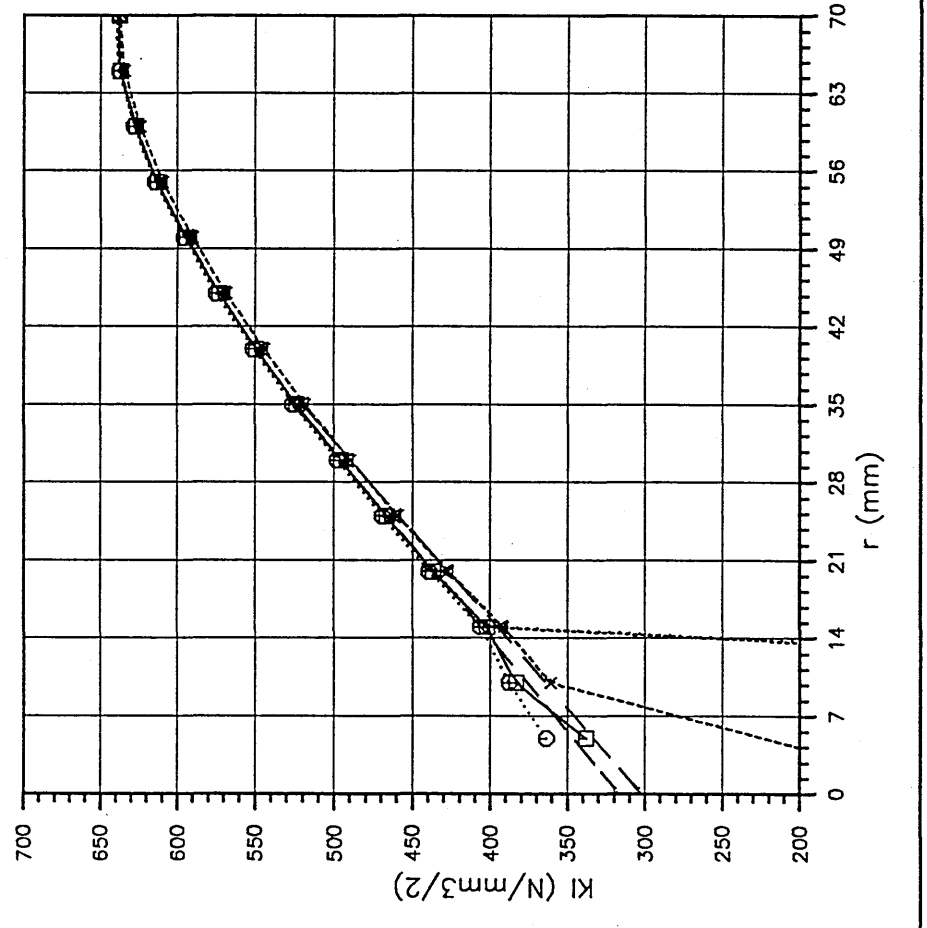

Fig.(9.19) KI SIF calculated from Stress Extrapolation by using 9-Node, Standard, Crack-tip, and (1/SQR2) Finite Elements.

FRAMEC

Run on 7-JUN-90, At 18:07:18

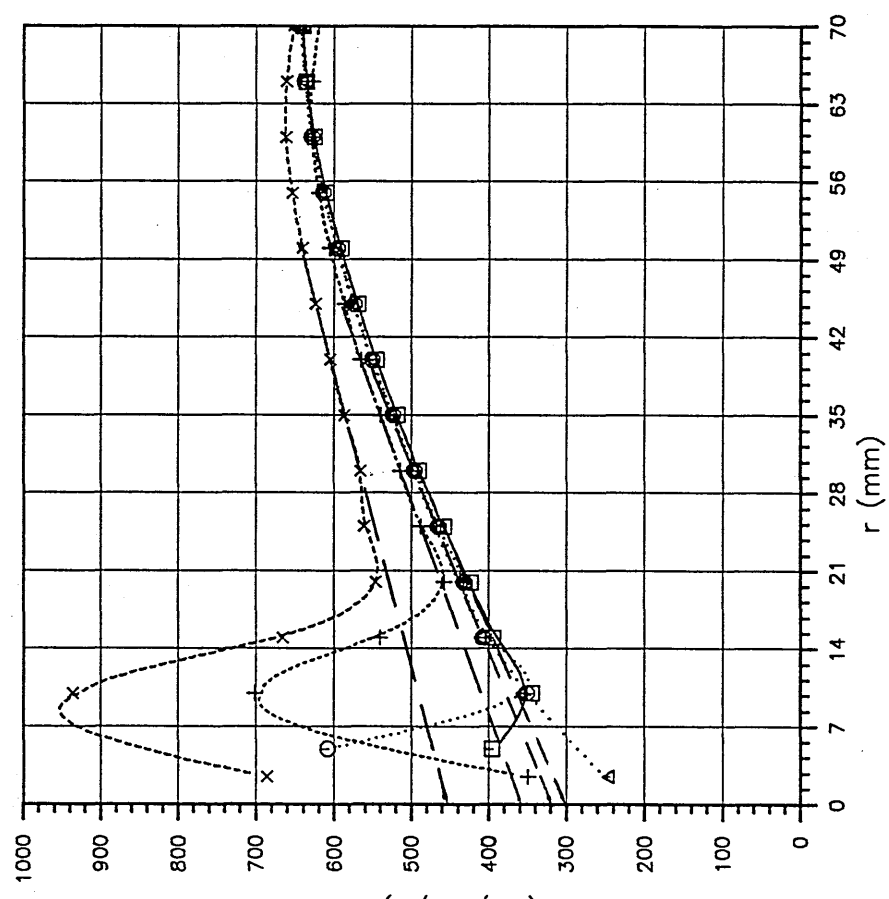

Fig.(9.20) SIF's for CC Plate calculated by Stress Extrapolation from 6-Node, Standard, Crack-tip, and Collapsed Finite Elements.

FRAMEC

Run on 7-JUN-90, At 18:13:33

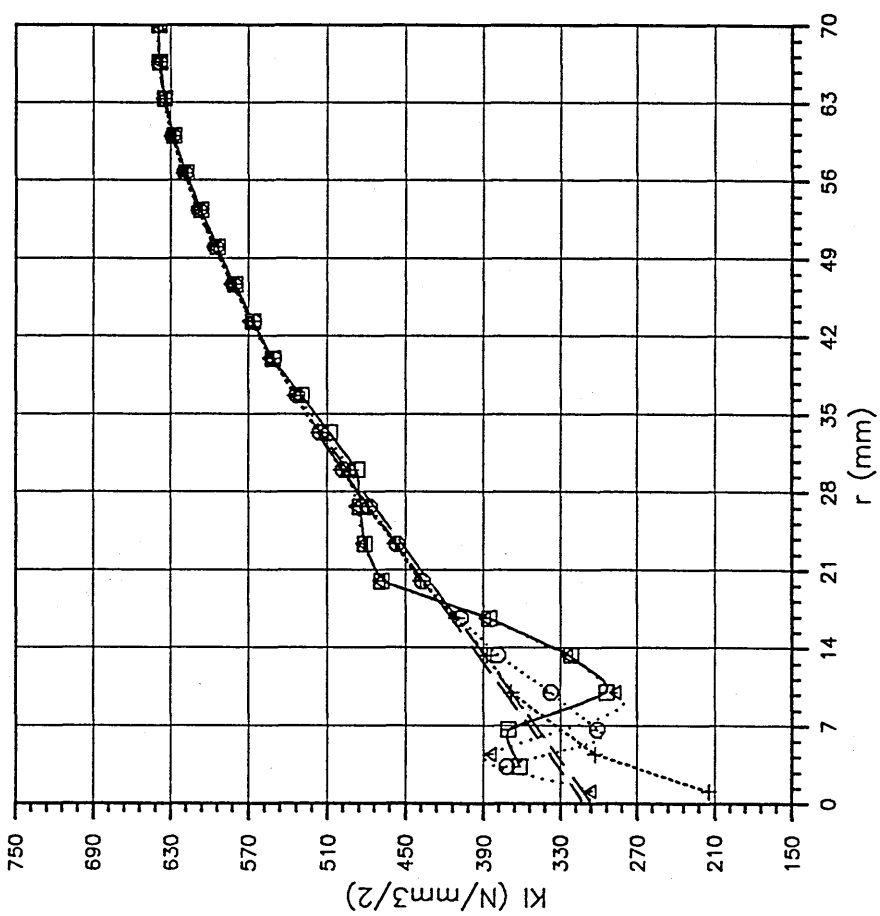

Fig.(9.21) KI SIF's for CC Plate calculated from Extrapolation by using 12-Node & 10-Node Standard & Crack-tip Finite Elements.

FRAMEC

Run on 7-JUN-90, At 18:29:14

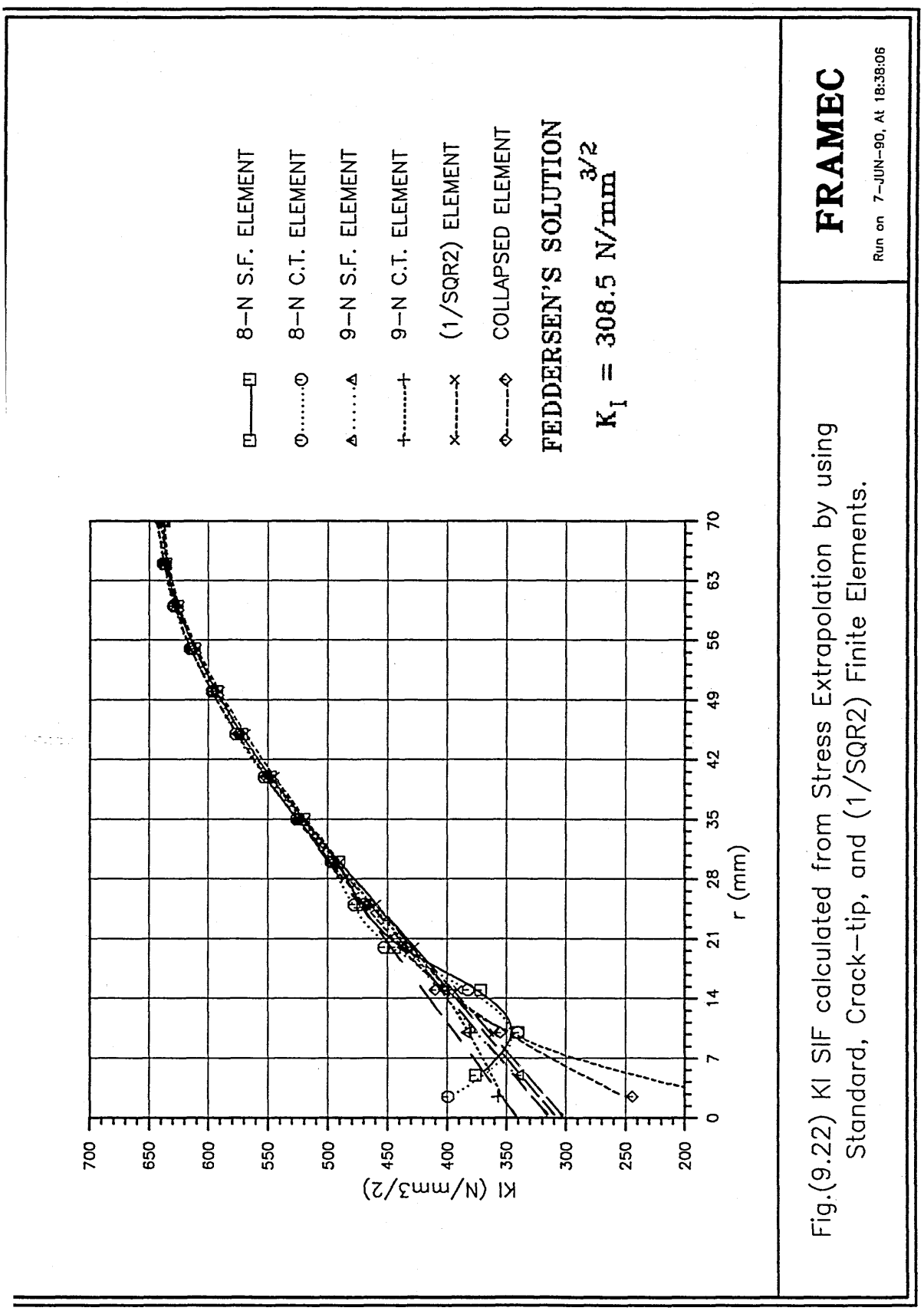

Fig.(9.22) KI SIF calculated from Stress Extrapolation by using Standard, Crack-tip, and (1/SQR2) Finite Elements.

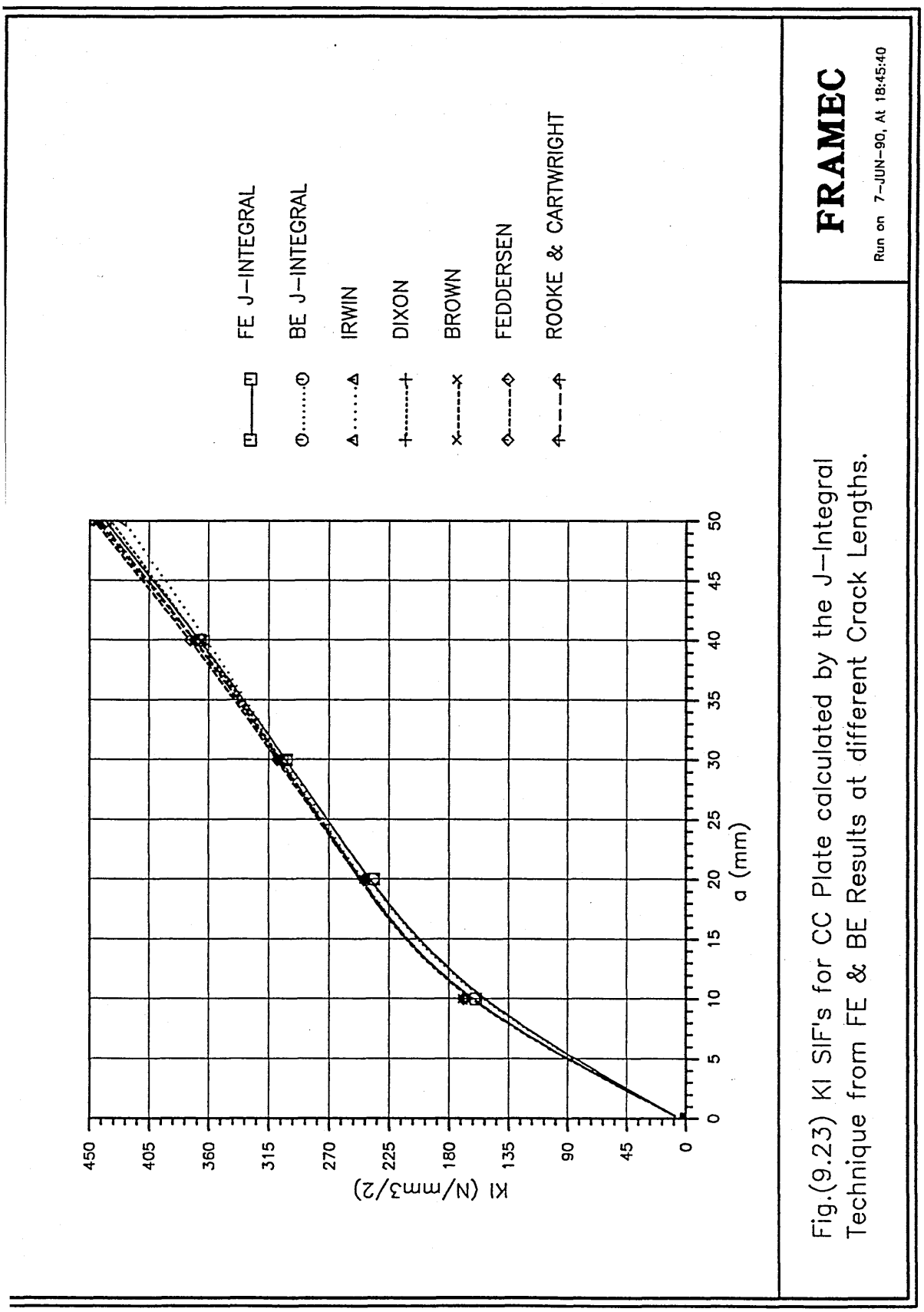

Fig.(9.23) KI SIF's for CC Plate calculated by the J-Integral Technique from FE & BE Results at different Crack Lengths.

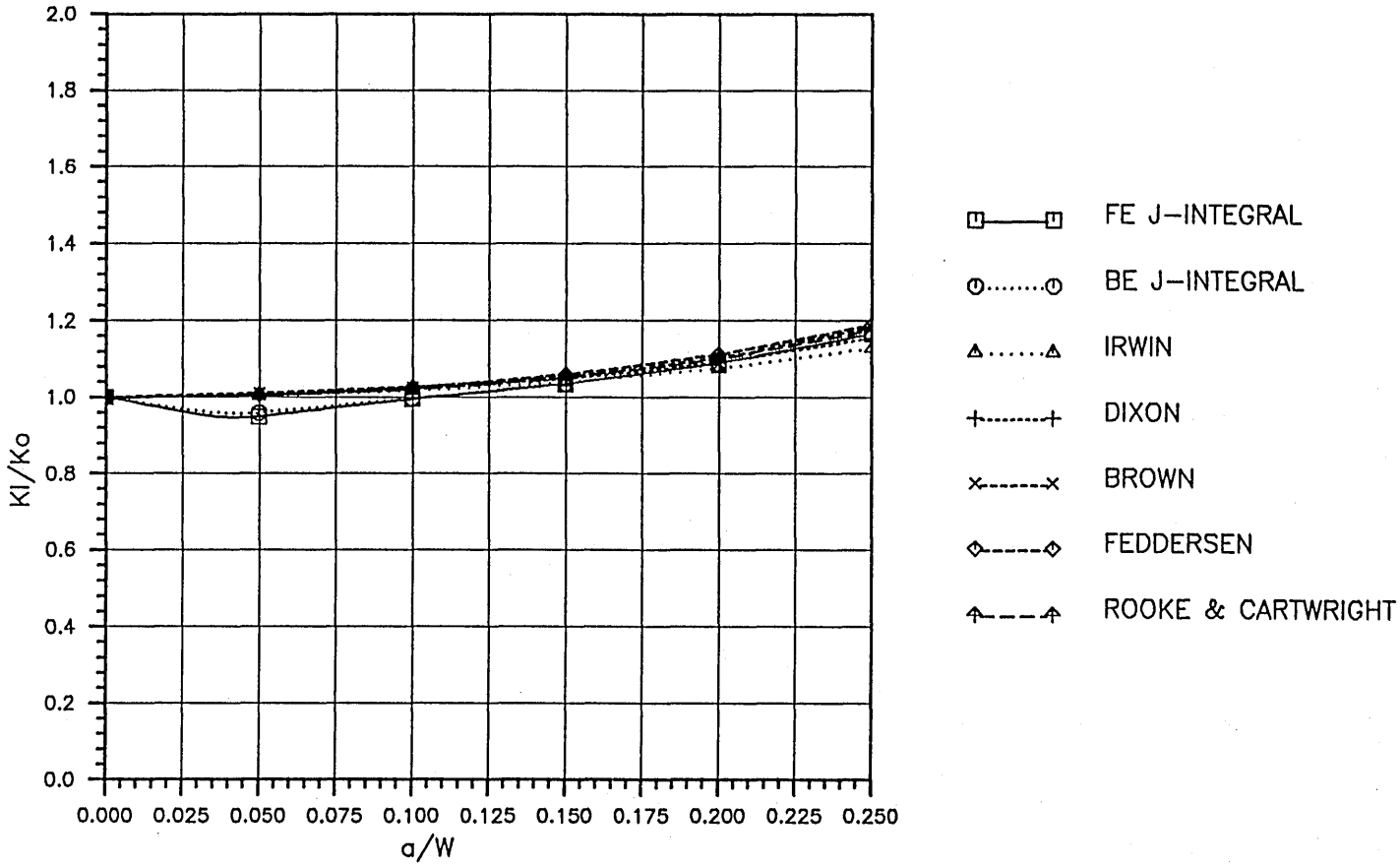

Fig.(9.24) Non-dimensional SIF's for CC Plate calculated by J-Integral Tech. from FE & BE Results at different Crack Ratios.

FRAMEC

Run on 7-JUN-90, At 18:51:44

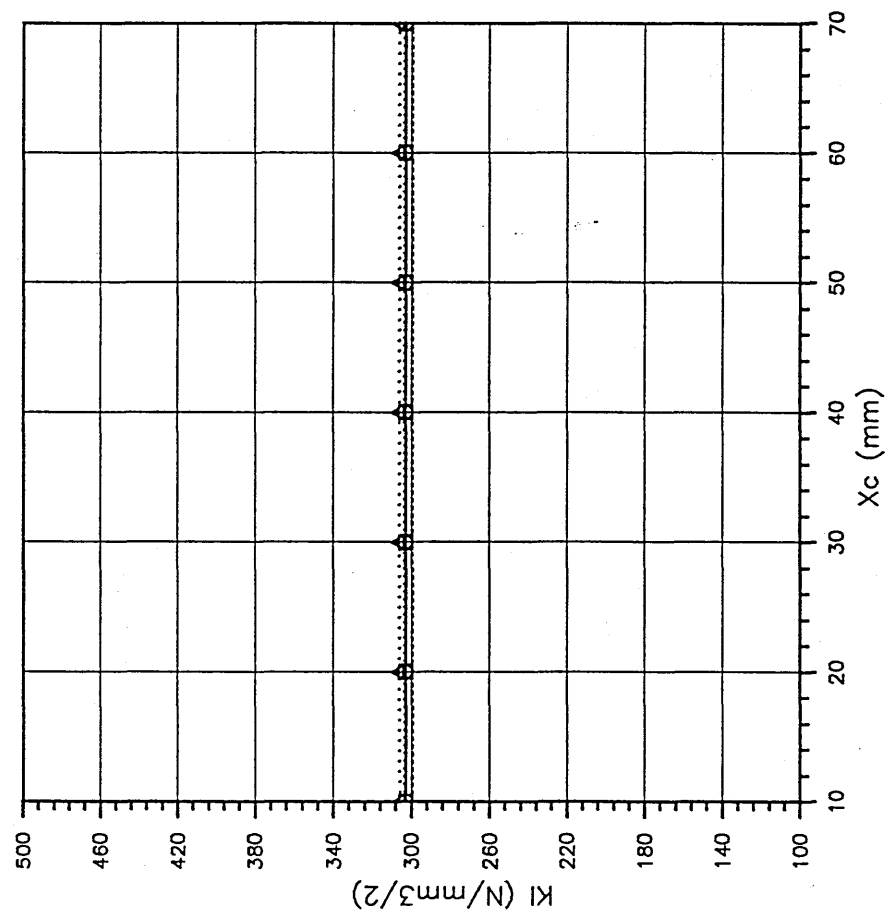

Fig.(9.25) SIF for CC Plate calculated by the J-Integral from 9-N and (1/SQR2) Elements at different Contour Distances from the Crack Tip.

FRAMEC

Run on 7-JUN-90, At 18:56:08

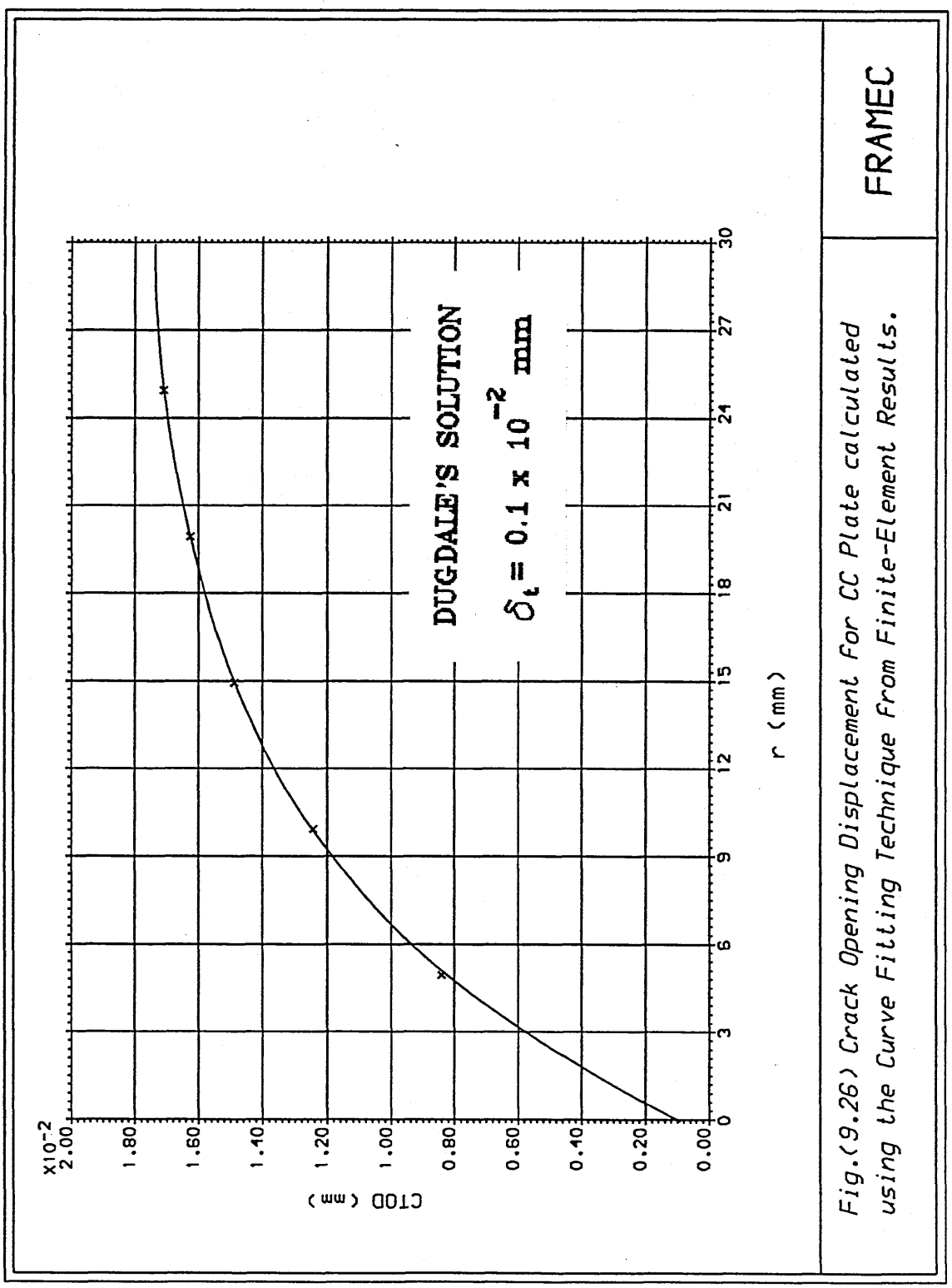

Fig.(9.26) Crack Opening Displacement For CC Plate calculated using the Curve Fitting Technique From Finite-Element Results.

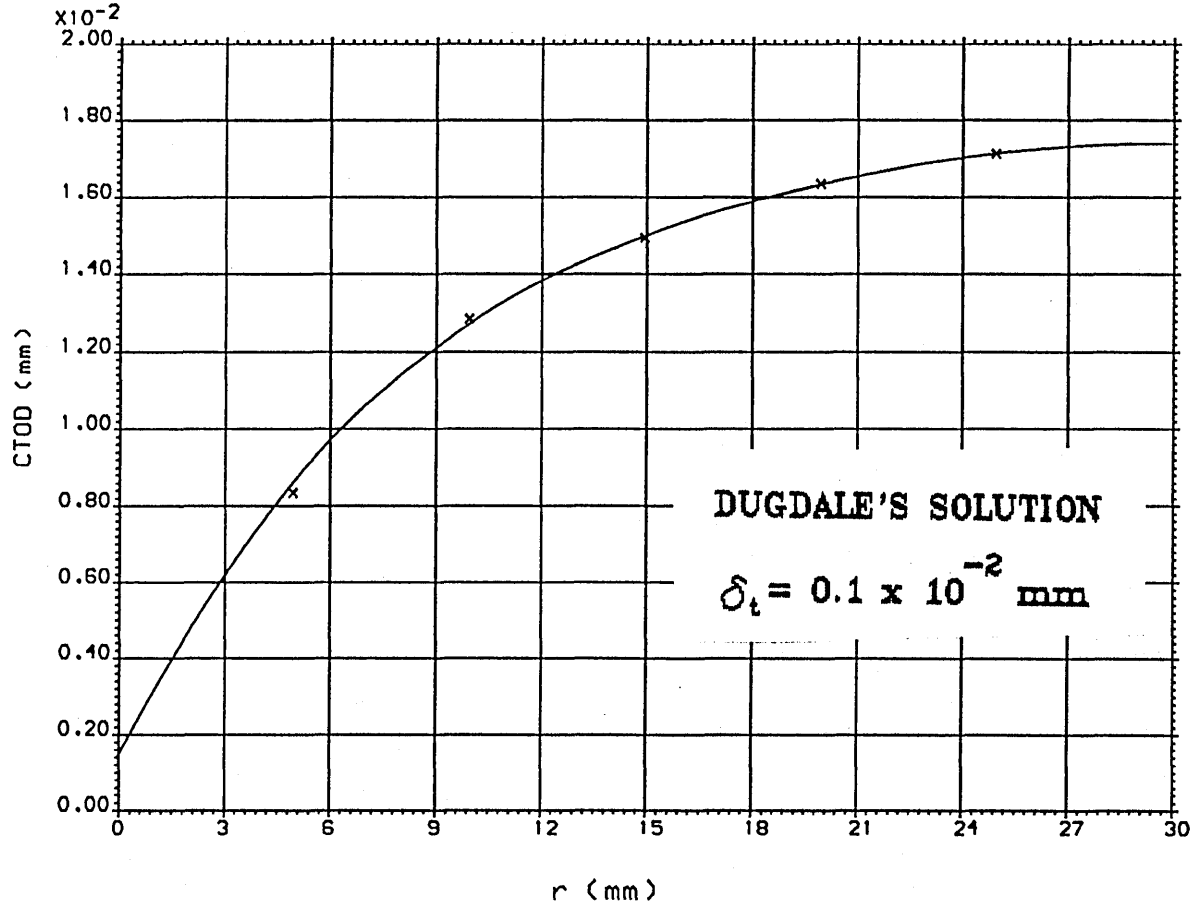

Fig.(9.27) Crcak Opening Displacement For CC Plate calculated using the Curve Fitting Technique From Boundary-Element Results.

FRAMEC

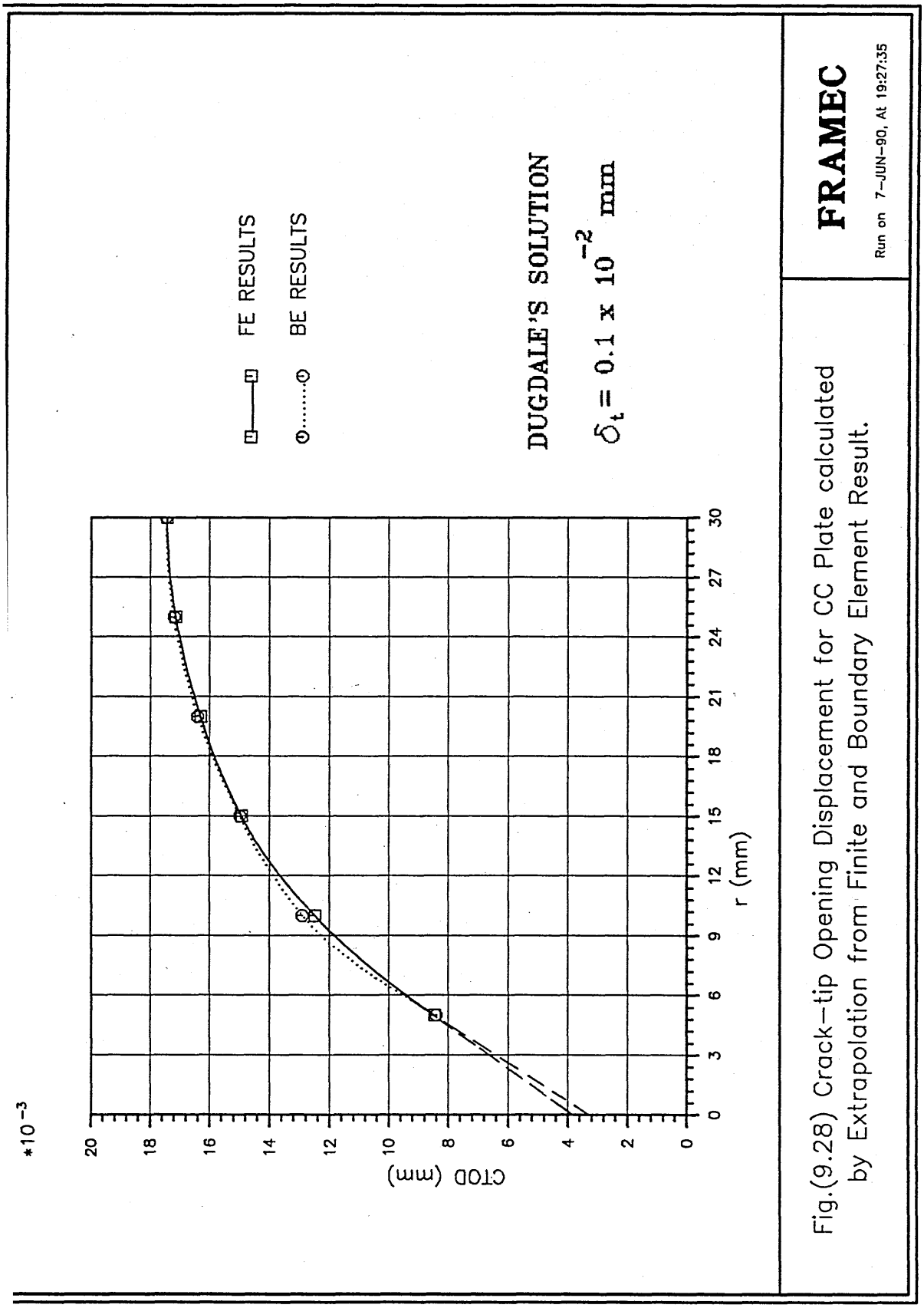

Fig.(9.28) Crack-tip Opening Displacement for CC Plate calculated by Extrapolation from Finite and Boundary Element Result.

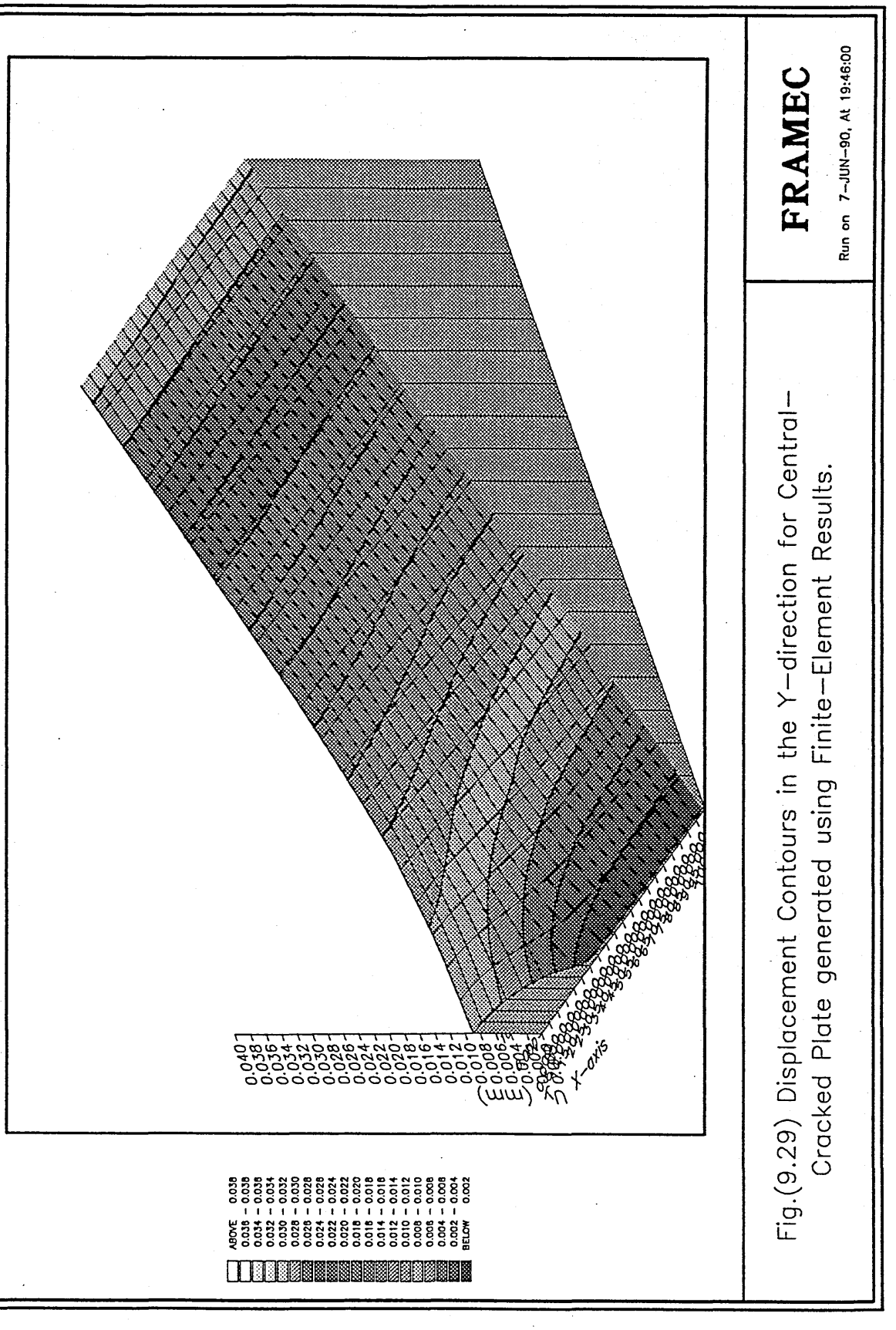

Fig.(9.29) Displacement Contours in the Y-direction for Central-Cracked Plate generated using Finite-Element Results.

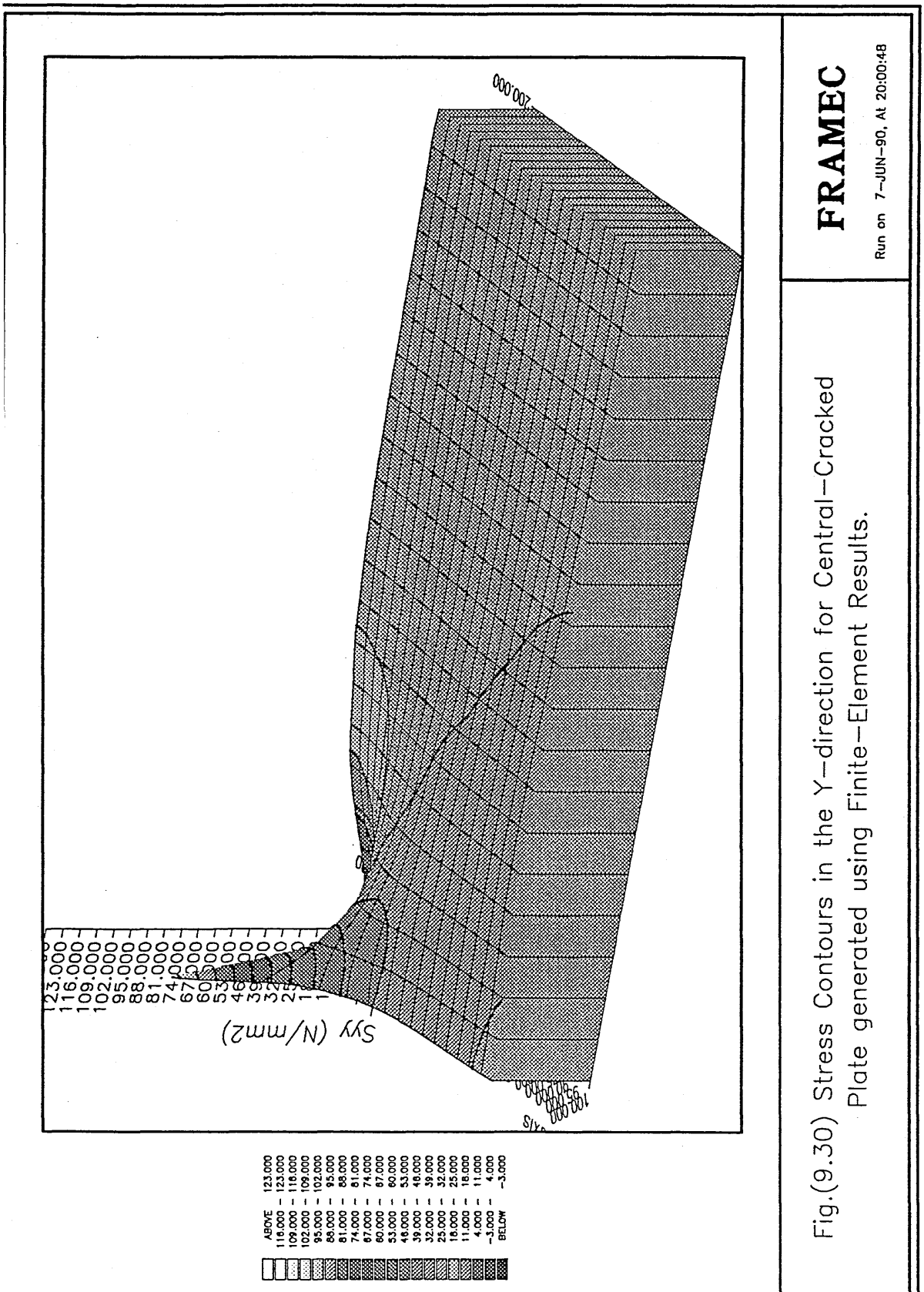

Fig.(9.30) Stress Contours in the Y-direction for Central-Cracked Plate generated using Finite-Element Results.

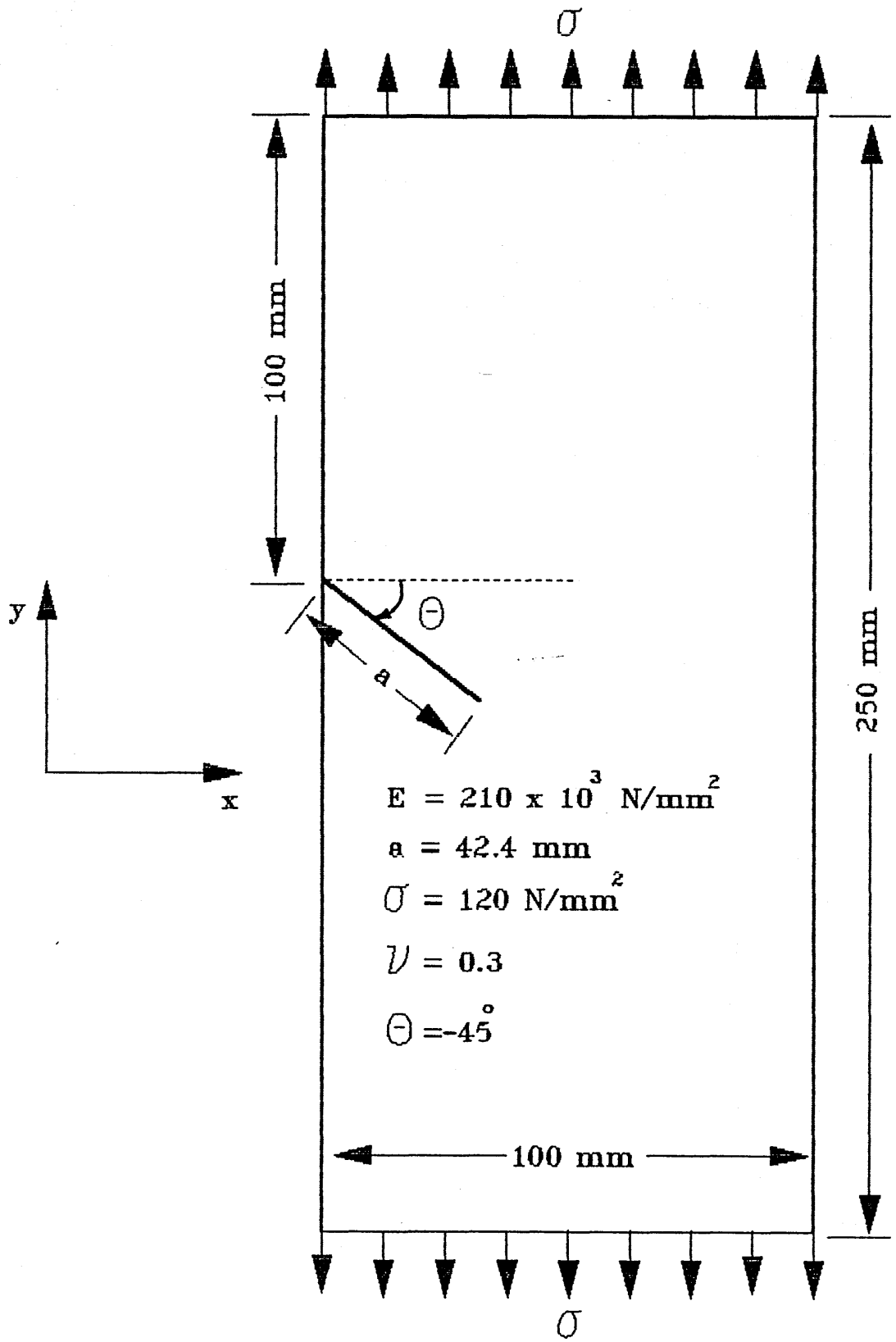

Fig.(9.31) Single-Edge Cracked Plate under Uniform Tension.

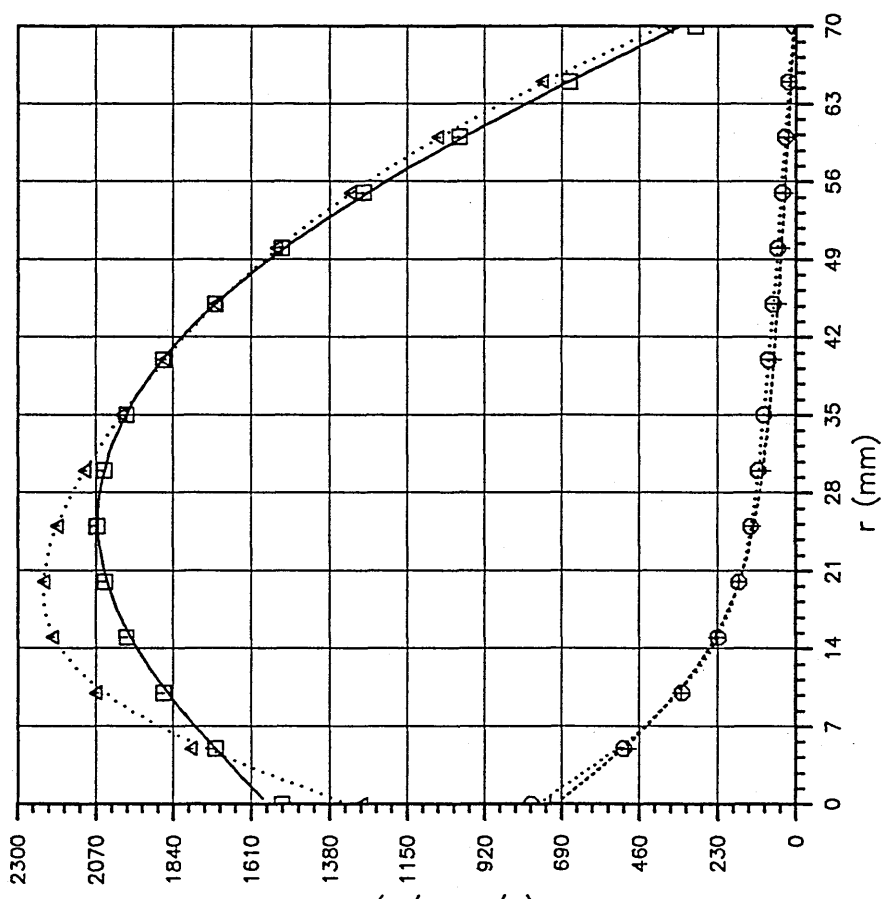

Fig.(9.32) SIF's for SEC Plate calculated using Stress Extrapolation Curve Fitting from Sy & Sx Stress Components.

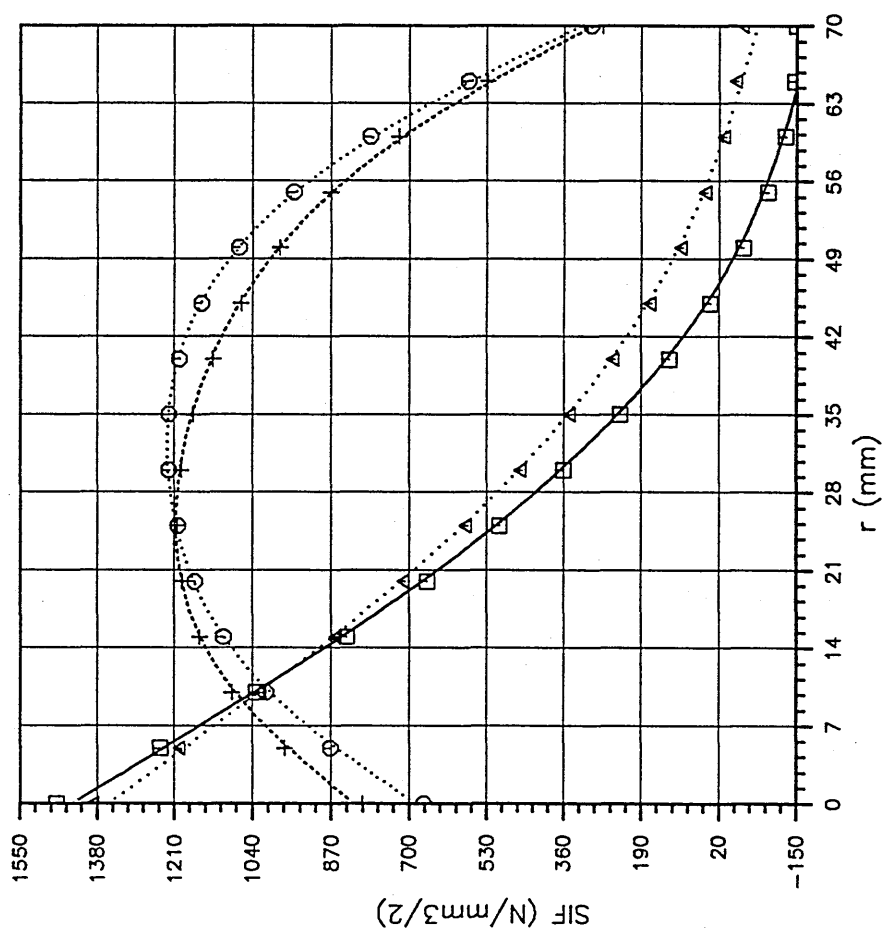

Fig.(9.33) SIF's for SEC Plate calculated using Stress Extrapolation Curve Fitting from Sx & Ss Stress Components.

FRAMEC

Run on 8-JUN-90, At 16:26:06

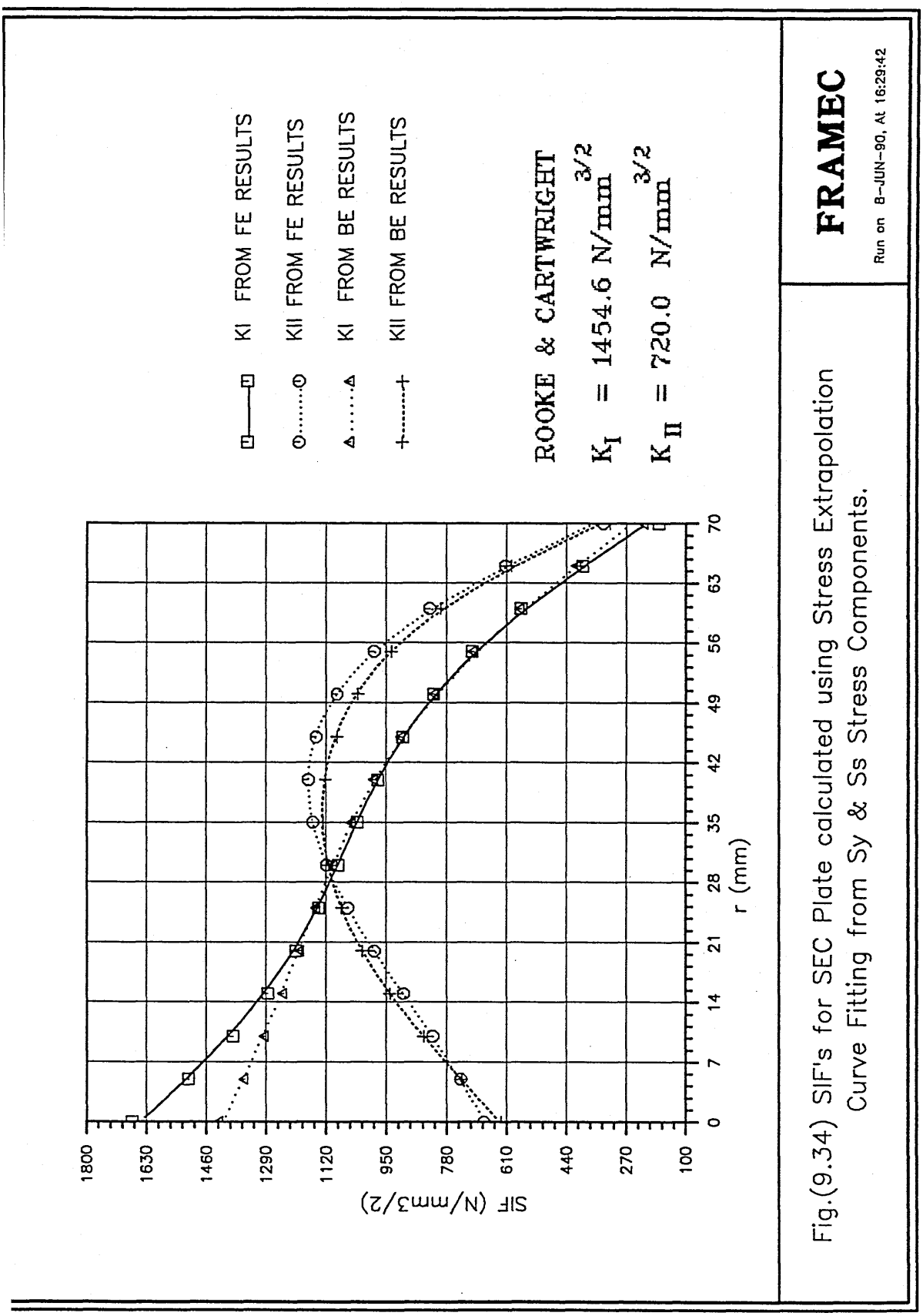

Fig.(9.34) SIF's for SEC Plate calculated using Stress Extrapolation Curve Fitting from Sy & Ss Stress Components.

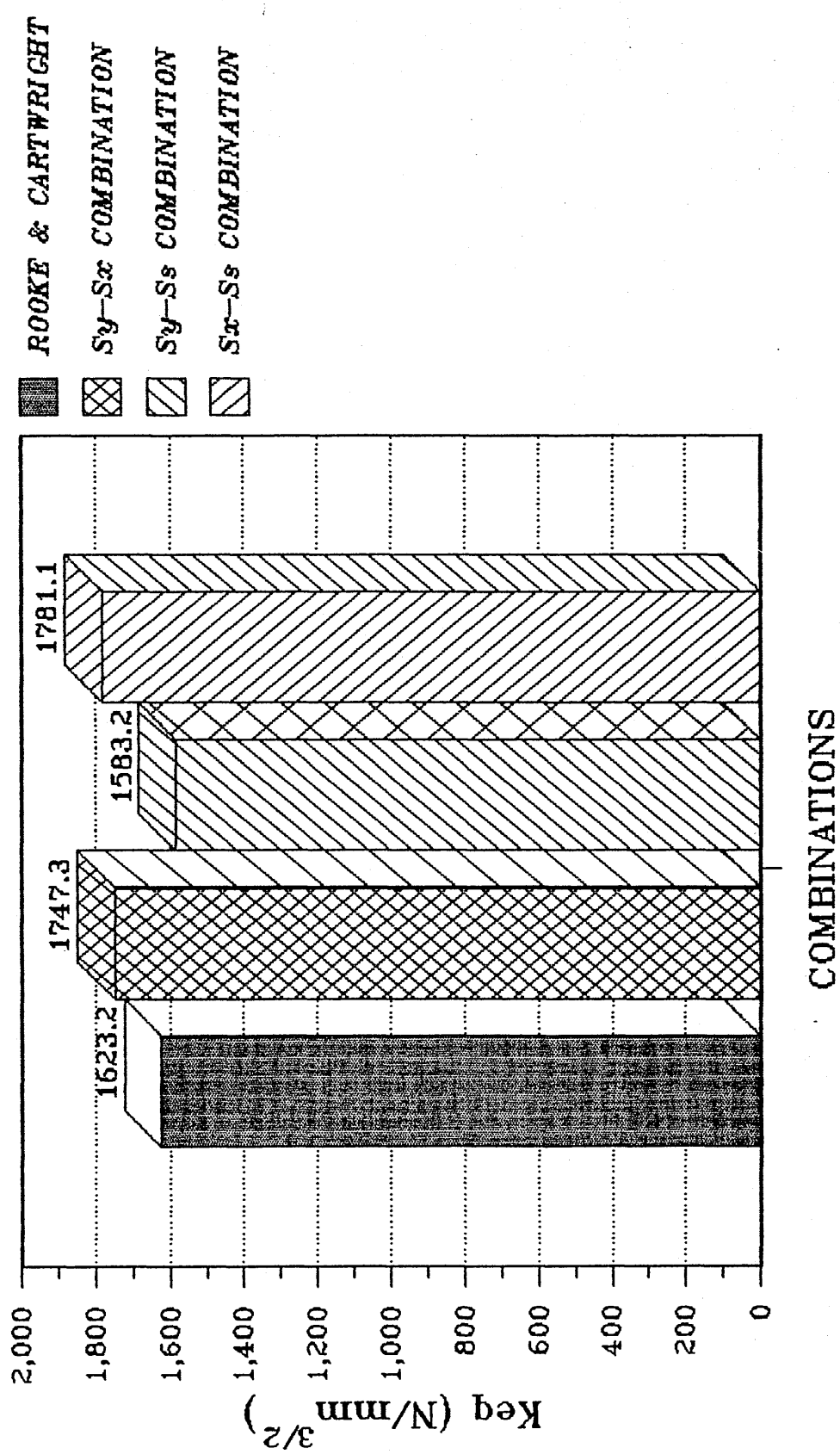

Fig.(9.35) Keq SIF's for SEC Plate calculated using Stress Extrapolation Curve Fitting from Finite-Element Results.

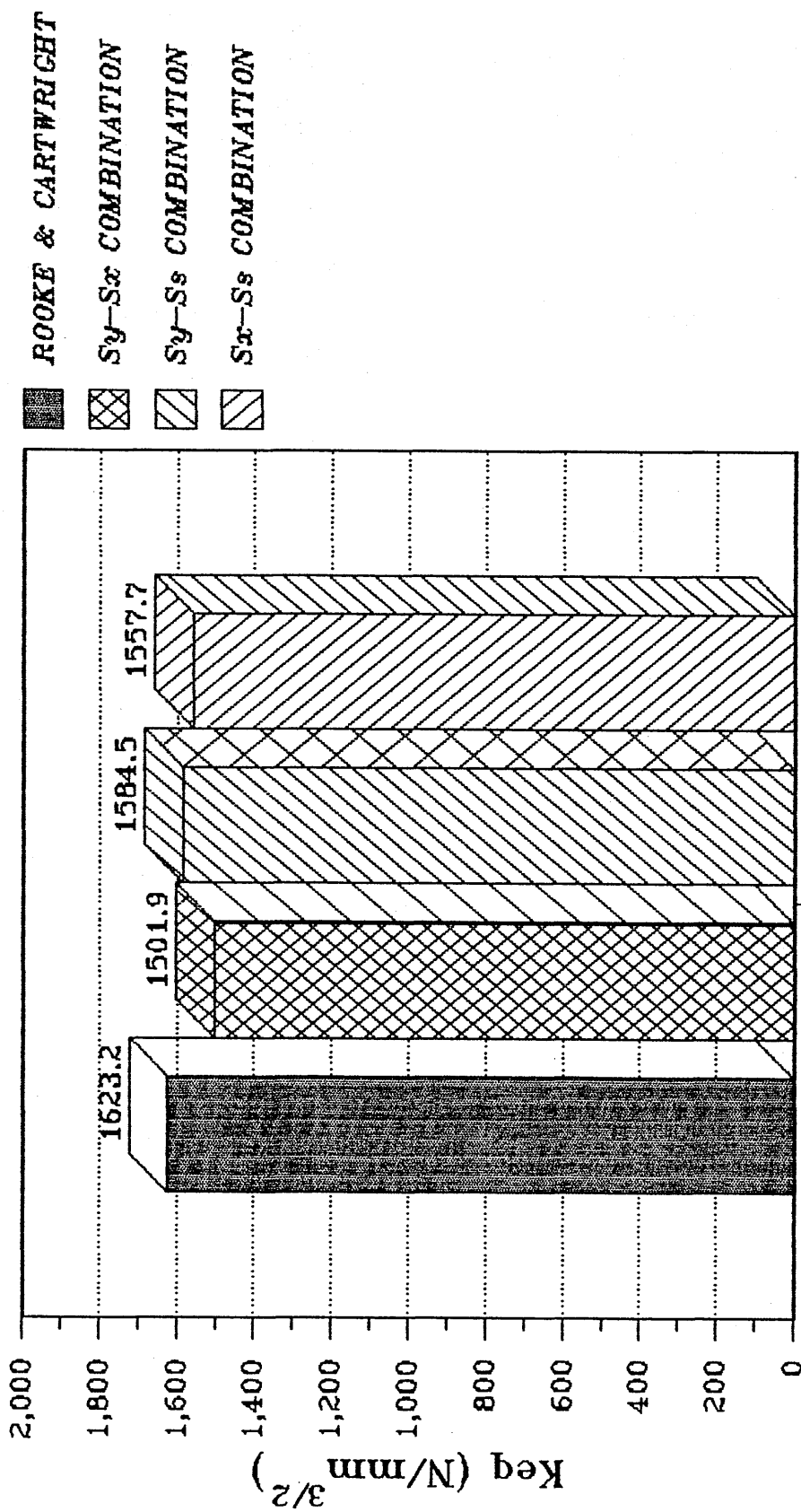

Fig.(9.36) Keq SIF's for SEC Plate calculated using Stress Extrapolation Curve Fitting from Boundary-Element Results.

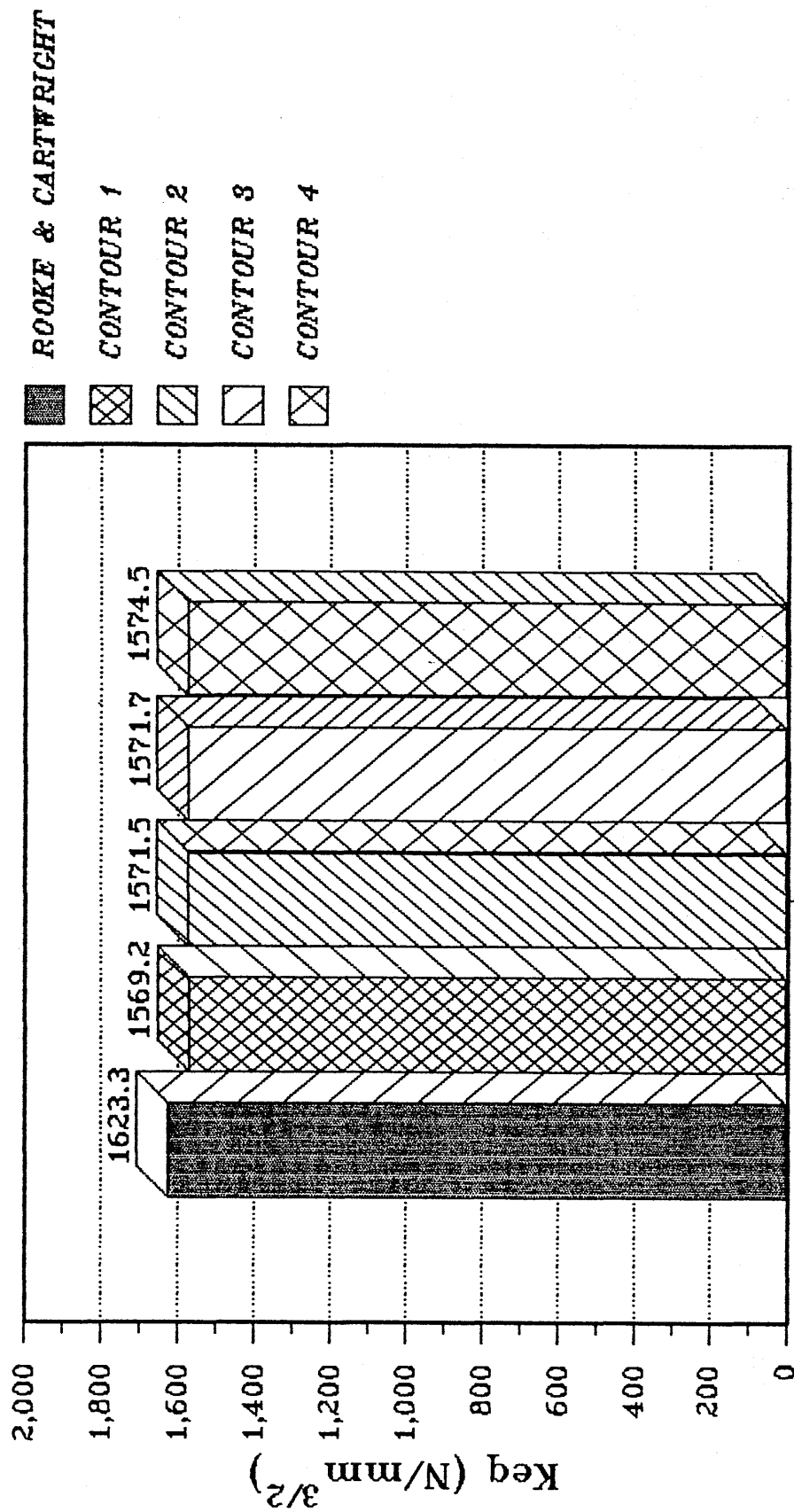

Fig.(9.37) Keq SIF's for SEC Plate calculated by the J-Integral Technique from FE Results at different Contours around the Crack Tip.

Fig.(9.38) Comparison between the SIF's for SEC Plate calculated by the J–Integral Technique from Finite and Boundary Element Results.

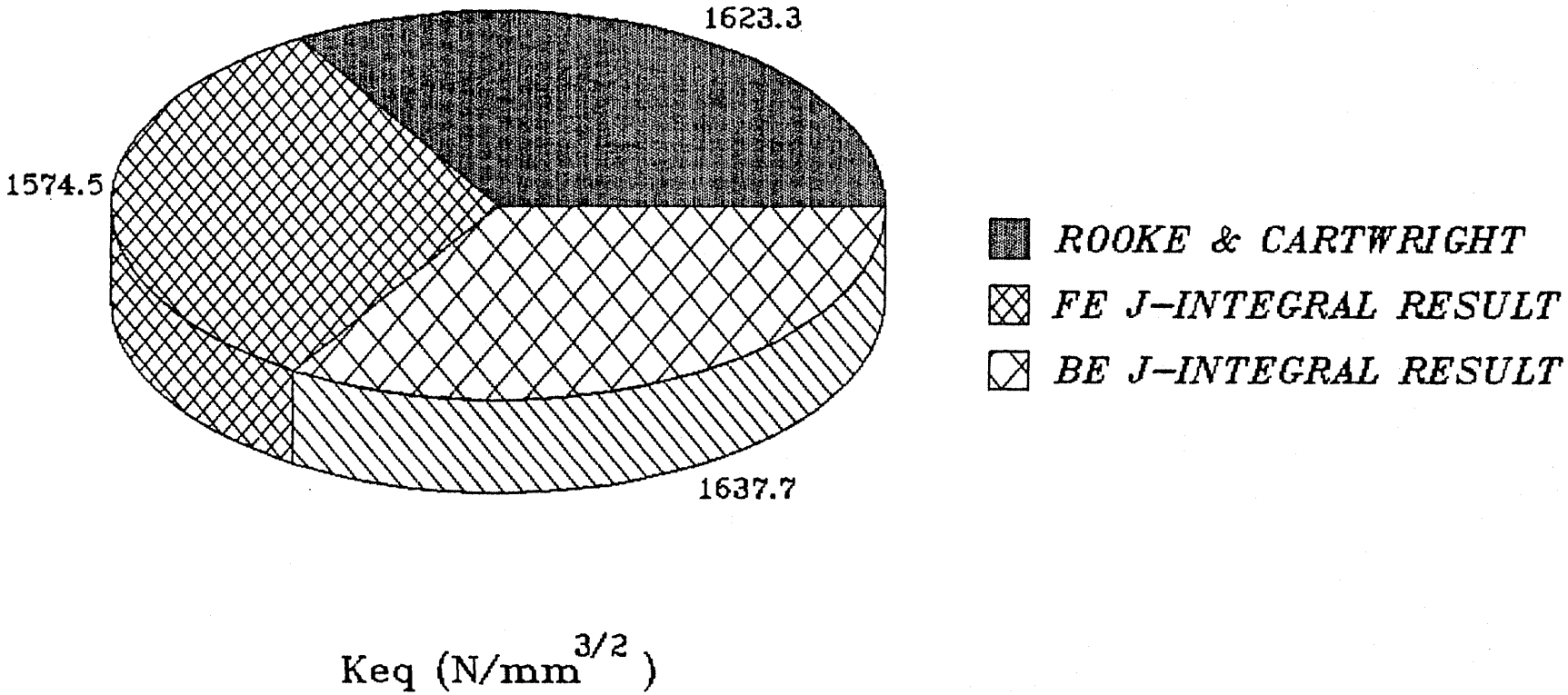

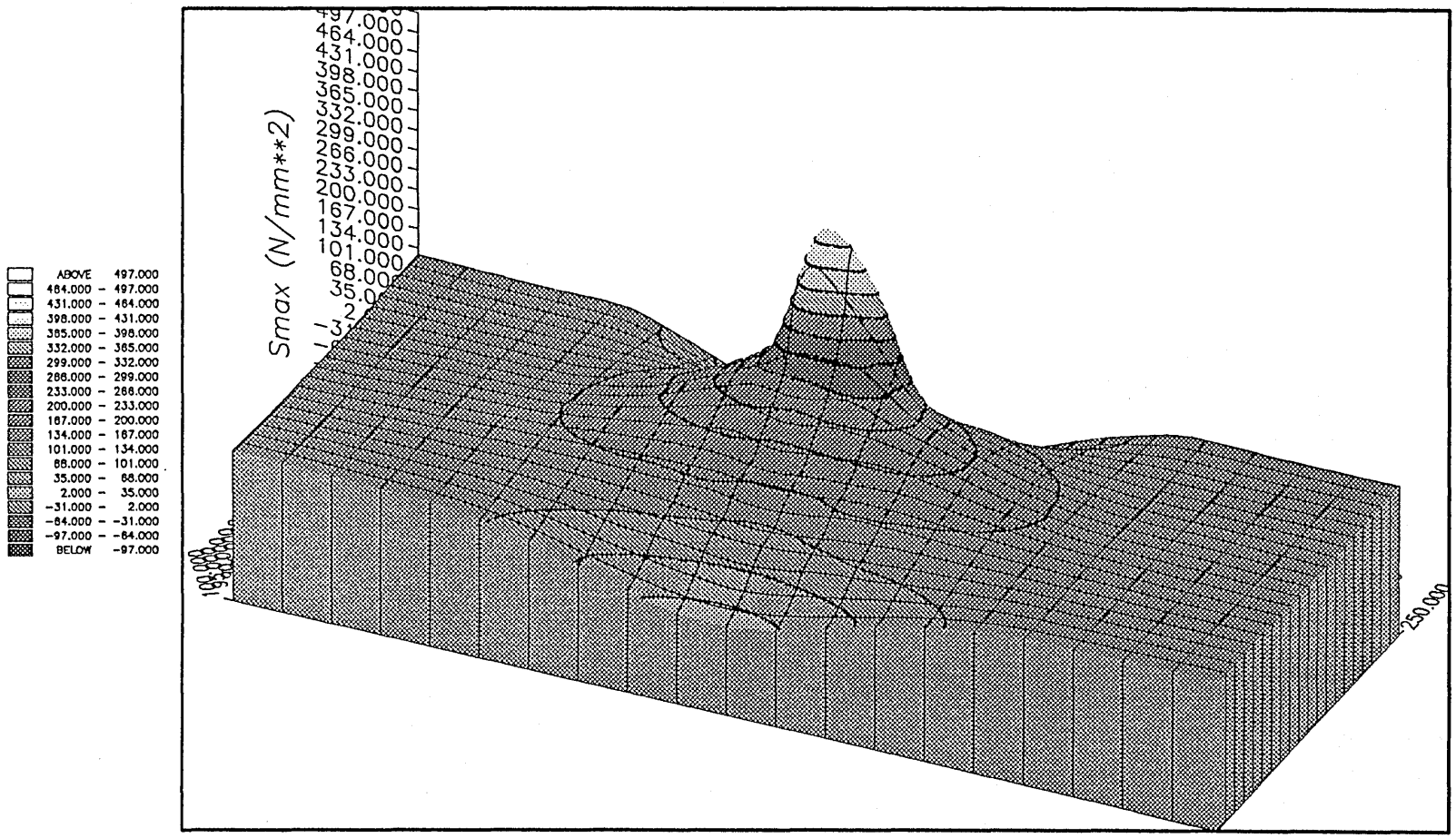

Fig.(9.39) Maximum Stress Contours for Single–Edge Cracked Plate generated from Finite–Element Results.

FRAMEC

Run on 8–JUN–90, At 16:34:55

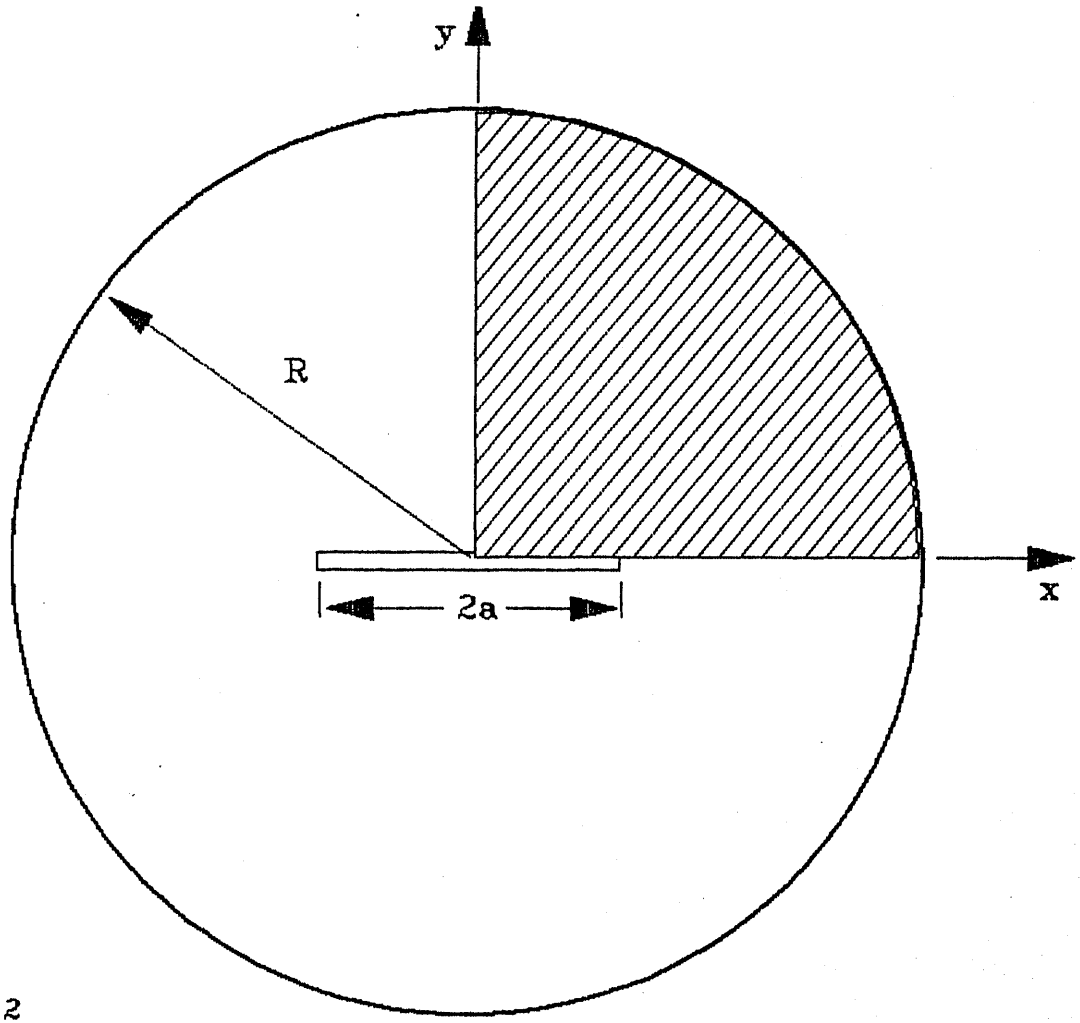

ν = 0.3
ω = 20 rad/s
ρ = 0.025 kg/mm^3
R = 20 mm
E = 1.0 x 10^4 N/mm^2

Fig.(9.40) Central–Cracked Rotating Disc.

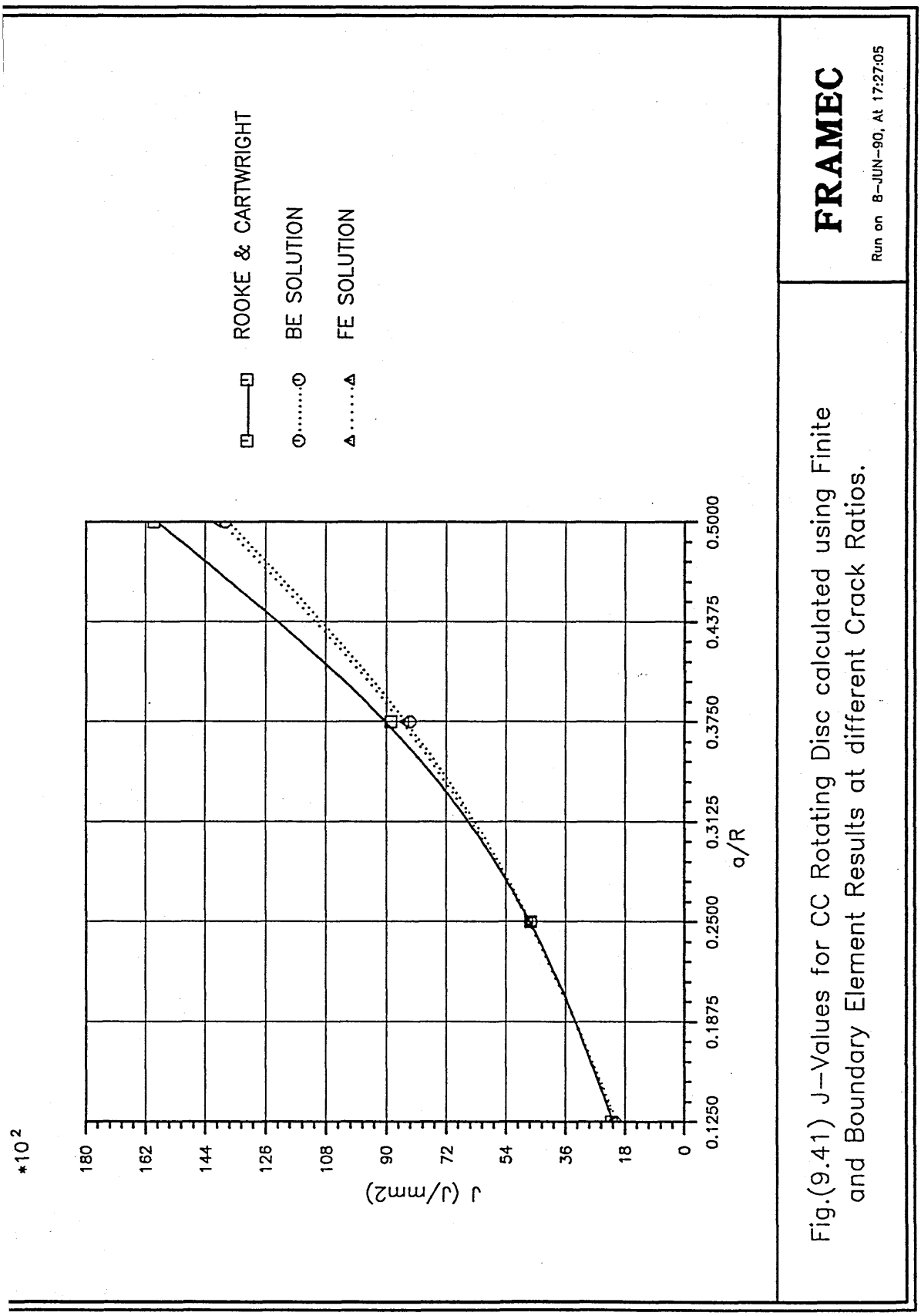

Fig.(9.41) J-Values for CC Rotating Disc calculated using Finite and Boundary Element Results at different Crack Ratios.

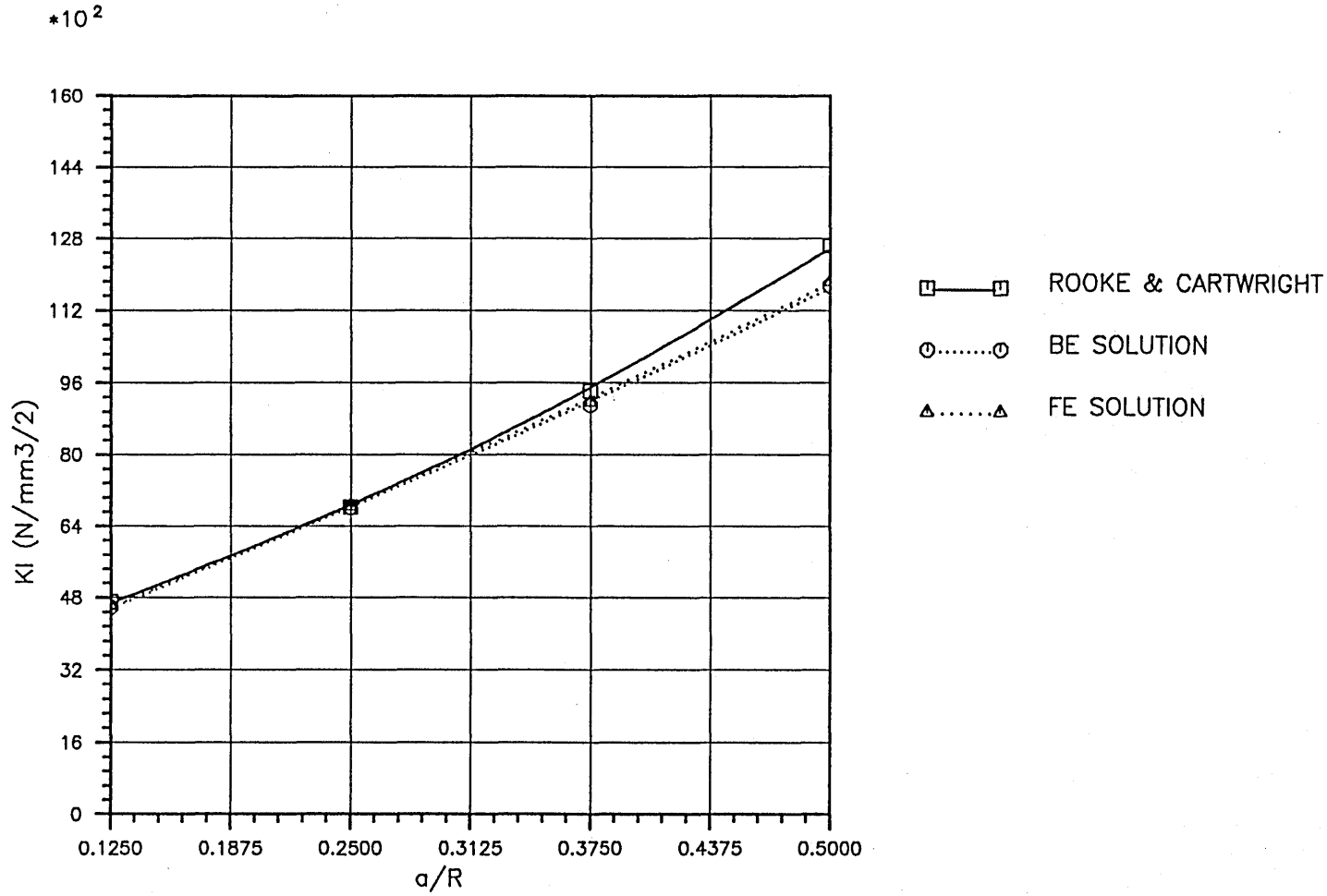

Fig.(9.42) KI SIF for CC Rotating Disc calculated using Finite and Boundary Element Results at different Crack Ratios.

FRAMEC

Run on 8-JUN-90, At 17:31:26

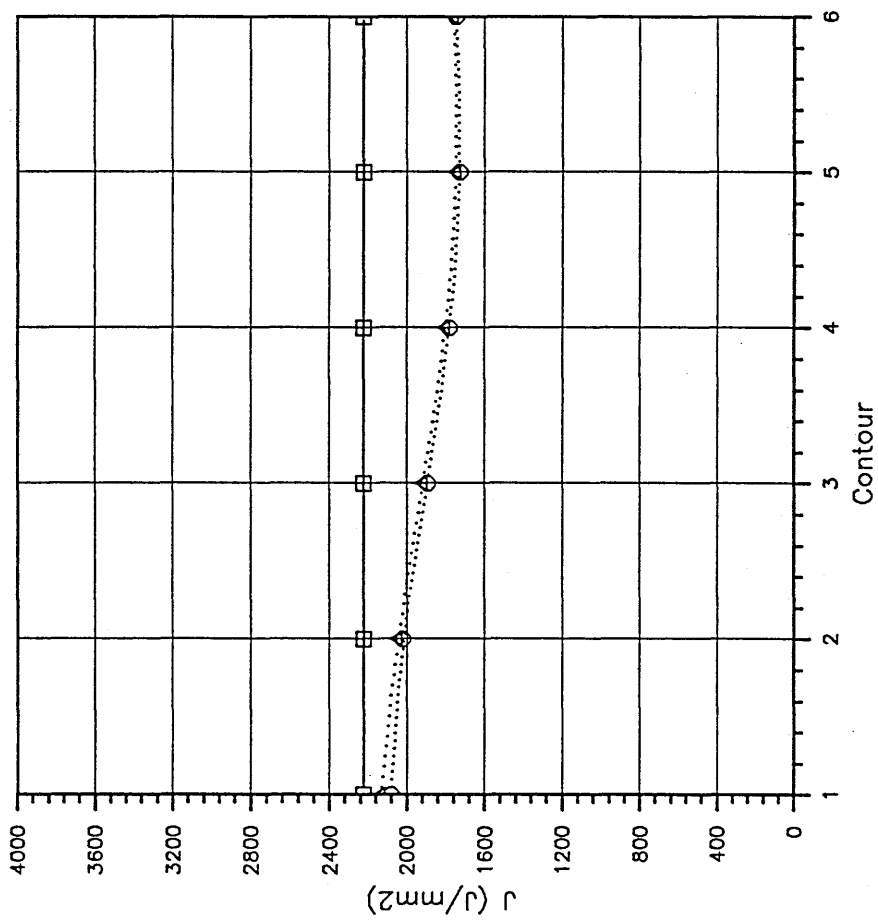

Fig.(9.43) J–Values for CC Rotating Disc calculated using FE & BE Results at different Contours around the Crack Tip (a/R = 0.125).

FRAMEC

Run on 8-JUN-90, At 17:36:56

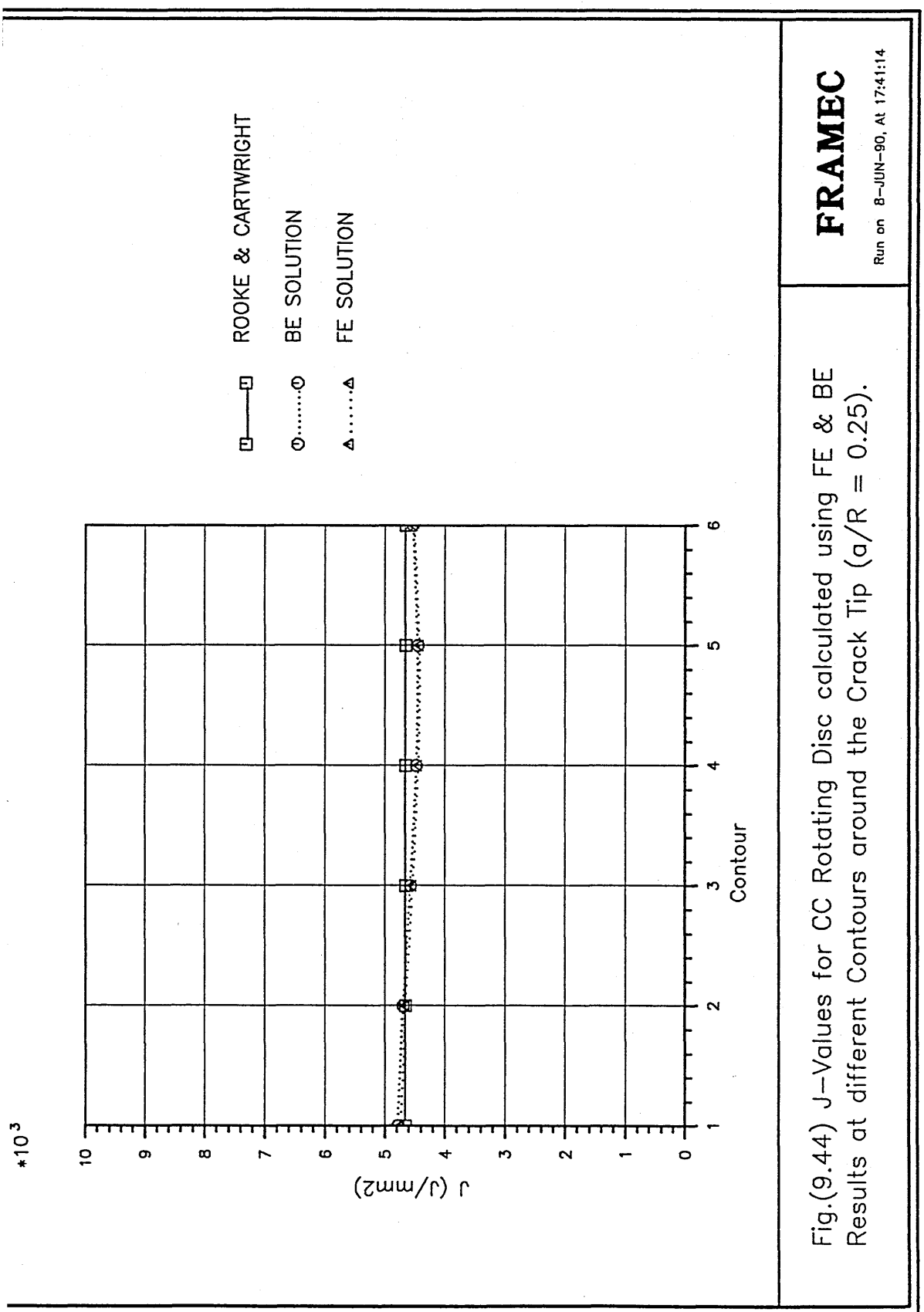

Fig.(9.44) J-Values for CC Rotating Disc calculated using FE & BE Results at different Contours around the Crack Tip (a/R = 0.25).

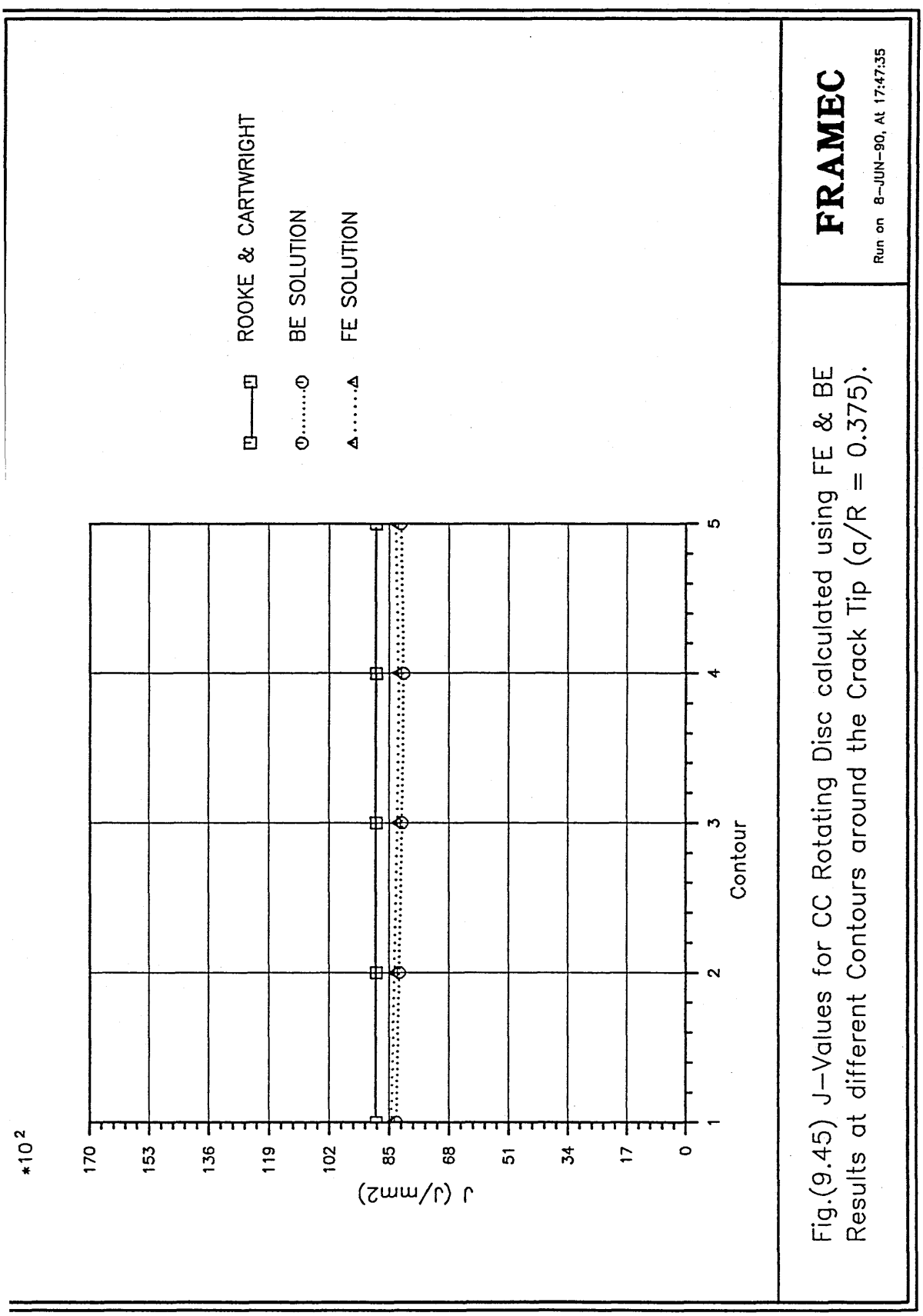

Fig.(9.45) J-Values for CC Rotating Disc calculated using FE & BE Results at different Contours around the Crack Tip (a/R = 0.375).

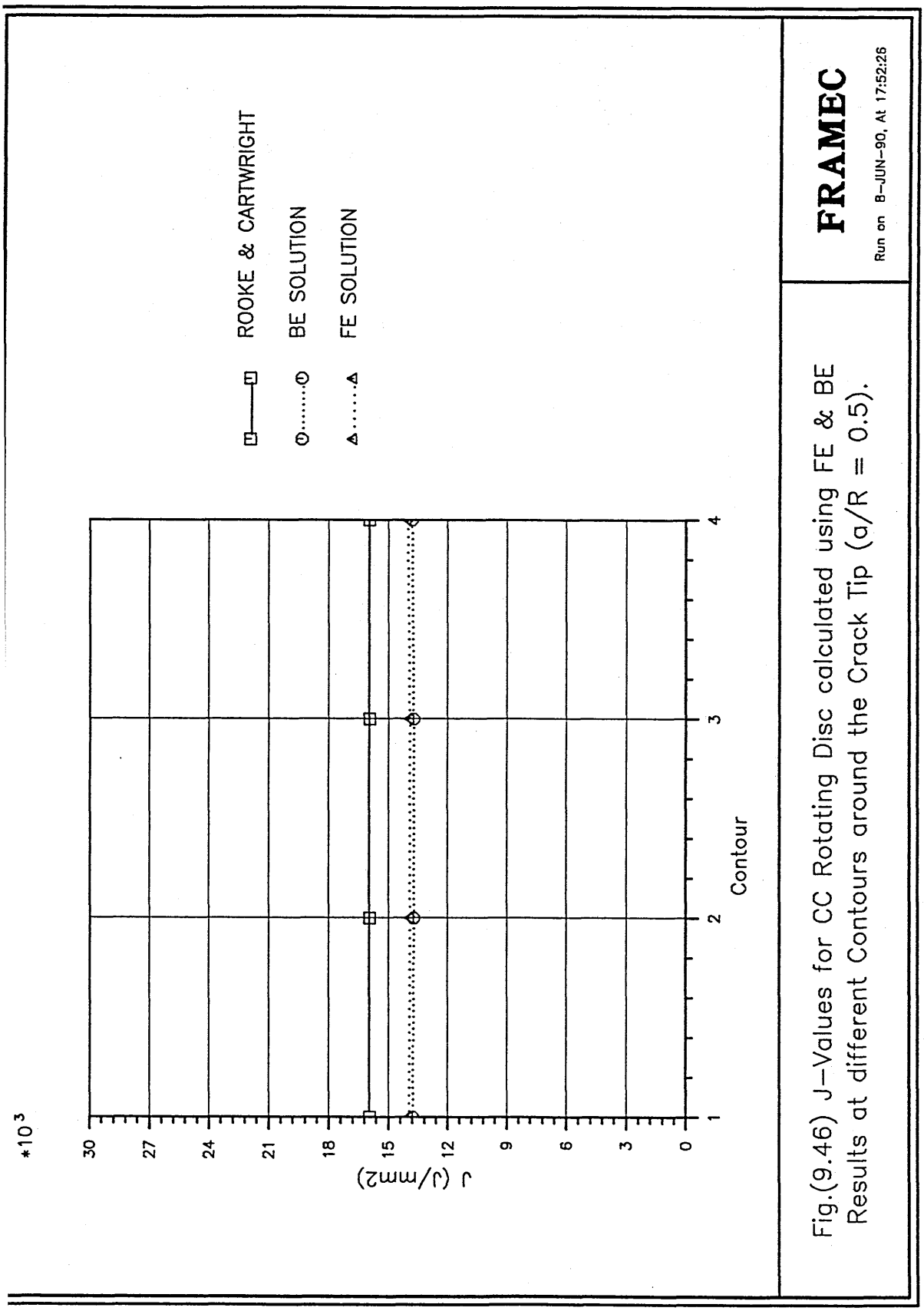

Fig.(9.46) J-Values for CC Rotating Disc calculated using FE & BE Results at different Contours around the Crack Tip (a/R = 0.5).

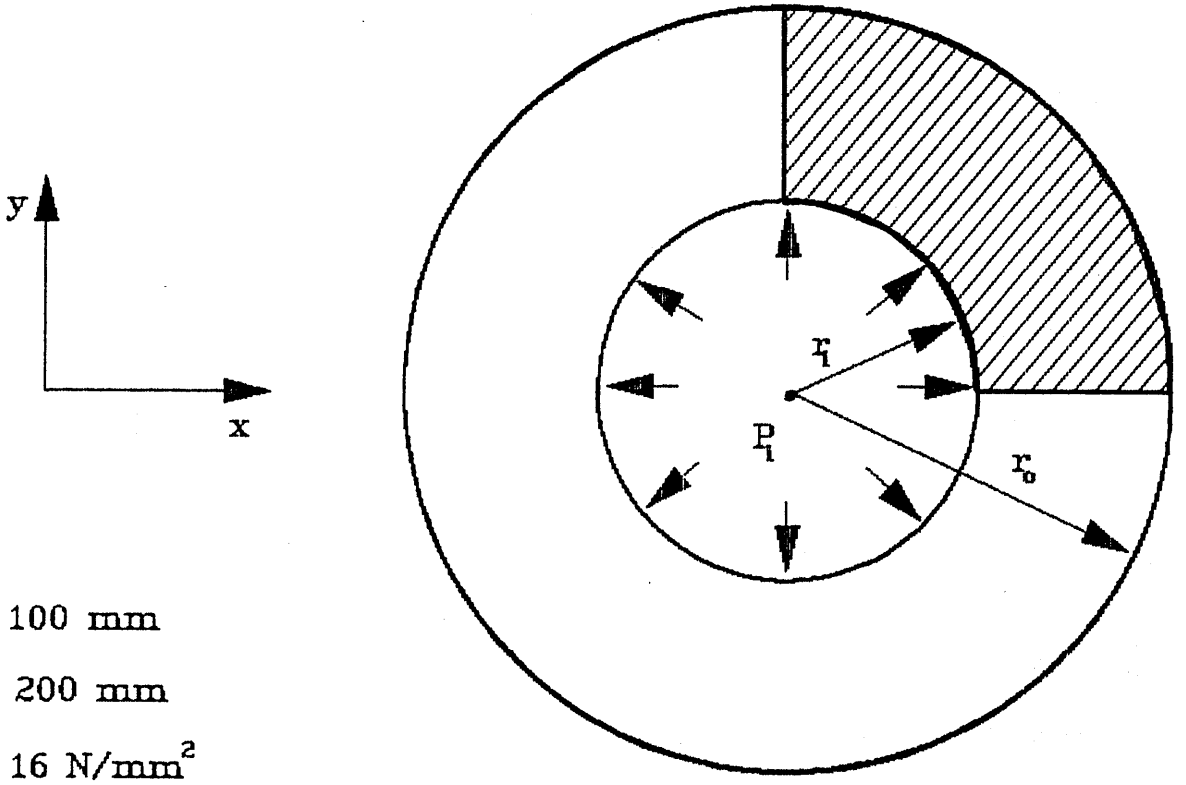

r_i = 100 mm

r_o = 200 mm

P_i = 16 N/mm^2

E = 2.1 x 10^4 N/mm^2 , ν = 0.3

Y = 24 N/mm^2 , H' = 0

Fig.(9.47) Pressurized Cylinder used for the Validation of the Finite-Element Elasto-Plastic Program.

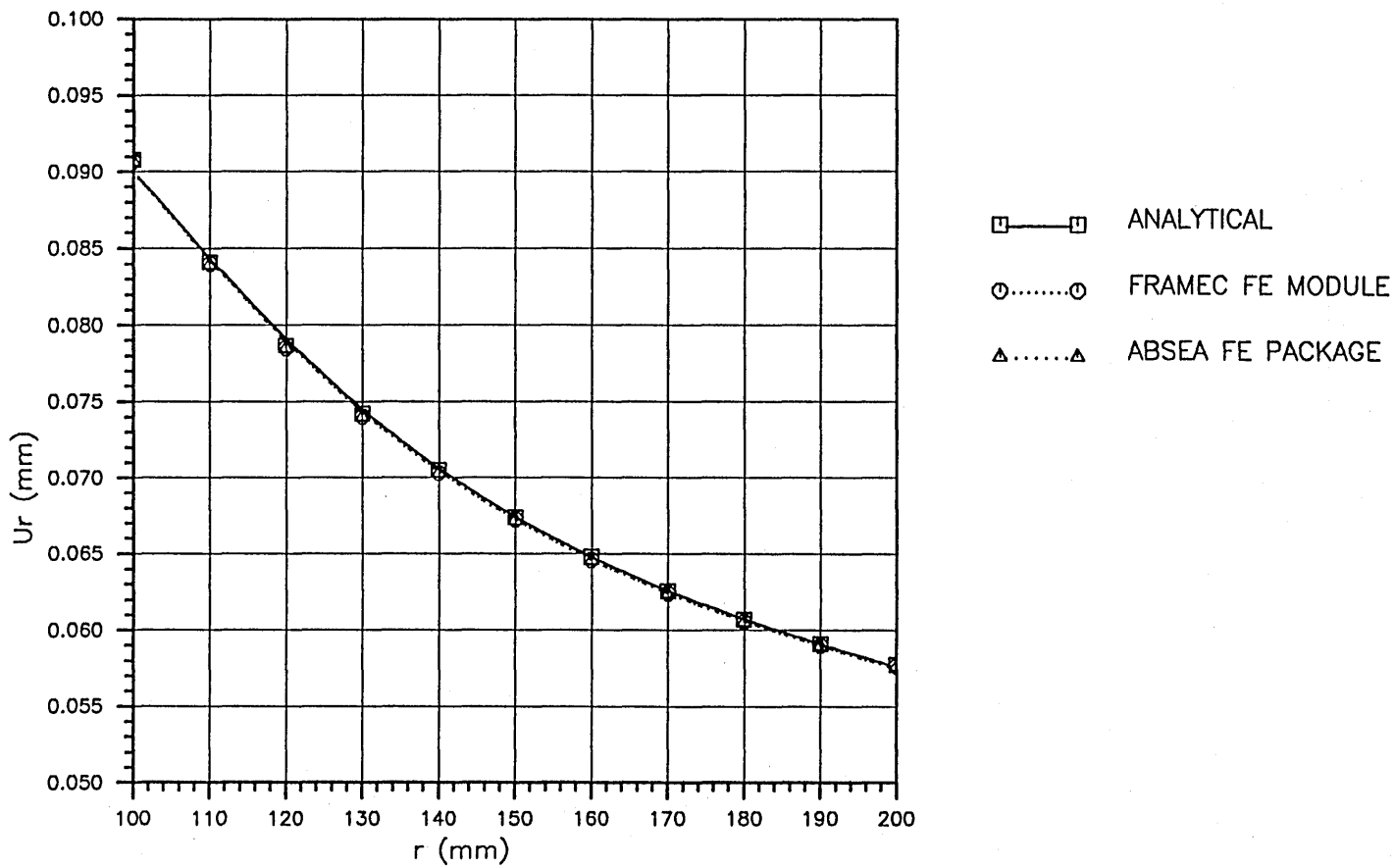

Fig.(9.48) Elastic Radial Displacements for Pressurized Cylinder calculated by Elasto–Plastic FE Analysis at Pi = 10 N/mm2.

FRAMEC

Run on 10–JUN–90, At 16:20:01

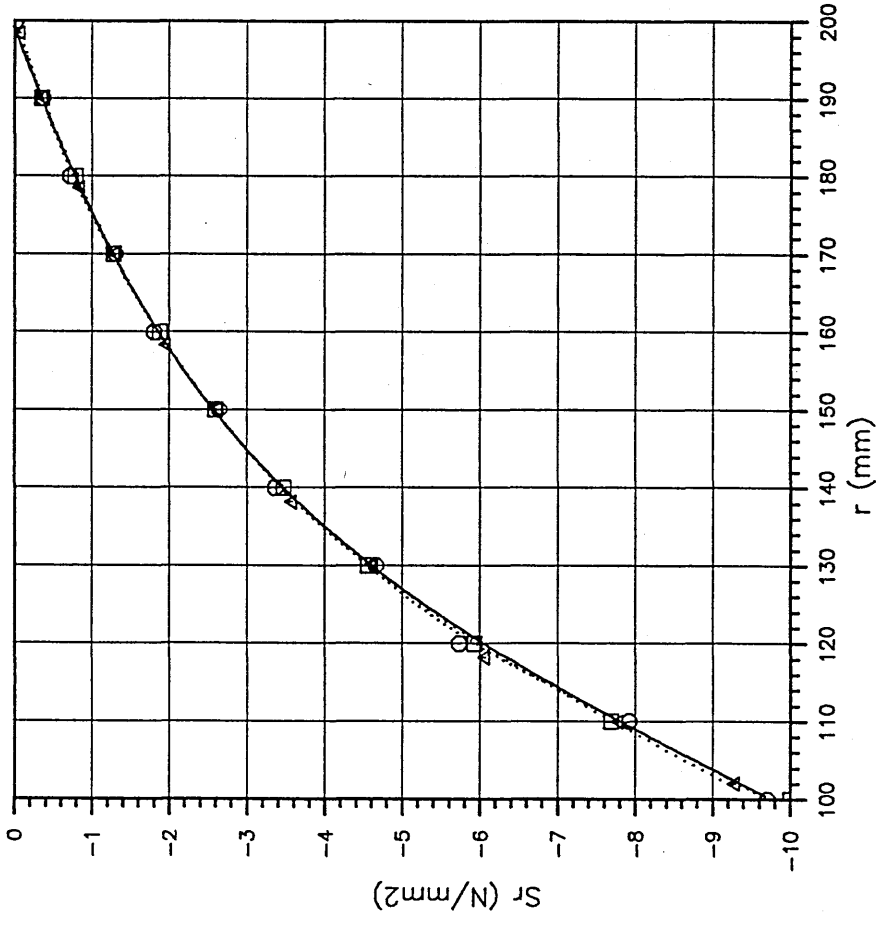

FRAMEC

Run on 10-JUN-90, At 16:23:28

Fig.(9.49) Elastic Radial Stresses for Pressurized Cylinder calculated by Elasto-Plastic FE Analysis at Pi = 10 N/mm2.

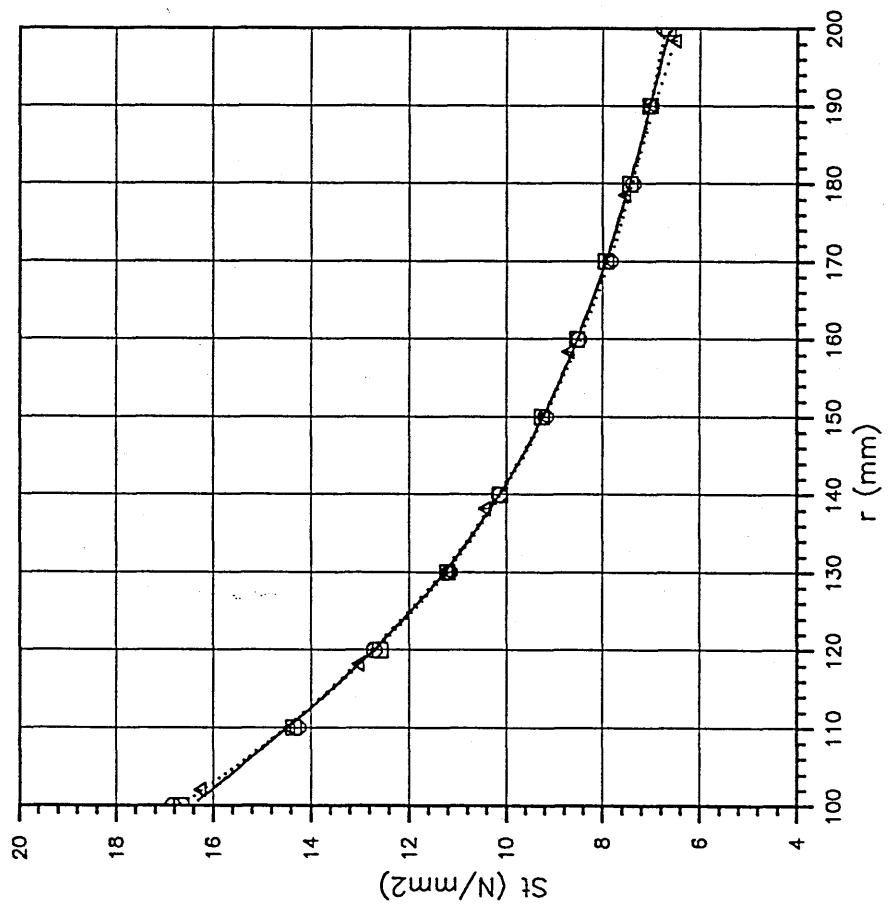

FRAMEC

Run on 10-JUN-90, At 16:27:58

Fig.(9.50) Elastic Hoop Stresses for Pressurized Cylinder calculated by Elasto-Plastic FE Analysis at Pi = 10 N/mm2.

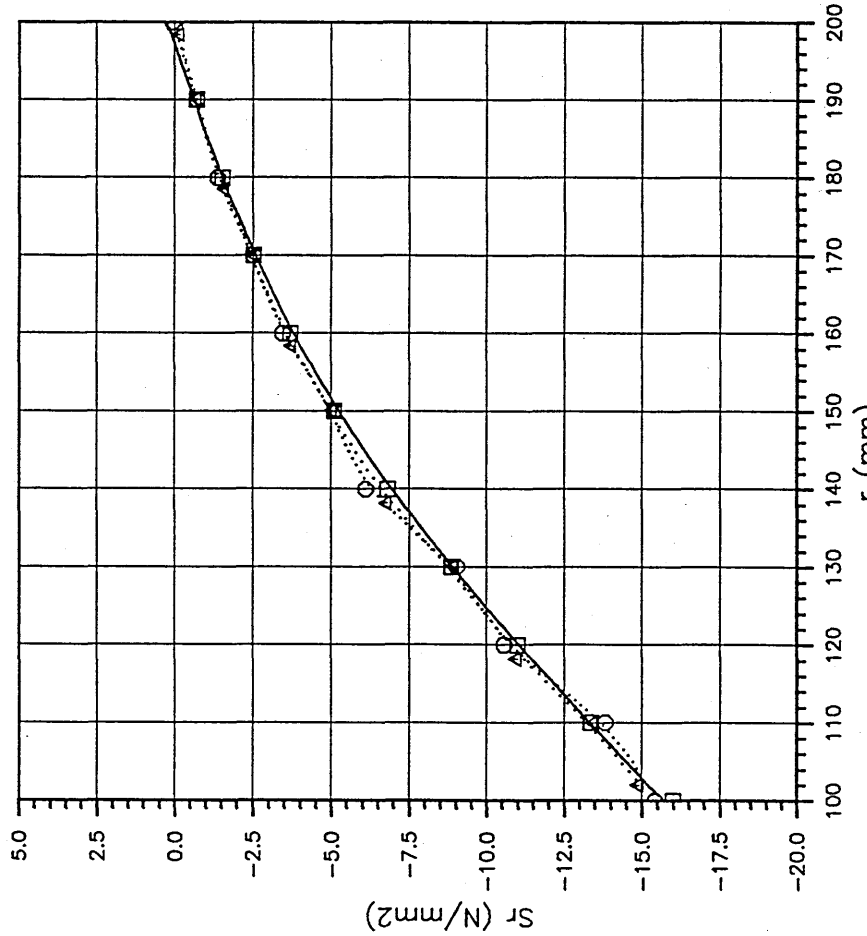

Fig.(9.51) Elasto-Plastic Radial stresses for Pressurized Cylinder calculated by Elasto-Plastic FE Analysis at Pi = 16 N/mm2.

FRAMEC

Run on 10-JUN-90, At 16:31:42

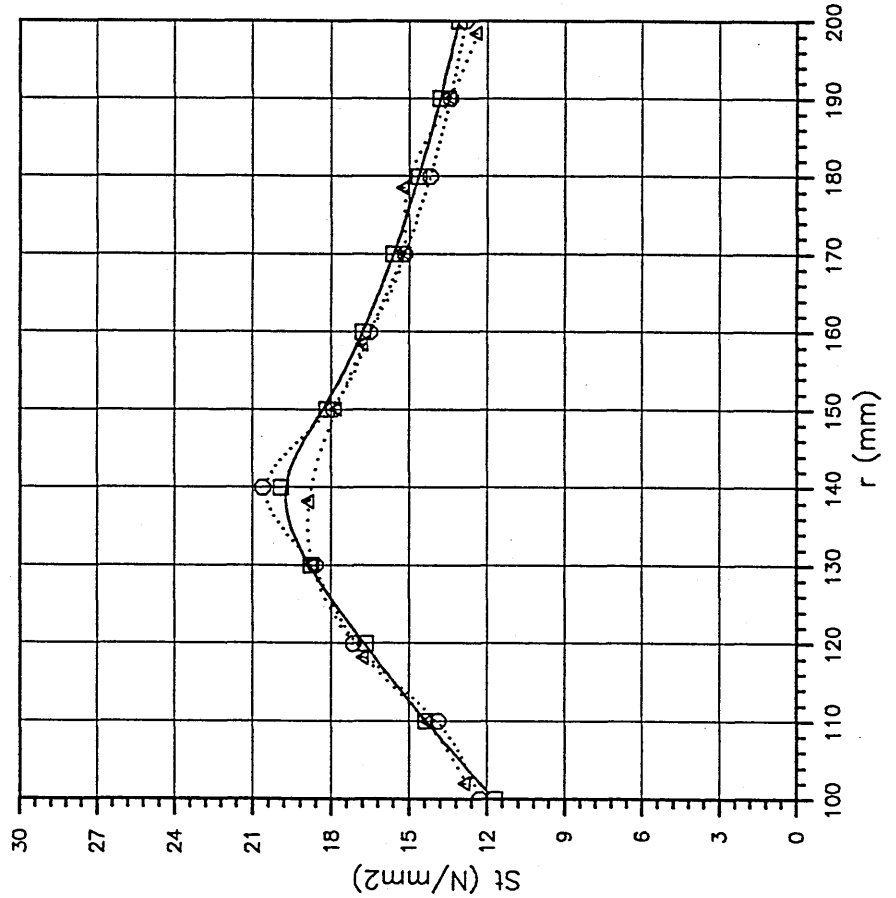

FRAMEC

Run on 10-JUN-90, At 16:34:56

Fig.(9.52) Elasto-Plastic Hoop Stresses for Pressurized Cylinder calculated by Elasto-Plastic FE Analysis at Pi = 16 N/mm2.

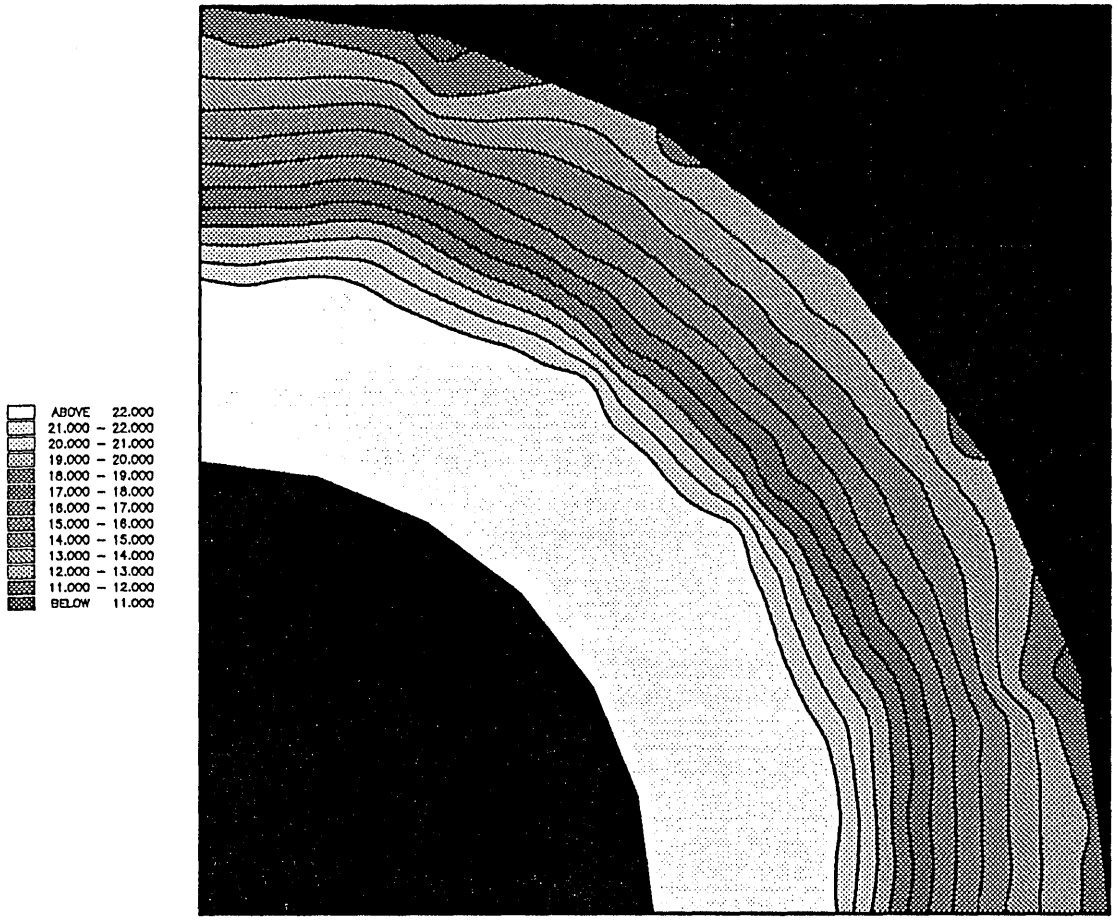

Fig.(9.53) Equivalent von Mises Stress Contours for Pressurized Cylinder Calculated at Pi= 16 N/mm2 & Y= 24 N/mm2.

FRAMEC

Run on 12-JUN-90, At 20:00:52

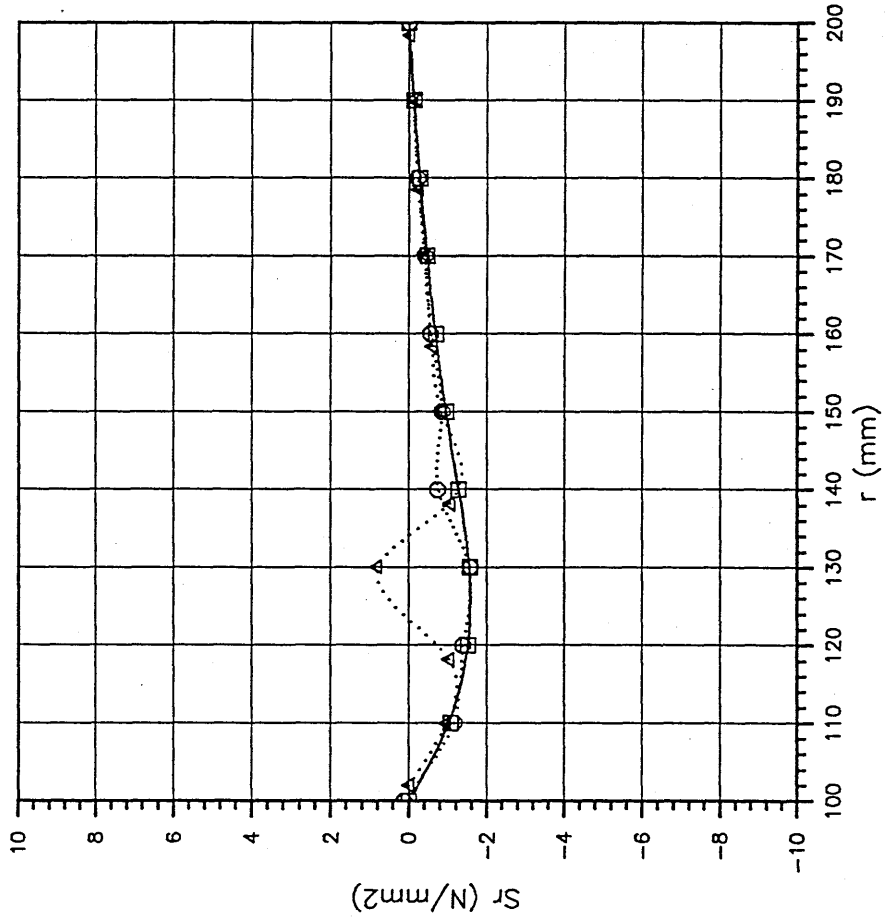

FRAMEC

Run on 10-JUN-90, At 16:46:08

Fig.(9.54) Residual Radial Stresses for Pressurized Cylinder calculated by Elasto-Plastic FE Analysis at Pi = 16 N/mm2.

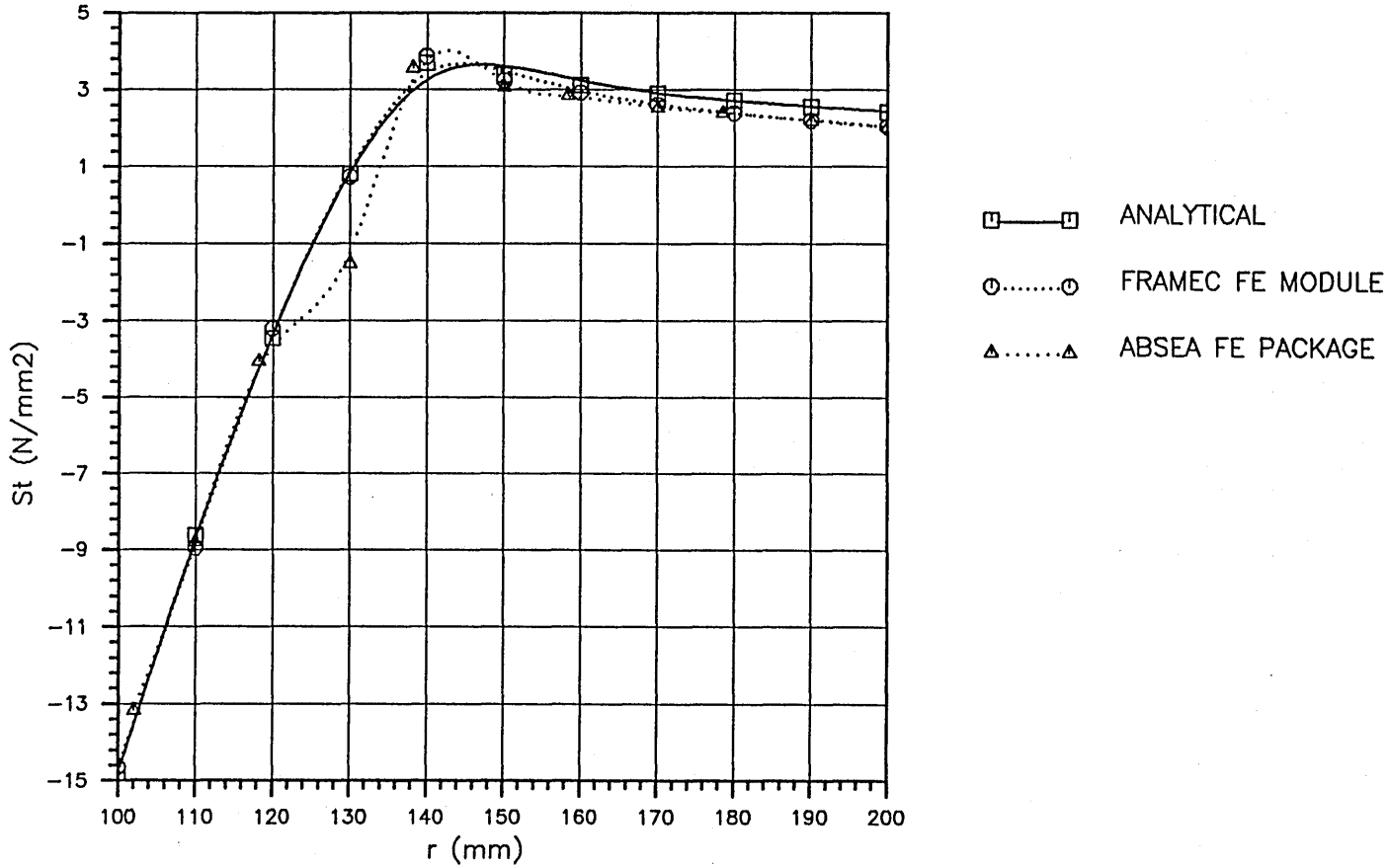

Fig.(9.55) Residual Hoop Stresses for Pressurized Cylinder calculated by Elasto-Plastic FE Analysis at Pi = 16 N/mm2.

FRAMEC

Run on 10-JUN-90, At 16:48:34

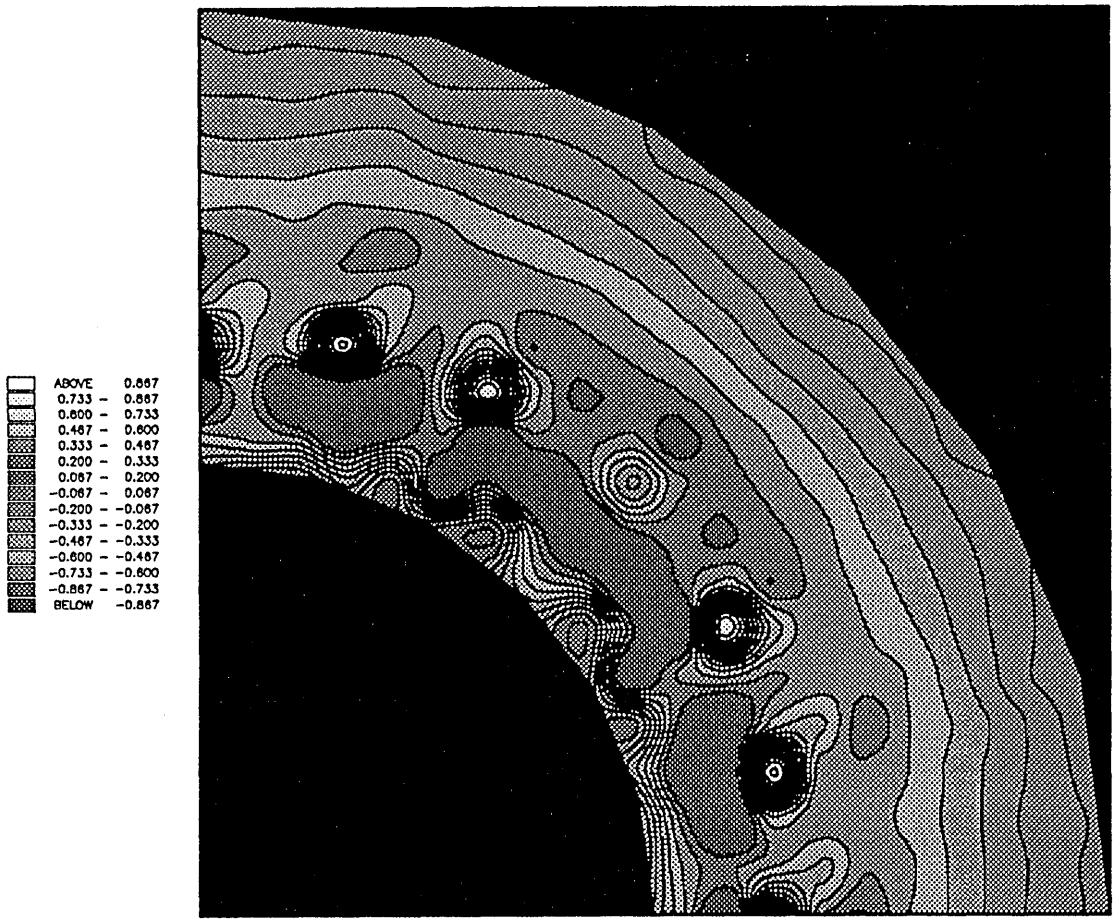

Fig.(9.56) Residual Radial Stress Contours for Pressurized Cylinder at Pi = 16 N/mm2 (Von Mises Criterion).

FRAMEC

Run on 10-JUN-90, At 17:01:00

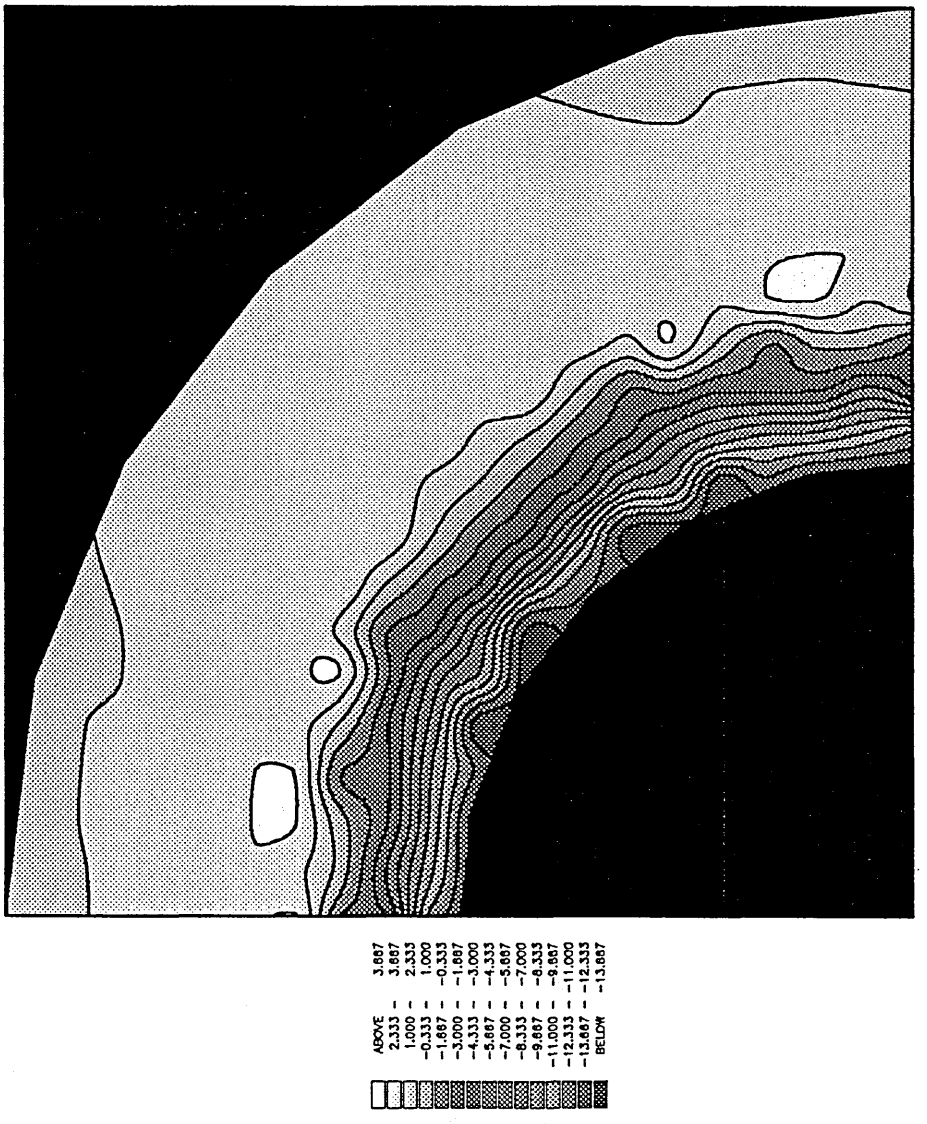

Fig.(9.57) Residual Hoop Stress Contours for Pressurized Cylinder at Pi = 16 N/mm2 (Von Mises Criterion).

FRAMEC

Run on 10-JUN-90, At 17:05:01

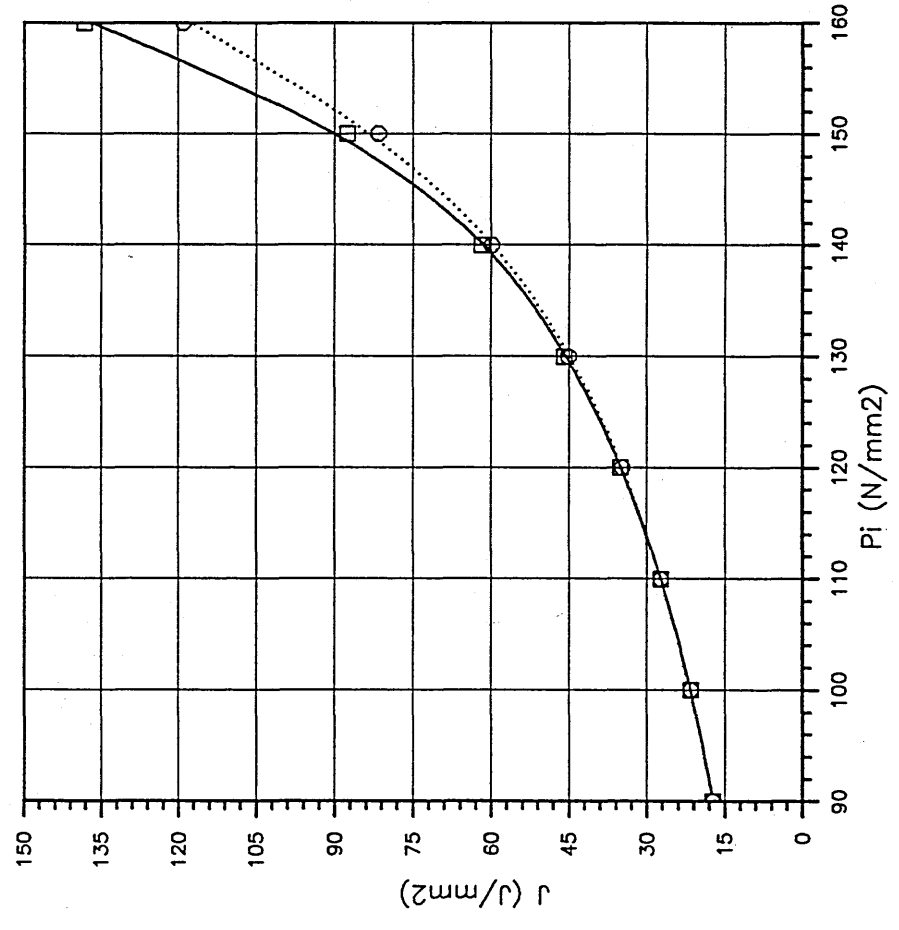

FRAMEC

Run on 10-JUN-90, At 17:09:30

Fig.(9.58) Elasto-Plastic J-Value's for Pressurized Cylinder calculated at different Pressure Intensities (Plane/Stress).

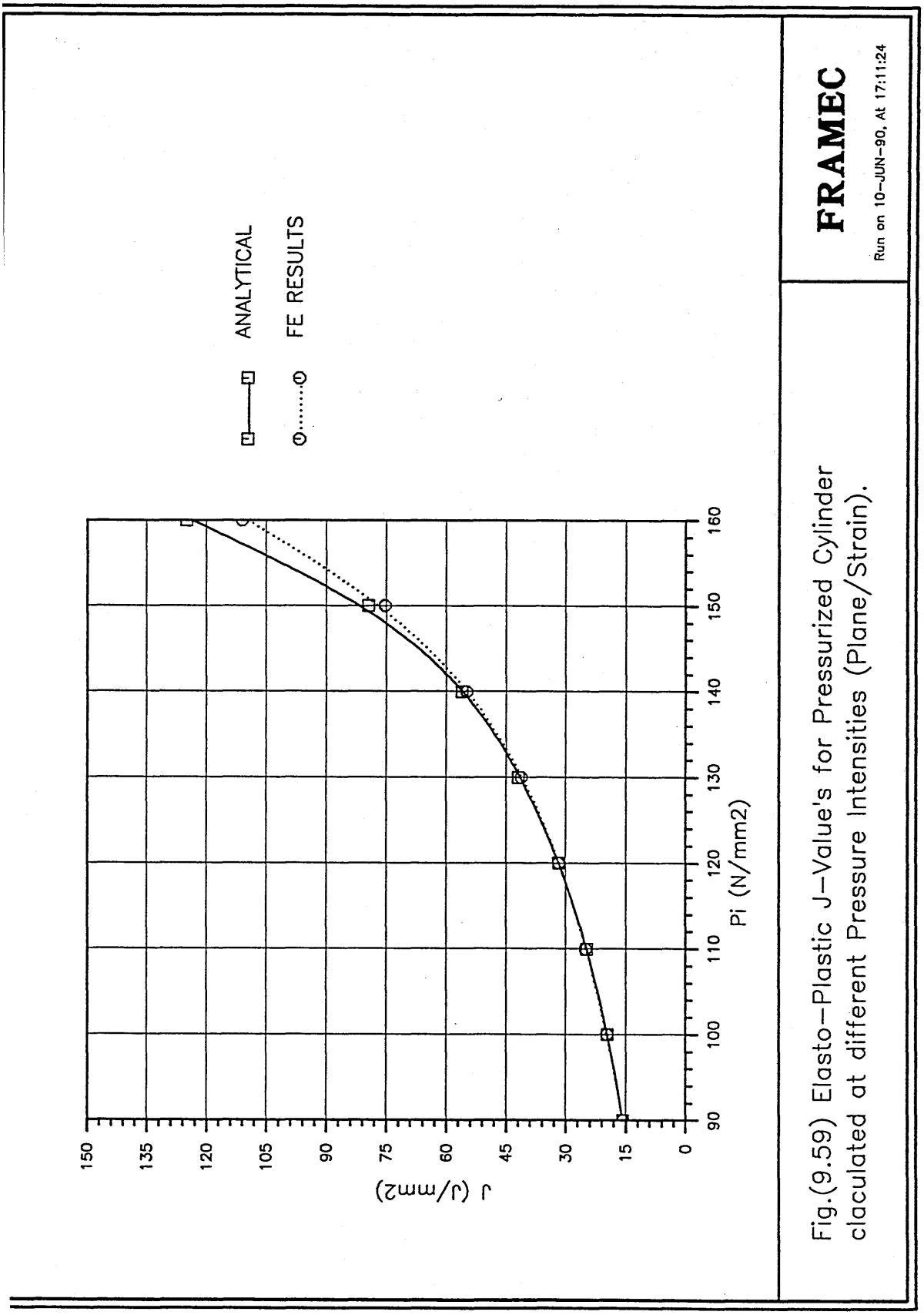

Fig.(9.59) Elasto-Plastic J-Value's for Pressurized Cylinder claculated at different Pressure Intensities (Plane/Strain).

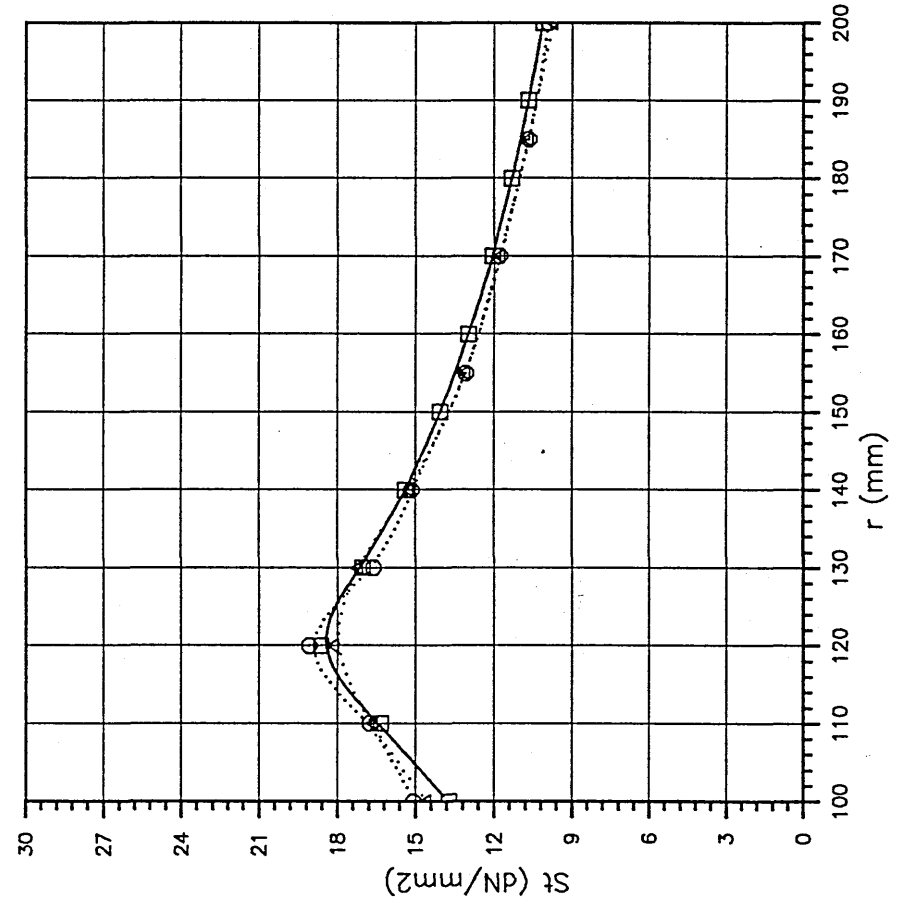

Fig.(9.60) Hoop Stress Distribution for Pressurised Thick Cylinder obtained by Elasto-Plastic Analysis at P= 14 dN/mm2.

FRAMEC

Run on 12-JUN-90, At 11:56:27

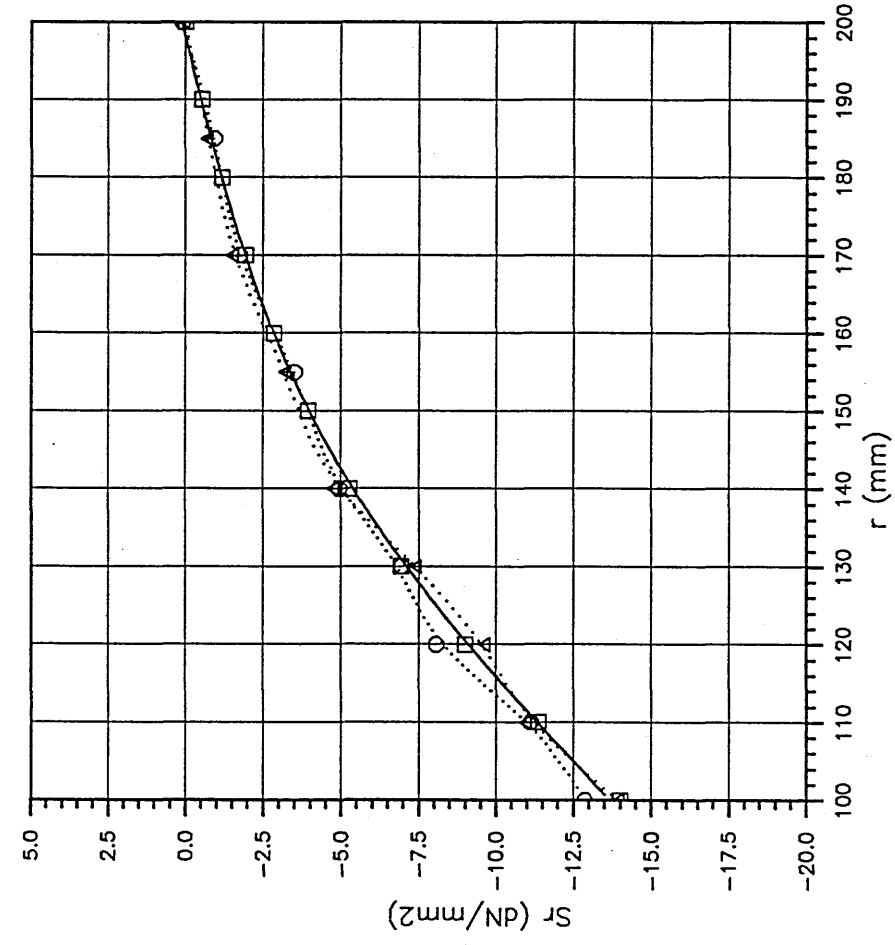

Fig.(9.61) Radial Stress Distribution for Pressurised Thick Cylinder obtained by Elasto-Plastic Analysis at P= 14 dN/mm2.

FRAMEC

Run on 12-JUN-90, At 11:59:31

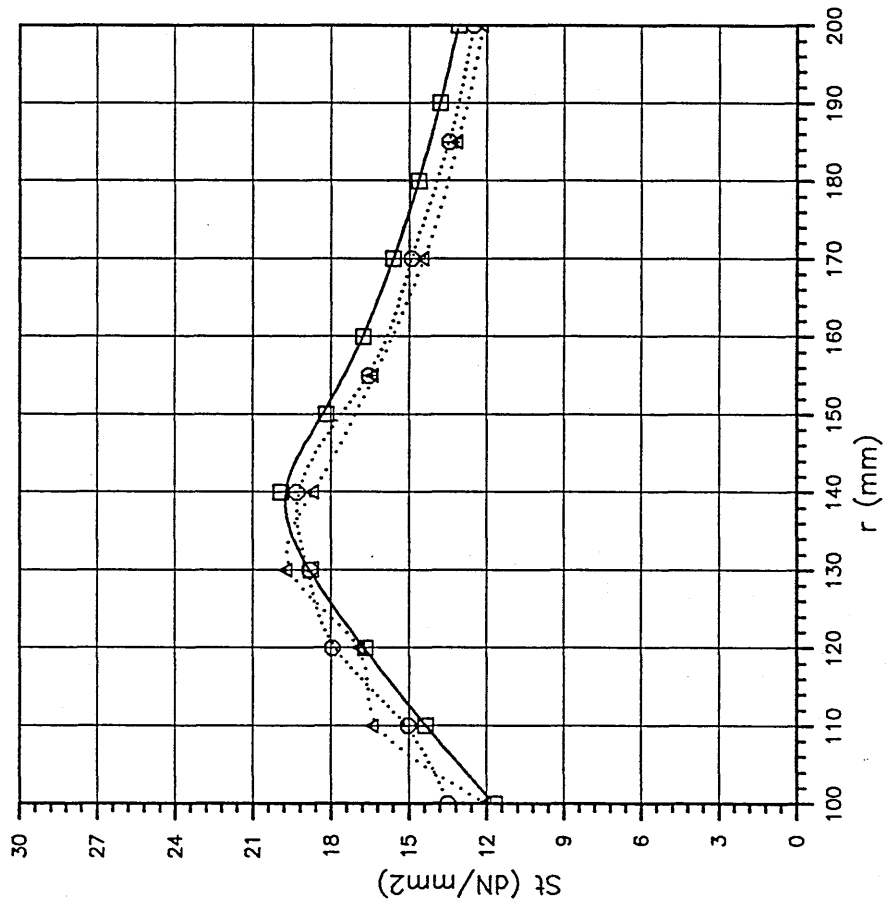

FRAMEC

Run on 12-JUN-90, At 12:03:40

Fig.(9.62) Hoop Stress Distribution for Pressurised Thick Cylinder obtained by Elasto-Plastic Analysis at P= 16 dN/mm2.

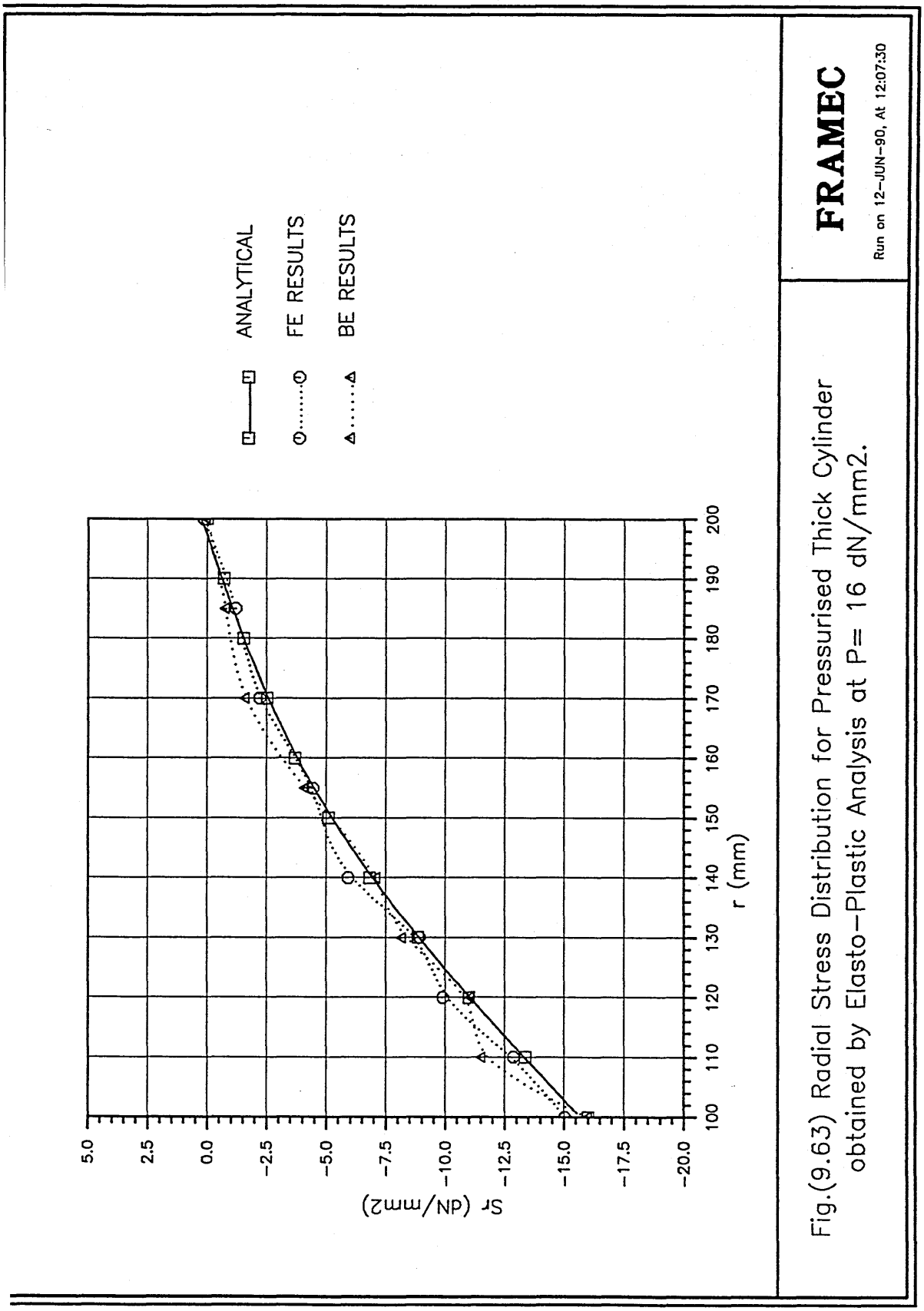

Fig.(9.63) Radial Stress Distribution for Pressurised Thick Cylinder obtained by Elasto-Plastic Analysis at P= 16 dN/mm2.

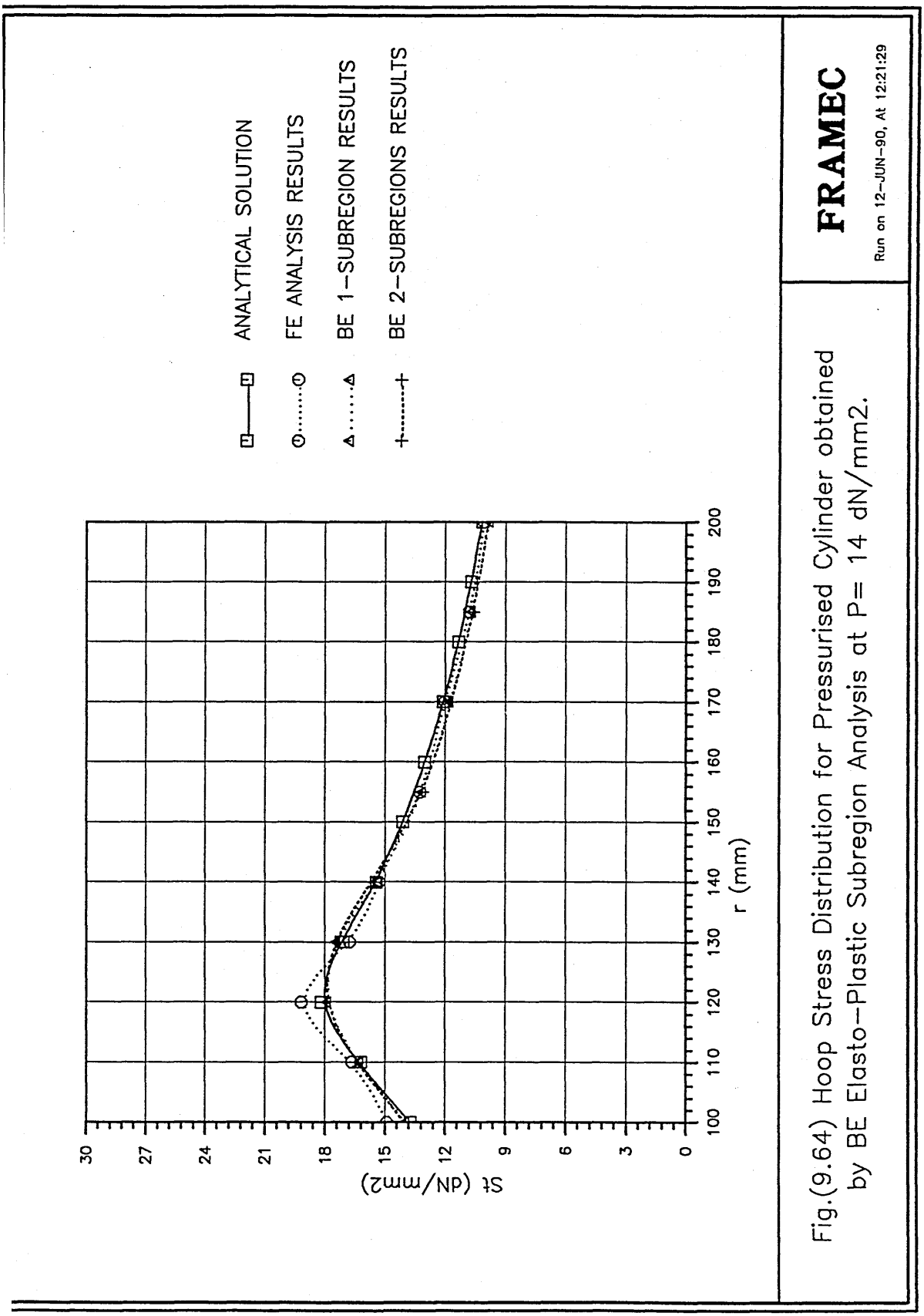

Fig.(9.64) Hoop Stress Distribution for Pressurised Cylinder obtained by BE Elasto-Plastic Subregion Analysis at P= 14 dN/mm2.

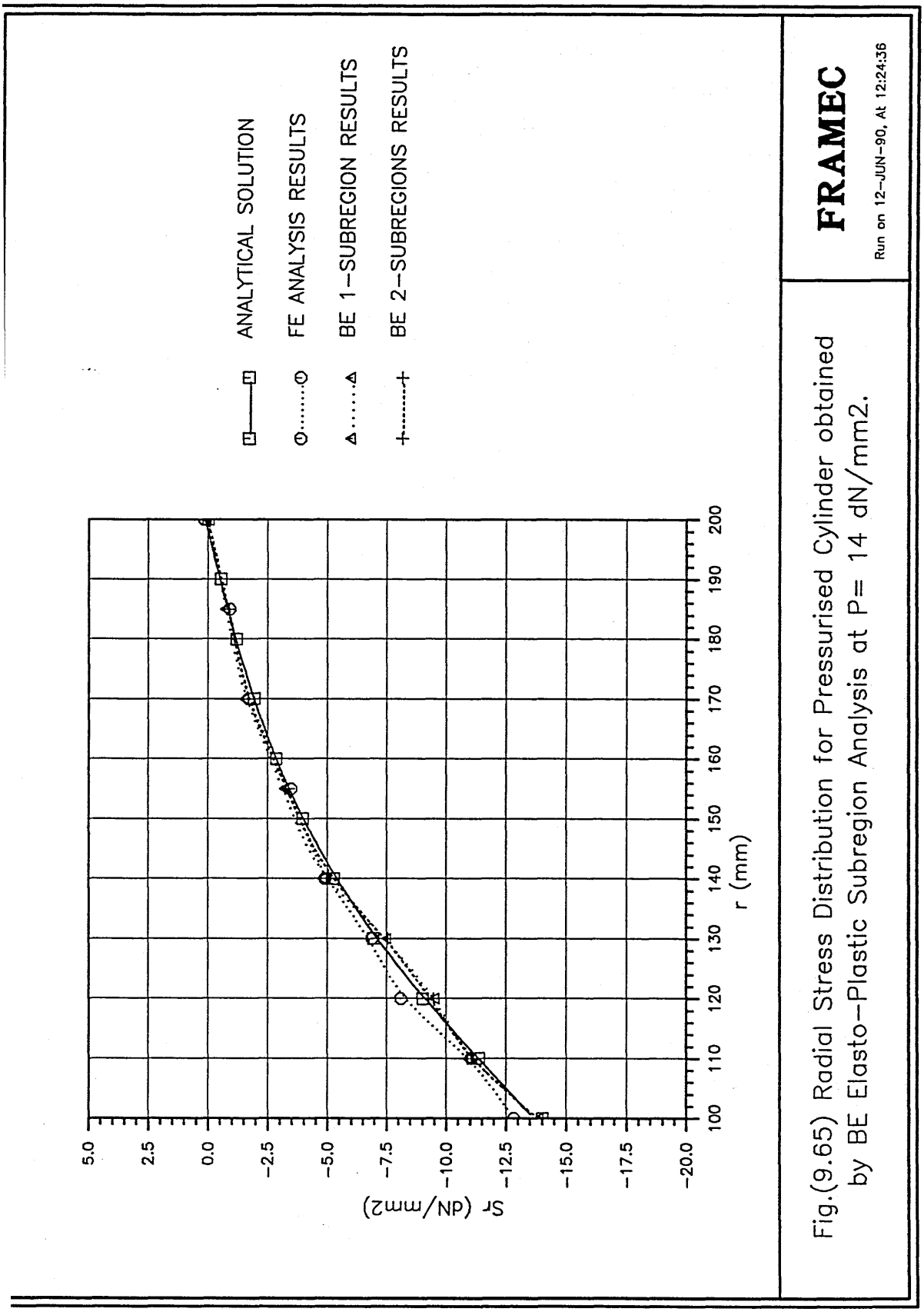

Fig.(9.65) Radial Stress Distribution for Pressurised Cylinder obtained by BE Elasto-Plastic Subregion Analysis at P= 14 dN/mm2.

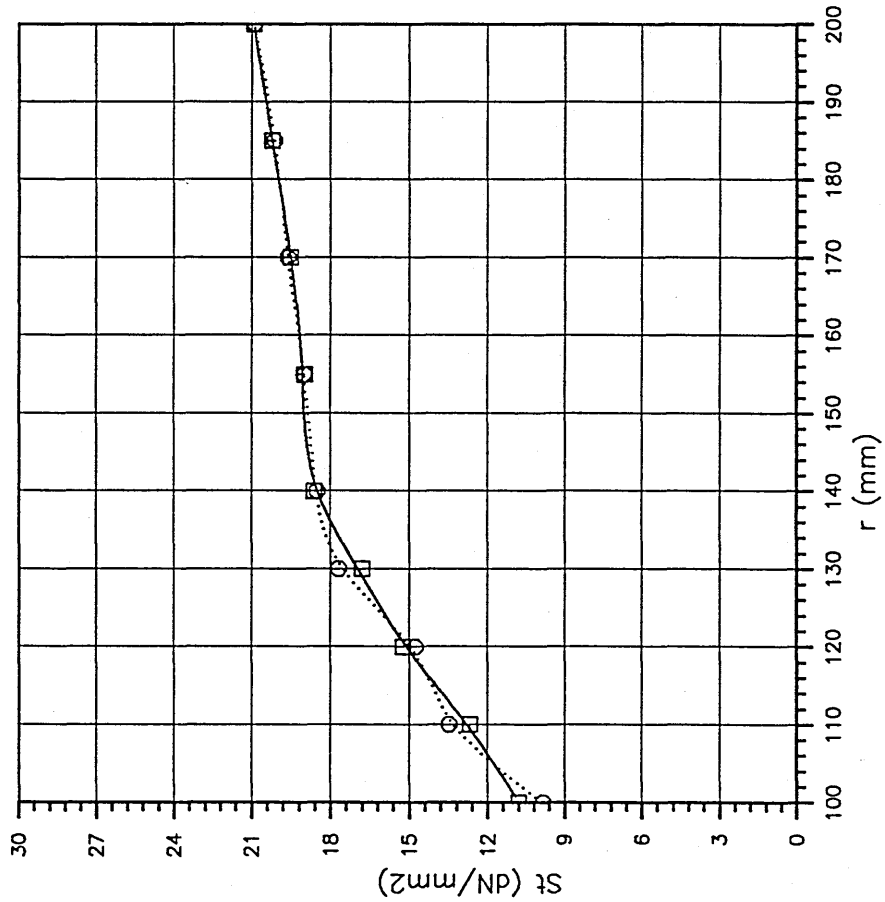

FRAMEC
Run on 12-JUN-90, At 12:28:51

Fig.(9.66) Hoop Stress Distribution for Cylinder under Pressure and Thermal Loading (Analysis at P= 18 dN/mm2 & dT= 100 C).

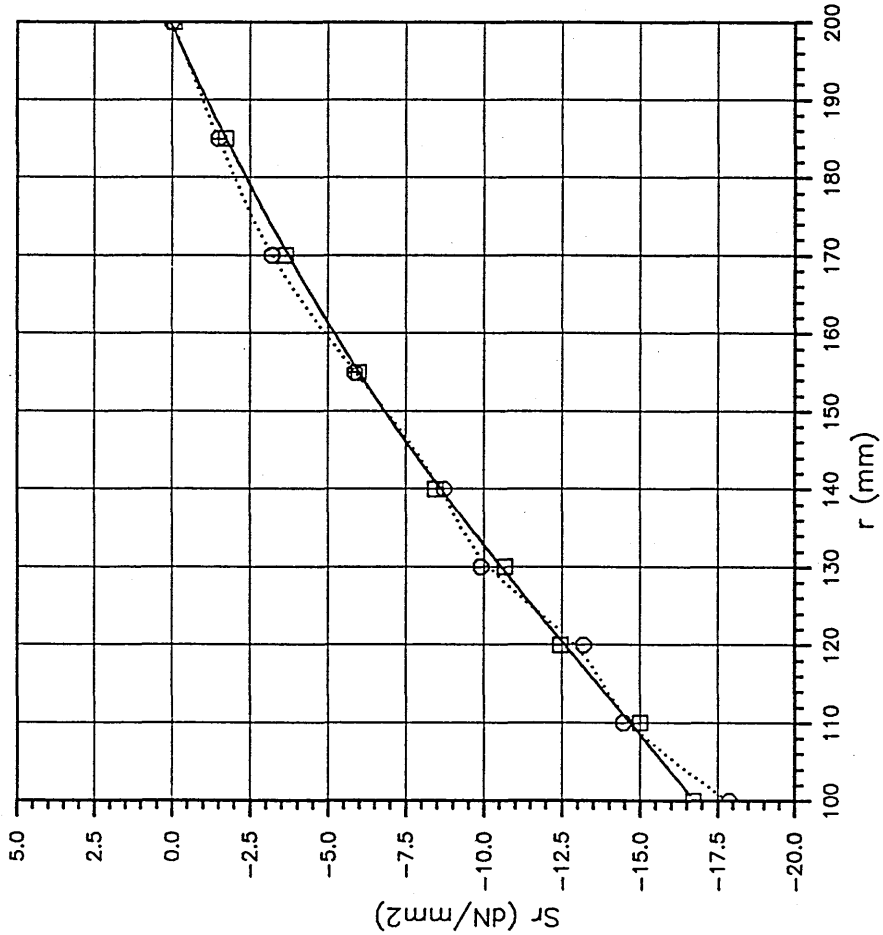

Fig.(9.67) Radial Stress Distribution for Cylinder under Pressure ant Thermal Loading (Analysis at P= 18 dN/mm2 & dT= 100 C).

FRAMEC

Run on 12-JUN-90, At 12:31:57

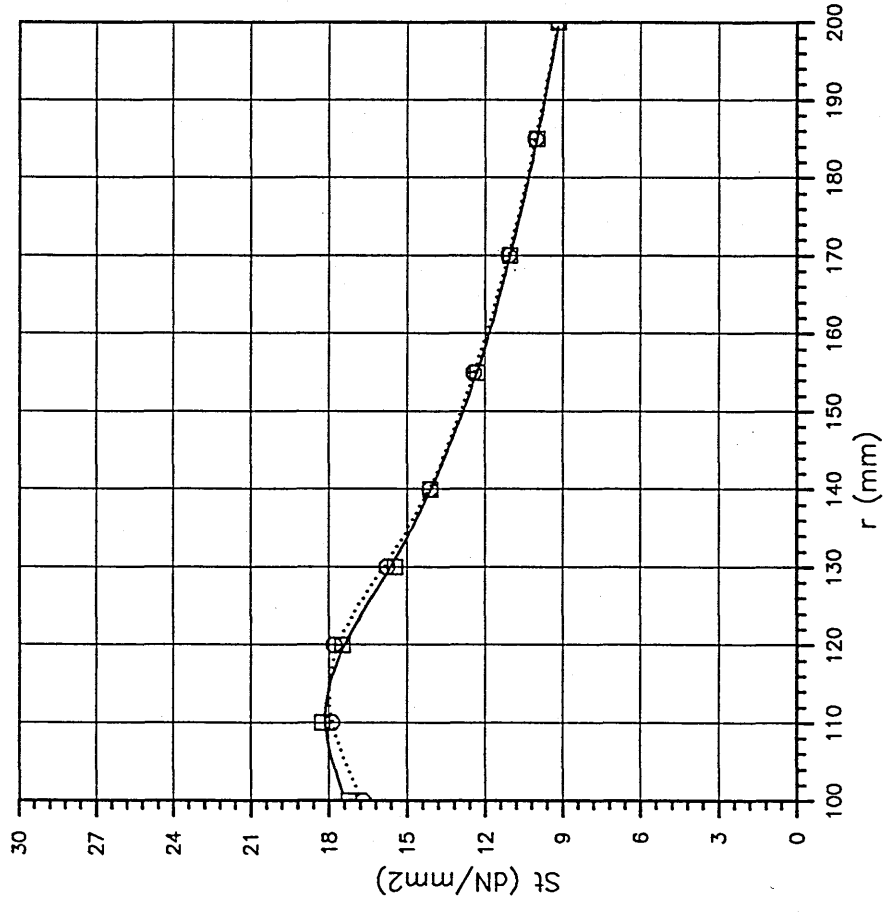

FRAMEC

Run on 12-JUN-90, At 12:34:56

Fig.(9.68) Hoop Stress Distribution for Cylinder under Pressure and Domain Loading (Analysis at P= 11 dN/mm2 & w= 1 rad/s).

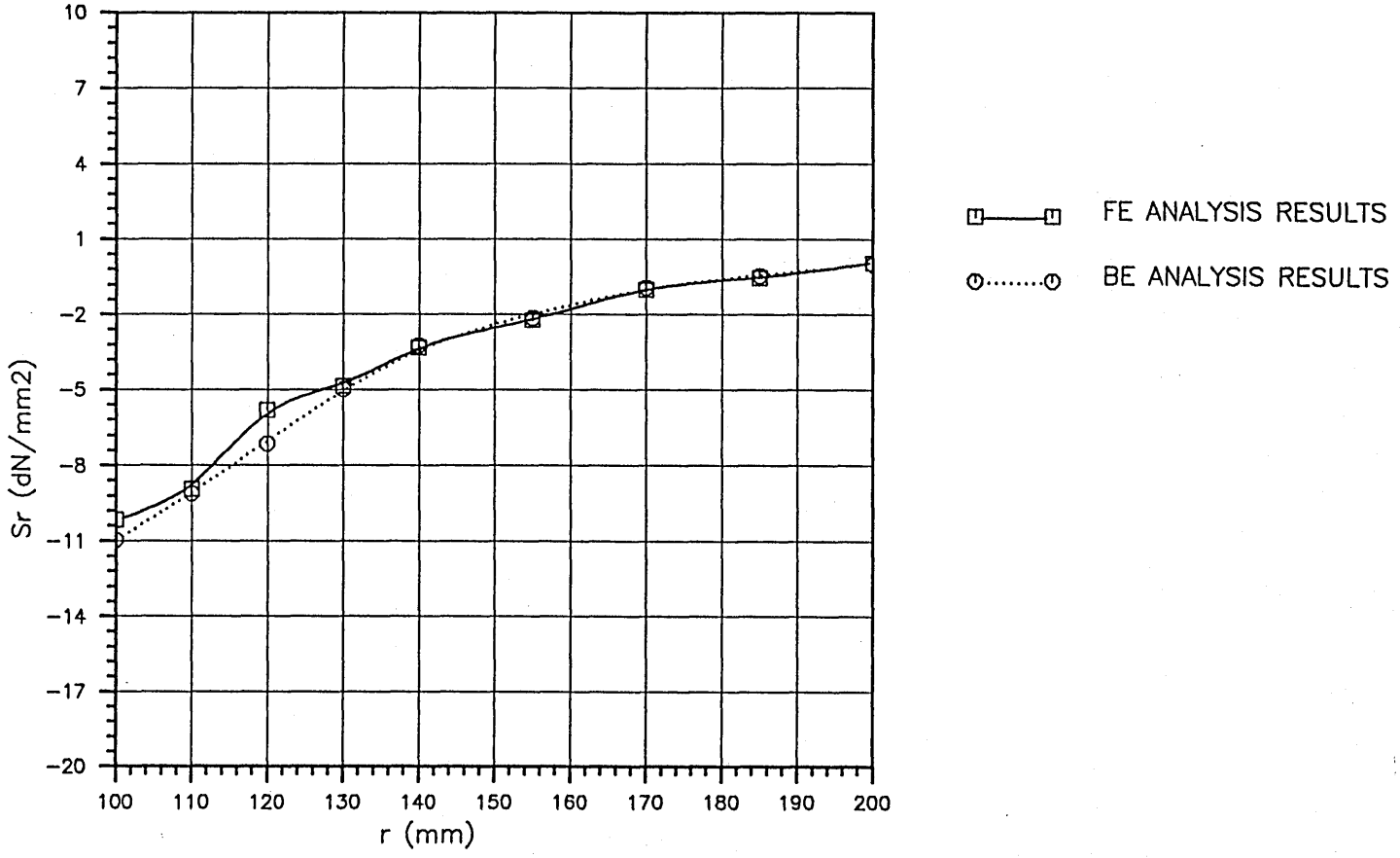

Fig.(9.69) Radial Stress Distribution for Cylinder under Pressure ant Domain Loading (Analysis at P= 11 dN/mm2 & w= 1 rad/s).

FRAMEC

Run on 12-JUN-90, At 12:37:53

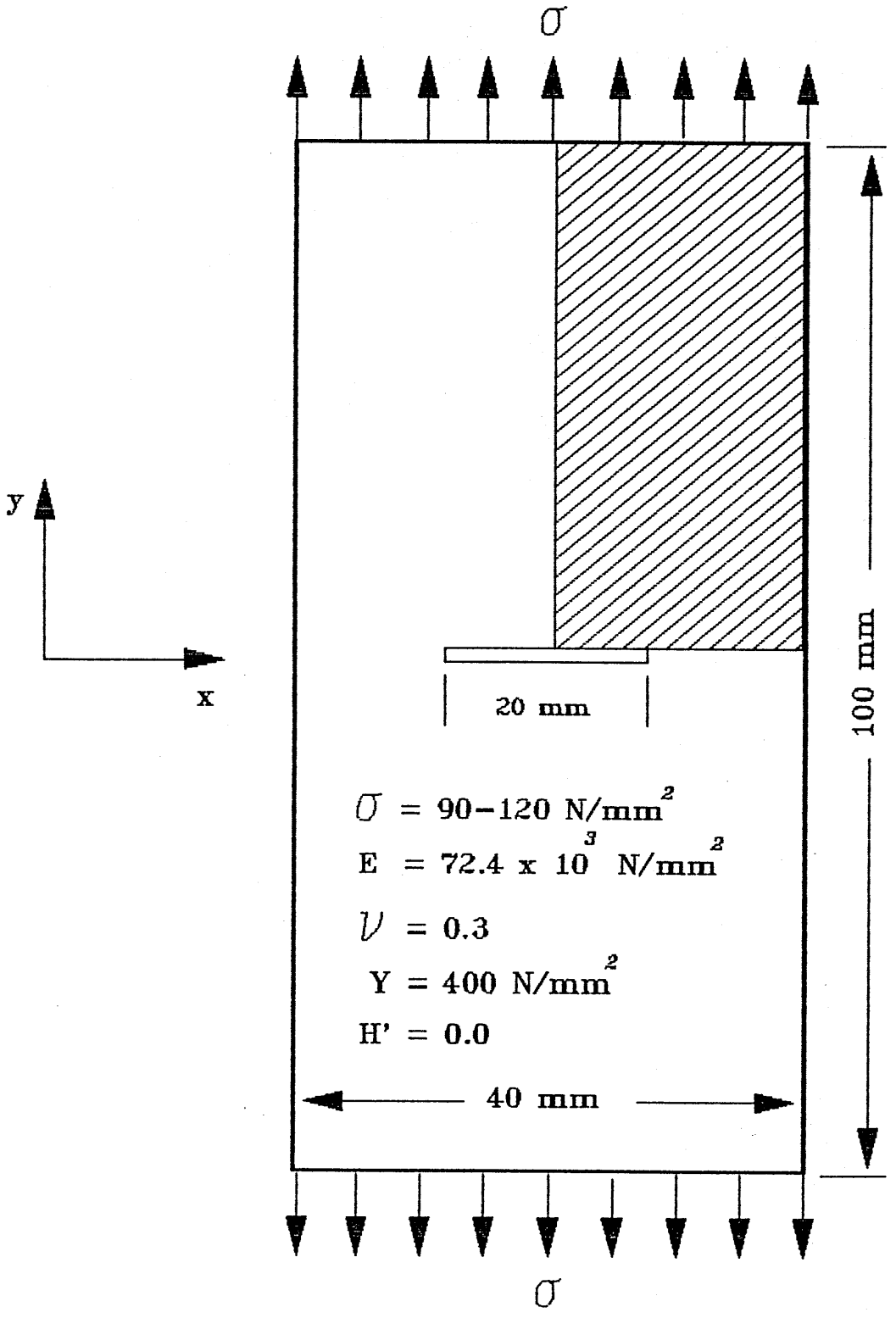

Fig.(9.70) Central-Cracked Plate under Uniform Tension used for Elasto-Plastic FE & BE Analyses.

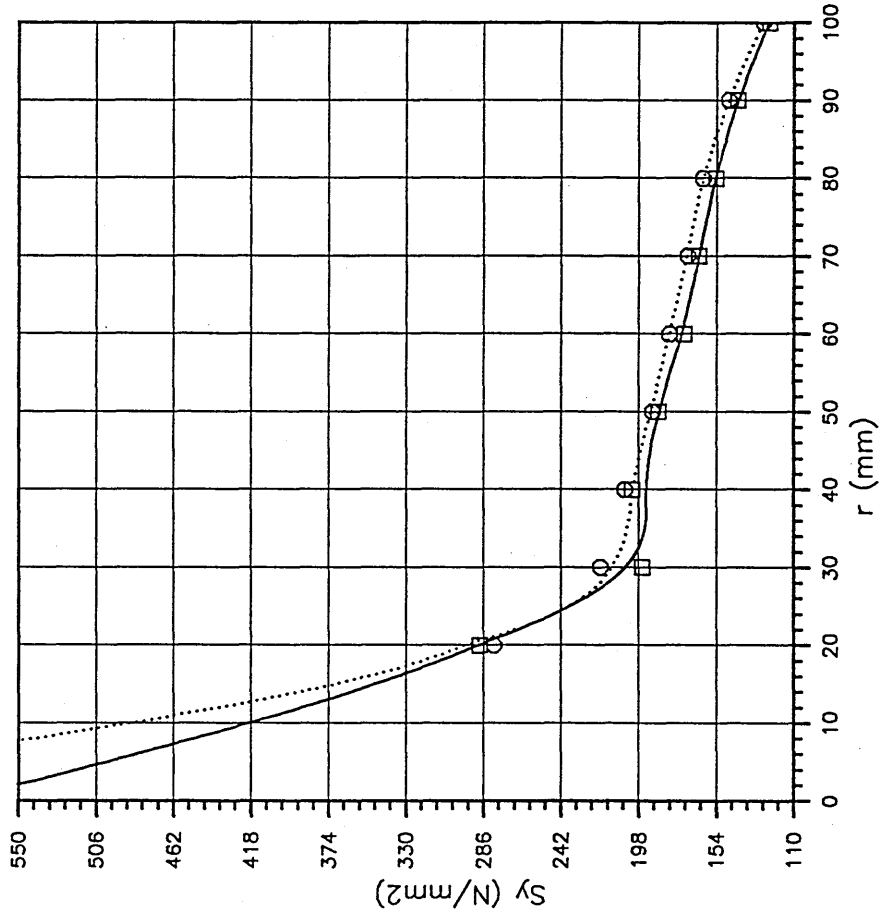

Fig.(9.71) Comparison between FE and BE SIGMA-Y Stress Distribution for Centarl-Cracked Plate at So=120 N/mm2 (Elasto-Plastic Analysis).

FRAMEC

Run on 12-JUN-90, At 13:06:47

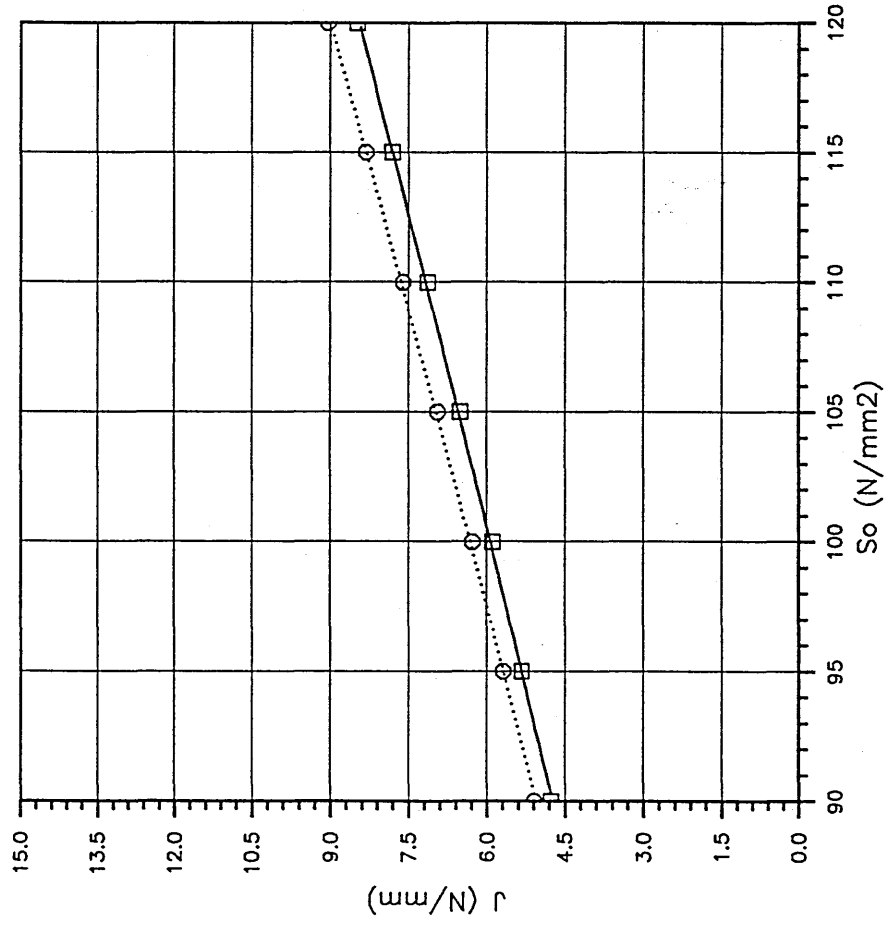

Fig.(9.72) Comparison between FE and BE J-Integral Values for Centarl-Cracked Plate (Elasto-Plastic Analysis).

FRAMEC

Run on 12-JUN-90, At 13:05:01

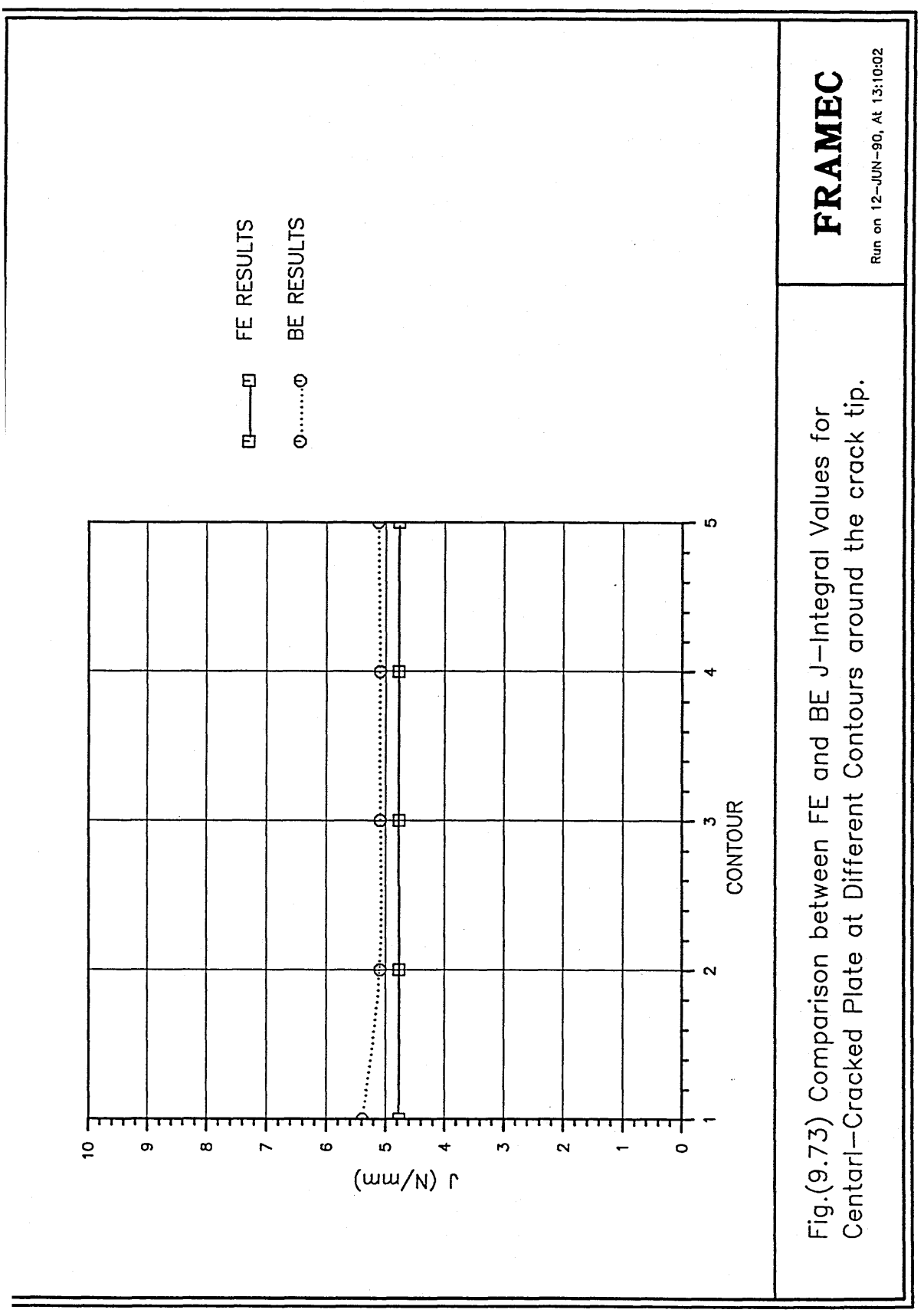

Fig.(9.73) Comparison between FE and BE J-Integral Values for Centarl-Cracked Plate at Different Contours around the crack tip.

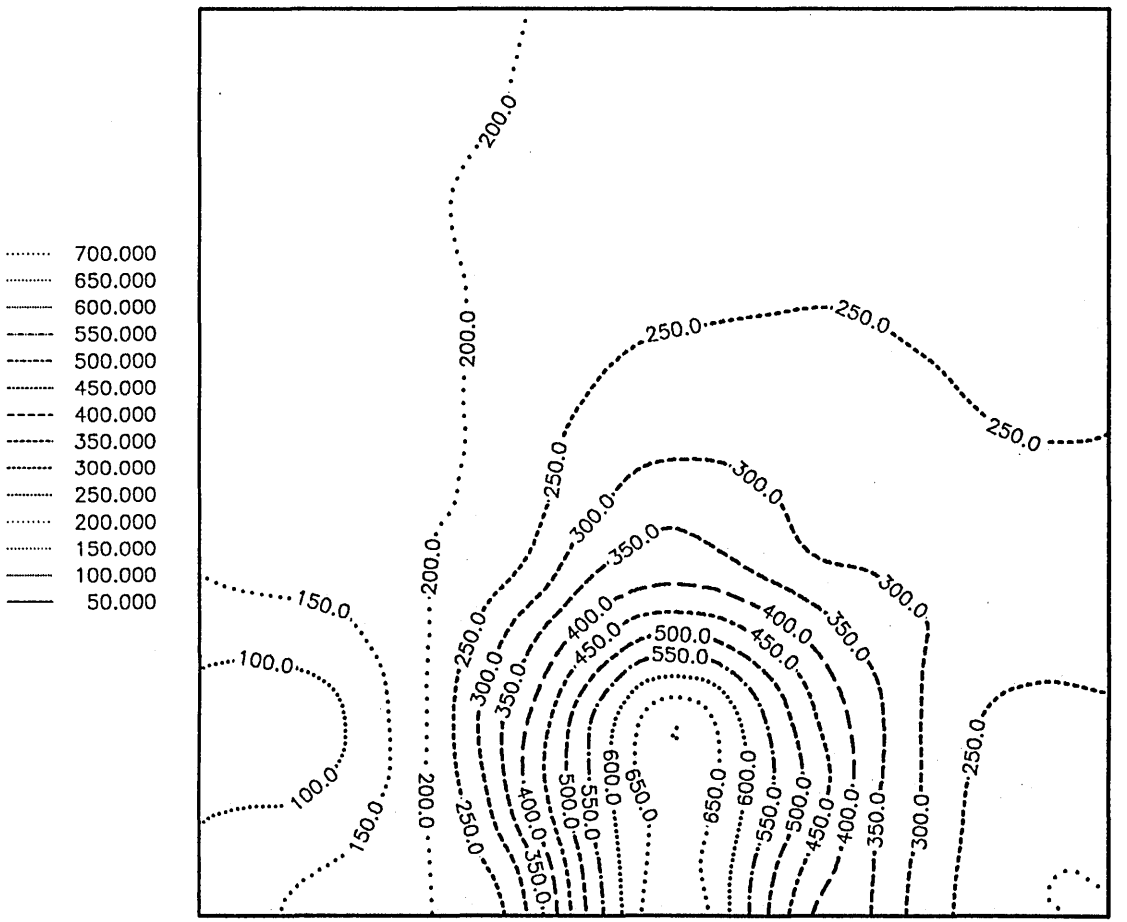

Fig.(9.74) Von Mises Equivalent Stress Contours for CC Plate generated by Elasto-Plastic FE Analysis (So=120, Y=400 MN/m2).

FRAMEC

Run on 12-JUN-90, At 13:21:23

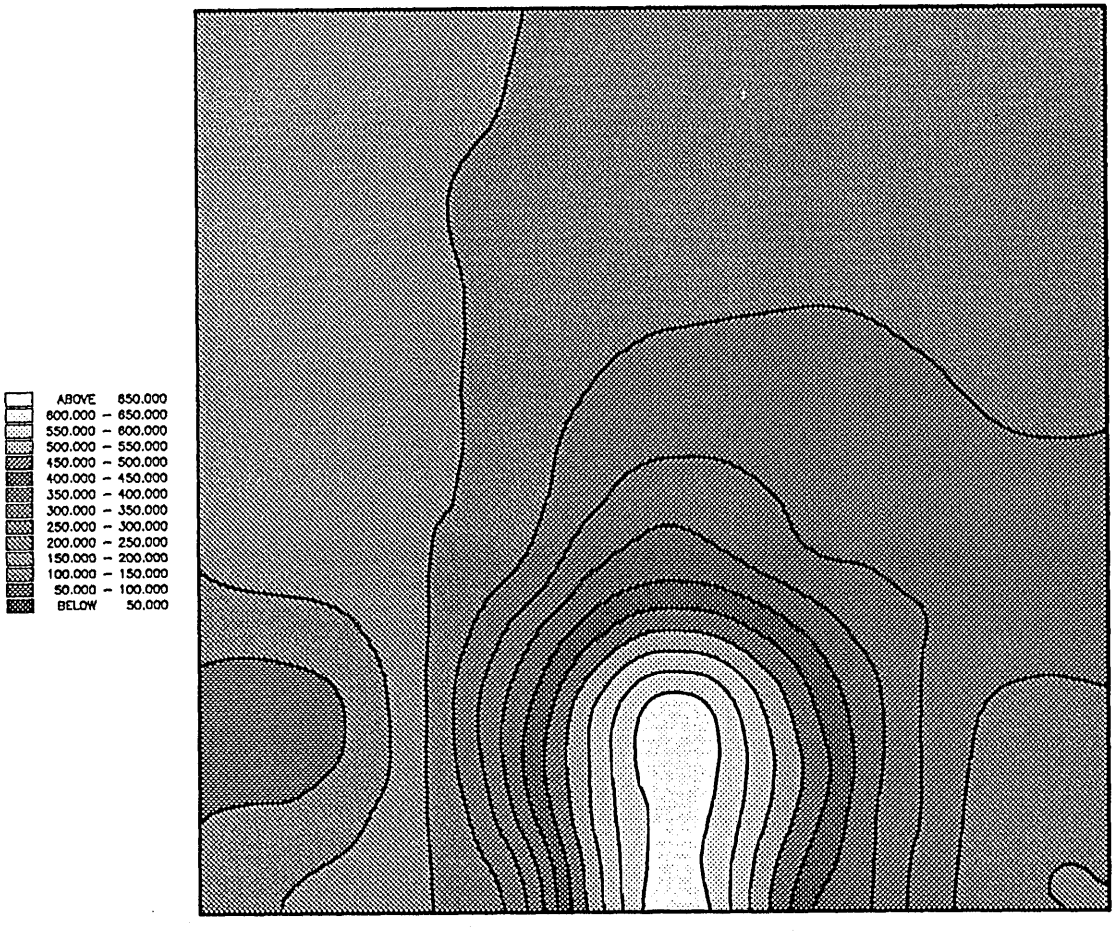

Fig.(9.75) Von Mises Equivalent Stress Contours for CC Plate generated by Elasto-Plastic FE Analysis (So=120, Y=400 MN/m2).

FRAMEC

Run on 12-JUN-90, At 13:30:46

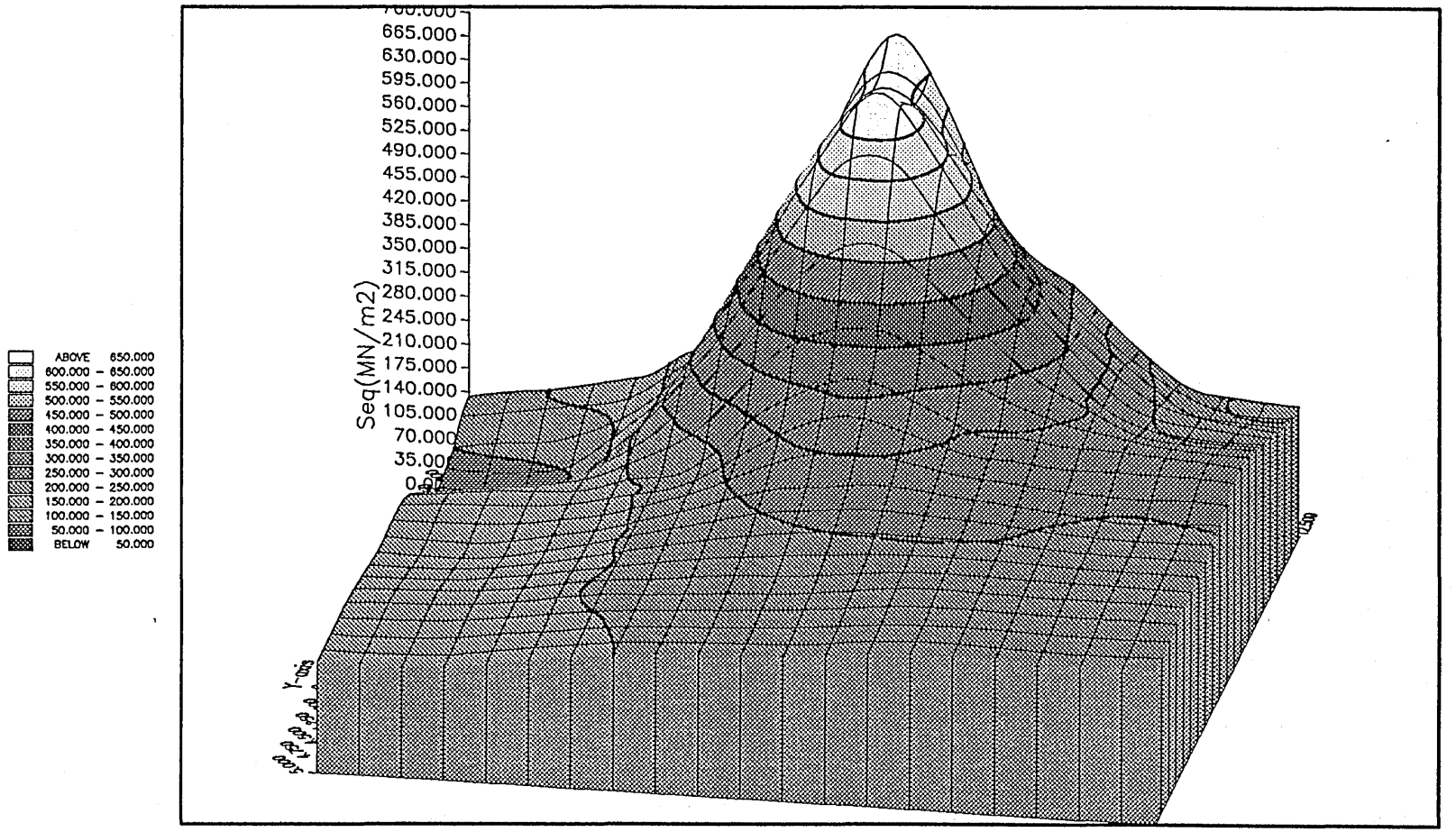

Fig.(9.76) Von Mises Equivalent Stress Contours for CC Plate generated by Elasto-Plastic FE Analysis (So=120, Y=400 MN/m2).

FRAMEC

Run on 13-JUN-90, At 12:37:44

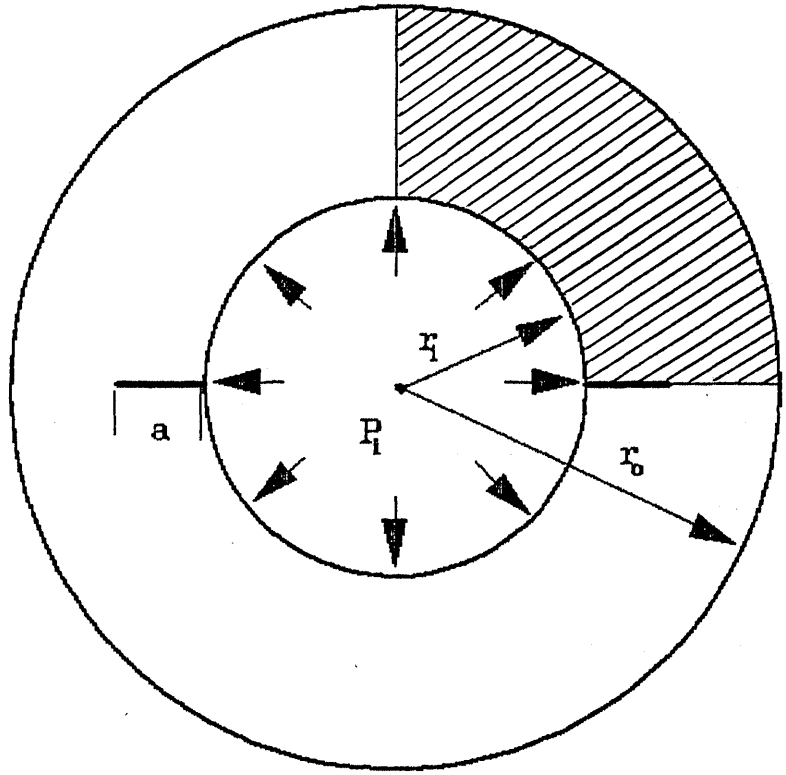

a = 40 mm

r_i = 100 mm

r_o = 200 mm

P_i = 5–9 N/mm^2

E = 2.1 x 10^4 N/mm^2 , ν = 0.3

Y = 24 N/mm^2 , H' = 0

Fig.(9.77) Case Study of Symmetrically Cracked Pressurized Cylinder.

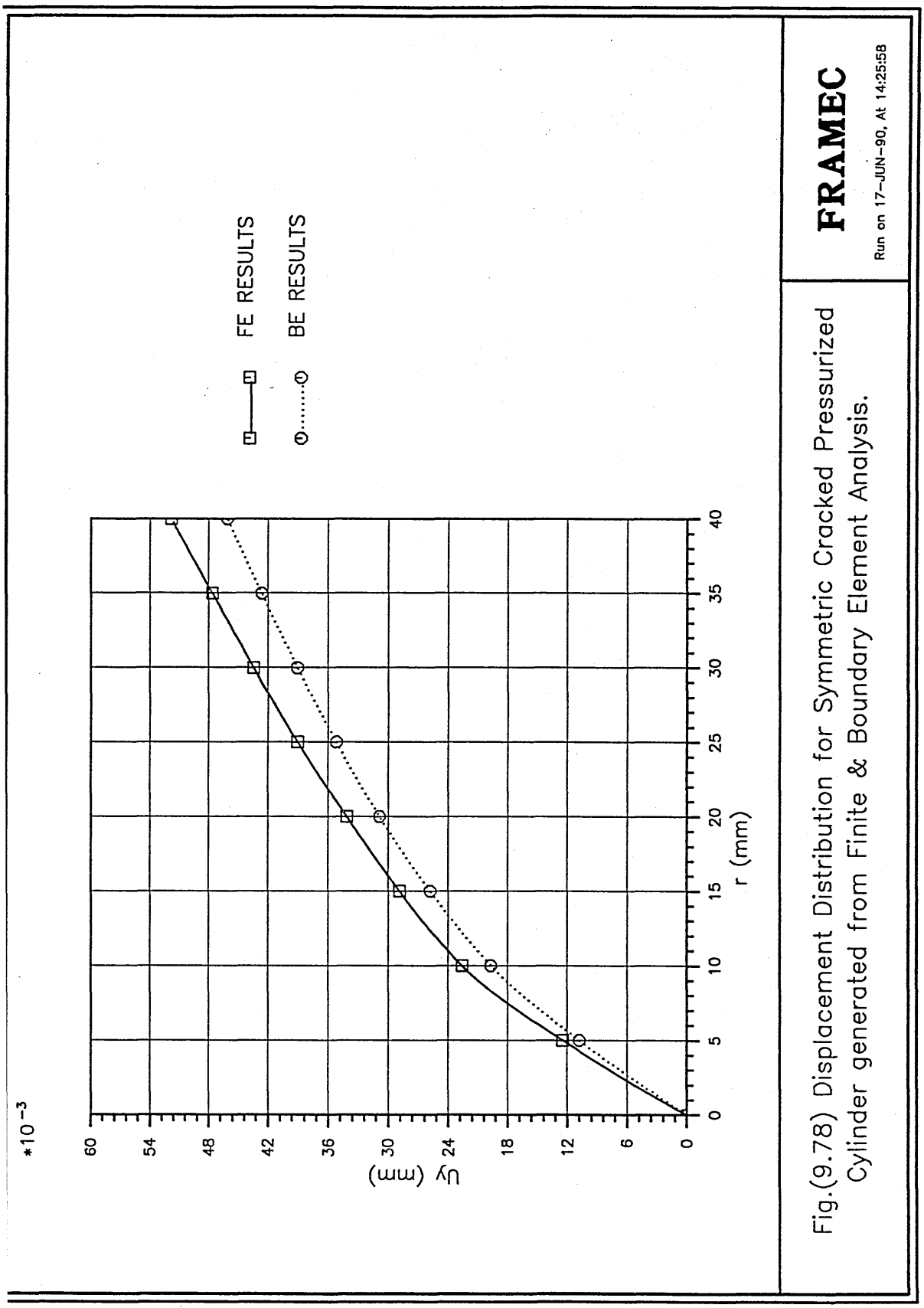

Fig.(9.78) Displacement Distribution for Symmetric Cracked Pressurized Cylinder generated from Finite & Boundary Element Analysis.

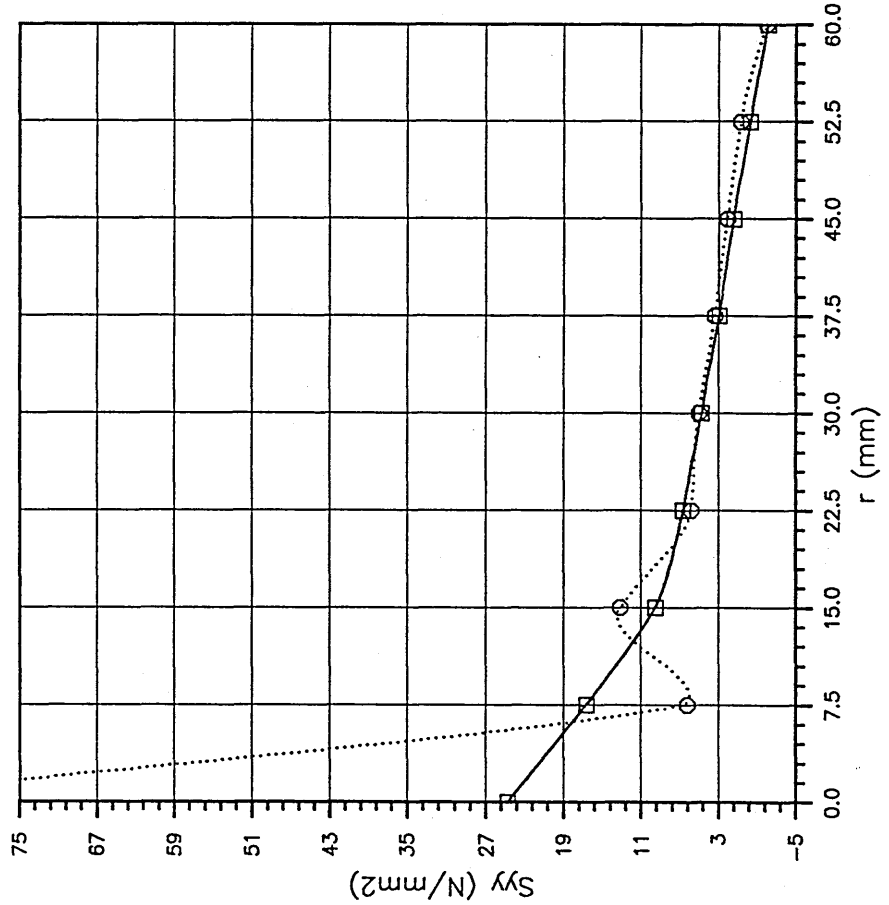

Fig.(9.79) Syy Stress Distribution for Symmetric Cracked Pressurized Cylinder generated from Finite & Boundary Element Analysis.

FRAMEC

Run on 17-JUN-90, At 14:26:36

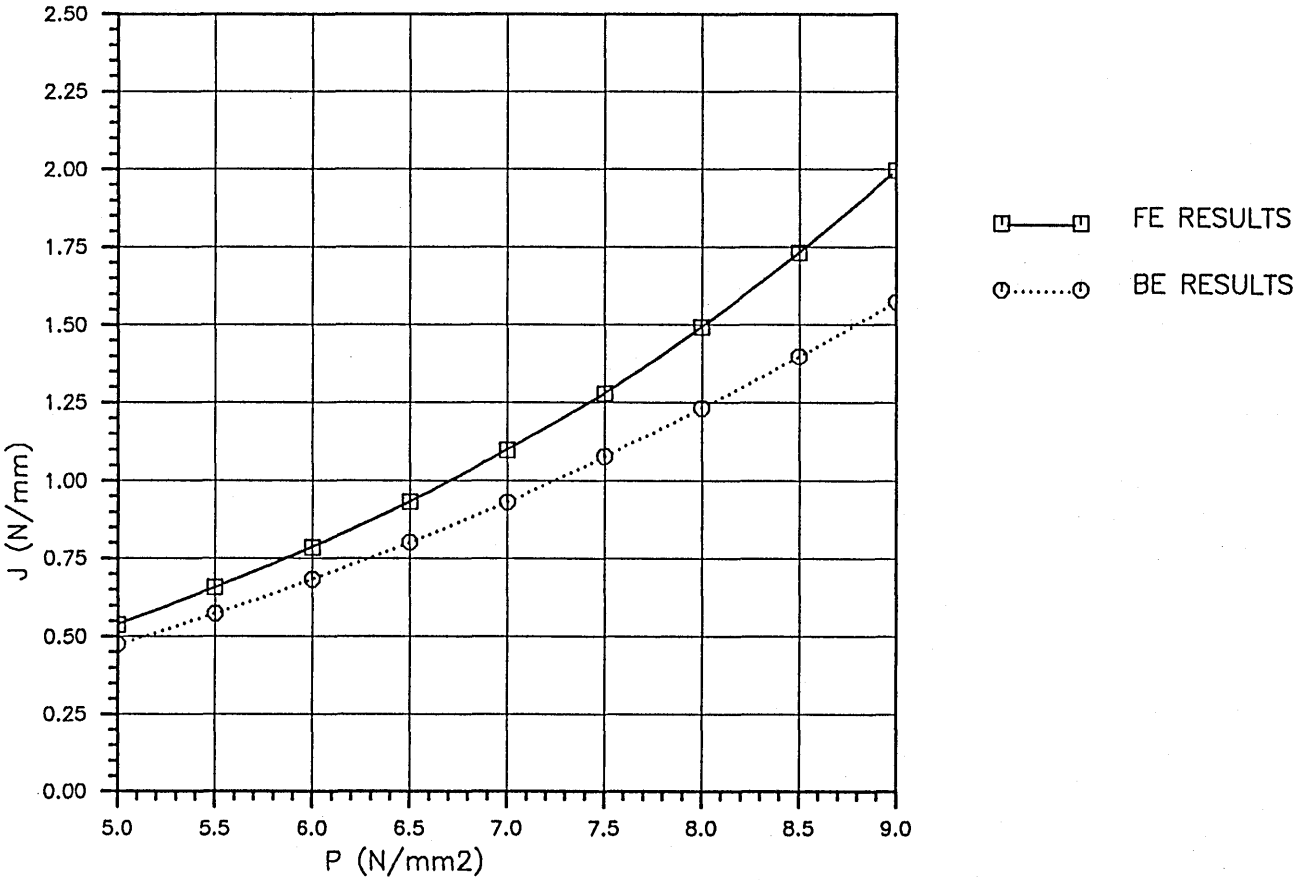

Fig.(9.80) J–Values for Symmetric Cracked Pressurized Cylinder generated using FE & BE Analysis at Different Load Increments.

FRAMEC

Run on 17–JUN–90, At 14:27:17

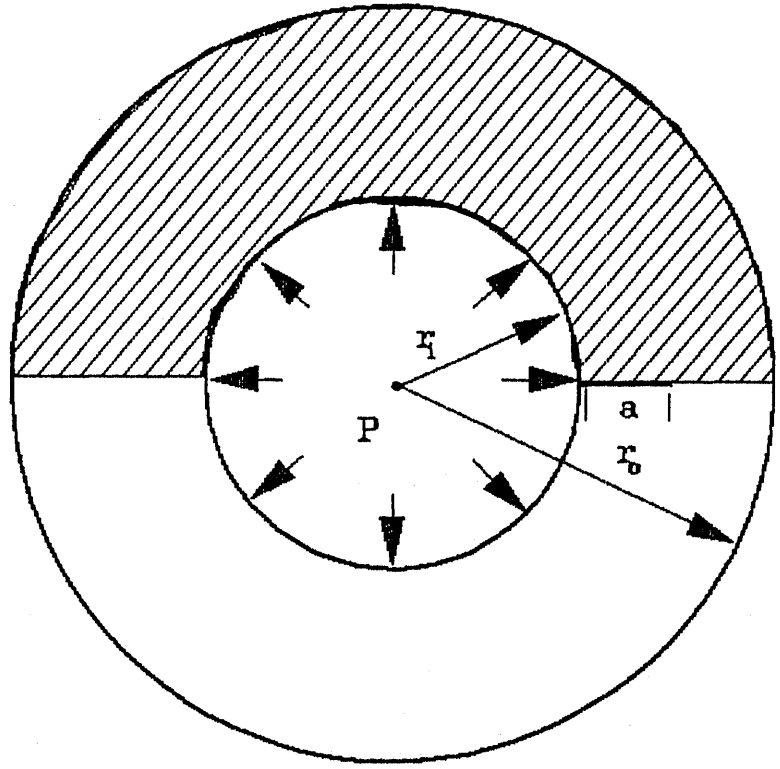

a = 50 mm

r_i = 100 mm

r_o = 200 mm

P = 165 N/mm^2 , Y = 275 N/mm^2

E = 2.148 x 10^5 N/mm^2, ν = 0.3

Fig.(9.81) Case Study of Cracked Thick-Walled Pressurized Cylinder.

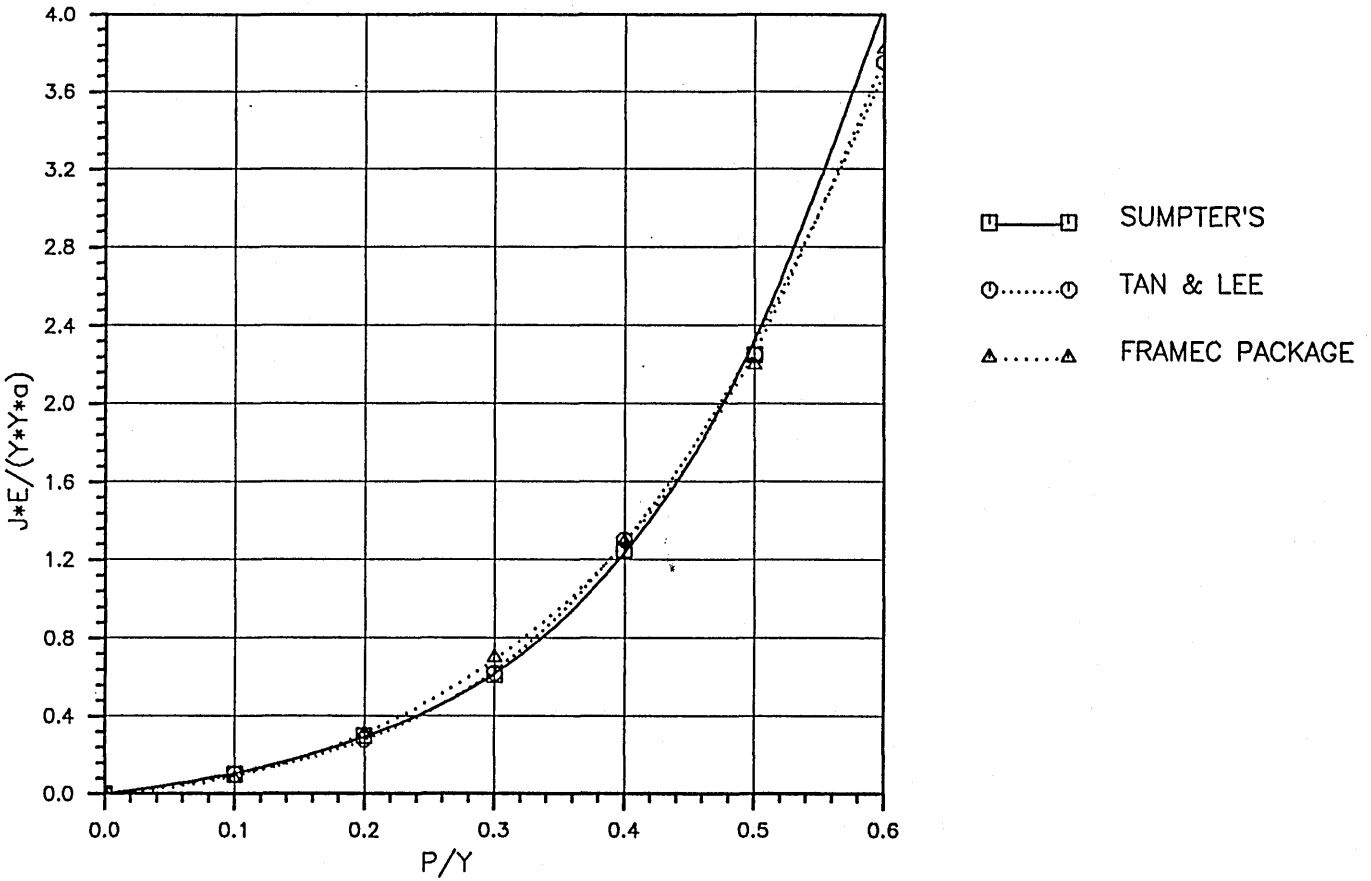

Fig.(9.82) Nondimensional J–Integral for Cracked Thick–Walled Cylinder calculated using FE Elasto–Plastic Analysis for different Load Ratios.

FRAMEC

Run on 17–JUN–90, At 14:51:50

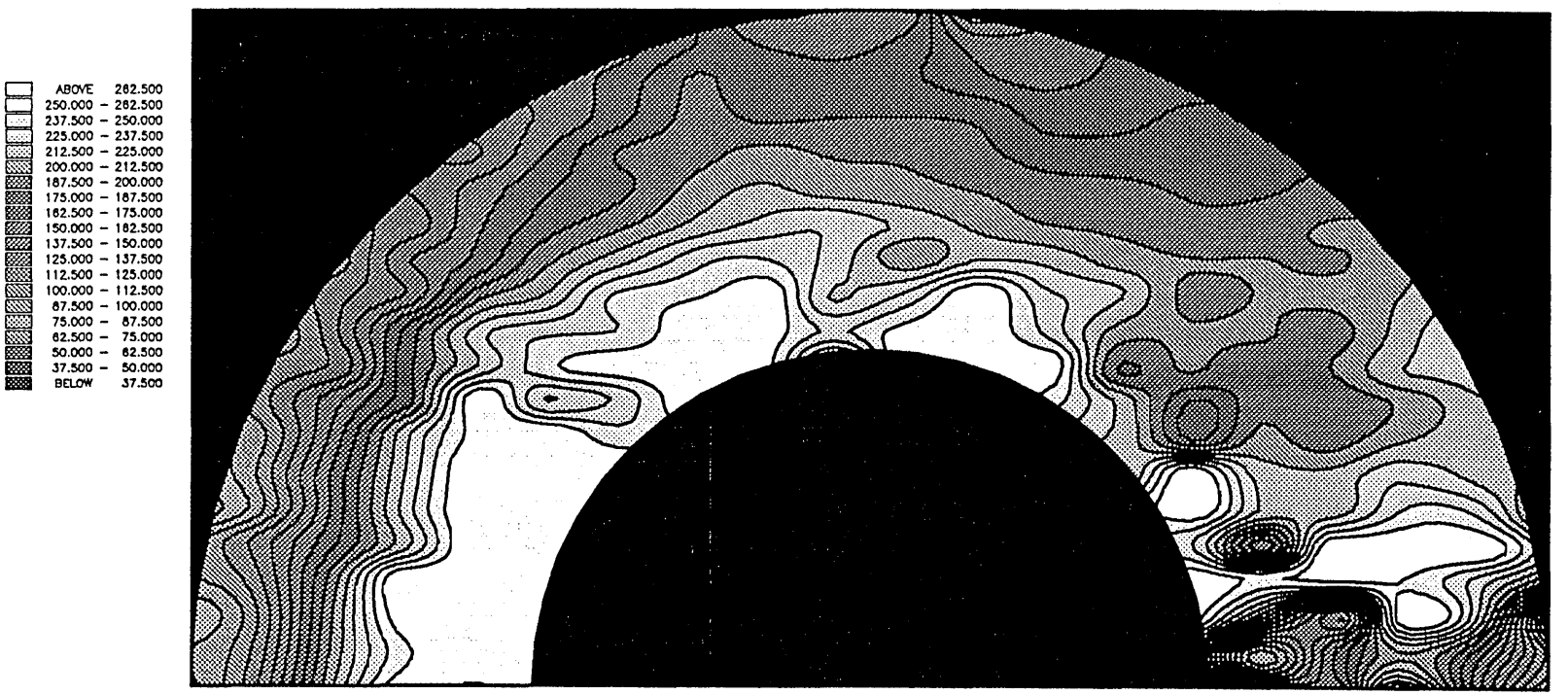

Fig.(9.83) Equivalent Stress Contours for Cracked Thick-Walled Cylinder Plotted for P = 165 MN/m2, and Y = 275 MN/m2.

FRAMEC

Run on 17-JUN-90, At 15:02:04

CHAPTER 10

CONCLUSIONS

CONCLUSIONS

From previous analysis and discussions, one can conclude that the basic objective of the work, aiming at the development of an efficient elastic, and elasto-plastic fracture mechanics package, based upon finite and boundary element methods, has been achieved.

When using the package for fracture mechanics analysis of some case studies, the following conclusions have also been envisaged:

(a) Package characteristics and facilities, such as controllability, modularity, pre- and post-processors, different types of elements, different types of loading,... etc., have proved to be very useful tools for carrying out such analysis.

(b) New crack-tip elements developed in this work have shown to be very efficient and can lead to an accurate estimation of linear-elastic fracture mechanics parameters.

(c) Accurate values for stress intensity factors can be obtained by means of the extrapolation-curve-fitting technique developed in this work.

(d) New algorithms derived for the calculation of J-integrals, have proved to be very efficient and advantageous for both linear-elastic and elasto-plastic fracture mechanics.

(e) The subregion technique, presented in this thesis, provides an indispensable facility to fracture analysis of components with non-symmetric and oblique cracks by means of the boundary element method. It has also proved to be

very useful for reducing computer *CPU* time during elasto-plastic boundary element analysis.

(*f*) The boundary element method has shown to be more efficient, in terms of accuracy, *CPU* time and human effort, than the finite element method, for linear-elastic fracture mechanics analysis. However, for elasto-plastic conditions, an accurate boundary element analysis may require *CPU* time larger than that for corresponding finite element analysis with the same accuracy level.

(*g*) Fracture analysis of components with short cracks may require very fine meshes in the vicinity of crack tips.

Recommendations for Future Work:

(*a*) Efficient solvers for boundary element analysis are required to be developed, specially for cases with elasto-plastic conditions.

(*b*) A proper coupling between finite and boundary element methods for an efficient analysis of non-linear problems should be investigated.

(*c*) Some experimental work is to be carried out for the validation of results showing some deviation from published analytical solutions.

(*d*) Fracture mechanics analysis, presented in this work, could be extended to cover fracture dynamics and fatigue crack growth.

REFERENCES

REFERENCES

1. Timoshenko S.P., "History of The Strength of Materials", McGraw-Hill, NewYork, 1953.

2. Todhunter I., Pearson K., "History of The Theory of Elasticity and of The Strength of Materials from Galileo to The Present Time", Cambridge University Press, 1886.

3. Fawkes A.J., "Finite elements applied to crack tip singularities", PhD Thesis, University College of Swansea, 1976.

4. Inglis C.E., "Stress in a plate due to the presence of cracks and sharp corners", Proced. Inst. Naval Architects, Vol. 60, 1913.

5. Griffith A.A., "The phenomena of rupture and flow in solids", Phil. Trans. R. Soc. A221, 163-198, 1921.

6. Westergaard H.M., "Bearing pressure and cracks", J. of Applied Mechanics, Vol. 66, A49-A52, 1939.

7. Ewalds H.L., Wanhill R.J.H., "Fracture Mechanics", Edward Arnold Pub., London, 1986

8. Irwin G.R., "Fracture Dynamic",in "Fracturing of Metals", ASM Cleveland, 1948.

9. Irwin G.R., "Analysis of stresses and strains near the end of a crack traversing a plate", Trans. ASME, J. of Appl. Mech., 1957.

10. Tracey D.M.,"Finite elements for determination of crack tip stress intensity factors" Engg. Fracture Mechanics, Vol. 3, 255-265, 1971.

11. Blackburn W.S., "In the mathematics of finite elements and applications", Brunel University, 327-336, 1973.

12. Blackburn W.S., Hellen T.K., "Calculation of stress intensity factors in three dimensions by finite element methods", Int. J. of Numerical Methods in Engg., Vol. 11, 211-229, 1977.

13. Henshell R.D., Shaw K.G., "Crack tip finite elements are unnecessary", Int. J. for Numerical Methods in Engg., Vol. 9, 495-509, 1975.

14. Barsoum R.S., "On the use of isoparametric finite elements in linear fracture mechanics", Int. J. for Numerical Methods in Engg., Vol. 10, 25-37, 1976.

15. Hibbitt H.D., "Some properties of singular isoparametric elements", Int. J. for Numerical Methods in Engg., Short Communication, Oct., 1975.

16. Tracey D.M., Cook T., "Analysis of power type singularity using finite elements", Int. J. for Numerical Methods in Engg., Vol. 11, 1225-1233, 1977.

17. Barsoum R.S., "Triangular quarter-points elements as elastic and perfectly-plastic crack tip elements", Int. J. for Numerical Methods in Engg., Vol. 11, 85-98, 1977.

18. Gallagher R.H., "A review of finite element technique in fracture mechanics", Proced. Conf. on Numerical Methods in Fracture Mechanics, 1-25, 1978.

19. Stern M., Becker E.B., "A conforming crack tip element with quadratic variation in the singular fields", Int. J. for Numerical Methods in Engg., Vol. 12, 279-288, 1978.

20. Pu S.L., Hussain M.A., Lorenson W.E., "The collapsed cubic isoparametric element as a singular element for crack problems", Int. J. for Numerical Methods in Engg., Vol. 12, 1727-1742, 1978.

21. Fawkes A.J., Owen D.R., Luxmoore A.R., "An assessment of crack tip singularity models for use with isoparametric elements", Engg. Fracture Mechanics, Vol. 11, 143-159, 1979.

22. Heymann F.J., "A review of the use of isoparametric finite elements for fracture mechanics", Engg. Application of Fracture Mechanics, Proced. of the 1st. Int. Conf. on Fracture, 371-387, 1979.

23. Morris J.L., Wait R., "Crack-tip elements with curved boundaries and variable nodes", Appl. Math. Modelling, Vol. 3, 259-262, 1979.

24. Lin K.Y., Tong P., "Singular finite elements for the fracture analysis of V-notched plate", Int. J. for Numerical Methods in Engg., Vol. 15, 1343-1354, 1980.

25. Blandford G.E., "Two-dimensional stress intensity factor computations using the boundary element method", Int. J. for Numerical Methods in Engg., Vol. 17, 387-404, 1981.

26. Benitez F.G., Ruiz C., "Boundary element method for two-dimensional fracture mechanics problems", Fourth Int. Seminar, 428-456, 1982.

27. Smith R.N., Mason J.C.,"A boundary element method for curved crack problems in two dimensions", Fourth Int. Seminar, 472-484, 1982.

28. Saouma V.E., Schwemmer D., "Numerical evaluation of the quarter-point crack tip element", Int. J. for Numerical Methods in Engg., Vol. 20, 1629-1641, 1984.

29. Banks-Sills L., Bortman Y., "Reappraisal of the quarter point quadrilateral element in linear elastic fracture mechanics", Int. J. of Fracture, Vol. 25, 169-180, 1984.

30. Wahba N.N., "On the use of singular displacement finite elements for cracked plate in bending", Int. J. of Fracture, Vol. 27, 3-30, 1985.

31. Hellen T.K., "A noval approach to crack-tip singularity solutions", Computer & Structures, Vol. 22, No. 5, 743-747, 1986.

32. Al-Edani A.A., "Two-dimensional linear elastic fracture mechanics using singular finite and boundary elements", MSc Thesis, SME, CIT, 1987.

33. Cartwright D.J., Rooke D.P., "Compendium of Stress Intensity Factors", London, Her Majesty's Stationary Office, 1976.

34. Mendelson A., "The use of parabolic variation and the direct determination of stress intensity factors using the B.I.E. method", Symposium Application of Computer Method in Engg., 1-16, 1977.

35. Takao Y., Kawata K., "Mechanical behaviour of single-edge crack", Inst. of Space and Aeronautical Science, Vol. 44, 43-55, 1979.

36. Vainshtok V.A., "Virtual crack variation method for determination of stress intensity factors for cracks of mixed mode and variable length", Innovative Numerical nalysis for the Engg. Science, Proced. of the 2nd. Int. Symposium, 797-803, 1980.

37. Woo C.W., Kuruppu M.D., "Use of finite element method of determining stress intensity factors with a conic-section simulation model of crack surface", Int. J. of Fracture, Vol. 20, 163-178, 1982.

38. Rooke D.P., Hutchins S.M., "Stress intensity factors for cracks at loaded holes-effect of load distribution", J. of Strain Analysis, Vol. 19, No. 2, 81-96, 1984.

39. Ogen G., Schiff B., "Stress intensity factors for two-dimensional crack problems using constrained finite elements", Int. J. of Fracture, Vol. 28, 55-68, 1985.

40. Walsh R.M., Pipes R.B., "Strain energy release rate determination of stress intensity factors by finite element method", Engg. Fracture Mechanics, Vol. 22, No. 1, 17-33, 1985.

41. Clech J.P., Lewis J.L., Keer L.M., "A finite element technique for determining mode I stress intensity factor: Application to no-slip bimaterial cracks problems", Computer & Structures, Vol. 23, No. 6, 715-724, 1986.

42. Banks-Sills L., Sherman D., "Comparison of methods for calculating stress intensity factors with quarter-point elements", Int. J. of Fracture, Vol. 32, 127-140, 1986.

43. Baker A.A., Parker A.P., "Modelling short cracks using the boundary element method", Presented at One-Day Seminar of the Institution of Mechanical Engg., London, 1986.

44. Wells A.A., "Unstable crack propagation in metal: Damage and fast fracture", Proced. of the Crack Propagation Symposium, Cranfield, The college of Aeronautics, Vol. 1, 210-230, 1962.

45. Burdekin F.M., Stone D.E.W., "The crack opening displacement approach to fracture mechanics in yielding", J. of Strain Analysis, Vol. 1, 145-153, 1966.

46. Rice, J.R., " A path independent integral and the approximate analysis of strain concentrations by notches and cracks", Trans. ASME, J. Appl. Mech., Vol. 35, 379-386, 1968.

47. Knott J.F., "The fracture toughness of metals", J. of Strain Analysis, Vol. 10, No. 4, 201-206, 1975.

48. Turner C.E., "Yielding fracture mechanics", J. of Strain Analysis, Vol. 10, 207-215, 1975.

49. Sakata M., Aoki S., Kishimoto K., "Extension of J-integral and its application to the estimation of structural strength", Proced. of the USA-JAPAN Joint Seminar, 23-34, 1979.

50. Miyoshi T., Shiratori M., "Relation between J-integral and crack-opening displacement", "proced of the USA-JAPAN Joint Seminar, 99-107, 1979.

51. Beryer C., Keller H.P., Munz D., "Determination of fracture toughness with linear-elastic and elasto-plastic methods", Elastic-Plastic Fracture Symposium, ASTM, 378-406, 1979.

52. Kishimoto K., Aoki S., Sakata M., "Dynamic stress intensity factors using J-integral and finite element method", Engg. Fracture Mechanics, Vol. 13, 387-494, 1980.

53. Dodds R.H., Read D.T., Wellman G.W., "Finite-element and experimental evaluation of the J-integral for short cracks", Fracture Mechanics, Fourteenth Symposium, ASTM, Vol. 1, I520-I542, 1983.

54. Sladek V., Sladek J., "Three-dimensional curved crack in an elastic body", Computer & Structures, Vol. 19, No. 5, 425-436, 1983.

55. Kishitani K., Hirai T., Murukami K., "J-integral method in analysis of stress intensity factor using boundary elements", J. of the Faculty of Engg., The University of Tokyo, Vol. XXXVII, No. 3, 529-547, 1984.

56. Dodds R.H., Read D.T., "Experimental and analytical evaluation of the J-integral for tensile panels containing short centre cracks", Int. J. of Fracture, Vol. 28, 39-54, 1985.

57. Zenkiewicz O.C., Valliappan S., King I.P., "Elasto-plastic solutions of engineering problems 'initial stress', finite element approach", Int. J. for Numerical Methods in Engg., Vol. 1, 75-100, 1969.

58. Miyamoto H., Shiratori M., Miyoshi T., "Elasto-plastic response at the tip of a crack", 1st. Int. Conf., Kyoto, Japan, Vol. 1, 433-445, 1971.

59. Tracey D.M., "Finite element solution for crack-tip behaviour in small-scale yielding", Trans. of the ASME, 146-150, 1976.

60. Miller K.J., Kfouri A.P., "A comparison of elastic-plastic fracture parameters in biaxial stress states", Elastic-plastic Fracture, Symposium sponsored by ASTM, 214-228, 1979.

61. Hammouda M.M., Miller K.J., "Elastic-plastic fracture mechanics analysis of notches", Elastic-plastic Fracture, Symposium sponsored by ASTM, 703-719, 1979.

62. Pilcer S., Ohlson N.G., "An elastic-plastic analysis of relationships between K_I, J , and *CTOD* ", 4th Int. Conf. of Mechanical Behaviour of Materials, Vol. 2, 959-965, 1983.

63. Dodds R.H., Rolfe S.T., Wellman G.W., "Finite-element Predictions of J and *CTOD* for non-linear fracture mechanics", Proced. Int. Conf. Finite Elements in Computational Mechanics, Bombay, India, Vol. 2, 909-922, 1985.

64. Groves S.E., Allen D.H., Haister W.E., "An efficient and accurate alternative to subincremenation for elastic-plastic analysis by the finite element method", Computer & Structures, Vol. 20, No. 6, 1021-1031, 1985.

65. Yagawa G., Takahashi Y., "Some applications of the finite element method to nonlinear fracture mechanics", Computer Methods in Applied Mechanics & Engg., Vol. 51, 51-69, 1985.

66. Cruse T.A., Polch E.Z., "BIE analysis of crack tip plastic zones", Structures Structural Dynamics & Materails, Conf., Part 1, 251-258, 1985.

67. Braudel H.J., Abouaf M., Chenot J.L., "An implicit and incremental formulation for the solution of elasto-plastic problems by the finite element method", Computer & Structures, Vol. 22, No. 5, 801-814, 1986.

68. Cruse T.A., Polch E.Z., "Application of an elastoplastic boundary element method to some fracture mechanics problems", Engg. Fracture Mechanics, Vol. 23, No. 6, 1085-1096, 1986.

69. Cruse T.A., Polch E.Z., "Elastoplastic *BIE* analysis of cracked plates and related problems Part 1: Formulation", Int. J. for Numerical Methods in Engg., Vol. 23, 249-437, 1986.

70. Cruse T.A., Polch E.Z., "Elastoplastic *BIE* analysis of cracked plates and related problems Part 2: Numerical Results", Int. J. for Numerical Methods in Engg., Vol. 23, 439-452, 1986.

71. Cruse T.A., "Boundary Element Analysis in Computational Fracture Mechanics", Kluwer Academic Pub., 1988.

72. El-Zafrany A.M., "Plasticity", Lecture Notes, SME, CIT, 1989.

73. Hearn E.J., "Mechanics of Materials", Vol. 1, Pergamon Press, 1985.

74. Atluri S.N., "Computational Methods in the Mechanics of Fracture", Vol. 2, in the Computational Methods in Mechanics, North-Holland Pub., 1986.

75. Owen D.R.J., Fawkes A.J., "Engineering Fracture Mechanics: Numerical Methods and Applications", Pineridge Press, 1983.

76. Parker A.P., "The Mechanics of Fracture and Fatigue: An Introduction", SPON Ltd. Pub., 1981.

75. Eshelby J.D., "The Continuum Theory of Lattice Defects", Solid State Physics, Vol. 3, F. Seitz and D. Turbull (Eds.), Academic Press Pub., 79-141, 1956.

76. Cherepanov G.P., "Crack propagation in continuous media", USSR, J. Appl. Math. and Mech. Translation, Vol. 31, 1967.

77. Rice J.R., "Mathematical analysis in the mechanics of fracture", Fracture An Advanced Treatise, Vol. II, H. Liebowitz (Ed.), Academic Press Pub., 191-308, 1968.

78. Kanninew M.F., Popelar C.H., "Advanced Fracture Mechanics", Oxford University Press, 1985.

79. El-Zafrany A.M., "Boundary Element Method", Lecture Notes, SME, CIT, 1986.

80. El-Zafrany A.M., "Finite Element Techniques for Engineering Analysis", A Book to be Published by Ellis Horwood.

81. Brebbia C.A., "The Boundary Element Method for Engineers", Pentech Press, London, 1980.

82. Cookson R.A., El-Zafrany A.M., "State of the Art review of the boundary element method", Presented at one-day Seminar of the Institution of Mechanical Engineering, London, 1986.

83. El-Zafrany A.M., "Techineques of Boundary Element Method for Engineers", A Book to be Published by Ellis Horwood.

84. Banerjee P.K., Butterfield R., "Boundary Element Method in Engineering Science", McGraw-Hill, 1981.

85. El-Zafrany A.M., Cookson R.A., Iqbal M., "Boundary element stress analysis with domain type loading", Presented at one-day Seminar of the Institution of Mechanical Engineering, London, 1986.

86. El-Zafrany A.M., "Fast Front Solver for Asymmetric Equations", Lecture Notes, SME, CIT, 1988.

87. Liebowitz H., Moyer E.T., "Finite Element Methods in Fracture Mechanics", Computers & Structures, Vol. 31, No. 1, 1-9, 1989.

88. Hearn E.J., "MECHANICS OF MATERIALS", 2nd Edition, Vol. 1, Pergamon Press, 1985.

89. Sumpter J.D.G., "Elastic-plastic fracture analysis and design using the finite element method", PhD Thesis, Imperial Collage, London, 1973.

90. Tan C.L., Lee K.H., "Elastic-plastic stress analysis of a cracked thick-walled cylinder", IMechE, 50-57, 1983.

APPENDIX A

APPENDIX A

A.1 Integration By-Parts Theorems:

Let $f(x,y)$ and $g(x,y)$ be continuous functions with continuous first order derivatives defined in a domain Ω with boundary Γ, then:

$$\text{(a)} \quad \iint_{\Omega} f \frac{\partial g}{\partial x} \, dA = \oint_{\Gamma} \ell \, f \, g \, ds - \iint_{\Omega} \frac{\partial f}{\partial x} \, g \, dA \qquad \text{(A.1)}$$

$$\text{(b)} \quad \iint_{\Omega} f \frac{\partial g}{\partial y} \, dA = \oint_{\Gamma} m \, f \, g \, ds - \iint_{\Omega} \frac{\partial f}{\partial y} \, g \, dA \qquad \text{(A.2)}$$

where, $\ell \, ds = dy$, $m \, ds = - \, dx$.

The proofs of the above theorems are shown in Ref.[79].

A.2 Useful Theorems:

A.2.1. Theorem (1):

Let a parameter ζ exists such that $\underline{u} = \underline{u}(x,y,\zeta)$, then, for a stationary structure defined in terms of the domain Ω, it can be shown that:

$$\iint_{\Omega} \underline{\sigma}^{t} \frac{\partial \underline{\varepsilon}}{\partial \zeta} \, dA = \oint_{\Gamma} \underline{T}^{t} \frac{\partial \underline{u}}{\partial \zeta} \, ds + \iint_{\Omega} \underline{X}^{t} \frac{\partial \underline{u}}{\partial \zeta} \, dA \qquad \text{(A.3)}$$

where Ω is a closed two-dimensional domain with a boundary Γ.

(a) Result (1):

$$\iint_{\Omega} \underline{\sigma}^t \, \Delta\underline{\varepsilon} \, dA = \oint_{\Gamma} \underline{T}^t \, \Delta\underline{u} \, ds + \iint_{\Omega} \underline{X}^t \, \Delta\underline{u} \, dA \qquad (A.4)$$

(b) Result (2):

Defining $\Pi = U + V = U -$ Work done by external loads, then:

$$\Delta\Pi = \iint_{\Omega} t \, \Delta W \, dA - \iint_{\Omega} t \, \underline{\sigma}^t \, \Delta\underline{\varepsilon} \, dA \qquad (A.5)$$

where $W = \dfrac{dU}{dvol} = \dfrac{1}{t} \dfrac{dU}{dA}$.

A.2.2 Theorem (2):

Let a parameter ζ exist such that $\underline{u}$, $\underline{\sigma}$, $\underline{\varepsilon}$, $\underline{T}$, and $\underline{X}$ are all functions of ζ, then in the absence of dissipation energy, for a moving structure defined by means of the domain Ω, it can be proved that:

$$\iint_{\Omega} \left(\frac{\partial W}{\partial \zeta} + \frac{\partial \mathcal{K}}{\partial \zeta} \right) dA = \oint_{\Gamma} \frac{\partial \psi}{\partial \zeta} \, ds + \iint_{\Omega} \frac{\partial \mathcal{B}}{\partial \zeta} \, dA \qquad (A.6)$$

(a) Result (1):

For a constant system of surface and body forces:

$$\iint_{\Omega} \left(\frac{\partial W}{\partial \zeta} + \frac{\partial \mathcal{K}}{\partial \zeta} \right) dA = \oint_{\Gamma} \underline{T}^t \frac{\partial \underline{u}}{\partial \zeta} \, ds + \iint_{\Omega} \underline{X}^t \frac{\partial \underline{u}}{\partial \zeta} \, dA \qquad (A.7)$$

(b) *Result (2):*

Dividing equation (A.5) by $t\Delta\zeta$ and taking the limits, it can be deduced that:

$$\frac{1}{t}\frac{d\Pi}{d\zeta} = \iint_{\Omega} \frac{\partial W}{\partial \zeta}\, dA - \iint_{\Omega} \underline{\sigma}^{t}\, \frac{\partial \underline{\varepsilon}}{\partial \zeta}\, dA \qquad (A.8)$$

(c) *Result (3):*

Substituting equation (A.3) into (A.8), it can be shown that:

$$\frac{1}{t}\frac{\partial \Pi}{\partial \zeta} = \iint_{\Omega} \frac{\partial W}{\partial \zeta}\, dA - \oint_{\Gamma} \underline{T}^{t}\, \frac{\partial \underline{u}}{\partial \zeta}\, ds - \iint_{\Omega} \underline{X}^{t}\, \frac{\partial \underline{u}}{\partial \zeta}\, dA \qquad (A.9)$$

APPENDIX B

APPENDIX B

FRAMEC PACKAGE LIBRARY OF FINITE ELEMENTS

B.1 Standard Family of Elements:

Element No. 1

4-Node Isoparametric Element.

$$N_1 = \mathcal{L}_1^2(\xi)\ \mathcal{L}_1^2(\eta)$$

$$N_2 = \mathcal{L}_2^2(\xi)\ \mathcal{L}_1^2(\eta)$$

$$N_3 = \mathcal{L}_2^2(\xi)\ \mathcal{L}_2^2(\eta)$$

$$N_4 = \mathcal{L}_1^2(\xi)\ \mathcal{L}_2^2(\eta)$$

where,

$$\mathcal{L}_i^n(z) = \prod_{\substack{r=1 \\ r\neq i}}^{n} \left[\frac{(n-1)\ z - (r-1)}{i-r} \right]$$

Element No. 2

6-Node Quadrilateral Element.

$$N_1 = \mathcal{L}_1^3(\xi)\ \mathcal{L}_1^2(\eta)$$

$$N_2 = \mathcal{L}_2^3(\xi)\ \mathcal{L}_1^2(\eta)$$

$$N_3 = \mathcal{L}_3^3(\xi)\ \mathcal{L}_1^2(\eta)$$

$$N_4 = \mathcal{L}_3^3(\xi)\ \mathcal{L}_2^2(\eta)$$

$$N_5 = \mathcal{L}_2^3(\xi)\ \mathcal{L}_2^2(\eta)$$

$$N_6 = \mathcal{L}_1^3(\xi)\ \mathcal{L}_2^2(\eta)$$

Element No. 3

8-Node Isoparametric Element.

$$N_1 = \mathcal{L}_1^3(\xi)\ \mathcal{L}_1^2(\eta) + \mathcal{L}_1^2(\xi)\ \mathcal{L}_1^3(\eta) - \mathcal{L}_1^2(\xi)\ \mathcal{L}_1^2(\eta)$$

$$N_2 = \mathcal{L}_2^3(\xi)\ \mathcal{L}_1^2(\eta)$$

$$N_3 = \mathcal{L}_3^3(\xi)\ \mathcal{L}_1^2(\eta) + \mathcal{L}_2^2(\xi)\ \mathcal{L}_1^3(\eta) - \mathcal{L}_2^2(\xi)\ \mathcal{L}_1^2(\eta)$$

$$N_4 = \mathcal{L}_2^2(\xi)\ \mathcal{L}_2^3(\eta)$$

$$N_5 = \mathcal{L}_3^3(\xi)\ \mathcal{L}_2^2(\eta) + \mathcal{L}_2^2(\xi)\ \mathcal{L}_3^3(\eta) - \mathcal{L}_2^2(\xi)\ \mathcal{L}_2^2(\eta)$$

$$N_6 = \mathcal{L}_2^3(\xi)\ \mathcal{L}_2^2(\eta)$$

$$N_7 = \mathcal{L}_1^3(\xi)\ \mathcal{L}_2^2(\eta) + \mathcal{L}_1^2(\xi)\ \mathcal{L}_3^3(\eta) - \mathcal{L}_1^2(\xi)\ \mathcal{L}_2^2(\eta)$$

$$N_8 = \mathcal{L}_1^2(\xi)\ \mathcal{L}_2^3(\eta)$$

Element No. 4

9-Node Lagrangian Element.

$$N_1 = \mathcal{L}_1^3(\xi)\ \mathcal{L}_1^3(\eta)$$

$$N_2 = \mathcal{L}_2^3(\xi)\ \mathcal{L}_1^3(\eta)$$

$$N_3 = \mathcal{L}_3^3(\xi)\ \mathcal{L}_1^3(\eta)$$

$$N_4 = \mathcal{L}_3^3(\xi)\ \mathcal{L}_2^3(\eta)$$

$$N_5 = \mathcal{L}_3^3(\xi)\ \mathcal{L}_3^3(\eta)$$

$$N_6 = \mathcal{L}_2^3(\xi)\ \mathcal{L}_3^3(\eta)$$

$$N_7 = \mathcal{L}_1^3(\xi)\ \mathcal{L}_3^3(\eta)$$

$$N_8 = \mathcal{L}_1^3(\xi)\ \mathcal{L}_2^3(\eta)$$

$$N_9 = \mathcal{L}_2^3(\xi)\ \mathcal{L}_2^3(\eta)$$

Element No. 5

8-Node Quadrilateral Element.

$$N_1 = \mathcal{L}_1^4(\xi)\ \mathcal{L}_1^2(\eta)$$

$$N_2 = \mathcal{L}_2^4(\xi)\ \mathcal{L}_1^2(\eta)$$

$$N_3 = \mathcal{L}_3^4(\xi)\ \mathcal{L}_1^2(\eta)$$

$$N_4 = \mathcal{L}_4^4(\xi)\ \mathcal{L}_1^2(\eta)$$

$$N_5 = \mathcal{L}_4^4(\xi)\ \mathcal{L}_2^2(\eta)$$

$$N_6 = \mathcal{L}_3^4(\xi)\ \mathcal{L}_2^2(\eta)$$

$$N_7 = \mathcal{L}_2^4(\xi)\ \mathcal{L}_2^2(\eta)$$

$$N_8 = \mathcal{L}_1^4(\xi)\ \mathcal{L}_2^2(\eta)$$

Element No. 6

10-Node Quadrilateral Element.

$$N_1 = \mathcal{L}_1^4(\xi)\ \mathcal{L}_1^2(\eta) + \mathcal{L}_1^3(\xi)\ \mathcal{L}_1^2(\eta) - \mathcal{L}_1^2(\xi)\ \mathcal{L}_1^2(\eta)$$

$$N_2 = \mathcal{L}_2^4(\xi)\ \mathcal{L}_1^2(\eta)$$

$$N_3 = \mathcal{L}_3^4(\xi)\ \mathcal{L}_1^2(\eta)$$

$$N_4 = \mathcal{L}_4^4(\xi)\ \mathcal{L}_1^2(\eta) + \mathcal{L}_2^2(\xi)\ \mathcal{L}_1^3(\eta) - \mathcal{L}_2^2(\xi)\ \mathcal{L}_1^2(\eta)$$

$$N_5 = \mathcal{L}_2^2(\xi)\ \mathcal{L}_2^3(\eta)$$

$$N_6 = \mathcal{L}_2^2(\xi)\ \mathcal{L}_3^3(\eta) + \mathcal{L}_4^4(\xi)\ \mathcal{L}_2^2(\eta) - \mathcal{L}_2^2(\xi)\ \mathcal{L}_2^2(\eta)$$

$$N_7 = \mathcal{L}_3^4(\xi)\ \mathcal{L}_2^2(\eta)$$

$$N_8 = \mathcal{L}_2^4(\xi)\ \mathcal{L}_2^2(\eta)$$

$$N_9 = \mathcal{L}_1^4(\xi)\ \mathcal{L}_2^2(\eta) + \mathcal{L}_1^2(\xi)\ \mathcal{L}_3^3(\eta) - \mathcal{L}_1^2(\xi)\ \mathcal{L}_2^2(\eta)$$

$$N_{10} = \mathcal{L}_1^2(\xi)\ \mathcal{L}_2^3(\eta)$$

Element No. 7

12-Node Isoparametric Element.

$$N_1 = \mathcal{L}_1^4(\xi)\ \mathcal{L}_1^2(\eta) + \mathcal{L}_1^2(\xi)\ \mathcal{L}_1^4(\eta) - \mathcal{L}_1^2(\xi)\ \mathcal{L}_1^2(\eta)$$

$$N_2 = \mathcal{L}_2^4(\xi)\ \mathcal{L}_1^2(\eta)$$

$$N_3 = \mathcal{L}_3^4(\xi)\ \mathcal{L}_1^2(\eta)$$

$$N_4 = \mathcal{L}_4^4(\xi)\ \mathcal{L}_1^2(\eta) + \mathcal{L}_2^2(\xi)\ \mathcal{L}_1^4(\eta) - \mathcal{L}_2^2(\xi)\ \mathcal{L}_2^4(\eta)$$

$$N_5 = \mathcal{L}_2^2(\xi)\ \mathcal{L}_2^4(\eta)$$

$$N_6 = \mathcal{L}_2^2(\xi)\ \mathcal{L}_3^4(\eta)$$

$$N_7 = \mathcal{L}_2^2(\xi)\ \mathcal{L}_4^4(\eta) + \mathcal{L}_4^4(\xi)\ \mathcal{L}_2^2(\eta) - \mathcal{L}_2^2(\xi)\ \mathcal{L}_2^2(\eta)$$

$$N_8 = \mathcal{L}_3^4(\xi)\ \mathcal{L}_2^2(\eta)$$

$$N_9 = \mathcal{L}_2^4(\xi)\ \mathcal{L}_2^2(\eta)$$

$$N_{10} = \mathcal{L}_1^4(\xi)\ \mathcal{L}_2^2(\eta) + \mathcal{L}_1^2(\xi)\ \mathcal{L}_4^4(\eta) - \mathcal{L}_1^2(\xi)\ \mathcal{L}_2^2(\eta)$$

$$N_{11} = \mathcal{L}_1^2(\xi)\ \mathcal{L}_3^4(\eta)$$

$$N_{12} = \mathcal{L}_1^2(\xi)\ \mathcal{L}_2^4(\eta)$$

Element No. 8

3-Node Triangular Element.

$$N_1 = L_1 = 1-\xi-\eta$$

$$N_2 = L_2 = \xi$$

$$N_3 = L_3 = \eta$$

Element No. 9

6-Node Triangular Element.

$$N_1 = \lambda_2^2(L_1)$$

$$N_2 = \lambda_1^2(L_1)\ \lambda_1^2(L_2)$$

$$N_3 = \lambda_2^2(L_2)$$

$$N_4 = \lambda_1^2(L_2)\ \lambda_1^2(L_3)$$

$$N_5 = \lambda_2^2(L_3)$$

$$N_6 = \lambda_1^2(L_3)\ \lambda_1^2(L_1)$$

where,

$$\lambda_s^n(L_r) = \prod_{t=0}^{s-1} \left[\frac{n\,L_r - t}{s-t} \right], \quad s = 1, 2, \ldots, n.$$

Element No. 10

10-Node Lagrangian Element.

$$N_1 = \lambda_1^3(L_1)$$

$$N_2 = \lambda_2^3(L_1)\ \lambda_1^3(L_2)$$

$$N_3 = \lambda_1^3(L_1)\ \lambda_2^3(L_2)$$

$$N_4 = \lambda_3^3(L_2)$$

$$N_5 = \lambda_2^3(L_2)\ \lambda_1^3(L_3)$$

$$N_6 = \lambda_1^3(L_2)\ \lambda_2^3(L_3)$$

$$N_7 = \lambda_3^3(L_3)$$

$$N_8 = \lambda_2^3(L_3)\ \lambda_1^3(L_1)$$

$$N_9 = \lambda_1^3(L_3)\ \lambda_2^3(L_1)$$

$$N_{10} = \lambda_1^3(L_1)\ \lambda_1^3(L_2)\ \lambda_1^3(L_3)$$

B.2 Transition Family of Elements:

Element No. 11

5-Node Quadrilateral Element.

$$N_1 = \mathcal{L}_1^3(\xi)\ \mathcal{L}_1^2(\eta)$$

$$N_2 = \mathcal{L}_2^3(\xi)\ \mathcal{L}_1^2(\eta)$$

$$N_3 = \mathcal{L}_3^3(\xi)\ \mathcal{L}_1^2(\eta)$$

$$N_4 = \mathcal{L}_2^2(\xi)\ \mathcal{L}_2^2(\eta)$$

$$N_5 = \mathcal{L}_1^2(\xi)\ \mathcal{L}_2^2(\eta)$$

Element No. 12

6-Node Quadrilateral Element.

$$N_1 = \mathcal{L}_1^3(\xi)\ \mathcal{L}_1^2(\eta)$$

$$N_2 = \mathcal{L}_2^3(\xi)\ \mathcal{L}_1^2(\eta)$$

$$N_3 = \mathcal{L}_3^3(\xi)\ \mathcal{L}_1^2(\eta) + \mathcal{L}_2^2(\xi)\ \mathcal{L}_1^3(\eta) - \mathcal{L}_2^2(\xi)\ \mathcal{L}_1^2(\eta)$$

$$N_4 = \mathcal{L}_2^2(\xi)\ \mathcal{L}_2^3(\eta)$$

$$N_5 = \mathcal{L}_2^2(\xi)\ \mathcal{L}_3^3(\eta)$$

$$N_6 = \mathcal{L}_1^2(\xi)\ \mathcal{L}_2^2(\eta)$$

Element No. 13

11-Node Lagrangian Element.

$$N_1 = \mathcal{L}_1^5(\xi)\ \mathcal{L}_1^3(\eta)$$

$$N_2 = \mathcal{L}_2^5(\xi)\ \mathcal{L}_1^3(\eta)$$

$$N_3 = \mathcal{L}_3^5(\xi)\ \mathcal{L}_1^3(\eta)$$

$$N_4 = \mathcal{L}_4^5(\xi)\ \mathcal{L}_1^3(\eta)$$

$$N_5 = \mathcal{L}_5^5(\xi)\ \mathcal{L}_1^3(\eta)$$

$$N_6 = \mathcal{L}_3^3(\xi)\ \mathcal{L}_2^3(\eta)$$

$$N_7 = \mathcal{L}_3^3(\xi)\ \mathcal{L}_3^3(\eta)$$

$$N_8 = \mathcal{L}_2^3(\xi)\ \mathcal{L}_3^3(\eta)$$

$$N_9 = \mathcal{L}_1^3(\xi)\ \mathcal{L}_3^3(\eta)$$

$$N_{10} = \mathcal{L}_1^3(\xi)\ \mathcal{L}_2^3(\eta)$$

$$N_{11} = \mathcal{L}_2^3(\xi)\ \mathcal{L}_2^3(\eta)$$

Element No. 14

13-Node Lagrangian Element.

$$N_1 = \mathcal{L}_1^5(\xi)\ \mathcal{L}_1^3(\eta)$$

$$N_2 = \mathcal{L}_2^5(\xi)\ \mathcal{L}_1^3(\eta)$$

$$N_3 = \mathcal{L}_3^5(\xi)\ \mathcal{L}_1^3(\eta)$$

$$N_4 = \mathcal{L}_4^5(\xi)\ \mathcal{L}_1^3(\eta)$$

$$N_5 = \mathcal{L}_5^5(\xi)\ \mathcal{L}_1^3(\eta) + \mathcal{L}_3^3(\xi)\ \mathcal{L}_1^5(\eta) - \mathcal{L}_1^3(\xi)\ \mathcal{L}_1^3(\eta)$$

$$N_6 = \mathcal{L}_3^3(\xi)\ \mathcal{L}_2^5(\eta)$$

$$N_7 = \mathcal{L}_3^3(\xi)\ \mathcal{L}_3^5(\eta)$$

$$N_8 = \mathcal{L}_3^3(\xi)\ \mathcal{L}_4^5(\eta)$$

$$N_9 = \mathcal{L}_3^3(\xi)\ \mathcal{L}_5^5(\eta)$$

$$N_{10} = \mathcal{L}_2^3(\xi)\ \mathcal{L}_3^3(\eta)$$

$$N_{11} = \mathcal{L}_1^3(\xi)\ \mathcal{L}_3^3(\eta)$$

$$N_{12} = \mathcal{L}_1^3(\xi)\ \mathcal{L}_2^3(\eta)$$

$$N_{13} = \mathcal{L}_2^3(\xi)\ \mathcal{L}_2^3(\eta)$$

Element No. 15

10-Node Quadrilateral Element.

$$N_1 = \mathcal{L}_1^5(\xi)\,\mathcal{L}_1^2(\eta) + \mathcal{L}_1^2(\xi)\,\mathcal{L}_1^3(\eta) - \mathcal{L}_1^2(\xi)\,\mathcal{L}_1^2(\eta)$$

$$N_2 = \mathcal{L}_2^5(\xi)\,\mathcal{L}_1^2(\eta)$$

$$N_3 = \mathcal{L}_3^5(\xi)\,\mathcal{L}_1^2(\eta)$$

$$N_4 = \mathcal{L}_4^5(\xi)\,\mathcal{L}_1^2(\eta)$$

$$N_5 = \mathcal{L}_5^5(\xi)\,\mathcal{L}_1^2(\eta) + \mathcal{L}_2^2(\xi)\,\mathcal{L}_1^3(\eta) - \mathcal{L}_2^2(\xi)\,\mathcal{L}_1^2(\eta)$$

$$N_6 = \mathcal{L}_2^2(\xi)\,\mathcal{L}_2^3(\eta)$$

$$N_7 = \mathcal{L}_2^2(\xi)\,\mathcal{L}_3^3(\eta) + \mathcal{L}_3^3(\xi)\,\mathcal{L}_2^2(\eta) - \mathcal{L}_2^2(\xi)\,\mathcal{L}_2^2(\eta)$$

$$N_8 = \mathcal{L}_2^3(\xi)\,\mathcal{L}_2^2(\eta)$$

$$N_9 = \mathcal{L}_1^3(\xi)\,\mathcal{L}_2^2(\eta) + \mathcal{L}_1^2(\xi)\,\mathcal{L}_3^3(\eta) - \mathcal{L}_1^2(\xi)\,\mathcal{L}_2^2(\eta)$$

$$N_{10} = \mathcal{L}_1^2(\xi)\,\mathcal{L}_2^3(\eta)$$

Element No. 16

12-Node Quadrilateral Element.

$$N_1 = \mathcal{L}_1^5(\xi)\,\mathcal{L}_1^2(\eta) + \mathcal{L}_1^2(\xi)\,\mathcal{L}_1^3(\eta) - \mathcal{L}_1^2(\xi)\,\mathcal{L}_1^2(\eta)$$

$$N_2 = \mathcal{L}_2^5(\xi)\,\mathcal{L}_1^2(\eta)$$

$$N_3 = \mathcal{L}_3^5(\xi)\,\mathcal{L}_1^2(\eta)$$

$$N_4 = \mathcal{L}_4^5(\xi)\,\mathcal{L}_1^2(\eta)$$

$$N_5 = \mathcal{L}_5^5(\xi)\,\mathcal{L}_1^3(\eta) + \mathcal{L}_2^2(\xi)\,\mathcal{L}_1^5(\eta) - \mathcal{L}_1^2(\xi)\,\mathcal{L}_1^2(\eta)$$

$$N_6 = \mathcal{L}_2^2(\xi)\ \mathcal{L}_2^5(\eta)$$

$$N_7 = \mathcal{L}_2^2(\xi)\ \mathcal{L}_3^5(\eta)$$

$$N_8 = \mathcal{L}_2^2(\xi)\ \mathcal{L}_4^5(\eta)$$

$$N_9 = \mathcal{L}_2^2(\xi)\ \mathcal{L}_5^5(\eta) + \mathcal{L}_3^3(\xi)\ \mathcal{L}_2^2(\eta) - \mathcal{L}_2^2(\xi)\ \mathcal{L}_2^2(\eta)$$

$$N_{10} = \mathcal{L}_2^3(\xi)\ \mathcal{L}_2^2(\eta)$$

$$N_{11} = \mathcal{L}_1^3(\xi)\ \mathcal{L}_2^2(\eta) + \mathcal{L}_1^2(\xi)\ \mathcal{L}_3^3(\eta) - \mathcal{L}_1^2(\xi)\ \mathcal{L}_2^2(\eta)$$

$$N_{12} = \mathcal{L}_1^2(\xi)\ \mathcal{L}_2^3(\eta)$$

Element No. 17

4-node Triangular Element.

$$N_1 = L_1\ (1 - 2L_2)$$

$$N_2 = 4\ L_1\ L_2$$

$$N_3 = L_2\ (2L_2 + 2L_3 - 1)$$

$$N_4 = L_3$$

Element No. 18

8-Node Triangular Element.

$$N_1 = L_2\ (2L_2 - 1) - \frac{8}{3}\ L_2\ L_3\ [2L_2\ (L_2 - L_3) - L_1\ (2L_2 - 1)]$$

$$N_2 = \frac{8}{3}\ L_2\ L_3\ [(4L_2 - 1)\ (2L_2 - 1) + (2L_3 - 1)\ (4L_3 - 3)]$$

$$N_3 = -\ 2\ L_2\ L_3\ [(4L_2 - 1)\ (4L_2 - 3) + (4L_3 - 1)\ (4L_3 - 3)]$$

$$N_4 = \frac{8}{3}\ L_2\ L_3\ [(4L_3 - 1)\ (2L_3 - 1) + (2L_2 - 1)\ (4L_2 - 3)]$$

$$N_5 = L_3\,(2L_3-1) - \frac{8}{3}\,L_2\,L_3\,[\,2L_3\,(L_3-L_2) - L_1\,(2L_2-1)]$$

$$N_6 = 4\,L_1\,L_3$$

$$N_7 = L_1\,(1 - 2L_2-2L_3)$$

$$N_8 = 4\,L_1\,L_2$$

B.3 Collapsed Crack-Tip Elements Family:

Element No. 1:

$$\xi' = \frac{\xi}{1-\eta} \quad , \quad \eta' = \eta$$

$$N_1 = \eta\,(2\eta-1)$$
$$N_2 = 4\,\eta\,(1-\xi-\eta)$$
$$N_3 = (1-\xi-\eta)\,(1-2\eta) - 2\xi + \frac{2\xi^2}{1-\eta}$$
$$N_4 = 4\xi - \frac{4\xi^2}{1-\eta}$$
$$N_5 = -\xi\,(1+2\eta) + \frac{2\xi^2}{1-\eta}$$
$$N_6 = 4\,\xi\,\eta$$

Element No. 2:

$$\xi' = \xi \quad , \quad \eta' = \frac{\eta}{\xi}$$

$$N_1 = (1-\xi)\,(1-2\xi)$$
$$N_2 = 4\xi\,(1-\xi)\,(1 - \frac{\eta}{\xi})$$
$$N_3 = (\xi-\eta)\,(-1 + 2\xi - 2\,\frac{\eta}{\xi})$$
$$N_4 = 4\eta\,(1 - \frac{\eta}{\xi})$$
$$N_5 = \eta\,(-3 + 2\xi + 2\,\frac{\eta}{\xi}\,)$$
$$N_6 = 4\eta\,(1-\xi)$$

Element No. 3:

$$\xi' = \frac{\xi}{\eta} \quad , \quad \eta' = \eta$$

$$N_1 = (1-\eta)\,(1-2\eta)$$
$$N_2 = 4\xi\,(1-\eta)$$
$$N_3 = \xi\,(-3 + 2\,\frac{\xi}{\eta} + 2\eta)$$
$$N_4 = 4\xi\,(1 - \frac{\xi}{\eta})$$
$$N_5 = (\eta-\xi)\,(-1 - 2\,\frac{\xi}{\eta} + 2\eta)$$
$$N_6 = 4\,(\eta-\xi)\,(1-\eta)$$

APPENDIX C

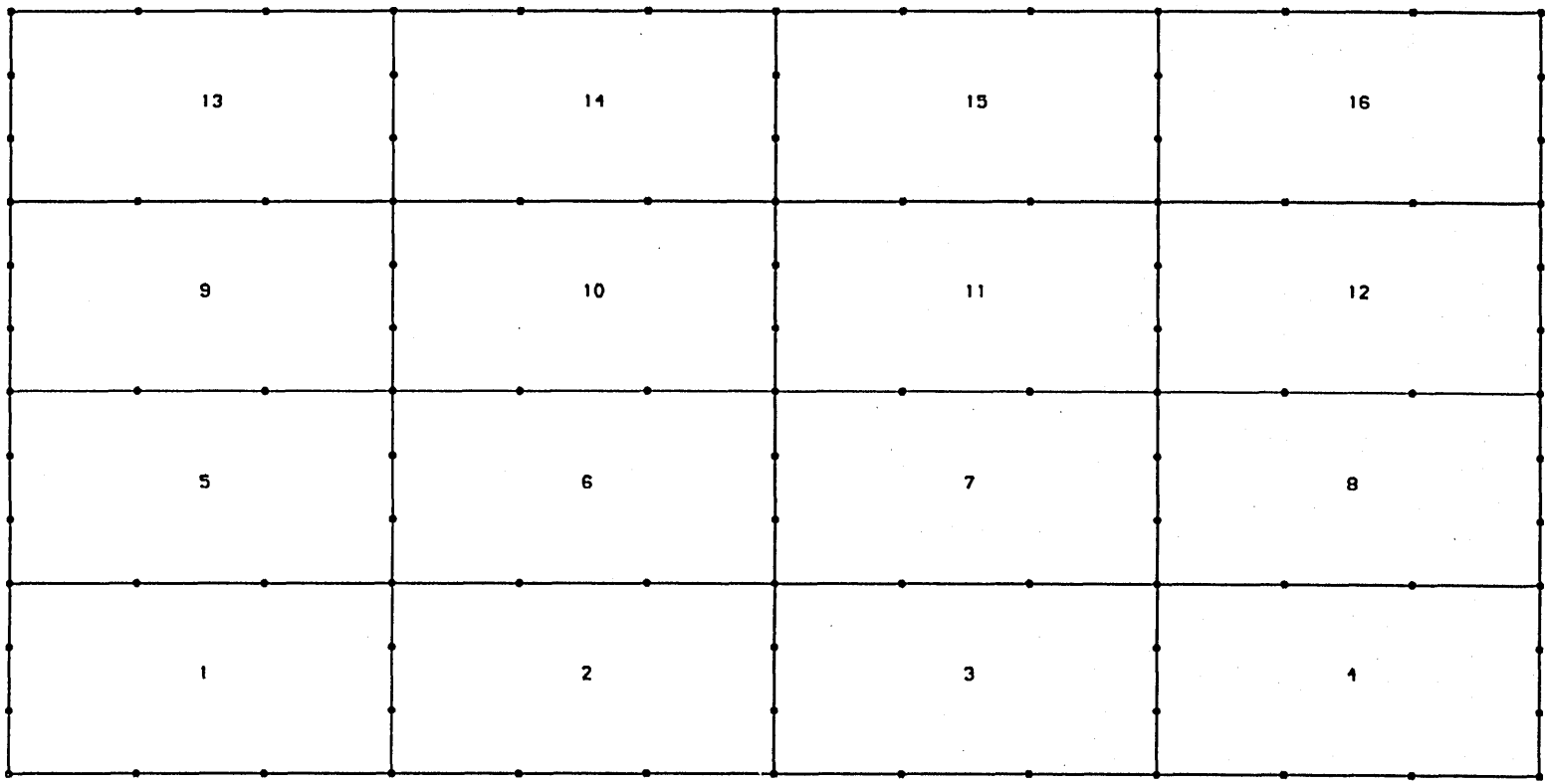

Fig.(C.1) Finite-Element Mesh For Plate under Tension generated using 12-Node Quadrilateral Finite Elements.

FRAMEC

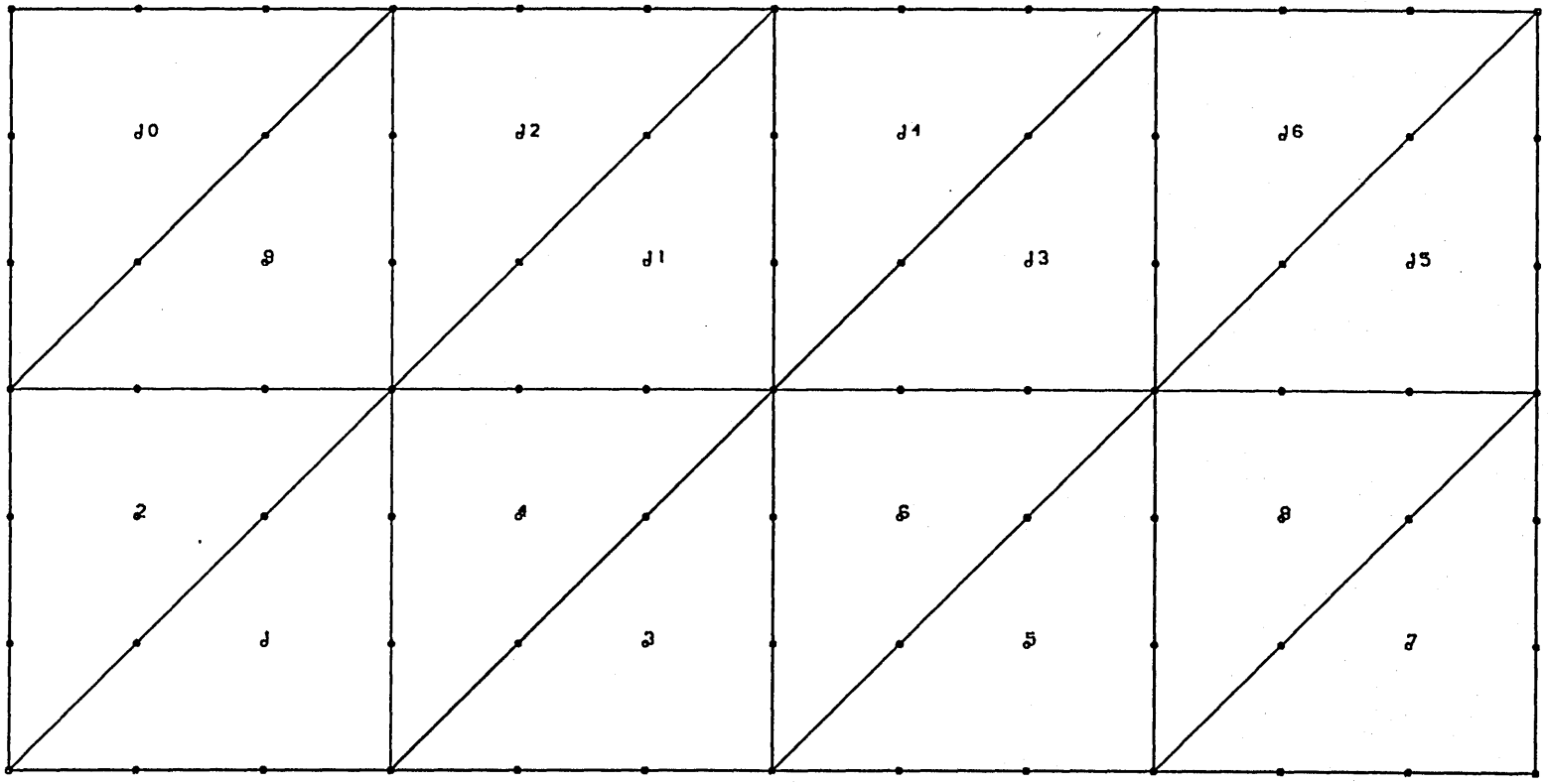

Fig.(C.2) Finite-Element Mesh For Plate under Tension generated using 10-Node Lagrangian Triangular Finite-Elements.

FRAMEC

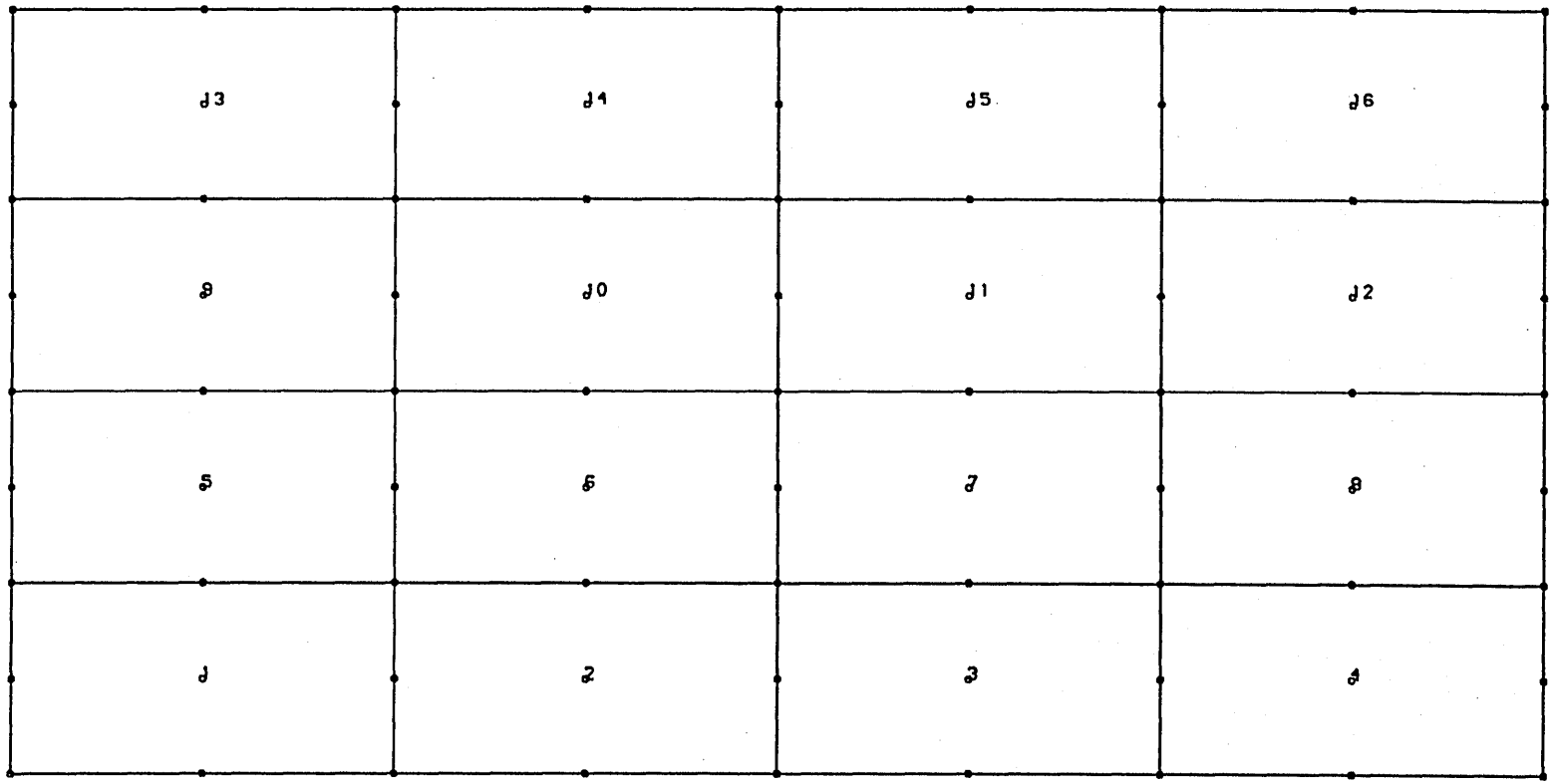

Fig.(C.3) Finite-Element Mesh For Plate under Tension generated using 9-Node Lagrangian Quadrilateral Finite Elements.

FRAMEC

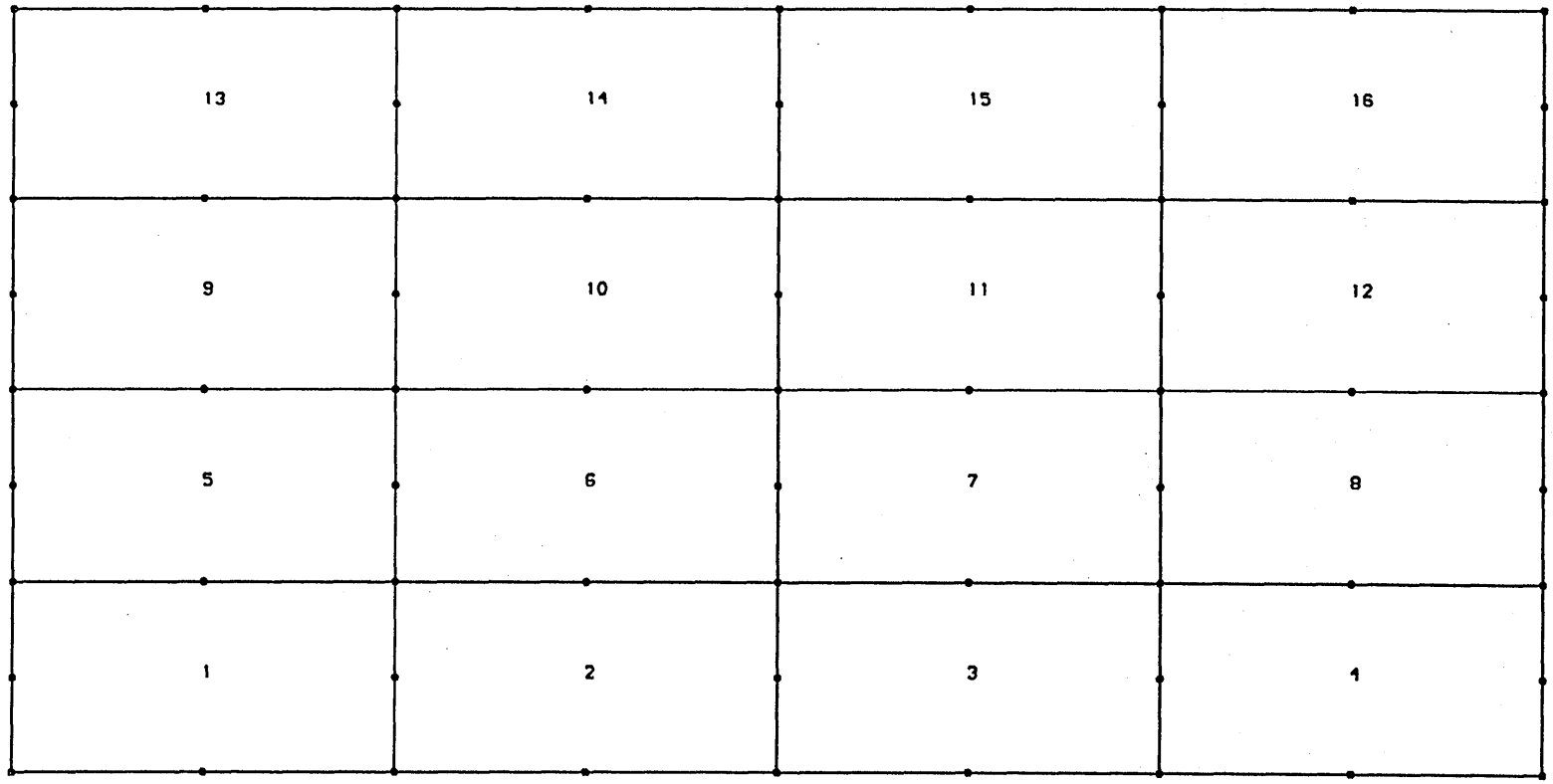

Fig.(C.4) Finite-Element Mesh For Plate under Tension generated using 8-Node Quadrilateral Finite Elements.

FRAMEC

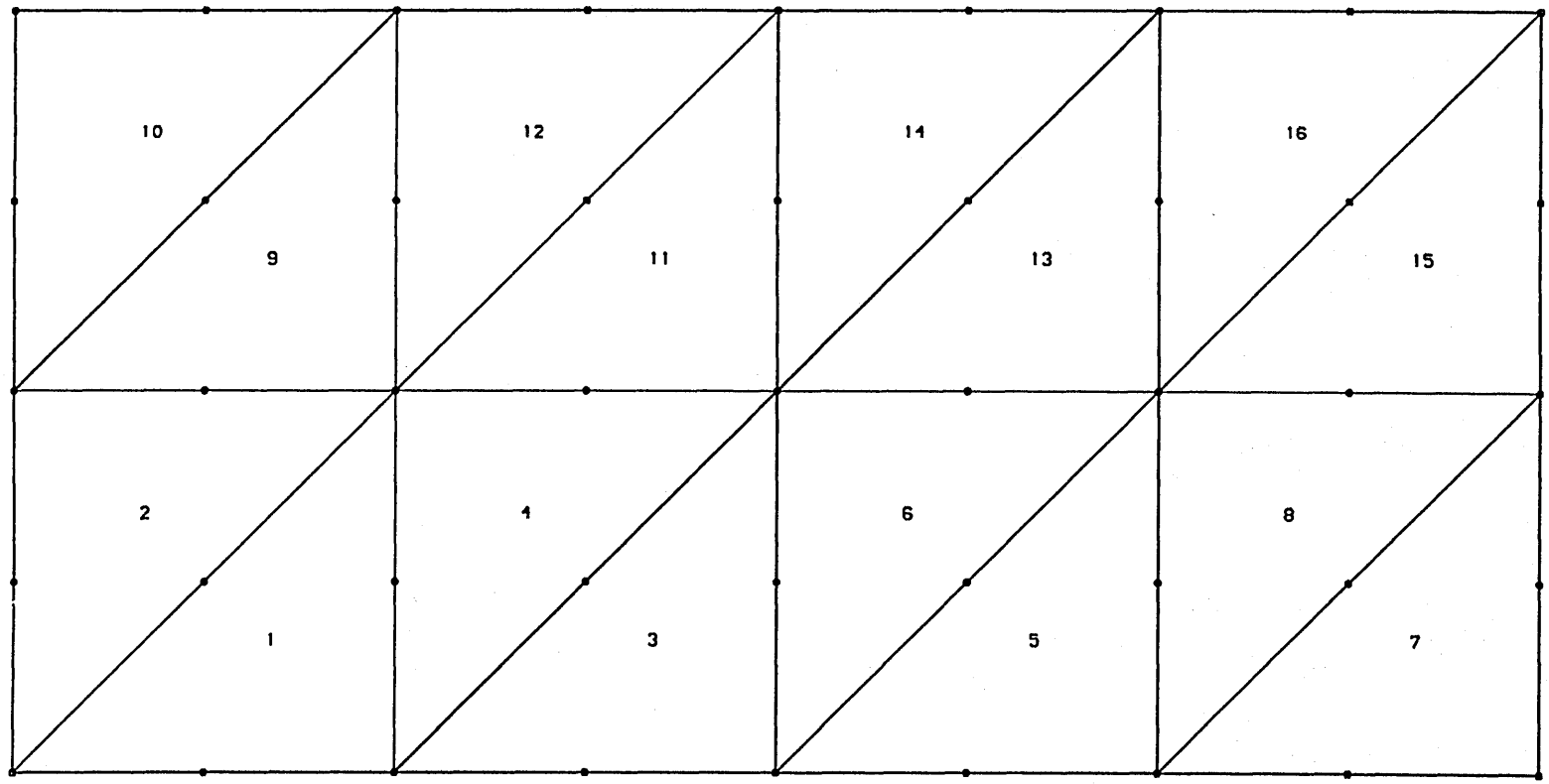

Fig.(C.5) Finite-Element Mesh For Plate under Tension generated using 6-Node Triangular Finite Elements.

FRAMEC

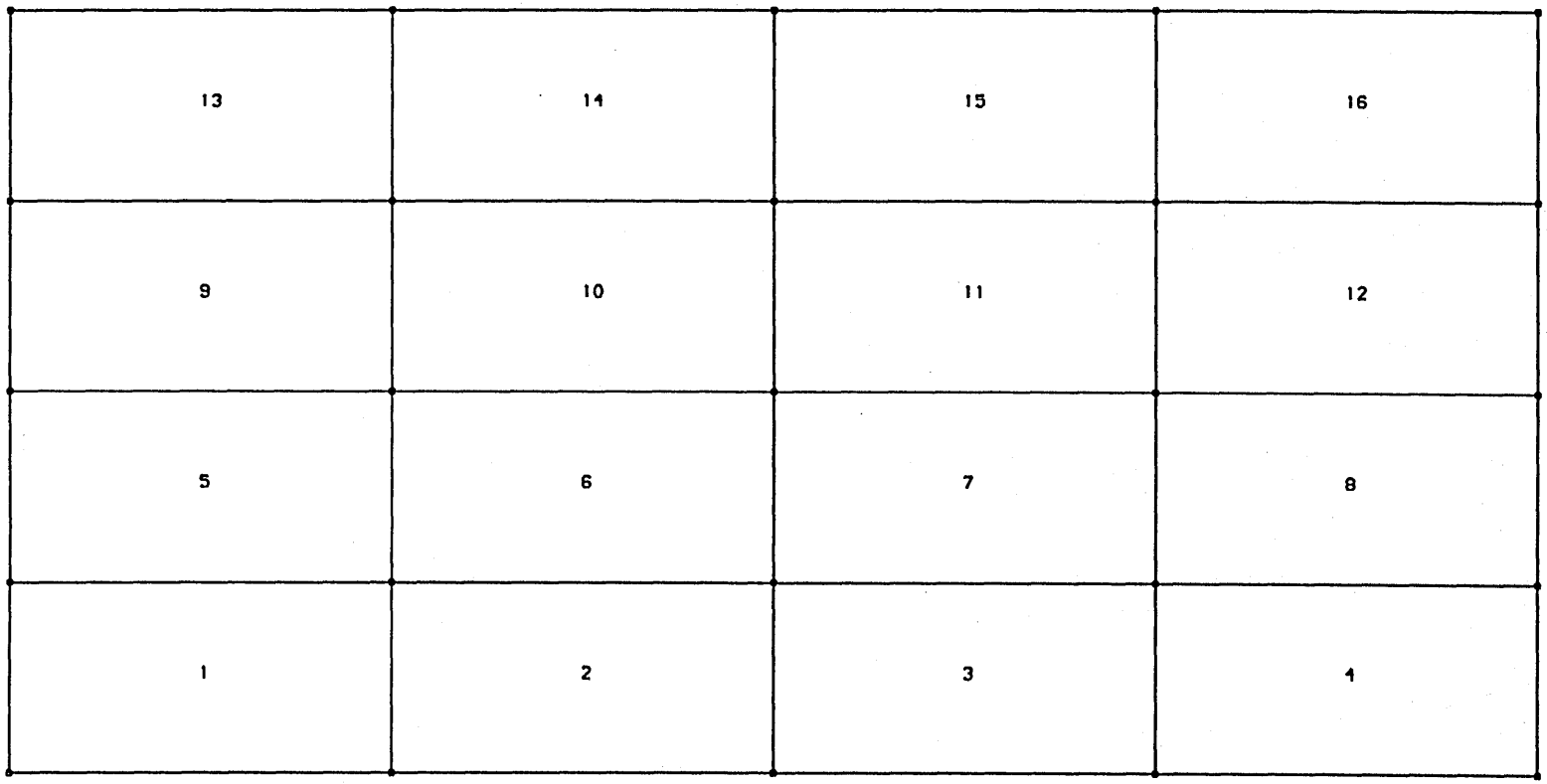

Fig.(C.6) Finite-Element Mesh For Plate under Tension generated using 4-Node Quadrilateral Finite Elements.

FRAMEC

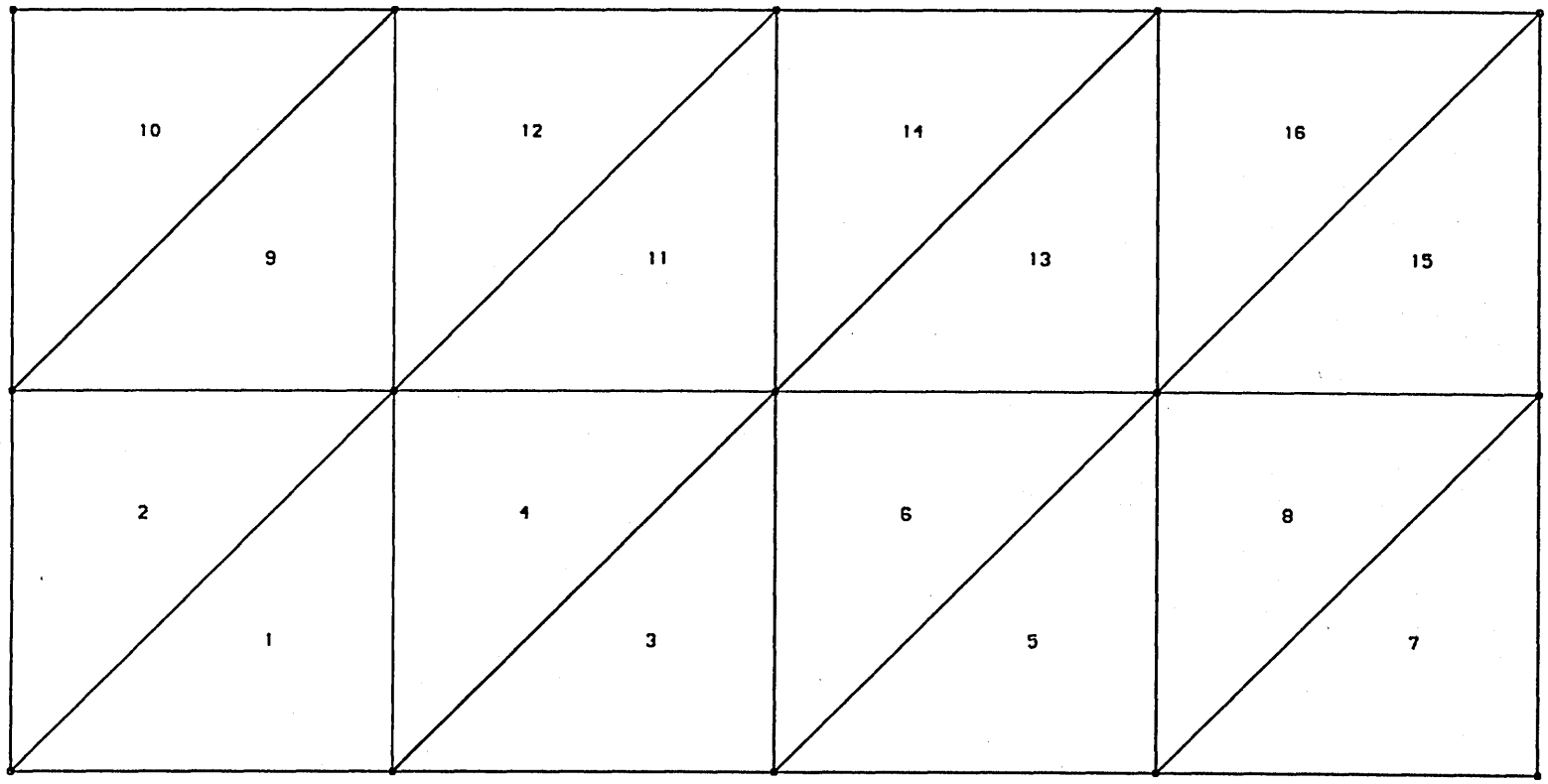

Fig.(C.7) Finite-Element Mesh For Plate under Tension generated using 3-Node Triangular Finite Elements.

FRAMEC

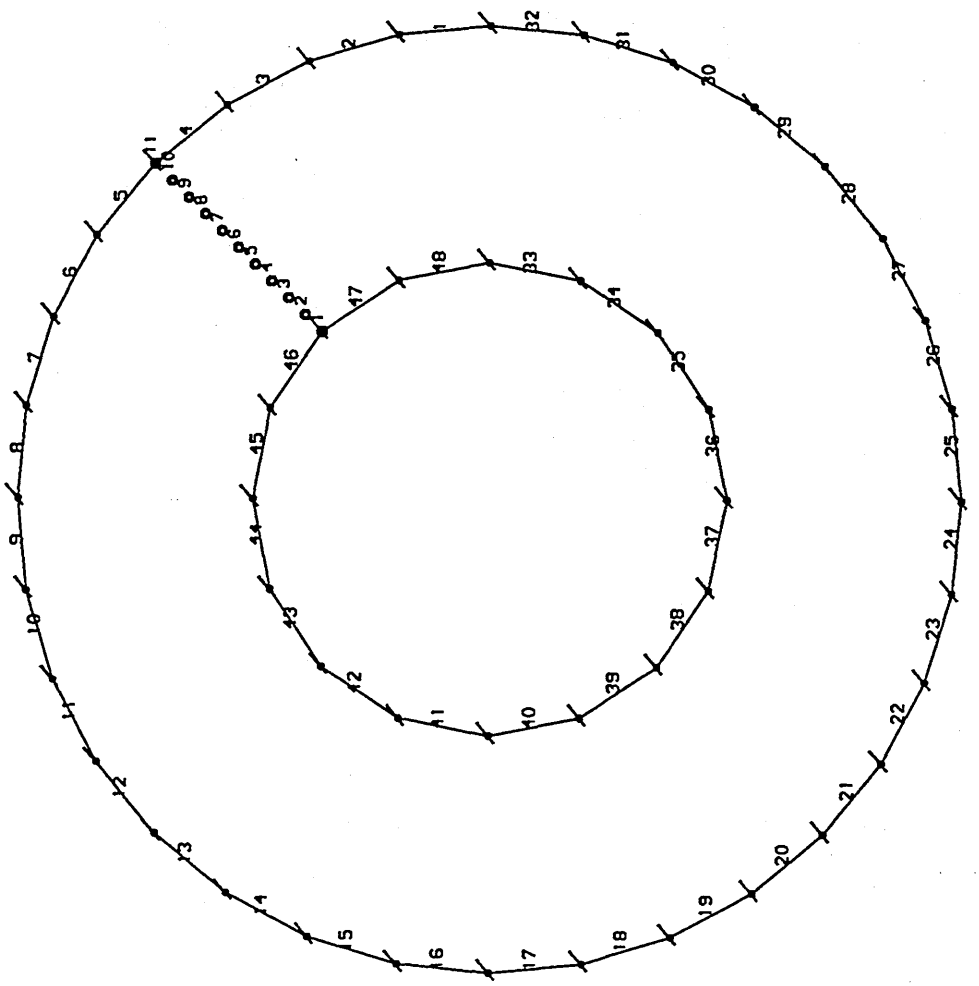

Fig.(C.8) Boundary-Element Mesh for Pressurized Cylinder generated using 2-Node Isoparametric Boundary Elements.

FRAMEC

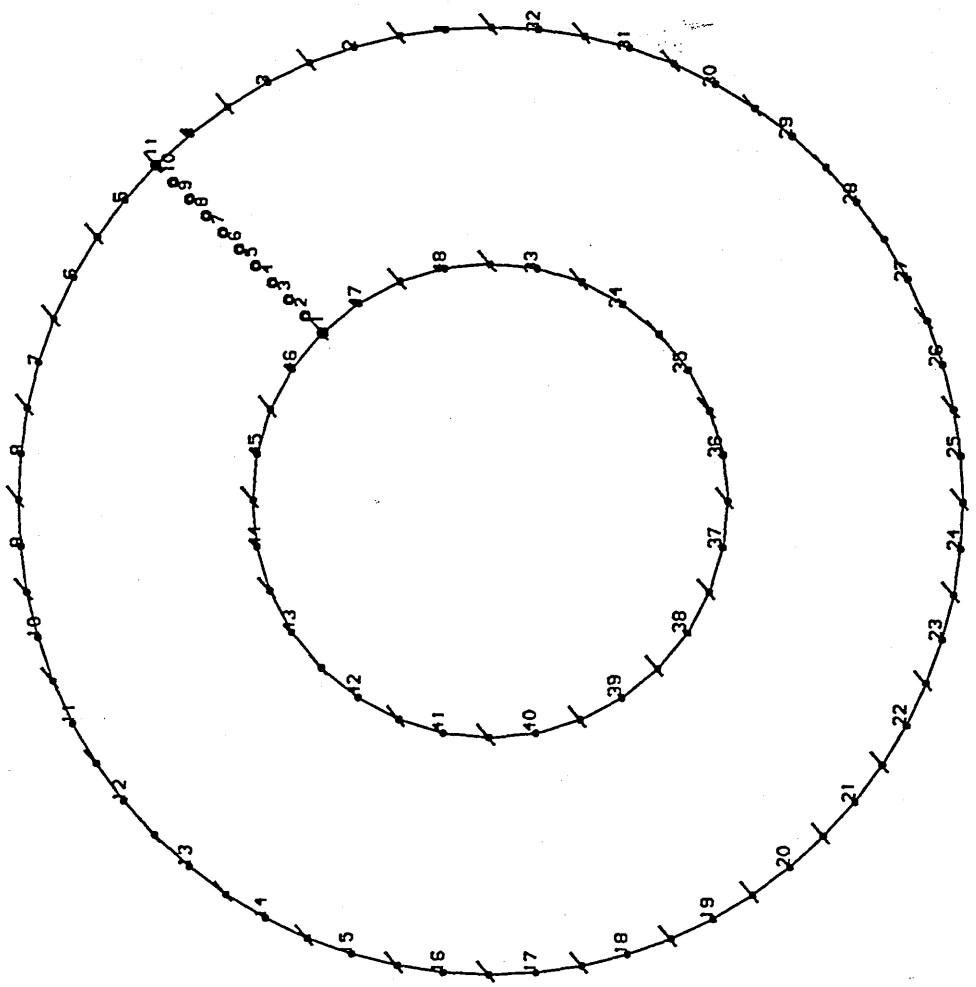

FRAMEC

Fig.(C.9) Boundary-Element Mesh For Pressurized Cylinder generated using 3-Node Isoparametric Boundary Elements.

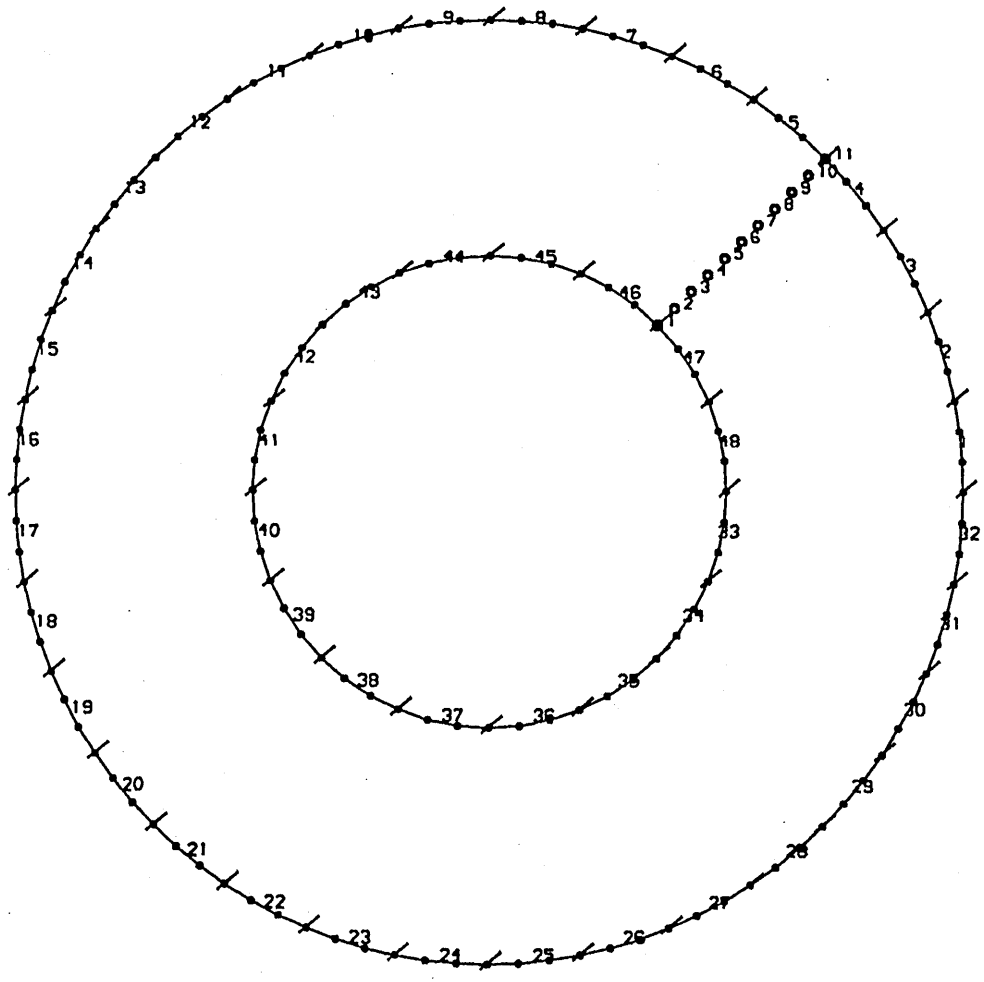

Fig.(C.10) Boundary-Element Mesh For Pressurized Cylinder generated using 4-Node Isoparametric Boundary Elements.

FRAMEC

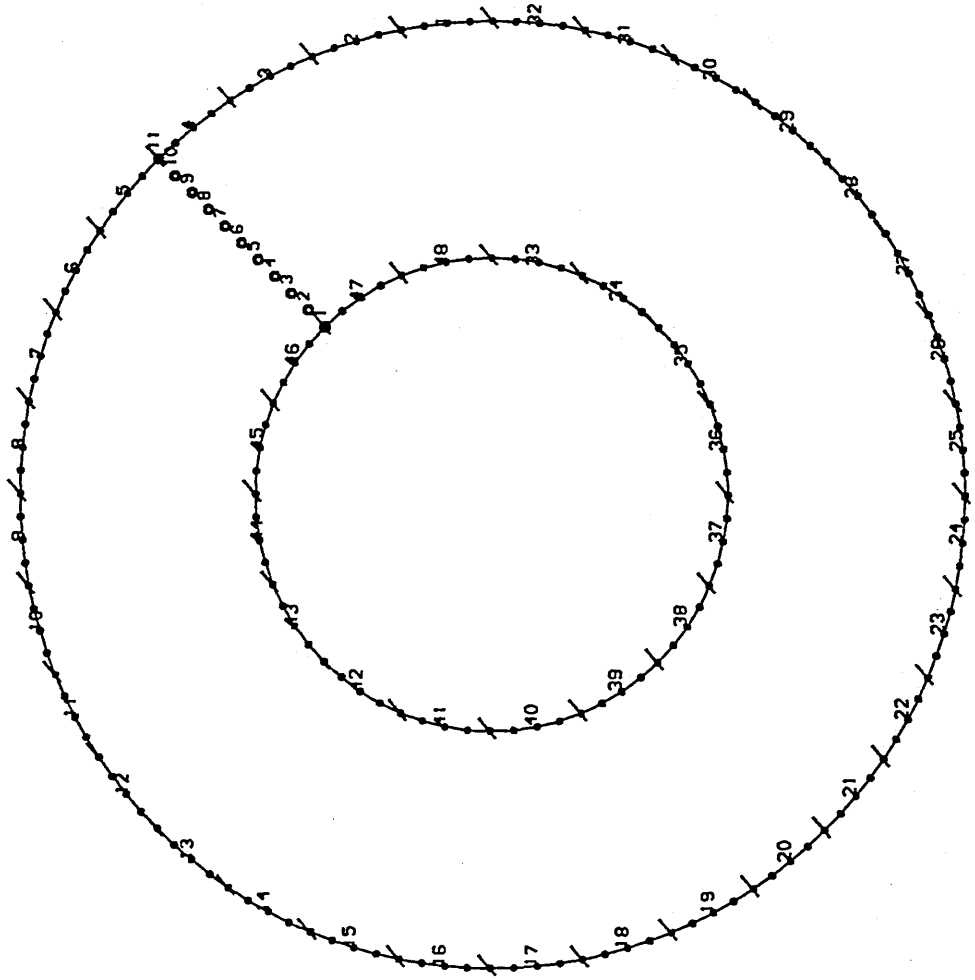

Fig.(C.11) Boundary-Element Mesh For Pressurized Cylinder generated using 5-Node Isoparametric Boundary Elements.

FRAMEC

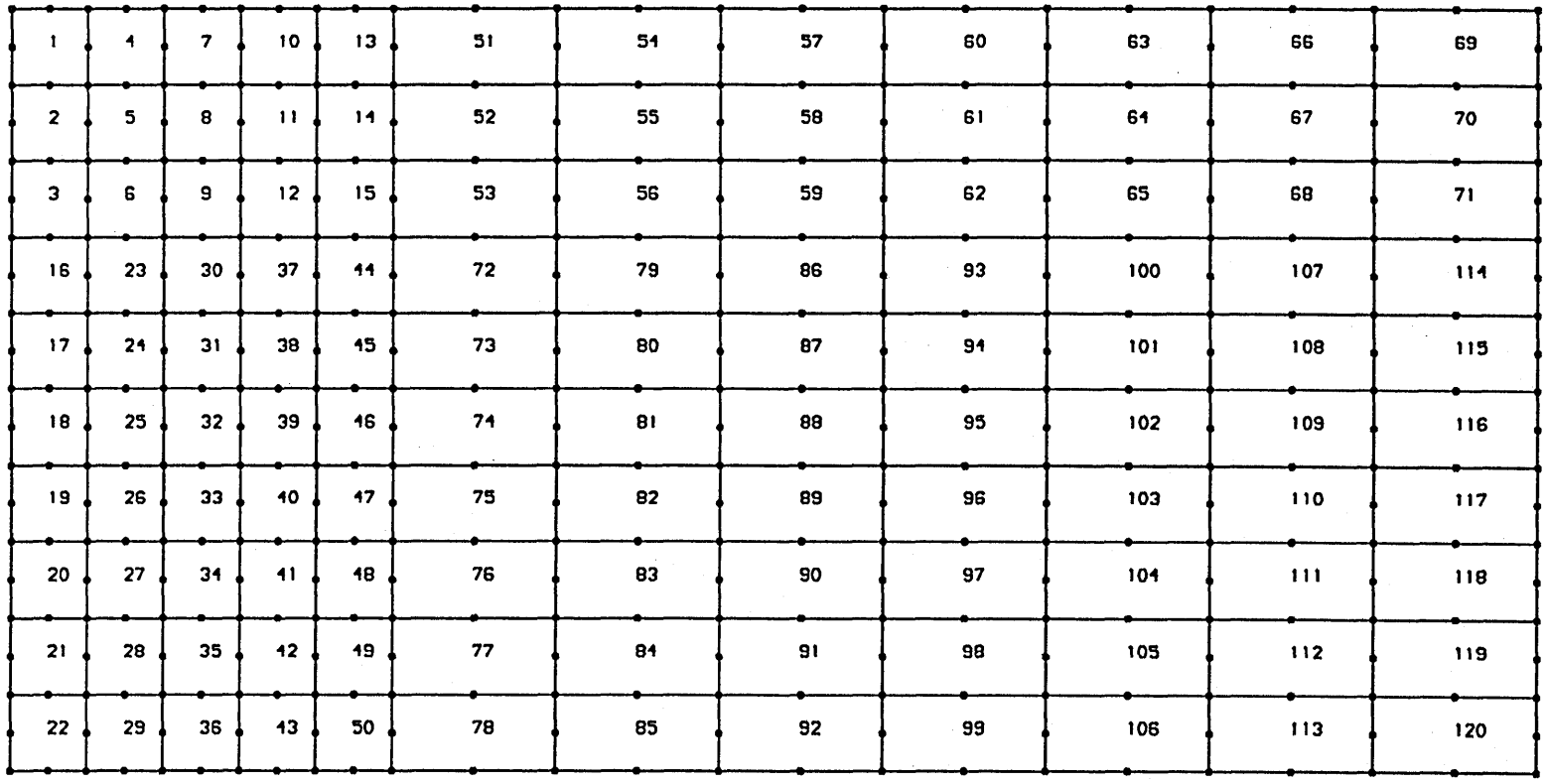

Fig.(C.12) Finite-Element Mesh For Central-Cracked Plate generated using 8-Node Quadrilateral Finite Elements.

FRAMEC

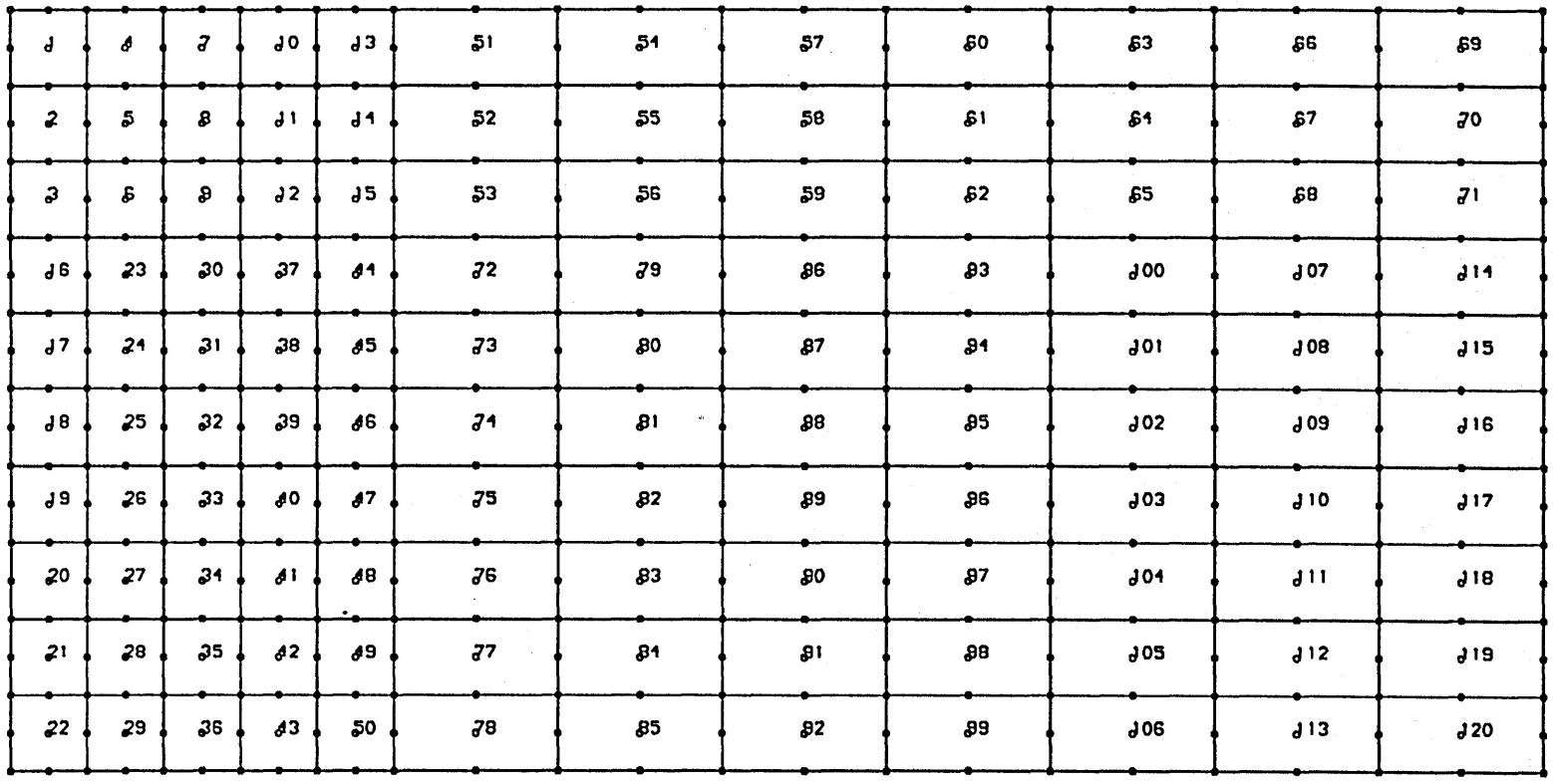

Fig.(C.13) Finite-Element Mesh For Central-Cracked Plate generated using 9-Node Lagrangian Quadrilateral Finite Elements.

FRAMEC

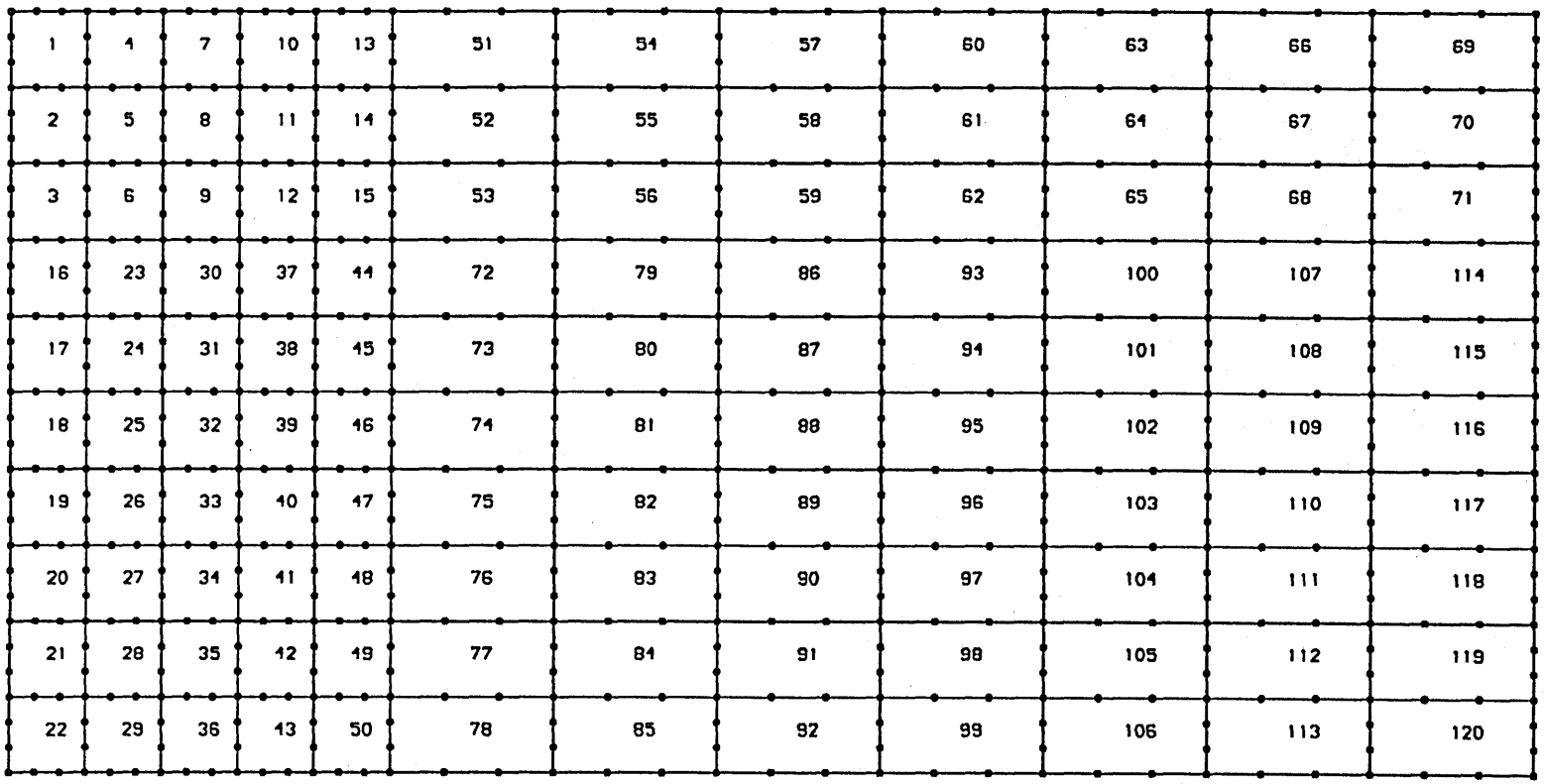

Fig.(C.14) Finite-Element Mesh For Central-Cracked Plate generated using 12-Node Quadrilateral Finite Elements.

FRAMEC

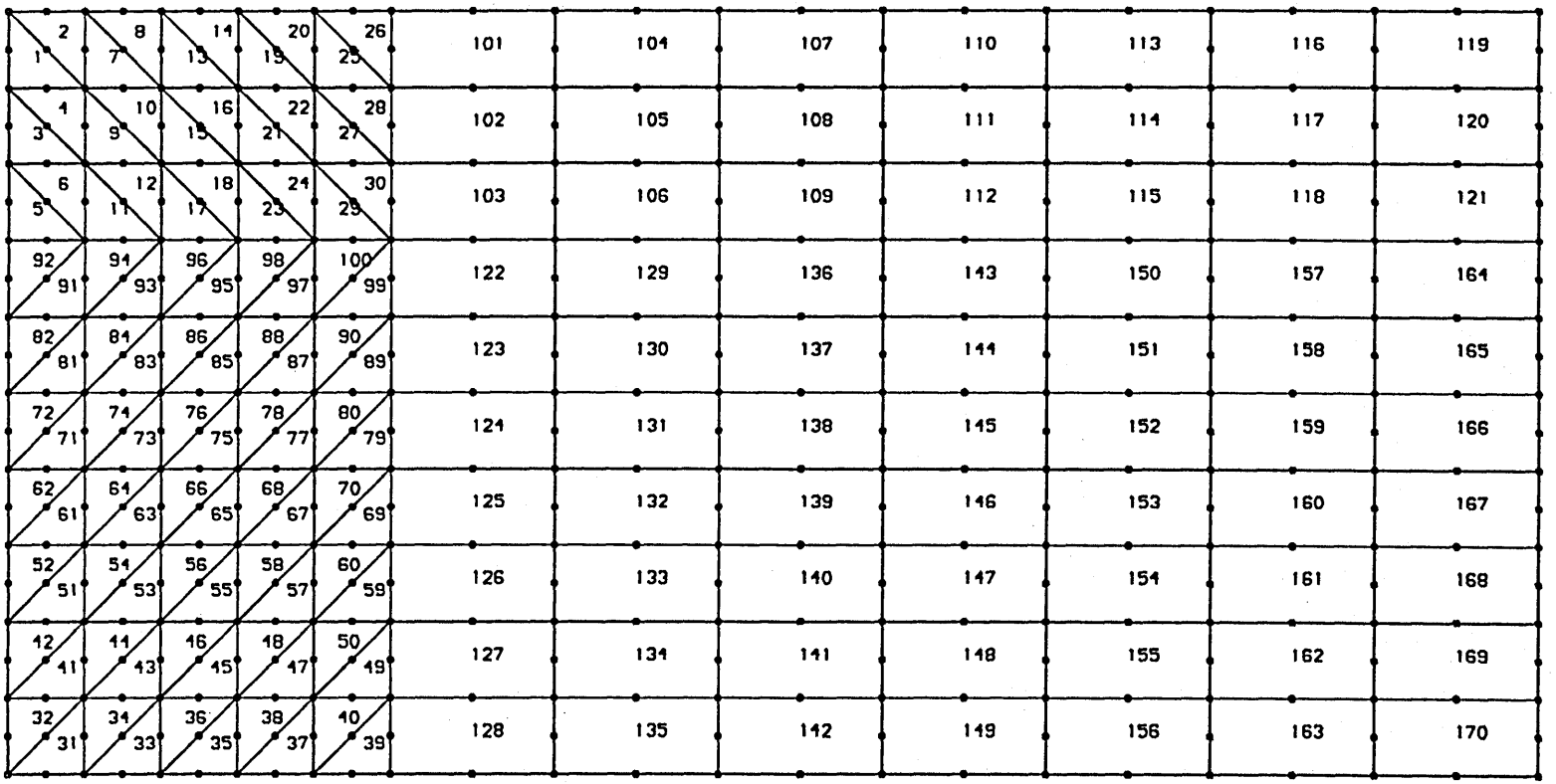

Fig.(C.15) Finite-Element Mesh For Central-Cracked Plate generated using 6-Node Triangular and 8-Node Quadrilateral Finite Elements.

FRAMEC

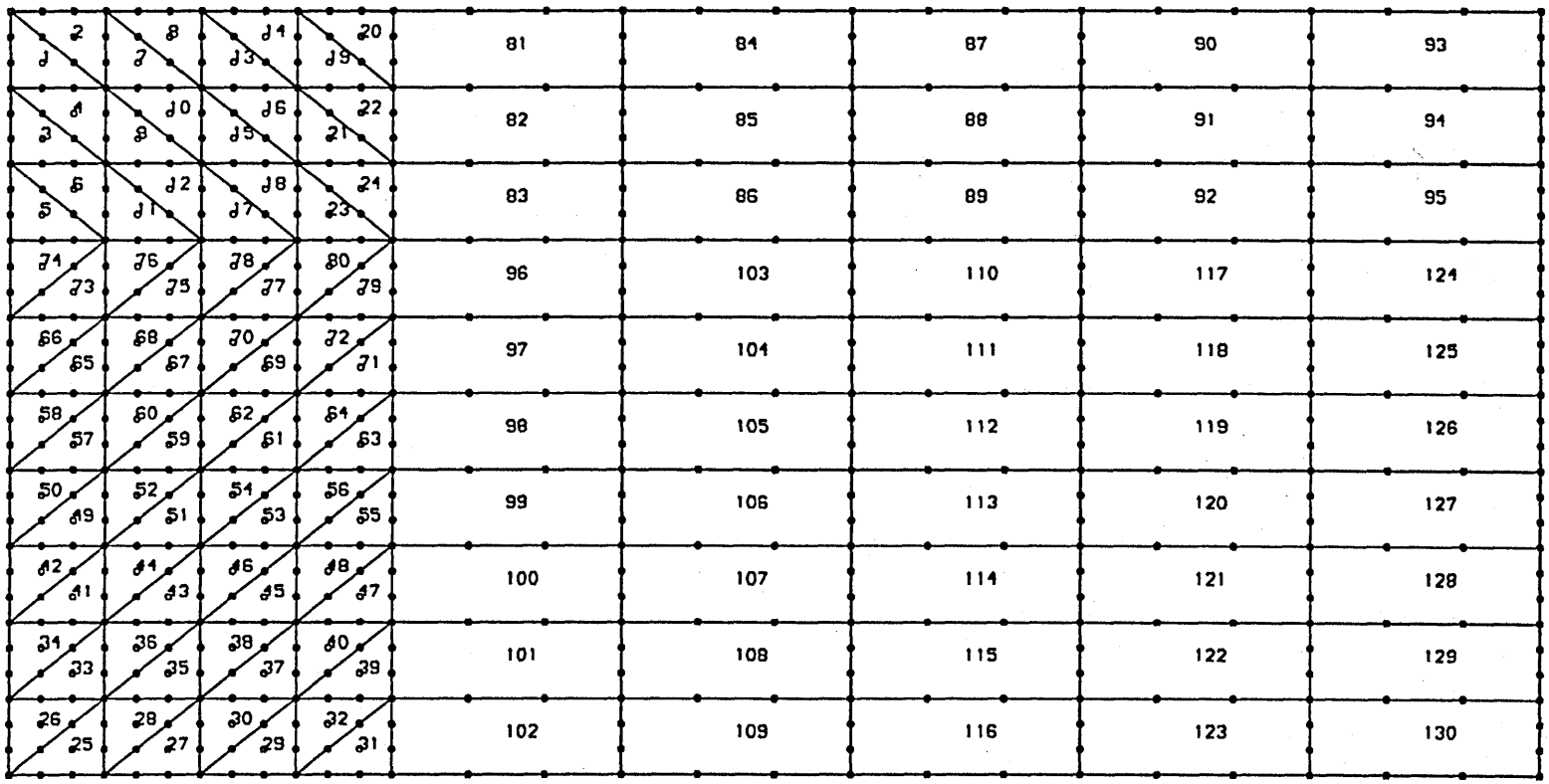

Fig.(C.16) Finite-Element Mesh For Central-Crcaked Plate generated using 10-Node Triangular and 12-Node Quadrilateral Finite Elements.

FRAMEC

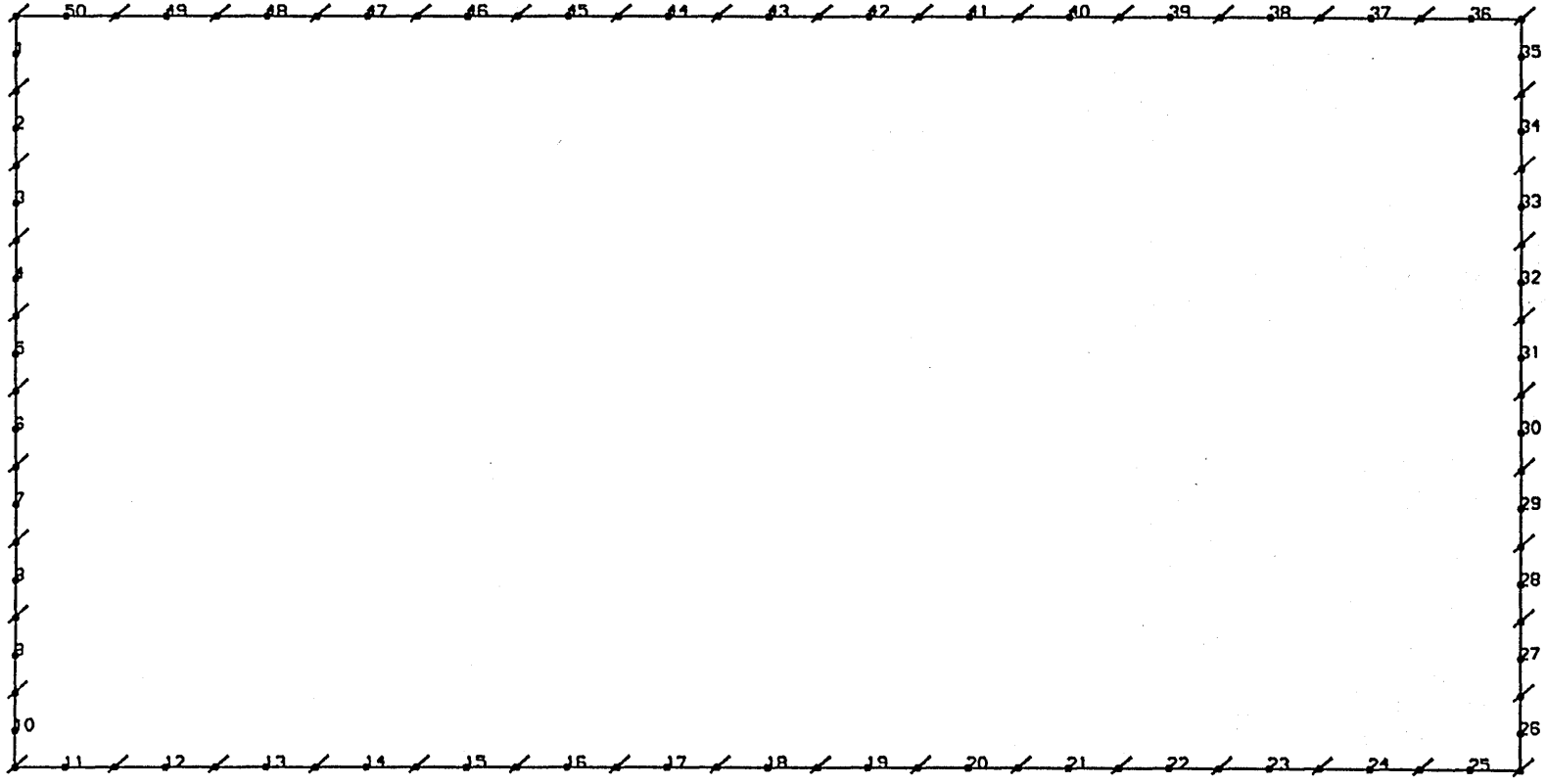

Fig.(C.17) Boundary-Element Mesh For Central-Cracked Plate generated using 3-Node Isoparametric Boundary Elements.

FRAMEC

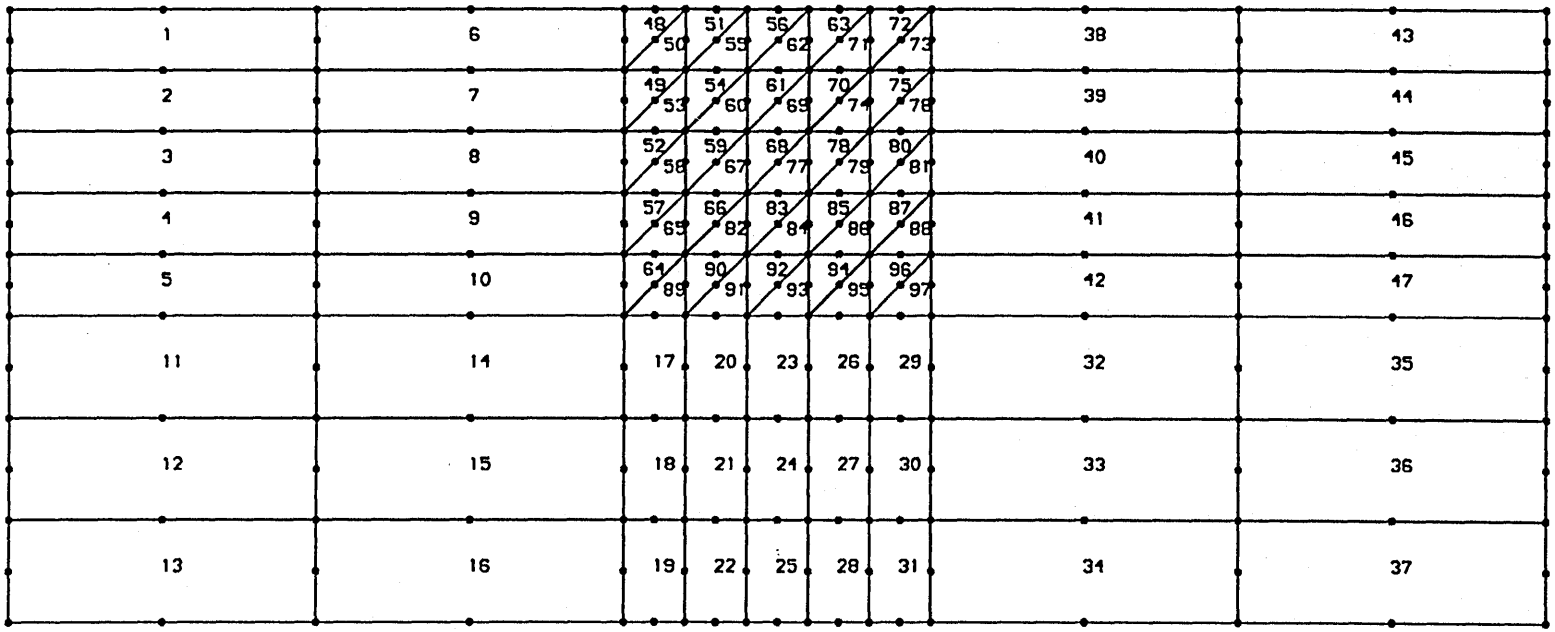

Fig.(C.18) Finite-Element Mesh For Single-Edge Crcaked Plate generated using 6-Node and 8-Node Finite Elements.

FRAMEC

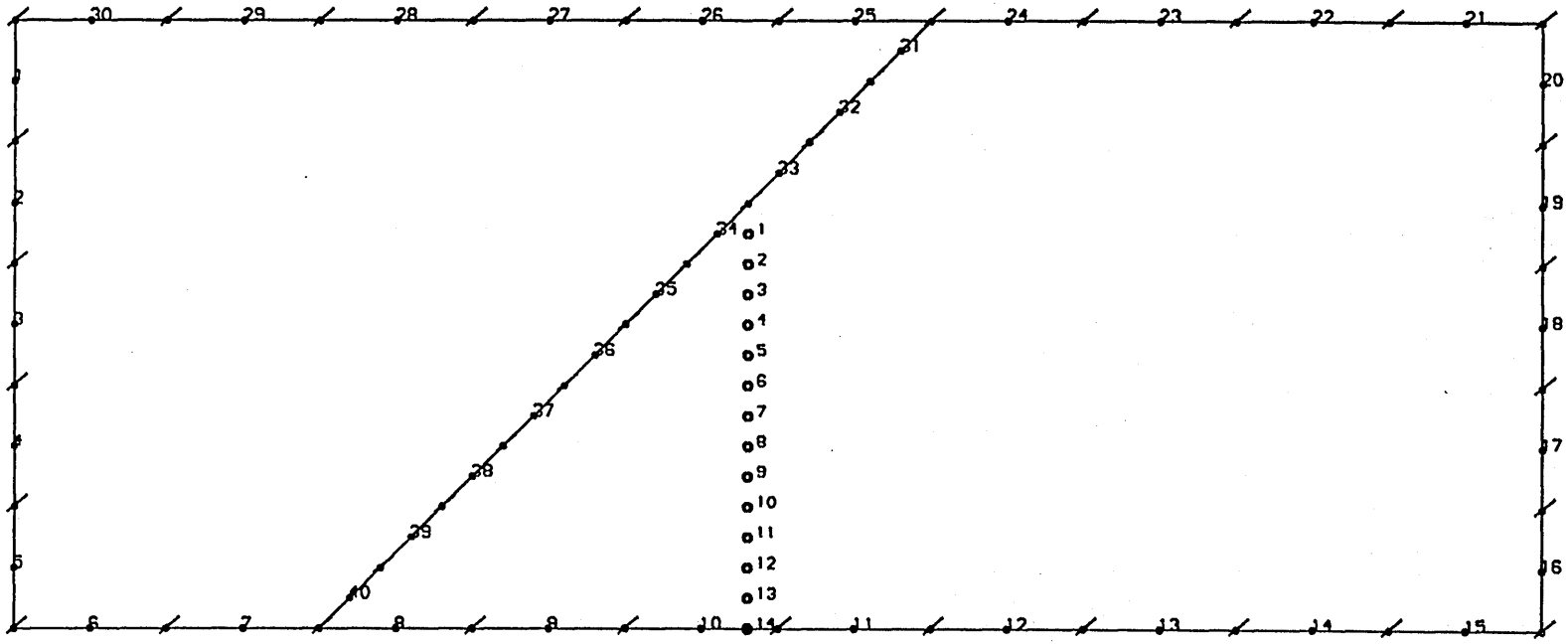

Fig.(C.19) Boundary-Element Mesh For Single-Edge Crcaked Plate generated using 3-Node Boundary Elements (Two Subregions).

FRAMEC

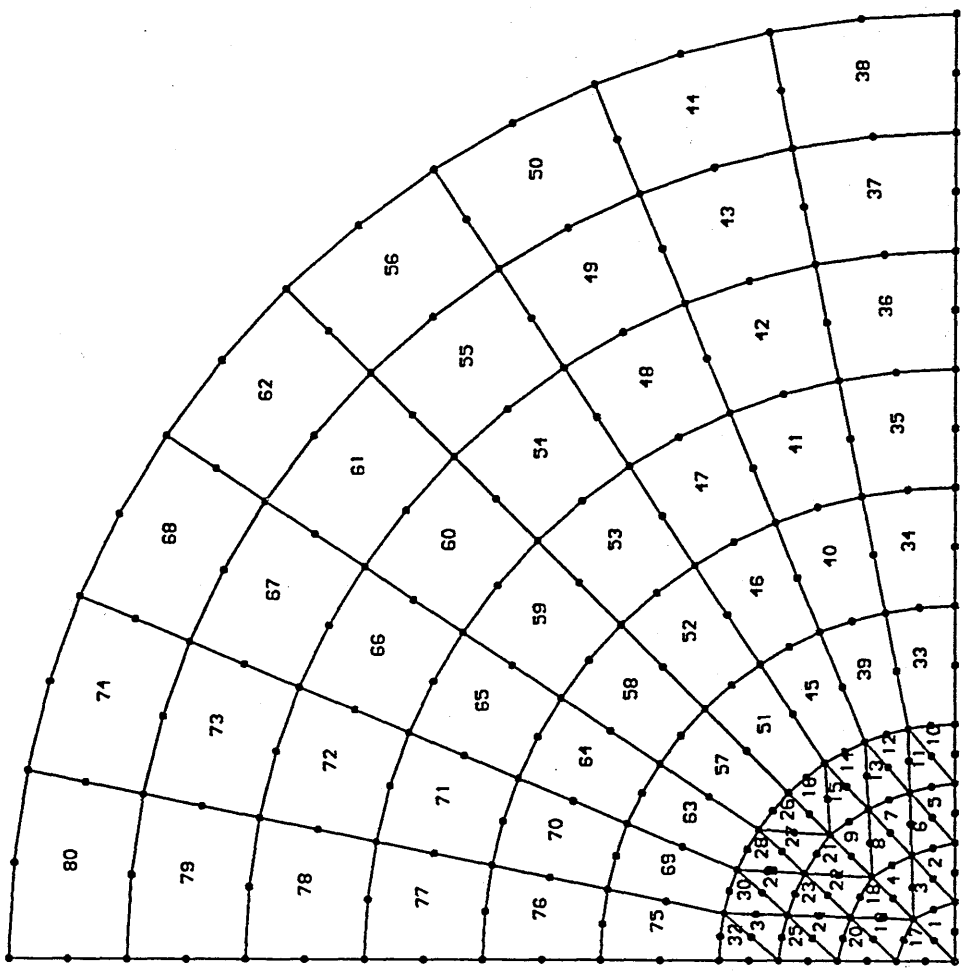

FRAMEC

Fig.(C.20) Finite-Element Mesh For Central-Crcaked Rotating Disc generated using 6-Node and 8-Node Finite Elements.

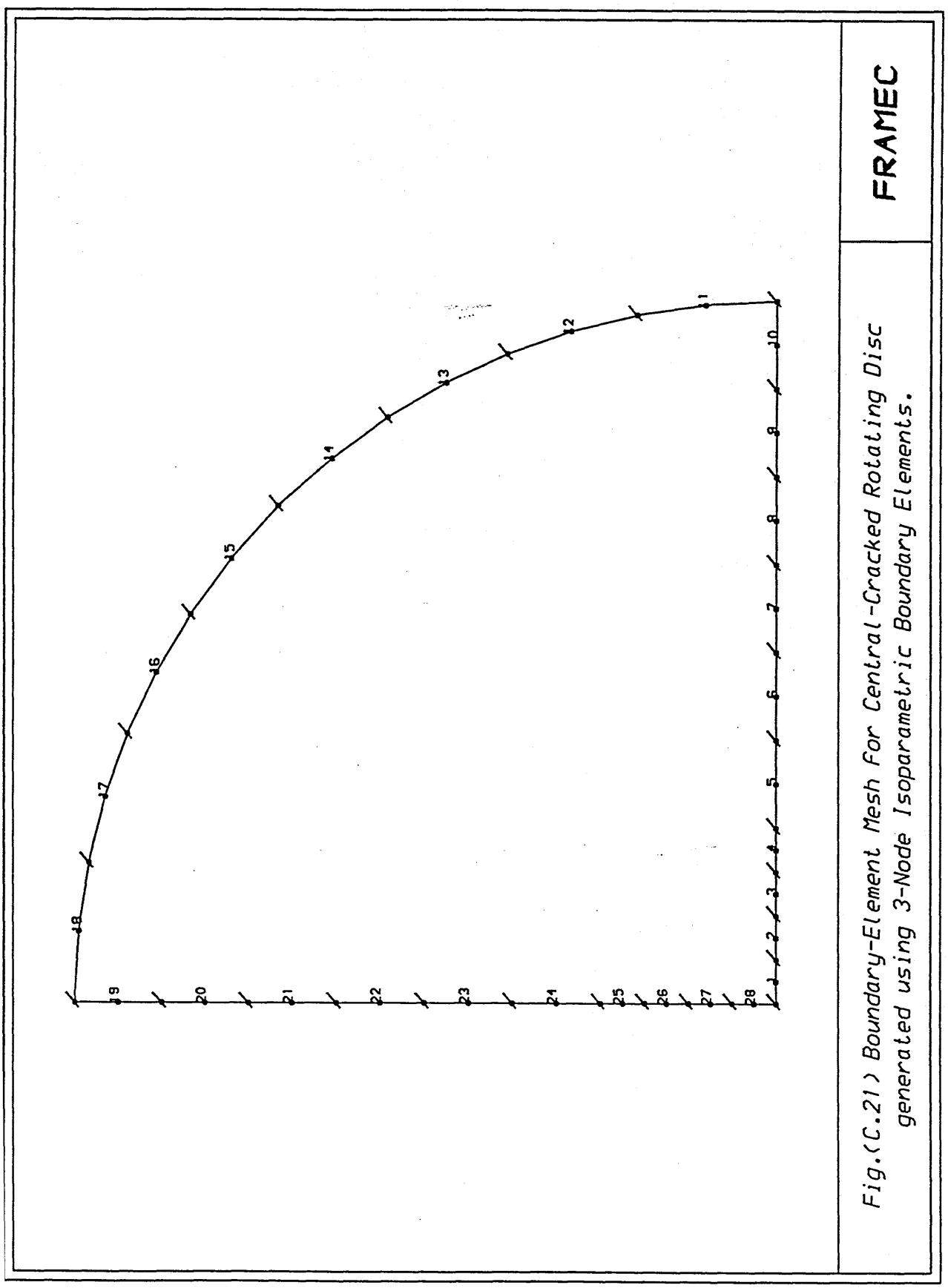

Fig.(C.21) Boundary-Element Mesh For Central-Cracked Rotating Disc generated using 3-Node Isoparametric Boundary Elements.

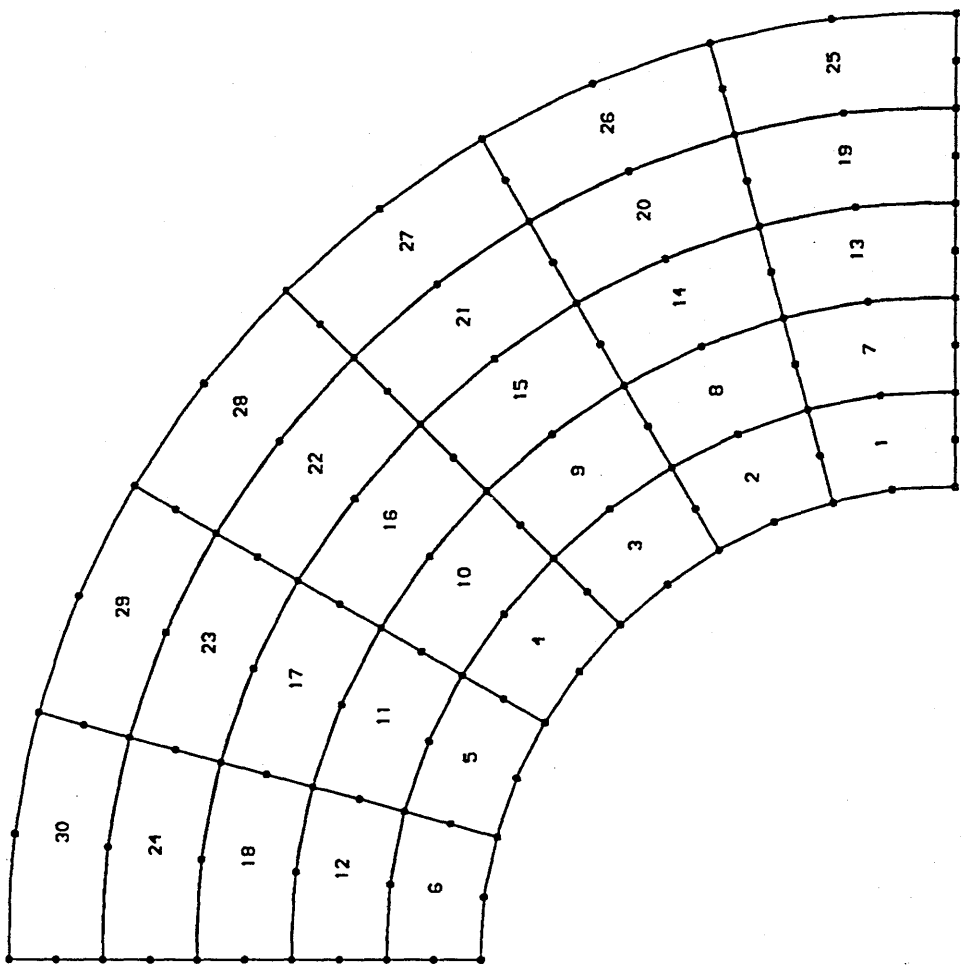

Fig.(C.22) Finite-Element Mesh For Pressurized Cylinder generated using 8-Node Quadrilateral Finite Elements.

FRAMEC

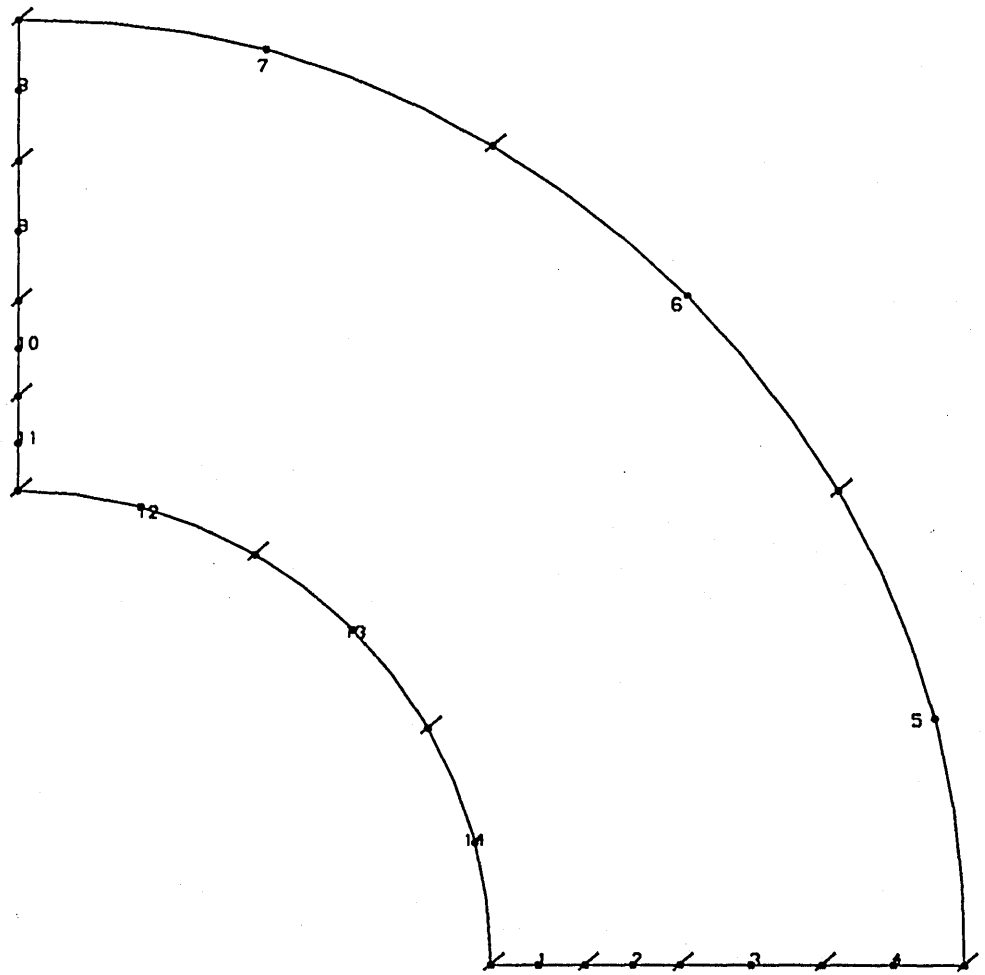

Fig.(C.23) Boundary-Element Mesh For Pressurized Thick Cylinder generated using 3-Node Isoparametric Boundary Elements.

FRAMEC

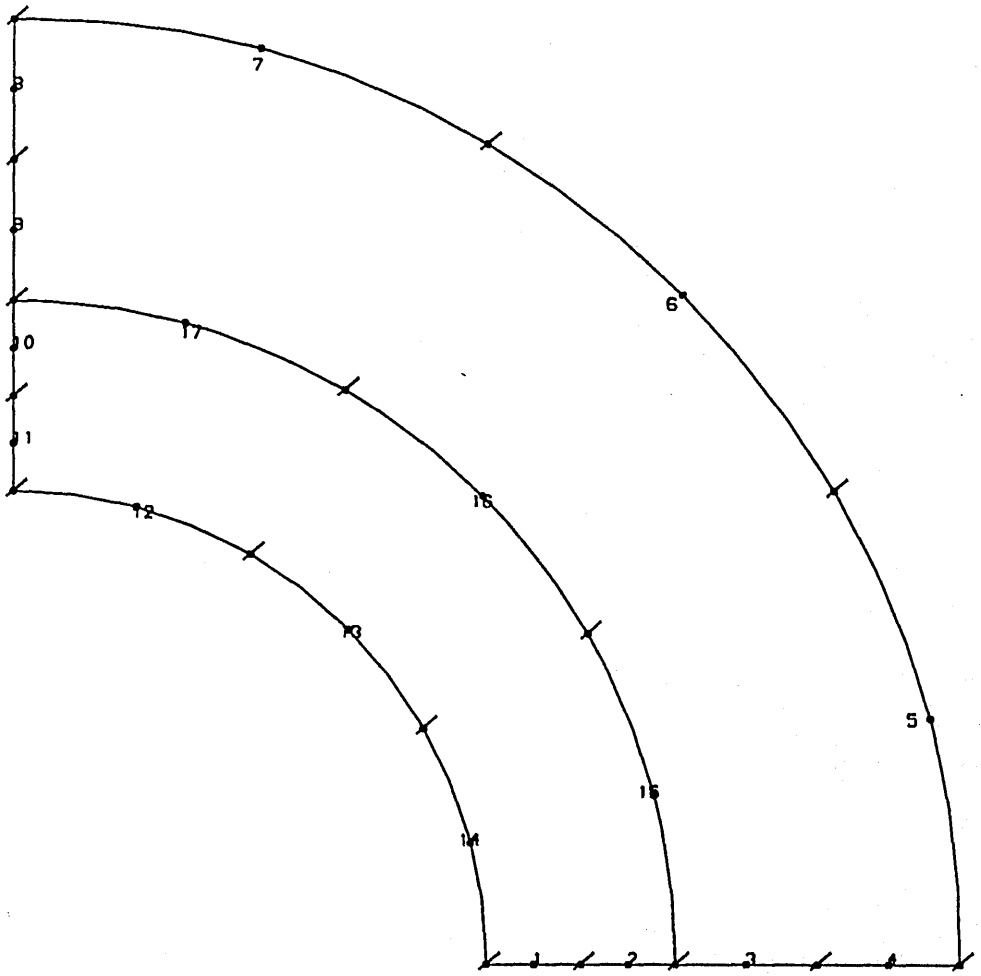

Fig.(C.24) Boundary-Element Mesh For Pressurized Thick Cylinder generated using 3-Node Boundary Elements (Two Subregions).

FRAMEC

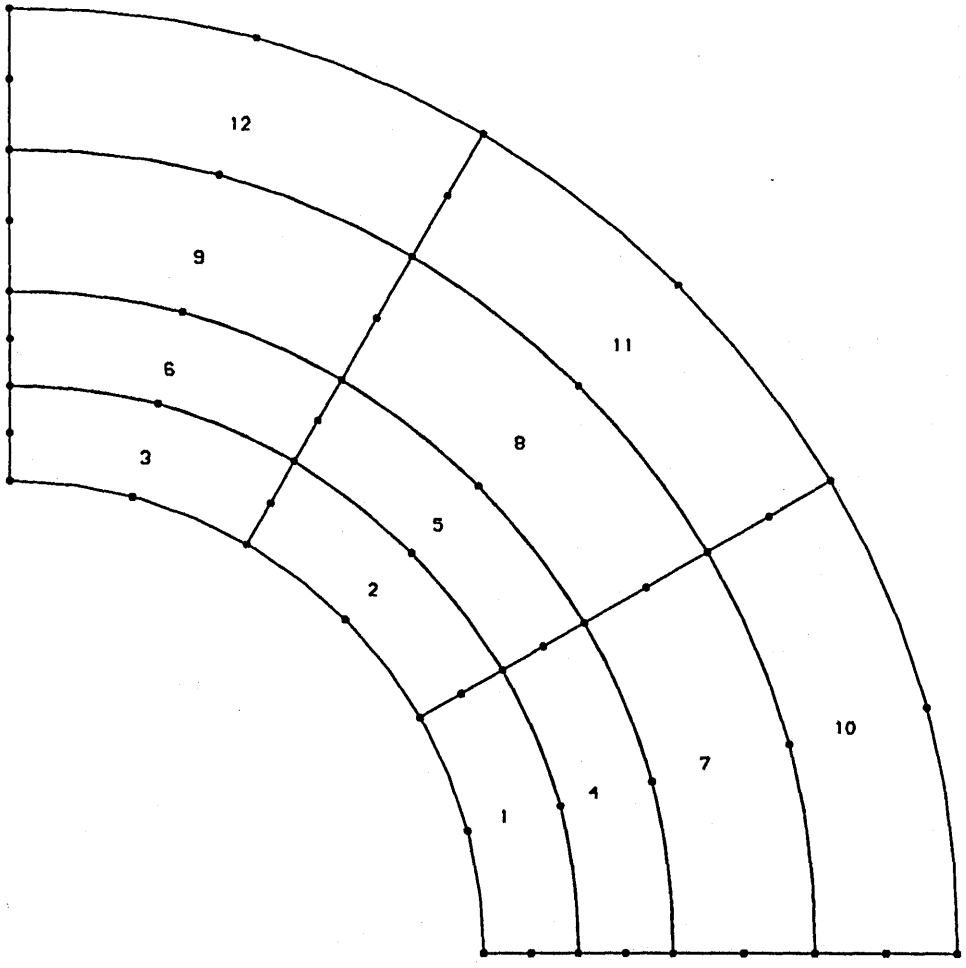

Fig.(C.25) Integration-Cell Mesh For Pressurized Thick Cylinder generated using 8-Node Quadrilateral Finite Elements.

FRAMEC

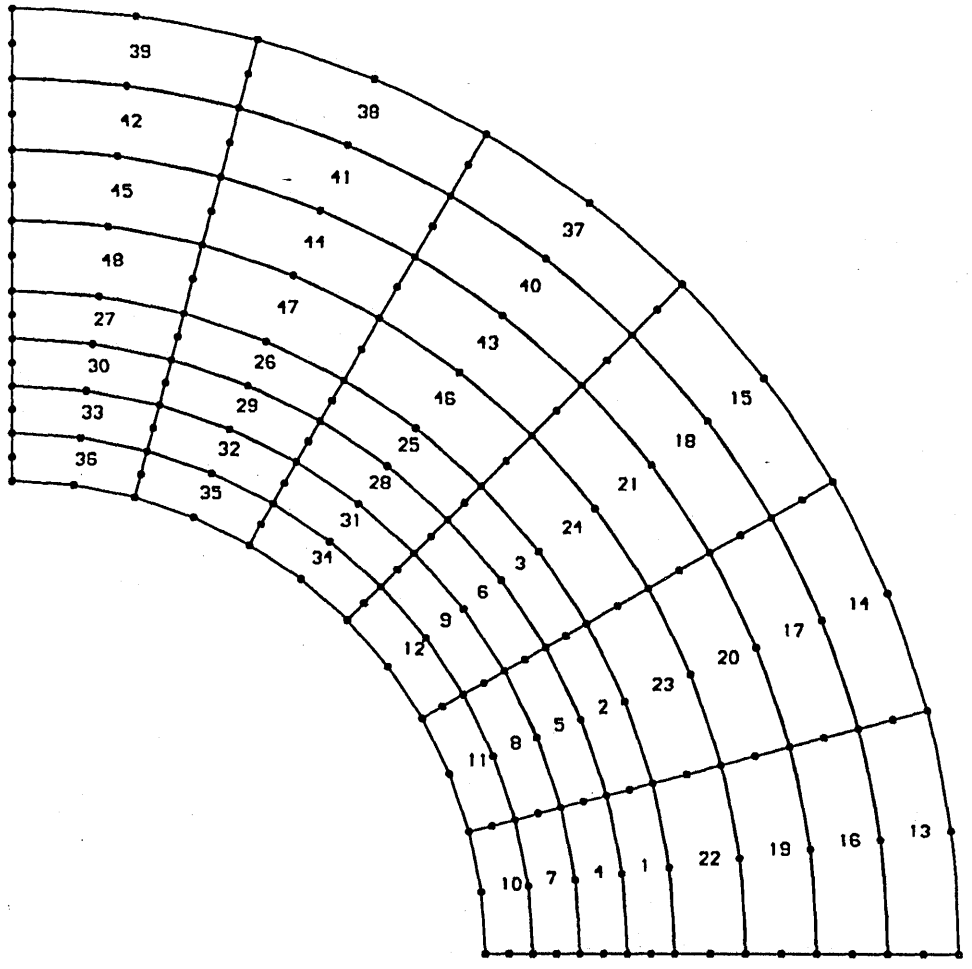

Fig.(C.26) Finite-Element Mesh For Symmetrically Cracked Pressurized Cylinder generated using 8-Node Quadrilateral Finite Elements.

FRAMEC

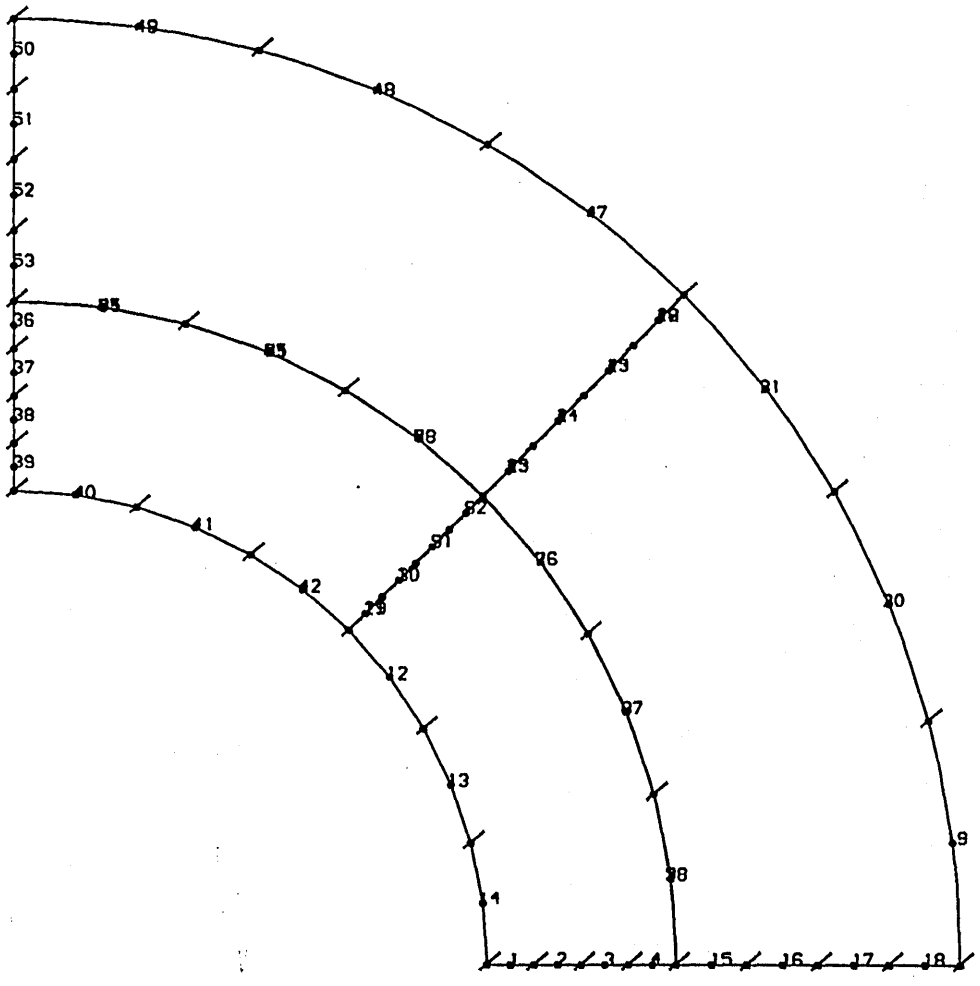

Fig.(C.27) Boundary-Element Mesh For Symmetrically Crcaked Pressurized Cylinder generated using 3-Node Boundary Elements (4-Subregions).

FRAMEC

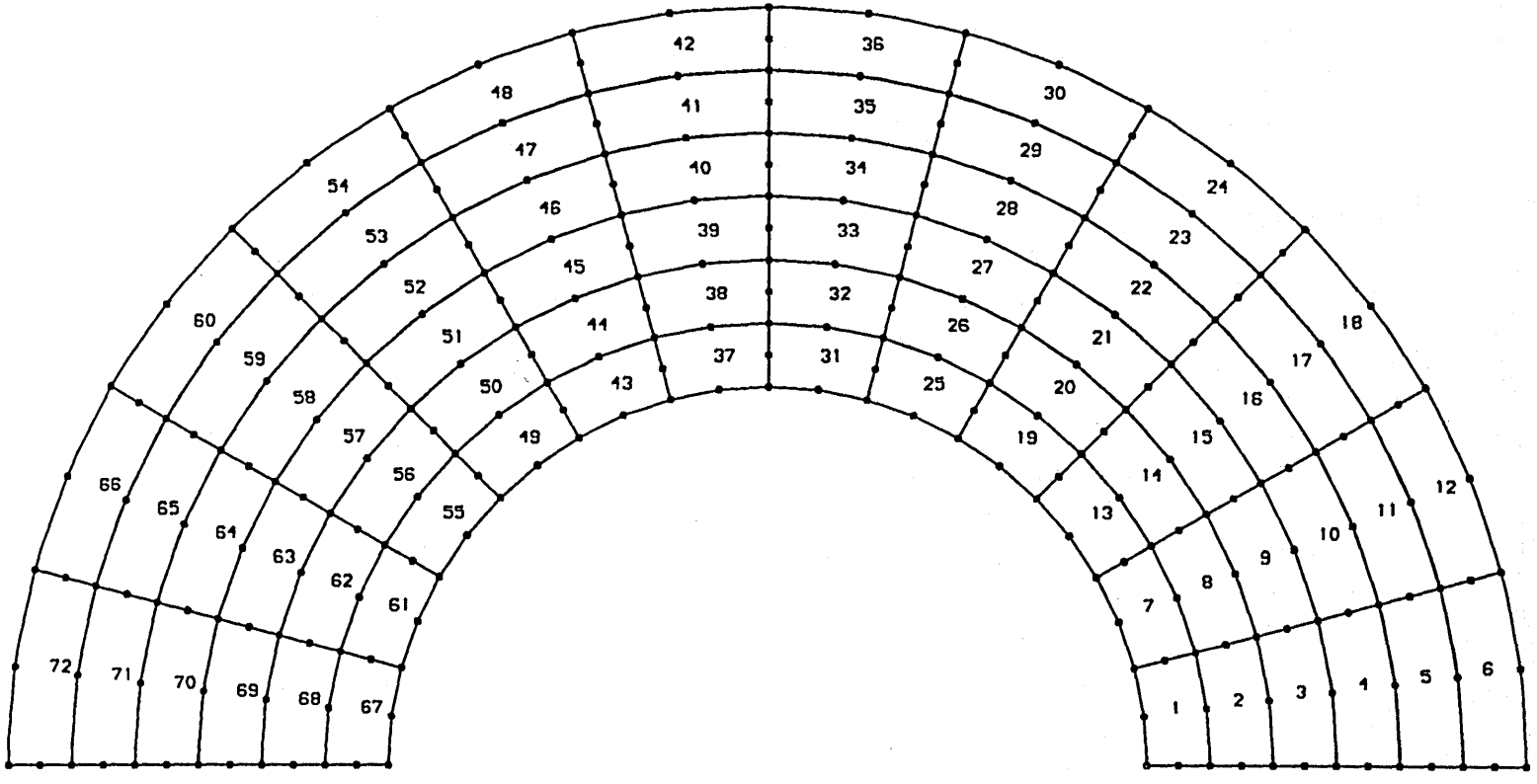

Fig.(C.28) Finite-Element Mesh For Pressurized Thick-Walled Cylinder generated using 8-Node Quadrilateral Finite Elements.

FRAMEC

APPENDIX D

APPENDIX D

Derivation of the Elasto-Plastic J-Integral Expressions for Pressurized Cylinder

For the case of pressurized cylinder as shown in Fig.(9.47), the *J*-integral expressions for plane stress and plane strain conditions can be derived as follows:

Considering the outer boundary of one quarter of the cylinder as the *J*-integral contour, and assuming that the structure contains a crack of zero length, then the *J*-integral expression for such a case can be written as follows:

$$J = \frac{1}{2} \int_{\Gamma} \underline{\sigma}^{t} \; \underline{\varepsilon} \; dy \qquad (D.1)$$

For this case:

$$dy = r_o \cos\theta \; d\theta \qquad (D.2)$$

where r_o is the outer radius of the cylinder.

Now, for the quarter cylinder, equation (D.1) can be expressed as follows:

$$J = \frac{1}{2} r_o \int_{o}^{\pi/2} \underline{\sigma}^{t} \; \underline{\varepsilon} \cos\theta \; d\theta \qquad (D.3)$$

Assuming Tresca criterion, the stress and strain relations for this case are given in Ref.[72] as follows:

(a) For Plane-Stress Condition:

$$\sigma_r = 0 \; , \qquad \tau_{r\theta} = 0$$

$$\sigma_\theta = \frac{YC^2}{r_o^2}, \qquad \varepsilon_\theta = \frac{Y}{E}\left(\frac{C}{r_o}\right)^2 \tag{D.4}$$

(b) For Plane-Strain Condition:

$$\sigma_r = 0, \qquad \tau_{r\theta} = 0$$

$$\sigma_\theta = \frac{YC^2}{r_o^2}, \qquad \varepsilon_\theta = \frac{Y}{E}\left(\frac{C}{r_o}\right)^2 (1-\nu^2) \tag{D.5}$$

where C is the radius of the plastic zone which can be estimated from the following expression:

$$\frac{2P_i}{Y} = 1 - \left(\frac{C}{r_o}\right)^2 + 2\log\left(\frac{C}{r_i}\right) \tag{D.6}$$

Now, by substituting from equations (D.4) and (D.5), the integration in equation (D.3) can be solved and expressions for the J-integral can be obtained as follows:

$$J = \frac{r_o}{2E} Y^2 \left(\frac{C}{r_o}\right)^4 \qquad \textit{for plane-stress condition,}$$

$$J = \frac{r_o}{2E} Y^2 \left(\frac{C}{r_o}\right)^4 (1-\nu^2) \qquad \textit{for plane-strain condition.}$$